Cranfield University

College of Defence Technology

Engineering systems department

PhD Thesis

Academic Year 2005

Dhanalakshmi Muniasamy

Behaviour of semi-rigid composite connections for steel framed buildings

Supervisor: Dr. M. P. Byfield

ABSTRACT

During propped construction the steel-concrete composite action resists dead as well as imposed loads. Conversely, the steel section alone resists the floor self-weight in unpropped beams. The major difference between propped and unpropped composite beams lies in the ductility requirements rather than in the strength requirements. Relatively few studies have been carried out to assess the rotation requirements for unpropped semi-continuous composite beams. The outstanding critical factor in the case of unpropped construction is the dead load stress that must be carried by the steel beam alone prior to hardening of the concrete.

This research overcomes the difficulties involved in modelling the composite and non-composite stages by using a numerical integration technique developed from the basic principles of structural mechanics. The method incorporates the fully non-linear material properties and requires very little assumption. The technique was initially validated using the experimental results from plain steel beam bending tests. The subsequent comparison between the model predictions and the results from the large-scale frame test carried out for this research purpose, showed that the method is capable of predicting non-elastic load vs. end rotation behaviour within a high degree of accuracy. Thus the model can be used with confidence in order to predict the connection rotation requirements for a wider range of loading configurations than is practically possible from experimental testing alone.

A parametric study is carried out using the numerical integration technique developed for the semi-continuous composite beam on a total of 2160 different beam configurations, utilising different steel grades and loading conditions. In this study the influence of dead load stress on the connection rotation requirement has been thoroughly evaluated along with several other factors including span to depth ratio, location within the building frame, ratio between the

support (connection) moment capacity and span (beam) moment capacity, loading type, steel grade and percentage of the beam strength utilised during design. The connection rotation capacity requirements resulting from this study are assessed to establish the scope for extending the use of composite connections to unpropped beams.

The large-scale experiment that has been carried out provided an opportunity to investigate the behaviour of a modified form of composite connection detail for use at perimeter columns (single-sided composite connections) with improved rebar anchorage. Additionally, another extensive parametric study is carried out using the numerical integration technique developed for the steel beam to establish the influence of strain-hardening on elastic-plastic frame instability design.

ACKNOWLEDGEMENT

I would like to thank my supervisor, Dr. Mike Byfield for his invaluable advice, guidance, constant encouragement and helpful criticism throughout the course of this research. I would like to acknowledge the contributions of Dr David Moore of the Building Research Establishment in the UK and Professor David Anderson of Warwick University, who were collaborators on the research presented herein, which was financed by the Engineering and Physical Sciences Research Council and the DETR. I would like to thank Dr. Graham Couchman of the Steel Construction Institute for his valuable time and constructive discussion and guidance in the critical part of this research. I would like to thank Dr. Hugh Goyder and Prof. Mike Davies for their valuable advice in modelling and computing.

I would like to thank all technical staffs at the Building Research Establishment, especially Mr. Dave White for his patient support in the experimental work. I would like to thank all my dear colleagues both staff and students of the Engineering Systems Department, and most particularly Prof. John Hetherington, Dr. Mike Iremonger and Mrs. Ros Gibson for their kind support in my student life.

I would like to thank Ron and Sue Colyer for their kindness and love without which it would have been difficult to study in a foreign land. Finally I would like to thank my family in India and in France for their constant encouragement and understanding. I would give special thanks to my husband, Dr. Lilian Bruyere, for his patience, moral and mental support during these years. I sincerely thank Jesus Christ for the grace and strength He has given me in this land.

Table of contents

List of Figures

List of Tables

Chapter 1 – Introduction

1.1 Background

Of all new multi-storey buildings in the developed countries, approximately 40% use composite floor construction. This type of construction is structurally efficient because it exploits the tensile resistance of the steel beams and the compressive resistance of the concrete slabs. This composite action increases the depth of the beam thereby increasing the flexural strength and stiffness and consequently results in reduced span-depth ratios. Research has shown that more savings, approximately 25% on weight and depth of individual beams, can be achieved if a composite connection could be employed. In such a connection, increased moment of resistance can be achieved by introducing slab reinforcement, which acts like an additional row of bolts in bare steel moment connections.

In semi-continuous frames the flexural strength of the composite connections is significantly less than that of the beams. Therefore, significant moment redistribution from the supports to the spans is necessary in order to permit the design sagging moment capacities to be attained in the composite beam section. This places a significant requirement on the rotation capacity of the connections. In order to determine the potential for moment redistribution, it is essential to know, not only the maximum rotation available from the connection (available rotation capacity), but also the beam end rotation required to achieve the design moment in the span (required rotation capacity). The available rotation capacity must be greater than the required rotation in order to utilise a given proportion of the flexural strength of the beam, typically between 0.85 and $1.0M_p$. Therefore, it is important to quantify both the available and required rotations during the development of design guides. Whilst connection performance is dependent on the detail selection, the rotation requirement demanded from the beam is specific to the given structural system. Considerable research work has been carried out to quantify these two parameters.

Johnson and HopeGill [1972, 1976a, 1976b and 1979] pioneered the development of continuous composite beams. Their research forms the basis of the Eurocode 4 [1994] rules governing the design of continuous composite beams. In this the allowable moment redistribution is calculated on the basis of section classification, based on section geometry and steel grade. The requirement for moment redistribution (often expressed as a percentage of the support moment) and, thus, the rotation required from the connection depends upon the connection moment capacity. Economic design is achieved by optimising the combination of connection and beam strengths. Practical methods are required to determine connection strength and ductility, as well as beam strength and the end rotation required to generate the necessary strength.

Extensive research has been carried out to predict the available rotation capacities of composite connections by Johnson [1988, 1991], Kemp [1991], Kubo [1988], SCI [1992], Xiao [1994] and Anderson [2000]. The most advanced model for calculating the rotation available from the connection, which depends on the tensile strain in the reinforcement, the slip at the steel-concrete interface and the compressive strain in the lower flange and web of the steel beam, is presented in COST C1 [1997].

Based on all these investigations, design and detailing rules [COST C1, 1997 and BCSA/SCI, 1998] have been developed. These take into account both strength and ductility requirements. In many situations it is necessary to limit the design moment in the span to $0.85M_p$, in order to ensure that the available rotation capacity exceeds the rotation requirements from the beams. SCI [1998] recommended rigid-plastic analysis where the composite joint is chosen to possess partial strength. The SCI design guide for composite connections [1998] is limited to partial strength composite connections in braced frames, where the connection between the beam and the column is of the flush end-plate type. The design guide also covers partial depth end-plate beam-to-beam connections and can be used for both manual and computer-aided design and detailing. The standard connections presented in the design guide [SCI, 1998] are capable of achieving more than 30% of the beam capacity. Hence, by choosing the right combination of steel grade, span to total

depth ratio, support to span moment ratio, design sagging moment and load arrangement it is possible to exploit the advantages of composite connections.

1.2 Objectives

A view widely held in industry is that the benefits offered by composite connections will not be fully used until this type of connection can be used efficiently in unpropped constructions and also composite connections to be developed at exterior columns.

At present, there are two major problems which prevent the industry exploiting the benefits offered by composite connections.

(a) The first problem is the performance of composite connections in the unpropped mode of construction. The current design rules for composite connections are focussed towards the propped mode of construction. However, the popular form of construction for continuous beams in the industry is unpropped because of the lower on-site construction costs, speed and convenience. Although the strength requirements for both forms of construction remain the same, the ductility requirement differs. It therefore becomes necessary to revise the design rules for composite connections which are currently focussed towards the propped mode of construction .

(b) The second problem is the fact that there are no standard connection details for composite connections employed at external beam-column connections. The few tests undertaken to simulate external column composite connections show that the problem of anchoring reinforcement restricts the moments that can be sustained [Tschemmernegg *et al.*, 1995]. The composite connection design guide [BCSA and SCI, 1998] recommends that connections to external columns should be non-composite to avoid this problem. The choice of non-composite connections at external locations generally results in an increase in the size of the connected beam and this can erode the benefits associated with composite connections.

The process of trying to solve these two problems, in order to facilitate the use of composite connections in the construction industry, forms the major objectives of this thesis.

During this process, experimental work has been undertaken on a large scale, semi-continuous composite subframe. In order to assess the current design rules, an extensive study needs to be undertaken which takes various parameters into consideration. A numerical model derived from basic structural mechanics principles has been developed as a part of this research to study the behaviour of semi-continuous composite beams. The model has been validated using the results of the experimental study carried out. The data obtained from the parametric study have been used to assess the practical limits for extending composite connections for use with the unpropped mode of construction. The results obtained from the experimental study on the behaviour of a new form of exterior composite connection detail has also been used to gain an understanding of the performance of this connection detail.

Along with the process of developing the numerical model for the study of semi-continuous composite beams, a basic model has been developed for the case of pure steel beams. The accuracy of this model was verified using the experimental results from the work of other researchers. This generic model of steel beams is used, as an additional objective to the major objectives, to characterise the strain-hardened performance of modern structural steels.

1.3 Scope of the investigation

During the last three decades, a considerable amount of research has been directed towards composite connections, with particular emphasis on propped construction and internal connections. Although the provision of a complete review of the development of composite connections is an arduous task, considerable effort has been made in the Chapter 2 to provide a 'state of the art' report on the experimental and analytical results in the development of key characteristics of composite connections. Chapter 2 clearly shows that current design guides for composite connections do not model the commonly

occurring unpropped construction well and also do not provide detail of single-sided moment resisting composite connections i.e. connections at the perimeter columns. These two problems greatly limit the direct use of composite connections in the construction industry.

Having identified the industrial need for further development in the design guides for composite connections, this study aims to solve these two major issues through a full-scale sub-frame test that was carried out at the Building Research Establishment, UK. The beams were unpropped during construction and one of the perimeter connections incorporated a modified form of composite connection. The test and its results are reported in the Chapter 3.

Although the test provided valuable data on the strength and ductility of internal composite connections in the case of unpropped construction, it is impossible to validate the design guide with one set of experimental data. Hence, a reliable mathematical model is needed in order to predict the elastic and plastic behaviour of composite connections under unpropped construction. A numerical model has been developed from the elementary principles of structural mechanics to predict the full moment vs. rotation response for laterally restrained steel beams, based on stress-strain data from mill tests. After expressing the stress-strain values as a polynomial function, the moment capacity for a given value of curvature is the determined by integrating the product of stress, area and lever arm throughout a given cross section. Thus, the moment vs. curvature relationship of a cross section is established. The curvature distribution along a member is then integrated to define the slope distribution, followed by further integration to define the deflected shape. The process is repeated incrementally to define the full moment vs. end-rotation and moment vs. mid-span deflection graphs. This straightforward approach is validated by the experimental work of other researchers and is documented in Chapter 4.

This numerical model of the steel beam has been extended in detail to cover composite beams under sagging and hogging moment for both propped and unpropped construction. The complete step-by-step approach of the method and its validation is presented in Chapter 5. The accuracy of the numerical model for semi-continuous composite beams in

predicting the non-elastic response of unpropped composite beams to loads generated during construction and subsequent operation, is established by comparing the calculated behaviour of the composite beams with the experimental results reported in Chapter 3.

Having established a good degree of accuracy for the numerical model in the prediction of the behaviour of semi-continuous composite beams, it was used to assess the ductility requirements of composite connections for use with unpropped composite beams. The major difference between propped and unpropped composite beams lies in the ductility requirements rather than in the strength requirements. The outstanding critical factor in the case of unpropped construction is the dead load stress that must be carried by the steel beam alone prior to hardening of the concrete. The effect of this factor on the ductility requirements of composite connections is assessed herein. The numerical model of the semi-continuous composite beam involves a 3D interpolation function of moment, curvature and beam stress under dead load in such a way that this function can be used to define the deflection and slope distribution along the beam. A parametric study has been carried out on a total of 2160 different beam configurations, utilising different steel grades and loading conditions. In this study the influence of dead load stress on the connection rotation requirement has been thoroughly evaluated along with several other factors including span to depth ratio, location within the building frame, ratio between the support (connection) moment capacity and span (beam) moment capacity, loading type, steel grade and percentage of the beam strength utilised during design. The connection rotation capacity requirements resulting from this study are assessed to establish the scope for extending the use of composite connections to unpropped beams. The details of the parametric study and the results from the assessment are presented in Chapter 6.

Having achieved a good degree of accuracy in predicting the end rotations of steel beams using the modelling technique presented in the Chapter 4, an extensive parametric study is carried out using this technique to establish the influence of strain-hardening on elastic-plastic frame instability design. This is presented in Chapter 7.

Chapter 2 - Literature review

2.1 Composite Construction

In modern multi-storey buildings the steel frame has become popular due to the high quality in fabrication and the speed of erection. This steel skeleton consists of beams and columns jointed through connections. In the early practice, the structural slab does not contribute to the load resistance capacity of the system. Thus structural steel beams need to resist all the applied flexural forces with the top halves subjected to compression, with the possibility of buckling, and with the bottom halves in tension. However, in the late 19^{th} century, the civil construction industry recognised the composite action that could be generated between steel and concrete by providing a bond at the interface. In the composite section, the steel element, which is effective in tension, will take care of the tensile forces and the concrete element, which is effective in compression, will resist the compressive forces. The first appearance of this practice was the Rock Rapids Bridge, Iowa in 1894 [Griffs, 1992].

The bond, which is crucial in composite action, was first achieved through the use of projecting shearing tabs into the beam flanges to the slab and was proposed by Julius Kahn in 1903. In 1929, Caughey and Scott proposed in a complete interaction theory that the bond so provided should resist the longitudinal shear. However, the bond should also prevent separation of the steel and concrete elements and ensure that the curvatures in the steel and concrete elements conform to each other. Present day stud shear connectors, whose strength is the same in all directions and which welded directly through the profiled sheeting, have the ability to resist the longitudinal shear by means of the shank & weld-collar, and the interface normal tensile force by means of the head. The design capacity formula proposed by the University of Illinois in 1956 was first used in Bad River Bridge in Pierre, South Dakota and later in IBM's Education Building in Poughkeepsie, New York [Narayanan 1988, Griffs 1992].

Meanwhile, in 1940, Swiss Engineers replaced solid slabs by profiled steel sheet slabs, in which the corrugated steel sheets satisfied two purposes - as permanent formwork, and as additional tensile reinforcement. The floors of the Nestle building in Vevey used this technique in 1959. [Wright, Evans & Harding 1987]

Thus this complementary behaviour of steel and concrete increases the depth of the beam thereby increasing the flexural strength and stiffness and consequently reducing span to depth ratios. According to SCI [1993], the composite section stiffness can be 3 to 5 times, and, the section modulus 1.5 to 2.5 times that of the steel section alone. It has also been estimated that savings in steel are of the order of 30 to 50% over non-composite beams. Reduction in the depth of section increases the integration of building. Furthermore, longer spans could be achieved through composite beams.

2.2 Composite connections

Composite connections resist moment by generating a couple between their tension and compression components. The mechanics are essentially the same as those for bare steel moment connections, with the slab reinforcement acting like an additional row of bolts in an extended end plate. In order to achieve their full potential, the reinforcing bars must be properly anchored and be capable of accommodating significant strain before fracture. A typical beam to column composite connection detail is shown in Figure 2-1.

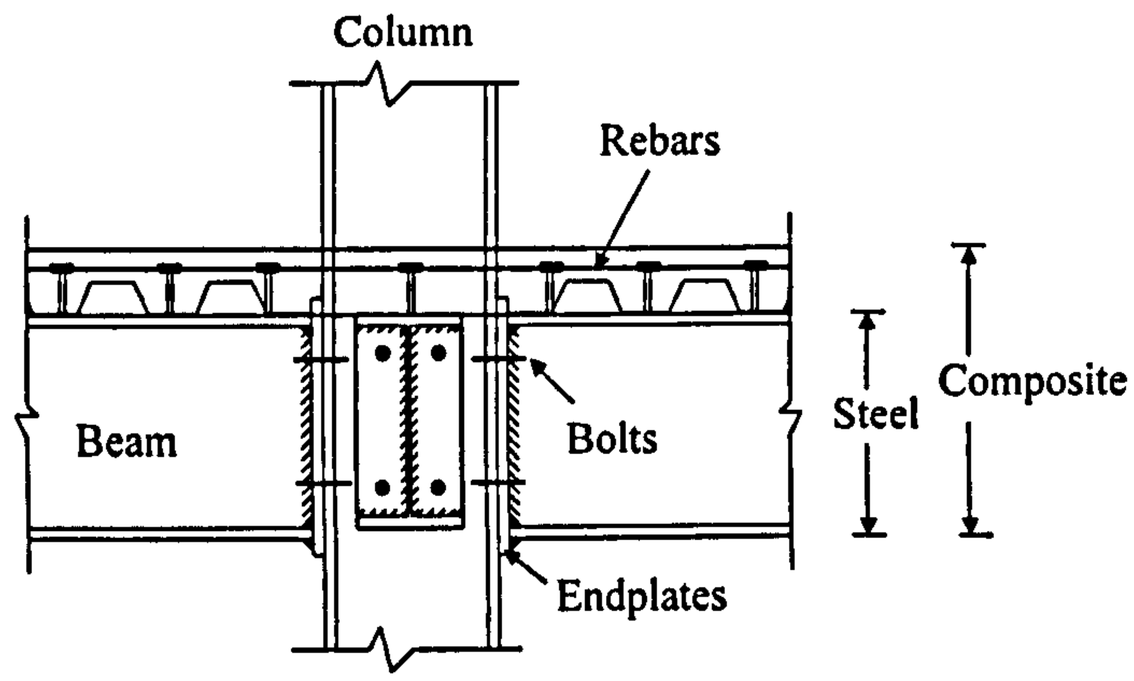

Figure 2-1. Composite connections

The classification of composite connections in braced frames based on their key characteristics is outlined below as in EC4. Composite connections can be classified as either: full strength/partial strength connections based on moment capacity, rigid/semi-rigid connections based on rotational stiffness and non-ductile/ductile based on rotation capacity. These are outlined as follows:

Full Strength Connection: A connection, which has a moment resistance at least equal to that of the beam section immediately adjacent to the connection.

Partial Strength Connection: A connection, which has a moment resistance, which is less than that of the beam section immediately adjacent to the connection

Rigid Connection: A connection is so designed that its deformation has no significant influence on the distribution of internal forces and moments in the structure, or on its overall deformation.

Semi-rigid Connection: A connection, which is too flexible to qualify as rigid, but is not a pin. A semi-rigid connection is one that provides a predictable degree of interaction between members, but is neither rigid nor nominally pinned. In Eurocode 4, no application rules are given for the use of semi-rigid connections, which are the subject of much current research.

Ductile Connection: A connection that has sufficient rotation capacity to act as a plastic hinge.

Figure 2-2 shows boundaries between rigid/semi-rigid, full strength/partial strength, and non-ductile/ductile, in addition to a typical composite connection response. The typical curve indicates that composite connections are normally ductile, rigid and partial strength [SCI 1998].

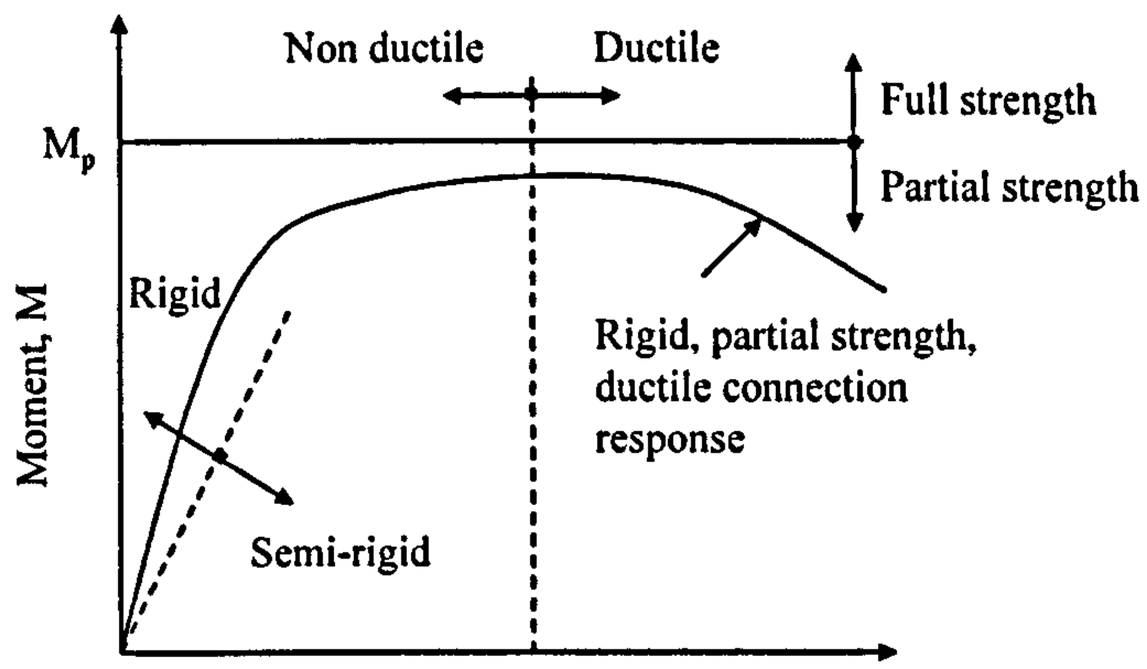

Figure 2-2. Classification of connections, SCI 1998

2.3 Composite frame design

Recognising the structural benefits from the composite beams, the present construction market exploits the efficiency of the composite floor construction. It is worthy of note that the floor system will always constitute the highest proportion of the total cost [Barnard, 1970]. The floor system could be designed in three possible ways.

Simple composite construction

Continuous composite construction

Semi-continuous composite construction

Table 2-1 Types of composite construction based on the classification of connections

Type of framing	Method of Analysis	Classification of connections
Simple	Statically determinate	Nominally pinned
Continuous	Elastic global analysis	Rigid
	Rigid-plastic analysis	Full strength
Semi-continuous	Elastic global analysis	Semi rigid
	Rigid-Plastic analysis	Partial strength
	Elastic-Plastic analysis	Semi-rigid and partial strength
		Semi-rigid and full strength
		Rigid and partial strength

The assumptions made in the design of the members in the floor system should be consistent with the method for global analysis and with the anticipated behaviour of the connections [EC4, 1992]. Thus the choice of construction is down to the behaviour of connections, Table 2-1.

Although structural behaviour is three dimensional, the usual presence of stiff floor slabs normally allows neglect of out-of-plane and torsional deformations of the joint. The joint characterisation is usually on the basis of the moment-rotation behaviour i.e. the in-plane response. The key joint parameters are:

(a) The design moment resistance

(b) The initial stiffness

(c) The design rotation capacity

The principles of each construction are explained in detail in the following sub sections.

2.3.1 Simple composite construction

It is common practice during the design of composite frames to assume that the floor system is simply supported. Such design assumes no continuity between the beams and columns and the connection is required to transfer only beam end shears. Connections are also required to have a defined tensile load capacity to provide tying forces to improve robustness [BSI, 1990]. The member forces and moments in simple composite frames can be determined using elastic or plastic analysis, as it is a statically determinate system. It is normally found that span-to-depth ratios are in the range of 18-22, the depth being the overall depth of the beam and the slab.

2.3.2 Continuous composite construction

When the floor systems are designed to be continuous a further increase in stiffness and load resistance and hence minimum material usage will result. However, structural steel is basically a simply supported material. It may be possible to achieve continuity by running an unbroken length of steel section over two or more spans [Brett, Nethercot & Owens 1987], but in usual practice the continuity of beams is cut by joints with the

columns. Continuity can then be achieved by the appropriate design of the joints. When the connections are subjected to hogging moments, as they usually are at the columns, resistance is provided between the steel beam section and the column, as well as properly anchored tension reinforcement within the effective breadth of the slab. Such joints are termed composite connections in Eurocode 4 [1994]. The mechanics are similar to those for bare-steel moment connections, with the slab reinforcement acting like an additional row of bolts. This slab reinforcement is in tension and is located further from the neutral axis, resulting in much higher initial stiffness and ultimate moments. These connections behave linearly after some initial yielding and provide substantial rotational restraint to the columns. In addition to the savings in materials achieved by transferring some of the mid-span moment to the supports and providing additional restraint to the columns, the slab steel provides an excellent method to control live load deflections and slab cracking [Echeta & Owens 1981]. The span-to-depth ratios are then in the range 22-25 for end spans and 25-30 for internal spans [Lawson & Wickens 1992]. A continuous composite frame can be analysed either elastically or plastically.

2.3.2.1 Elastic Analysis of continuous construction

Elastic global analysis of continuous beams, according to BS 5950 Part 3 and EC4 Part 1, may be carried out by two different approaches:

Using the section properties of either the gross uncracked section throughout the length of the beam or using the section properties of the cracked section for negative moments for a length of 15% of the span on each side of internal supports and elsewhere the section properties of the gross uncracked section.

In an elastic analysis of continuous beams, the support moments are approximately double the span moments. This implies the support (hogging) section should have larger moment capacity than the span (sagging) section. However, composite beam's moment capacity in sagging is typically 1.3 times the hogging moment capacity. Therefore, designing composite beams on a purely elastic basis means that the potentially large sagging moment capacities available from composite action can never actually be utilised.

Therefore, the resulting negative moment at any support may be reduced (except adjacent to cantilevers) by an amount not exceeding the appropriate maximum percentage given in Table 2-2.

Table 2-2. Limits to the redistribution of hogging moments (percentage of the initial value of the bending moment to be redistributed in elastic global analysis)

Codes	Method of analysis	Section Classification				
		Class 4 slender	Class 3 semi-compact	Class 2 Compact	Class 1 Plastic	
					Non-reinforced	generally
BS5950	Uncracked	10	20	30	50	40
Part 3.1	Cracked	0	10	20	40	30
EC4	Uncracked	10	20	30	40	40
Part 1	Cracked	0	10	15	25	25

To maintain equilibrium with the applied loads, corresponding increases should then be made to the positive moments. Both BS5950: Part 3.1 and Eurocode 4 permit the redistribution of support moments, depending on the method used and the classification of the section at each internal support. It is worthy of note that these codes assume the bare steel connection is fully rigid. Imposed loads need to be arranged in the most unfavourable realistic pattern for each case. For example, in continuous beams subjected to uniformly distributed imposed loads, the loading patterns to be considered are: a. alternate spans loaded, and b. two adjacent spans loaded.

The moment of resistance of composite sections in the support region is normally greater according to uncracked analysis in comparison with the cracked approach. It therefore follows that the requirement for redistribution for cracked analysis is less than that for uncracked analysis, as can be seen in Table 2-2. BS5950: Part 3.1 permits 10% less redistribution if the cracked section method is used for all section classifications. Subsequently, this reduction in moment redistribution for the cracked approach has been revised in EC4, based on the section classification. In EC4, the same difference is allowed for semi-compact and slender beams, and 15% more redistribution is allowed for plastic and compact sections. This can be explained, according to Anderson & Johnson, as the ratio of depth of slab to depth of steel section increases the difference between support

moment given by uncracked and cracked analysis increases. Furthermore, this ratio is generally higher for plastic and semi-compact sections [Anderson & Johnson, 1992].

2.3.2.2 Plastic analysis of continuous construction

Plastic global analysis may be carried out using either the rigid-plastic or elastic-plastic methods. According to EC4, elastic-plastic methods should account for the load-slip behaviour of the shear connection. No application rules are given for these methods. However, to analyse continuous beams by rigid-plastic analysis demands that the rotation capacity should be sufficient to enable the required hinge rotation to develop. This requirement is assumed to be satisfied if all effective cross sections at the hinge locations are Class 1; and all other effective cross-sections are Class 1 or Class 2. The fundamental assumption in rigid-plastic design is that sufficient rotation capacity is available in the plastic hinges (except the last to form) for a full collapse mechanism to develop.

Thus, in the rigid-plastic analysis of continuous beams, full strength connections have to be provided so that the plastic resistance moment of the beam can be attained in the region of the joint. Such connections may not offer the most economical solution due to the high fabrication costs involved. Furthermore, [Nethercot, 1995] provides an explanation as to why the use of full strength connections in continuous beams is not always the optimum solution. In continuous composite beams, the first plastic hinges will form at the support. This places a substantial portion of the steel section in compression. If the full sagging moment is to be developed in the mid-span region, then the support hinges must rotate at a sensibly constant moment level as further load is accommodated by redistribution of moments from the supports. This requires that the sections be restricted to the class 1 limits, so as to ensure a sufficiently long plateau on the moment-rotation response. According to BS5950, the compression flange may be assumed to be Class 1 if the width to thickness ratio is less than 9.5ε for hot rolled sections. Similarly the limiting width to thickness ratio for webs is 64ε under pure bending, or less than 32ε when subject to compression throughout the depth, where, $\varepsilon = (275/\rho_y)^{1/2}$.

Flange properties, b/T, of the standard range of UK UB sections vary between 4.11 and 8.82. Web properties, d/t, of all sections vary between 24.1 and 57.2. If the web is under full compression then the maximum d/t ratio limit is 28, which makes most of the UB sections not suitable for plastic design. Only certain sections will be suitable for plastic design (shallower sections) due to this limiting ratio. A comparison of the flange outstand b/T and web d/t limits for all standard UK beam sections with the class 1 limits of the current British Code is shown in Figure 2-3 and Figure 2-4. [These figures have been reproduced based on Nethercot's research for the purpose of this review].

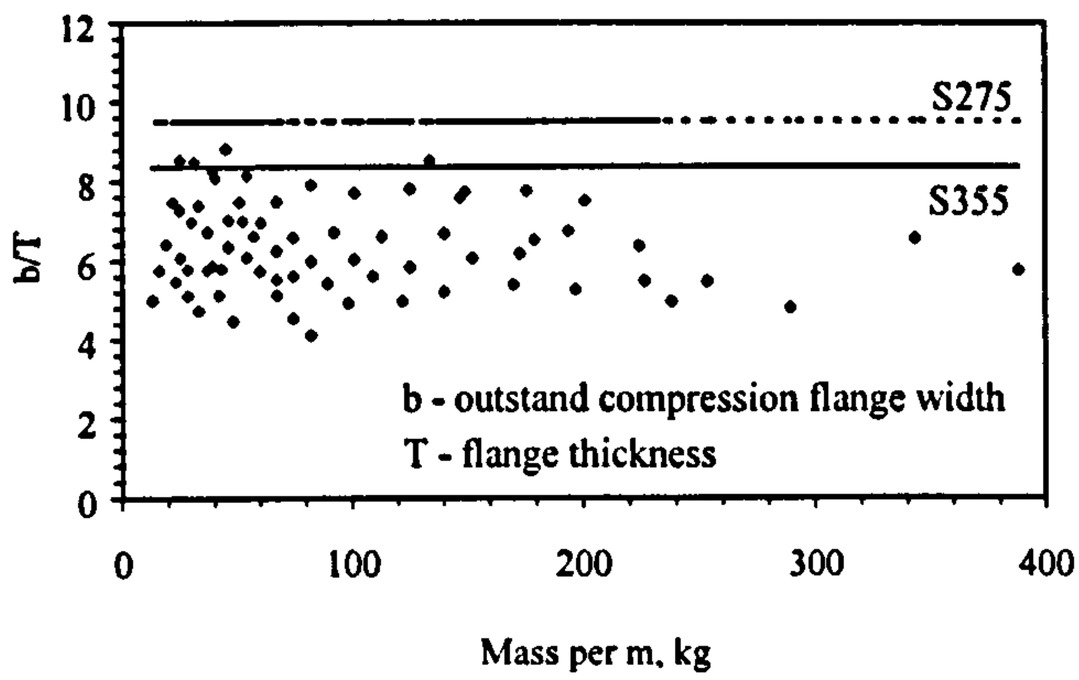

Figure 2-3. Comparison of flange properties of UK UB rolled sections with plastic cross-sectional limits of BS5950: Part 3 composite beams – flanges, Nethercot 1995

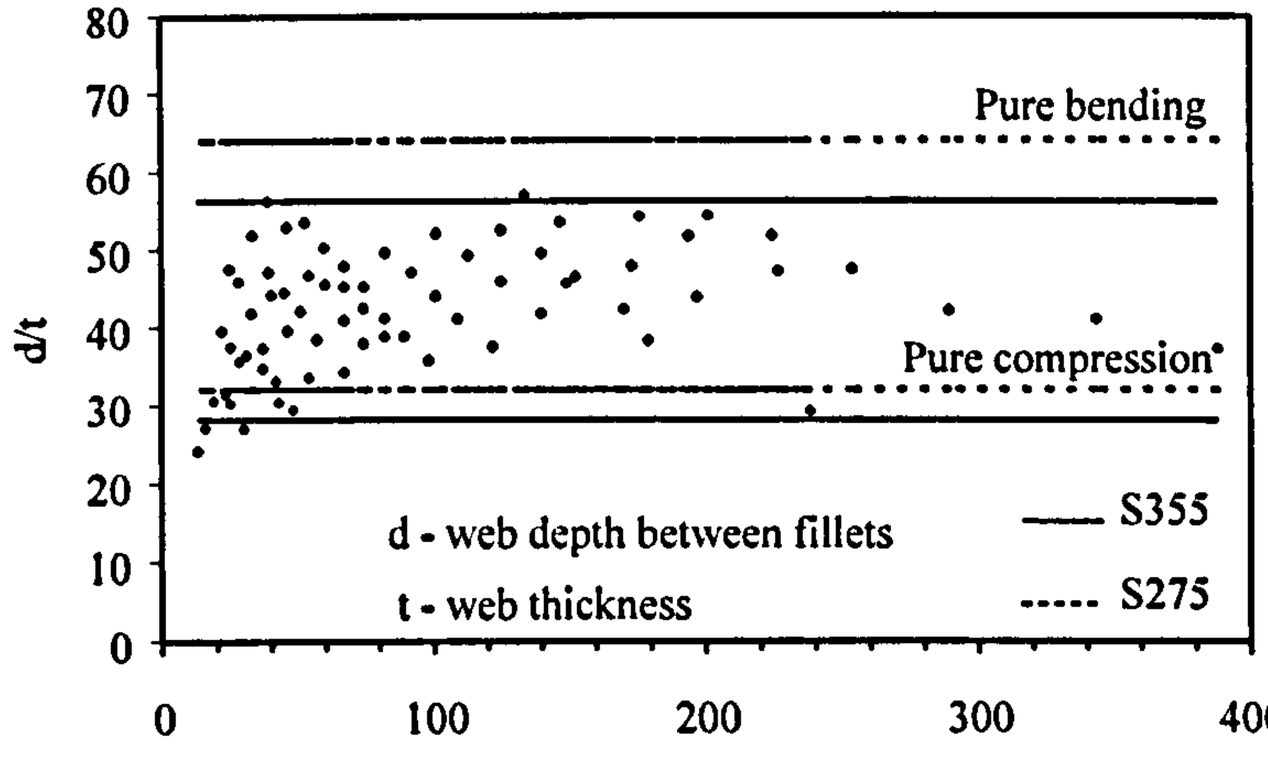

Figure 2-4. Comparison of web properties of UK UB rolled sections with plastic cross-sectional limits of BS5950: Part 3 composite beams – webs, Nethercot 1995

It can be seen clearly from the figures that almost no sections have flange proportions outside the limiting values for either grade 43 or grade 50 steel. Similarly for a section under pure bending where half the web is in compression, almost all sections fall within the limitations. However, efficiently designed composite beams in hogging are likely to have the neutral axis located close to or within the concrete slab. This leads to a far greater depth of web being in compression with the result is that almost no standard UK UB sections are suitable for plastic design.

2.3.3 Semi-continuous composite construction

It has been understood that continuous composite construction creates high fabrication costs and importantly, it places most of the steel web in compression adjacent to the connections. Since the section classification requirements are thus more onerous than for resistance against sagging moments, the standard range of UB sections do not possess the ductility required to redistribute moments. This implies that demanding the first plastic hinge to form at the hogging section limits the choice of section. This will in many circumstances inevitably lead to uneconomic designs. Thus, partial strength connections become attractive, since fabrication costs are lower and most importantly, the first plastic hinge will form at the connection rather than the adjacent hogging beam section.

In this type of beam full continuity is not achieved and it is normally referred to as semi-continuous composite construction. It is no longer required for the support section to achieve plastic rotations, since ductility is provided by the connections, which are designed to achieve the rotations required for sufficient moment redistribution to permit the design sagging moment capacities to be attained in the beam section. Eurocode 3 and Eurocode 4 both permit 'semi-continuous' construction in which the connections exhibit characteristics of partial strength, ductility, and either full or semi-rigidity. Moreover, by limiting the strength of the connections, problems common to fully restrained connections, such as local buckling and brittle failures by fracture can be avoided [Anderson and Najafi, 1994]. Thus it can be understood that the concept of semi-continuous composite construction requires a more precise statement of the joint

behaviour. Semi-continuous composite beams can be analysed in three different possible ways based on the appropriate classification of joint model, Table 2-3.

Table 2-3 Methods of global analysis of semi-continuous composite beams

Method of Global Analysis	Classification of joint
Elastic global analysis	Semi rigid joint
Rigid-Plastic analysis	Partial strength
Elastic-Plastic analysis	Semi-rigid and partial strength
	Semi-rigid and full strength
	Rigid and partial strength

The following review will outline the basic principles for all the three possible methods of analysis.

2.3.3.1 Elastic-global analysis of semi-continuous construction

Elastic analysis, which is required for serviceability verifications, is widely used in the design of simple and continuous multi-storey frames. However, the elastic analysis of semi-continuous beams demands a quantification of connection stiffness, which may prove difficult in practice. Although less convenient than rigid-plastic analysis, it is of more general application. In particular, as long as the frame remains elastic, only negligible rotation capacity will be required from the joints. The distribution of internal forces and moments is affected by load patterns. However, following Eurocode 4, these may be reduced to consideration of either: (a) imposed load in adjacent spans, or (b) imposed load on alternate spans.

Conventionally, the finite size of the joint has been ignored in global analysis. In advanced calculation methods, the joint is represented as a separated element, which most realistically, is of finite size. There are finite size models [Innsbruck component model, Tschemmernegg, 1997], which represent the actual behaviour of the joint. However, the ECCS Technical Committee 11 for composite structures [1999] has proposed a model that represents the overall joint behaviour by rotational springs and at the same time would be simple enough for everyday design. Such models for steel joints are described

in the Revised Annex J of Eurocode 3 [1998]. In case of double-sided joint configurations, two separate but interacting joints may be modelled. Each joint takes into account the behaviour of the column web panel in shear as well as the behaviour of the relevant connection (Figure 2-5). To avoid the web deformation being taken into account twice, a transformation parameter is introduced which can be determined from COST-C1 [1997] and Eurocode 3 [1998]. Equivalent beam stubs with appropriate bending stiffness may substitute this rotational spring, if software is used that does not support flexural springs. More details of this simplified modelling can be found in the ECCS Technical Committee report 11 for composite structures [1999].

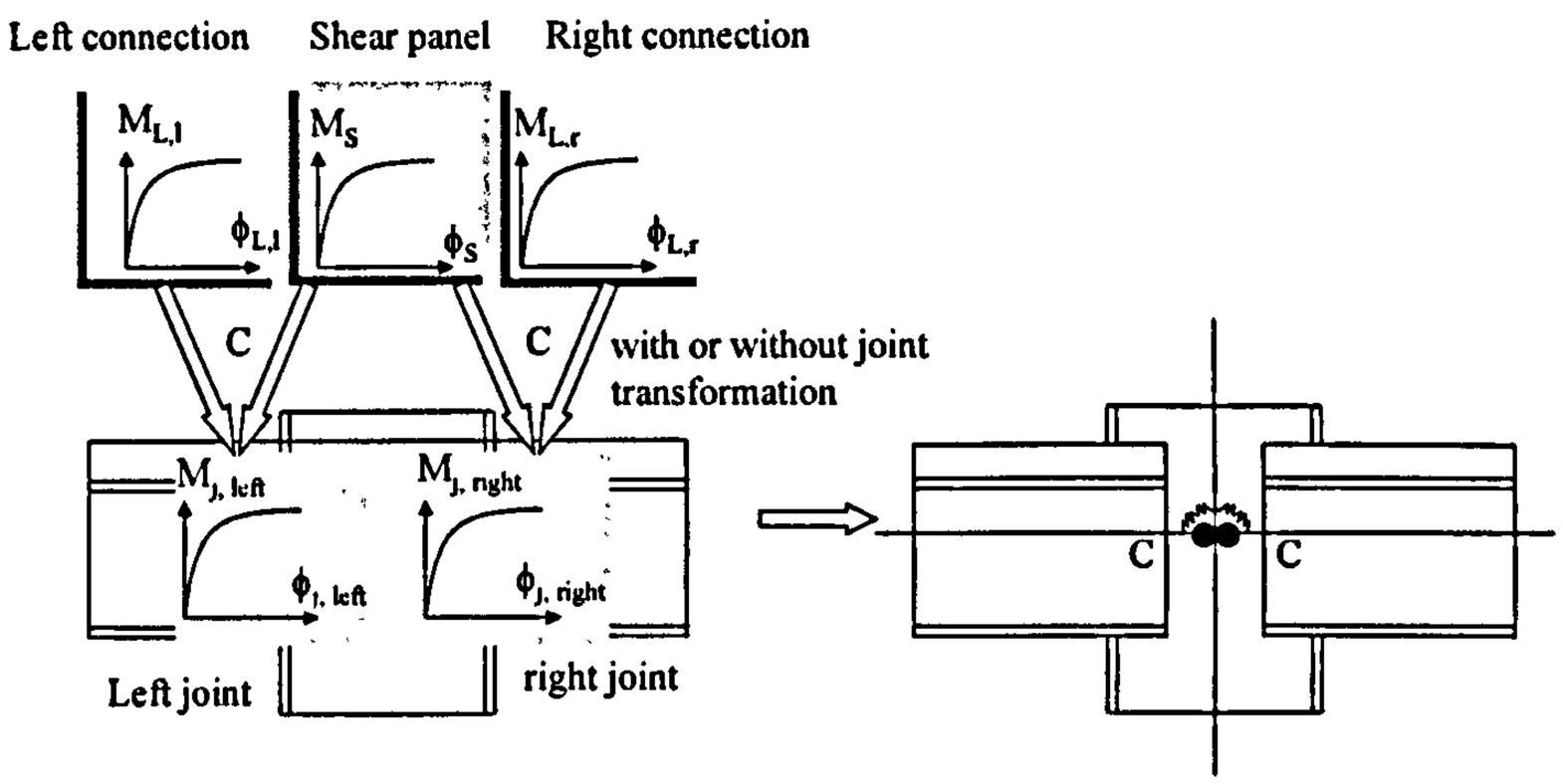

Figure 2-5. Simplified joint modelling, COST C1 1997

The actual moment-rotation response of the joint is non-linear. According to EC3, the (non-linear) moment-rotation design curve consists of three parts, as shown in Figure 2-6. Up to a level of 2/3 of the design moment of resistance ($M_{j,Rd}$), the curve is assumed to be linear elastic. The corresponding stiffness is the so-called initial stiffness $S_{j,ini}$. Between 2/3 $M_{j,Rd}$ and $M_{j,Rd}$, the curve is non-linear. After the moment in the joint reaches $M_{j,Rd}$, a yield plateau is assumed. The end of this moment-rotation curve indicates the rotation capacity of the joint.

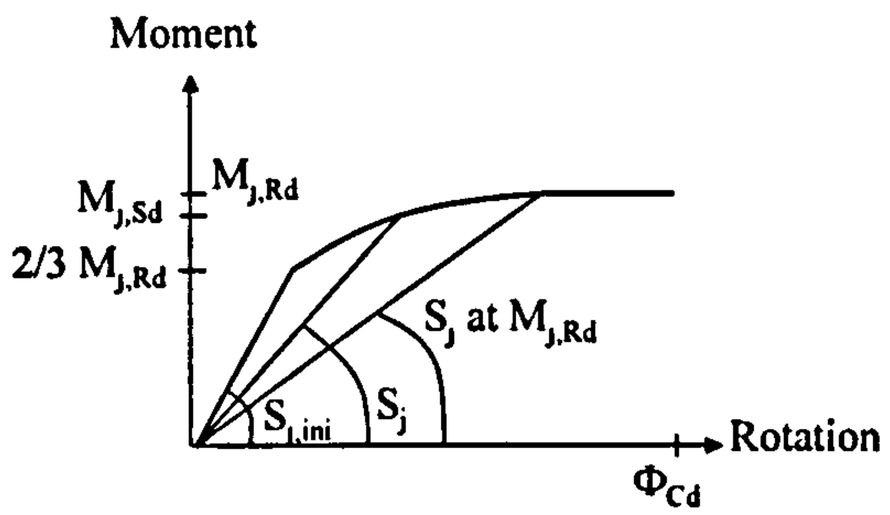

Figure 2-6. Non-linear M-ϕ curve, COST C1 1997

The characterisation adopted by Eurocode 3 assumes a fixed ratio between the initial stiffness $S_{j,ini}$ and the secant stiffness at the intersection between the non-linear part and the yield plateau (S_j at level $M_{j,Rd}$), see Figure 2-6. For composite joints with bolted endplates, this ratio is taken as equal to 3.0. Contact plate joints have a less gradual increase in stiffness and the ratio is taken as 2.0. The shape of the non-linear part for a bending moment $M_{j,Sd}$ between 2/3 $M_{j,Rd}$ and $M_{j,Rd}$ can be found with the following interpolation formula [ECCS, 1999]:

$$S_j = \frac{S_{J.ini}}{\left(\frac{1.5\,M_{J.Sd}}{M_{J.Rd}}\right)^{\psi}}$$

where $\psi = 2.7$ for joints with bolted flush end-plates and 1.7 for joints with contact plates. In this interpolation formula, the value of S_j is therefore dependent on $M_{j,Sd}$. However, the use of such curves requires sophisticated programs for frame analysis. For practical application, the non-linear shape of the moment-rotation curve may be idealised into a bi-linear or tri-linear representation. In general, it is conservative to take the simplified curve as lying below the non-linear curve.

The simplest approximation is to represent the joint characteristic by a bi-linear curve. The joint stiffness is constant for bending moments lower than the design moment. An appropriate stiffness can be calculated by dividing the initial joint stiffness $S_{j,ini}$ by a modification factor, denoted η. This depends on the type of steelwork connection and on the joint configuration.

The simplified model neglects the finite size of the joint. For elastic analysis, the joint is therefore modelled as a spring located at the end of the supported member. The key joint characteristic is the rotational stiffness, S_j. As long as the design resistance moment is not exceeded, a single secant stiffness $S_{j,ini} / \eta$ can be used.

2.3.3.2 Rigid-plastic analysis of semi-continuous construction

The plastic analysis of continuous beams was pioneered by [JF Baker, 1956], although the earliest work into plastic bending strengths was by [Ewing, 1899]. Plastic analysis is based on the assumption that plastic hinges form at critical points in a frame, the rotation of which allows for the redistribution of moments. When a rigid plastic analysis is used, it is the flexural bending strength of beams and their connections, rather than stiffness that is critical. Connection strength can be predicted with sufficient accuracy using current methods [BS5950 (1990), EC3 (1992), EC4 (1994), Eureka Cimsteel (1992)]. However, an assessment of ductility is also required in order to determine the degree of moment redistribution that can be accommodated. Typical collapse mechanisms will be of beam type, where hinges are formed at the joints first and then the mid-span. In other words, in the case of plastic analysis of semi-continuous composite frames in utilising the full beam capacity, moment redistribution should be defined as a function of connection ductility. In order to determine the available amount of moment redistribution, it is essential to know not only the maximum rotation capacity available from the connection (available rotation capacity), but also the end rotation required from the beam to achieve a desired level of moment of resistance in the span (required rotation capacity). Moreover, the available rotation capacity from the connections has to be always greater than the rotation required capacity in order to develop the design moment in the span. Therefore it is important to quantify both the available and the required rotation capacities.

The degree of moment redistribution required and thus the rotation required in the joint depends upon the moment capacity of the joint. Economic design is achieved by optimising the combination of joint strength and ductility with the beam sagging moment capacity. Thus practical methods are required to determine joint strength and ductility, as well as beams strength and the end rotation required to generate that strength. Whilst

connection performance is dependent on the detail selection, the rotation requirement demanded from the beam is specific to the given structural system.

The available rotation capacity may be limited by the ductility of the reinforcement. In an attempt to increase joint ductility the 'X' type reinforcement can be specified. According to BS4449 [1988] on the elongation limits for reinforcement, the minimum elongation at fracture is no less than 14%. Tests [COST-C1, 1997, SCI, 1998] and numerical studies [Li *et al.*, 1996, Najafi *et al.*, 1997] show that adequate capacity can be readily achieved with commercially available reinforcement. However, the ductility in tests has been substantially greater than the maximum specified for high-quality reinforcement, which is 5% elongation at maximum force [Eurocode 2, 1992]. Therefore greater elongation of reinforcement can only be used when the supplier can demonstrate that this can be achieved in the bars to be provided.

2.3.3.3 Elastic-plastic analysis of semi-continuous construction

A third possibility is to combine stiffness and resistance considerations in an elastic-plastic analysis. Suitable software is increasingly available. Such an analysis has the advantage that it provides the required rotation capacity for the specific structure being designed. In general it will be easier to satisfy these instead of the more general values derived from parametric studies [Li *et al.*, 1996, Najafi *et al.*, 1997]. For elastic-plastic analysis the key joint characteristics are the rotational stiffness and the moment resistance. If the curve at $M_{j,Rd}$ is idealised as an unlimited plateau, then a check is required to ensure that the joint rotations given by the analysis do not exceed the design rotation capacity. Eurocode 4 allows simplified elastic-plastic analysis through redistribution of moments. Demands may then be placed on the rotation capacity of the joints, although they are difficult to quantify in a form suitable for design [ECCS, 1999].

2.4 Connections in use in the UK

The only connections currently covered by design rules for partial strength design are extended end plate and flush end plate connections. This is because they can achieve

effective transfer of compression at the bottom flange and the connections possess good rotation capacity. A commonly used form of connections for frames in the UK, they provide stiffness for the frame during construction and a considerable amount of research has been carried out on their performance, both as steel and composite connections.

The different forms of fabricated steel beam to column connections that are widely used in the UK are listed in Table 2-4 [Lawson & Gibbons, 1995].

Table 2-4 Available steel beam to column connections in UK

Category	Type	Classification
End plate	Extended end plates (with bolts above and below the beam top flange)	Partial strength or rigid
	Flush end plates (with bolts contained within the beam depth)	Partial strength or semi-rigid
	Partial depth end plates (with the plate not directly connected to the complete depth of the web, or to both flanges)	Simple (nominally pinned)
	Haunched connection with a local deepening of the beam section	Full strength or rigid
Angle cleat	Web cleats in pairs attached to the web	Simple
	Web cleats and a bottom seating cleat	Simple
	Web cleats and top and bottom cleats	Semi-rigid
Fin plate		Simple

2.4.1 Standardisation of design and detailing of connections

Within UK construction, the Latham enquiry [1994] challenged traditional attitudes and practices. It argued that the industry need to seek more rapid ways of meeting the challenging targets it set, if the construction industry was to flourish into the new millennium. For steel frame construction, connection design and detailing is arguably the single most influential item in the complex chain of activities needed to produce the final product. Adopting greater standardisation of connections has the potential to reduce design time, simplify drawing production, improve handling efficiency in the fabrication shop and reduce erection times. It should also improve information flow, reduce

confrontation, facilitate the more effective use of IT and assist in the development of a more integrated approach to the whole design and construction process.

In 1988 it was recognised in the UK [Nethercot, 1995] that the climate was right for the standardisation of connection design and details. The importance of connection type on frame costs and programme was recognised and it was accepted that appropriate standardisation would benefit all parties. Thus the BCSA/SCI Connections Group was established, in parallel with developments within the CIMSteel Project. Reflecting on this decade of developments permits the benefits achieved thus far to be identified. It can be concluded that these extend far beyond the obvious improvement to the specific task of connection design and detailing; once that particular activity is accepted as a 'standard operation', achieving the Latham targets for the production of steel frames becomes closer to a reality.

2.4.2 Range of standard connections

For ordinary projects, it is usually neither practicable nor economic to test specific connection details on a routine basis. However, it is possible to use a range of standard details whose characteristics have been demonstrated by testing. A range of composite connections suitable for use in semi-continuous frames was developed at the SCI [1997].

A series of tests at the University of Abertay, Dundee [Bose and Hughes, 1995] confirmed the characteristics of these connections. These connections were originally developed for use in unbraced frames designed using the wind moment method. Because the wind loads on frames may reverse, the connections in a wind moment frame need to be symmetrical so that they can resist both hogging and sagging moments. Connections in a braced frame do not experience a reversal of moment, so the standard connections differ slightly from those given by Bose and Hughes. Standard composite 'plastic' connections suitable for use in semi-continuous composite frame (plastic global analysis – partial strength connections: plastic hinges form in the connections) have a similar form:

- Connections with flush end plate details using M20 8.8 bolts & M24 8.8 bolts
- For each steel detail, a range of 8 reinforcement options is given

- ϕ16mm (4,6,8 &10 No.); ϕ20mm (4,6,8 &10 No.) reinforcement bars
- Reinforcement strength of 460 N/mm^2 is assumed.

Standard composite connections recommended by the SCI are partial strength, rigid and plastic (ductile) connections. Plastic frame analysis is recommended because of its economy and simplicity.

2.5 Research into the key characteristics of composite connections

Having understood the advantage of composite connections in the design of multi-storey buildings and the lack of design guidance for this connection, more recent research has focused on testing composite connections and frames and developing design methods for frames with semi-rigid connections, with particular emphasis on propped construction and internal connections. Today advanced computational modelling supplements experimental investigations. Hence much of the research is advanced through the use of numerical modelling. Zandonini [1989] reviewed the development of composite connections prior to 1986. Furthermore, Xiao [1994] presented a review of composite connections research from 1986 to 1993. As part of this review an attempt was made to cluster the experimental and analytical results, providing more up-to-date information on previous work.

The key characteristics that are required for the composite connection in overall frame design are moment capacity (strength), rigidity (stiffness) and rotational capacity (ductility). Much recent research has been focused towards the development of methods to calculate the moment capacity of composite connections. Design equations have been developed to cover a comprehensive set of possible modes of failure. Conversely, considerably less research effort has been expended on the prediction of rigidity and ductility, which necessitates further research.

The following review presents the research background of the present day design methods for assessing the key characteristics of composite joints. These characteristics include:

- Moment capacity
- Available rotation capacity

- Required rotation capacity

2.5.1 Moment capacity of composite connections

As a pioneer in the development of continuous composite beams, Johnson [1972] first suggested a simple equation to quantify the moment capacity for a flush end plate composite connection. In this method, the connection moment capacity is calculated by simply multiplying the tensile force in the reinforcement by the lever arm (distance from the centre of the reinforcement to the centre of the compression flange). In this approach, the connection ultimate strength is either under or over estimated because of the simple fixed lever arm value and neglection of the variation of the neutral axis position due to the reinforcement ratio and the possible influence of the bolts tension. The proposed equation is mainly applicable for flexible steel connections. In this proposed equation the contribution of rebar is only considered.

Subsequently, Johnson [1981] improved the equation for calculating the connection moment capacity by adding the moment capacity of the steel connections. It was proven from the tests undertaken [Johnson and Law, 1981] that the influence of shear lag and slip in the composite beams (due to the deformation of the beams, the slab and the shear connectors) on the plastic moment of the joint is small. Yield load of the bolts and the endplate exceeds that of the column flanges, as thin-flanged steel members are likely to be used in composite columns. Yield load of the flanges is calculated for the bare steel beam-column connection according to Packer [1977] and the predicted plastic moment is calculated by adding the moment capacity of the steel connection to Johnson & Hope-Gill's prediction formula.

In 1992, separate calculation procedures for web side plate (fin plate), flush end plate and partial depth end plate composite connections were published [Xiao, Nethercot and Choo, 1992]. These were consistent with the BS5950 [1992] approach for composite beams and composite slabs. In these procedures assumptions were made which included:

(a) The tensile resistance of the cracked concrete was neglected,

(b) Strain hardening of the reinforcement was not considered, and

(c) Only the contribution of the beam section, reinforcement and connecting components to strength were considered.

In comparison to Johnson's work, Xiao's equation for the moment capacity of the joint included the variation in the neutral axis position due to the reinforcement ratio and the influence of the bolts tension. It has been recognised in the composite web side plate connection with neutral axis in the steel section that the yielding of the reinforcement acting in conjunction with the bearing capacity of the plate or beam web controls the failure. The shear and compression zone of the column web should also be checked using EC3. In this method only the contribution of the beam section, reinforcement and connecting components are included.

Anderson and Najafi developed a simple spring model to predict satisfactorily a bilinear moment-rotation curve for the composite connections, provided account is taken of the deformation of the shear connection. In this method, the depth of web under compression is determined by equilibrium. The moment capacity includes the tensile forces from the reinforcement and the bolts. The performance of the web under compression is deduced from the moment capacity of the joint. They confirmed that an extended endplate increases the moment of resistance and the rotation capacity of a composite connection, compared to a flush end plate [Anderson and Najafi, 1994].

Two years later, in 1994, Xiao *et al.* [1994] improved their previous model by defining the position of neutral axis for different connection types. The connection types include the fin-plate, cleated end-plate, partial depth end-plate and flush end-plate. Various neutral axis positions were considered, these included locations in the concrete slab, the top flange, between the top flange and the top bolt row and finally below the top row of bolts. Connection type and neutral axis position are consistent with the current Eurocode and the BSI code approaches.

Three more additional assumptions were made in comparison with the previous model:
(a) The influence of the metal decking was included for tension capacity if the profiling is oriented parallel to the beam direction.

(b) If the composite floor contained mesh only, the tensile strength of the reinforcement was neglected due to the comparatively low ductility exhibited by mesh type reinforcement.

(c) The presence of the shear force and axial force in the composite connection was neglected. The rigid-plastic stress block approach was used to locate the centroid of either the total tensile force or compressive force. This approach was also used to determine the lever arm and hence calculate the moment of resistance.

Ren and Crisinel proposed a method for calculating the moment capacity, which is based on Xiao *et al*'s [1992] method, but modified for the calculation of the compressive capacity of the steelwork connection, and extended to cover double web cleat connections. The moment resistance calculation, in the case of a flush end plate connection is based on the failure mode being controlled by the tension resistance of the reinforcement. It is assumed that full shear interaction is provided between the slab and the steel beam. The bolt tension resistance is determined in accordance with Annex J of Eurocode 3. The available compression resistance at the compressive zone of the steelwork connection is determined by the critical section of the beam flange or the effective column web. A similar procedure to that of flush end-plate connections is adopted for the prediction of the moment resistance of the double-angle web cleat composite connections [Ren and Crisinel 1995].

Following Ren's work, Li *et al* proposed a method to calculate the moment capacity of flush end-plate connections using the procedure specified in Annex J of EC3 for the steel connections by considering the reinforcement as an extra row of bolts. It is known that the calculation of the potential bolt row forces and column web-buckling load in Annex J of EC3 is relatively complex. Therefore, an attempt was made to simplify the calculation of these forces. In these calculations, failure mode 1 specified in Annex J of EC3 was assumed and bolt failure was neglected [Li, Nethercot and Choo 1996].

In 1998, the SCI and BCSA published a design guide for composite connections in which a design procedure for composite connections subjected to hogging moments in braced frames is presented. The design method is applicable to both beam-to-column connections

and to beam-to-beam connections. In the guide the composite connection has been conveniently divided into three separate zones, see Figure 2-7.

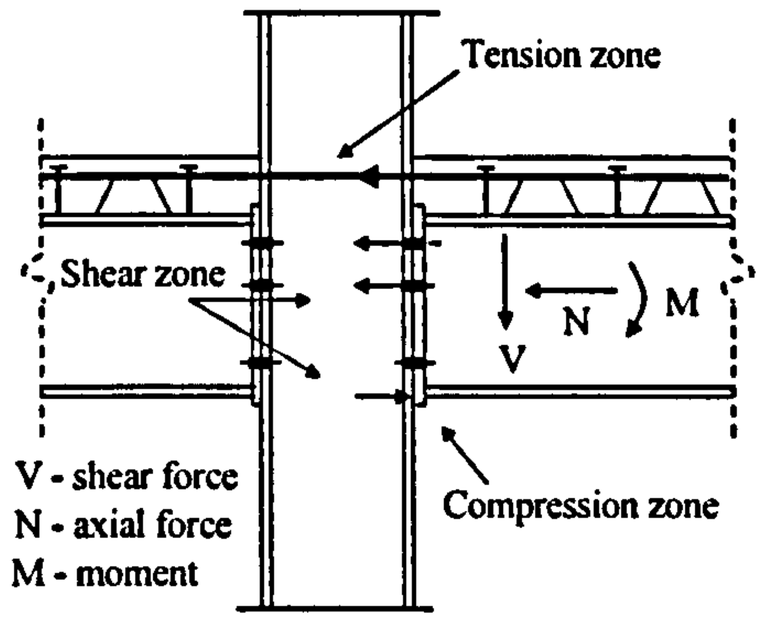

Figure 2-7. Composite endplate beam to column connection, SCI 1998

These include the tension zone, compression zone and shear zone. In the tension zone the reinforcement strength is calculated. The resistances of bolt rows are governed by three failures: (i) complete flange or end plate yielding, (ii) bolt failure with flange/endplate yielding, and (iii) bolt failure. In the compression zone comparatively few checks are required. As column web crushing (bearing) and buckling are both non-ductile failure mechanisms, a check is required to ensure that neither of these failure modes govern the behaviour of a plastic connection. Furthermore, a check of the beam flange crushing (bearing) capacity is required. Moreover, if column web crushing is critical then the column requires compression stiffening. In the shear zone, for a two-sided connection with balanced moments, the shear is zero, but in the case of a connection with unbalanced moments the shear is the difference between the two opposing forces. In such case, the column web must resist the resultant of the shears. These checks are needed for (major axis) connections to column flanges. They are not relevant for (minor axis) connections to column webs. Whilst calculating the moment capacity, the reinforcement and bolt row resistances can only be fully realised if sufficient resistance in the compression zone is available [SCI & BCSA, 1998].

The latest publication by the ECCS technical committee 11 for composite structures [1999], design provisions are provided based on the component method for steel joints described in the revised Annex J of Eurocode 3 [1998]. The proposed component model

for a composite joint is based on known force-deformation curves of the individual components, which have to be derived through component characterisation. The transfer from force-deformation curves of individual components to moment-rotation curves is achieved by fulfilling the requirements of compatibility and equilibrium and limitations on the resistance of components and their deformation capacity [Huber, 1998].

Eurocode 3 already provides expressions for the design resistance of all the tension, compression and shear components except reinforcement in tension. To simplify calculation, plastic theory is used to determine the design moment of resistance. This moment is therefore taken as the maximum evaluated on the basis of the following criteria: (a) the internal forces are in equilibrium with the forces applied to the joint, (b) the design resistance of each component is not exceeded, (c) the deformation capacity of each component is not exceeded, and (d) compatibility is neglected. A detailed procedure for calculating the moment of resistance by component models can be seen from chapter 8 of ECCS publication [1999].

2.5.2 Available Rotation Capacity of composite connections

As discussed earlier, in continuous composite beams both the hogging end resistance and mid-span sagging moment of resistance should be exploited in an economical design. This places a substantial requirement to redistribute the end moments. Ductility of composite joints is needed for that redistribution. Available ductility from the joint is the rotation that can be developed without the bending moment falling below the design moment resistance of the joint [Kemp and Dekker, 1991]. This capacity is dependent on several parameters and values exceeding 30mrad (1.2 degree) may be required to develop 90% of the sagging plastic moment of resistance in propped construction [Najafi and Anderson, 1997]. Test results [Anderson *et al.*, (1997), Bode *et al.*, (1996), Aribert *et al.*, (1994)] have shown that such values can be achieved, but it is clearly important that available rotation capacity can also be calculated [Anderson *et al.*, 2000]. Considerable research effort has been carried out to determine this key characteristic of the composite joint.

From the previous section on moment capacity it can be understood that the most recent model [ECCS, 1999] incorporates all the components which comprise the composite connection and studied all components behaviour in order to develop a design procedure for the moment resistance calculation. That simplified model does not make explicit allowance for either: (a) slab concrete bearing against the column, (b) transverse slab reinforcement, and (c) slip at the steel concrete interface. Account is taken of these actions through detailing rules to exclude their influence or (for slip) by a reduction factor on the stiffness [ECCS, 1999]. Moreover, the development of the full tensile force in the reinforcement depends on the longitudinal shear force being transferred from the beam to the slab via the shear connectors and concrete. BS 5950: Part 3 requires full shear connection to be provided in the negative moment region [SCI, 1998]. Thus the effect of slip is not considered explicitly in the moment resistance calculation. However, in the calculation of available rotation capacity, the contribution of slip in the shear connectors is considered. With conventional headed studs, some slip deformation will still occur. Since the available rotation capacity is dependent on the failure mode of the joint, this slip makes a useful and dependable contribution to the rotation capacity [Anderson *et al.*, 2000]. Furthermore, the detailing rules from the composite connection guide [SCI, 1998] specify that the first shear connector should be at least 100mm from the face of the column in order to ensure that reinforcing bars are strained over a substantial length, so that sufficient rotation can take place prior to failure.

The available rotation capacity model developed by the SCI assumed that the compression zone is located in the steel beam and the ultimate reinforcement strain is 2%. Based on this assumption, available rotation is calculated in two steps. In the first step, the elongation of the rebar over a length from half depth of the column to the first shear connector and beyond is calculated. This rebar elongation divided by the composite beam depth defines the available rotation. The contributions from the slip of shear connectors and bolts are neglected in this model [SCI, 1992].

Two years later, Najafi and Anderson proposed a spring model to represent the deformation of both the reinforcement and the shear connection. The equilibrium and compatibility equation for available rotation capacity is given as in Figure 2-8 where the

deformation of both shear connection and reinforcement is considered. It has been assumed that the slip at the connection depends initially on the nearest stud to the column. Under increasing load this stud provides resistance to slip, until it becomes plastic. Its force then remains constant and equal to its maximum resistance. Additional load is then assumed to be resisted by the next stud deforming elastically until the plastic resistance of that stud is reached also. Further load will then be carried by the next stud and so forth [Najafi and Anderson 1994]. However, in this model only the deformations of the tension components are considered.

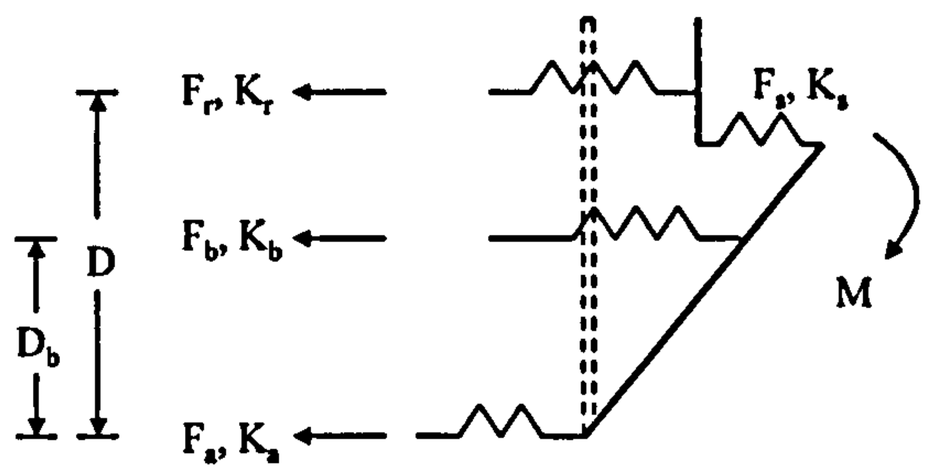

F - represents force ; K - represents stiffness

available rotation = $(F_r/K_r + F_s/K_s)/D = (F_b/K_b)D_b$

Figure 2-8. A spring model for available rotation capacity - Najafi and Anderson 1994

Xiao *et al.* have proposed a method similar to the SCI 1992 method. The model required modifications after comparison against the experimental results. Firstly, it neglected deformation of the compression zone, which had been observed as being quite substantial in many tests. Secondly, it assumed a fixed rotation point at the bottom flange of the beam, which does not accord with the deformation behaviour of different steel details and is not consistent with the approach to the calculation of moment capacity. To overcome these shortcomings the following assumptions were made: (1) strain hardening of the reinforcement was neglected, (2) concrete tensile strain was neglected, and (3) the rotation point of the connection was located on the neutral axis. The first two rows of studs can be defined as the plastic zone when determining the elongation of the reinforcement. It was found later that the elongation of the reinforcement in the elastic zone has no effect on the rotation capacity and should be neglected. Another important contribution to the rotation capacity is slip of the shear studs (Figure 2-9). Xiao *et al.*

[1994] have derived the specific rotation capacity for different composite connections and for different neutral axis position. The main defect of the above model is that the depth considered for the calculation of rotation capacity becomes larger than the beam depth and is sometimes greater than the combined beam and slab depth, when compared with the test results. This is not acceptable, since it implies that the beam is rotating without having any physical contact with the column.

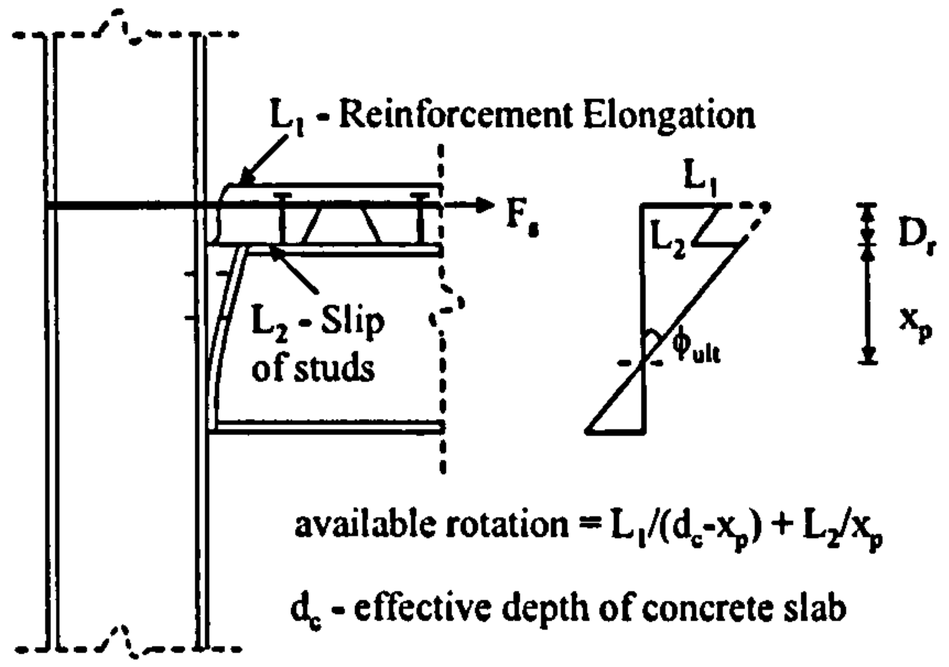

Figure 2-9. Beam to column rotation capacity model, Xiao *et al.* 1994

Similar to Najafi's [1994] method, a more comprehensive approach was proposed by Ahmed *et al.* In this method, as the depth of the compression beam web is determined, the contribution towards the available rotation from the rebars, shear studs and bolts could be calculated more precisely, see Figure 2-10. However, the contribution of compression component is neglected in this approach [Ahmed and Nethercot, 1997].

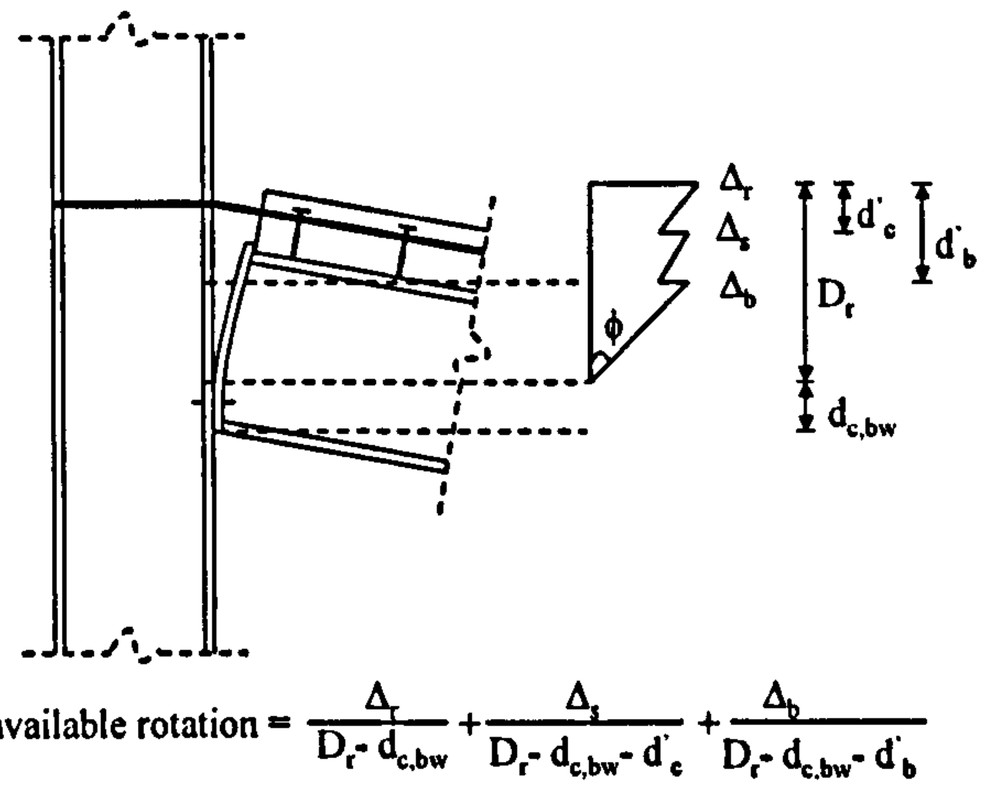

Figure 2-10. Available rotation capacity model, Ahmed and Nethercot 1997

The recent model developed by Anderson [2000] has been recognised by the ECCS technical committee for composite structures [1999]. This detailed approach incorporated contributions from both the tension and compression components (Figure 2-11). The failure mode of the connection determines the available rotation capacity.

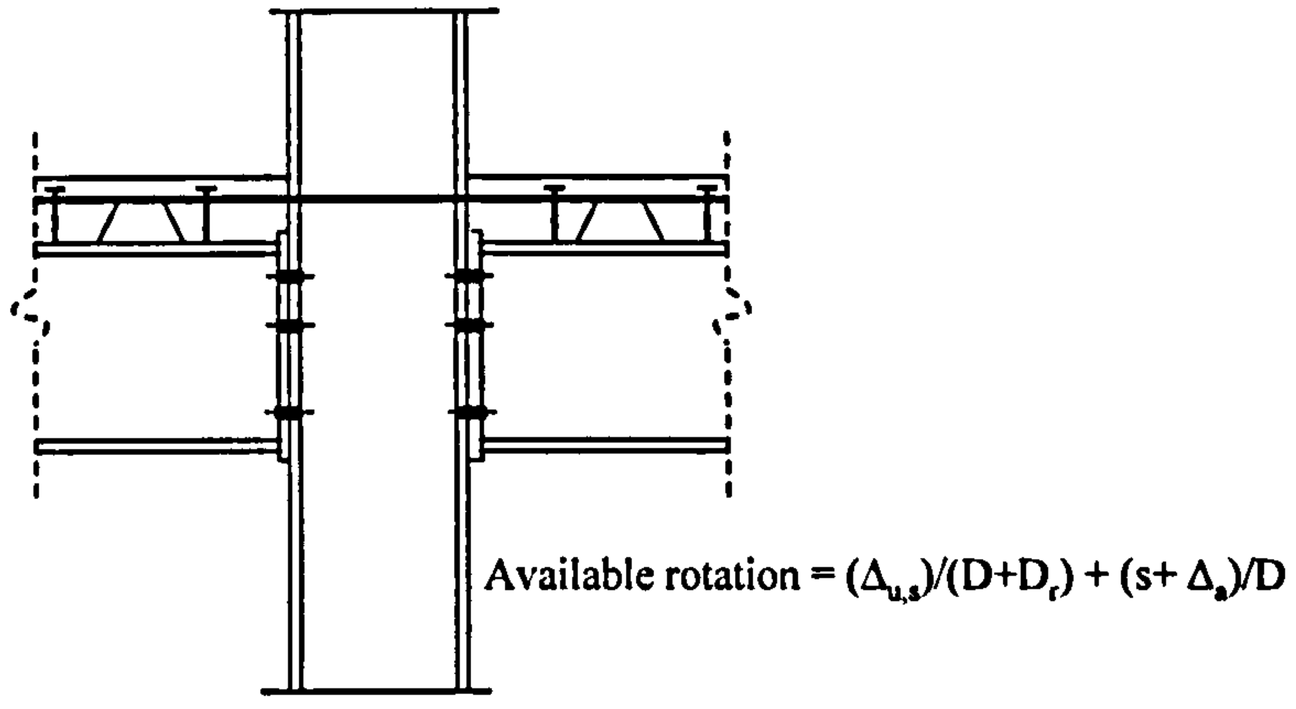

Figure 2-11. Available rotation capacity model by Anderson *et al.*, 2000

If redistribution of moment is required, the joint must deform in a dependable manner. This can be achieved through the in-elastic elongation of the reinforcement and through slip of the shear connection at the end of the beam. As the force required to achieve yielding of the reinforcement or loss of interaction is comparatively easy to compute, the designer can proportion other parts of the joint to avoid the premature loss of rotation capacity that would result from their failure. For comparison with test results, it is also necessary to make allowance for plastic compression in the beam flange immediately adjacent to the joint. For the slab reinforcement, the deformation capacity is limited by rupture of the bars. Importantly, the bond between the concrete and the reinforcement causes yielding only at crack locations. Rupture usually occurs at a transverse crack between the end support of the composite beam and the first shear connector in the direction of the span. The proposed calculation model is not an exact representation of the complex physical behaviour in a composite joint. However, reasonable agreement has been shown between calculated and measured total rotations limited by rupture of the slab reinforcement or by attainment of limiting slip capacity [ECCS, (1999) & Anderson *et al.*,

(2000)]. The calculated rotation based on this model can therefore be taken as the available rotation capacity of the joint.

2.5.3 Required support and connection rotations

It can be understood from the previous review that certain levels of rotation must be accommodated at the support sections of continuous beams and frames in order to mobilise a profitable amount of sagging moment of resistance in the span section. If the support section possesses a larger rotation capacity than is required, the desirable moment of resistance can be achieved in the span by utilising the majority of the sagging moment capacity of the composite section. However, if the available rotation capacity is lower than the required rotation capacity, then the amount of moment of resistance in the span has to be controlled in accordance with the available rotation capacity. Thus to determine the achievable moment resistance in the span or the degree of moment redistribution on the basis of rotation compatibility at the support, both the available rotation capacity in a given connection type and the required rotation capacity in a structural arrangement should be known. This section presents the development of required rotation capacity.

The rotation capacity of Class 1 sections, which may be required to achieve a plastic mechanism of collapse or an identified percentage redistribution of elastic moment, is obtained by non-linear analysis. The original studies of required rotation capacity in plastic design were undertaken by Driscoll [1957]. Several researchers [Johnson (1961), Hope Hill (1976, 1979), and Ansourian (1981, 1982)] have investigated the required hinge rotations in plastically designed, continuous composite beams [Kemp, 1987].

Following their investigation, Kemp and Dekker [1990] constructed a chart to determine the non-dimensional required rotation value [actual required rotation / hypothetical elastic rotation] from elastic-plastic analysis of the moment distribution in two equal span beams, and assuming plastic hinges are developed on both sides of the internal support. This hypothetical elastic rotation was determined for the ultimate moment resistance over the negative moment region. It was concluded that the requirements of EC4 [1989] relating to

the allowable redistribution of moments were consistent with this independent evaluation of required rotation capacity [Kemp & Dekker, 1991].

In 1992 Gibbons [1992] examined the connection rotation capacity required to achieve the assumed collapse mechanism (in the case of plastic global analysis) or the assumed distribution of elastic design moments (in the case of elastic global analysis). In the plastic global hinge analysis, the rotational capacity required at the supports of composite beams with partial strength connections was dependent on a number of factors. These included the shape of the free bending moment diagram, the shape factor of the section, beam length, support moment to mid-span moment ratio (k), elastic and plastic curvature and whether or not the beam is propped during construction. The end rotation comprises elastic and plastic components. The maximum plastic strain required at the position of maximum moment necessary to mobilise 95% of M_p of the composite section was determined as $3\varepsilon_y$ for a propped beam and $6\varepsilon_y$ for an unpropped beam (ε_y: yield strain). Theoretically mobilisation of the remaining moment of resistance demands high values of strain, which are possible, however, this model did not include the strain- hardening factor. Furthermore, this calculation takes into account the stress conditions that exist in the bare steel beam at the end of the construction stage. It was assumed that the beam was propped only at mid-span. It was shown that the 'locked-in' stresses at a prop location have a beneficial effect i.e. a low additional plastic strain is required. In the proposed formulae for calculating the required rotation capacity, to take into account of the construction stage stress conditions, a factor Ω has been introduced. Also, to take into account the unpropped mode of construction, the total rotation was multiplied by a factor α. The proposed equations are presented in Table 2-5.

Table 2-5. Gibbon's required rotation capacity equation, 1992

Uniform loading	Two point loading	Single point loading
$\phi_{total} = \alpha \frac{p_y L}{ED}\left\{0.33 - 0.21k + \frac{0\,22\Omega}{(1+k)^{1/2}}\right\}$	$\phi_{total} = \alpha \frac{p_y L}{ED}\left\{0.33 - 0.21k + \Omega\left(0.3 + \frac{0.07}{1+k}\right)\right\}$	$\phi_{total} = \alpha \frac{p_y L}{ED}\left\{0.25 - 0.325k + \frac{0.1\Omega}{(1+k)}\right\}$

when propped, $\alpha = 1.0$ and $\Omega = 1.0$; when unpropped, $\alpha = 0.7$ and $\Omega = 2.5$;

p_y: yield stress of the steel; E: young's modulus; L: beam span;

D: depth of steel section; k: joint moment / plastic moment resistance in midspan.

An attempt was also made to provide a more conservative equation by simplifying the three separate equations into a single equation, which is given in Table 2-6 [Gibbons, 1992].

Table 2-6. Gibbon's simplified required rotation equation, 1992

$\phi_{total} = \frac{p_y L}{ED}\{0.7\mu - 0.2k\}$	Values of μ	
	Propped	Unpropped
Two point loading	1.0	1.25
Uniform loading	0.8	0.9
Single point loading	0.5	0.5

Subsequently, in 1992 Najafi made an attempt to improve on Gibbon's equation. He developed a computer program, initially developed by Johnson [1982] for fixed-end beams, to include the effect of semi-rigid joints. The program first derived the moment-curvature relationship for the beam's cross-section in hogging and sagging bending from geometric data and material properties. To obtain the moment-curvature relationships, values of curvature were varied. For each value, the position of the neutral axis was altered until equilibrium of direct forces was achieved; the moment was then calculated. The maximum value was taken to correspond to a limiting stress in the steel of 1.3 times the yield value (strain hardening does not start until 6-8ε_y) or to a limiting concrete strain in compression of 0.0035. An initial value was assumed for the support moment. Load was then applied and the program varied the support moment until the slope at mid span was equal to zero. The percentage redistribution of moments was calculated by comparing the support moment with the elastic support moment of the fixed-end beam. The slope at mid-span was equal to the rotation of the joint plus the integration of curvature along half the span of the beam. Therefore, the model was applicable to symmetrical load only. In the elasto-plastic analysis of the program, it was assumed that full shear connection existed and that zero slip occurred at the steel-concrete interface. In addition, the contribution of the decking and the effect of tension stiffening in the concrete were ignored. The stress strain curves used for concrete and reinforcement were as given in BS5400 [1984]. The strain hardening of steel was allowed for by assuming a decreased

modulus of elasticity, usually taken as the ratio E/33 at 8 times the yield strain. The residual stresses in the steel section were also taken into consideration in this program, with a compressive stress of $\sigma_y/2$ at the tips of the flanges. For design considerations, the partial safety factors of 1.15 for reinforcement, 1.50 for concrete and 1.00 for structural steel were used. Furthermore, the EC4 recommendations for the effective width of the concrete slab were included in the program.

This program could analyse both propped and unpropped situation. For propped construction, no initial strain and stress are assumed in the section. Also it is assumed that no rotation occurred in the steel connection during the construction stage, although it is known that in reality some rotation may occur depending on the spacing of the props. For unpropped construction, initial elastic sagging and hogging moments are input, representing load on the steel section at the end of construction. Initial strains were added to those due to the residual stresses. In generating the moment-curvature relationships, initial total strains (not stresses) were assumed to exist in the section. Thus the resulting moment at each stage includes the initial bending moment due to lack of propping. The initial rotation in the steelwork connection was found by using the beam line method with the initial secant stiffness of the steel joint, which is input as data. The composite connection was assumed to possess this initial rotation after construction was completed. Two different cases (full strength connections and partial strength connections) that may occur in the plastic hinge analysis of a composite beam with semi-rigid connections have been included in the program. The program was also modified so that it could deal with both a solid slab and a composite slab. Since the program developed plasticity in all slices of the steel section, the program could deal with only composite beams with Class1 sections.

Najafi suggested an optimum amount of 1% reinforcement with respect to the area of concrete slab (above decking) within an effective breadth in order to provide a rotation capacity which corresponds to that required from the joint. The total rotation that occurred at the joint was taken as the resultant of elastic and plastic rotations along the length of the beam. Najafi derived formulae to calculate the required rotation following Gibbons work [1992]. However, Najafi did not consider the factor (α) for unpropped construction as in

Gibbons equation. In the derivation, it was assumed that only 95% of sagging moment of resistance was reached, as this is sufficient in the design of composite beams. These formulae are presented in a table format, see Table 2-7.

Table 2-7. Formulae for calculating required rotations by Najafi [1992]

	Propped	Unpropped
Grade 43	$\phi = \frac{f_y L}{ED}(0.33 - 0.21k + 0.38(1+k)^{-1/2}$	$\phi = \frac{f_y L}{ED}(0.33 - 0.31k + 0.55(1+k)^{-1/2}$
Grade 50	$\phi = 0.88\frac{f_y L}{ED}(0.33 - 0.21k + 0.38(1+k)^{-1/2}$	$\phi = 0.88\frac{f_y L}{ED}(0.33 - 0.31k + 0.55(1+k)^{-1/2}$

where,

f_y: yield stress of the steel; E: young's modulus; L: beam span

D: depth of steel section; k: joint moment / plastic moment resistance in mid-span.

As discussed above, both Gibbons and Najafi considered the effect of unpropped construction on the required rotation capacity to a limited extent. Gibbons proposed a single equation to determine the required rotation capacity for both propped and unpropped beam which includes a factor, 'μ' (varies from 0.5 to 1.25 for different loading conditions), to take into account of the construction stage stress conditions. However there is no publication to explain the method of assessing the 'μ' factor and therefore it is not possible to directly compare Gibbon's approach with that presented in this thesis. The latest model by Najafi using Johnson's computer program uses the basic structural mechanics principle of deriving moment-curvature relationship for each given cross section along the span subjected to either hogging and sagging moments, using the geometric data and material properties. The connection rotation is determined by integrating the curvature along the beam. Although the model presenting in Chapter 5 of this thesis, is similar in principle to Najafi's, three major contrasts exist between the two models, listed below.

1. Najafi's model manually calculates the connection (steel) moment-rotation during the construction stage using the beam line method with the initial secant stiffness of the steel joint and gives the construction rotation as an input value to the program. Whereas the model presenting herein calculates the construction stage connection rotation using steel

section material properties using the program in the first phase and incorporates that in the composite stage. Therefore there is no need for manual calculation.

2. Najafi's model is applicable to symmetrical boundary conditions only as it always considers the slope at mid-span to be equal to zero. Hence the integration of curvature along half the span of the beam is equal to the required rotation of the connection. In contrast, the author's model determines rotation as an integration of curvature to the point of maximum deflection i.e. zero slope which can occur at any point of the beam with respect to the boundary condition and can be used for either internal or external beam locations within the frame. This allows for a more generic model.

3. Najafi's model considers the connection rotation due to construction stage loading in the unpropped construction as a single value and does not study the variation of dead load stress along the beam. In contrast the author's model considers the fact that the moment-curvature relationship for the beam is dependent on the degree of dead load stress locked into the beam during construction and uses a 3D function of moment-curvature and dead load stress to calculate the required rotation of the connection.

These three major differences set out the precise limitations in the existing Gibbon and Najafi's work compared to the author's work presented in this thesis.

Finally, design charts were produced for determining the required rotation capacity in the composite connections of semi-continuous frames for different steel grades. It was concluded that the maximum percentage redistribution of moments, given as 40%, in EC4 and BS5959: Part 3.1, is an appropriate value for both propped and unpropped composite beams. However, more redistribution of moments may be possible in conservatively designed beams, although values greater than 40% are not advisable. Moreover, it is possible to reduce the rotation requirements by not utilising the full sagging moment of resistance of the composite beam. Also it has been concluded that the flexibility of partial strength connections does not influence the rotation needed for plastic mechanism, rather its resistance determines the required rotation. Moreover, very flexible connections may cause the first hinge to form at mid-span.

In order to predict the rotation capacities for the connections of the continuous and semi-rigid frames, a step-by-step method was proposed by Li [1995]. This model can only be applied directly to propped beams, because it is assumed that the composite beam supports both dead and imposed loads. In this method, the required rotation analysis for the whole structure is divided into the analysis of the equivalent single span beam and the equivalent column. The connection rotation requirement is equal to the difference between the beam end rotation and the column rotation. Assuming the column is rigid or loading is balanced, the required rotation is calculated from the equivalent single span beam only. According to this method, the required rotations contributed by beam deformation are sub-divided into the elastic and plastic components, these being integrals of the respective elastic and plastic curvatures that occur in the span. As the accurate evaluation of flexural stiffness for the hogging region is not available, the average flexural stiffness of the cracked and uncracked sections is used as the flexural stiffness of the hogging moment region. Owing to the step-by-step characteristics of this analysis method, it is possible to analyse the required connection rotations for complicated frame structures. Subsequently, this approach was simplified so that it could be incorporated into a design procedure in an empirical equations format, catering for a variety of load types and support conditions [Li *et al.*, 1995]. The detailed approach could be obtained from Li's 1995's publication. In order to present an empirical equation Li conducted orthogonal tests and selected only those parameters which have the greatest influence on the required end rotation. A sample equation to calculate the required rotation for a uniformly distributed load, with equal end moments is given:

$$\theta_r = \left(0.344 - 0.225R' + 0.561\left(\frac{M_d - M_y}{M_p - M_y}\right)^2 \frac{1}{\sqrt{1+R'}}\right)\frac{M_d L}{EI} \text{ where}$$

θ_r : required rotation capacity; M_d : span design moment

R' : support moment to span design moment ratio; M_y : span yield moment

M_p : span plastic moment resistance; L : beam span length

EI : positive bending flexural stiffness.

Thus the main factors affecting the non-dimensional required rotations are support-to-span moment ratio, relative moment ratio $\frac{M_s - M_y}{M_p - M_y}$ and in some other load conditions, span yield moment-to-design moment ratio. Li's model was used as the basis for the background study leading to the 'Green Book' detailing rules [SCI, 1998].

Based on the single beam analysis, an alternative approach for predicting the required connection rotations was also proposed [Lawson and Gibbons, 1995]. The analysis was concerned with the end rotations due to the development of a plastic hinge in the mid-span zone of a beam, in addition to the pure elastic behaviour of the beam. The analysis took into account the span to depth ratio of the beam, the load pattern along the beam, and the steel strength. Assuming the beam to be a uniform section and using moment area method, the theoretical equations for calculating the elastic required rotation were given for three conditions of uniformly distributed load, two concentrated loads at third points and a single concentrated load at mid-span.

Further to that it was assumed that the plastic neutral axis of the composite beam section was located at the top of the steel and a fixed ultimate strain (3 times the yield strain) at the bottom flange of the steel beams. Based on the Nottingham [Li, 1995] and Warwick [Najafi, 1992] research, the authors found that the minimum required end rotation of a composite beam necessary to develop the plastic moment resistance, M_{pc}, of the composite beam in mid span may be determined from the following approximate formulae shown in Table 2-8. This is a function of the moment resistance, M_{cc}, in the connections for a span to depth ratio less than or equal to 20, and for three different load cases.

Table 2-8. Lawson's simple equations to calculate the required rotation [1995]

Uniformly distributed load	Two point loads	Central point load
$\theta_{required} = 0.03\left[1 - 0.5\frac{M_{cc}}{M_{pc}}\right]\left(\frac{\rho_y}{355}\right)$	$\theta_{required} = 0.04\left[1 - 0.5\frac{M_{cc}}{M_{pc}}\right]\left(\frac{\rho_y}{355}\right)$	$\theta_{required} = 0.02\left[1 - \frac{M_{cc}}{M_{pc}}\right]\left(\frac{\rho_y}{355}\right)$

It was concluded that the adequacy of the composite connections is dependent primarily on a geometric parameter (span to depth ratio). As there is a relationship between span and depth for well-designed composite beams, it is more convenient to use span as the determining parameter. The longer the beam span, the greater the required end rotation to develop the plastic mechanism. In elastic terms, the longer the beam, the lower the percentage of moment redistribution that is permitted before the connection rotation capacity is exceeded. A maximum beam span has therefore been established for a given maximum percentage redistribution of moment in elastic global analysis, see Table 2-9.

Table 2-9. Maximum percentage redistribution of negative moment for elastic global analysis, and maximum spans for use of these redistributions, SCI 1995

Case		Section classification			
		Class1		Class 1 or 2	Class 1,2 or 3
Continuous steel section (BS 5950 Pt 3)		50%		30%	20%
Composite connections (p > 1.0%)		50%	40%	30%	20%
Maximum span of beam (m)	S355 steel	10	12	15	17
	S275 steel	12	14	17	20

p = percentage of slab reinforcement (ignoring the mesh)

From the Table 2-9, it can be understood that a small degree of redistribution means that the composite connection has to be designed for a relatively high moment, and hence the amount of reinforcement that is needed in the slab is relatively high. A high degree of redistribution means that plasticity may develop in the connections, which also affects the serviceability performance. Table 2-9 also presents the maximum span of beam, corresponding to the maximum redistribution of negative moment that is permitted in each case. In principle, longer spans are permitted if the percentage moment redistribution is reduced. For example, S355 Class 1 or 2 beams could be analysed for 30% moment redistribution for spans up to 15m. Reducing the steel grade increases the maximum span permitted for a given percentage redistribution of moment.

Although there are equations available for calculating the rotation capacity, due to the complexity in the prediction of available and required rotations, it is impractical to directly check the rotation requirement for every connection during design. Li *et al.*,

[2000] therefore suggested a method allowing for the indirect evaluation of connection rotation requirements. This indirect method permits designers to establish whether a connection rotation requirement is satisfied without involving complicated calculation. According to test results [Xiao *et al.*, (1994), Li *et al.*, (1996) & Anderson *et al.*, (1994)] and the methods developed [SCI, (1992), Xiao *et al.*, (1993) & Ahmed *et al.*, (1997)] for predicting connection rotation capacity, it is known that 20mrad can be taken as the lower bound of the available rotation capacity of composite connections, provided the connections are designed appropriately. If the required rotation capacity for a composite connection is below this limit, then the connection rotation requirement would be automatically satisfied. However, the tests also demonstrated that most composite connections are capable of achieving a rotation capacity of 30mrad provided at least 1% reinforcement (rebar to concrete slab area ratio) is used in the negative moment region and column web buckling failure is prevented. This implies that a properly designed composite connection is quite ductile and can meet the rotation requirements for unpropped construction. According to the method developed [Li *et al.*, 1995] for predicting required connection rotations, it is possible to obtain general indications for the span to depth ratio and connection/span moment ratio for a given value of required connection rotation. The paper by [Li *et al.*, 2000] aimed at developing simple rules which facilitate the use of Eurocode 4 Annex J [1992] as well as SCI Green Book [1998], and uses the calculated required connection rotations in order to propose limitations on the span to depth ratio of composite beams when using semi-continuous construction. A table has also been presented by Li to establish a relationship between the maximum span to depth ratio of a composite beam, the available rotation capacity of the connection and the connection/span moment ratio. From these relationships, the rotation requirement for a connection can easily be checked to see whether it is satisfied or not. A summary of the maximum span to depth ratios is given for discussion in Table 2-10. For example, take an internal composite beam with span to depth ratio of 20 with steel grade (S275) subjected to UDL, $M'/M_d = 0.25$ and $M_d \leq 0.9M_p$ and with a minimum available rotation capacity of 25mRad. From Table 2-10, it can be seen that the maximum span to depth ratio for this beam is 25. Since the actual span to depth ratio of the beam (i.e. 20) is much smaller than the maximum value allowed, the connection meets the rotation requirement and no further checks are necessary [Li *et al.*, 2000].

Table 2-10. Summary of maximum span to depth ratio of composite beams with semi-rigid connections for M'/$M_d \geq 0.25$ and connection rotation capacity greater than 25 mRad and $M_d = 0.9M_p$, propped construction

Steel grade	M''	UDL	2PL	1PL
235	M'	29.0	21.0	55.0
	0.0	29.0	21.0	50.0
275	M'	25.0	19.0	47.0
	0.0	26.0	31.0	43.0
355	M'	20.0	17.0	37.0
	0.0	20.0	24.0	34.0

where, M_d: span design moment, M_p : plastic moment of resistance of span section;
M': connection moment capacity; M'': other end connection moment capacity
UDL: uniformly distributed load; 2PL: two points loads; 1PL: single point load

SCI [1998] recommended rigid-plastic analysis where the composite joint is chosen to possess partial strength. The design guide for composite connections by SCI [1998] is limited to partial strength composite connections in braced frames, where the connection between the beam and the column is of the flush end-plate type. The design guide also covers partial depth end-plate beam-to-beam connections and can be used for both manual and computer-aided design and detailing. The design method is in the form of an easy to use step-by-step checklist for a set of standard composite connections, which is based on the latest design theories and practical aspects associated with current fabrication and erection practice in the UK. These design checks are supplemented by quick look up tables and worked examples for each connection type. Finally, the method is compared with available experimental evidence for practical composite connections and it is concluded that the new method is safe and gives reasonable estimates of strength [Moore and Couchman, & SCI, 1998]. There are three restrictions in order to ensure that the rotation requirement does not exceed that available. These include:

- Design sagging resistance of the beam is limited to 0.85 Mp to limit rotation requirement.
- Connection moment capacity should not be less than 30% of the beam moment capacity in sagging as the demand on rotation requirement increases with the moment redistribution.

- Span (L) to total depth (D) ratio of the beam should satisfy the following limits:

$L/D \leq 25$ for beams subjected to UDL, multiple point loads or a central load

$L/D \leq 20$ for beams subject to two point loads

This is because the extension or the spread of plastic moment region along the span differs for different load cases and thereby influence the rotation requirement.

The Standard connections presented by the SCI are capable of achieving more than 30% of the beam capacity. Hence by choosing the right combination of steel grade, span to total depth ratio, support to span moment ratio, design sagging moment and load arrangement it is possible to exploit the advantages of composite connections.

The recent publication by ECCS Technical Committee 11 in Design of Composite Joints for buildings recommends elastic-plastic analysis. It gives a design aid for the elastic-plastic analysis of semi-continuous composite construction. At the time of drafting EC4 Part 1.1, no detailed provisions were made for the design of composite joints, although a 'composite connection' was defined in section 1; it was also suggested in section 4.10 that some use could be made of Annex J of ENV 1993-1-1. Design of braced frames with partial strength composite connections is one option given in Section 4.9.2.4 of EC4 Part 1.1. Annex J of Eurocode 3 was revised during the EC4 period. It adopted a 'component' approach, partly to facilitate extension to composite joints. The model design provisions given hereafter built on the revised EC3 annex, which has now been published as part of Amendment 2 [1998] to EC3 1993 Part1.1.

Composite joints are attractive when they increase resistance and stiffness for little additional effort in construction. In practice therefore columns are unlikely to be heavily stiffened. Thus clauses for steel backing plates, supplementary web plates and other forms of stiffening are not included in the model clauses. Eurocode 3 may be used for the design of these steel elements, if required. As the provisions are 'model' clauses, they do not fully address all types of composite joint, for example those with fully welded steel connections or with angle cleats. The component approach, adopted in the model clauses, does however enable the designer to extend the provisions to these types of joint, making use of Amendment 2 of Eurocode 3 for component properties. Similarly, joints to

columns with rectangular or circular hollow sections may be designed, using the literature to determine appropriate component properties. No separate required rotation model has been presented as this publication is primarily intended for elastic-plastic analysis. However, summarising all the previous works on required rotation capacity, the following conclusions have been drawn regarding the required rotations of composite joints [ECCS, 1999].

(a). The overall required rotation is unaffected by the stiffness of the joint and therefore calculation can be performed on an isolated beam

(b) The rotation is significantly affected by the moment resistance of the joint relative to that of the beam in sagging bending.

(c) The rotation is significantly affected by the strength grade of the steel beam section.

(d) The rotation is significantly affected by the beam span to depth ratio; an increase from 20 to 30 in the ratio causes the required rotation to increase by approximately 30%.

(e) When other parameters are the same, equal point loads at third-points along the span requires the largest rotation; a central point load requires the smallest rotation; a uniformly distributed load requires an intermediate values. Compared with an udl, the required rotation can increase by the order 50% if point loads act at the one-third points.

(f) When one end-moment is zero, the required rotations are smaller compared to equal end moments when the beam supports equal point loads at third points, and larger under a central point load.

(g) When one end-moment is zero, the rotations are almost the same compared to equal end-moments when the beam supports a uniformly distributed load.

(h) When other parameters are constant, a variation of steel beam size has little effect on the rotation.

(i) As plastification spreads in the mid-span region, the demands on rotation capacity increase sharply.

(j) The rotation is increased with un-propped construction.

(k) Provided that the span to overall depth ratio of the composite beam does not exceed 30, the limits in Table 2-11 can be used in design. For unpropped construction, the rotations are those at the composite stage.

Table 2-11. Limits for available rotation capacity (θ_{ava}) and the design moment (M_{design})

	Uniformly distributed load	Two point loads
Propped	$\theta_{ava} \geq 22$mrad and $M_{design} \leq 0.9M_p$	$\theta_{ava} \geq 33$mrad and $M_{design} \leq 0.9M_p$
Unpropped	$\theta_{ava} \geq 22$mrad and $M_{design} \leq 0.85M_p$	$\theta_{ava} \geq 33$mrad and $M_{design} \leq 0.85M_p$

Where θ_{ava}: Available rotation capacity; M_{design}: span design moment; M_p: span plastic moment resistance

2.6 Research into unpropped construction

In a propped beam, the dead and live loads are supported by the composite beam itself. In the case of unpropped beams, the dead load (or construction stage) is carried only by the steel beam and the live load is resisted by the composite action. According to COST C1 [1997] and ECCS [1999], during the construction phase joints should be modeled in accordance with Eurocode 3 [1992 & 1998]. Research work discussed so far in this review chapter was intended mainly for propped construction. Design rules [plastic global hinge analysis (SCI, 1998) & elastic-plastic analysis (ECCS, 1999)] that have been developed for composite connections in frame structures are also for propped construction. However, widespread use of composite connections is unlikely before they can be used with unpropped beams, which are popular because of the lower on-site construction costs, speed and convenience. Thus it is important to validate the use of the design guidance for composite connections for unpropped construction.

In unpropped construction, the steel beam alone supports the dead load and this leads to greater strain and curvature in the beam sagging region. During construction significant dead load compressive stresses are locked into the top half of the steel section. Additional curvature is necessary to convert these compressive stresses to tensile yield stresses. Since the end rotation is given by the integral of curvature, an increase in the required rotation capacity will result. This increase is significant because the bottom flange strains are non-elastic and therefore produce large curvatures. Researchers [Anderson *et al.*, (1997), Couchman (1995) & Gibbons (1992)] suggest that this increase could be as high as 40% compared with the propped case. It is worthy of note that this increase in the required

rotation for the unpropped construction depends totally on the dead load supported by the steel beam. However, what is not clearly understood is the level of dead load strain that this 40% increase could occur. In order to revise the design rules, it becomes necessary to know the effect that this dead load strain will have on the percentage increase of required rotation in the unpropped case. Also, in unpropped construction the connection reinforcing bars resist only post-construction loads. Therefore, the end rotations resulting from dead loading place no strain on the reinforcement, thus increasing the available rotation capacity. This increase has been quantified as between 10 to 15% in comparison with propped construction [Couchman and Way, 2000]. However, this improvement in performance is more than offset by a substantial increase in the rotation requirement. It is understood that although the strength requirement for both forms of construction remains the same, the ductility requirement differs. It therefore becomes necessary to revise the design rules for composite connections in the unpropped mode of construction.

Chapter 3 – Full-scale test on composite connections in unpropped composite floors

---

Papers published based on this chapter:

1. Dhanalakshmi, M., Byfield, M. P. and Couchman, G. H. (2002). Composite connections at perimeter locations in unpropped composite floors, *International Conference on Advances in Steel Structures (ICASS 02)*, HongKong, December, Volume 1, 261-268.

2. Dhanalakshmi, M. and Byfield, M.P. (2002). "Strength and Ductility of Composite connections", The Structural Engineer, Volume 80, Number 20.

3. Byfield, M. P., Dhanalakshmi, M and Goyder, H. G. D. (2004). "Modelling of unpropped semi-continuous composite beams", Journal of Constructional Steel Research, Volume 60, 1353-1367.

3.1 Introduction

It is understood from chapter 2 that most of the composite connection research considered propped beams, being based on cruciform tests, which by their very nature model the propped construction condition. Therefore, due to the absence of unpropped test data, the existing composite connection design and detailing rules [SCI (1998) and EC4 (1994)] can currently only be used with beams that are propped during construction. Moreover, the widespread use of composite connections with propped construction is unlikely, because unpropped construction is generally a preferred and more economic method.

Due to the lack of test data the guides do not adequately model the commonly occurring unpropped situation and the concern amongst steelwork designers and fabricators is such that without a proper validation of this model this beneficial form of construction will

remain largely unused. Furthermore, according to the industry standard composite connection design guide [BCSA and SCI, 1998], it is recommended that connections to perimeter columns should be non-composite, to avoid problems in anchoring the reinforcement. The provision of composite connections at the perimeter locations will minimise the external beam depth. Thus for applications where it is important to minimise beam depth, even if this is at the expense of heavier perimeter columns, practical details are also required for single sided moment resisting connections. Thus it is necessary to solve these two problems i.e. (1) extend composite connections for use with unpropped composite floors, and (2) develop composite connections for use at perimeter column locations. In order to investigate these two problems a full-scale sub-frame test was carried out at the Building Research Establishment, UK. The beams were unpropped during construction and one of the perimeter connections incorporated a modified form of composite connection. This test is reported in this chapter.

A background study on composite connection research during the last three decades reveals that more than 120 various types of composite connections have been tested [Xiao, 1994]. However, to take advantage of composite connections behaviour it is essential to examine the interactions between beams and their connections through to failure of the complete system. Full-scale testing is the only method of obtaining accurate and believable data on these interactions. Numerical modelling techniques can be developed [Ahmed and Nethercot, 1995], but they will need to be calibrated against test data and furthermore they do not always offer reliable solutions at present.

Several researchers have carried out experimental studies to investigate the behaviour of semi-rigid steel frames [Nethercot (1989), Davidson (1987), Gibbons (1990), Stelmack *et al.* (1986), Lloyd *et al.* (1992)]. Furthermore, large-scale experimental studies on to the behaviour of semi-rigid composite frames incorporating propped beams have also been carried out [Leon (1987), Li (1994) and Armer (1994)]. However, very few tests have been undertaken on unpropped construction. Thus, the research reported herein was carried out in collaboration with Building Research Establishment (BRE), Steel Construction Institute (SCI) and Warwick University to investigate the behaviour of composite connections. The project aimed to determine the ductility characteristics of

standard composite connections under the unpropped situation, in addition to investigating the performance of a new form of exterior composite connection detail. It has been decided to unify these problems in one test frame.

Accordingly, a sub frame was tested to simulate a subsection of a multi-storey building. The frame was 3.8m wide and comprised two bays each 11.4m long. It employed standard composite connections at the interior joints, and a new form of composite connections at the exterior joint. A standard pin connection was used at the other exterior joint. The props were removed before the casting of concrete slab, which allowed the test to simulate the unpropped method of construction. At both construction and composite stages, measurements were taken comprehensively to record the connections strength and ductility, member deflections and moment distributions. The test provides data on ductility, exterior connections and unbalanced loading.

3.2 Design of the composite frame specimen

It is important to state at this stage of this thesis the responsibilities of different parties involved in carrying out this test from the initial design stage to the testing and the analysis of the test results. The lay out of the sub-frame, member sizing (composite beams, columns, and composite slabs), internal composite connection detailing, and instrument locations for the test have been developed and designed by BRE, SCI and Dr. Mike Byfield and are outside the scope of the author's responsibility. The new form of exterior composite connection detail, Figure 3-8, was developed and designed by author's supervisor Dr. Mike Byfield for the purpose of this research and was incorporated into the test frame. The author is involved with BRE and SCI in the decision making of test procedure, construction of test frame, installation of the instrumentation and carrying out the test. The main responsibilities of the author in this experiment are in reporting the behaviour of internal and external composite connections and the overall test frame behaviour, and subsequently to analyse the test data.

3.2.1 Lay out of the frame specimen

The general lay out of the test frame is shown in Figure 3-1.

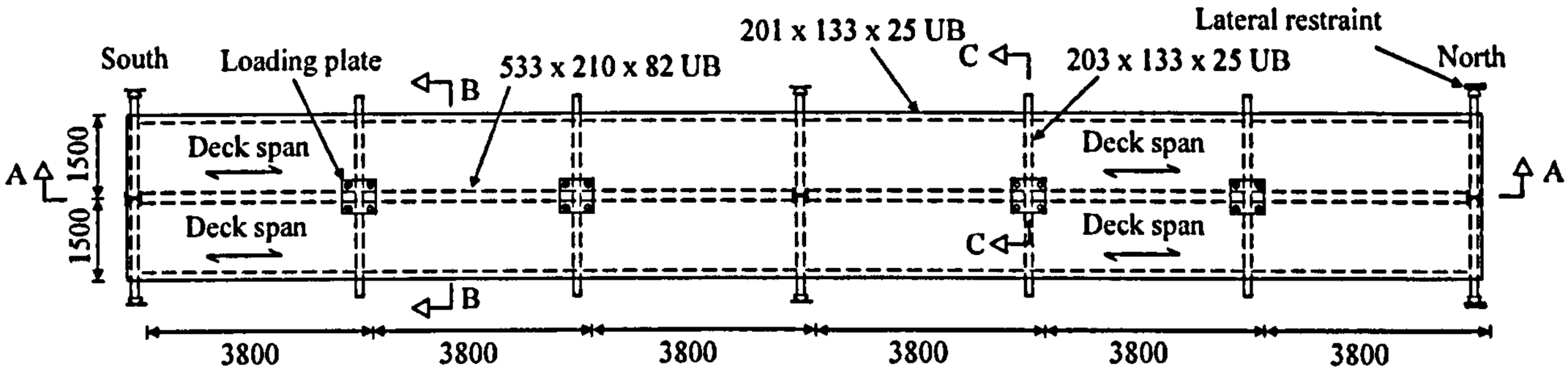

Figure 3-1. Plan view of test frame

A relatively deep beam was selected because there is very little data available on the ductility of composite connections with deep beams. The overall dimensions of the test specimens are a compromise between the following conflicting requirements:

(a) The need to provide a practical arrangement for the chosen beam size

(b) The constraints within the BRE laboratory

A beam length 11.4m has been chosen, as this is the practical span for a 533x210UB and to fit within the overall length, and grid of loading holes in the structures testing lab at the BRE. The test specimen represents part of a multi-storey, braced frame and therefore the length of the supporting columns was selected to reflect the span between the points of contra-flexure that occur approximately at mid-height in the columns of multi-storey buildings. Thus, the column height reflects a half-storey below and above the slab (Figure 3-2).

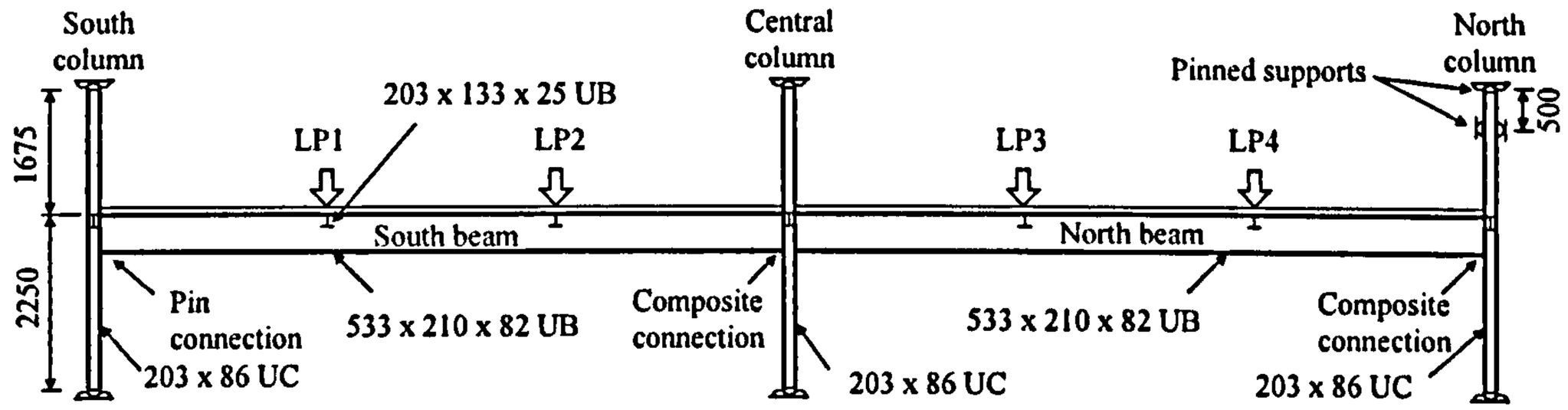

LP: Load point

Figure 3-2. Side elevation of test frame (Section A-A)

The slab width was chosen to be the effective width for the span of the beam i.e. span/4 and the depth of the slab is 130mm (Figure 3-3).

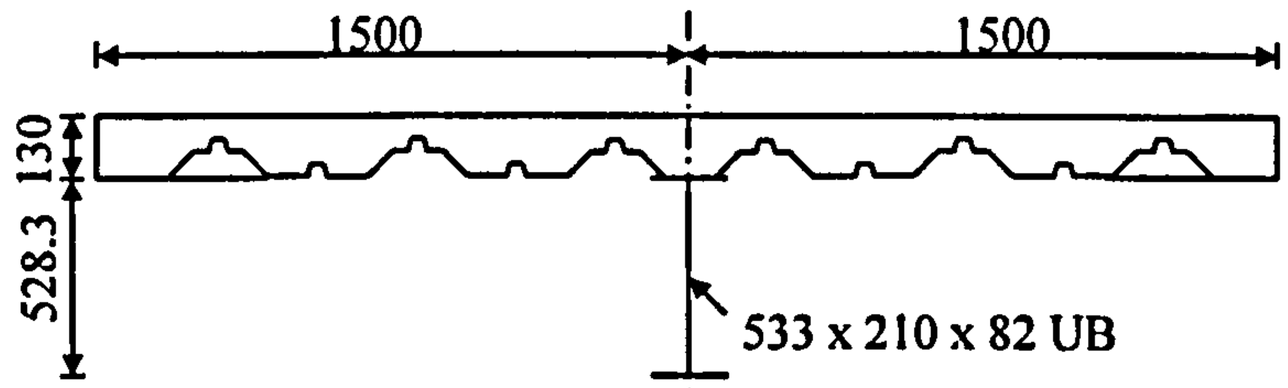

Figure 3-3. Cross section through the slab (Section B-B)

Primary beams (533x210x82UB) were connected to the major axis of the column (203x203x86UC). Secondary beams (203x133x25UB) were connected to the web of the primary beam (533x210x82UB) through supporting beams fabricated from a circular hollow steel section (Figure 3-4).

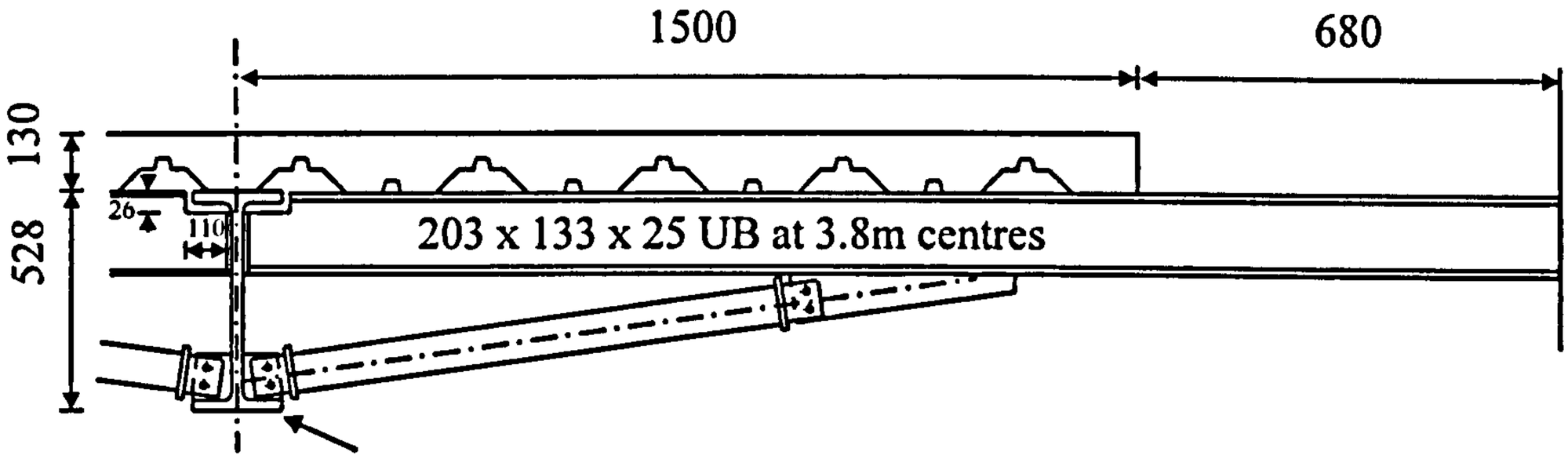

Figure 3-4. Cross-section through deck (Section C-C)

Multi deck profile sheet (type 60x1.2) was placed parallel to the beams and therefore required additional transverse reinforcement in the high shear zone of the slab. The transverse reinforcement enable the concrete flange to resist the longitudinal shear transmitted by the shear connectors, both immediately adjacent to the shear connectors and elsewhere within its effective breadth. A total of 6Nos. of 12mm ϕ high yield steel reinforcement bars were provided at the high shear zone (at the connection) and mesh reinforcement was provided throughout, Figure 3-14. Headed shear studs of 19mm diameter and clear height of 100mm were used to affect the shear connection between steel and concrete.

In the plastic design of composite beams with full shear connection the longitudinal shear force to be transferred between the points of zero and maximum sagging moment should be the smaller of the tensile resistance of the steel section (R_s) or the compressive resistance of the concrete slab (R_c). In the hogging moment region, the development of the full tensile force in the reinforcement (R_r) depends on longitudinal shear force being transferred from the beam to the slab via the shear connectors and concrete. The design strength of the headed shear connectors in the positive moment region is 80% of the characteristic strength whereas only 60% is taken in the negative moment region.

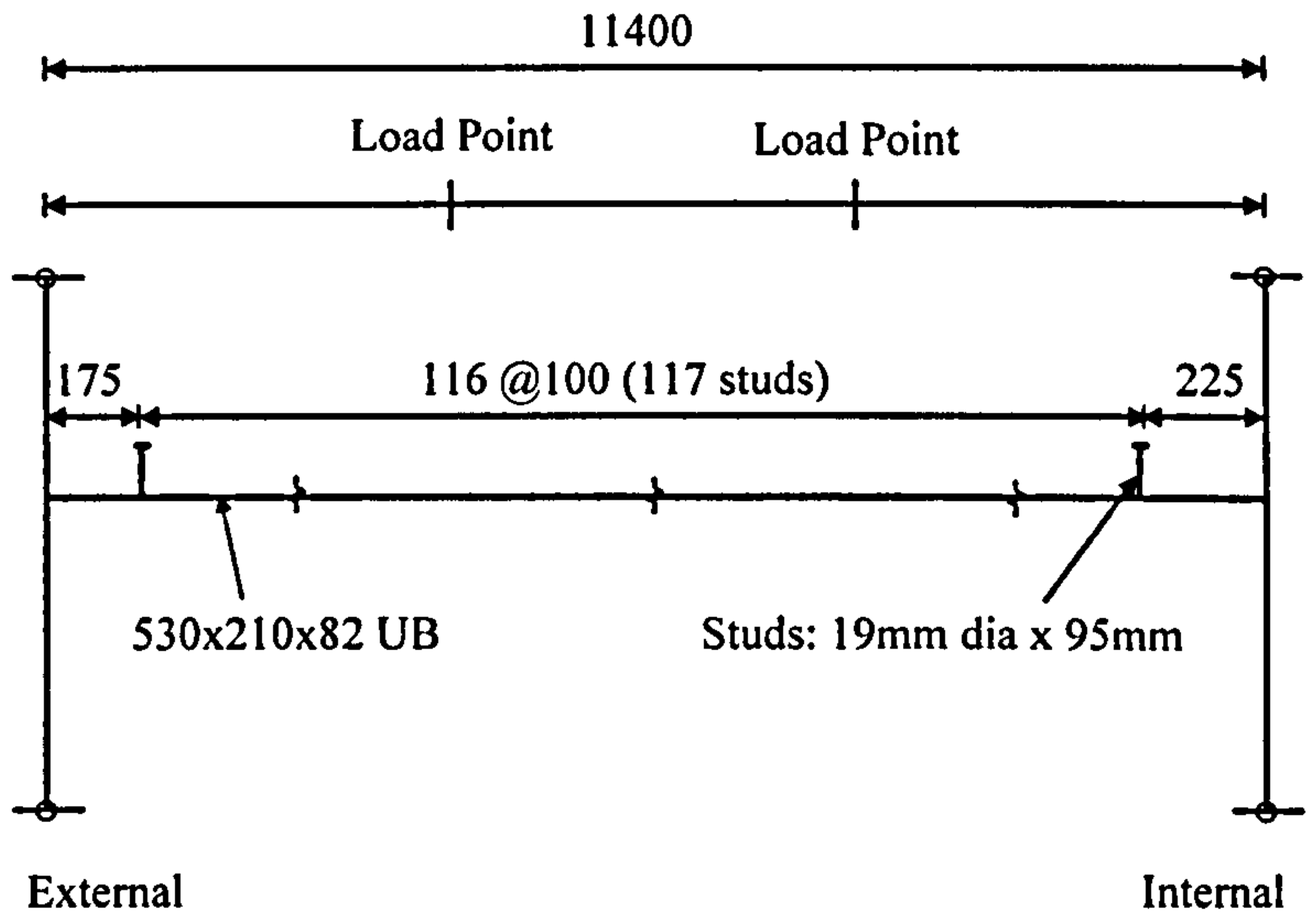

Figure 3-5. Shear stud layout - Main beam (100%)

In the test beam, the required number of shear connectors on both sides of the maximum sagging moment was calculated to be 68 in order to provide full shear connection. Also the required number of shear connectors in the hogging moment region considering the boundary conditions of the beam was calculated to be 7. In order to develop the full plastic moment of resistance, a total of 117 shear studs were used at a spacing of 100mm, see Figure 3-5. The secondary beams which are at every 3.8m centre had shear studs at 323mm spacing, Figure 3-6

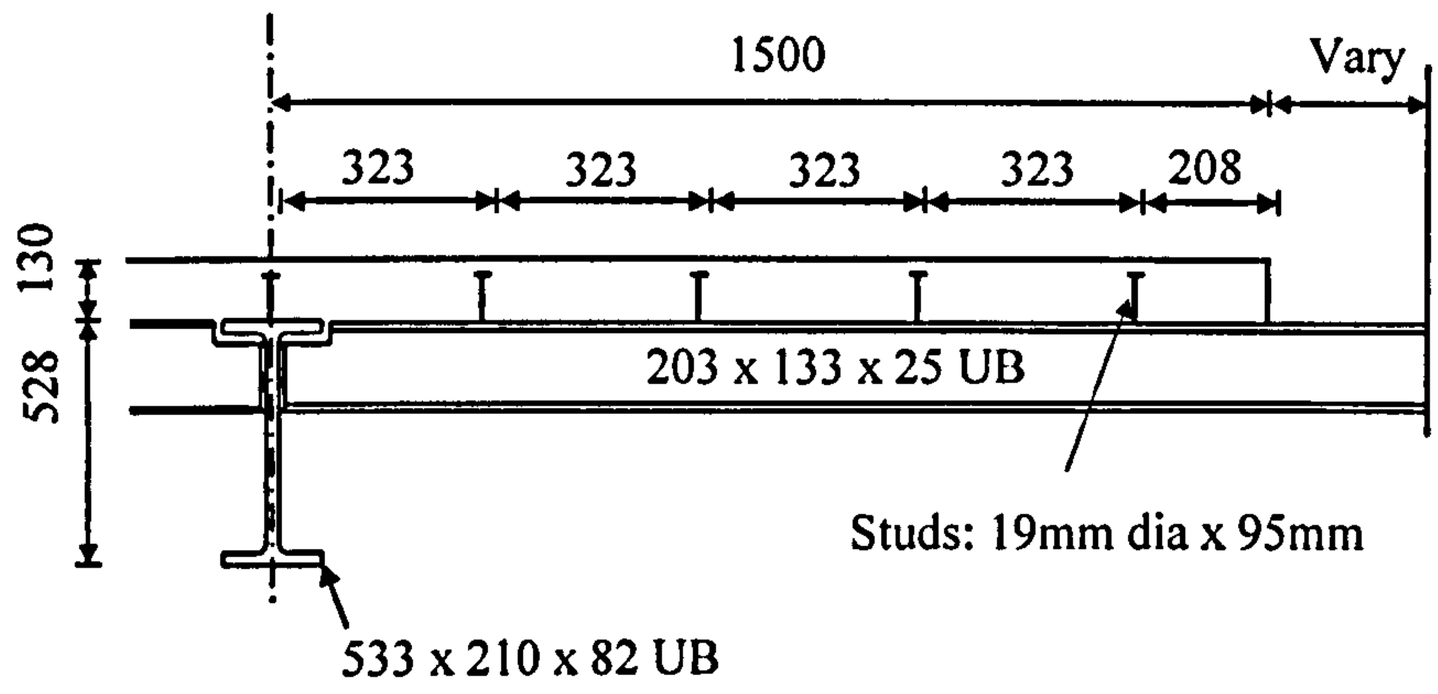

Figure 3-6. Shear stud layout - All cross beams

The reaction frame was designed to provide a simple support to the top and bottom of each of the three supporting columns. It consisted of a steel portal frame braced out of plane by two sets of diagonal tension cables. The simple supports at the top and bottom of

each column are achieved by connecting a 150mm diameter half round to the top and bottom of the column and supporting this between two additional half rounds connected to either the rafter of the portal frame or the column's base plate [Moore, 1999]. This detail is shown in Figure 3-7.

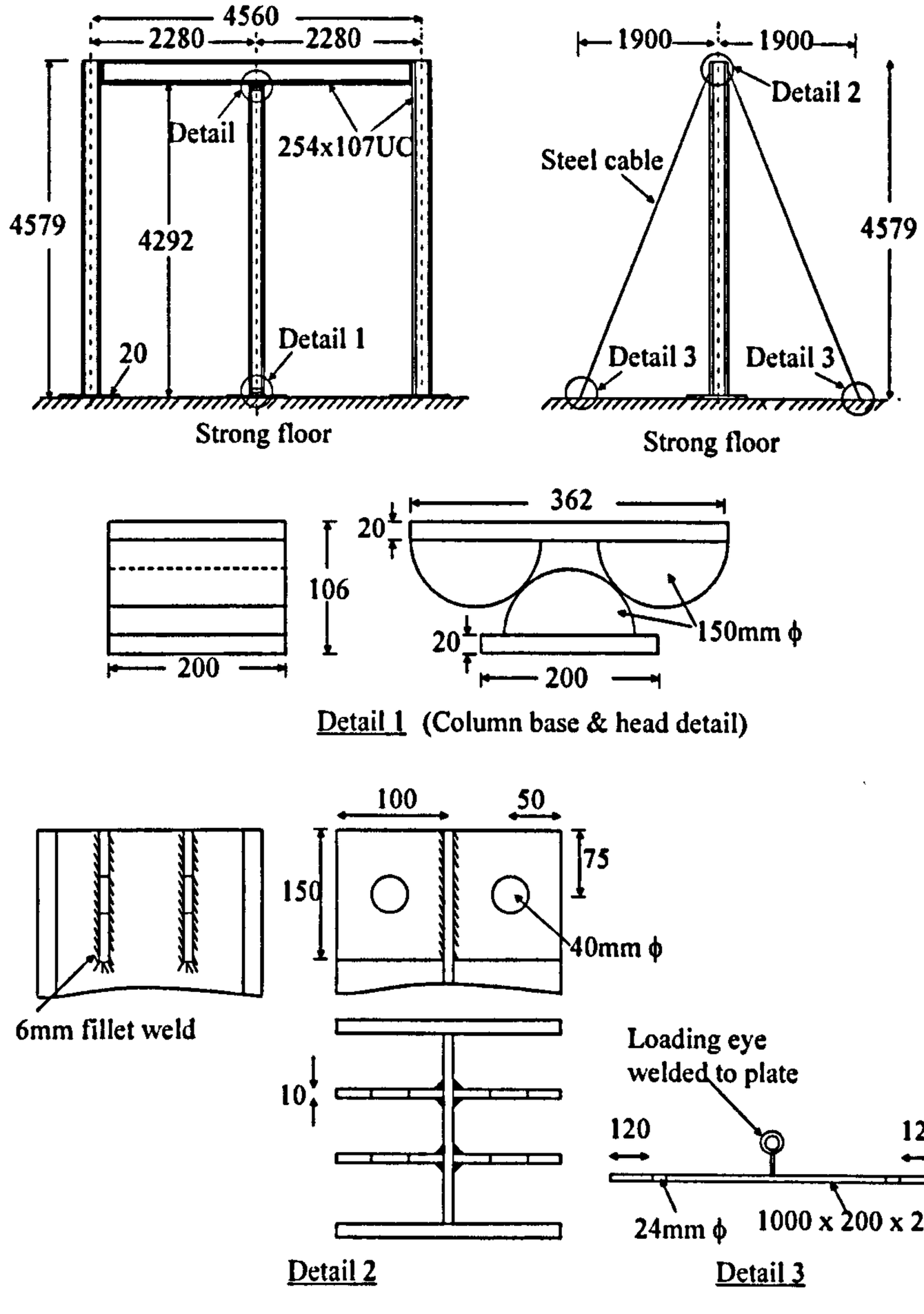

Figure 3-7. Column reaction frames

The props were removed before the casting of the slab, which allow the test to simulate the unpropped situation. This frame employed standard composite connections at the interior joints and a new form of composite connection at the exterior joint located at the "North" column, see Figure 3-8.

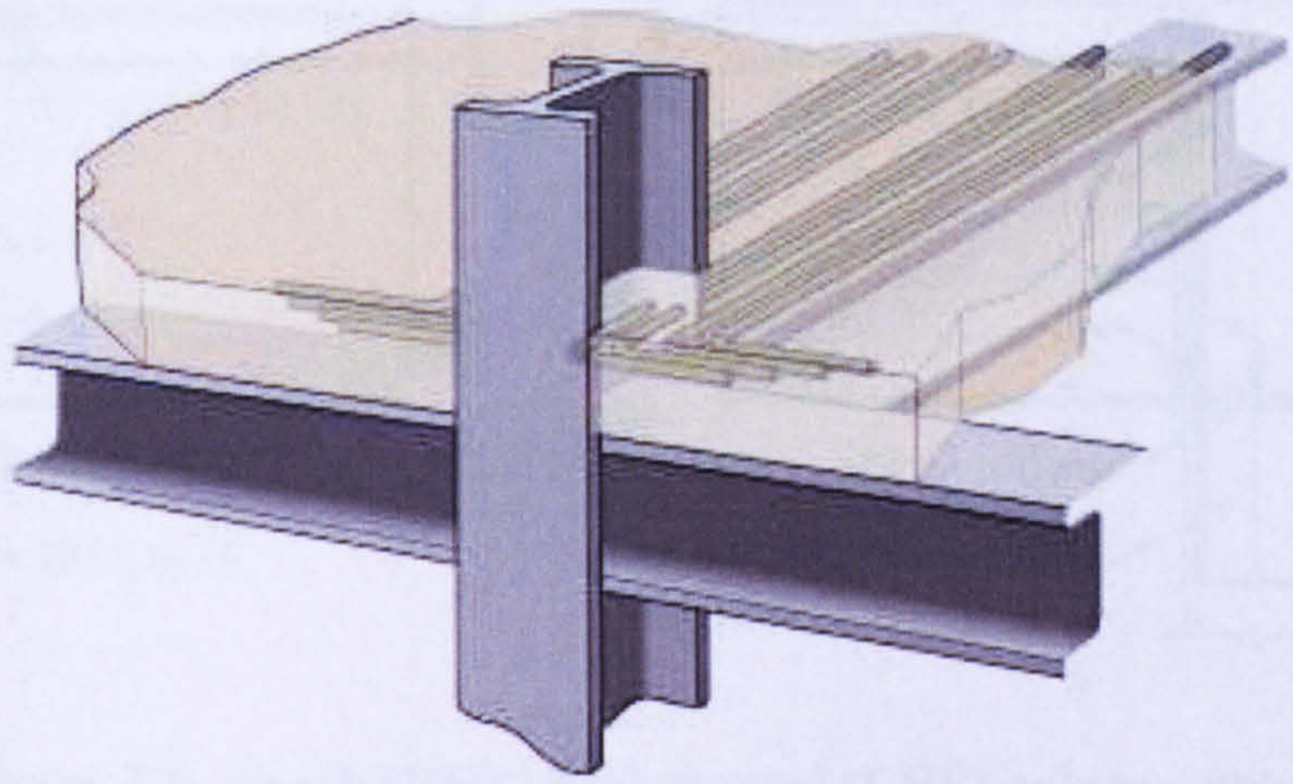

Figure 3-8. Novel perimeter column connection

Central column (composite) connections

The internal composite connections were designed in accordance with the SCI/BCSA composite connection design guide [1998]. The interior connection detail is shown in Figure 3-9, using 2 rows of M20 8.8 bolts with a 200x12 (S275) flush end plate. It also includes 4No. 16mm ϕ high yield steel reinforcement bars. These were the X-type bars recommended for use with composite connections due to their high ductility being able to achieve strains of up to 10% prior to fracture [SCI/BCSA, 1998]. All flange welds were full strength, with a minimum visible fillet of 10mm and all web welds were continuous 8mm fillets. The first shear connector was located at a distance of 100mm from the face of the column. This ensures that reinforcing bars could strain over a substantial length, so that sufficient rotation could take place. A 20mm web stiffener was used to prevent buckling of the column. Design tables in the Appendix B to the guide [BCSA and SCI, 1998] reveal a design moment capacity of 354kNm for this particular connection.

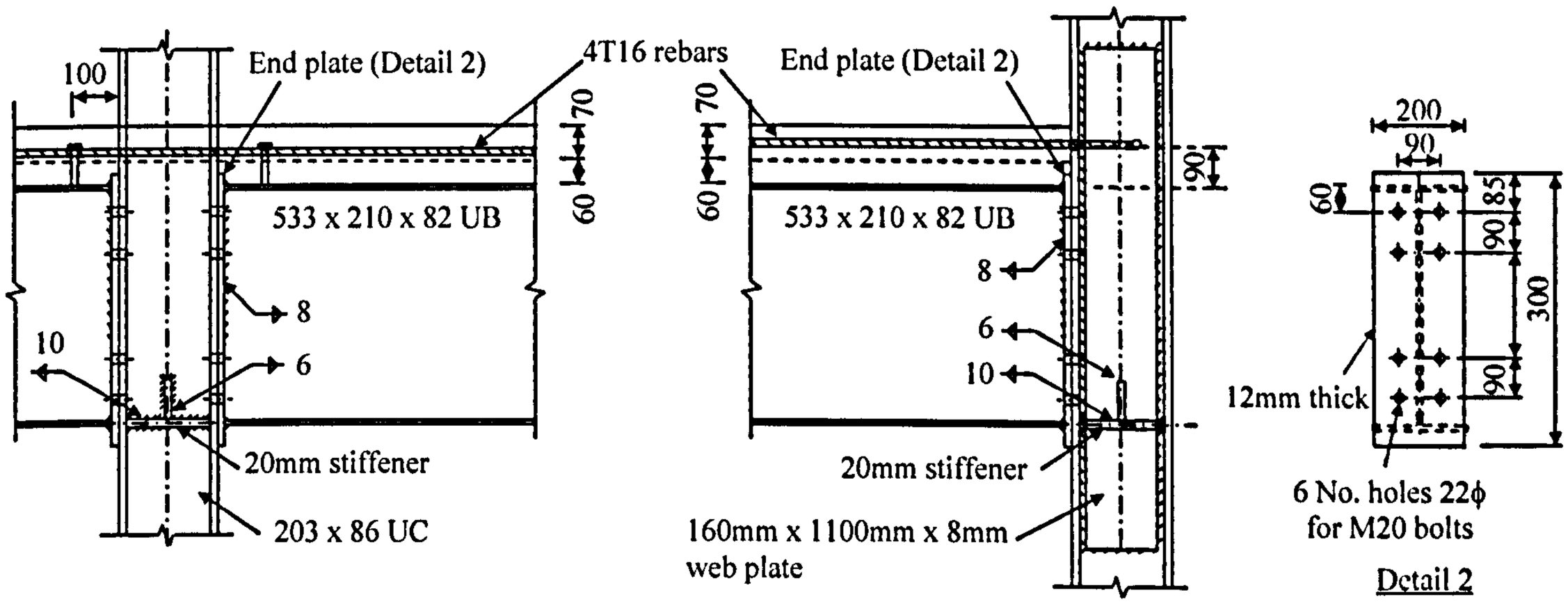

Figure 3-9. North (RHS) and central (LHS) column details

North column (composite) connection

The composite connection at the exterior joint detail, see Figure 3-9, was similar to the central composite connection, comprising the identical endplate and bolt arrangement, together with a total of 4No. 16mm ϕ high yield steel reinforcement bars, which passed through 22mm ϕ holes drilled through the interior flange of the column. The design of the rebar anchorage for the North Column was in accordance with the BS8110 requirements and involved cranking the bars at two points through a total of 90°. Since the connection was unbalanced it was necessary to stiffen the column web to prevent a shear failure. This was achieved with a web plate stiffener applied to one side of the column web, in accordance with the recommended details listed in the moment connections design guide [BCSA and SCI, 1995]. Assuming that the design tables in the Appendix B to the design guide [BCSA and SCI, 1998] are applicable to this novel connection detail, then the design moment capacity would again be 354kNm.

South column (nominally pinned) connection

An industry standard flexible end plate connection [BCSA and SCI, 1995] was used at the exterior joint connecting to the "South" column comprising 2 rows of M20 8.8 bolts with a 200x12 (S275) partial depth end plate, see Figure 3-10.

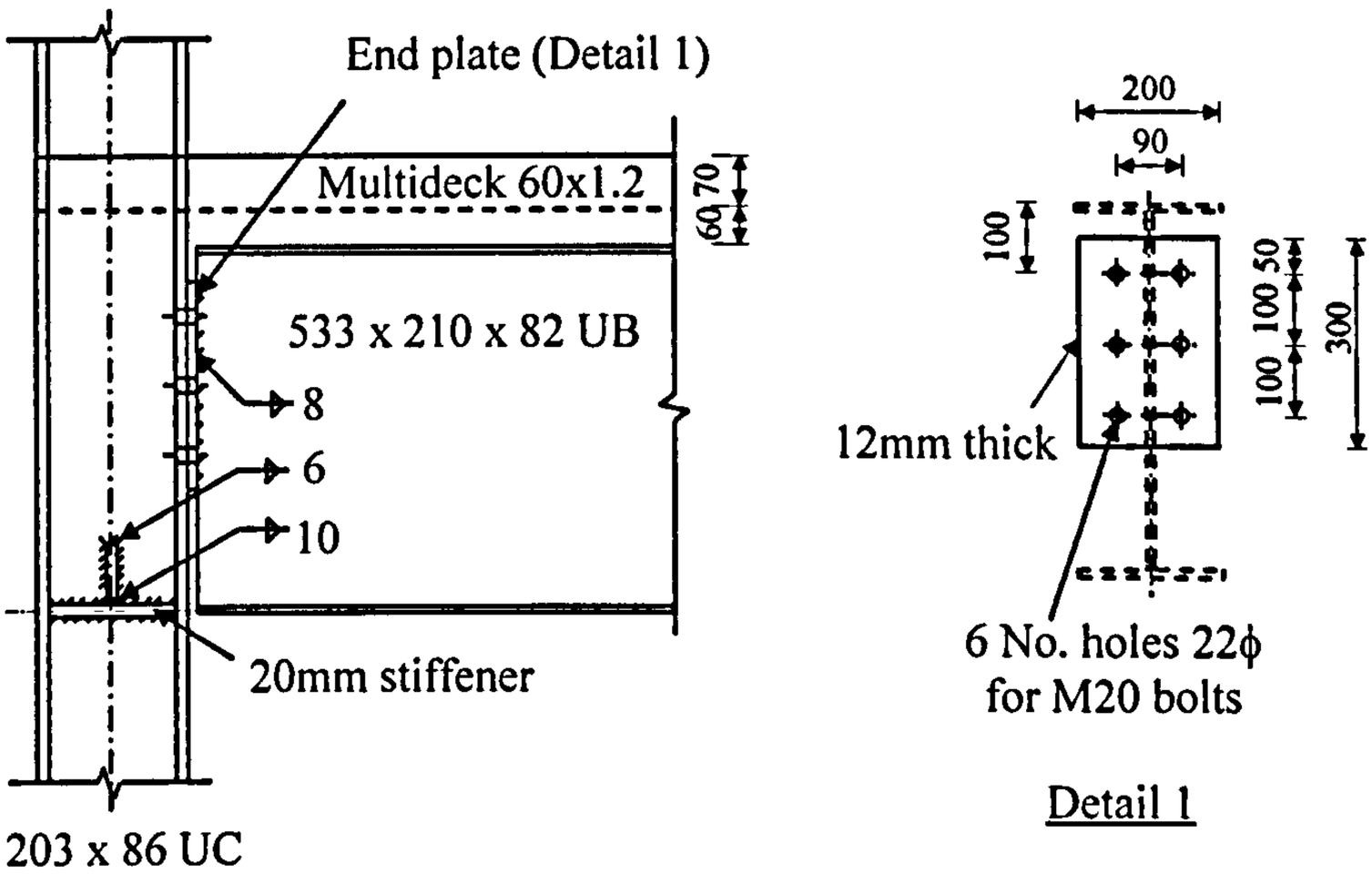

Figure 3-10. South (pinned) column connection detail

3.2.2 Frame construction

In order to assess the behaviour of the frame, instrumentations such as strain gauges, deflectometers and inclinometers at necessary locations were attached before the test frame was erected. The instruments were initialised when the frame was unloaded, with bolts left untightened. The central, south and north portal frames were held down and the base plates were tightened respectively. The bolts in the test frame were tightened using a torque spanner to 75N.m. The inner and outer secondary props were released respectively. After the steel erection was completed, the concrete slab was cast in a single day. The concrete was poured and tamped at the 1st quarter south end of the frame and continued through until the south side was completed. Subsequently the north slab pouring commenced from the centre column through to the south side slab.

3.2.3 Material properties

Grade 43 (S275) steel was used for all the steel beams, columns and endplates. High yield reinforcement bars were used and the strength of normal weight concrete (NWC) – stiff mix concrete was designed to be C30. Three steel coupons were taken from the top and bottom flange and web of the north beam, south beam and the column, i.e. 9 in total. The tensile mill tests were carried out at the Corus (British Steel) Lackenby Mill and were

in accordance with the British Specification BS EN 10025. Similarly, three test pieces were cut off from each type of reinforcement. Three concrete cubes were water tank cured and six were site cured. All the material, steel, reinforcement and concrete, test results are summarised in Table 3-1, Table 3-2 and Table 3-3 respectively.

Table 3-1. Material properties of the beams and columns

Location	Yield strength (N/mm^2)			Ultimate strength (N/mm^2)		
	Top	Bottom	Average	Top	Bottom	Average
South beam flange	298	290	294	477	477	477
North beam flange	305	300	302	480	480	480
South beam web	343	-	330	495	-	497
North beam web	317	-	330	499	-	497
Column flange	266	268	267	466	466	466
Column web	280	-	280	462	-	462

Table 3-2. Material properties of the reinforcement bars

Coupons	Yield strength (N/mm^2)					Ultimate strength (N/mm^2)					% Elongation			
	1	2	3	4	Avg.	1	2	3	4	Avg.	1	2	3	4
Rebar T10	482	488	486	481	484	557	559	558	558	558	27.1	30.9	30.9	28.8
Rebar T16	556	556	556	-	556	644	642	642	-	643	25.6	25.6	23.3	-

Table 3-3. Concrete cube strengths at 28 days

Load number	Mean strength (N/mm^2)	
	Standard cured	Site cured
Mix 1	41	35
Mix 2	43	33

Mix 1: Three cubes standard cured; Six cubes site cured

Mix 2: Three cubes standard cured, Six cubes site cured

Site curing: under wet hessian and polythene sheet adjacent to the composite frame for 28 days

Standard curing: in water at 20°C for 28 days.

The stress-strain curves from the coupon tests are shown in Figure 3-11.

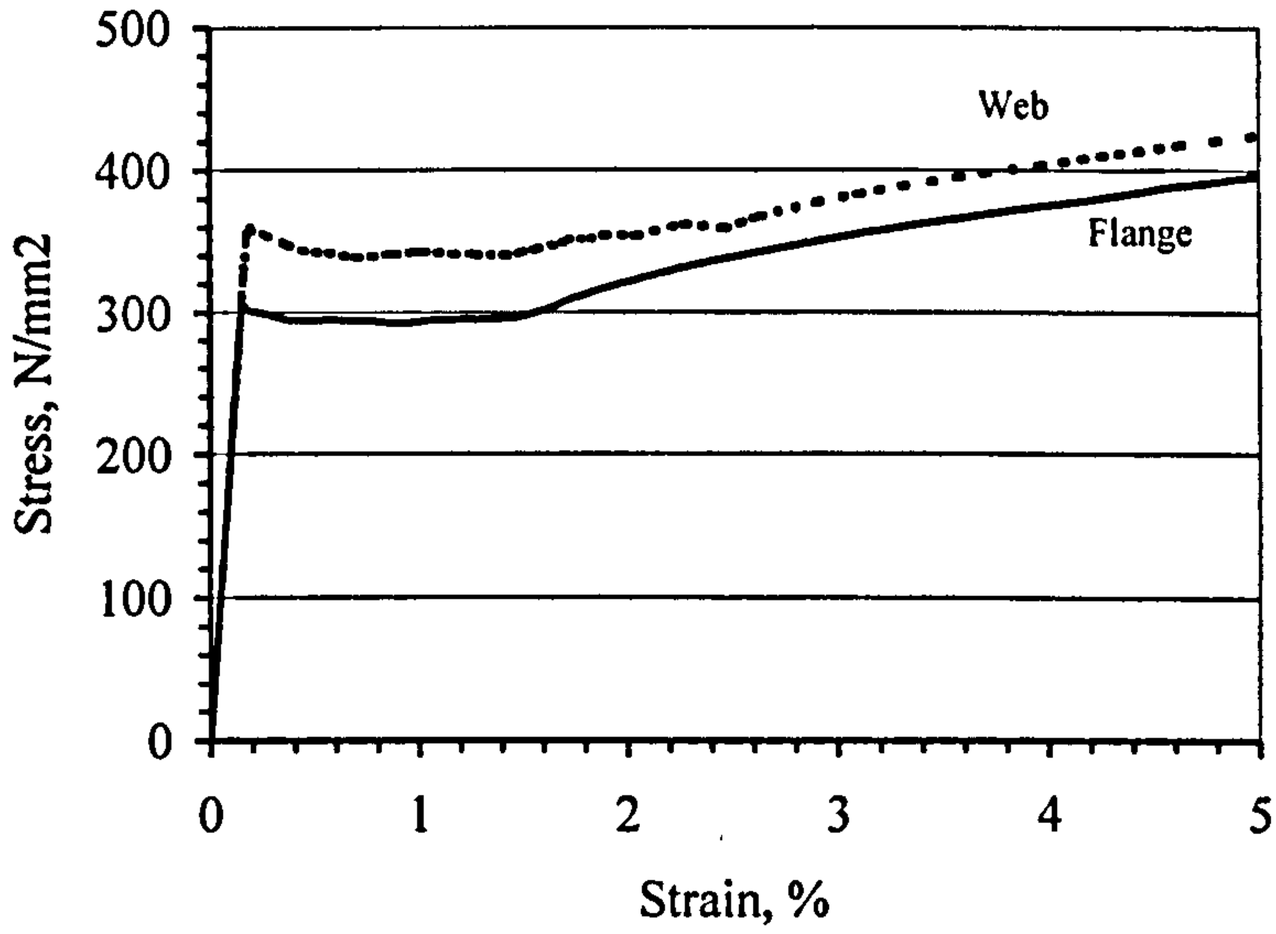

Figure 3-11. Average stress-strain curve for the test beam

3.2.4 Measurement of the frame moment distribution

The frame moment distribution could be calculated either from measured beam strains or column strains and load measurements. Calculating the moment of the composite beam from the measured beam strain is complicated due to the indeterminate characteristics of the concrete stress-strain, effects of slip and concrete cracking. Hence, the frame bending moment distributions have to be calculated from the column strain measurements and load measurements. However, this was found to be the most effective method because the columns remained largely elastic during the loading, whereas the beams entered the plastic stage, thus preventing an accurate measurement of strain for the type of strain gauges used during the test. In order to record the moment distribution along the column at least two section moments have to be known above and below the slab level. In this test, the strain-gauged sections on the column were located 480mm above and below the centreline of the beams, to avoid local deformation of the columns affecting the column moment calculations. At each column section, six strain readings were taken from the flanges and web. Thus a total of 72 column section strains were measured to obtain the moment distribution of all the columns. The positions of the strain gauges on the columns are shown in Figure 3-12.

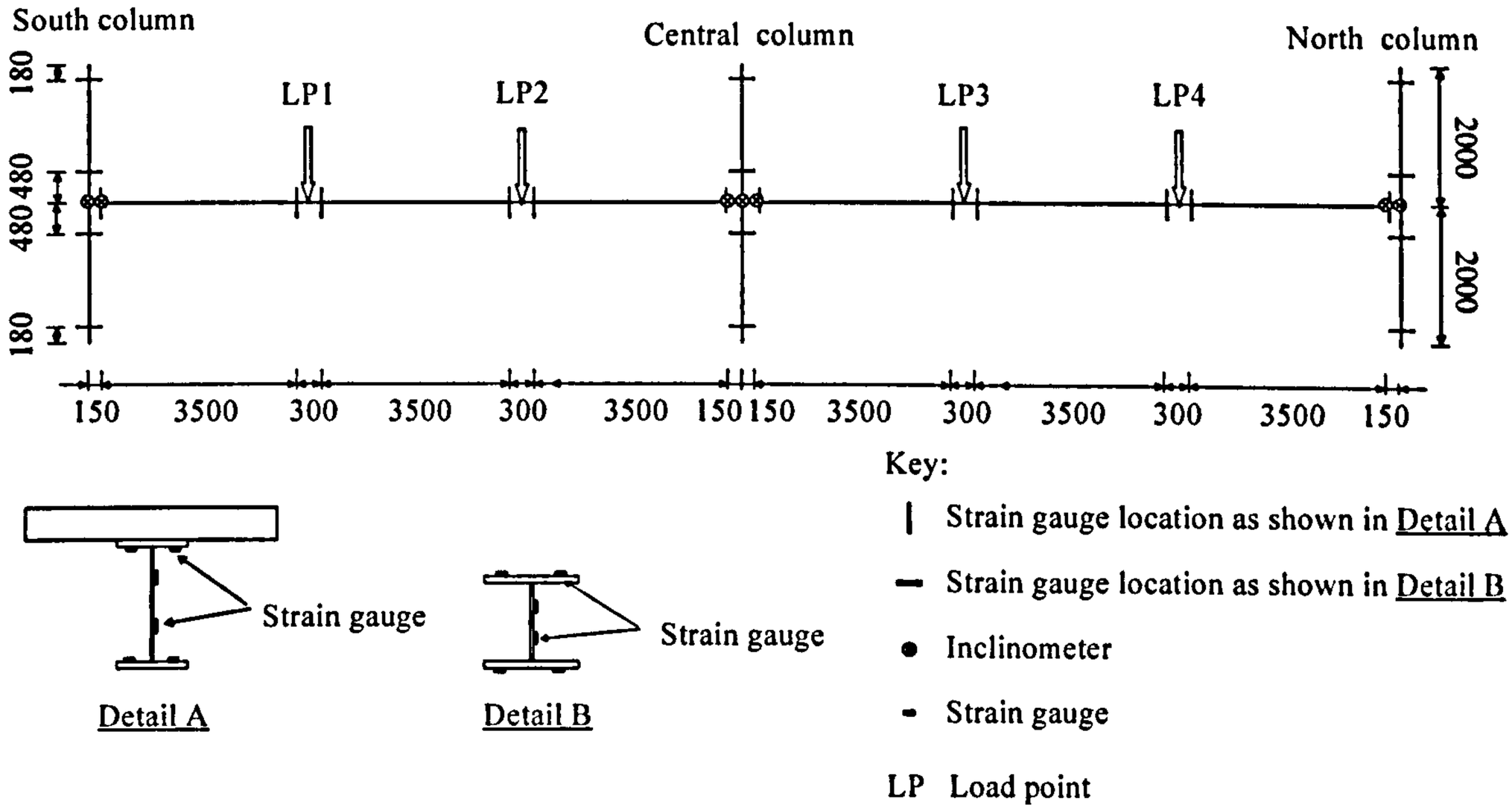

Figure 3-12. Side elevation of frame showing strain gauge and inclinometer locations

Strains were measured at six different sections along each primary beam in order to establish the moment distribution along the beams. At each beam section, six strain readings were measured from the flanges and web. Thus a total of 72 beam section strains were measured. However, strains were not measured on the concrete slab. The detailed locations of the composite beam strain gauges are shown in Figure 3-12.

3.2.5 Measurement of the connection rotation

The connection in-plane rotations were recorded using inclinometers. Four inclinometers were required for the external beam-column connections and three inclinometers for the internal beam-column connections. The measured beam and column rotations were used to calculate the net (connection) rotation. The arrangement of the inclinometers is shown in Figure 3-12.

3.2.6 Measurement of frame deflections

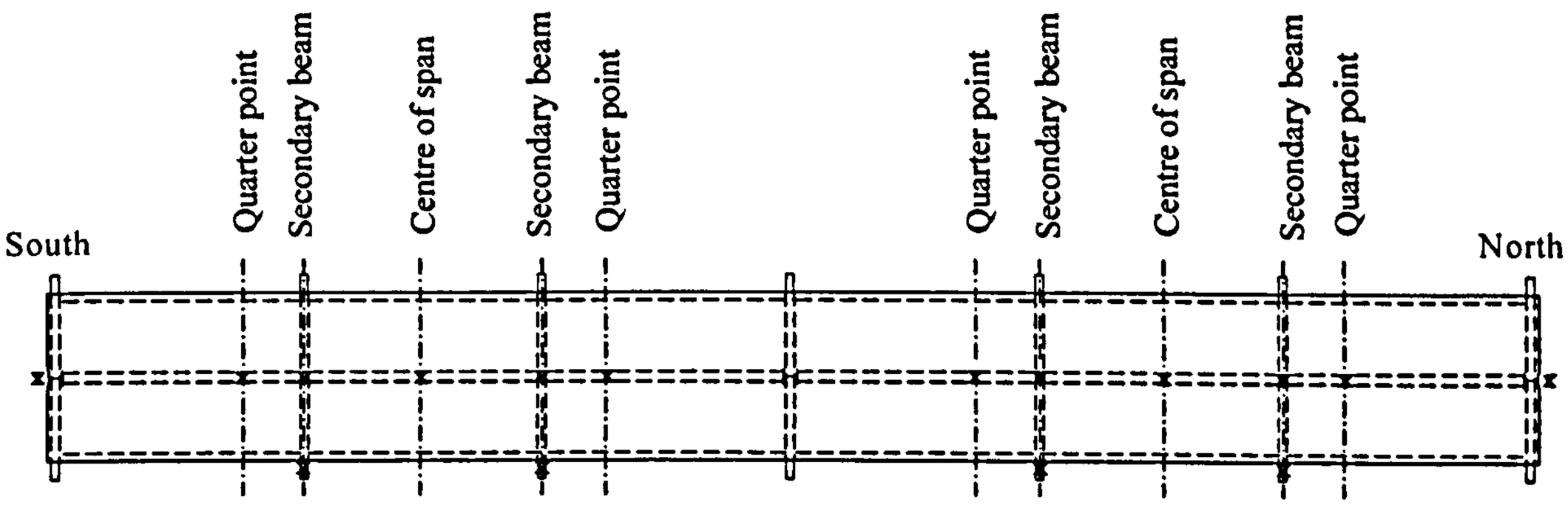

Key: ⧗ Vertical displacement
⧗ Horizontal displacement

Figure 3-13. Plan view of test frame showing locations of displacement transducers

Beams deflections were measured at quarter, mid, and three-quarter points within the span. They were also recorded at all four loading points. Vertical deflections were also measured at the end of the each secondary beam of the West Side. In total, 14 displacement transducers were used for the vertical deflection measurements. Horizontal deformations were also measured at the horizontal neutral axis of the exterior beam-column connections. The arrangement of the displacement transducers is shown in Figure 3-13.

3.2.7 Measurement of rebar strain

The arrangement of the reinforcement for all the connections and the slab is shown in detail in Figure 3-14, which is in accordance with SCI [1998] rebar detailing. At the central connection, 4 Nos. of 16mm diameter rebars were placed longitudinally, approximately 20mm above the top of the decking, to ensure adequate concrete cover. These longitudinal bars were uniformly spaced within a specified effective area (2 x width of the column flange) from the column centre line.

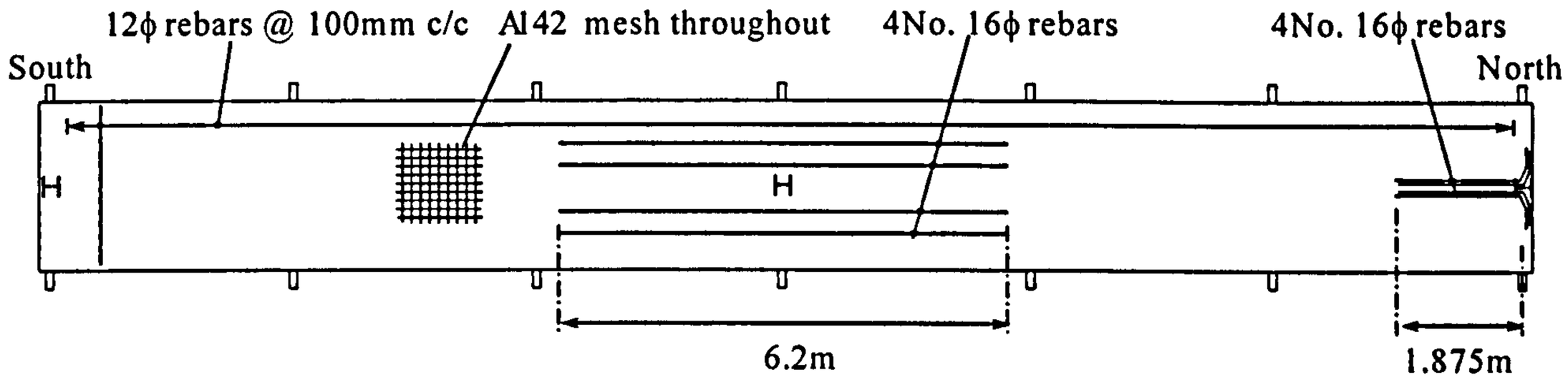

Note, high tensile reinforcement throughout (f_y = 460N/mm²)

Figure 3-14. Rebar layout

These rebars were anchored within the compression zone of the slab at a distance of 3.1m from the central connection (which is greater than 0.2 x beam span + anchorage length for 16mm diameter rebar according to BS8110). Furthermore, 6 Nos. of 12mm diameter transverse rebars were placed above the longitudinal rebars. These were provided with adequate cover to the decking and the top of the slab. The transverse bars were uniformly spaced either side of the column within a specified effective area (3 x width of the column flange) from the column face. Reinforcing mesh (type A142) was provided throughout the slab to control cracking. A total of 22 strain gauges were fixed to measure the central rebar strains, see Figure 3-15.

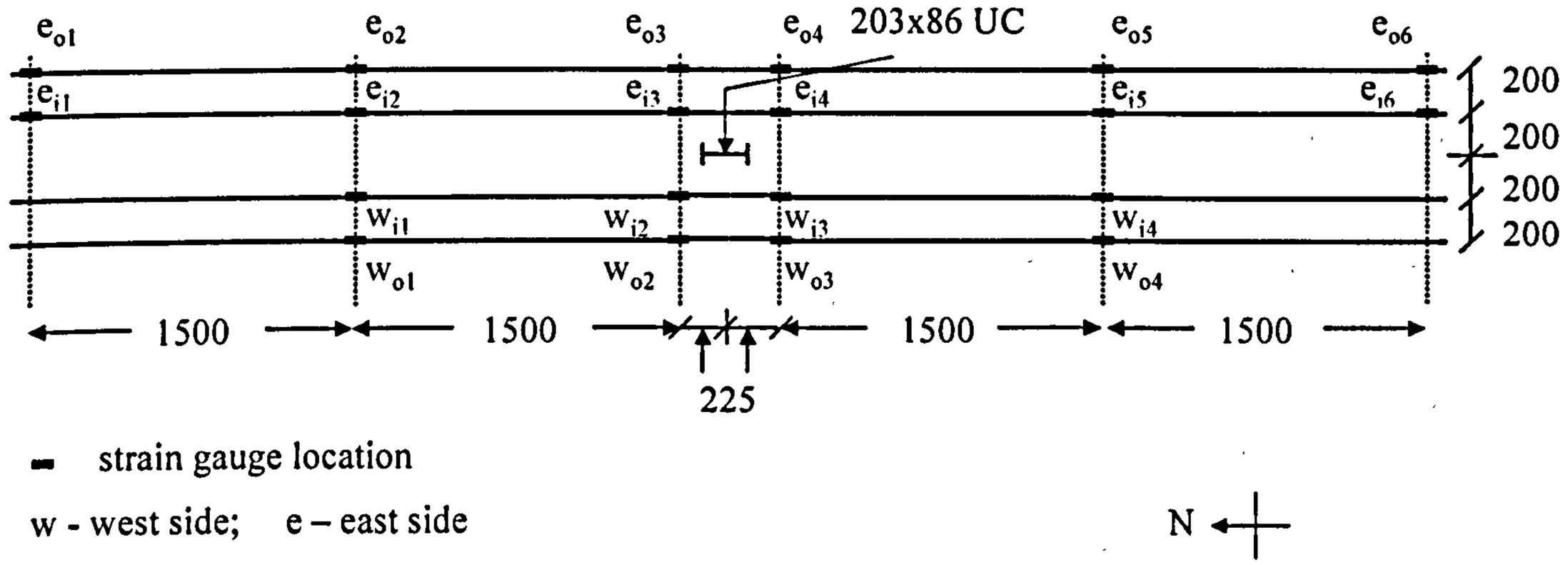

Figure 3-15. Measurement of strain reading at the central column rebars

Also a total of 6 strain gauges were fixed to measure the north column rebar strains, see Figure 3-16.

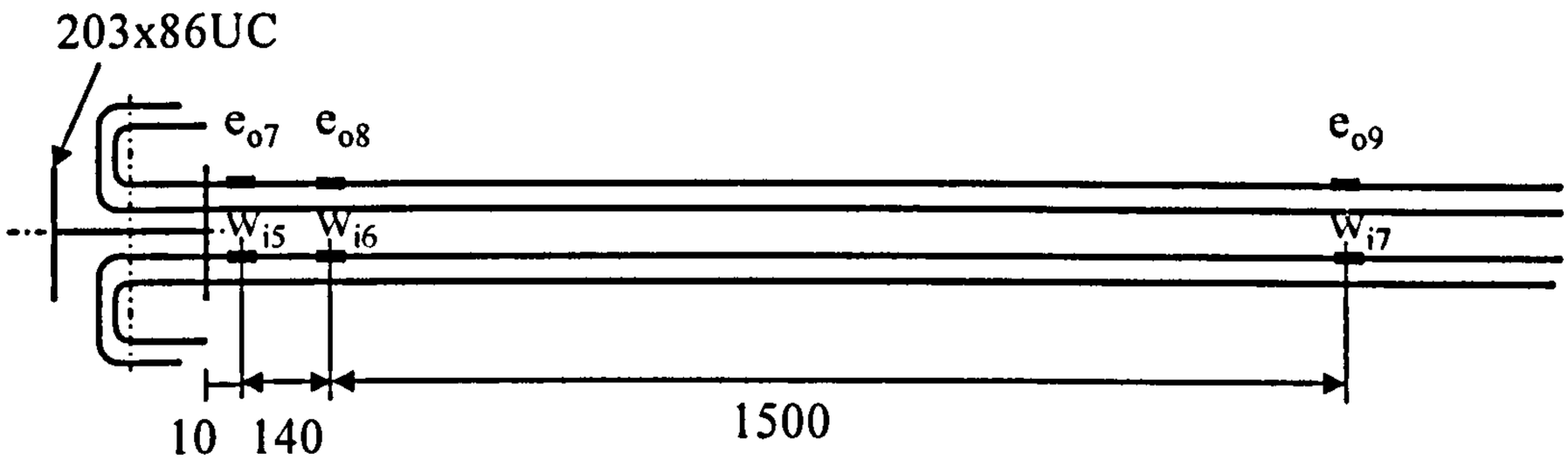

Figure 3-16. Measurement of strain reading at the north column rebars

3.2.8 Loading mechanism and applied force measurements

A series of hydraulic jacks positioned below the laboratory floor were used to apply the load to the frame. Details of the loading system are shown in Figure 3-17. This loading arrangement consisted of a 300kN hydraulic ram, which reacted against a transverse–loading beam fabricated from a rectangular hollow steel (400x200x16 RHS) section. The loading beam is supported by two 38mm diameter Macalloy Bars, which have a working load of approximately 768kN. These bars passed through a grid of holes in the strong floor and were secured in position by a nut and washer assembly. The load was applied to each of the third points by a single 300kN hydraulic ram which was controlled by a single servo-control valve from a fixed displacement gear pump, capable of delivering 23 litres of oil per minute at a pressure of 3000psi. The load cells located below the RHS beams measured the force. Thus, two concentrated loads at the one third and two third points loaded the primary beams respectively; see Figure 3-2 [Moore, 1999].

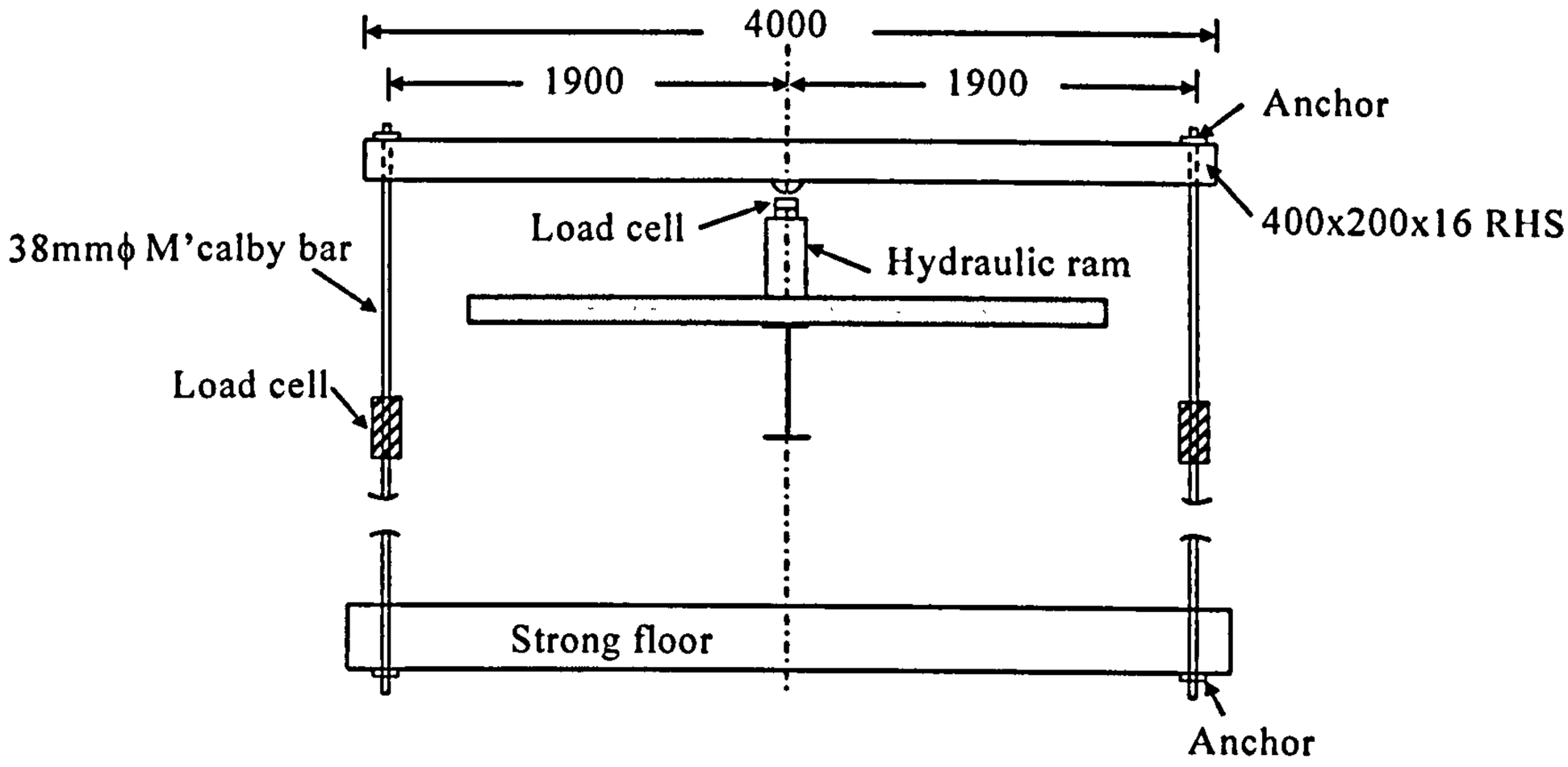

Figure 3-17. Arrangement of loading mechanism

3.2.9 Data logging

A data logger was used to record strains, rotations and displacements, as well as to monitor the applied loads. The raw data recorded in the test were transferred into an EXCEL spread sheet and use for further processing of data.

3.3 Test Procedures

Prior to casting of the slab, all monitoring channels for strain gauges, deflection transducers and inclinometers were scanned. After the slab was cast, the readings were again scanned and recorded. Then the loading arrangement was installed at every loading location and the readings were scanned and recorded for each installation. Once the frame was ready for the test, two pre test runs were carried out in order to make sure that all the instruments were working effectively. After all the instrumentation was checked, the actual test was subdivided into 5 different phases, see the load history shown in Figure 3-18. Before the load was applied, all the monitoring channels were scanned to record the initial values.

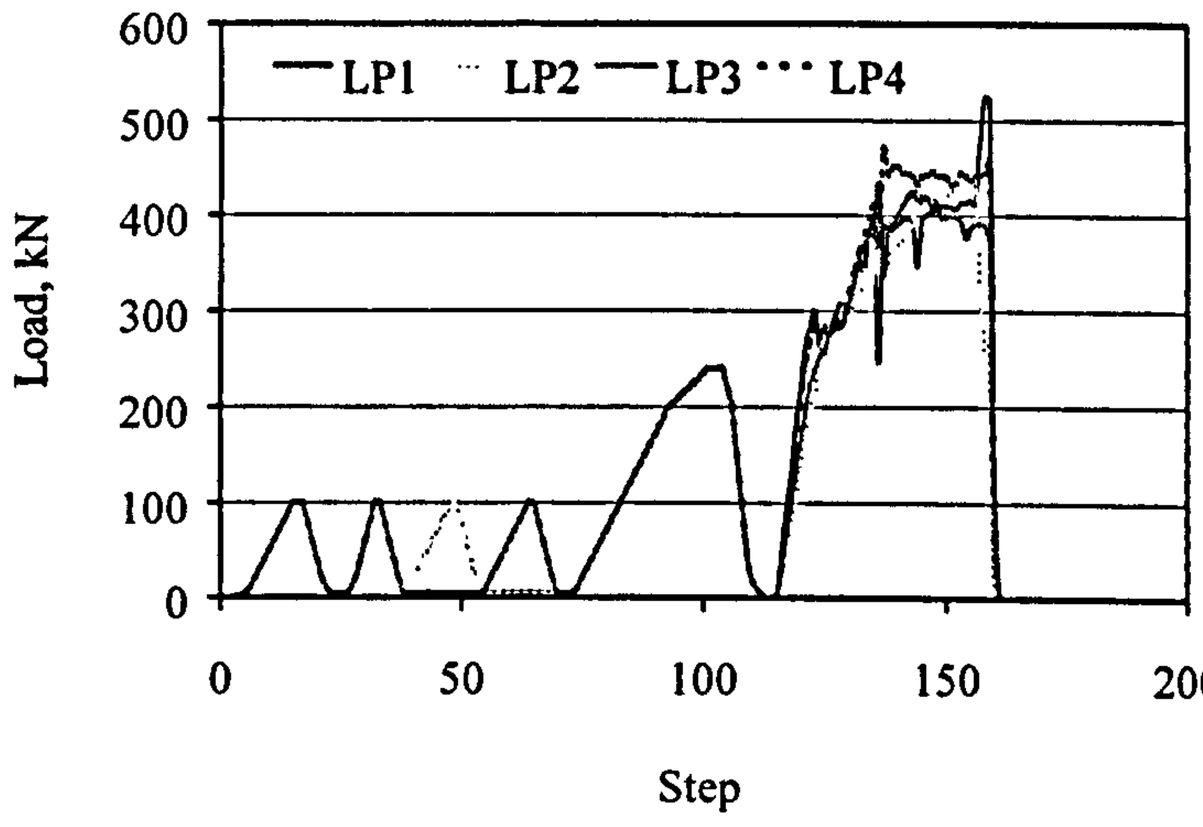

Figure 3-18. Load history

Phase 1

Loads were increased in 5kN increments to 100kN and returned to 5kN on both spans. During this phase the readings indicated the need to restrain the slab against lateral movement at the central column. Following the provision of this additional restraint the test was repeated successfully. All the deflections, strains and rotations followed a linear variation i.e. within the elastic limit for this loading. Furthermore, all the readings returned to their initial values after all the loads were restored to zero.

Phase 2

The south beam loading was maintained at 5kN and the north beam was loaded to 100kN and subsequently returned to 5kN. All the channels were scanned and the readings were recorded.

Phase 3

The north beam loading was maintained at 5kN and the south beam was loaded to 100kN and returned to 5kN. Subsequently, the north beam loading was kept as 5kN and the south beam was loaded to 100kN and return to 5kN. All the channels were scanned and the readings were recorded.

Phase 4

Before the start of this phase the north column had an additional restraint installed as a safety precaution. The restraint was located 500mm below the head of the column (see Figure 3-2). During this phase both beams were simultaneously loaded to 240kN at each load point in increments of 5kN and later unloaded again. This test was carried out primarily to investigate the behaviour of the frame under the serviceability conditions, although the beams did yield under the applied load.

Phase 5

During this phase the frame was loaded through to failure, see Figure 3-19. Consequently, the loading was switched from load control to displacement control. All the channels for strain, rotation and deflection were scanned and the readings were recorded for the subsequent frame analysis.

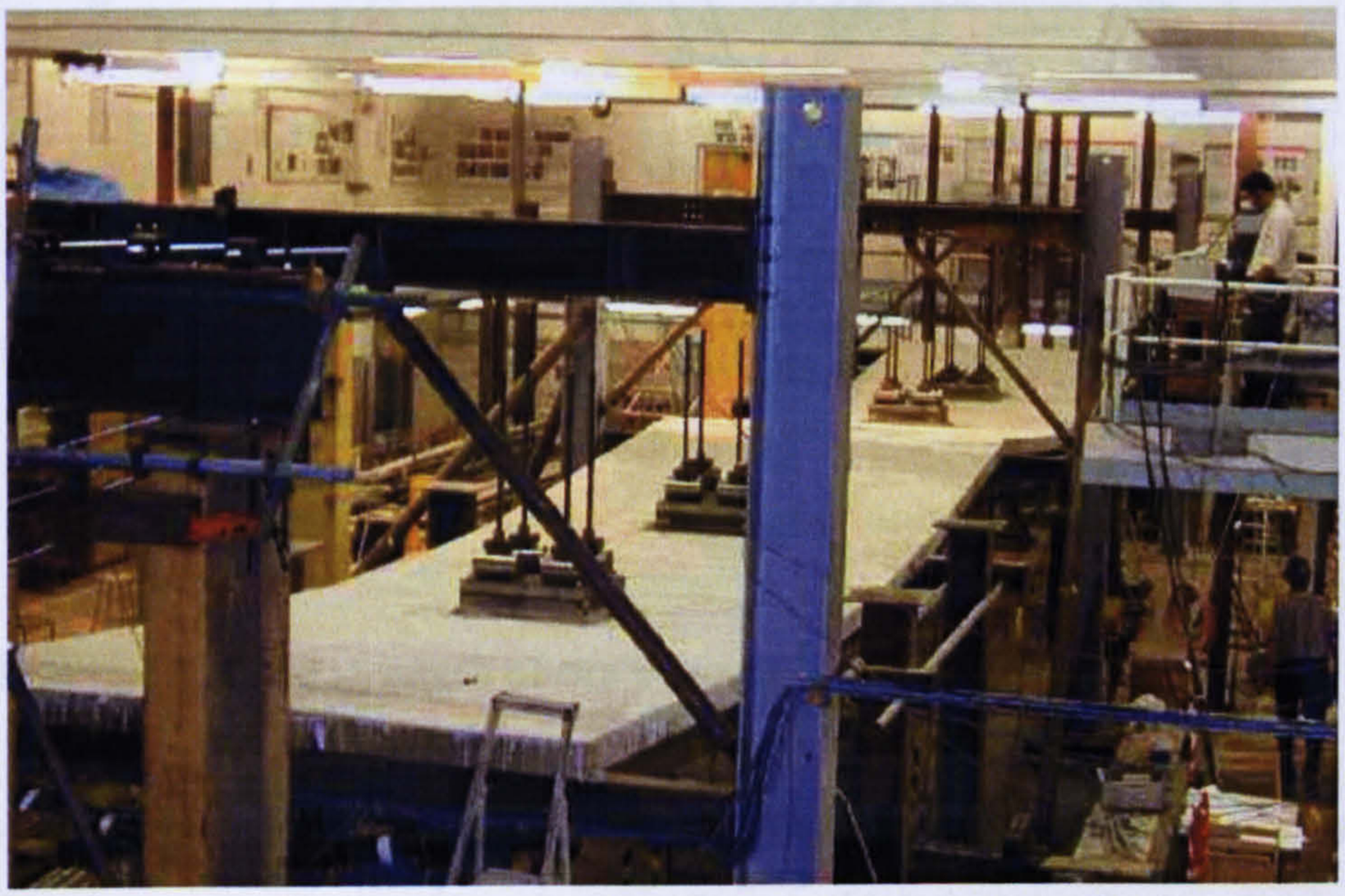

Figure 3-19. Test frame after failure

3.4 Results

The horizontal displacements recorded at the perimeter beam column connections are shown in Figure 3-29. The figure demonstrates that significant in-plane movement of the

columns was observed, as the bottom flanges of the beams reacted against the columns. This resulted in significant bending moments in the perimeter columns. The moment vs. rotation performance of the connections are shown in Figure 3-21 and Figure 3-25, where the rotation is the net rotation of the connection (i.e. beam rotation – column rotation). The observed behaviour of the connections is considered in detail below. Based on the measured column strain and load values, frame moment distribution through to failure of the test frame was calculated and is shown in Figure 3-20 for a range of load increments through to failure.

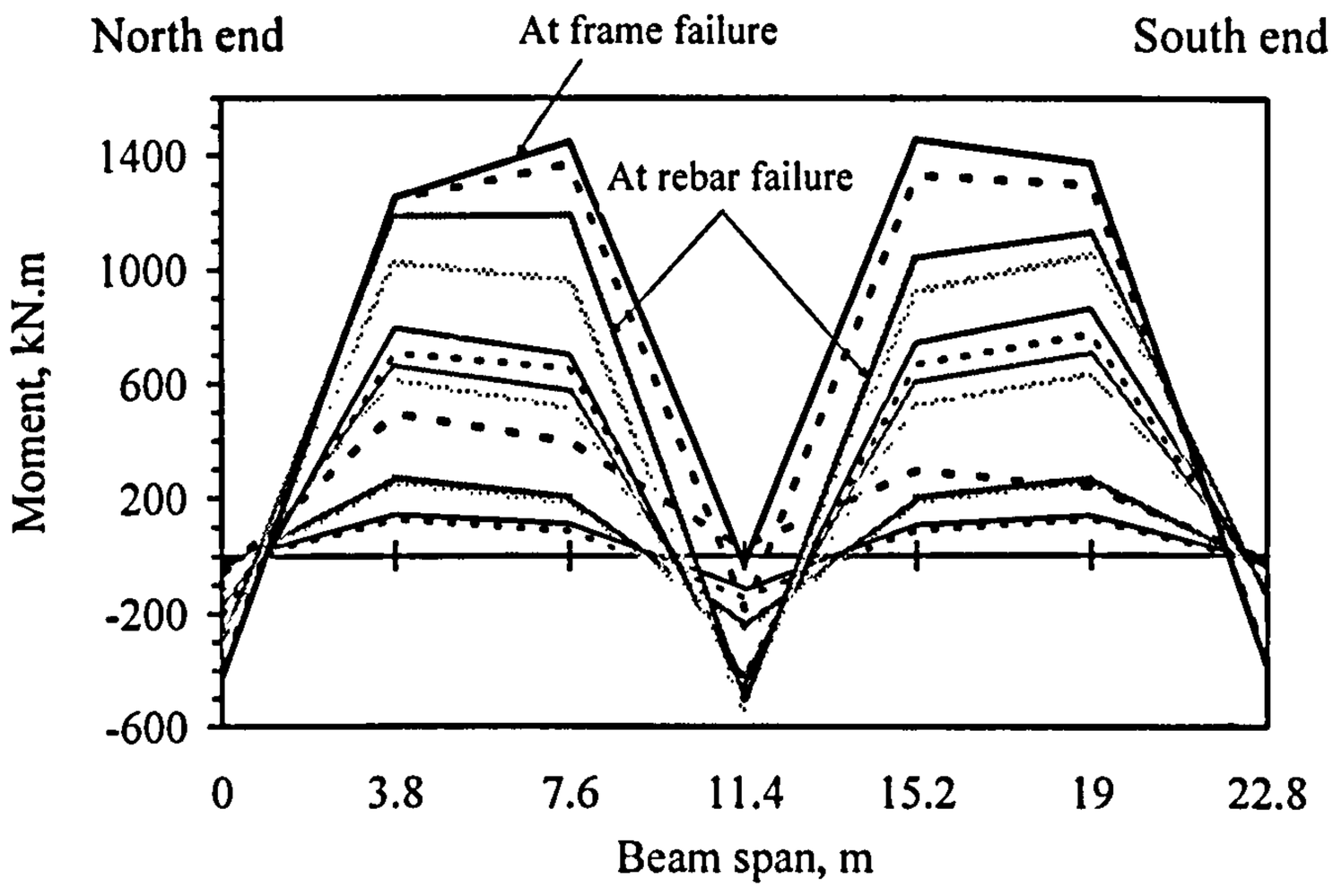

Figure 3-20. Experimentally observed bending moment diagrams

3.4.1 Observed flexural strength of the beams

The maximum observed flexural strengths of the north and south beams were 1448kN.m and 1454kN.m respectively. This is significantly higher than the nominal moment capacities of 933kN.m and 960kN.m for the north and south beams respectively (see calculations in Appendix A). This significant increase in strength can be attributed to the following factors:

- Conservatism in the calculation of the effective width of the slab.

- Over strength steel, since the actual material properties exceed the nominal strengths by a significant margin. This is particularly important in the web.
- Strain hardening in the lower beam flange and in the web.

If the flexural strength was calculated assuming the full 3m width of the slab contributed to the flexural strength, and using the measured material and geometric properties of the test specimen, then the expected flexural strength was 1214kN.m (see calculations in Appendix A).

However, this omits any strengthening effects from strain hardening. It is not possible to determine the actual strain within the lower beam flange that corresponds to the maximum flexural strengths, but given the high degree of deformation, a maximum strain of 3% would not seem unreasonable and would correspond with strains shown to be present in the plastic hinges of non-composite beams [Byfield and Nethercot, 1998]. Thus assuming 3% strain in the lower flange and including the effects of strain hardening in the web, the expected flexural strength in the beams would be 1400kN.m (see calculations in Appendix A) which corresponds more closely with the observed behaviour.

Table 3-1 shows varying yield strength for the flanges and the web of the north and south beam. Research by Byfield and Nethercot [1997] on the yield stress of hot rolled sections shows that the average yield stress observed was considerably higher than that assumed in design. It was proved that the average yield stress is higher than the nominal value by 16% for flange thickness greater than 10mm and by 37% for thinner flanges. Since web material often has a thickness of less than 10mm, this additional strength can be expected to contribute significantly to the overall moment capacity of the section and it could be the explanation for the over strength observed in the test beam.

3.4.2 Flexural strength of the 'nominally pinned' south column connection

Figure 3-21 shows that this connection behaved as a nominally pinned connection during the construction phase, but subsequently stiffened considerably after the concrete slab was cast. The bending moments generated during rotations of up to 40mrads exceeded those

predicted by the conventional design rules of BS5950-1. At rotations of greater than 45mrads the connection strength increased up to bending moments in excess of 300kN.m, as beam rotation caused the bottom flange of the beam to react against the face of the column. This effect caused considerable sideways movement in the column as shown in Figure 3-22. It is also observed that all the bolts are in intact and that there was no bottom flange buckling or web buckling after the test frame failure, see Figure 3-22.

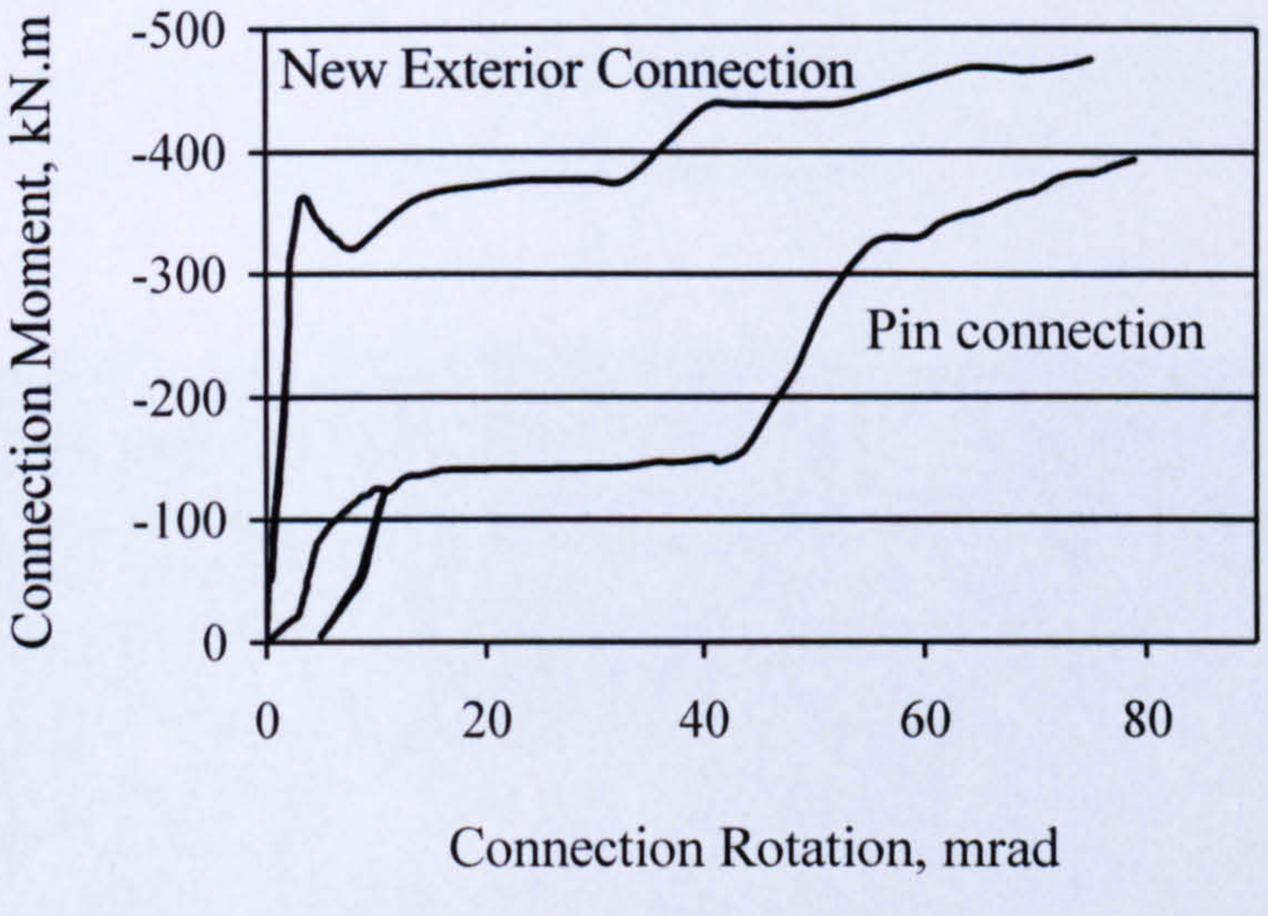

Figure 3-21. Moment vs. rotation for exterior beam column connections

Figure 3-22. South side pin connection after test frame failure

3.4.3 Flexural strength of the north column composite connection

Figure 3-21 shows the strength, ductility and stiffness characteristics of this novel connection detail. The stiffness was lower than the internal connections (Figure 3-25) although the ductility was improved. The design moment capacity of this connection (calculated in accordance with the composite connections design guide, BCSA/SCI (1998), using the measured material and geometric properties recorded for the test frame) was 406kN.m. Inspection of Figure 3-21 shows that the test specimen failed to reach this design moment within an acceptable degree of rotation.

Figure 3-23. North side composite connection after test frame failure

The following physical observations were made on this connection after the test frame failure, see Figure 3-23.

(a) The top row of bolts failed and fractured completely.

(b) The second row of bolts lost their strength. The thread was stripped, and the head moved up to 3mm on east side and greater than 3mm on west side. In short, the bolt was on the verge of failure.

(c) The endplate buckled.

(d) All bottom bolts remained in good condition.

(e) End rotation of the beam caused considerable sideways movement of the column, resulting in plastic deformation of the north column.

(f) No bottom flange buckling.

Figure 3-24 shows the cracks developed on the slab. Whilst considerable movement is observed the photograph indicates the rebar remained intact.

Figure 3-24. Cracks observation in the exterior composite connection side

3.4.4 Flexural strength of the interior composite connections

Figure 3-25 shows the moment-rotation behaviour of the central connections. The maximum observed strength of 650kN.m exceeded the nominal design strength of 406kN.m. The south side connection began to fail after a post construction rotation of 23mrads. However, the identical north side connection achieved considerably more rotation before failure.

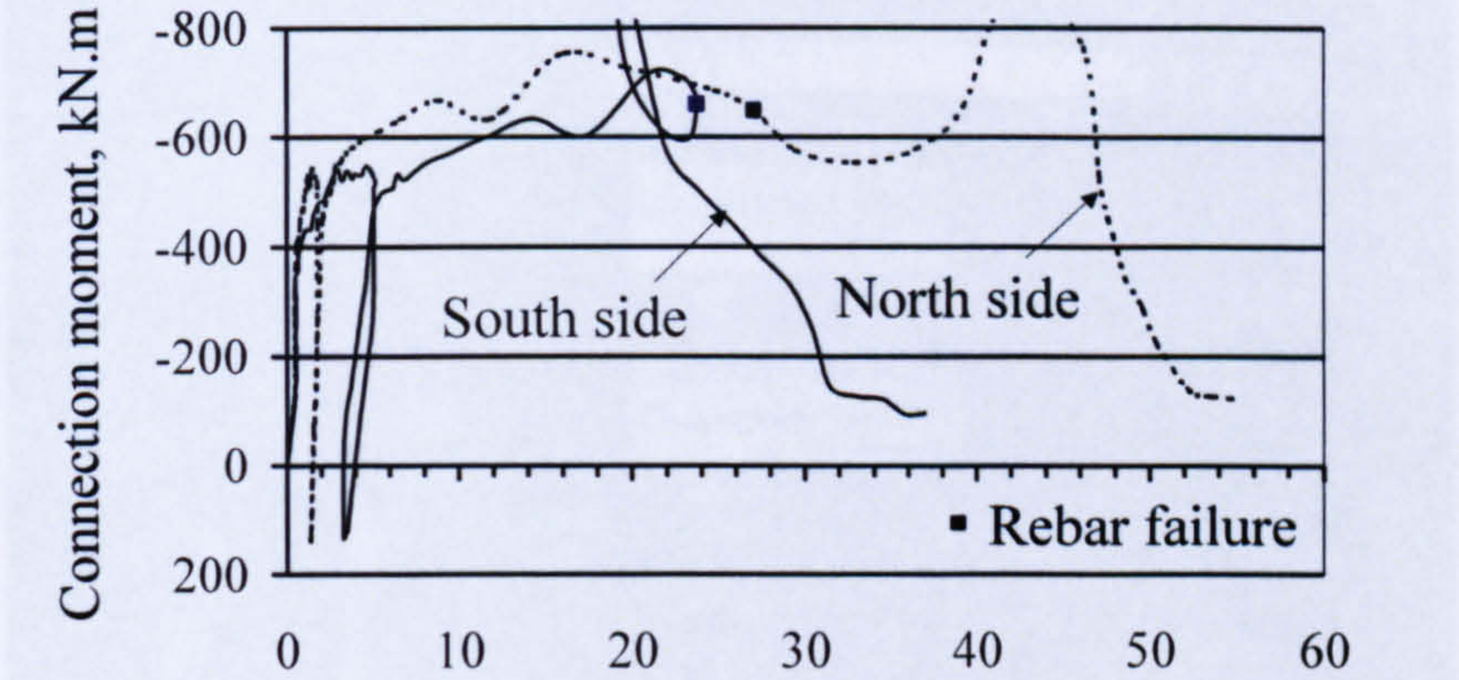

Figure 3-25. Moment vs. rotation for interior beam column connections

Figure 3-26 shows the slab cracking after the test. It clearly shows the rebar failure on the east side of the slab and the survived rebars on the west side of the slab. The failure of the rebar initiated the decline in strength which is clearly identifiable on the connection moment-rotation graph, Figure 3-25 .

Figure 3-26. Cracks and rebar failure at the interior composite connection

Figure 3-27. Interior composite connection (moment connection side) after test frame failure

Figure 3-28. Interior composite connection (pin connection side) after test frame failure

The observed failure of each component in this connection is shown in Figure 3-27 and Figure 3-28. The main observations included:

(a) Top row of bolts were completely fractured

(b) Bottom flange buckling extended to a length of 400mm along the beam from the column face

(c) Web buckling extended to a length of 350mm from the column face

The localised distortions of the plate elements, coupled with the line junctions remaining straight, characterise local buckling [Oehlers and Bradford, 1995].

3.4.5 Load vs. horizontal displacement

The horizontal displacements recorded at the perimeter beam-column connections are shown in Figure 3-29.

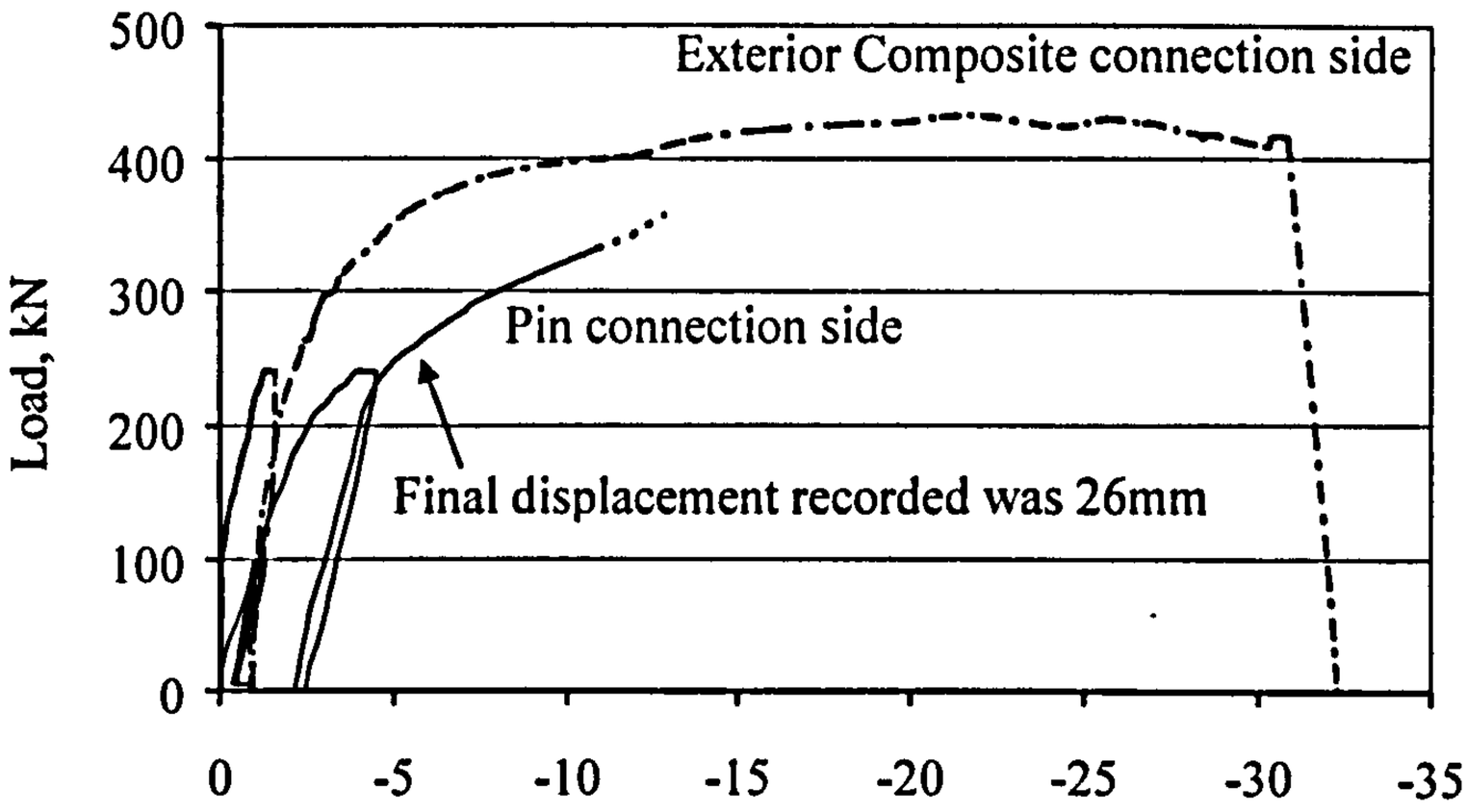

Figure 3-29. Load vs. Horizontal displacement

The figure demonstrates that a horizontal displacement of 30mm was observed at the exterior composite connection side. The movement is as a result of the bottom flange of the beams pushing against the column flanges as the ends of the beams rotate under load. The movement of the south (flexible end plate connection) was slightly less than 26mm because the end plate did not extent to the bottom flange, leaving an 8mm gap.

3.4.6 Load vs. rotation

The load vs. rotation data recorded from the inclinometers shown in Figure 3-30 is presented in Table 3-4, where the load represents the load applied from the loading jack located closest to the particular inclinometer. Generally beam rotations are greater than column rotations. It can be seen in Figure 3-30 that the beam end rotation at the exterior connection is greater than the beam end rotation at the interior connection. This is due to the higher moments generated at the central columns. Interior column rotation is much lower than exterior column rotations. Connection rotation is calculated from the measured beam end rotation minus the column rotation.

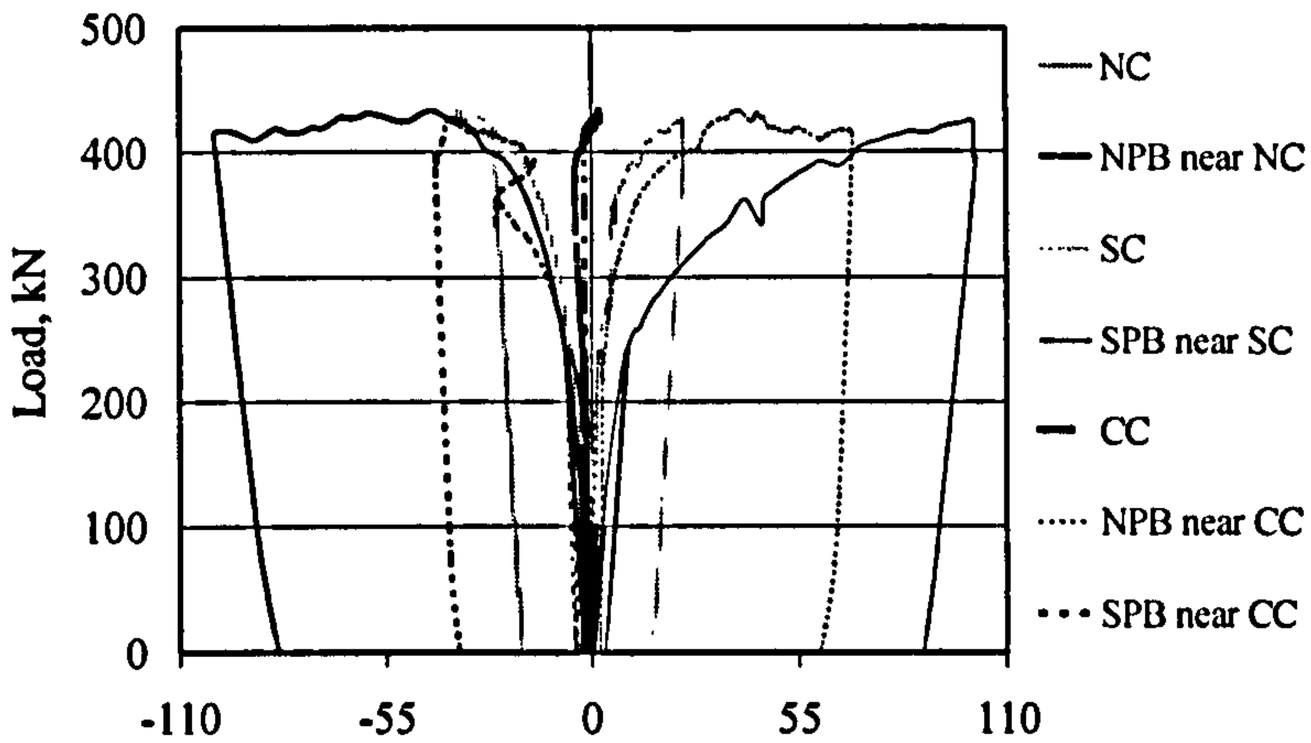

Figure 3-30. Load vs. rotation as recorded by inclinometers (see Figure 3-12)

NC - north column rotation; SC - south column rotation; CC - central column rotation

NPB near NC - north primary beam rotation near north column

SPB near SC - south primary beam rotation near south column

NPB near CC - north primary beam rotation near central column

SPB near CC - south primary beam rotation near central column

3.4.7 Load vs. deflection

Figure 3-31 shows the load vs. mid-span deflection for each span, where the load is the average load applied to each span by the hydraulic jacks.

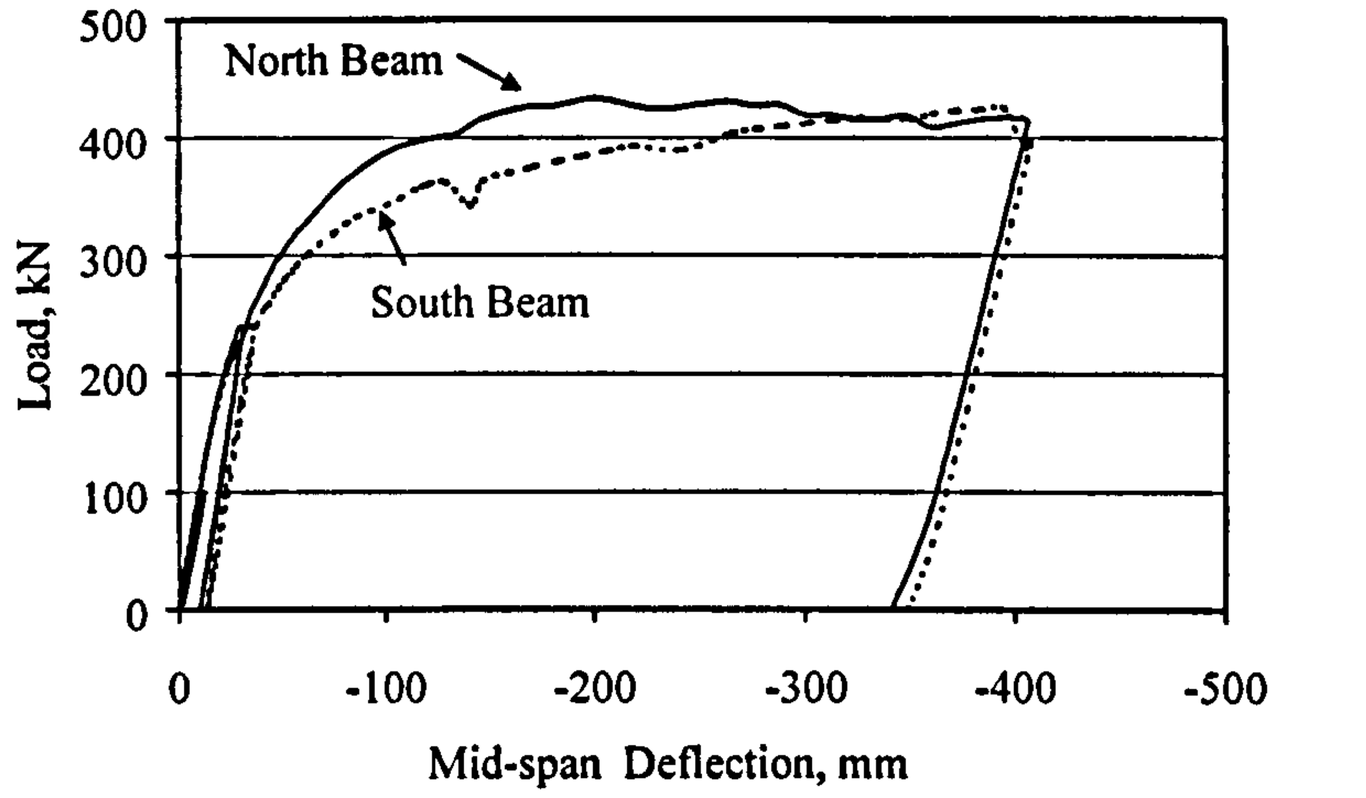

Figure 3-31. Load vs. mid-span deflection

The figure demonstrates that the north beam deflected less than the south beam for the same load in the first half of the test. During the latter half of the test the south beam stiffened as the south beam connection stiffened due to the ductility problems discussed in section 3.4.1. The vertical and horizontal deflection as measured at every quarter span of the beam during the test is also shown in Figure 3-32 and the raw data is presented in Table 3-5.

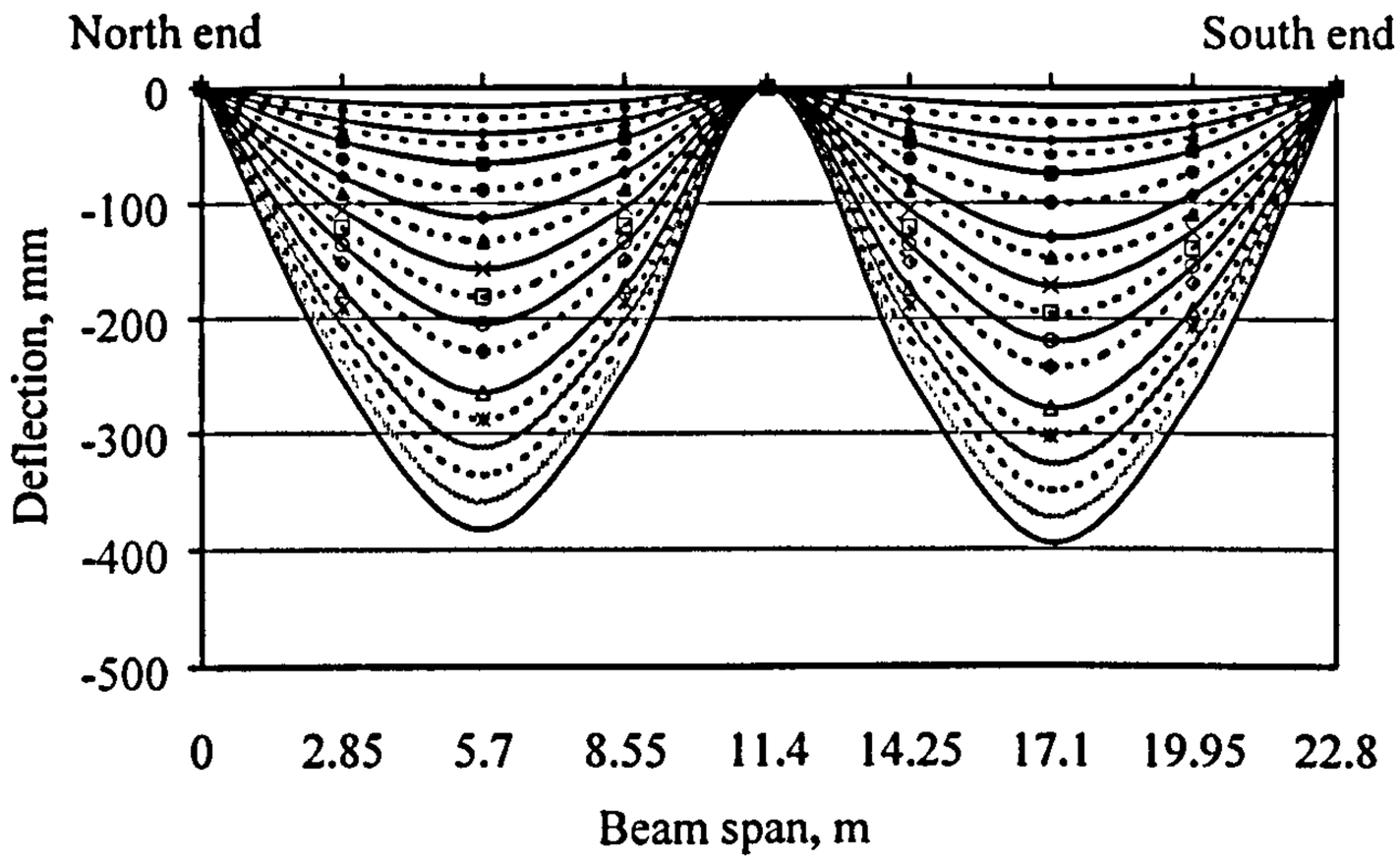

Figure 3-32. Experimentally measured deflections along the span at various load levels

Prior to the rebar failure the south beam mid-span deflection was 147mm (can be see as a small dip Figure 3-31) which is 15mm greater than the north beam. After the rebar failure, the stiffness of the frame was adversely affected. The deflection measured at the mid-span after the frame failure was 407mm for both south and north beams. Figure 3-19 clearly shows the deflected shape of the frame after failure.

3.5 Discussion and conclusions

The reported test provides important information on the strength and ductility of composite connections when used with unpropped beams. The standard composite connections used at the interior column were shown to achieve their design moment capacity comfortably, although the limit on post-construction ductility was shown to be 23mrads. Thereafter, failure of the connection reinforcing bars initiated a decline in strength, and this sudden failure of the rebars highlights the ductility problems associated with composite connections.

The flexural strength of the perimeter composite connection was shown to achieve almost the same nominal strength as that predicted for an equivalent connection located at an internal joint. Importantly, the cranks in the reinforcement provided additional ductility to the connection, at the expense of absolute flexural strength.

Significantly, bolts were shown to have failed at all of the composite connections after the sudden rebar fracture, which again raises questions concerning the ductility of this form of connection detail. Though failure of bolts is a concern in the ductility of this form of connection detail, it was initiated only after the sudden fracture of rebars. It is important to understand that the cause of this sudden rebar fracture is in part due to the relatively low percentage of reinforcement, 1.15%, that has been used in this critical hogging connection. As a consequence of the rebar fracture, the load path has been redirected to the bolt and obviously the bolts are not designed to take the sudden increase in tension and their complete fracture ensues. According to the SCI standard connection guide, the minimum area of reinforcement needed to ensure the connections considered can undergo sufficient rotation to strain the reinforcement to yield is 750mm^2 (1.07%).

The major contribution to the available rotation capacity of composite connections is from the rebar elongation. Slip and beam deformation contributes to additional capacity. The importance of sufficient percentage reinforcement to avoid sudden fracture of reinforcement can be explained. The embedded reinforcement normally provides higher stiffness and a lower overall ductility compared to reinforcement acting alone. The stress and strain concentrations that occur in the slab near the joint (due to discontinuities caused by the connection and the column) determine the location of the first and main crack. The occurrence of the first crack and subsequent cracks (thereby increasing the elongation of the slab) depends on the parameters that influences the behaviour of reinforced concrete in tension and on the position of the first shear connector.

If low amount of reinforcement is used then only one main crack will form at the joint and the rebar will yield directly at the location of the main crack eventually lead to the fracture of the rebar during further rotation of the joint. If higher percentage of reinforcement is used then the elongation length of the slab (rebar) increases (however it will be limited by the location of the main crack and the position of the first shear connector). In the reinforced concrete the first/main crack occurs when reinforcement <= 0.8%. For a composite slab reinforcement >=0.8% would give safe results [Anderson *et al.*, 2000]. However to achieve greater elongation of reinforcement and there by greater rotation capacity it is important to have higher percentage of reinforcement which is found to be from previous experiments at least 1.4%. In the case of unbraced frames excessive unbalanced moments causes local concrete crushing and therefore reinforcement amount to be limited. Bur for braced frames, where unbalanced moments will not be excessive, maximum reinforcement area limitations should not be restrictive. However it needs to be restricted to keep the compression zone in the lower half of the steel beam. Or else compression stiffeners in the column may be necessary. Most of the composite frames are braced frames where unbalanced moments are not excessive and by providing compression stiffeners (if necessary), there may not be a requirement to limit the amount of reinforcement.

The maximum area of reinforcement to keep the compression zone in the lower half of the steel beam (to avoid compression stiffening) for this connection form from the SCI guide is 817 mm^2 (1.17%). The amount of reinforcement used is 804mm^2 (1.15%). Though it is within the maximum reinforcement recommended by SCI but it is certainly less than the normal reinforcement for composite connections i.e. 1.4%. The standard connection detail from SCI seems to recommend a low percentage reinforcement which consequently accounts for the lack of ductility in the connections. Therefore it is right to conclude that the observed lack of ductility in the test composite connections is mainly due to the low percentage of reinforcement and the bolt fracture can be eventually avoided if there is an adequate provision of reinforcement.

Importantly, the nominally pinned connection was shown to possess a considerable moment capacity, formed by a couple between the bolts and the bottom flange of the beam after only relatively low beam end rotations. The compressive force at the bottom flange is the prying action developed as the bottom flange of the beam pressed against the face of the column at a small beam end rotation. Subsequently this couple imposed considerable strain on the bolt/end plate assembly, which could have led to a sudden connection failure since the connection was designed to resist only shear loading. Since the allowed gap between bottom beam flange and column flange is approximately 10mm in the standard pin connection detail, the prying action becomes unavoidable. Thus, the ductility of this standard form of connection was shown to be lacking.

The analysis clearly shows that the flexural strength of the test beam substantially exceeds the nominal beam strength. This was due to conservative design assumptions regarding material and geometric properties. The test was terminated due to concern regarding the rupturing of connection bolts. However at this stage the beam has achieved a large mid-span deflection of 300mm and hence the calculated flexural strength of the beam can be regarded as a conservative measure of the true flexural strength. It is possible that the test beam would have demonstrated more strength if the test had been continued. Though this would have demonstrated the possible enhancement in the flexural strength of the composite beam due to over-strength steel and strain-hardening effect, neither could be relied on for practical designs. Further testing might also have endangered the frame

robustness. The robustness of frames depends on the harmonious interaction between the weak beam members and strong connections. Continuation of the test could have transferred of weak point of the frame from the beams to the connection i.e. it may have caused the complete flexural failure of the pin connection due to the prying force.

Table 3-4. Applied load, calculated moment and recorded rotation during test

Applied Load in kN				Moment in kN.m						Rotation in mrad								
LP1	LP2	LP3	LP4	S_{con}	SC_{con}	NC_{con}	N_{con}	S_{beam}	S_{col}	S_{con}	SC_{beam}	SC_{col}	SC_{con}	NC_{beam}	NC_{col}	NC_{con}	N_{beam}	N_{col}	N_{con}
Construction stage load				-18.20	-110.00	-107.00	-47.60	1.77	-0.58	2.35	-0.95	-0.54	-0.42	0.12	0.24	0.36	-1.03	-0.85	0.19
13.60	14.20	14.50	14.60	-19.19	-116.90	-110.90	-49.72	2.18	-0.46	2.64	-1.30	-0.86	-0.44	0.27	0.14	0.41	-1.24	-0.98	0.26
18.42	19.14	19.20	19.62	-20.35	-122.85	-113.72	-50.61	2.56	-0.22	2.78	-2.10	-1.64	-0.46	1.05	-0.63	0.42	-1.75	-1.34	0.41
23.65	24.36	24.41	24.83	-21.51	-128.81	-116.54	-51.87	2.71	-0.17	2.88	-2.24	-1.75	-0.49	1.17	-0.74	0.43	-1.75	-1.32	0.43
33.51	34.23	34.33	34.80	-23.82	-140.77	-122.17	-54.02	2.96	-0.05	3.01	-2.21	-1.74	-0.47	1.16	-0.73	0.43	-1.95	-1.46	0.49
43.69	44.38	44.43	44.94	-29.38	-160.88	-142.38	-59.16	3.20	0.05	3.15	-2.23	-1.71	-0.52	1.13	-0.70	0.43	-2.15	-1.62	0.53
53.72	54.40	54.42	54.98	-34.74	-202.50	-184.01	-64.37	3.44	0.14	3.30	-2.26	-1.72	-0.54	1.14	-0.71	0.44	-2.34	-1.79	0.55
63.76	64.45	64.44	65.04	-39.79	-216.33	-198.16	-69.15	3.67	0.19	3.48	-2.26	-1.74	-0.52	1.17	-0.73	0.44	-2.56	-1.95	0.61
73.81	74.47	74.43	75.07	-45.11	-231.82	-213.72	-73.80	3.92	0.28	3.64	-2.26	-1.76	-0.50	1.20	-0.75	0.45	-2.75	-2.12	0.63
83.86	84.50	84.47	85.15	-50.20	-278.36	-260.49	-78.78	4.17	0.49	3.68	-2.28	-1.76	-0.52	1.20	-0.75	0.45	-2.95	-2.31	0.65
93.88	94.51	94.46	95.18	-55.49	-303.06	-285.43	-83.91	4.39	0.56	3.84	-2.28	-1.77	-0.51	1.21	-0.76	0.45	-3.15	-2.46	0.69
103.95	104.57	104.48	105.24	-60.27	-334.78	-317.47	-88.76	4.64	0.60	4.04	-2.30	-1.81	-0.50	1.25	-0.80	0.46	-3.35	-2.62	0.74
113.70	114.32	114.23	115.04	-65.55	-347.43	-330.43	-93.81	4.88	0.74	4.14	-2.32	-1.80	-0.52	1.25	-0.79	0.46	-3.56	-2.79	0.78
123.71	124.33	124.22	125.09	-71.18	-355.68	-338.79	-99.48	5.13	0.83	4.30	-2.45	-1.80	-0.64	1.25	-0.79	0.46	-3.78	-2.97	0.81
133.76	134.37	134.22	135.15	-77.14	-383.92	-367.20	-105.72	5.40	0.92	4.48	-2.48	-1.80	-0.68	1.30	-0.79	0.51	-4.01	-3.14	0.86
143.78	144.38	144.27	145.21	-81.66	-419.51	-403.19	-112.20	5.74	1.09	4.66	-2.79	-1.83	-0.96	1.38	-0.82	0.56	-4.26	-3.33	0.94
153.85	154.42	154.29	155.28	-85.64	-432.01	-415.76	-118.63	6.12	1.13	4.99	-2.95	-1.82	-1.13	1.44	-0.81	0.63	-4.53	-3.54	0.99
163.87	164.43	164.29	165.33	-89.73	-431.32	-415.18	-124.76	6.52	1.21	5.31	-3.24	-1.83	-1.41	1.54	-0.82	0.72	-4.83	-3.76	1.07
173.87	174.42	174.27	175.37	-93.49	-460.25	-444.41	-131.39	6.89	1.30	5.59	-3.42	-1.84	-1.58	1.60	-0.83	0.77	-5.09	-3.97	1.12
183.93	184.47	184.29	185.44	-97.50	-482.43	-467.05	-137.36	7.34	1.36	5.98	-3.71	-1.81	-1.90	1.70	-0.80	0.90	-5.38	-4.19	1.19
193.97	194.51	194.29	195.47	-101.30	-483.43	-468.68	-143.01	7.82	1.35	6.47	-3.99	-1.86	-2.14	1.80	-0.85	0.95	-5.67	-4.42	1.25
203.99	204.51	204.30	205.55	-104.98	-513.40	-499.46	-149.31	8.29	1.42	6.87	-4.35	-1.86	-2.49	1.91	-0.85	1.06	-5.99	-4.67	1.32
214.04	214.56	214.33	215.59	-108.48	-543.03	-530.11	-156.70	8.80	1.43	7.37	-4.76	-1.83	-2.93	2.00	-0.82	1.18	-6.33	-4.93	1.40
218.90	219.42	219.17	220.49	-110.51	-527.39	-514.90	-160.82	9.08	1.54	7.54	-5.00	-1.90	-3.10	2.07	-0.89	1.18	-6.51	-5.07	1.44
224.04	224.56	224.30	225.63	-112.70	-518.71	-506.79	-165.54	9.33	1.45	7.88	-5.17	-1.91	-3.25	2.13	-0.91	1.23	-6.67	-5.21	1.46
228.94	229.45	229.19	230.55	-114.73	-539.78	-529.17	-170.42	9.56	1.40	8.16	-5.47	-1.94	-3.52	2.23	-0.94	1.29	-6.87	-5.37	1.50
234.07	234.57	234.27	235.65	-116.82	-521.23	-512.12	-175.30	9.85	1.45	8.40	-5.75	-1.93	-3.82	2.33	-0.92	1.40	-7.06	-5.53	1.54
238.96	239.46	239.21	240.58	-118.91	-532.97	-525.40	-180.58	10.10	1.50	8.60	-6.00	-2.06	-3.94	2.41	-1.05	1.36	-7.26	-5.69	1.57
244.14	244.63	244.36	245.75	-120.23	-529.77	-523.87	-187.66	10.48	1.26	9.22	-6.52	-2.18	-4.34	2.57	-1.17	1.39	-7.53	-5.90	1.63
249.01	249.49	249.20	250.61	-122.45	-545.12	-539.93	-193.29	10.75	1.26	9.49	-6.74	-2.21	-4.53	2.64	-1.20	1.44	-7.75	-6.08	1.67
254.13	254.60	254.34	255.74	-125.00	-546.27	-542.89	-200.71	11.06	1.27	9.79	-7.04	-2.30	-4.74	2.76	-1.29	1.47	-7.97	-6.27	1.71
254.17	254.66	254.37	255.79	-125.30	-519.46	-518.51	-210.56	11.41	1.03	10.38	-7.76	-2.60	-5.16	3.34	-1.59	1.75	-8.21	-6.42	1.79
254.19	254.65	254.35	255.79	-125.03	-507.86	-508.11	-215.67	11.52	0.96	10.57	-7.74	-2.67	-5.07	3.47	-1.66	1.81	-8.25	-6.51	1.74
254.20	254.66	254.37	255.81	-124.40	-509.78	-510.38	-219.27	11.60	0.91	10.69	-7.86	-2.81	-5.05	3.58	-1.80	1.78	-8.38	-6.58	1.79
234.13	234.62	234.32	235.71	-113.63	-436.72	-437.04	-210.85	11.16	0.70	10.46	-7.86	-2.79	-5.07	3.60	-1.78	1.82	-8.02	-6.28	1.74
214.09	214.60	214.34	215.65	-102.81	-395.23	-395.33	-200.96	10.69	0.56	10.13	-7.87	-2.80	-5.06	3.60	-1.79	1.80	-7.62	-5.96	1.65
163.92	164.47	164.28	165.36	-76.17	-265.60	-264.62	-174.89	9.45	0.06	9.39	-7.79	-2.80	-4.99	3.57	-1.79	1.78	-6.60	-5.17	1.43
113.74	114.36	114.21	115.09	-51.42	-150.10	-148.13	-147.45	8.17	0.49	8.66	-7.30	-2.78	-4.52	3.47	-1.77	1.70	-5.55	-4.37	1.17
63.81	64.48	64.41	65.08	-27.67	-7.11	-4.13	-116.91	6.86	-0.07	6.79	-6.72	-2.74	-3.98	3.25	-1.73	1.52	-4.46	-3.56	0.89
33.72	34.41	34.40	34.94	-14.06	86.94	90.69	-97.92	6.02	-0.29	5.73	-6.29	-2.67	-3.62	3.10	-1.66	1.44	-3.77	-3.06	0.72
23.72	24.42	24.41	24.91	-9.78	124.61	128.27	-91.95	5.74	-0.43	5.30	-6.15	-2.65	-3.49	3.05	-1.65	1.40	-3.53	-2.89	0.64

Table 3-4. continued...

Applied Load in kN				Moment in kN.m				Rotation in mrad										
LP1	LP2	LP3	LP4	S_{con}	SC_{con}	NC_{con}	N_{con}	S_{beam}	S_{col}	S_{con}	SC_{beam}	SC_{col}	SC_{con}	NC_{beam}	NC_{col}	NC_{con}	N_{beam}	N_{col}	N_{con}
18.55	19.27	19.26	19.73	-7.63	120.01	123.55	-88.43	5.58	-0.43	5.15	-6.10	-2.68	-3.42	3.04	-1.67	1.37	-3.40	-2.78	0.62
13.61	14.28	14.49	14.86	-5.48	134 84	138.33	-85.72	5.44	-0.52	4.92	-6.06	-2.69	-3.37	3.01	-1.68	1.33	-3.29	-2.71	0.59
14.24	14.83	15.07	15.01	-4.80	131.76	134.39	-80.22	5.42	-0.50	4.92	-5.86	-2.60	-3.27	2.97	-1.59	1.38	-3.20	-2.60	0.60
36.28	52.17	43.60	43.31	-17.76	40.08	41.80	-92.06	6.09	-0.17	5.92	-5.87	-2.58	-3.28	3.02	-1.58	1.45	-3.77	-3.01	0.75
65.13	97.86	86.73	77.76	-35.38	-68.22	-66.56	-110.68	6.98	0.14	7.13	-5.97	-2.62	-3.36	3.15	-1.61	1.54	-4.57	-3.60	0.97
94.25	139.55	130.67	108.28	-52.57	-169.80	-167.80	-130.77	7.85	0.40	8.25	-6.42	-2.58	-3.84	3.29	-1.57	1.72	-5.34	-4.17	1.17
121.09	189.21	171.27	143.30	-70.80	-267.57	-266.37	-152.80	8.78	-0.12	8.90	-6.89	-2.61	-4.27	3.41	-1.60	1.81	-6.13	-4.77	1.37
150.97	230.26	213.81	175.37	-88.12	-339.95	-338.38	-174.95	9.65	0.20	9.46	-7.28	-2.65	-4.64	3.56	-1.64	1.92	-6.92	-5.35	1.57
179.91	274.96	257.96	207.38	-105.24	-453.53	-452.46	-197.23	10.54	0.49	10.05	-7.67	-2.69	-4.98	3.77	-1.68	2.09	-7.71	-5.98	1.72
208.44	300.56	282.12	238.53	-121.21	-495.54	-499.67	-222.66	11.49	0.82	10.67	-8.43	-2.94	-5.48	4.46	-1.94	2.52	-8.55	-6 68	1.87
226.49	314.70	302.24	253.68	-126.24	-506.06	-516.20	-250.39	13.37	1.81	11.56	-9.48	-3.28	-6.20	4.98	-2.27	2.71	-9.42	-7.42	2.00
274.11	271.30	287.80	268.34	-131.70	-513.10	-523.87	-258.80	14.77	2.63	12.14	-9.64	-3.37	-6.26	5.10	-2.36	2.73	-9.60	-7.56	2.04
279.89	280.53	298.63	273.37	-134.90	-533.45	-547.44	-292.17	15.66	3.00	12.66	-10.03	-3.57	-6.45	5.43	-2.56	2.86	-9.98	-7.85	2.13
280.69	291.44	289.73	291.93	-135.90	-521.14	-539.02	-312.93	16.64	3.53	13.11	-10.55	-3.75	-6.79	5.64	-2.75	2.89	-10.43	-8.23	2.20
280.56	308.41	309.39	296.39	-136.18	-536.62	-557.19	-320.24	18.05	3.99	14.06	-11.35	-3.89	-7.46	6.06	-2.88	3.18	-11.14	-8.79	2.35
304.40	296.30	301.37	321.10	-139.01	-547.86	-568.96	-326.19	19.70	4.34	15.36	-11.86	-3.97	-7.89	6.40	-2.97	3.44	-11.76	-9.29	2.47
308.76	321.62	333.44	323.63	-141.38	-570.23	-596.63	-337.64	23.44	4.96	18.48	-13.76	-4.24	-9.52	7.82	-3.24	4.59	-13.10	-10.40	2.70
320.64	343.47	358.91	344.92	-141.53	-601.65	-632.70	-360.51	28.77	5.53	23.24	-16.33	-4.56	-11.77	10.18	-3.55	6.63	-15.44	-12.32	3.11
323.20	369.30	377.39	369.89	-142.28	-633.30	-666.87	-362.58	33.27	5.08	28.19	-19.07	-4.76	-14.30	12.61	-3.76	8.85	-17.98	-14.35	3.63
357.07	355.13	395.10	383.21	-142.97	-602.54	-633.30	-355.35	37.78	5.14	32.65	-22.18	-4.73	-17.44	15.64	-3.72	11.92	-20.38	-16.31	4.07
347.37	396.25	411.35	392.26	-147.11	-717.03	-751.14	-347.09	41.02	5.43	35.59	-25.81	-4.76	-21.05	19.66	-3.75	15.91	-22.84	-18.35	4.50
342.94	408.14	425.53	394.79	-147.27	-708.15	-726.98	-341.54	43.21	5.72	37.50	-27.28	-4.35	-22.93	22.99	-3.34	19.65	-25.32	-20.38	4.94
451.74	259.70	383.69	448.06	-150.35	-683.10	-683.86	-334.33	47.10	6.26	40.84	-27.15	-3.55	-23.60	27.35	-2.54	24.81	-29.19	-23.58	5.61
348.17	404.39	483.24	350.77	-147.39	-659.99	-648.58	-335.21	47.71	6.40	41.31	-26.83	-3.05	-23.77	29.10	-2.04	27.05	-29.72	-23.99	5.74
369.91	396.71	456.48	401.93	-153.85	-600.15	-575.97	-329.89	50.39	7.09	43.29	-25.74	-2.31	-23.43	30.74	-1.30	29.44	-32.15	-26.08	6.07
376.78	400.98	465.70	407.47	-166.10	-599.12	-552.58	-329.41	52.70	8.23	44.47	-23.25	-0.93	-22.32	32.81	0.08	32.89	-34.68	-28.33	6.34
382.82	404.29	465.28	416.00	-190.67	-642.02	-577.06	-326.39	55.16	9.04	46.12	-20.54	0.40	-20.94	35.05	1.41	36.45	-37.29	-30.63	6.66
386.06	410.11	458.72	424.46	-221.68	-726.32	-654.56	-322.83	57.67	9.30	48.37	-18.51	1.19	-19.71	37.06	2.20	39.26	-39.75	-32.77	6.98
395.32	410.76	458.87	433.11	-258.64	-882.95	-814.47	-320.32	60.26	10.12	50.14	-17.40	1.53	-18.92	38.45	2.53	40.99	-42.37	-34.84	7.53
404.84	408.89	455.70	438.68	-284.13	-932.24	-864.09	-321.65	62.93	11.24	51.68	-16.88	1.78	-18.66	40.22	2.79	43.01	-45.05	-36.77	8.28
447.68	359.77	447.33	430.16	-326.05	-820.56	-764.88	-361.72	68.12	12.66	55.45	-18.31	1.88	-20.19	43.33	2.89	46.22	-51.06	-37.30	13.76
426.12	410.31	455.47	431.56	-330.15	-576.75	-525.15	-374.16	73.56	14.06	59.50	-20.20	1.78	-21.99	44.33	2.79	47.12	-57.82	-36.87	20.95
431.10	421.45	456.20	428.20	-352.13	-383.19	-343.18	-378.28	81.54	16.59	64.95	-26.39	1.05	-27.44	46.53	2.06	48.59	-68.50	-35.29	33.21
432.06	424.43	455.42	412.30	-358.58	-329.70	-293.02	-435.38	84.24	17.54	66.70	-28.50	0.66	-29.16	47.86	1.67	49.52	-73.12	-33.07	40.05
437.33	424.05	454.08	414.27	-364.72	-248.96	-223.05	-438.07	86.88	18.53	68.35	-30.19	0.26	-30.44	49.15	1.27	50.42	-76.09	-32.95	43.13
434.95	423.52	447.13	413.32	-368.35	-145.54	-138.64	-437.59	89.57	19.53	70.04	-32.39	-0.96	-31.43	52.22	0.05	52.27	-79.47	-32.84	46.64
444.76	430.57	451.46	401.54	-389.30	-96.50	-96.69	-468.60	100.39	23.22	77.17	-38.85	-1.81	-37.04	63.12	-0.80	62.32	-93.65	-27.32	66.34

LP1, LP2, LP3 & LP4 – Loads at one third points on South and North primary Beams respectively.

S-South; SC- South - Central; NC - North-Central; N- North;

Subscripts: $_{con}$ – Connection; $_{col}$ – Column; $_{beam}$ – Beam

Table 3-5. Applied load, recorded vertical and horizontal deflection during test

Load in kN				Vertical Deflection in mm						Horizontal Deflection in mm	
				South Beam			North Beam			South Column	North Column
LP1	LP2	LP3	LP4	¼ span	½ span	¾ span	¼ span	½ span	¾ span	@ neutral axis	@ neutral axis
	Construction stage load			-3.5	-7.67	-5.7	-4.2	-6.57	-2.92	-	-
13.60	14.20	14.50	14.60	-2.45	-9.16	-2.19	-1.51	-7.76	-1.59	-0.27	-0.17
18.42	19.14	19.20	19.62	-3.55	-10.42	-3.34	-3.2	-9.97	-3.11	-0.91	-0.21
23.65	24.36	24.41	24.83	-3.6	-10.53	-3.36	-3.18	-9.91	-3.11	-0.75	-0.08
33.51	34.23	34.33	34.80	-3.78	-10.86	-3.68	-3.37	-10.27	-3.14	-0.77	-0.11
43.69	44.38	44.43	44.94	-4.36	-11.78	-4.35	-3.85	-11.08	-3.7	-0.81	-0.08
53.72	54.40	54.42	54.98	-4.87	-12.74	-5.04	-4.33	-11.92	-4.31	-0.91	-0.11
63.76	64.45	64.44	65.04	-5.38	-13.47	-5.73	-4.85	-12.74	-4.94	-0.94	-0.08
73.81	74.47	74.43	75.07	-5.88	-14.27	-6.42	-5.3	-13.55	-5.57	-1	-0.09
83.86	84.50	84.47	85.15	-6.4	-15.11	-7.08	-5.79	-14.36	-6.28	-1.05	-0.09
93.88	94.51	94.46	95.18	-6.92	-16.01	-7.74	-6.31	-15.17	-6.92	-1.16	-0.11
103.95	104.57	104.48	105.24	-7.43	-17.14	-8.42	-6.84	-15.98	-7.48	-1.23	-0.15
113.70	114.32	114.23	115.04	-7.97	-18.14	-9.09	-7.33	-16.8	-8.01	-1.29	-0 17
123.71	124.33	124.22	125.09	-8.46	-18.92	-9.76	-7.82	-17.58	-8.57	-1.4	-0.2
133.76	134.37	134.22	135.15	-9.02	-19.78	-10.45	-8.42	-18.52	-9.28	-1.48	-0.28
143.78	144.38	144.27	145.21	-9.74	-20.7	-11.2	-9.03	-19.49	-10.09	-1.56	-0.33
153.85	154.42	154.29	155.28	-10.44	-21.71	-12.06	-9.66	-20.49	-10.84	-1.65	-0.38
163.87	164.43	164.29	165.33	-11.21	-22.91	-12.98	-10.37	-21.65	-11.71	-1.77	-0.45
173.87	174.42	174.27	175.37	-12.05	-24.32	-14	-11.19	-22.87	-12.61	-1.95	-0.56
183.93	184.47	184.29	185.44	-12.87	-25.52	-14.94	-12.01	-24.07	-13.47	-2.11	-0.64
193.97	194.51	194.29	195.47	-13.76	-27	-16.06	-12.8	-25.25	-14.28	-2.23	-0.74
203.99	204.51	204.30	205.55	-14.76	-28.56	-17.18	-13.63	-26.53	-15.29	-2.38	-0.82
214.04	214.56	214.33	215.59	-15.81	-30.24	-18.39	-14.47	-27.88	-16.3	-2.61	-0.96
218.90	219.42	219.17	220.49	-17.02	-32.09	-19.78	-15.43	-29.37	-17.39	-2.81	-1.02
224.04	224.56	224.30	225.63	-17.64	-33.07	-20.52	-15.93	-30.16	-18.02	-2.9	-1.05
228.94	229.45	229.19	230.55	-18.28	-34.06	-21.26	-16.47	-30.91	-18.54	-3.04	-1.07
234.07	234.57	234.27	235.65	-19.12	-35.45	-22.22	-17.09	-31.8	-19.09	-3.26	-1.12
238.96	239.46	239.21	240.58	-19.95	-36.63	-23.1	-17.79	-32.7	-19.65	-3.42	-1.17
244.14	244.63	244.36	245.75	-20.72	-37.87	-23.98	-18.37	-33.6	-20.23	-3.56	-1.24
249.01	249.49	249.20	250.61	-21.89	-39.74	-25.37	-19.22	-34.83	-21.42	-3.82	-1.33
254.13	254.60	254.34	255.74	-22.58	-40.9	-26.11	-19.81	-35.76	-22	-4.01	-1.37
254.17	254.66	254.37	255.79	-23.47	-42.3	-27.09	-20.46	-36.79	-22.69	-4.17	-1.46
254.19	254.65	254.35	255.79	-24.76	-44.22	-28.42	-21.37	-38	-23.53	-4.55	-1.68
254.20	254.66	254.37	255.81	-25.23	-44.78	-28.88	-21.62	-38.41	-23.87	-4.7	-1.7
234.13	234.62	234.32	235.71	-25.46	-45.19	-29.19	-21.91	-38.82	-24.23	-4.74	-1.73
214.09	214.60	214.34	215.65	-24.85	-44.27	-27.97	-21.04	-37.37	-23.31	-4.67	-1.73
163.92	164.47	164.28	165.36	-23.8	-42.56	-26.63	-20.09	-35.76	-22.11	-4.5	-1.72

Table 3-5. continued...

LP1	LP2	LP3	LP4	¼ span	½ span	¾ span	¼ span	½ span	¾ span	@ neutral axis	@ neutral axis
113.74	114.36	114.21	115.09	-20.92	-37.65	-23.12	-17.49	-31.54	-18.82	-4.11	-1.67
63.81	64.48	64.41	65.08	-17.96	-32.89	-19.53	-14.73	-27.1	-15.54	-3.62	-1.4
33.72	34.41	34.40	34.94	-14.94	-27.9	-15.77	-11.84	-22.58	-12.19	-3.2	-1.18
23.72	24.42	24.41	24.91	-12.96	-24.81	-13.42	-9.96	-19.68	-10.01	-2.85	-1.1
18.55	19.27	19.26	19.73	-12.37	-23.89	-12.62	-9.4	-18.71	-9.33	-2.77	-1.09
13.61	14.28	14.49	14.86	-12.04	-23.34	-12.23	-9.15	-18.25	-8.96	-2.74	-1.1
14.24	14.83	15.07	15.01	-11.61	-22.74	-11.73	-8.75	-17.59	-8.53	-2.42	-1.05
36.28	52.17	43.60	43.31	-11.6	-22.75	-11.75	-8.72	-17.57	-8.52	-2.42	-1.04
65.13	97.86	86.73	77.76	-12.94	-24.84	-13.63	-10.06	-19.85	-9.78	-2.62	-1.03
94.25	139.55	130.67	108.28	-15.28	-28.42	-16.21	-12.35	-23.35	-12.47	-2.91	-1.07
121.09	189.21	171.27	143.30	-17.4	-31.65	-18.65	-14.52	-26.66	-14.82	-3.34	-1.23
150.97	230.26	213.81	175.37	-19.76	-35.42	-21.35	-16.68	-30.07	-17.31	-3.7	-1.42
179.91	274.96	257.96	207.38	-21.96	-38.72	-23.84	-18.97	-33.47	-19.72	-4.07	-1.71
208.44	300.56	282.12	238.53	-24.2	-42.44	-26.43	-21.07	-36.91	-22.31	-4.4	-1.98
226.49	314.70	302.24	253.68	-27.03	-46.33	-29.24	-23.88	-40.87	-25.12	-5.01	-2.37
274.11	271.30	287.80	268.34	-30.01	-50.58	-32	-26.77	-45.25	-28.05	-5.68	-2.6
279.89	280.53	298.63	273.37	-30.54	-52.7	-34.26	-26.83	-45.65	-28.52	-5.86	-2.71
280.69	291.44	289.73	291.93	-31.96	-54.84	-35.89	-28.25	-47.56	-29.76	-6.18	-2.82
280.56	308.41	309.39	296.39	-33.38	-57.11	-37.42	-29.06	-49.26	-31.08	-6.53	-2.84
304.40	296.30	301.37	321.10	-35.69	-60.52	-39.78	-31.3	-52.62	-33.21	-7.01	-3
308.76	321.62	333.44	323.63	-38.6	-66.12	-44.1	-33.99	-57.32	-37.17	-7.54	-3.43
320.64	343.47	358.91	344.92	-42.32	-71.7	-47.88	-37.45	-62.37	-40.09	-8.36	-3.7
323.20	369.30	377.39	369.89	-49.62	-83.71	-56.29	-45.03	-73.85	-48.06	-9.82	-4.62
357.07	355.13	395.10	383.21	-56.77	-95.01	-64.04	-52.29	-85.45	-55.77	-11.15	-5.49
347.37	396.25	411.35	392.26	-64.56	-109.38	-75.51	-59.61	-96.51	-63.22	-12.17	-6.64
342.94	408.14	425.53	394.79	-75.33	-126.53	-87.21	-67.01	-108	-70.72	-13.09	-7.95
451.74	259.70	383.69	448.06	-82.72	-138.4	-95	-74.89	-119.81	-78.34	-13.01	-9.48
348.17	404.39	483.24	350.77	-86.39	-150.37	-109.05	-82.41	-134.32	-89.9	-12.59	-11.63
369.91	396.71	456.48	401.93	-92	-155.94	-111.39	-89.08	-140.65	-91.87	-12.36	-12.15
376.78	400.98	465.70	407.47	-99.72	-168.16	-118.67	-96.8	-152.2	-99.13	-11.5	-13.8
382.82	404.29	465.28	416.00	-107.47	-180.34	-126.23	-104.74	-164.56	-106.87	-9.74	-16.07
386.06	410.11	458.72	424.46	-115.14	-192.5	-133.68	-112.6	-176.95	-114.53	-8.02	-18.29
395.32	410.76	458.87	433.11	-122.82	-204.27	-141.07	-120.2	-188.65	-121.8	-6.89	-19.77
404.84	408.89	455.70	438.68	-130.49	-216.2	-148.6	-127.69	-200.53	-129.59	-6.06	-21.09
447.68	359.77	447.33	430.16	-137.92	-228.11	-156.27	-135.11	-212.31	-137.33	-5.25	-22.25
426.12	410.31	455.47	431.56	-153.63	-251.1	-171.11	-150.14	-236.47	-153.28	-4.99	-24.46
431.10	421.45	456.20	428.20	-183.39	-299.21	-201.57	-180.13	-284.21	-184.66	-5.46	-26.89
432.06	424.43	455.42	412.30	-190.97	-311.29	-209.24	-187.24	-295.91	-192.23	-5.64	-27.1
437.33	424.05	454.08	414.27	-198.54	-323.05	-216.78	-194.53	-307.87	-200.29	-5.68	-28.23
444.76	430.57	451.46	401.54	-236.78	-381.19	-254.58	-232.48	-367.4	-239.91	-6.8	-30.42

LP1, LP2, LP3 & LP4 – Loads at one third points on South and North primary Beams respectively.

Chapter 4 – Numerical modelling for steel beams using mill test data

---

Papers published based on this chapter:

1. M.P. Byfield, Dhanalakshmi, M. (2002). Analysis of strain hardening in steel beams using mill tests. *International Conference on Advances in Steel Structures (ICASS 02)*, HongKong, 139-146.

2. M.P. Byfield, J.M. Davies, Dhanalakshmi. M. (2004). Calculation of the strain hardening behaviour of steel structures based on mill tests, Journal of Constructional Steel Research, vol. 61, 133-150.

4.1 Introduction

A numerical modelling technique for predicting the moment vs. deformation for steel sections is presented. The technique uses neither stiffness matrices nor finite element analysis but numerical integration based on the full mill test stress strain curves. Using the stress-strain values as a polynomial function, the moment capacity for a given value of curvature is defined by integrating the product of stress, area and lever arm throughout a given cross section. Thus, the moment curvature relationship of a cross section is established. The curvature distribution along a member is integrated to define the slope distribution, followed by further integration to define the deflected shape. The process is repeated incrementally to define the full moment vs. end-rotation and moment vs. mid-span deflection graphs. The model is constructed from first principles and achieves a high degree of accuracy.

The method does not account for the weakening effects of lateral torsional and local buckling on the moment curvature relationship. This decision is justified on the evidence from bending tests on class 1 cross-sections presented by Byfield and Nethercot [1998],

which showed that lateral torsional and local buckling have little significant effect on the moment vs. curvature relationship where the end rotation is limited to 6 degrees and where the non-dimensional slenderness is below the limit allowed for plastic design ($\bar{\lambda}_{LT}$ = 0.4). Techniques are available for calculating the available rotation capacities of class 1 and 2 cross-sections for use in portal frame structures *inter alia*, Kemp and Dekker [1991], and can be used to limit the analysis to calculated maximum rotations, beyond which buckling will limit strength increases due to strain hardening and thus cause the model to overestimate strength. No attempt is made to account for the weakening effects of local buckling, the method is therefore only justified for use with class 1 (plastic) cross-sections, as defined in Eurocode 3 Part 1.

4.2 Modelling of moment vs. Curvature using mill tests (M-ϕ)

Figure 4-1A shows a cross-section subjected to a pure sagging moment applied about the major axis.

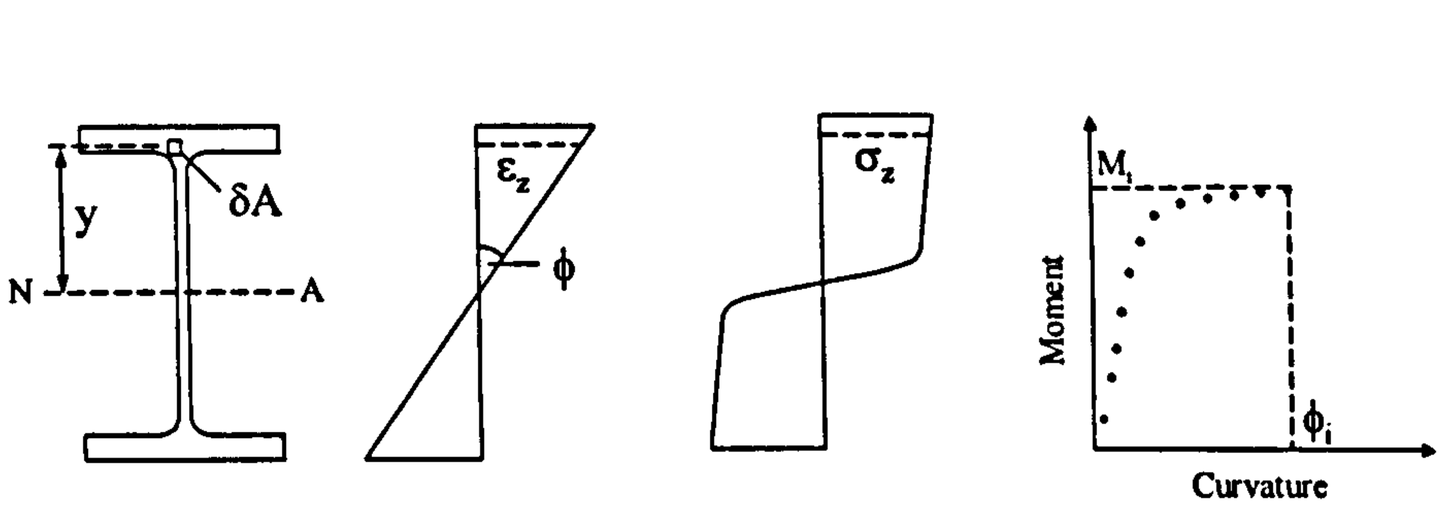

A. Define cross-section | B. Define strain distribution | C. Define stress distribution | D. Define M-ϕ

Figure 4-1. Description of steps for calculating M-ϕ relationship

A fibre of the beam (δA) is located a distance y from the neutral axis, which is located at half the depth of the cross-section assuming that: (a) the section is symmetrical, (b) zero axial load, and (c) that the stress strain relationship for steel is equal for compression and tension. Given that plane sections can be assumed to remain plane, then the strain (ε_z) in the fibre (δA) is equal to:

$$\varepsilon_z = \phi y \tag{1}$$

Where ϕ is the curvature, see Figure 4-1B. The mill test stress strain relationship is converted into a polynomial function, and used to define the stress σ_z for the fibre (δA), Figure 4-1C. By this means the distribution of stress for the given value of curvature can be derived, Figure 4-1C. The moment due to the normal force in a fibre (δA) is equal to the product of force and distance from the neutral axis. The integral of all such moments across the entire cross-section provides the total moment, i.e.:

$$M = \int_A \sigma_z y \, dA \tag{2}$$

The curvature is increased gradually and the corresponding moment for each curvature is calculated. Using this technique the moment curvature relationship is characterised for a given section, Figure 4-1D.

4.3 Modelling of moment vs. end rotation (M-θ)

Once the M-ϕ relationship for the cross-section is determined it is relatively simple to establish the distribution of curvature. For every loading increment (Figure 4-2A), the distribution of bending moments is calculated (Figure 4-2B), which is converted into the distribution of curvature using the M-ϕ relationship (Figure 4-2C). The curvature distribution is then integrated to define the distribution of slope, Figure 4-2D, which is integrated again to define the distribution of deflection, Figure 4-2E, i.e.

$$\theta = \int \phi \, dz \tag{3}$$

and

$$v = \iint \phi \, dz \tag{4}$$

Where θ is the end rotation and v is the deflection. The process is repeated incrementally to define the full moment vs. mid-span deflection or end-rotation for a member. The

bending moment diagram shown in Figure 4-2B is symmetrical. This is a convenient situation to analyse since the end rotation is equal to the integral of curvature between the support and the centre of the span. Where loading is non-uniform it is easier to double integrate curvature using the support displacements as boundary conditions, in order to define the displacement distribution. Slope distribution can then be defined by differentiating the deflection.

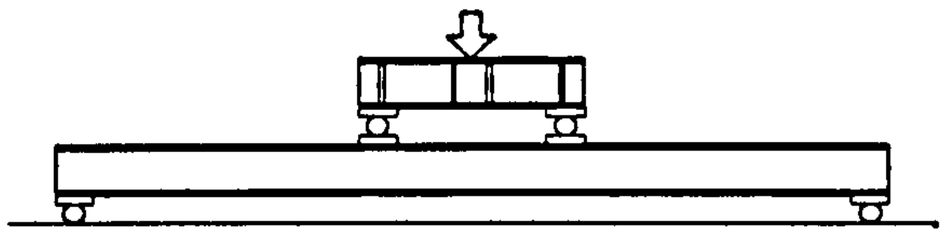

A. Define load set up

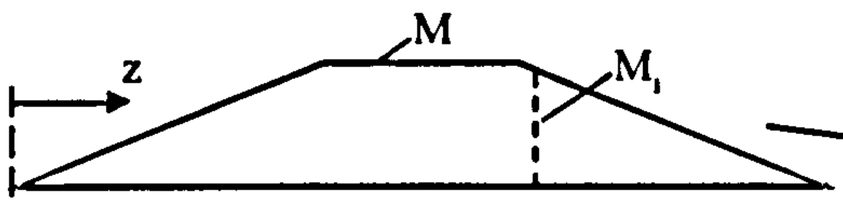

B. Define bending moment distribution

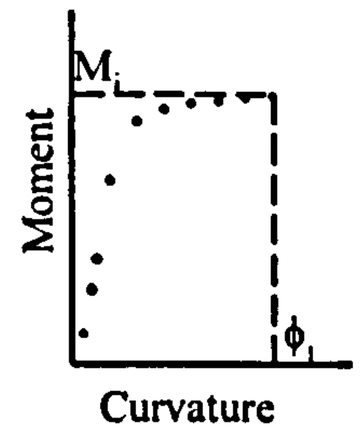

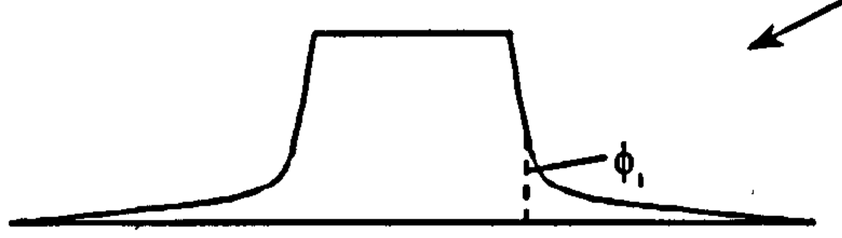

C. Define distribution of curvature, ϕ

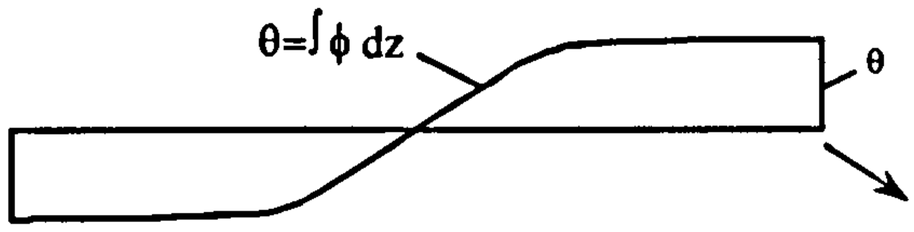

D. Define distribution of slope, θ

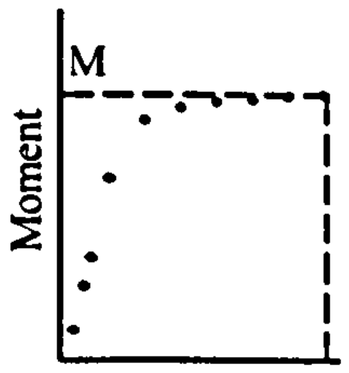

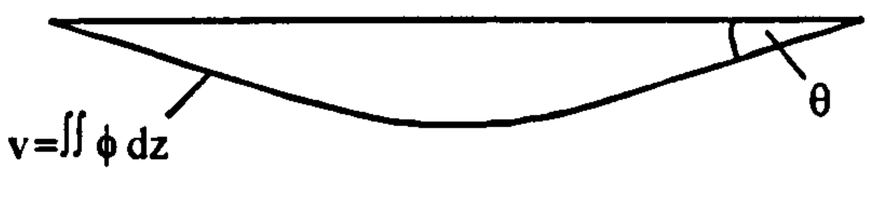

E. Define distribution of deflection

Figure 4-2. The calculation of slope and deflection

4.4 Nottingham test [Byfield and Nethercot (1998)]

Byfield and Nethercot [1998] demonstrated that the plastic moment of resistance design formula substantially underestimates the bending strength class 1 hot-rolled open sections. As a part of their study, they carried out a series of four-point bending tests on 12 nos. of fully laterally restrained beams and 20 nos. of partially laterally restrained beams. 203x102x23UB and 152x152x30UC beam sections were considered for the study. The geometric and material properties of each test specimen were recorded. Experimental moment vs. end rotation is recorded throughout the test.

A comparison between their predicted and experimental resistances showed that the function underestimates the bending strength of class 1 I-section beams by an average of 16% for partially restrained beams and 22% for fully restrained beams.

4.5 Verification of Numerical model

The accuracy of the numerical model presented in this chapter has been assessed using the Nottingham test [Section 4.4] results for fully restrained beams of sections 203x102x23UB and 152x152x30UC. The experimental data are based on the average results from 6 identical bending tests for each of the beam sections.

Theoretical predictions used the mill test [BS EN10002-1,1990] stress strain curves taken from the 6 test specimens (2 tests per specimen) for each of the beam sections, see Figure 4-3 (a) and (b). Thus, statistical variations are reduced which allows the method to fully demonstrate the degree of accuracy with which it is able to predict large deformations.

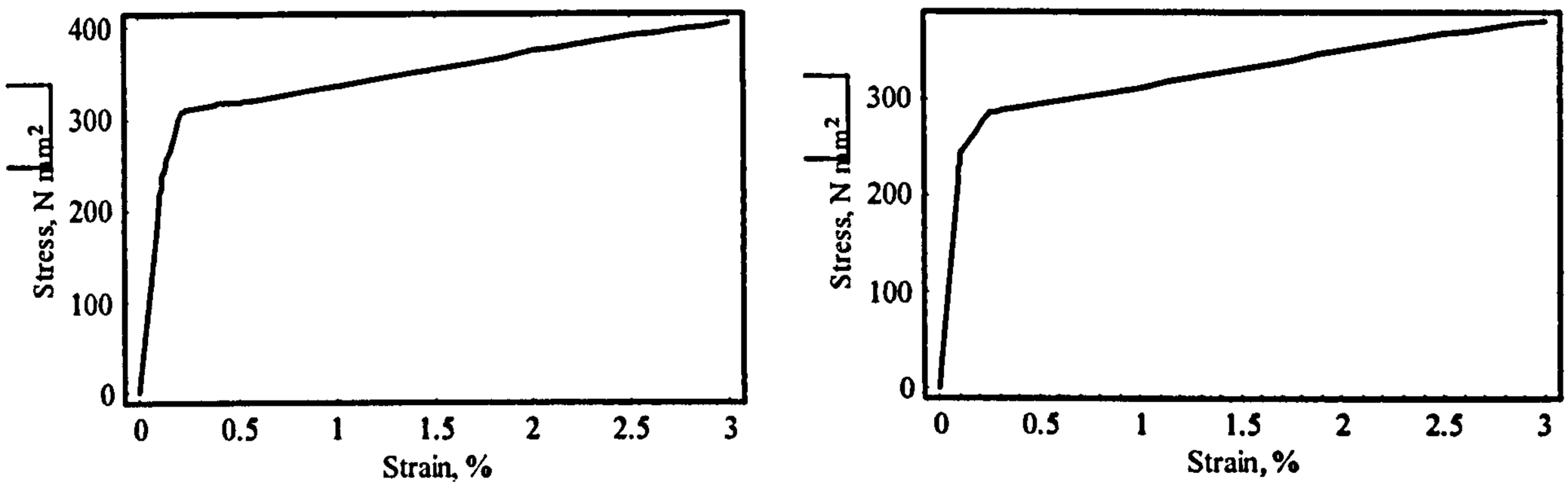

(a) 203 x 203 x 23 UB section

(b) 152 x 152 x 30 UC section

Figure 4-3. Stress-strain interpolation function for Nottingham test beam sections

Theoretical moment-curvature relationship for each of the beam sections are shown in Figure 4-4 (a) and (b).

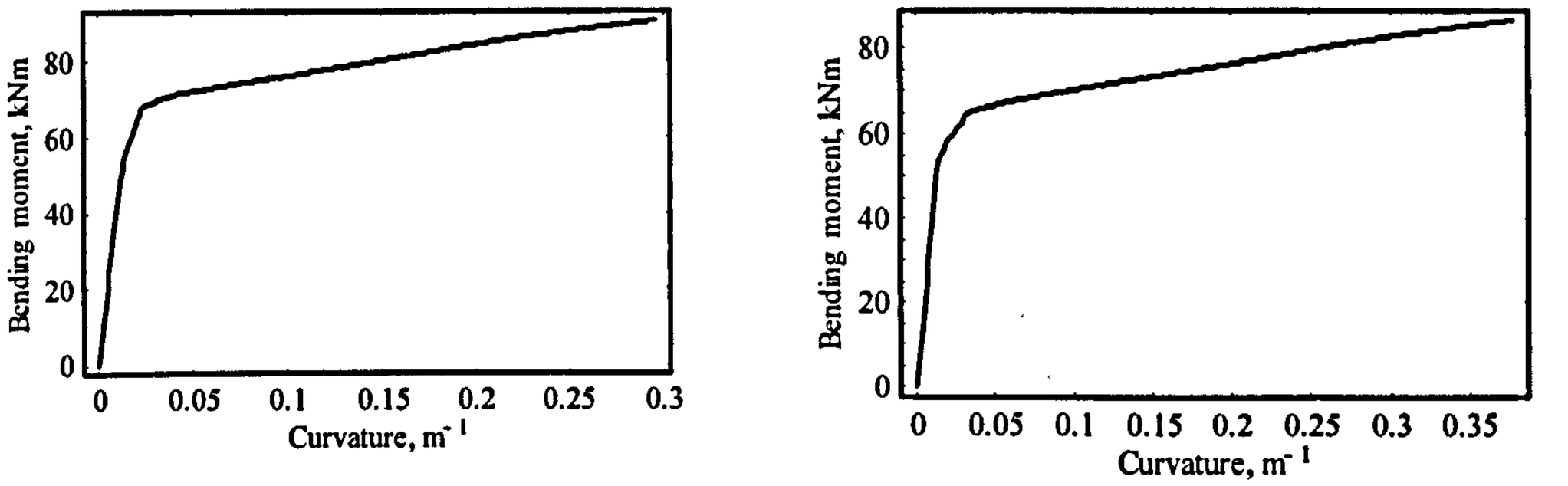

(a) 203 x 203 x 23 UB section

(b) 152 x 152 x 30 UC section

Figure 4-4. Moment-curvature relationship for the Nottingham test sections

The theoretical distributions of moment, curvature, deflection and slope for each of the test beam sections are shown in Figure 4-5 (a) and (b).

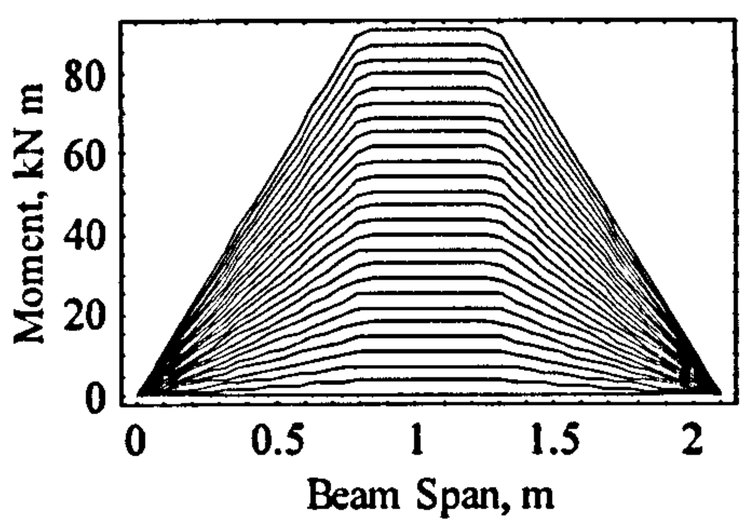

(i) Moment distribution

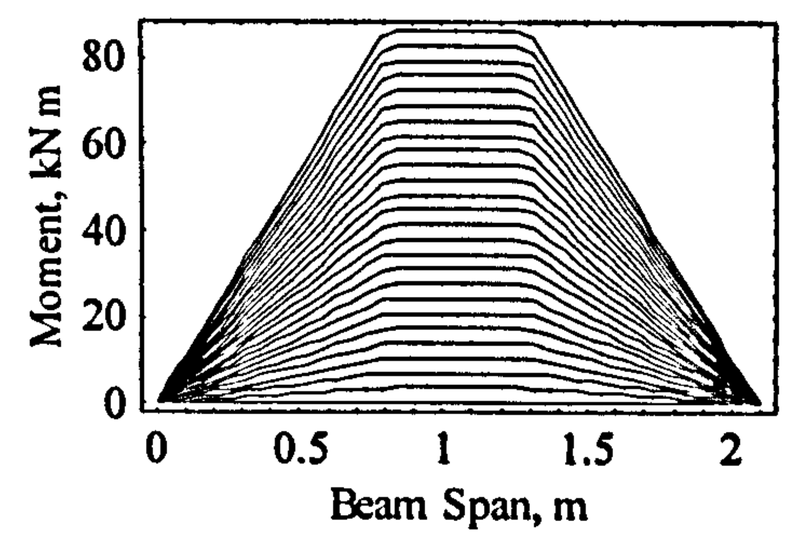

(i) Moment distribution

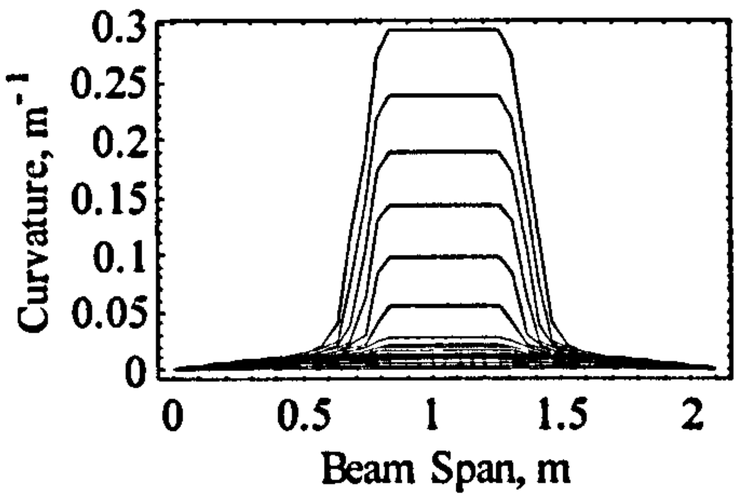

(ii) Curvature distribution

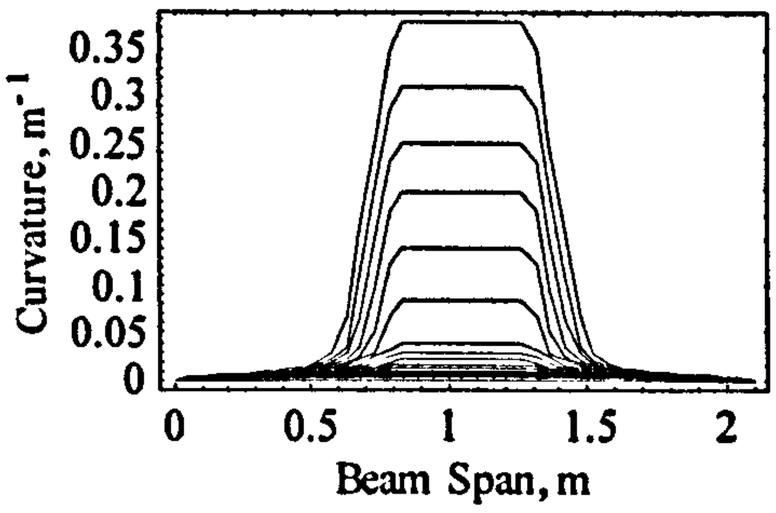

(ii) Curvature distribution

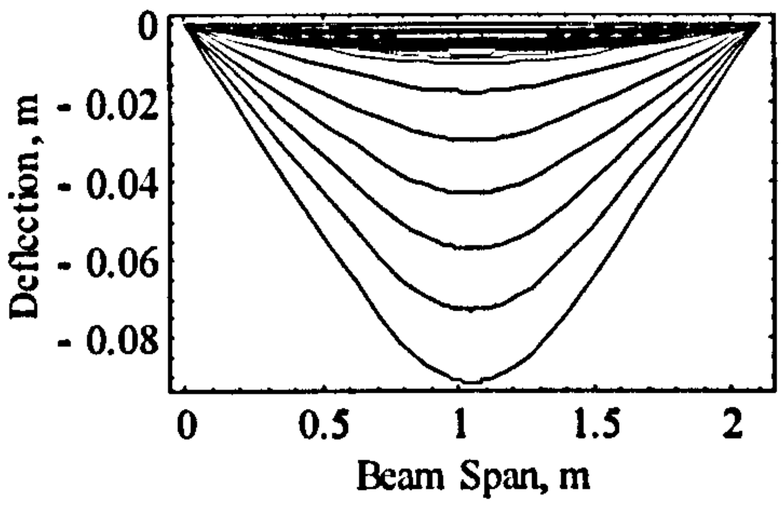

(iii) Deflection distribution

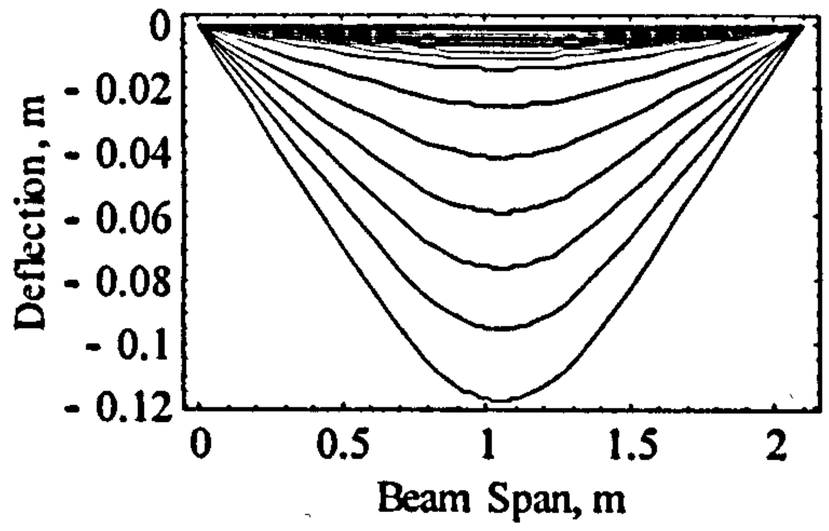

(iii) Deflection distribution

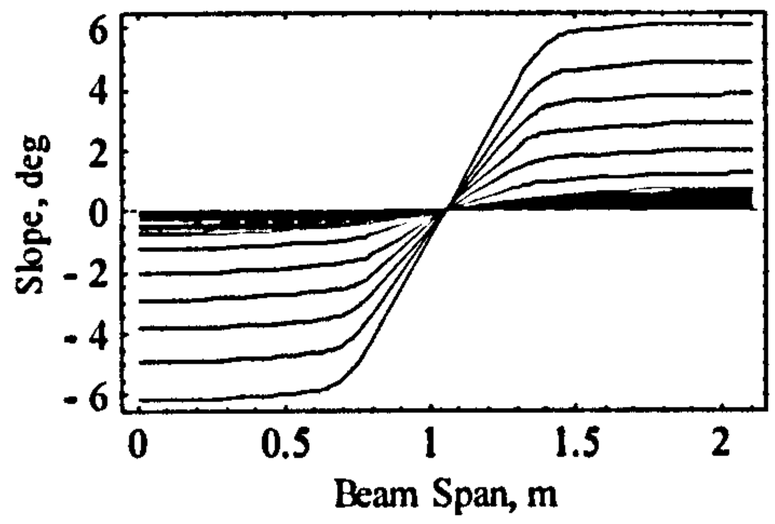

(iv) Slope distribution

(a) 203 x 203 x 23 UB section

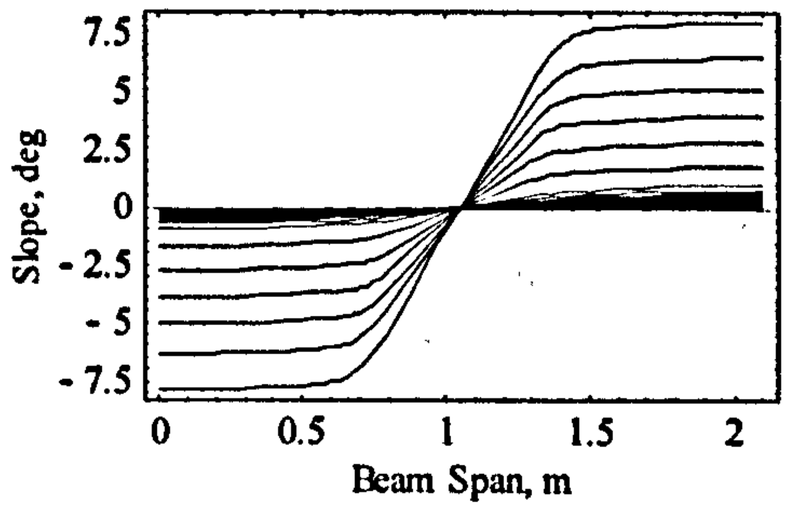

(iv) Slope distribution

(b) 152 x 152 x 30 UC section

Figure 4-5. Moment, curvature, deflection and slope distribution of Nottingham test sections

The capability of the model to produce accurate predictions of large deformations for each of the test beam sections is shown in Figure 4-6 and Figure 4-7, where the model predictions are compared with the experimental moment vs. end rotation for fully restrained beams. The model can clearly be seen to achieve a good degree of conformity with experimental behaviour of both test beam sections.

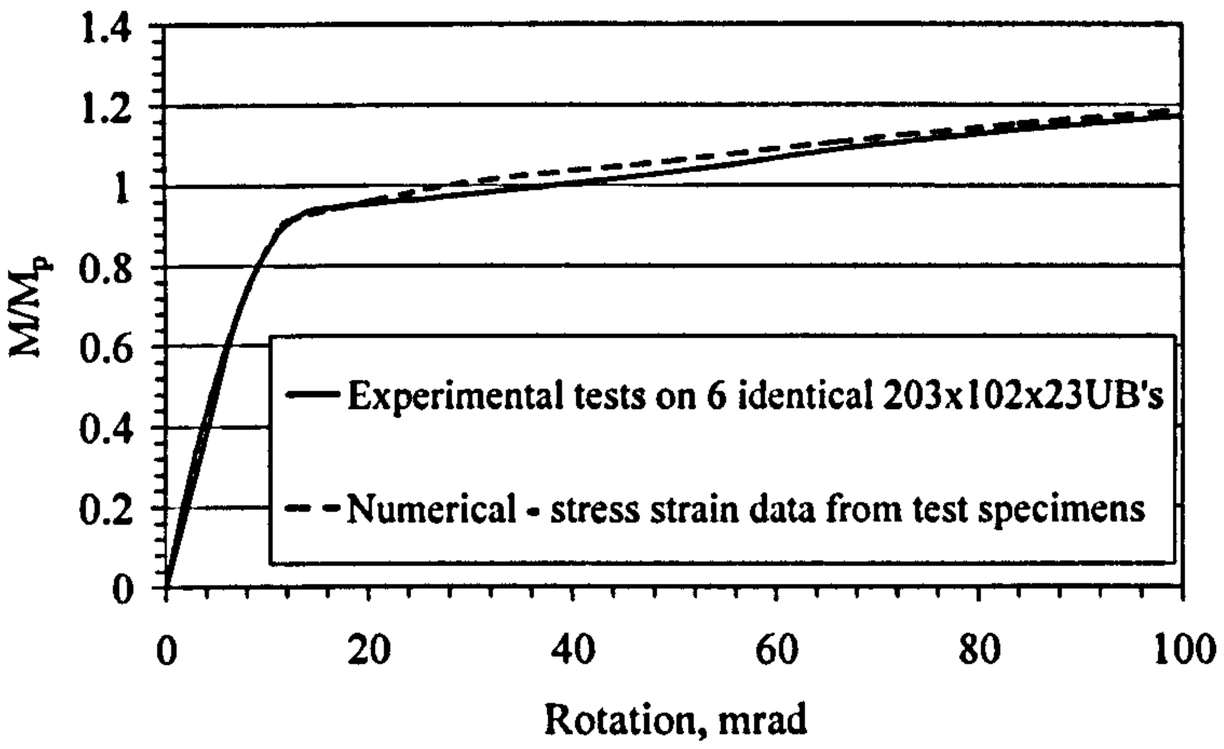

Figure 4-6. Comparison between experimental and predicted M-θ for 203x102x23UB test beam

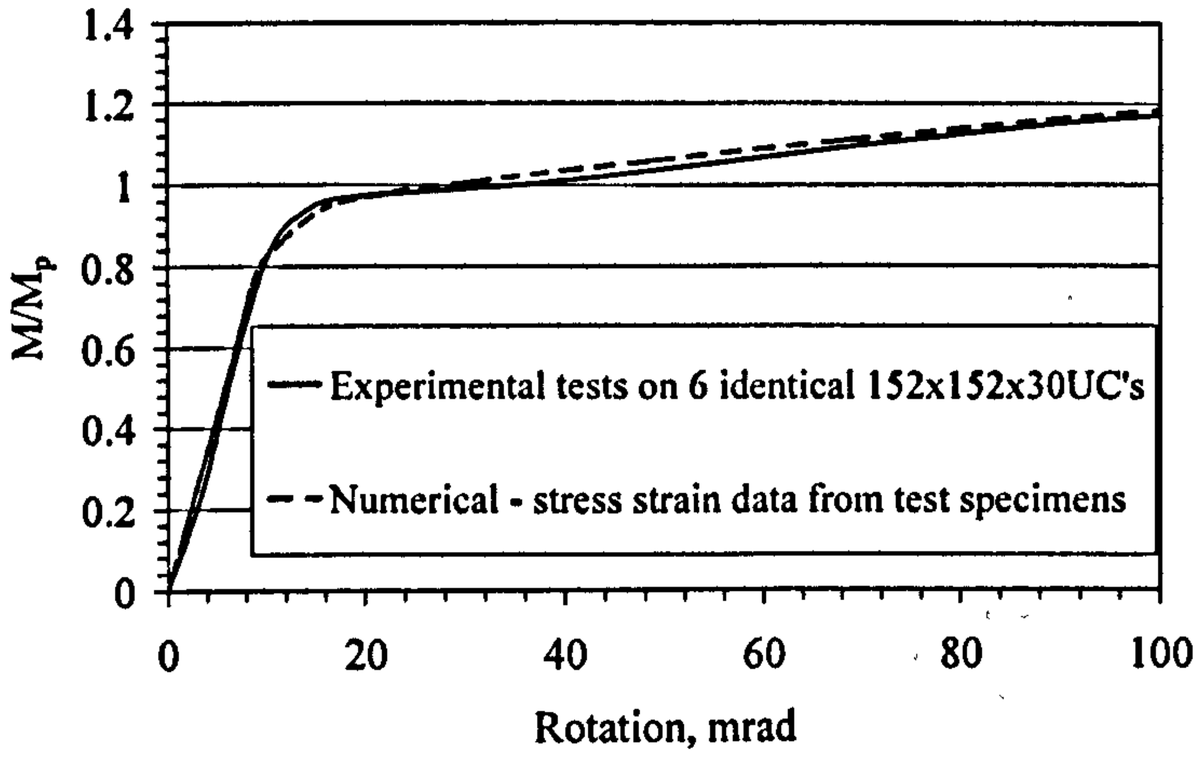

Figure 4-7. Comparison between experimental and predicted M-θ for 203x102x23UB test beam

4.6 Conclusions

A method for predicting the full (non-linear) moment-rotation curves for laterally restrained steel beams, based on stress-strain data from mill tests is presented. The accuracy of the method has been established by comparing the predicted moment vs. end rotation behaviour of restrained steel beams with the behaviour observed through 6 identical bending tests on each of different beam sections carried out in Nottingham. The results demonstrate that the numerical model, based on mill test data, provides accurate predictions of actual response to load.

Having achieved a very high degree of accuracy in predicting the end rotations of steel beams using the modelling technique presented in this chapter, an extensive parametric study is carried out using this technique to establish the influence of strain-hardening on elastic-plastic frame instability design which is presented in Chapter 7.

The same first principles used in this modelling technique are further extended to predict the non-linear member behaviour of semi-continuous composite beams as presented in Chapter 5.

Chapter 5 - Modelling of unpropped semi-continuous composite beams

---

Papers published based on this chapter:

1. M.P. Byfield, Dhanalakshmi, M and H.G.D. Goyder, Modelling of unpropped semi-continuous composite beams, Journal of Constructional Steel Research, Volume 60, Pages 1353-1367, 2004.

5.1 Introduction

The numerical model technique presented in Chapter 4 has been demonstrated to predict strength and ductility of steel beams with good accuracy, using the characteristic values of stress strain data obtained from the mill test data. Consequently, this model has been extended herein intensively to predict the load-deformation behaviour of composite beams unpropped during construction and incorporating composite connections at the supports. This involves incorporation of the effect of unpropped construction in the steel and composite beam stresses and the effect of semi-rigid composite connections in the beam behaviour under loading.

In unpropped construction, the steel section alone supports the weight of the concrete slab during casting. The subsequent applied loading is resisted by the composite action of the steel and concrete. This mode of construction results in significant stresses built into the steel section. This configuration creates difficulties in numerical modelling and may account for the relatively few studies carried out to assess the rotation requirements of connections in these circumstances [Anderson & Najafi(1997), SCI(1992)].

The numerical modelling technique presented here involves the development of a 3D function to define the relationship between moment, curvature and the beam stress under dead load. This function is useful because the moment-curvature relationship for the beam is dependent on the degree of dead load stress 'locked' into the beam during construction.

Clearly, the dead load stress varies with the bending moment. The 3D function permits the corresponding variation in moment-curvature response to be accurately modelled. A similar technique is also employed to define the moment-curvature response of the beam subjected to hogging moments. Subsequently, the moment-curvature functions are used to define the distribution of curvature for any given bending moment distribution. Deflected shape is obtained by double integrating the distribution of curvature along the beam, with the end displacements providing boundary conditions. This end rotation is obtained as a by product of this process.

The accuracy of the technique has been assessed experimentally using the test data reported in detail in Chapter 3. The model predictions of end rotations and displacements are shown to be in good agreement with observed experimental values. This model has subsequently been used in a parametric study to establish the scope for extending the use of composite connections to unpropped beams as in Chapter 6.

5.2 Modelling of moment-curvature

For the beam shown in Figure 5-1 the modelling of moment-curvature can be divided into three regions. A three-dimensional moment-curvature-dead load strain relationship is calculated for Regions B and C shown in Figure 5-1.

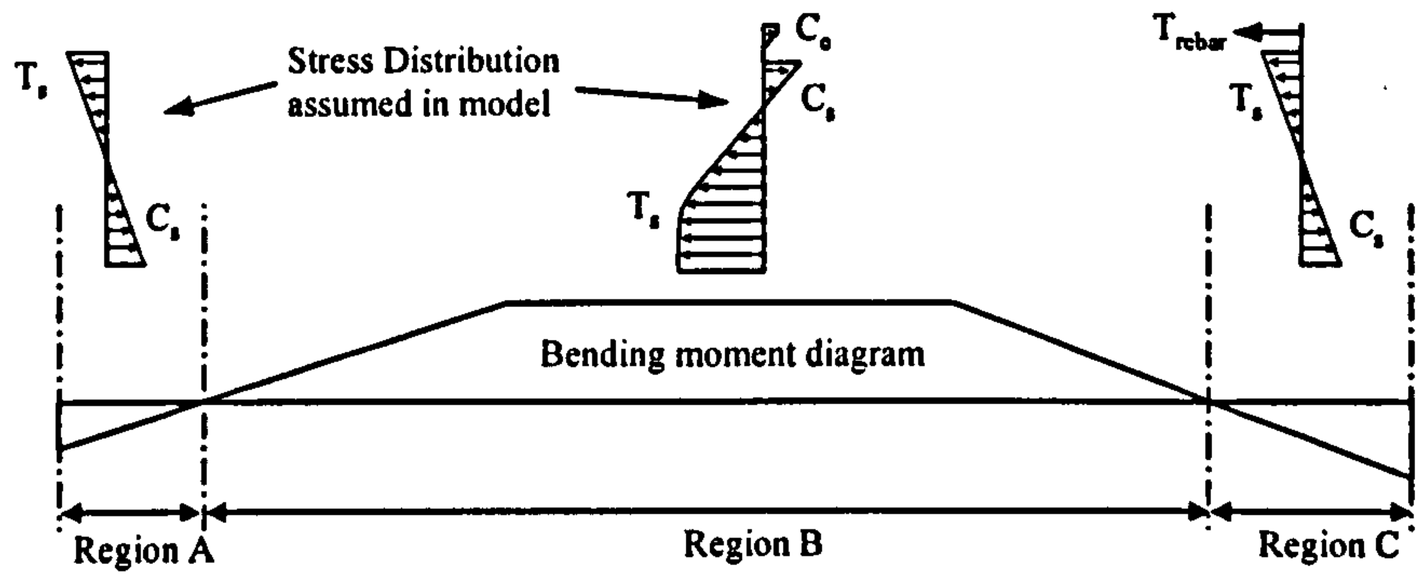

Region A - section in hogging next to pinned connection
Region B - section in sagging
Region C - section in hogging next to composite connection

Figure 5-1. Cross-sections considered in the composite stage analysis

While for region A, a two-dimensional moment-curvature relationship was used to model the small hogging moments developed by simple connections, such as partial depth end plate connections.

Material and geometric properties. In the model, the non-linear stress-strain relationships for each material (determined from testing) are expressed in the form of interpolation functions, enabling the material non-linearity for the steel, concrete and rebar to be accurately modelled. The non-linear stress-strain relationship, defined in BS8100 [1997], is used to model the concrete response to compression. The stress-strain interpolation functions used for the model of the test frame are shown in Figure 5-2.

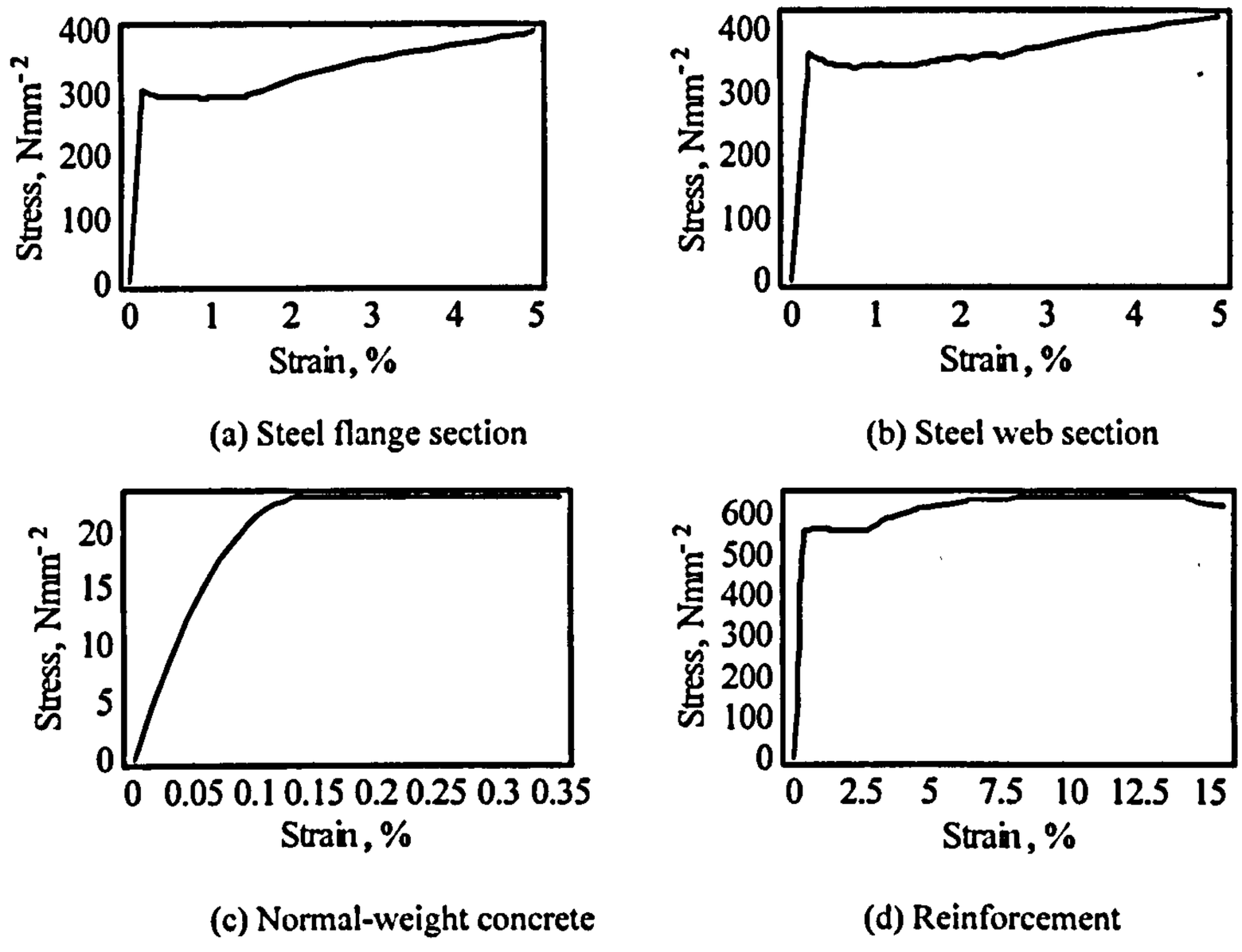

Figure 5-2. Stress-strain interpolation functions for material properties

Figure 5-2a and b were determined from the average stress strain behaviour determined from coupon tests of beam material. Figure 5-2c shows the assumed stress-strain curve for concrete in compression. Figure 5-2d is the experimentally derived stress-strain curve for the reinforcement.

Assumptions. A full shear connection at the steel-concrete interface is assumed. Li [1994, 1993] and Couchman [1995] have studied the effect of shear connections on the rotation capacity and have concluded that the degree of shear connection does not significantly influence the rotation capacity. According to Li [1994], if unfactored material strength is used, the curvature of composite beams between the yield and ultimate moments is little affected by the degree of shear connection. Also, according to Couchman [1995], variations in the degree of shear connection have no influence on the ability of a beam to form a mechanism, provided the available rotation capacity is sufficient for beams with full shear connection. This assumption is also consistent with BS 5950: Part 3 [1990], which requires full shear connections to be provided in the hogging moment region in order to develop the full tensile force in the reinforcement. The other assumptions used in the modelling are as follows.

- The effective width of the slab is one quarter of the length of the beam.
- The area of concrete located within the troughs of the profiled metal decking is included if in compression and within the effective width of the slab.
- The strength of the profiled steel deck is ignored.
- The weakening effects of local buckling are ignored.
- The steel section is assumed to be formed from rectangular elements, with no root radius at the web-flange intersection.
- Concrete strength under tension is neglected.
- Plane sections remain plane.
- The properties of steel in tension and compression are identical.

5.2.1 Modelling of unpropped composite beams subjected to sagging moments

The modelling technique is illustrated in Figure 5-3, which also shows the notation system used. Consider a fibre of a composite beam with a cross-sectional area δA, located at a distance y below the top of a slab (Figure 5-3a). Under a dead load in an unpropped construction the steel beam resists all of the load and remains elastic, producing a strain in the fibre δA of $\varepsilon_{z.d}$ (Figure 5-3b). Under an imposed load, zero slip is assumed at the steel-concrete interface (Figure 5-3c). Assuming plane sections remain plane and no net

axial force is present, then the strain distribution due to any subsequent loading can be calculated in terms of the neutral axis position *Yi*.

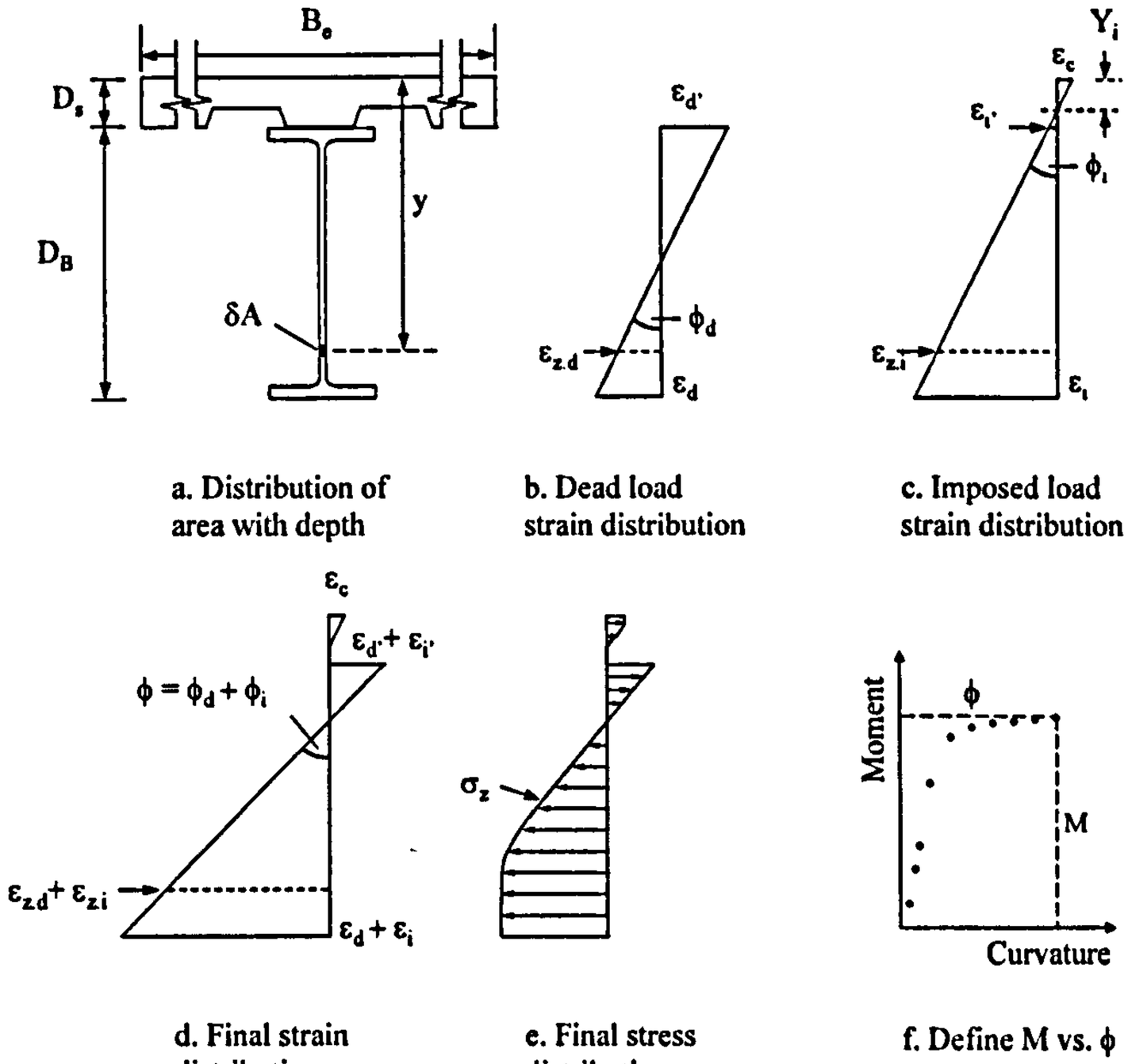

a. Distribution of area with depth

b. Dead load strain distribution

c. Imposed load strain distribution

d. Final strain distribution

e. Final stress distribution, σ_z

f. Define M vs. ϕ

Figure 5-3. Modelling of unpropped beam in a sagging moment region

The final strain distribution (Figure 5-3d) is equal to the combined effects of the dead and imposed load strains. Once a strain distribution is specified, a stress distribution can be calculated using the non-linear stress-strain interpolation functions described previously. Clearly, at locations where $y < D_s$, the concrete stress-strain interpolation function is used for compression, with any tensile stress equal to zero. At locations where $y \geq D_s$, the steel stress-strain interpolation function is used. This produces a distribution of stress throughout the cross-section as illustrated in Figure 5-3e. The normal force in the fibre δA is $\sigma_z \delta A$ and since the beam is subjected to pure bending the resultant normal force on the complete cross-section must be zero, i.e.:

$$\int_A \sigma_z dA = 0 \tag{1}$$

The tensile and compressive normal forces maybe calculated as a function of dead load strain, imposed load strain and neutral axis depth. The position of the neutral axis Y_i lies at a depth where the sum of steel tensile forces balances the concrete compressive forces. This depth can be found by means of an iterative procedure. The moment due to the normal force in a fibre is equal to the product of force and distance from the neutral axis, and the integral of all such moments across the entire cross-section is equal to the applied moment, i.e.:

$$M = \int_A \sigma_z y \, dA \tag{2}$$

Finally, the curvature (ϕ) for this moment is equal to the sum of dead and imposed load curvatures, i.e:

$$\phi = (\varepsilon_d + \varepsilon_i - \varepsilon_{d'} - \varepsilon_{i'})/d \tag{3}$$

By this means the moment-curvature relationship is characterized (Figure 5-3f).

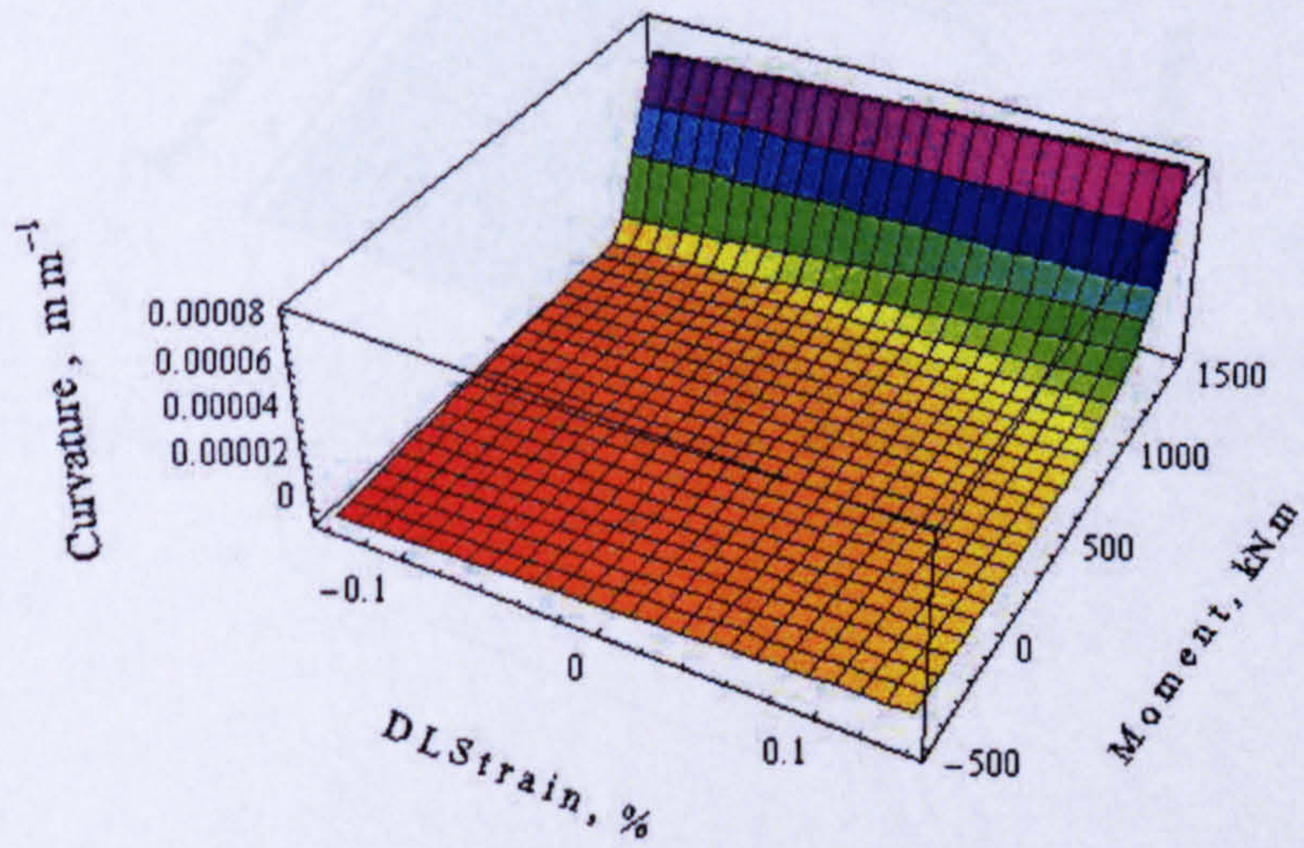

Figure 5-4. Moment-curvature-dead load strain relationship for the experimental unpropped composite beam section subjected to sagging moment

During the modelling, the section moment is calculated as a function of bottom flange dead load strain (ε_d) and imposed load strain to form a 3D moment-curvature-dead load strain distribution for the cross section, Figure 5-4. This 3D relationship may be expressed as an interpolating function so that it can be used in subsequent rotation and deflection calculations. Since the moment, curvature and strain obtained are not in the form of 3D-interpolation functions, a series of 2D moment-curvature interpolation relationships are generated for a range of strain values. Subsequently, grids of 2D-interpolation functions are used to form a 3D-interpolation function as shown in Figure 5-4. Thus, for each value of moment and dead load strain, a curvature value can be obtained from this 3D interpolation function.

Effect of dead load strain on the curvature

A parametric plot, Figure 5-5, is presented to illustrate the variation in the neural axis depth for the test composite beam under sagging moment for different combinations of dead load strain and imposed load strain.

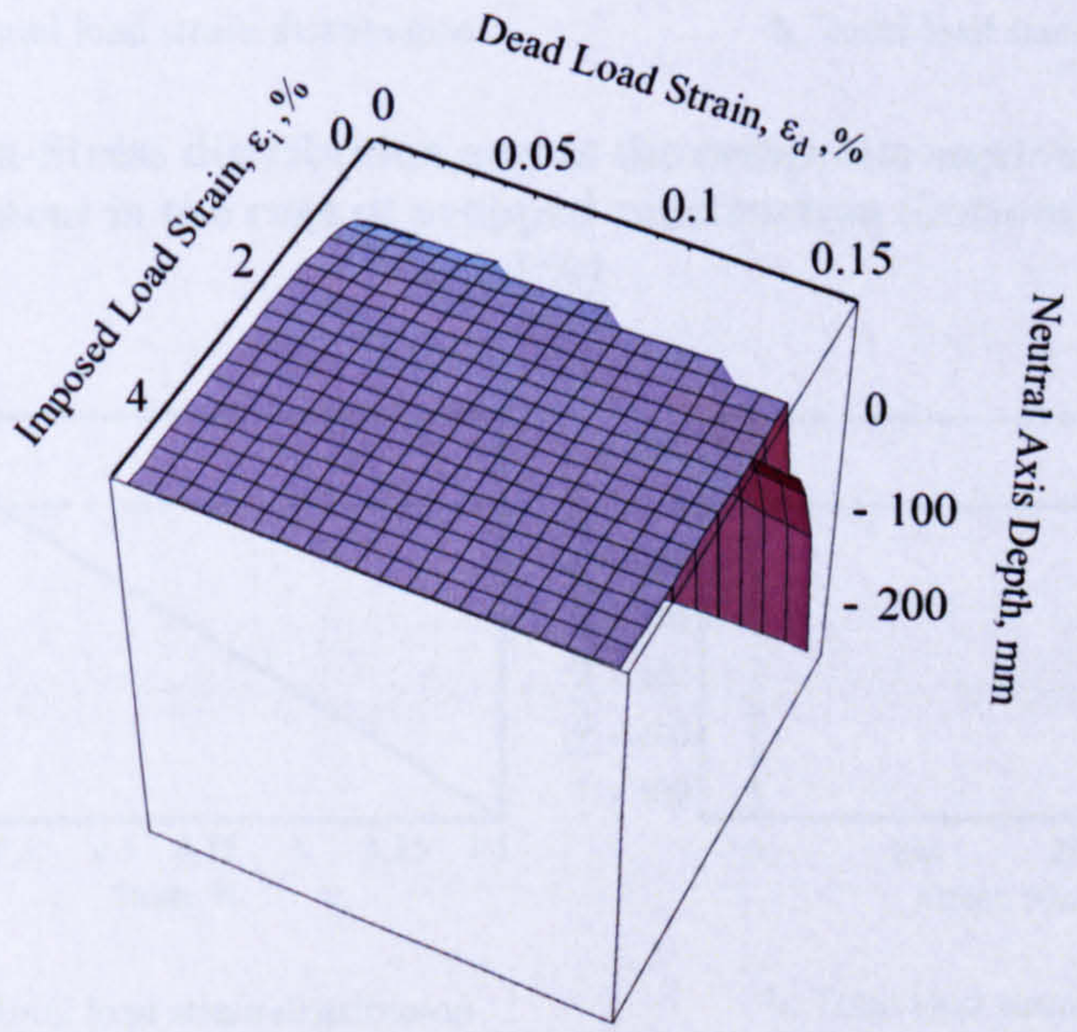

Figure 5-5. Parametric plot of variation in the neutral axis depth with different combination of dead load strain and imposed load strain for the experimental unpropped composite beam under sagging moment

In this figure, neutral axis in the steel section is presented as negative sign and neutral axis in the concrete slab is presented as positive sign. For a dead load strain of up to 0.15% (i.e. the yield strain of the steel section), the neutral axis moves from the steel web to concrete flange as the imposed load strain increases above 1%.

Figure 5-6 and Figure 5-7 show the total load stress distribution throughout the composite cross-section in the case of PROPPED construction, for example, using the test beam material and geometric properties for a bottom flange strain of 1.1% and 1.5% respectively. In both cases the neutral axis lies in the concrete slab with moment and curvature of 1437kN.m, 0.0208m^{-1} and 1448.5kN.m, 0.0283m^{-1} respectively.

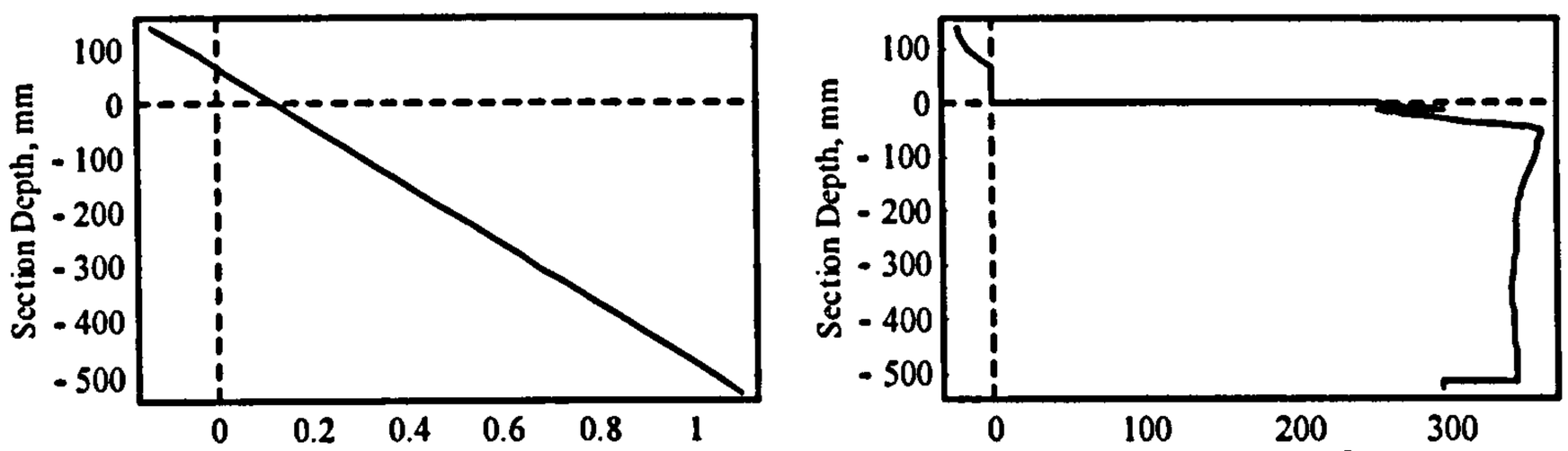

a. Total load strain distribution

b. Total load stress distribution

Figure 5-6. Strain-Stress distribution across the composite section depth subjected to sagging moment in the case of propped construction (bottom flange strain= 1.1%)

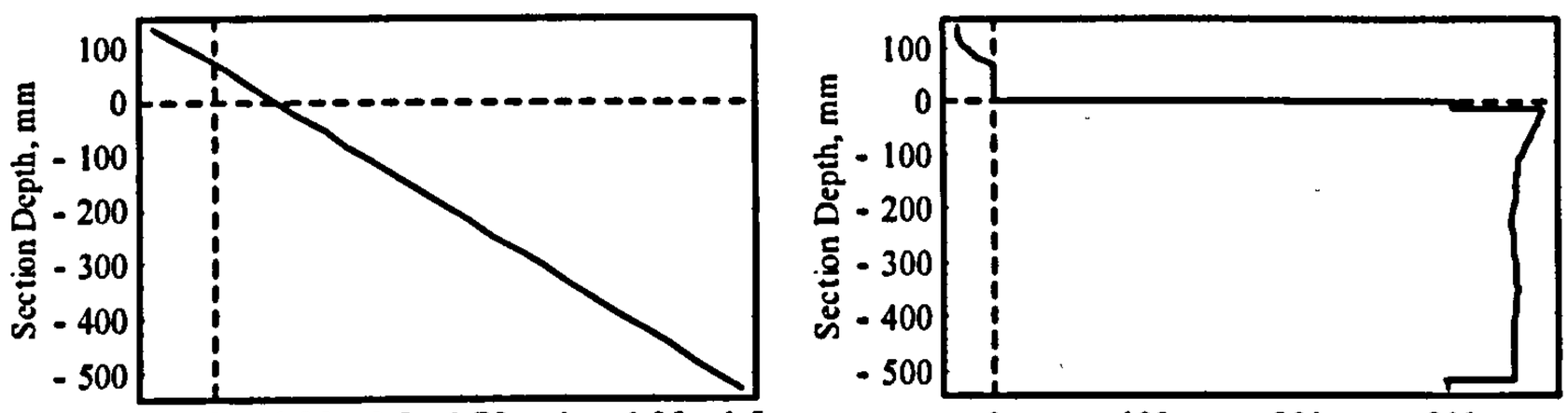

a. Total load strain distribution

b. Total load stress distribution

Figure 5-7. Strain-Stress distribution across the composite section depth subjected to sagging moment in the case of propped construction (bottom flange strain= 1.5%)

Figure 5-8 and Figure 5-9 show the total load stress distribution throughout a composite cross-section of the test beam itself, calculated for an imposed load strain in the lower flange of 1% at maximum dead load strains of 0.1% and 0.5% respectively. Thus achieving the final strain at the bottom flange of 1.1% and 1.5% respectively. These figures show the influence of dead load strain distribution in the unpropped construction.

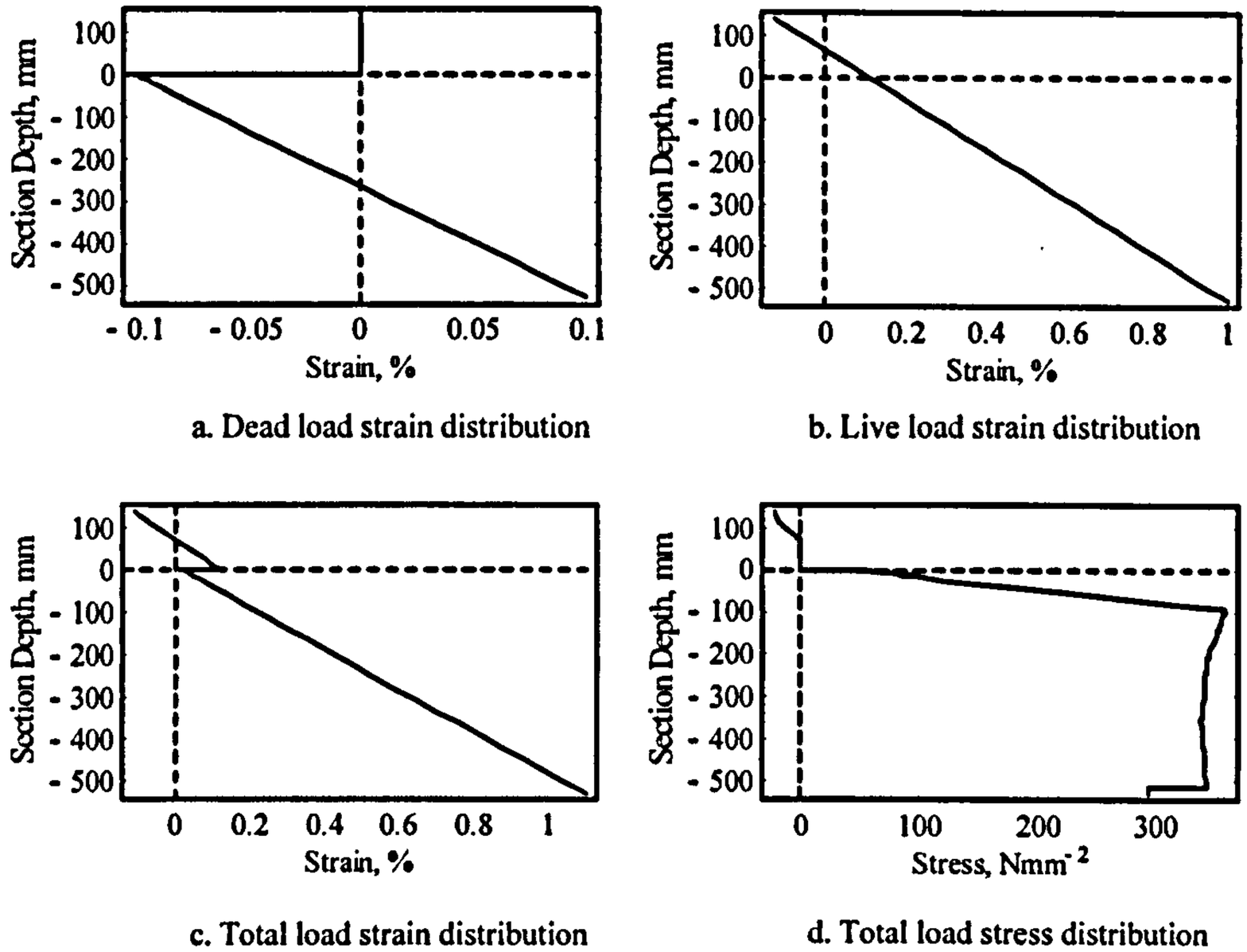

a. Dead load strain distribution

b. Live load strain distribution

c. Total load strain distribution

d. Total load stress distribution

Figure 5-8. Strain-Stress distribution across the composite section depth subjected to sagging moment (ε_d = 0.1% and ε_l =1%)

In the case of dead load strain of 0.1% (Figure 5-8c & d), the neutral axis of the composite section lies 73mm above the steel-concrete interface in the concrete slab i.e. the compressive capacity of the concrete slab over its effective width is greater than the tensile capacity of the steel section. The moment capacity and the curvature of the composite beam at this stress condition are 1421kN.m and 0.0227m^{-1}. Though considerable compressive stresses are locked into the top half of the steel section (Figure 5-8a) under the additional composite loading of strain 1% these locked up compressive stresses are converted into tensile stresses. This required an additional curvature of 0.0019m^{-1} i.e. 9% increase in curvature than the propped construction case (Figure 5-6).

In the case of a dead load strain of 0.5% (Figure 5-9c & d), the neutral axis of the composite section lies 98mm below the steel-concrete interface, in the steel web i.e. the compressive capacity of the concrete slab over its effective width is less than the tensile capacity of the steel web section. The moment capacity and the curvature of the composite beam at this stress condition are 1372kN.m and 0.0378m^{-1} in the case of higher dead load strain level, even the additional live loading strain of 1% is insufficient to convert the steel beam top compressive stresses into yield stresses. This results in a reduction in the lever arm and thus results in a lower moment capacity. It can be noted that at a strain of 1.5% in the bottom flange, in a 34% increase in curvature is required to convert the compressive top flange stresses into tensile yield stresses.

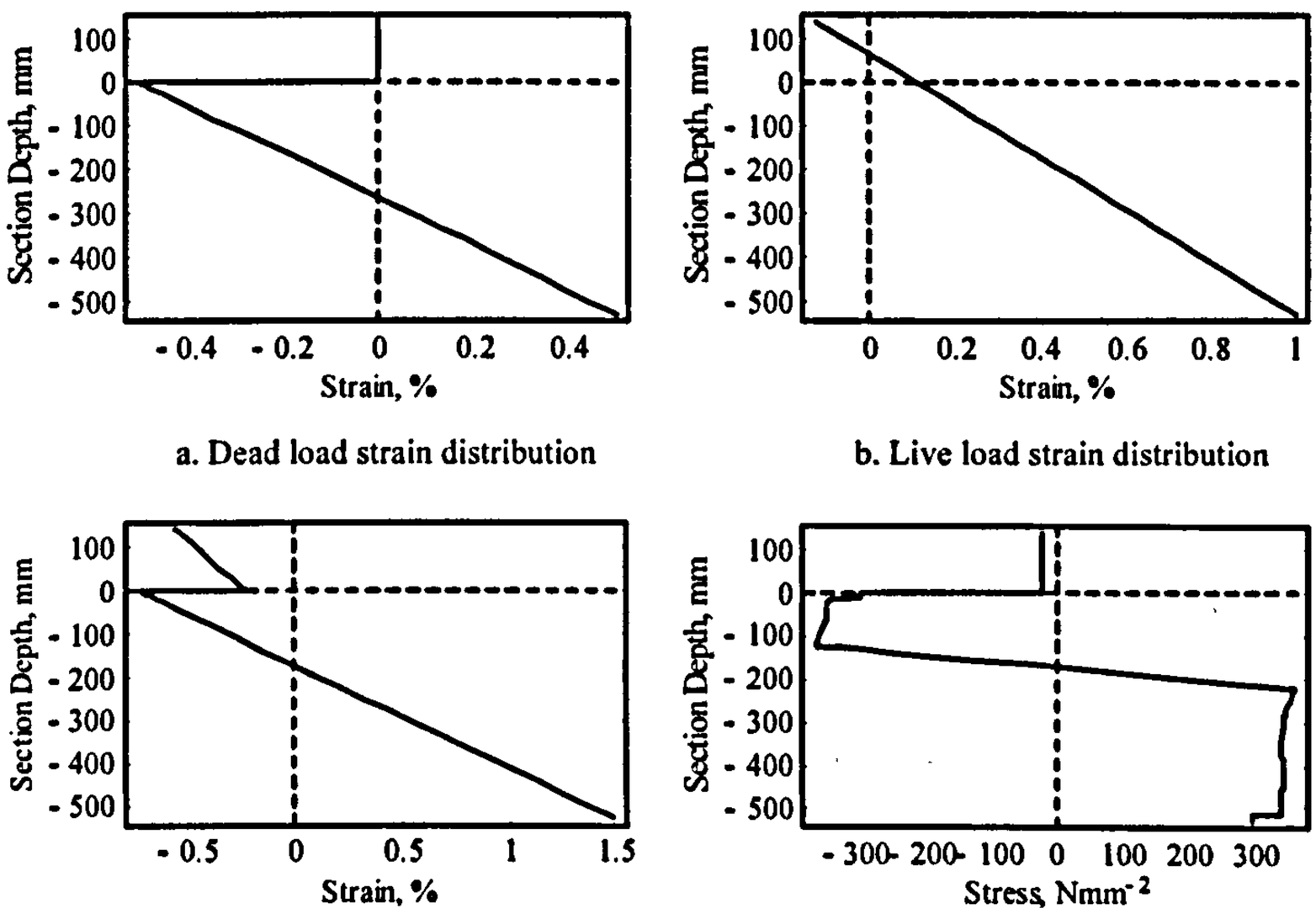

Figure 5-9. Strain-Stress distribution across the composite section depth subjected to sagging moment (ε_d = 0.5% and ε_l =1%)

The above discussion illustrates increase in curvature resulting from the unpropped mode of construction. Since the end rotation is given by the integral of curvature, an increase in the required rotation capacity will result. This increase is significant because the bottom flange strains are non-elastic and therefore produce disproportionately large curvatures.

5.2.2 Composite section in hogging

A similar procedure as that outlined in section 5.2.1 is repeated to determine the 3D interpolation function relating moment, curvature and dead load strain for the unpropped experimental composite section under hogging. For each value of moment and dead load strain, a curvature value can be obtained from this 3D interpolation function, Figure 5-10 .

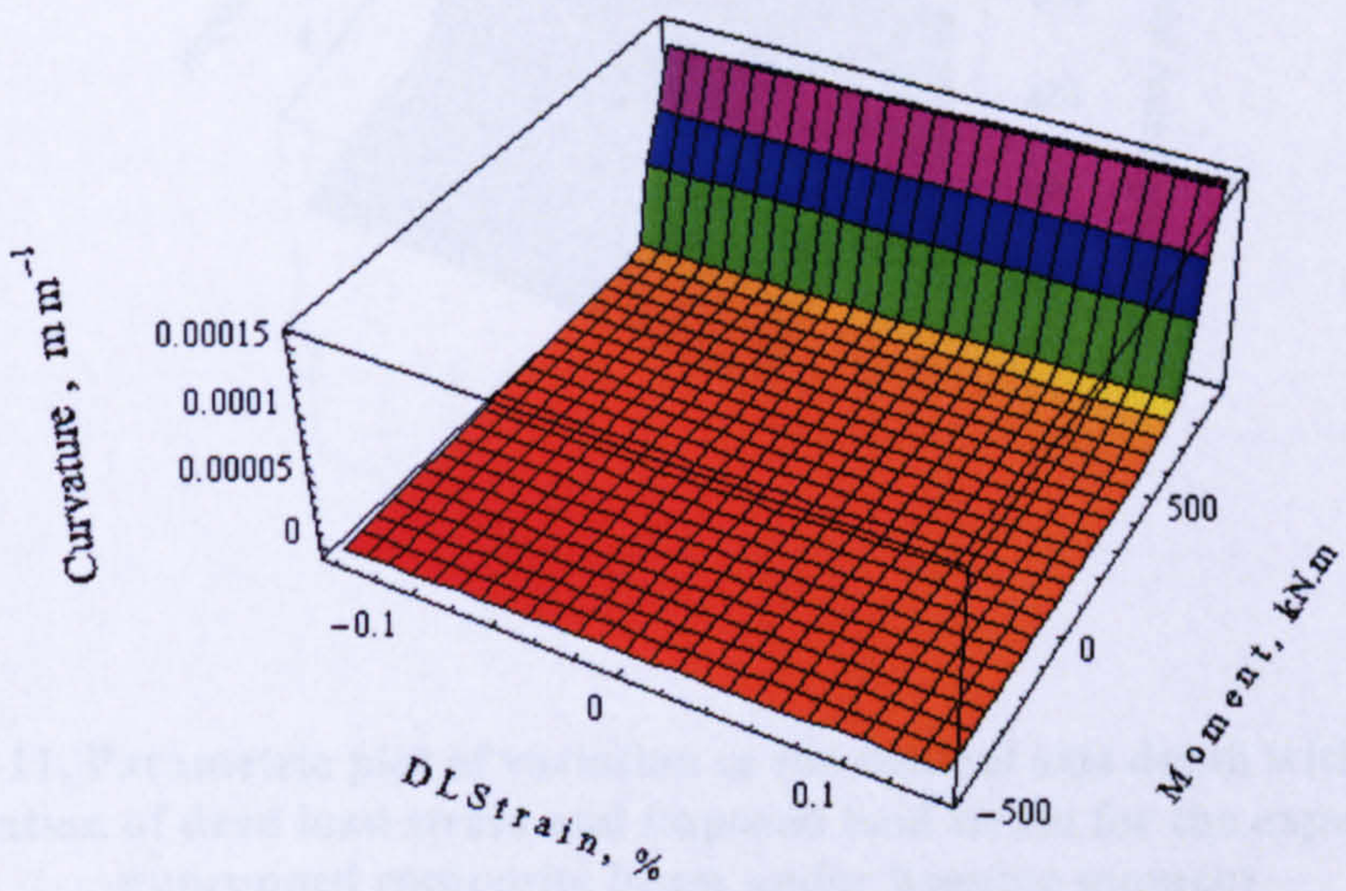

Figure 5-10. Moment-curvature-dead load strain relationship for the experimental unpropped composite beam section subjected to hogging moment

The tensile forces in the reinforcement bars that comprise the composite connection are included in the moment calculations. This is justified because the reinforcement bars are anchored past the point of contra-flexure. The position of the neutral axis is adjusted during the analysis until the normal forces balance. The concrete is assumed to be cracked and to have zero tensile stress. As previously, the strain distribution throughout the section is assumed to be linear.

Effect of dead load strain on the curvature

A parametric plot, Figure 5-11, is presented to illustrate the variation in the neural axis depth for the test composite beam under hogging moment for different combinations of dead load strain and imposed load strain.

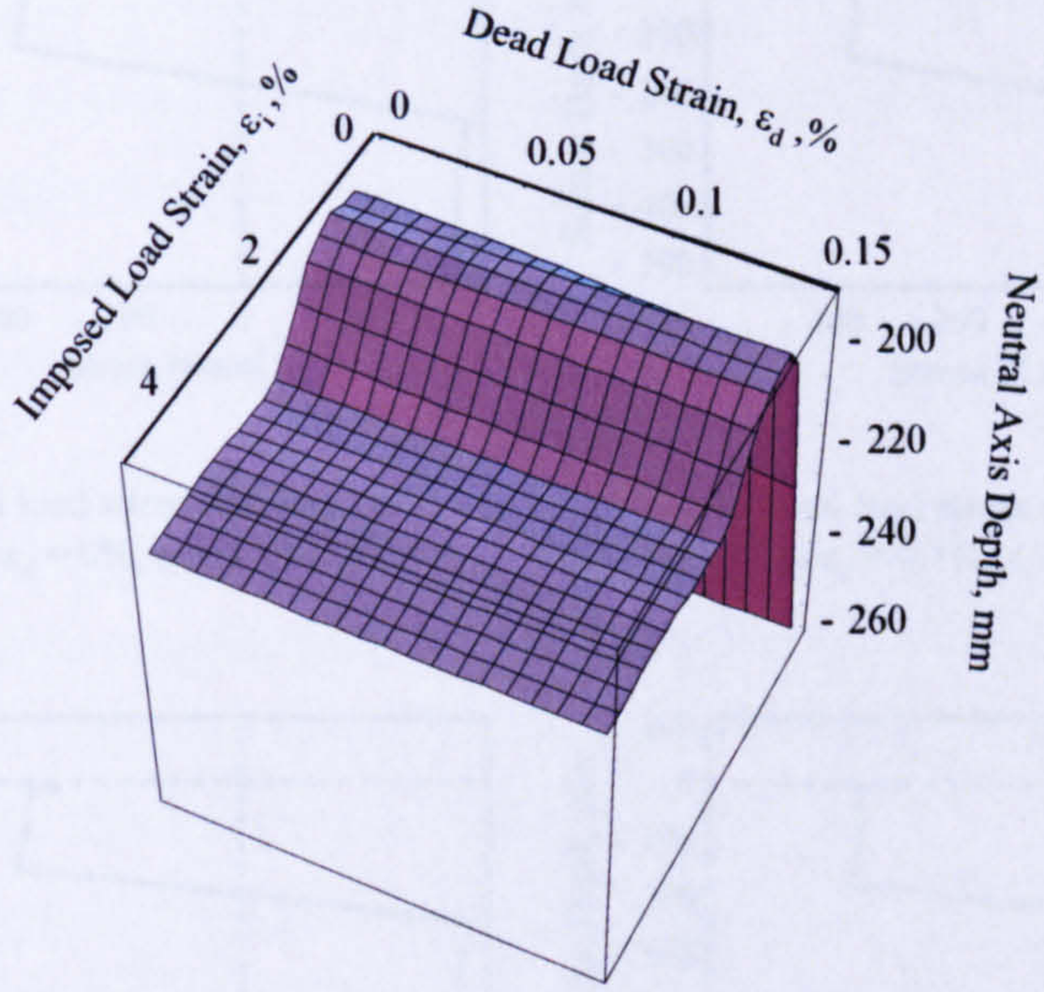

Figure 5-11. Parametric plot of variation in the neutral axis depth with different combination of dead load strain and imposed load strain for the experimental unpropped composite beam under hogging moment

In this figure, neutral axis in the steel section is presented with a negative sign and neutral axis in the concrete slab is presented with a positive sign. Unlike the composite beam section under sagging moment, for a dead load strain of up to 0.15% (i.e. the yield strain of the steel section), the neutral axis always lies in the steel section regardless of the imposed load strain increase. This is due to the fact that both under the construction and composite stage loading the rebar and the top part of the steel section will be under tension and the bottom part of the steel section remains under compression. The test composite beam flange and web section are Class 1 (plastic) i.e. a plastic hinge can be developed with sufficient rotation capacity to allow redistribution of moments within the structure prior to local buckling. In the test beam, a plastic hinge was developed and allowed the redistribution of moments at the internal composite connections. Significant flange and web local buckling was observed at the internal composite connections at the frame failure. However, in the model the weakening effects of local buckling were

ignored because the test beam is Class 1 section and the composite connections are partial strength.

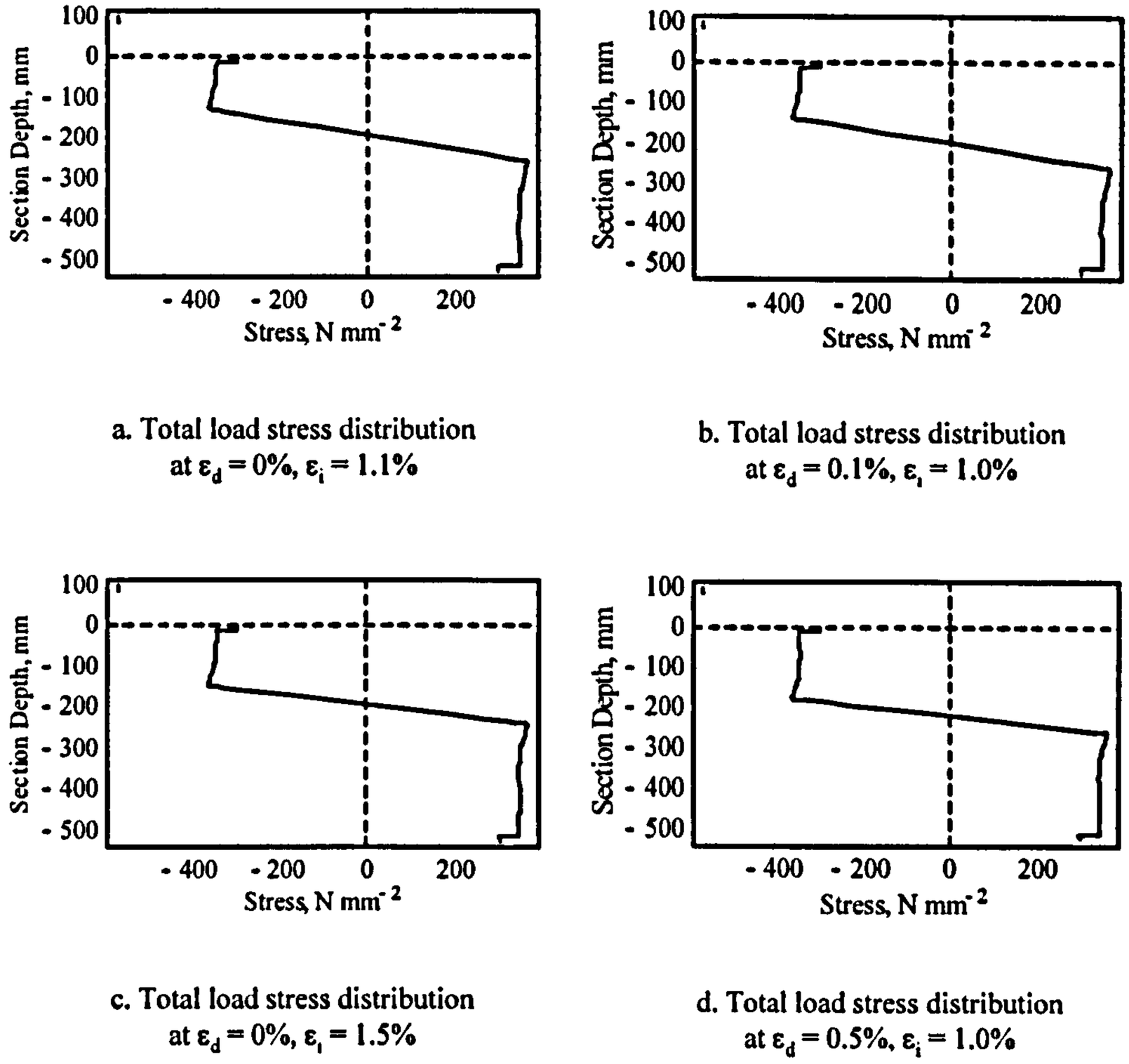

a. Total load stress distribution at $\varepsilon_d = 0\%$, $\varepsilon_i = 1.1\%$

b. Total load stress distribution at $\varepsilon_d = 0.1\%$, $\varepsilon_i = 1.0\%$

c. Total load stress distribution at $\varepsilon_d = 0\%$, $\varepsilon_i = 1.5\%$

d. Total load stress distribution at $\varepsilon_d = 0.5\%$, $\varepsilon_i = 1.0\%$

Figure 5-12. Comparison of total load stress distribution across the composite section depth subjected to hogging moment in the case of propped construction (a&c) and unpropped construction (b&d)

Figure 5-12 b&d shows a typical stress distribution for the test beam calculated for a cross-section located next to a composite connection, i.e. Region C in Figure 5-1 where there is hogging. This figure was calculated for the same extreme fibre strain as in the sagging configuration shown in Figure 5-8 and Figure 5-9, although in the hogging case the neutral axis lies within the steel web. The stress in the reinforcement is calculated for an imposed load strain in the lower flange of 1% at maximum dead load strains of 0.1% and 0.5% respectively and can be seen at the top of the figure. In both cases the neutral axis lies in the steel web with moment and curvature of 767kN.m, 0.0329m^{-1} and 768kN.m, 0.0452m^{-1} respectively.

Figure 5-12 a&c shows a typical stress distribution for the case of propped construction using the same the test beam material and geometric properties for a bottom flange strain of 1.1% and 1.5% respectively. In both cases the neutral axis lies in the steel web with moment and curvature of 767kN.m, 0.0329m^{-1} and 768.5kN.m, 0.0452m^{-1} respectively. This comparison shows that the effect of dead load strain on the curvature in the case composite section under hogging moment is negligible.

5.2.3 Steel section without composite action

The procedure outlined in section 5.2.1 is repeated for a section subjected to hogging moments, and adjacent to a nominally pinned connection, as in Region A in Figure 5-1. All stresses in the concrete were ignored. The steel section 2-D moment-curvature interpolation function for the test beam is shown in Figure 5-13 where for each value of moment, a curvature value can be obtained. This relationship is used in the construction stage analysis and also for the composite section in hogging adjacent to the pinned connection.

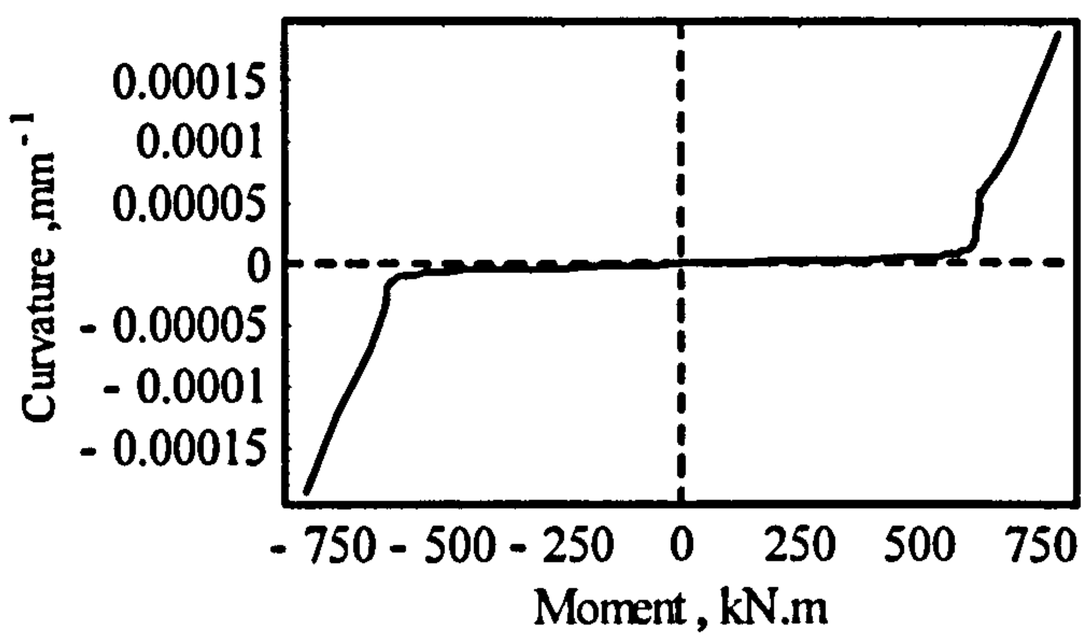

Figure 5-13. Moment-curvature relationship for the experimental steel section without composite action

5.3 Modelling of load-deformation relationship

Once interpolation functions have been established to model the interaction between moment, curvature and dead load strain, it is a relatively trivial process to calculate the distribution of curvature and deflection under either construction or post-construction loads. The beam subjected to a dead load during construction is analysed to determine the moment-rotation and load-deflection responses using the 2-D steel section moment-curvature-dead load strain relationships. Subsequently, the composite beam subjected to imposed load is analysed using the 3-D moment-curvature-dead load stress relationships.

Construction stage. The loading and beam boundary conditions enable the moment distribution along the beam to be calculated at a number of locations. The 2-D moment-curvature interpolation function for the steel section enables the curvature distribution to be calculated. The distribution of deflection, v, is defined by double integrating the curvature distribution using the support displacements as boundary conditions, i.e.:

$$v = \iint \phi \, dz \tag{4}$$

where L is the length of the beam. The slope distribution can then be defined by differentiating the deflection, i.e.:

$$\theta = \frac{dv}{dz} \tag{5}$$

Composite stage. The moment distribution along the beam can be calculated from the applied loading and the dead load strain distribution imposed during the construction stage. This enables the curvature distribution along the beam to be calculated for each of the regions shown in Figure 5-1. The distribution of deflection and slope can then be calculated from the curvature in the same manner as described for the construction stage. Consequently the overall deformation is deduced from both the construction and composite stage responses.

5.4 Comparisons between experimental and analytical studies

Results for the north composite beam and the south composite beam from the full-scale composite sub frame test [Dhanalakshmi *et al.*, 2002] unpropped during construction as reported in Chapter 3 were used for assessing the accuracy of the model.

5.4.1 Experimental north beam

The theoretical distributions of dead load strain, moment, curvature, slope and deflection for the experimental north beam condition at the construction stage loading and also composite loading corresponding to sagging moments of $0.85M_p$, M_p and $1.15M_p$ are shown in Figure 5-14. The value of M_p (beam plastic design moment) was calculated using the measured material and geometric properties of a test specimen. Comparison of the results for the predicted and experimental deflection and rotation responses to the same load are presented in Table 5-1.

Table 5-1. Comparison of calculated and measured deflections and end rotations for the north beam

	Deflection (mm)						Beam end rotation (°)			
	Quarter span		**Mid-span**		**Third quarter span**		**Adjacent to exterior column**		**Adjacent to internal column**	
Loading	Num.	Exp.	Num.	Exp.	Num.	Exp.	Num.	Exp.	Num.	Exp.
Construction stage	4.12	4.20	5.62	6.57	2.79	2.92	0.066	0.059	0.004	0.007
$0.85M_p$	31.23	39.05	44.75	55.80	29.03	36.53	0.67	0.69	0.57	0.44
$1.00\ M_p$	90.19	90.83	143.80	134.08	95.40	88.16	1.84	1.64	1.89	1.66
$1.15M_p$	132.42	128.55	192.21	193.96	113.81	126.77	2.38	2.37	1.93	2.20

The curvature distribution (Figure 5-14:1b) is obtained using the 2D M-ϕ interpolation function (Figure 5-13) for the moment distribution due to dead load (Figure 5-14:1a). Deflections and end rotations (Figure 5-14:1c&d) are calculated from the curvature distribution as explained in Section 5.3 for the construction stage loading. Comparison of the theoretical values with the measured experimental results shows good accuracy.

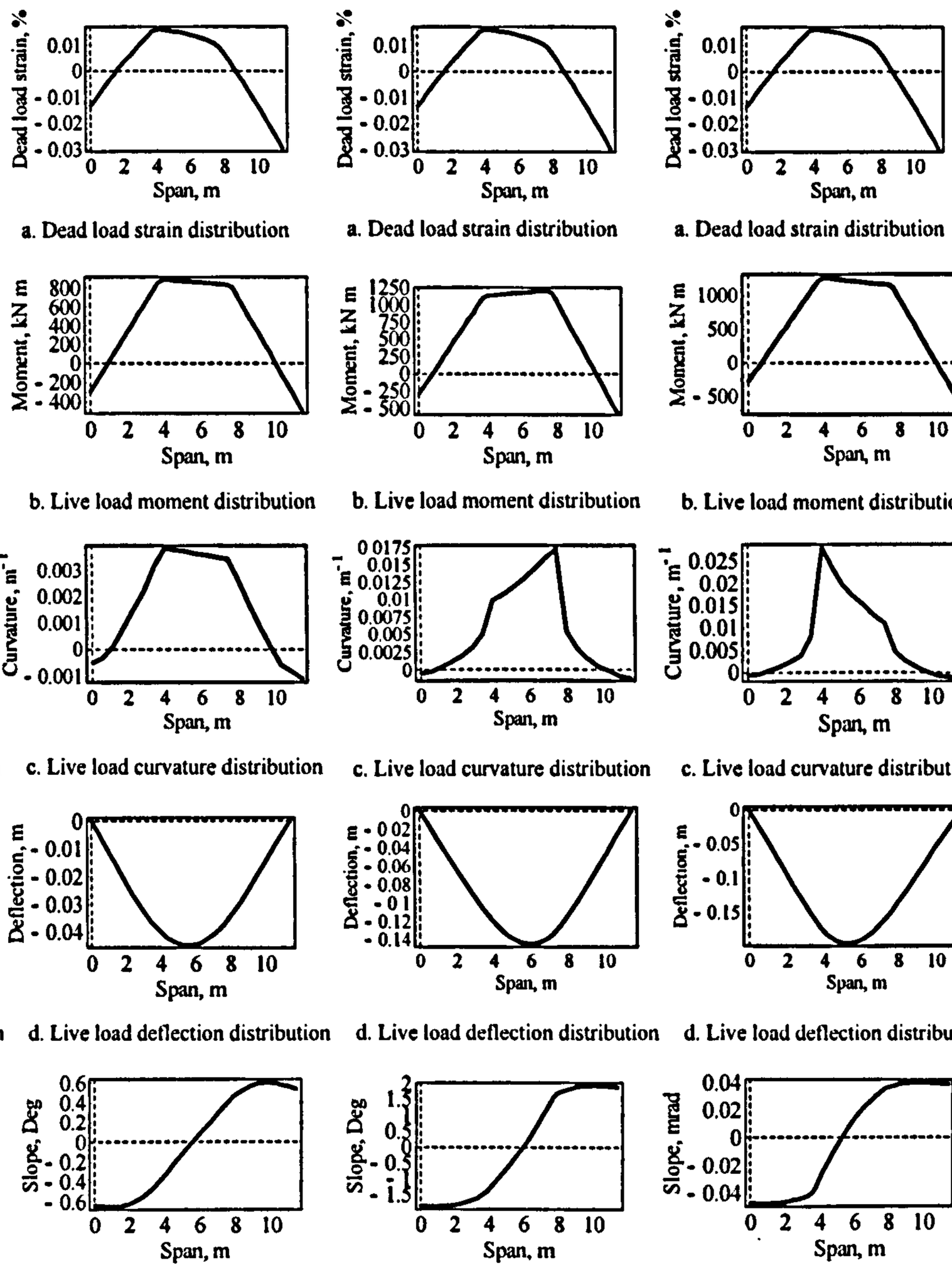

a. Dead load strain distribution | a. Dead load strain distribution | a. Dead load strain distribution

a. Dead load moment distribution | b. Live load moment distribution | b. Live load moment distribution | b. Live load moment distribution

b. Dead load curvature distribution | c. Live load curvature distribution | c. Live load curvature distribution | c. Live load curvature distribution

c. Dead load deflection distribution | d. Live load deflection distribution | d. Live load deflection distribution | d. Live load deflection distribution

d. Dead load slope distribution | e. Live load slope distribution | e. Live load slope distribution | e. Live load slope distribution

1. Construction stage loading | 2. 0.85Mp loading | 3. 1.00Mp loading | 4. 1.15Mp loading

Figure 5-14. Dead load strain, moment, curvature, deflection and slope distribution for the north beam under construction stage and composite stage loading corresponding to sagging moments of $0.85M_p$, $1.0M_p$ and $1.15M_p$

As it can be seen in Figure 5-14:1a, the dead load strain (or stress) at the sagging region is only 10% of the yield strain (or stress) which implies very low dead load compared to the practical situation. For this dead load strain distribution in combination with the moment

distribution at loads corresponds to sagging moment of $0.85M_p$ (Figure 5-14:1b) deflections and end rotations are calculated using the 2D M-ϕ and 3D M-ϕ-ε_d interpolation functions. Similarly deflections and end rotations are calculated for loads correspond to $1.0M_p$ and $1.15M_p$.

Figure 5-14 :2b, 3b & 4b show that the curvature adjacent to the connections is very small in comparison to that in the central section of the beam. Therefore, deflection and slope are most influenced by the non-elastic deformation of the mid-section of the beam. Comparison of the results (Table 5-1) for the predicted and experimental responses to loads corresponding to sagging moments of 0.85, 1.00 and $1.15M_p$ show good accuracy. The comparison between predicted and experimental values of deflection is shown graphically in Figure 5-15 for a load level corresponding to $1.0M_p$.

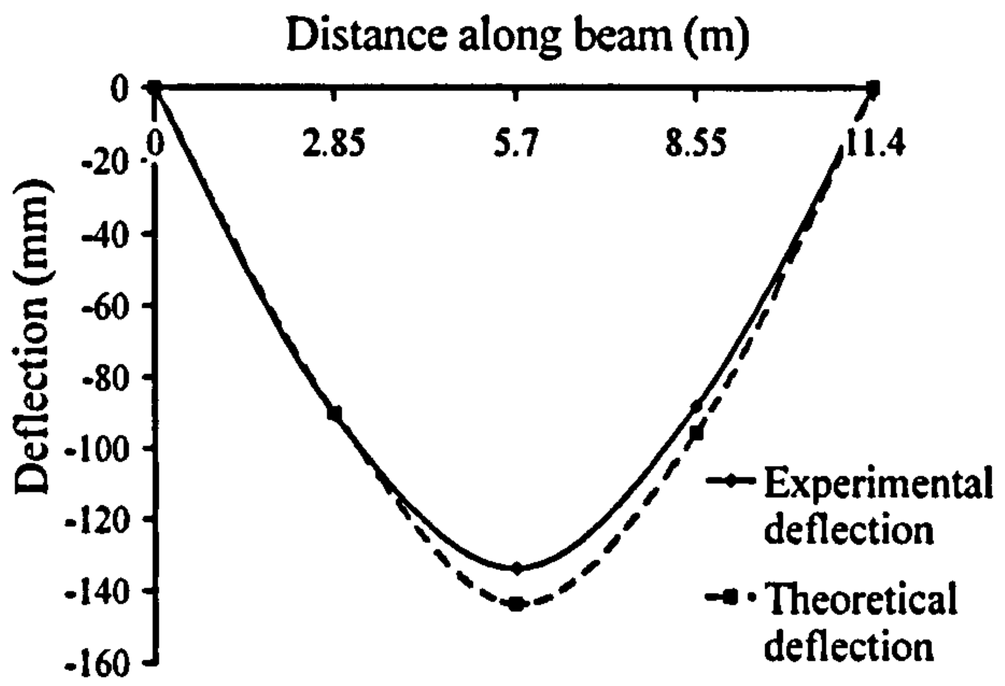

Figure 5-15. Comparison between theoretical and experimental deflections at loading corresponding to $1.0M_p$ for the north beam

In theory, $1.0M_p$ should represent the maximum moment generated in the beam. The primary reason M_p was exceeded during the test was because the yield stress ($294N/mm^2$) was calculated using coupon tests of flange material. The web material has a significantly higher yield stress than the flange ($343N/mm^2$). This additional strength made a significant contribution to the beam sagging moment capacity. The model accounted for this effect because it employed separate stress-strain interpolation functions for the flange and web. Furthermore, the maximum strain in the flange at $1.15M_p$ was approximately

1.8% (calculated from the numerical model). This level of strain would have resulted in significant strain hardening, raising the flange stress to around 316N/mm^2. This effect would also have contributed to the over strength performance observed in the test.

The data in Table 5-1 shows that the predicted rotations compare closely to the measured values, even at the large deformations associated with loading of 1.15M_p. Thus it can be seen the theoretical model is a reliable predictor of end rotation and deflection. It can therefore be used for assessing connection rotation requirements for composite beams with composite connections at both ends.

As discussed previously, the concrete stress-strain relationship presented in BS8110 [1997] was used for modelling purposes. The results from the model show that the plastic plateau of this relationship, Figure 5-2c, was only reached at sagging moments beyond 1.0M_p. At a moment of 0.85M_p the maximum strain in the concrete was 0.04%. Therefore, inaccuracies in the concrete stress-strain function e.g. ignoring the tension stiffening of concrete [Kemp, 1998], should not affect the ability of the model to predict rotation requirements for design moments up to 1.0M_p.

5.4.2 Experimental south beam

The theoretical distributions of dead load strain, moment, curvature, slope and deflection for the experimental north beam condition at the construction stage loading and also composite loading corresponding to sagging moments of 0.85M_p, M_p are shown in Figure 5-16. The value of M_p (beam plastic design moment) was calculated using the measured material and geometric properties of a test specimen.

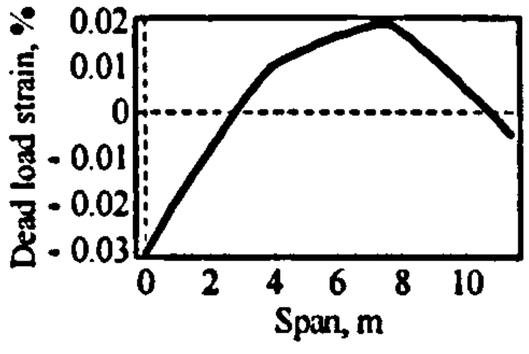

a. Dead load strain distribution

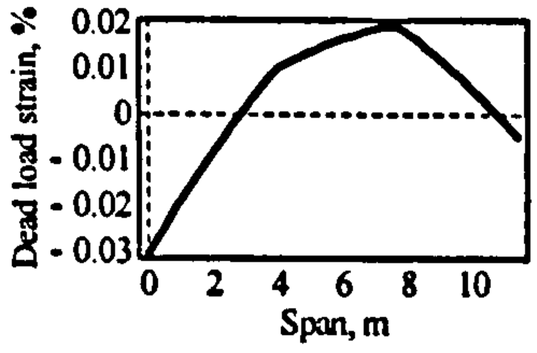

a. Dead load strain distribution

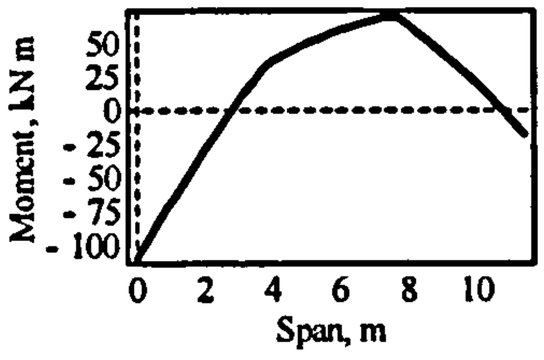

a. Dead load moment distribution

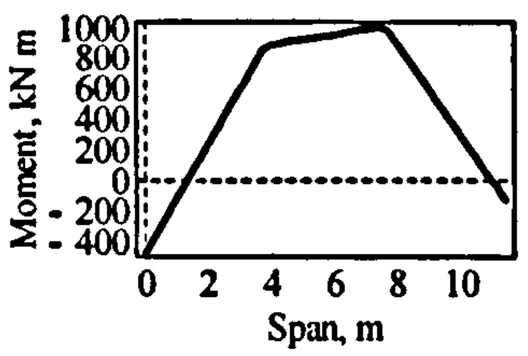

b. Live load moment distribution

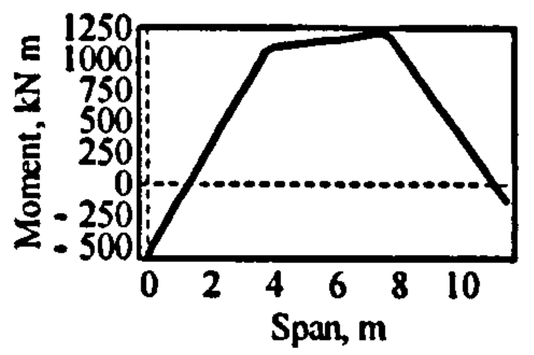

b. Live load moment distribution

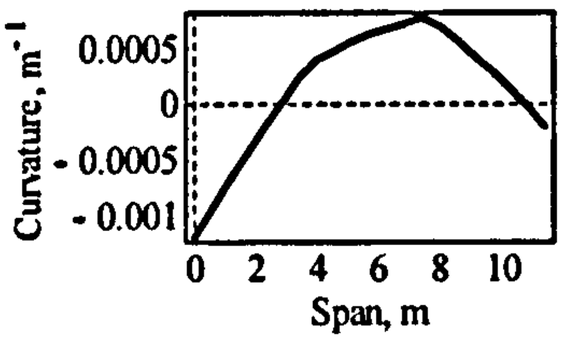

b. Dead load curvature distribution

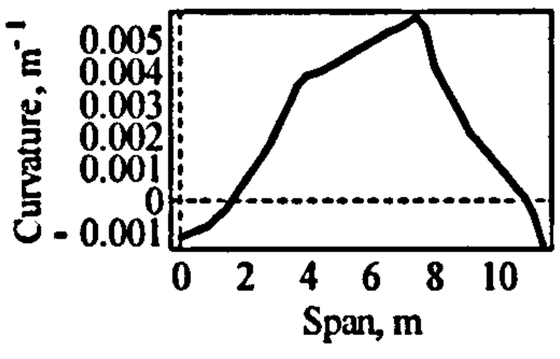

c. Live load curvature distribution

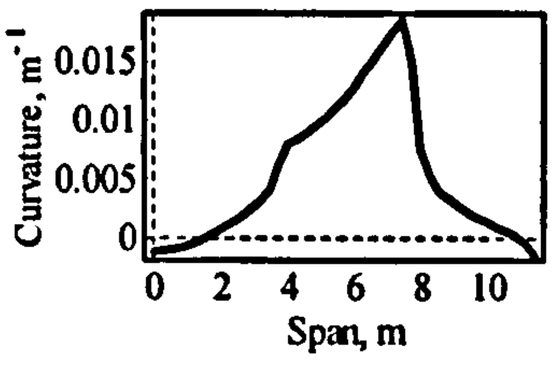

c. Live load curvature distribution

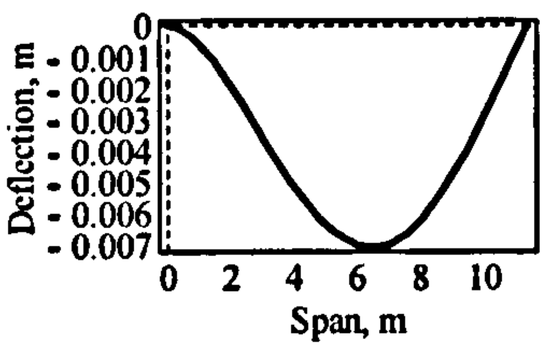

c. Dead load deflection distribution

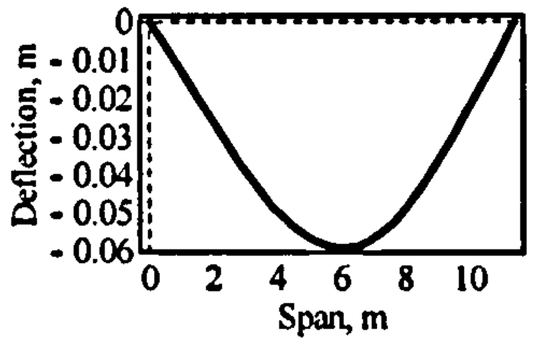

d. Live load deflection distribution

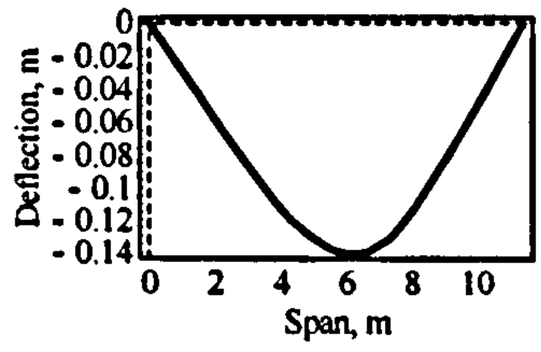

d. Live load deflection distribution

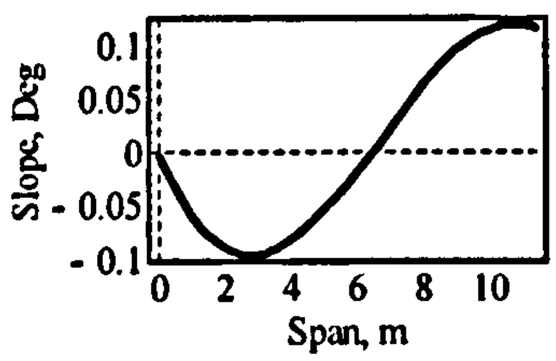

d. Dead load slope distribution

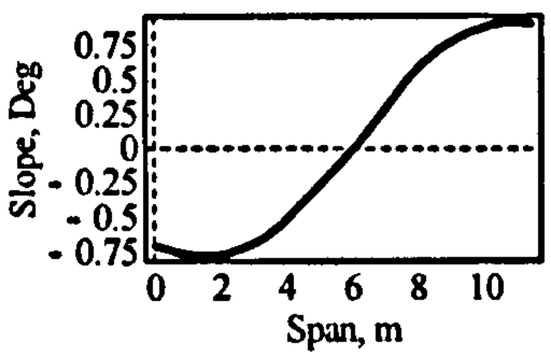

e. Live load slope distribution

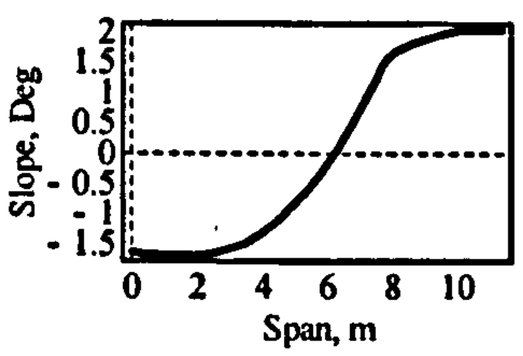

e. Live load slope distribution

1. Construction stage loading 2. 0.85Mp loading 3. 1.00Mp loading

Figure 5-16. Dead load strain, moment, curvature, deflection and slope distribution for the south beam under construction stage and composite stage loading corresponding to sagging moments of 0.85Mp and 1.0Mp

Comparison of the results for the predicted and experimental deflection and rotation responses to the same loads are presented in Table 5-2.

Table 5-2. Comparison of calculated and measured deflections and end rotations for the south beam

	Deflection (mm)						Beam end rotation (°)			
	Quarter span		**Mid-span**		**Third quarter span**		**Adjacent to exterior column**		**Adjacent to internal column**	
Loading	Num.	Exp.	Num.	Exp.	Num.	Exp.	Num.	Exp.	Num.	Exp.
Construction stage	3.30	3.50	6.83	7.67	5.51	5.72	0.117	0.100	0.004	0.055
$0.85M_p$	37.40	38.90	58.97	61.05	42.60	44.70	0.90	1.54	0.11	0.73
$1.00M_p$	83.40	88.50	138.90	145.30	97.70	108.20	2.01	2.63	1.65	1.48

As the measured strain values correspond to a sagging moment of $1.15M_p$ for the south beam are not reliable and so the results are. Therefore there is no comparison for the loading corresponds to $1.15M_p$ as in the case of north beam. The data in Table 5-2 shows that the predicted deflections and rotations compare closely to the measured values even at the plastic moment capacity level.

5.4.3 Comparisons with other existing test results

It is agreed in principle in the research community that any researcher's model has to be validated not only with the experimental results carried out by the same researcher but also against the existing test results by other researchers. The numerical model as presented in this chapter is built on the foundation principle of known material properties of steel flange, steel web and concrete. If the model is used to back-analyse a test result then the exact measured values of these parameters must be used. Hence the results of the model are sensitive to the variation in stress-strain properties of test steel section in the plastic range. If the design sagging moment considered is more than $0.85M_p$ then the role of strain-hardening becomes a critical factor in the required rotation. Though there are several experimental moment-rotation values for composite beams under propped construction (very few tests have been undertaken on unpropped construction) that are available from other researchers work, often there is no comprehensive report of the

measured material properties of the section used in the test. Because of the absence of sufficiently comprehensive information on measured material properties, it can be expected that a discrepancy would occur in the comparison between numerical and test results which could not then be attributed to limitations in the numerical model without some doubt on the role of uncertainties in important measured properties. Therefore a specific decision has been taken not to attempt any further validations of the model reported herein against other existing results.

5.5 Conclusions

A fully analytical method has been presented for modelling the non-elastic response of unpropped composite beams to loads generated during construction and subsequent operation. The method uses interpolation functions to model the non-linear material properties of the steelwork, reinforcement and concrete. These functions are used to construct 2D moment-curvature responses for composite beams resisting defined levels of dead load strain. A series of these 2D functions are compiled to form a 3D function of dead load strain, curvature and applied moment. A similar technique is used for characterising the moment-curvature relationship of composite beams subjected to hogging moments due to operating loads applied after construction. Thus, the distribution of curvature in a beam can be determined given the dead and imposed load bending moment distributions. The curvature distribution may be double integrated, with support displacements as boundary conditions, to determine deflected shape. Similarly, end rotation is determined by differentiating the distribution of deflection. The approach combines state-of-the-art numerical integration software with well-established principles of structural mechanics and non-linear material properties. The accuracy of the model was assessed via comparison with results from a 24m long double H-frame test carried out specifically for the investigation reported. The frame used unpropped composite beams and incorporated composite connections. The comparison between theoretical and experimental deflections and end rotations was carried out at loads up to and beyond the design load capacity of the frame. The results show that the modelling technique achieves a very high degree of accuracy and can therefore be used to assess the ductility requirements of composite connections for use with unpropped composite beams. The

technique can also be used to establish the response of composite beams to large sagging deformations.

Chapter 6 - Assessment of the use of composite connections with unpropped composite beams

Papers published based on this chapter:

1. Byfield, M. P., M. Dhanalakshmi and Couchman. G. H. (2004). "Assessment of the use of composite connections with unpropped composite beams", Journal of Constructional Steel Research, Volume 60, 1369-1386.

2. Byfield, M. P., M. Dhanalakshmi, Couchman, G. H. and Goyder, H. G. D. (2005) Limitations in the use of composite connections with unpropped construction, *Eurosteel 2005 conference*.

6.1 Introduction

In semi-continuous frames the flexural strength of the connections is significantly less than that of the beams. Therefore, significant moment redistribution from the supports to spans is necessary in order to utilise anything approaching the full flexural strength of the span. This places a significant requirement on the rotation capacity of the connections.

In order to determine the potential for moment redistribution it is essential to know not only the maximum rotation available from the connection (available rotation capacity), but also the beam end rotation required to achieve the design moment in the span (required rotation capacity). The available rotation capacity has to be greater than the required rotation in order to utilise a given proportion of the flexural strength of the beam, typically between 0.85 and $1.0M_p$. Therefore, it is important to quantify both the available and required rotations during the development of design guidance. Considerable research work has been carried out to quantify these two parameters. A comprehensive review of the research work on available and required rotations is presented in Chapter 2.

Based on the results of these investigations, design and detailing rules [COST C1 (1997) and SCI (1998)] have been developed. These take into account both strength and ductility requirements. In many situations it is necessary to limit the design moment in the span to $0.85M_p$, in order to ensure that the available rotation capacity exceeds the requirements from the beams. However, widespread use of composite connections is unlikely before they can be used with unpropped beams. Although the strength requirement for both forms of construction remains the same, the ductility requirement differs. It therefore becomes necessary to revise the design rules for composite connections, which are currently focussed towards the propped mode of construction [SCI, 1998].

The available rotation capacity is generally limited by the ductility of the reinforcement. In view of this it has also been found necessary in many cases to limit standard design guidance to use with high ductility reinforcement [SCI, 1998], sometimes referred to as X-type rebars. In unpropped construction the connection reinforcing bars resist only post-construction loads. Therefore, the end rotations resulting from dead loading place no strain on the reinforcement, thus increasing the available rotation capacity. However, this improvement in performance may be more than offset by a substantial increase in the rotation requirement. During construction significant compressive strains occur in the top half of the steel section. In order to develop the final state (composite beam) moment in the span, typically $0.85M_p$, significant curvature is required to raise the neutral axis to the region of the beam/slab interface. Since the end rotation is given by the integral of curvature, an increase in the required rotation capacity in comparison with propped construction will result. This increase can be very significant, because the bottom flange strains are non-elastic and therefore produce large curvatures.

Researchers [Anderson and Najafi (1997), Couchman (1992) and Gibbons (1992)] suggest that the increased rotation requirement could be as high as 40% compared with the propped case. What was not clearly understood prior to this investigation was at what level of dead load stress this increase would occur. In order to assess the design rules, it becomes necessary to know the effect that this dead load stress will have on the percentage increase in the required rotation associated with unpropped constructions.

Having achieved a very high degree of accuracy in predicting the end rotations and displacements of unpropped test composite beams using the modelling technique presented in Chapter 5, an extensive parametric study is presented, carried out using this technique to establish the scope for extending the use of composite connections to unpropped beams. The numerical model for this parametric study is presented in Appendix B.

This chapter presents the results from a parametric study carried out to assess under which conditions composite connections can be safely used with unpropped composite beams. A total of 2160 different beam configurations have been considered, utilising different steel grades and loading conditions. The critical factor affecting the required rotation capacity of the connections is found to be the level of dead load stress developed by a beam prior to hardening of the concrete, as this has a big influence on the beam deflections.

The influence of several other factors has also been assessed. These include:

1. Span to depth ratio
2. Location within the building frame
3. Ratio between the Support (connection) moment capacity and Span (beam) moment capacity ($M_{support} / M_{span}$)
4. Loading type
5. Steel grade and
6. Percentage of the beam strength utilised during design

The connection rotation capacity requirements resulting from this study are then compared with the rotation capacity of industry standard composite connection details.

6.2 Assessment of the rotation capacity requirements

The parametric study presented in this chapter has been carried out using the numerical model described in the Chapter 5 of this thesis and also published [Byfield, Dhanalakshmi and Goyder, 2004]. The model was validated using test results from a large (24m long),

unpropped double H-frame test carried out specifically as part of the present investigation. The experiment is reported in Chapter 3 of this thesis and is also published [Dhanalakshmi, Byfield and Couchman, 2002]. Comparison between experimental and theoretical response to load has shown excellent conformity, up to and beyond the design limit of the beam ($1.0M_p$). Using this model a range of different design scenarios have been considered in order to establish what can be considered as the worst-case design scenarios, thereby allowing simplified design rules to be developed for general use.

The parametric study was carried out on a medium size beam (406x178x60UB), supporting a slab 120mm deep, incorporating 50mm deep profiled metal decking. The composite connection details conform to industry standards [BCSA and SCI, 1998]. The concrete design strength was 30N/mm^2. Both exterior and interior beams have been studied. External refers to beams which have composite connections at one end and nominally pinned connections at the other. Internal beams have composite connections at both ends. All exterior connections were assumed to be partial depth end-plate, i.e. nominally pinned. Such connections are known to develop small bending moments [Dhanalakshmi, Byfield and Couchman, 2002]. Therefore a nominal bending moment of $0.05M_p$ has been assumed, where M_p is the design plastic moment of resistance of the composite section in sagging. The moment capacity of internal connections has been taken as $0.3M_p$, $0.4M_p$, $0.5M_p$ and $0.6M_p$.

The ratio between the maximum stress in the lower flange due to dead loads (prior to the hardening of the concrete) σ_{dl}, and the yield stress, σ_y, has been taken as 0.0, 0.25, 0.50, 0.75 and 1.0. Clearly, a σ_{dl}/σ_y ratio of 0.0 refers to a propped beam and a ratio of 1.0 represents the limit for an unpropped beam. Finally, the study determined the end rotations for beams subjected to mid-span design moments of 0.85, 0.90 and $0.95M_p$. The case of $1.0M_p$ was not considered because the rotation required from an unpropped beam to achieve this level of moment exceeds the practical limit for the connections.

A range of cases have been studied in a full combination of end conditions, support to span moment ratios and span to depth ratios. Each case has been carried out for both the S275 and S355 steel grades. A total of 720 unpropped beams were considered for values

of design moment corresponding to 0.85, 0.90 and 0.95M_p. Thus, the total number of unpropped beams considered was 2160. A flowchart describing the parameters covered in this study is shown in Figure 6-1.

The end rotation requirements from beams corresponding to a design moment of 0.85M_p, 0.90 M_p, and 0.95M_p are listed in Table 6-1, Table 6-2 and Table 6-3 respectively. Table 6-2 and Table 6-3 shows that the rotations required to achieve higher values of design moment are impractically high (see Section 6.2.4).

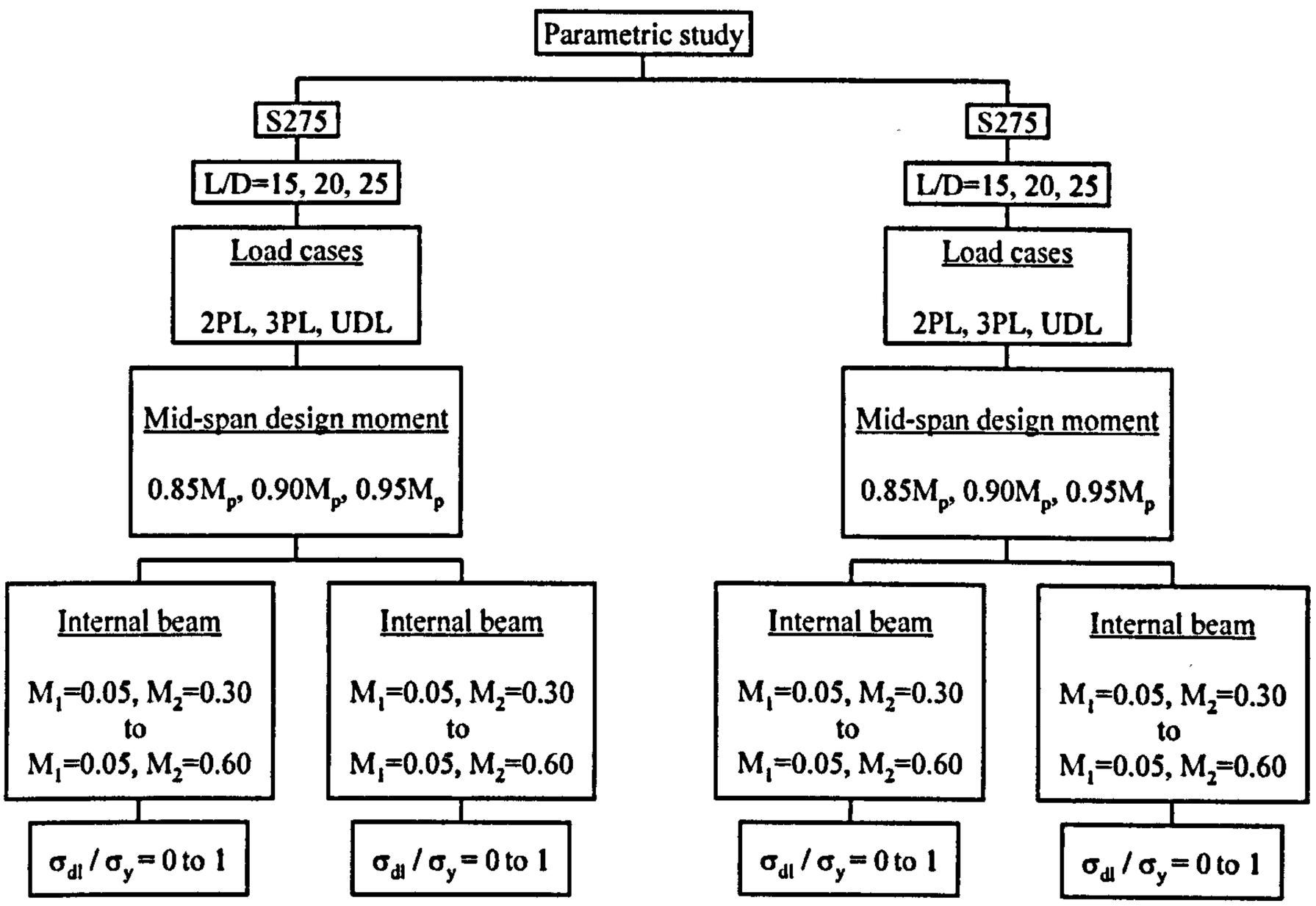

σ_{dl} Maximum stress under dead load and prior to the development of composite action
σ_y Yield stress
L Beam span
D Beam depth (inclusive of slab)
M_1 Ratio of first support to span design moment;
M_2 Ratio of second support to span

Figure 6-1. Flowchart of the factors considered in the parametric study

6.2.1 Effect of dead load stress on $\theta_{required}$

During unpropped construction the steel beam alone supports the entire dead load. In order to develop the design sagging moment additional curvature is required. The extent of this is demonstrated in Figure 6-2 and Figure 6-3, in which the beam moment-end rotation relationship is shown for varying degrees of maximum dead load stress for a typical internal and external beams comprising an S355 grade with $M_{support}/M_{span}$ = 0.3 and L/D = 20 respectively.

Figure 6-2 shows that required rotation capacity of the connection ($\theta_{required}$) to achieve $0.85M_p$ increases by 220% between the case of the fully propped (σ_{dl} = 0) and the case in which the yield stress is reached under construction loads ($\sigma_{dl} = \sigma_y$). The beam moment-end rotation relationship for all the other cases considered in the parametric study is shown in Appendix C.

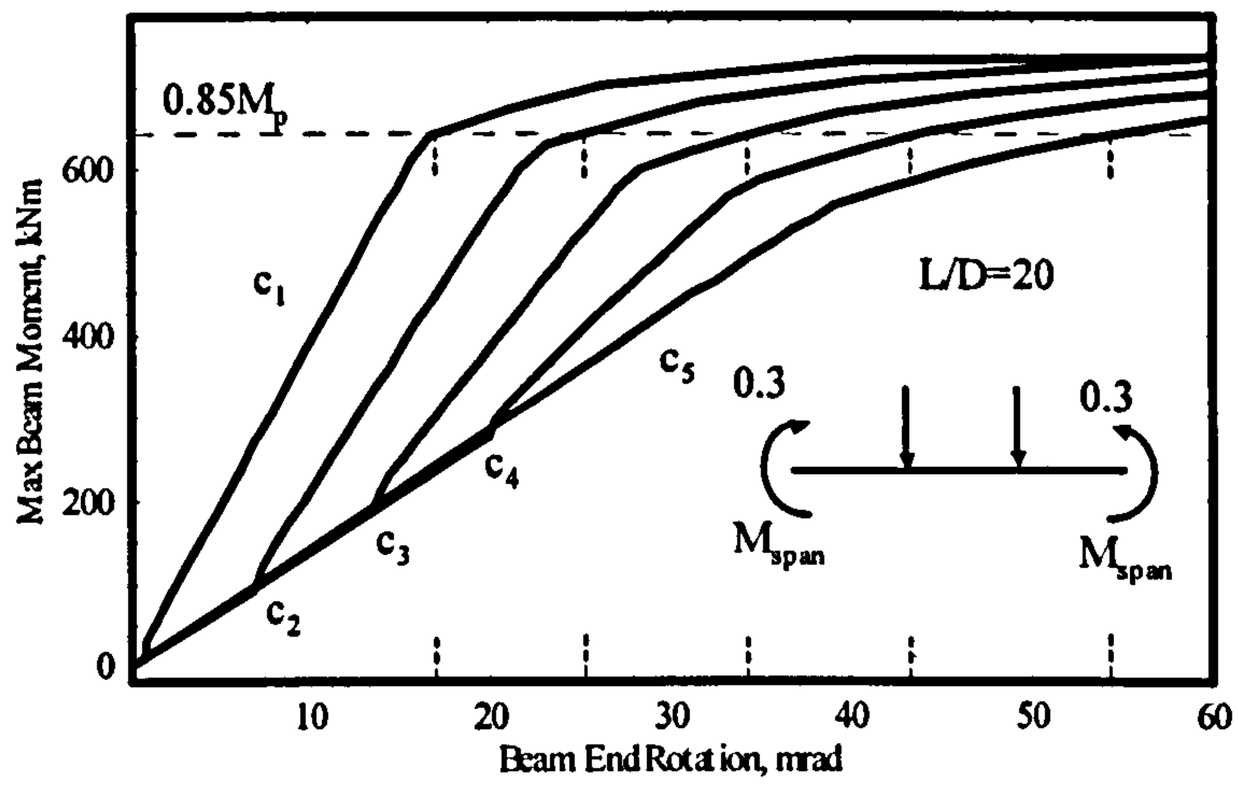

Figure 6-2. Moment vs. end rotation relationship for various maximum dead load stress levels for a typical internal beam, S355 (c_1 to c_5).

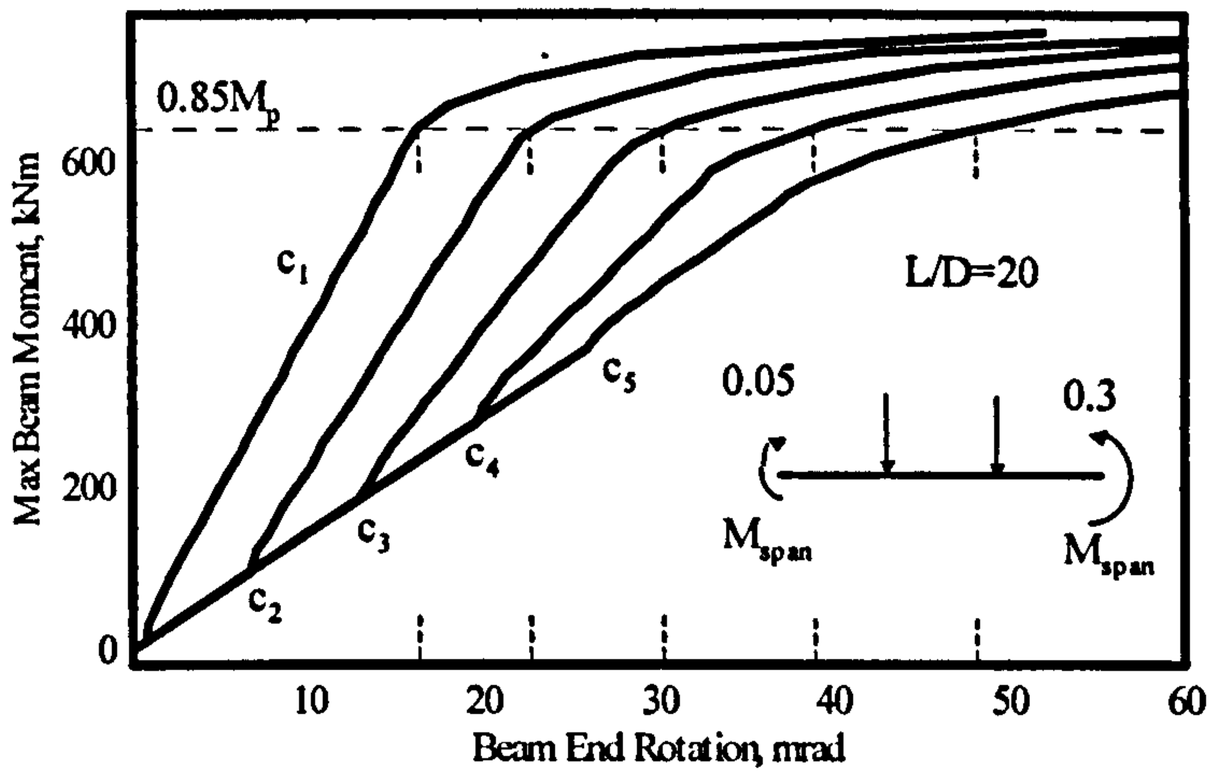

Figure 6-3. Moment vs. end rotation relationship for various maximum dead load stress levels for a typical external beam, S355 (c_1 to c_5)

Figure 6.2 and 6.3 Notes:

c_1: $\sigma_{dl} = 0$; c_2: $\sigma_{dl} = 0.25\sigma_y$; c_3: $\sigma_{dl} = 0.50\sigma_y$; c_4: $\sigma_{dl} = 0.75\sigma_y$; c_5: $\sigma_{dl} = \sigma_y$

An opportunity is taken at this stage to present typical values of the ratio of dead load stress to yield stress that could occur in construction practice. A worked example of the complete design of a typical unpropped semi-continuous composite beam is presented in Appendix D of this thesis. The size of the composite beam considered to suit the composite connection detail as given in the SCI 'Green book'. A beam span of 10m and steel grade S275 is considered. Steel beam size of 457x152x60UB is considered. The composite slab is 120 mm deep with 60 mm deep profiled metal decking as permanent soffit and spanning between beams spaced at 3m centres. An unfactored dead load of 3 kN/m^2 (the wet concrete weight, self-weight of the steel beam) and an imposed load of 0.5 kN/m^2 is considered as construction stage loading. An unfactored imposed load of 6 N/m^2 is considered under composite stage. The connection moment capacity at both construction stage and composite stage loading is considered to exceed 30% of the design beam moment capacity in sagging. Under construction loading, the steel beam meets the ULS and SLS requirements and under composite loading, the composite beam meets the ULS and SLS requirements. Refer Appendix D of this thesis for a complete design check. The main objective of this worked example is to show a typical value of dead load stress

to yield stress under unpropped construction and it is found to be in the range of 0.4 to 0.5 and therefore the third curve in Figure 6-2 will be more important.

Table 6-4 presents the percentage increase in required rotations from the case of fully propped to the case in which the yield stress is reached ender construction loads for all the cases analysed in the parametric study. It can be seen from Table 6-4 that the percentage increase in $\theta_{required}$ from propped to unpropped construction for S275 and S355 is almost similar for all different dead load stress levels.

Whether it is an internal or external composite beam, Table 6-4 shows:

$\theta_{required}$ increases 35-60% when the $\sigma_{dl} = 0.25\sigma_y$

$\theta_{required}$ increases 80-120% when the $\sigma_{dl} = 0.50\sigma_y$

$\theta_{required}$ increases 120-180% when the $\sigma_{dl} = 0.75\sigma_y$

$\theta_{required}$ increases 160-260% when the $\sigma_{dl} = 1.00\sigma_y$

Although with unpropped construction the composite parts of the connection (i.e. the reinforcement) are not strained under dead load, the substantially greater strains that occur in the steel section lead to plasticity at lower load levels, and hence much greater beam deflections and total end rotations.

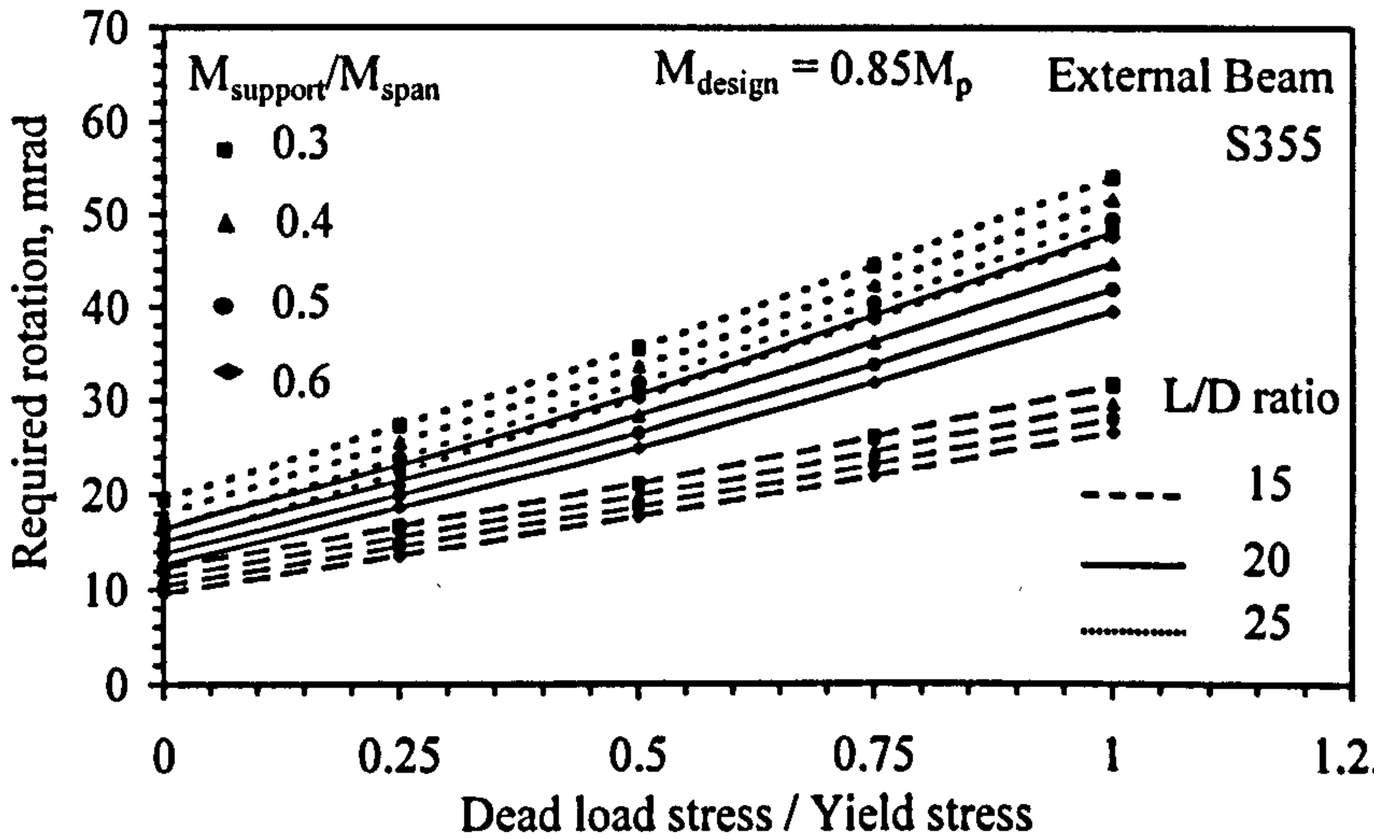

Figure 6-4. Required rotations to achieve $0.85M_p$ – S355, External beam

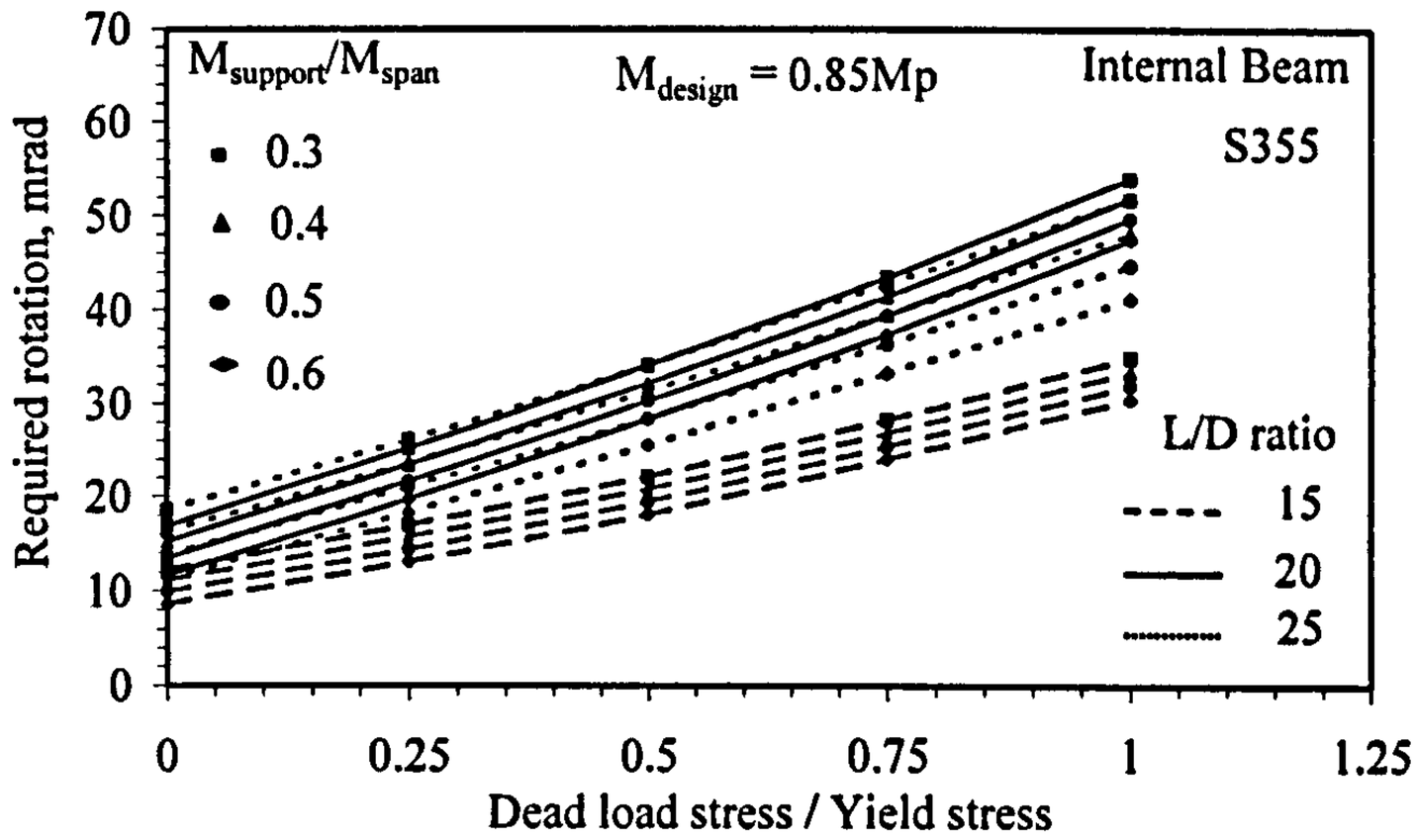

Figure 6-5. Required rotations to achieve $0.85M_p$ – S355, Internal beam

The relationship between $\theta_{required}$ and σ_{dl} is shown in Figure 6-4 and Figure 6-5 for a typical external and internal beams respectively. The relationship between $\theta_{required}$ and σ_{dl} for all the other cases considered in the parametric study is shown in Appendix C. The substantial increases in $\theta_{required}$ evident from these figures significantly limits the use of the connections with unpropped construction.

Analysis of the data listed in Table 6-1 shows that for the design moment of $0.85M_p$, on average $\theta_{required}$ increases by:

4mrads for every 0.25 increment in σ_{dl}/σ_y, when $L/D \leq 15$;
7mrads for every 0.25 increment in σ_{dl}/σ_y, when $L/D \leq 20$;
9mrads for every 0.25 increment in σ_{dl}/σ_y, when $L/D \leq 25$.

Analysis of the data listed in Table 6-2 shows that for the design moment of $0.90M_p$, on average $\theta_{required}$ increases by:

5mrads for every 0.25 increment in σ_{dl}/σ_y, when $L/D \leq 15$;
8mrads for every 0.25 increment in σ_{dl}/σ_y, when $L/D \leq 20$;
10mrads for every 0.25 increment in σ_{dl}/σ_y, when $L/D \leq 25$.

Analysis of the data listed in Table 6-3 shows that for the design moment of $0.95M_p$, on average $\theta_{required}$ increases by:

6mrads for every 0.25 increment in σ_{dl}/σ_y, when $L/D \leq 15$;
10mrads for every 0.25 increment in σ_{dl}/σ_y, when $L/D \leq 20$;
13mrads for every 0.25 increment in σ_{dl}/σ_y, when $L/D \leq 25$.

6.2.2 Effect of Steel Grade on $\theta_{required}$

Due to the increased strains, the rotation requirements will be more onerous for higher-grade steel. A typical comparison of the effect steel grade has on $\theta_{required}$ is shown in Figure 6-6 and Figure 6-7 for external and internal beams respectively. Comparison of the effect steel grade has on $\theta_{required}$ for all the other cases considered in the parametric study is shown in Appendix C.

Analysis of the data in Table 6-1, Table 6-2 and Table 6-3 shows $\theta_{required}$ is 10 to 20% higher for S355 in comparison with S275 beams irrespective of the mid-span design moment.

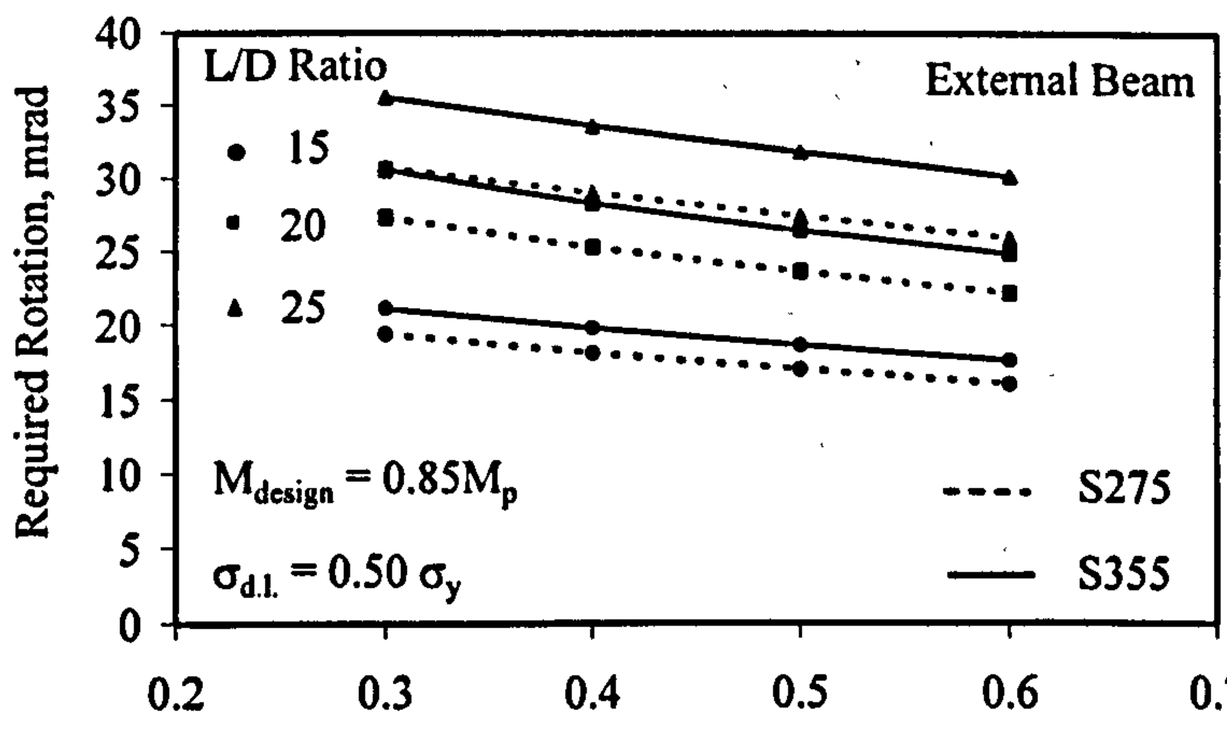

Figure 6-6. Effect of Steel grade on the required rotation of an External beam

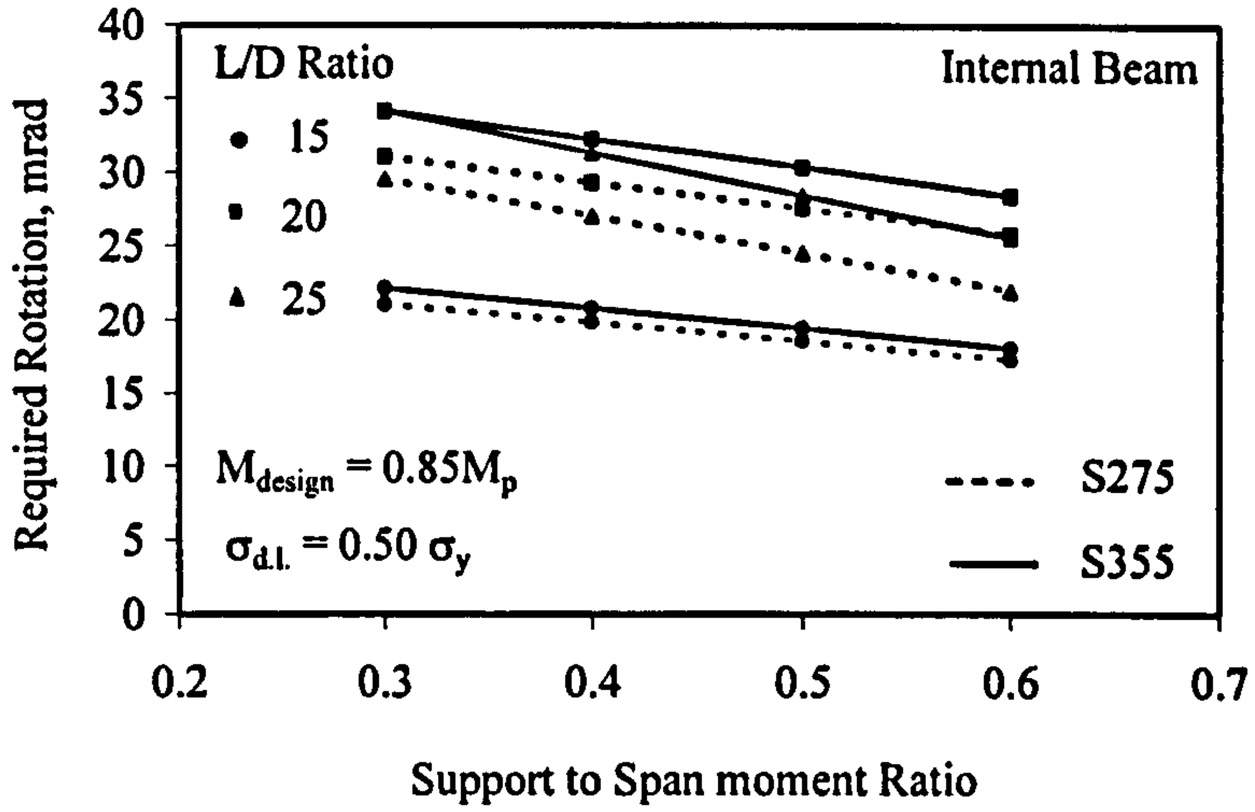

Figure 6-7. Effect of Steel grade on the Required Rotation of an Internal beam

6.2.3 Effect of $M_{support}/M_{span}$ on $\theta_{required}$

As would be expected $\theta_{required}$ increases as the requirement for moment redistribution increases, i.e., the ratio of $M_{support}/M_{span}$ decreases, see Figure 6-6 and Figure 6-7. This relationship was found to be irrespective of the steel grade, *L/D* ratio, end conditions, sagging design moment and degree of propping.

Typically, $\theta_{required}$ increased by 25% as $M_{support}/M_{span}$ decreased from 0.6 to 0.3. Figure 6-6 and Figure 6-7 also reveal that $\theta_{required}$ increases substantially with increased *L/D* ratio. Typically, $\theta_{required}$ increased by 10 to 90% as the *L/D* ratio increased from 15 to 25, depending on the design sagging moment and the steel grade. Comparison of the effect $M_{support}/M_{span}$ ratio has on $\theta_{required}$ for all the other cases considered in the parametric study is shown in Appendix C.

6.2.4 Effect of Design Sagging Moment on $\theta_{required}$

As the design sagging moment reduces from $0.95M_p$ and $0.90M_p$ to $0.85M_p$, there is a significant reduction observed in $\theta_{required}$. Figure 6-8 and Figure 6-9 demonstrate this trend

for a typical internal and external beam case, comprising an S355 grade with $M_{support}/M_{span}$ = 0.3 and L/D = 20, respectively.

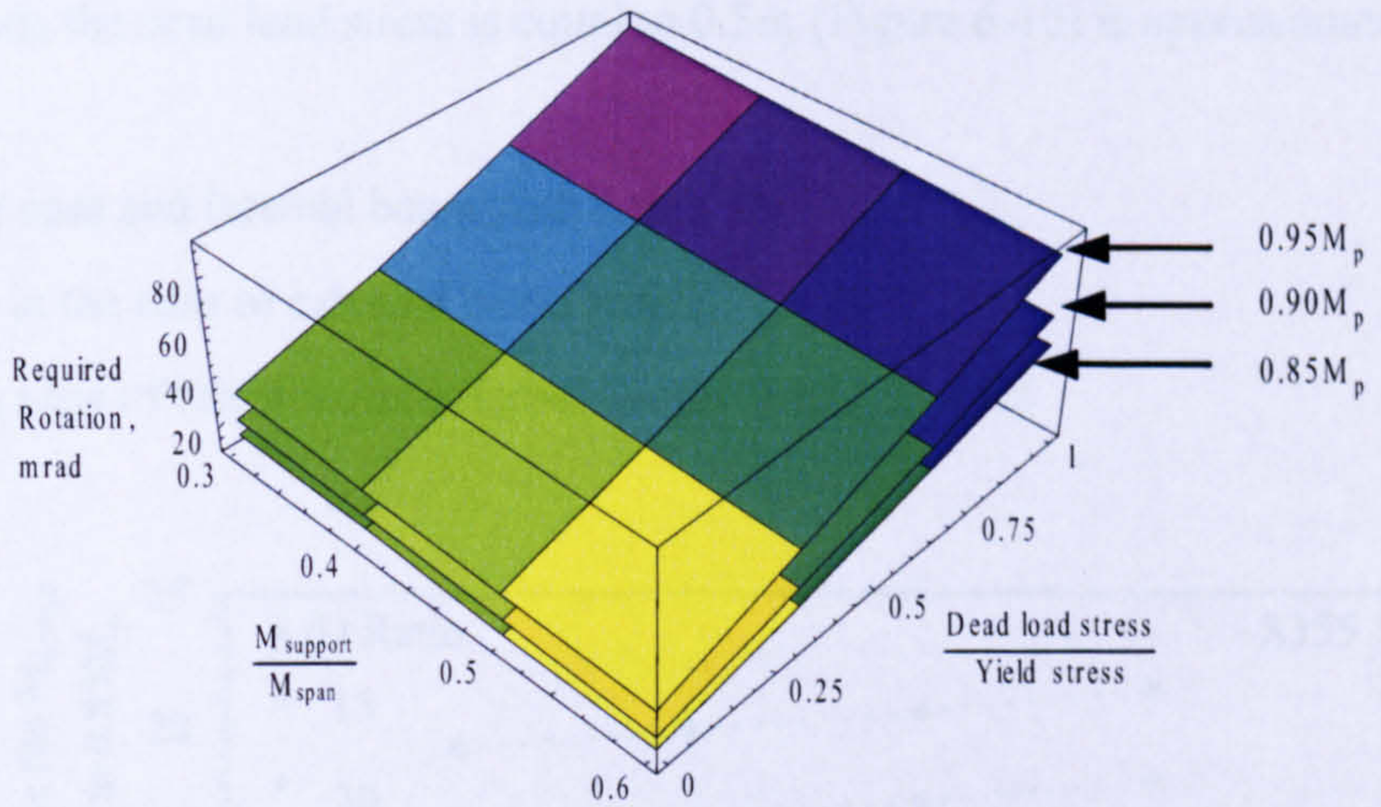

Figure 6-8. Relationship between required rotation capacity and design moment in an internal beam, S355 grade with $M_{support}/M_{span}$ = 0.3 and L/D = 20 for 2PL case.

Figure 6-8 and Figure 6-9 show that when the design sagging moment reduces from 0.95 to 0.85M_p, the percentage reduction in $\theta_{required}$ is typically:

Higher for internal beams than for external beams.

Higher as support to span moment ratio increases for internal beams.

Lower as support to span moment ratio increases for external beams.

Lower as the dead load stress to yield stress ratio increases.

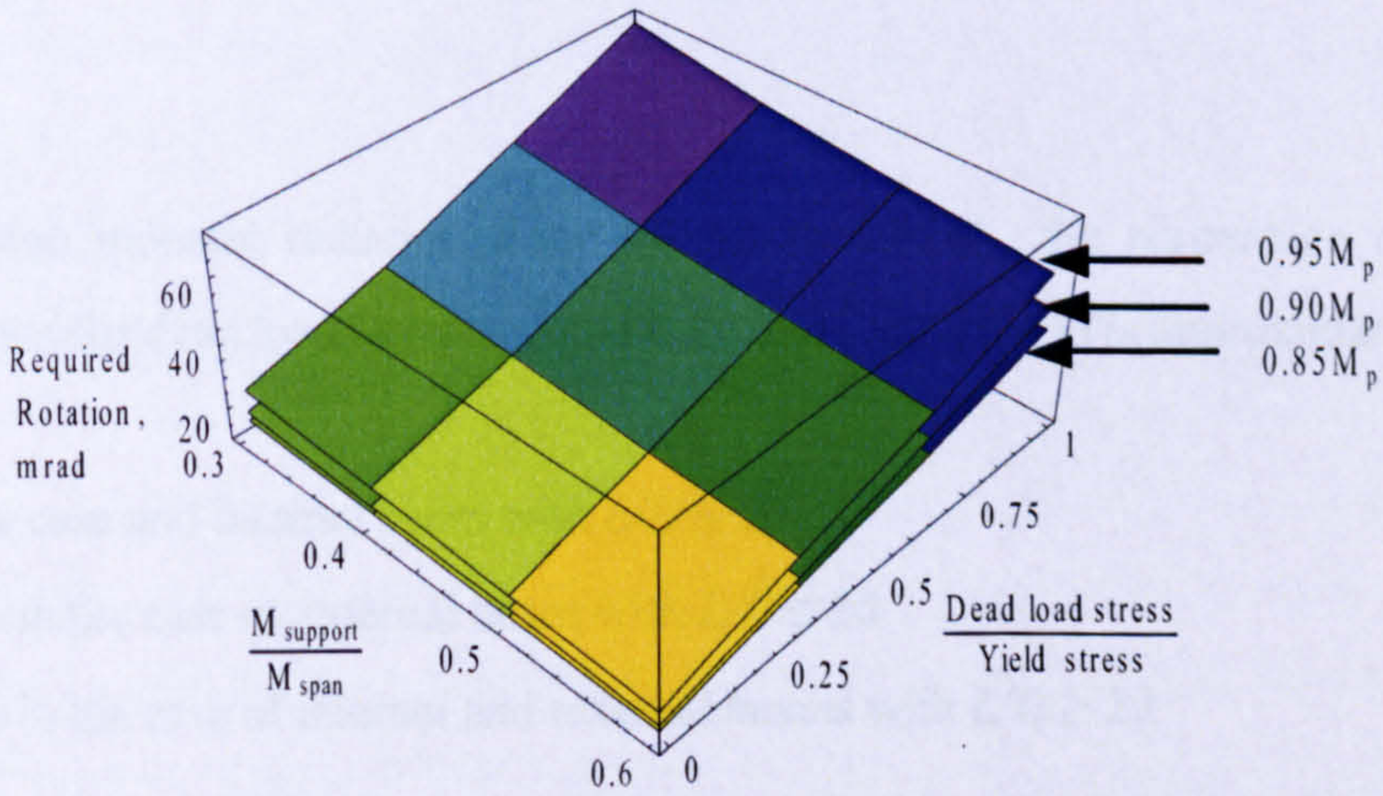

Figure 6-9. Relationship between required rotation capacity and design moment in an external beam, S355 grade with $M_{support}/M_{span}$ = 0.3 and L/D = 20 for 2PL case

For a design moment reducing from $0.90M_p$ to $0.85M_p$, the percentage reduction in $\theta_{required}$ when the dead load stress is equal to $0.5\sigma_y$ (Figure 6-10) is approximately:

20% in the case and internal beam with $L/D \leq 20$

10 to 15% in the case of external beam with $L/D \leq 20$

12% in the case of internal and external beams with $L/D \geq 20$

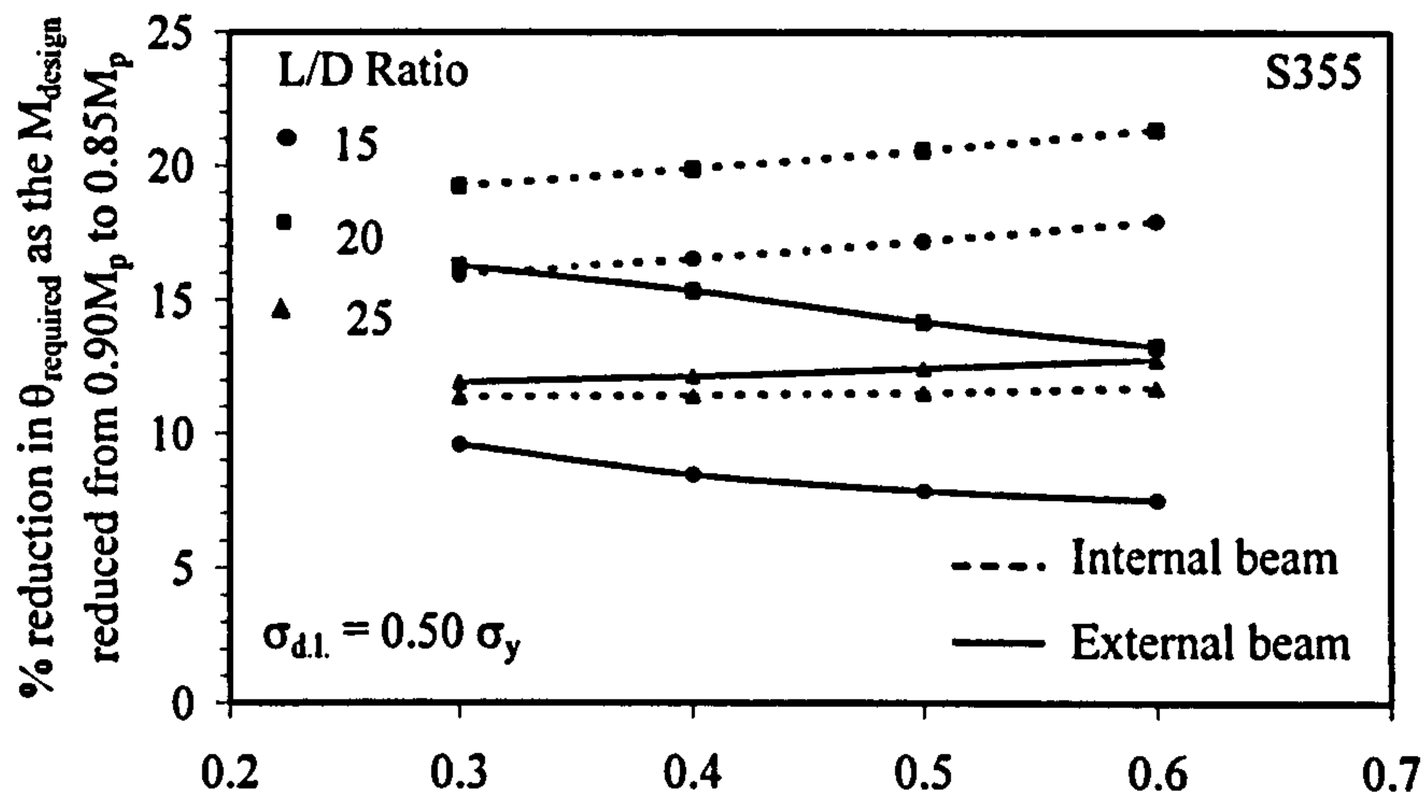

Figure 6-10. Percentage reduction in required rotation as the design moment reduced from $0.90M_p$ to $0.85M_p$ for unpropped form of construction: $\sigma_{dl} = 0.50\sigma_y$, S355 grade

For a design moment reducing from $0.95M_p$ to $0.85M_p$, the percentage reduction in $\theta_{required}$ when the dead load stress is equal to $0.5\sigma_y$ (Figure 6-11) is approximately:

45% in the case and internal beam with $L/D \leq 20$

20 to 40% in the case of external beam with $L/D \leq 20$

25 to 30% in the case of internal and external beams with $L/D \geq 20$

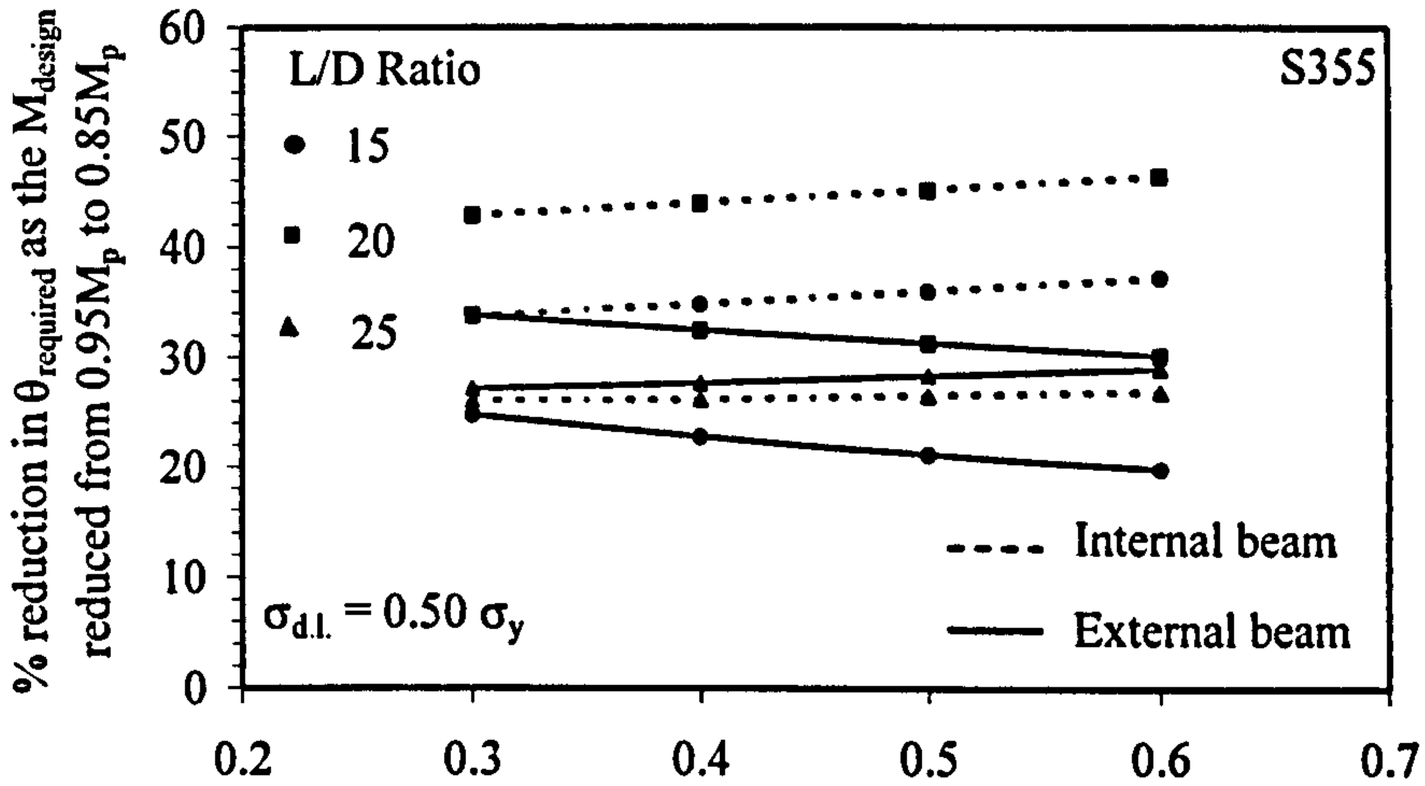

Figure 6-11. Percentage reduction in required rotation as the design moment reduced from $0.95M_p$ to $0.85M_p$ for unpropped form of construction: $\sigma_{dl} = 0.50\sigma_y$, S355 grade

Thus, the proportion of M_p utilised during design, together with *L/D* ratio and location within the building frame can significantly limit the increase in $\theta_{required}$ resulting from a move to unpropped construction.

6.2.5 Influence of the type of loading on $\theta_{required}$

The rotation requirement of internal beams resisting 2 point loads (at third span points) is greater than for beams supporting 3-point loads (at quarter span points). Figure 6-12-1(b) shows that for the 2-point load case, the plastic moment region extends over the mid one-third length of the span. Therefore the integral of curvature between the support and the point of maximum deflection is substantially greater than for the 3-point load case, Figure 6-12-2(b), in which the zone of plasticity is localised. On average, $\theta_{required}$ was 20-60% higher for the 2-point loads case. Internal beams subjected to a UDL, Figure 6-12-3(b), required slightly more end rotation than equivalent beams subjected to 3 point loads. This is as expected given that the zone of plasticity is extended for the UDL case. Less obvious was that externally located beams subjected to UDL's, Figure 6-13-3(b) required more end rotation than equivalent beams subjected to 2 point loads, Figure 6-13 –3(a).

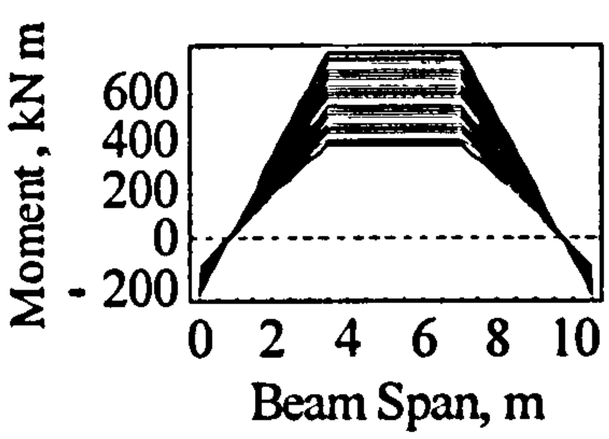

a. Moment distribution

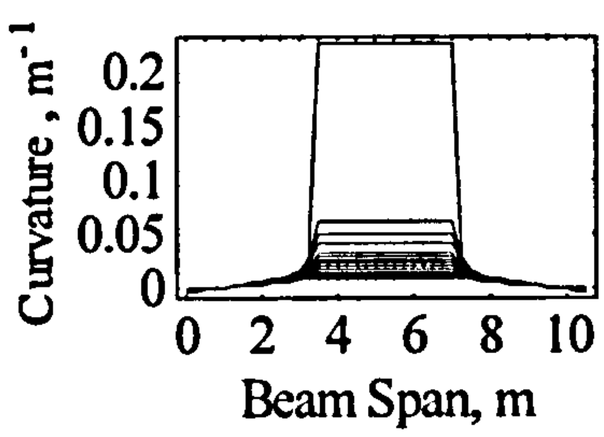

b. Curvature distribution

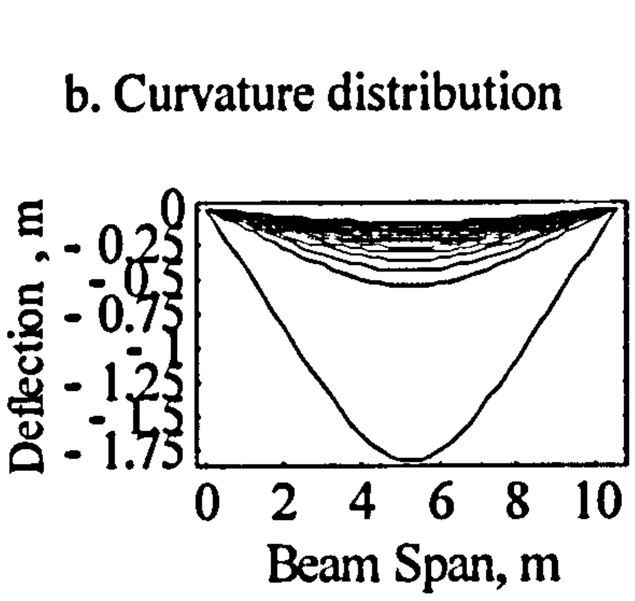

c. Deflection distribution

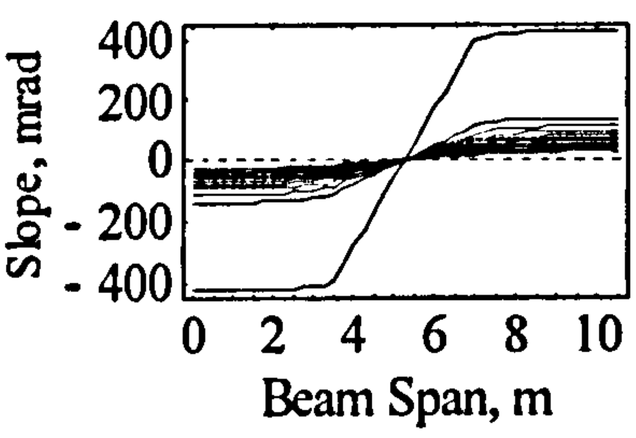

d. Slope distribution

1. Two point loads

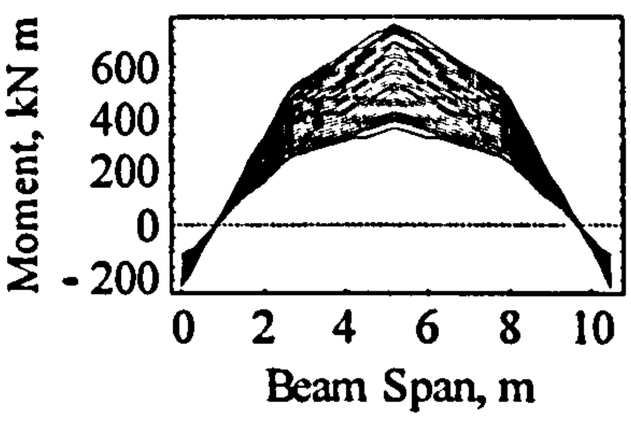

a. Moment distribution

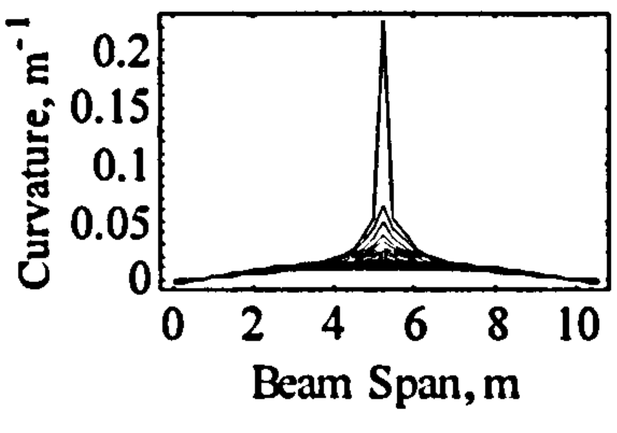

b. Curvature distribution

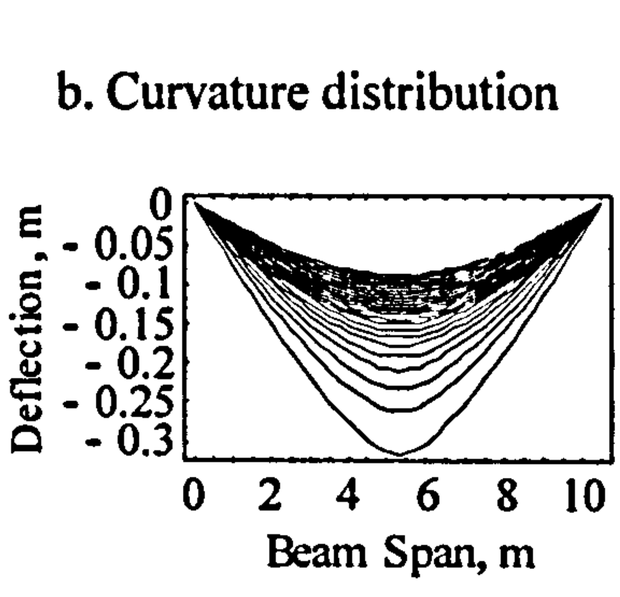

c. Deflection distribution

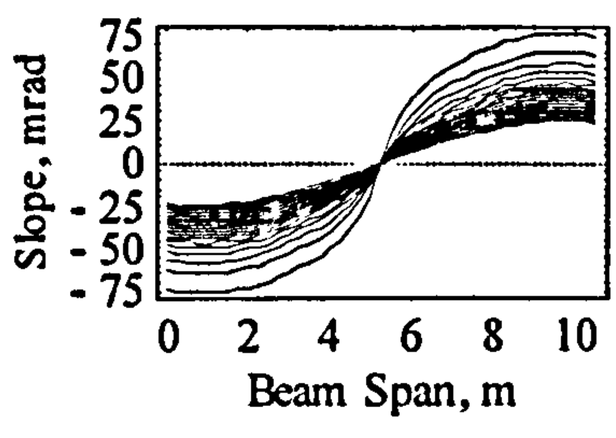

d. Slope distribution

2. Three point loads

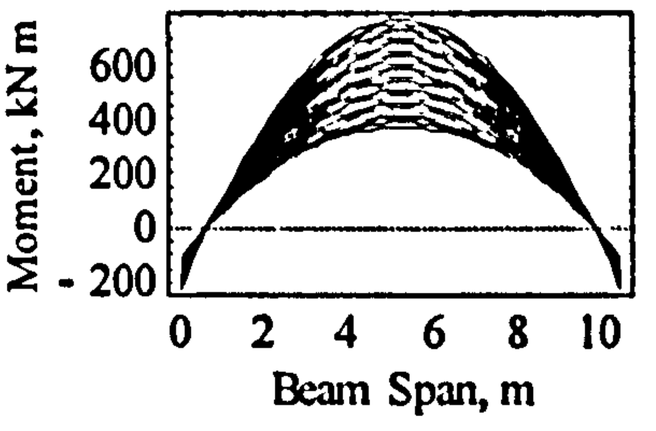

a. Moment distribution

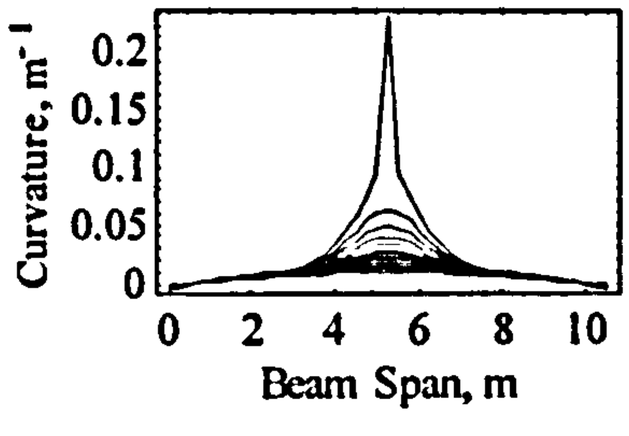

b. Curvature distribution

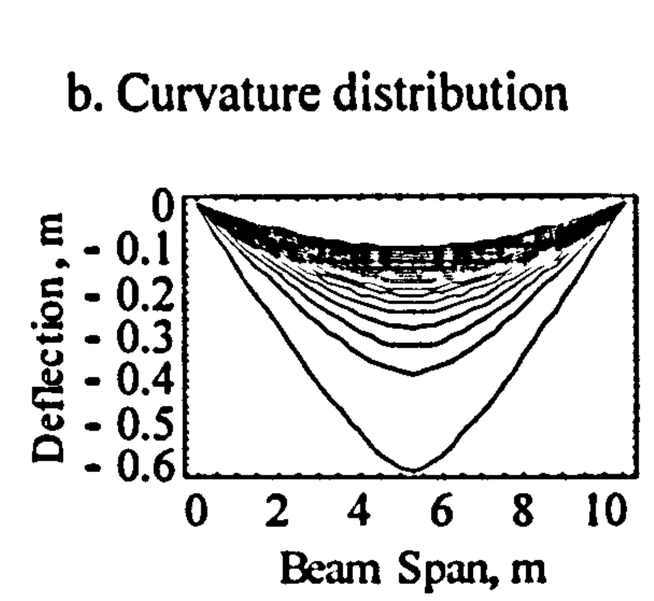

c. Deflection distribution

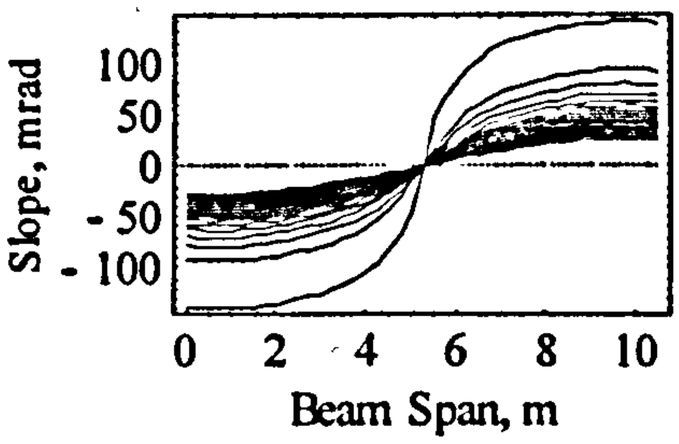

d. Slope distribution

3. Uniformly distributed loads

Figure 6-12. Moment, Curvature, Deflection and Slope distribution for an Internal beam of Steel grade S355, L/D=20 at $\sigma_{dl} = 1.0\sigma_y$

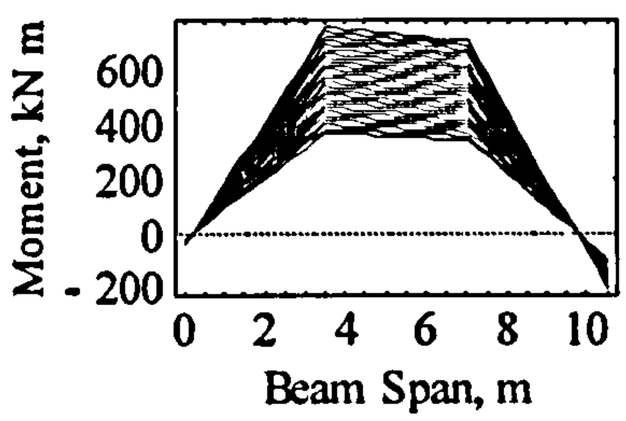

a. Moment distribution

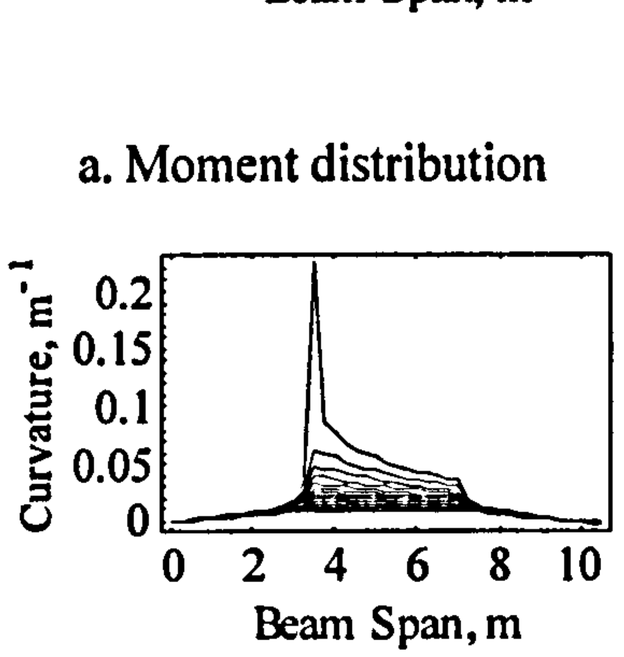

b. Curvature distribution

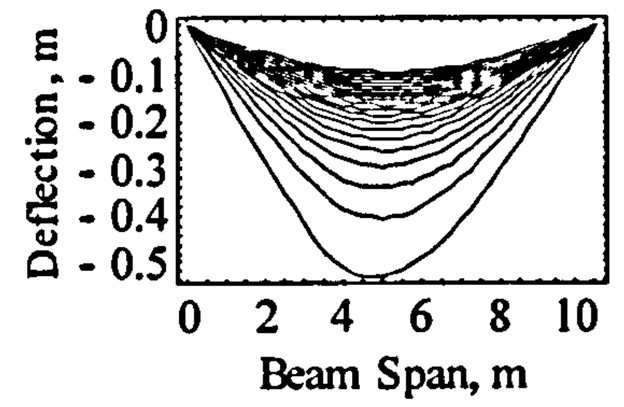

c. Deflection distribution

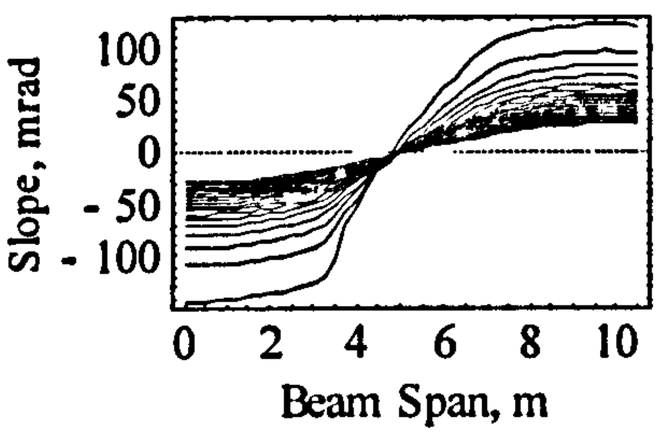

d. Slope distribution

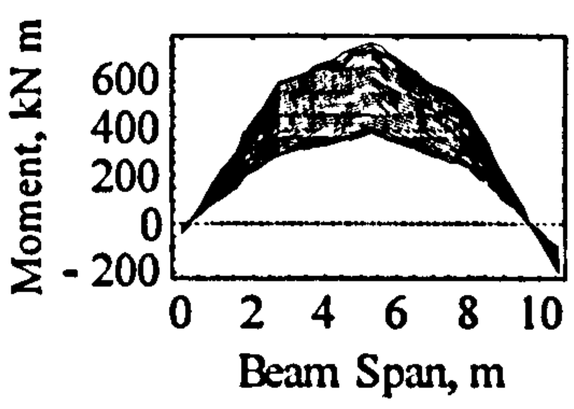

a. Moment distribution

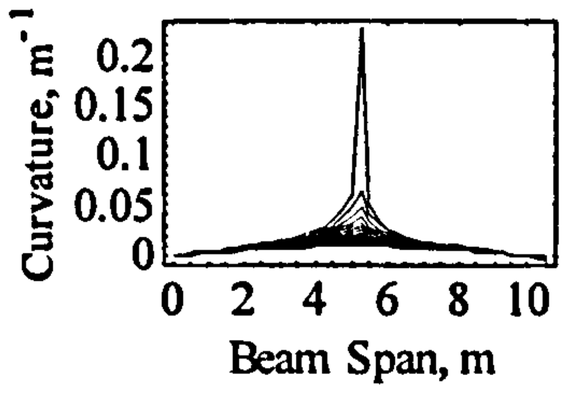

b. Curvature distribution

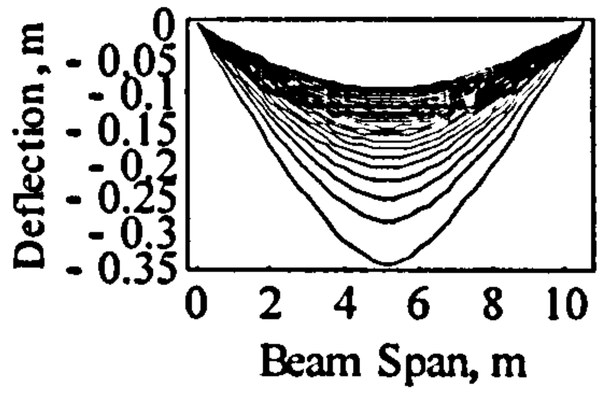

c. Deflection distribution

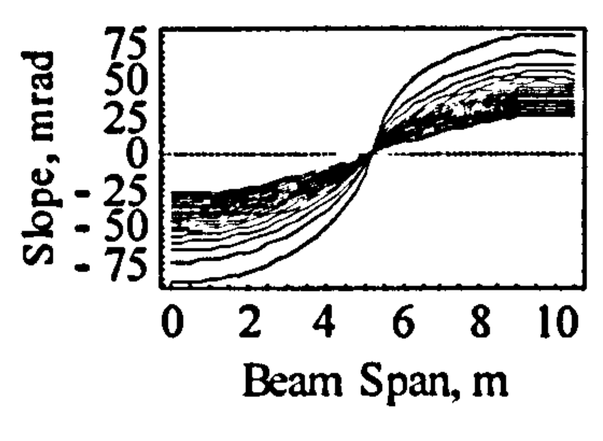

d. Slope distribution

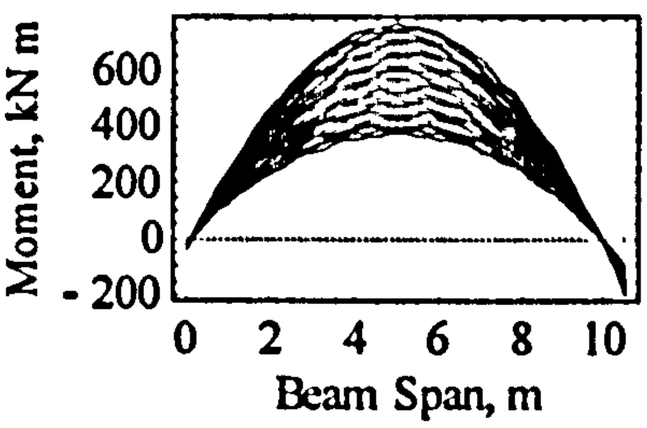

a. Moment distribution

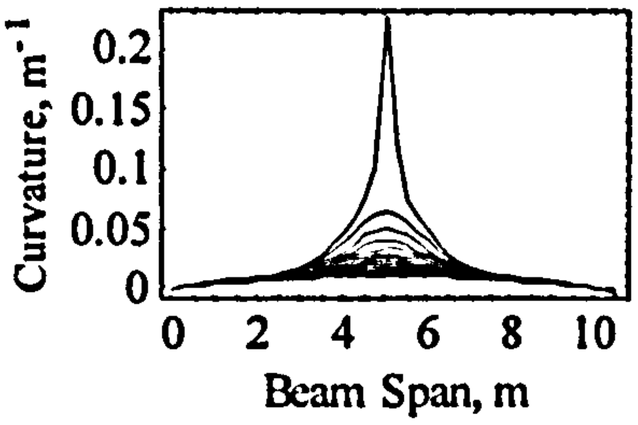

b. Curvature distribution

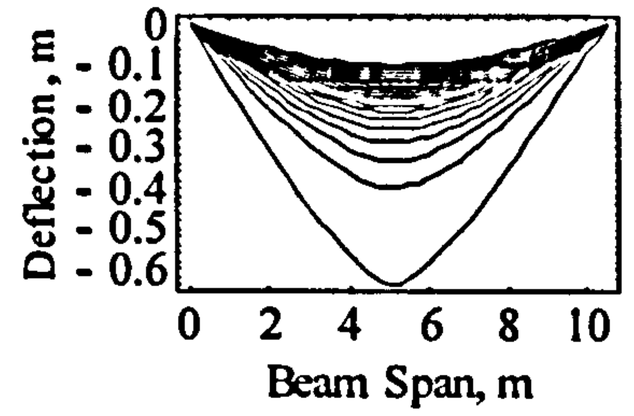

c. Deflection distribution

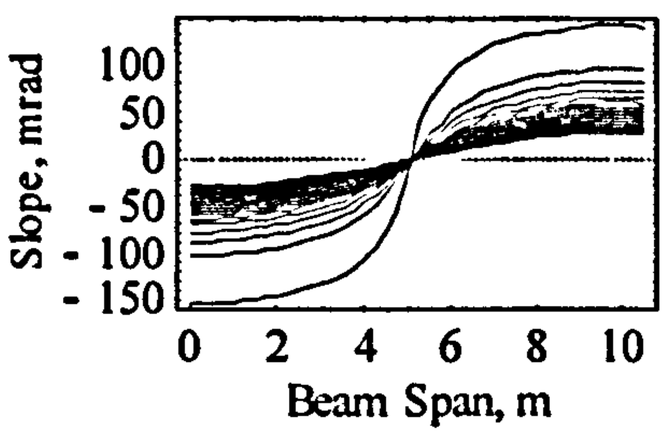

d. Slope distribution

1. Two point loads

2. Three point loads

3. Uniformly distributed loads

Figure 6-13. Moment, Curvature, Deflection and Slope distribution for an External beam of Steel grade S355, L/D=20 at $\sigma_{dl} = 1.0\sigma_y$

6.2.6 Effect of end conditions on $\theta_{required}$

The rotation requirement of internal beams subjected to 2-point loads, Figure 6-12-1(d), is substantially greater than that for external beams, Figure 6-13-1(d). This is due to the non-symmetrical distribution of curvature. Figure 6-13-1(b), 2(b) and 3(b) illustrate the curvature distributions of external beams. These figures demonstrate the effect that non-symmetrical end conditions have on curvature, in comparison with the distribution for the symmetrical beams, see Figure 6-12-1(b), 2(b) and 3(b). The lack of symmetry results in a reduction in the rotation requirement for beams located at external locations.

6.3 Rotation capacity of composite connections to unpropped beams

Anderson *et al* [2000] developed and validated their available rotation capacity model using composite connection tests which, by their very nature, represented a connection to a beam that was propped during construction. If this model is to be used to predict the rotation capacity available from standardised composite connections, then the implications of propping on the available rotation capacity needs due consideration.

When a beam is unpropped during construction, the steel beam alone supports the dead load. The slab only starts to behave structurally as the concrete gains strength. As far as the connection is concerned, the reinforcement is therefore not subject to strain due to dead load. The available rotation capacity of a given connection, assuming that capacity is governed by the ductility of the reinforcement, will therefore be greater when it is used on a beam that is unpropped during construction. In order to quantify this increase in capacity, the proportion of the total reinforcement strain that can be attributed to dead load in a propped situation must first be identified.

Li's analytical model [1992] for calculating required rotation capacity divided rotation into the elastic and plastic components. The first step in identifying the strain in the reinforcement due to dead load is to assess the relative magnitudes of the elastic and plastic components for a typical beam. Li derived plastic rotations from measured beam deflections [1992] for a series of composite beams tested in the 1960's [Chapman(1964),

Culver(1961) and Slutter(1965)]. Applying formulae [Young, 1989] to relate elastic deflections to elastic end rotations, corresponding values of elastic rotation have been determined for three of these tests. Elastic and plastic rotations are given in Table 6-5 (θ_{el} and θ_{pl}). It is assumed that the measured beam deflections from which these values are derived are associated with the attainment of an ultimate moment in the beam equal to M_p.

As shown previously, the total rotations required to achieve $0.85M_p$ in the span are significantly lower than those required to achieve $0.95M_p$. The decrease in total rotation comes entirely from a reduction in the plastic component. Values of θ_{pl} derived from test deflections must therefore be modified to obtain a true picture of the relative proportions of the elastic and plastic rotations that are relevant to the design condition of $0.85M_p$ advocated for standardised composite connection details prepared for industry [BCSA and SCI, 1998]. Such values are given in the column marked θ_{pl} in Table 6-5. The average value of $\theta_{el}/\theta_{pl}^{*}$ is 0.74. Given the limited data on which this value is based, a conservative value of 0.5 is assumed in the calculations that follow, so that one third of the total rotation, and therefore one third of the total strain in the reinforcement, is assumed to be due to elastic deformations of the beam. The conservatism of this value of 0.5, though necessary due to the limited information on which it is based, was confirmed by calculations using Li's formulae [2000]. However, future work in this area may justify a less conservative value, and thus allow the final conclusions in this chapter to be relaxed.

The proportion of the elastic strain that is due to dead load must be determined. Factored dead (w_d) is assumed to be half the factored imposed load (w_i), and connection strength is assumed to be equal to $0.4M_p$. The shape factor for the composite beam is taken as 1.45 so that the elastic limit is reached at a sagging moment of $0.7M_p$. Since the sagging moment is assumed to reach $0.85M_p$ under full dead plus imposed loading, the loading needed to attain $0.7M_p$ is given by:

$$w_d + \beta w_i = (0.7M_p + 0.4M_p)\, l^2/8 \qquad (1)$$

and with

$$w_d + w_i = (0.85M_p + 0.4M_p)\, l^2/8 \qquad (2)$$

$$w_i = 2w_d \quad (3)$$

Therefore $\beta = 0.8$ and the beam reaches its elastic limit once approximately 80% of the imposed load has been applied. More importantly, that part of the elastic strain in the reinforcement that is due to dead load is given by:

$$w_d/(w_d + \beta.w_i) = 0.4 \quad (4)$$

So 40% of the elastic strain is due to dead load, and the elastic strain is one third of the total strain. Removal of the dead load strain from the reinforcement, by adopting unpropped construction, therefore allows an effective increase in available rotation of approximately 15%. Using extreme combinations of support moment, w_d and w_i, this figure would fall to 10% [Couchman and Way, 2000].

Given that the difference in the available rotation capacity between propped and unpropped construction has been assessed, it becomes necessary to determine the available rotation capacity of practical composite connections. Thus, the rotation capacity of standardised composite connection details [BCSA and SCI, 1998] has been assessed using Anderson, Aribert and Kronenburger's model [2000], developed for use with propped beams. The results show that connections detailed according to the standardised rules [BCSA and SCI, 1998] are capable of achieving rotations of 29 and 23mrads for S355 and S275 steel respectively (propped). Applying the 10% increase in rotation capacity due to the unpropped mode of construction, these capacities rise to 32 and 25mrads for S355 and S275 steel. Interestingly, this degree of available rotation capacity was confirmed during the large-scale composite frame test carried out as part of the present study, in which composite connections (using S275 steel) were observed to fail after a rotation of 25.4mrad [Chapter3 and Dhanalakshmi *et al* (2002)]. Note that in applying the available rotation capacity model to establish detailing rules, the rotation capacity contribution from slip was calculated assuming shear connection stiffness compatible with studs in a solid slab. Variations when studs are used with some types of decking should not significantly affect the validity of the detailing rules, given that the rotation contribution due to slip is generally small [Li, 1992].

To achieve these rotation values, limitations are imposed on the detailing of the standardised connections [BCSA and SCI, 1998]. For all 'plastic' connections the first stud must be at least 100mm from the face of the column. This restriction ensures that the reinforcing bars are strained over a sufficient length to ensure ductility. In addition, the centre of the reinforcement should be approximately 70mm above the top of the steel section, in order to restrict the lever arm from the neutral axis to the bars. Lower bounds on reinforcement area, which are compatible with the detailing limitations, are also included. These vary as a function of the section size, steel grade and reinforcement ductility [BCSA and SCI, 1998].

6.4 Comparison between available and required rotation capacities

The comparison reveals that for unpropped construction the rotation requirements frequently exceed those available from standardised connection details. This seems surprising as it is often thought that, because composite connection rotation capacity is generally governed by the ductility of the reinforcement, and thus reinforcement is not strained under dead load with unpropped construction, that the more widely studied case of propped construction is more onerous. However, most of the strain in the reinforcement for a propped case has been shown to be due to imposed load (when components such as the steel beam have started to plastify, so deformations increase rapidly). There is therefore little additional rotation capacity available due to having avoided this dead load strain by using unpropped construction. On the other hand, when the construction is unpropped much greater strains develop in the steel section, which much alone support the dead load. The steel therefore plastifies at lower load levels, deflects more, and imposes significantly greater demands for end rotation. If we compare unpropped to propped we therefore have slightly more available rotation capacity trying to counter significantly more required rotation. Restrictions will need to be imposed to ensure design safety when combining composite connections with the unpropped mode of construction.

The basic restriction is that the maximum design sagging moment should be restricted to $0.85M_p$, since design moments exceeding this place significantly higher rotation demands on the connections. The second restriction is that the ratio between support and span moment must not be less than 0.3. Lower values require additional moment redistribution and therefore impose higher demands on the connection ductility. The study has shown that the required rotation capacity increases by between 4 and 9mrads (depending on the *L/D* ratio) for every 25% increase in the stress imposed on the beam prior to the development of composite action (σ_{dl}). Due to this rapid increase in the rotation requirement, it is found necessary to limit σ_{dl} during design. The results from the parametric study (Table 6-1) have been used to determine the limits on σ_{dl} required to ensure connections can meet the rotations demanded from the beams. The results from this comparison are presented in Table 6-6 for a range of different geometric configurations.

The restrictions imposed on σ_{dl} are less severe for S355 steel, as opposed to the S275 grade. This is because approximately 25% extra rotation capacity is available from S355 connections, whilst the rotation requirements increase by only 10 to 20%.

High values of σ_{dl} can be imposed on beams where the *L/D* ratio is no greater than 15. The parametric study has shown that the required rotation capacity increases by between 10 and 90% as this ratio increases from 15 to 25. The effect this has on the limiting values of σ_{dl} are:

When $L/D \leq 15$, $\sigma_{dl} \leq 0.89\sigma_y$ (S355) or $0.68\sigma_y$ (S275)

When $L/D \leq 20$, $\sigma_{dl} \leq 0.44\sigma_y$ (S355) or $0.31\sigma_y$ (S275)

When $L/D \leq 25$, $\sigma_{dl} \leq 0.21\sigma_y$ (S355) or $0.13\sigma_y$ (S275)

Values of σ_{dl} should be calculated under factored dead load because the implications of excess stress would be structural failure of the composite connections. These limits represent the worst-case scenarios of loading set up and position within the building frame. Less restrictive limits can be determined from Table 6-6 which presents values of

σ_{dl} for a range of different beam configurations. For example, σ_{dl} can be increased to $0.67\sigma_y$ for S355 beams supporting 3 point loads with a span to depth ratio of 20.

Inspection of Table 6-6 reveals that beams subjected to 3 point loads have the highest permissible values of σ_{dl}. This is due to a more concentrated zone of plasticity. In contrast, the extended zone of plasticity that would occur in beams subjected to 2 point loads and located internally within a building frame creates low values of σ_{dl}. Otherwise identical 2 point load beams located externally have higher σ_{dl} values because the bending moment diagram is unsymmetrical, thus reducing the zone of plasticity. For beams subjected to uniformly distributed loads, the position within a frame (internal or external) does not significantly effect σ_{dl}.

6.5 Conclusions and implications for design

Beams unpropped during construction have been found to require substantial end rotations in order to attain their design sagging moments. These rotation demands have been found to frequently exceed the rotations available from standardised connection details, which are only 10% (as a conservative lower bound) higher than when these connections are used with propped beams. Values of available rotation capacity for industry standard [BCSA and SCI, 1998] composite connections, when used with unpropped construction, are relatively limited at only 32mrad (with S355 beams) and 25mrad (S275). However it will be difficult to achieve higher values with practical levels of reinforcement. Therefore, limits have to be imposed on the use of composite connections with unpropped construction. The primary restriction is that the maximum design sagging moment in the beam must be restricted to $0.85M_p$. Furthermore, the ratio between the support and span design moments must not be less than 0.3.

During propped construction composite action resists dead, as well as imposed loads. Conversely, the steel section alone resists the floor self weight in unpropped beams. The ratio between the maximum bending stress (during this non composite stage) and the yield stress (σ_{dl}/σ_y) was found to have a critical effect on the rotation required from the connections. In S355 beams where the span to depth ratio is less than or equal to 15, $\sigma_{dl} \leq$

$0.89\sigma_y$. If less than or equal to 20, then the σ_{dl} limit falls to $0.44\sigma_y$. These limits can be relaxed for many configurations. For example the limits are less restrictive for beams supported by nominally pinned connections at one end. Lower limits are also placed on beams subjected to 3 point loads or uniformly distributed loads. When beams are made from S275 steel the stress limits are more onerous. Moreover, range of limiting σ_{dl}/σ_y ratios have been presented herein for design purposes. Before relying on the ductility of standard composite connections when used in unpropped construction, designers should pay careful attention to the values given and ensure that the factored dead load stresses fall within the implied limits. An increase in steel beam size, or strength, may be necessary.

Table 6-1: Composite connection rotation capacity requirement to reach $0.85M_p$ span moment

Steel grade	Load case	End moments		Span to depth ratio = 15 Maximum dead load stress, σ_{dl}					Span to depth ratio = 20 Maximum dead load stress, σ_{dl}					Span to depth ratio = 25 Maximum dead load stress, σ_{dl}				
		M_1	M_2	$0.0\sigma_y$	$0.25\sigma_y$	$0.5\sigma_y$	$0.75\sigma_y$	$1.0\sigma_y$	$0.0\sigma_y$	$0.25\sigma_y$	$0.5\sigma_y$	$0.75\sigma_y$	$1.0\sigma_y$	$0.0\sigma_y$	$0.25\sigma_y$	$0.5\sigma_y$	$0.75\sigma_y$	$1.0\sigma_y$
S275	2PL	0.05	0.30	12.1	15.6	19.4	23.9	29.0	16.1	21.2	27.3	34.6	42.1	19.7	26.4	34.4	43.8	53.5
		0.05	0.40	11.2	14.6	18.1	22.2	26.9	14.8	19.7	25.3	31.9	39.1	18.1	24.4	31.8	40.4	49.6
		0.05	0.50	10.3	13.6	17.0	20.9	25.2	13.6	18.3	23.6	29.7	36.4	16.6	22.7	29.6	37.5	46.3
		0.05	0.60	9.5	12.7	16.1	19.8	23.8	12.5	17.1	22.2	27.9	34.3	15.2	21.1	27.7	35.2	43.5
		0.30	0.30	12.2	16.3	21.1	26.7	32.4	16.7	23.4	31.1	39.1	47.8	20.6	29.3	39.2	49.4	60.7
		0.40	0.40	11.1	15.1	19.9	25.4	31.0	15.2	21.7	29.3	37.2	45.9	18.6	27.2	37.0	47.0	58.3
		0.50	0.50	9.9	13.9	18.6	24.1	29.6	13.6	20.0	27.6	35.4	44.0	16.6	25.1	34.8	44.7	55.9
		0.60	0.60	8.7	12.7	17.4	22.8	28.3	11.9	18.3	25.8	33.6	42.2	14.5	22.9	32.5	42.5	53.5
	UDL	0.05	0.30	12.6	16.2	20.1	24.5	29.2	16.8	22.2	28.3	35.0	42.0	20.6	27.6	35.6	44.1	53.3
		0.05	0.40	11.8	15.3	19.1	23.5	28.0	15.7	21.0	27.0	33.5	40.3	19.3	26.1	33.8	42.2	51.1
		0.05	0.50	11.1	14.5	18.3	22.5	26.9	14.7	19.9	25.7	32.1	38.8	18.0	24.7	32.3	40.5	49.2
		0.05	0.60	10.3	13.7	17.4	21.5	25.9	13.7	18.7	24.5	30.7	37.3	16.7	23.3	30.7	38.8	47.3
		0.30	0.30	12.3	15.9	19.8	24.1	28.8	16.4	21.8	27.8	34.4	41.4	20.2	27.1	34.9	43.4	52.5
		0.40	0.40	11.3	14.8	18.5	22.7	27.2	15.0	20.2	26.1	32.5	39.2	18.4	25.1	32.7	40.9	49.7
		0.50	0.50	10.2	13.6	17.2	21.4	25.7	13.5	18.5	24.3	30.5	37.1	16.5	23.0	30.4	38.5	47.0
		0.60	0.60	9.1	12.4	16.0	20.0	24.3	11.9	16.9	22.5	28.6	35.0	14.5	20.9	28.2	36.0	44.4
	3PL	0.05	0.30	11.5	14.7	17.9	21.4	25.1	15.1	19.7	24.6	30.0	35.6	18.5	24.4	30.8	37.7	45.0
		0.05	0.40	10.6	13.7	16.9	20.4	24.0	14.0	18.4	23.3	28.5	34.0	17.1	22.8	29.0	35.8	42.9
		0.05	0.50	9.8	12.9	16.0	19.4	23.0	12.9	17.2	22.0	27.1	32.5	15.7	21.3	27.4	34.1	41.1
		0.05	0.60	9.0	12.0	15.2	18.5	22.0	11.8	16.1	20.8	25.9	31.2	14.3	19.9	25.9	32.5	39.5
		0.30	0.30	11.0	14.1	17.3	20.7	24.2	14.5	18.9	23.7	28.8	34.2	17.7	23.4	29.6	36.2	43.2
		0.40	0.40	9.8	12.8	15.9	19.1	22.5	12.8	17.1	21.7	26.6	31.7	15.6	21.1	27.1	33.4	40.1
		0.50	0.50	8.5	11.4	14.4	17.6	20.8	11.1	15.3	19.7	24.4	29.4	13.4	18.8	24.5	30.7	37.1
		0.60	0.60	7.2	10.1	13.0	16.1	19.2	9.27	13.4	17.7	22.3	27.1	11.1	16.4	22.0	28.0	34.2

Notes: M_{design} is the design sagging moment ; M_1 is the ratio of first support to span design moment; M_2 is the ratio of second support to span design moment; Rotations in mrads

Table 6-1: Composite connection rotation capacity requirement to reach $0.85M_p$ span moment (continued)

				Span to depth ratio = 15					Span to depth ratio = 20					Span to depth ratio = 25				
Steel grade	Load case	End moments		Maximum dead load stress, σ_{dl}					Maximum dead load stress, σ_{dl}					Maximum dead load stress, σ_{dl}				
		M_1	M_2	$0.0\sigma_y$	$0.25\sigma_y$	$0.5\sigma_y$	$0.75\sigma_y$	$1.0\sigma_y$	$0.0\sigma_y$	$0.25\sigma_y$	$0.5\sigma_y$	$0.75\sigma_y$	$1.0\sigma_y$	$0.0\sigma_y$	$0.25\sigma_y$	$0.5\sigma_y$	$0.75\sigma_y$	$1.0\sigma_y$
S355	2PL	0.05	0.30	12.2	16.6	21.1	26.0	31.7	16.4	23.1	30.6	39.1	48.1	21.0	30.1	40.6	52.1	64.2
		0.05	0.40	11.3	15.5	19.9	24.5	29.7	15.1	21.4	28.3	36.2	44.8	19.1	27.6	37.3	48.2	59.8
		0.05	0.50	10.4	14.5	18.7	23.1	28.0	13.8	19.9	26.5	33.9	42.0	17.4	25.6	34.6	44.9	56.0
		0.05	0.60	9.6	13.6	17.7	22.0	26.6	12.6	18.6	24.9	31.9	39.6	15.8	23.7	32.4	42.1	52.7
		0.30	0.30	12.3	17.0	22.1	28.3	34.9	16.9	25.2	34.2	43.5	54.0	22.8	33.9	45.6	58.7	73.0
		0.40	0.40	11.1	15.7	20.8	26.9	33.4	15.2	23.4	32.3	41.4	51.8	20.6	31.6	43.2	56.1	70.1
		0.50	0.50	9.92	14.4	19.5	25.5	32.0	13.5	21.6	30.3	39.4	49.7	18.4	29.3	40.7	53.4	67.3
		0.60	0.60	8.63	13.1	18.1	24.1	30.5	11.7	19.7	28.4	37.4	47.5	16.1	26.9	38.2	50.9	64.4
	UDL	0.05	0.30	12.7	17.2	21.8	26.8	32.3	17.2	24.1	31.6	39.5	48.1	22.0	31.3	41.4	52.2	64.0
		0.05	0.40	11.9	16.3	20.8	25.6	31.0	16.0	22.8	30.1	37.8	46.2	20.6	29.6	39.4	50.0	61.5
		0.05	0.50	11.1	15.4	19.8	24.6	29.8	14.9	21.6	28.7	36.3	44.5	19.1	28.0	37.6	48.0	59.2
		0.05	0.60	10.4	14.6	18.9	23.6	28.7	13.8	20.4	27.4	34.8	42.9	17.7	26.5	35.9	46.0	57.0
		0.30	0.30	12.4	16.9	21.4	26.4	31.8	16.7	23.6	31.0	38.9	47.4	21.5	30.7	40.6	51.4	63.1
		0.40	0.40	11.4	15.7	20.1	24.9	30.1	15.2	21.9	29.1	36.7	45.0	19.5	28.5	38.1	48.5	59.8
		0.50	0.50	10.2	14.4	18.7	23.4	28.5	13.6	20.1	27.1	34.6	42.6	17.4	26.2	35.5	45.7	56.7
		0.60	0.60	9.0	13.1	17.4	22.0	26.9	11.9	18.3	25.2	32.5	40.2	15.3	23.8	33.0	42.9	53.5
	3PL	0.05	0.30	11.6	15.6	19.7	23.9	28.3	15.5	21.4	27.6	34.2	41.2	19.4	27.3	35.6	44.5	54.0
		0.05	0.40	10.7	14.6	18.6	22.7	27.0	14.2	20.0	26.1	32.5	39.3	17.9	25.5	33.6	42.3	51.6
		0.05	0.50	9.8	13.7	17.6	21.7	25.9	13.0	18.7	24.7	31.0	37.7	16.3	23.8	31.8	40.4	49.5
		0.05	0.60	9.0	12.8	16.7	20.7	24.9	11.9	17.5	23.4	29.7	36.3	14.8	22.2	30.2	38.6	47.7
		0.30	0.30	11.1	15.0	19.0	23.1	27.3	14.8	20.6	26.6	32.9	39.6	18.6	26.1	34.2	42.7	51.8
		0.40	0.40	9.8	13.6	17.5	21.4	25.4	13.0	18.6	24.4	30.5	36.9	16.3	23.6	31.3	39.5	48.2
		0.50	0.50	8.5	12.2	16.0	19.7	23.6	11.2	16.6	22.2	28.1	34.2	13.9	21.0	28.4	36.4	44.7
		0.60	0.60	7.1	10.8	14.4	18.1	21.9	9.2	14.5	20.0	25.7	31.6	11.3	18.3	25.6	33.3	41.2

Notes: M_{design} is the design sagging moment ; M_1 is the ratio of first support to span design moment; M_2 is the ratio of second support to span design moment; Rotations in mrads

Table 6-2: Composite connection rotation capacity requirement to reach $0.90M_p$ span moment

				Span to depth ratio = 15					Span to depth ratio = 20					Span to depth ratio = 25				
Steel grade	Load case	End moments		Maximum dead load stress, σ_{dl}					Maximum dead load stress, σ_{dl}					Maximum dead load stress, σ_{dl}				
		M_1	M_2	$0.0\sigma_y$	$0.25\sigma_y$	$0.5\sigma_y$	$0.75\sigma_y$	$1.0\sigma_y$	$0.0\sigma_y$	$0.25\sigma_y$	$0.5\sigma_y$	$0.75\sigma_y$	$1.0\sigma_y$	$0.0\sigma_y$	$0.25\sigma_y$	$0.5\sigma_y$	$0.75\sigma_y$	$1.0\sigma_y$
S275	2PL	0.05	0.30	13.2	17.6	22.7	28.3	34.3	18.7	25.7	33.5	41.8	50.8	23.2	32.2	42.1	52.8	64.2
		0.05	0.40	12.1	16.2	20.8	26.1	31.8	16.9	23.3	30.6	38.5	46.9	20.9	29.1	38.5	48.6	59.3
		0.05	0.50	11.2	15	19.3	24.2	29.6	15.4	21.3	28.1	35.6	43.6	19	26.6	35.3	45	55.2
		0.05	0.60	10.3	14	18	22.6	27.7	14.1	19.7	26	33.1	40.9	17.3	24.5	32.7	41.9	51.8
		0.30	0.30	14.5	20.3	26.3	32.9	40	22	30.4	39.6	49.4	59.9	27.3	37.9	49.6	62	75
		0.40	0.40	13.3	19.1	25	31.5	38.5	20.4	28.7	37.7	47.4	57.7	25.2	35.7	47.2	59.4	72.3
		0.50	0.50	12.1	17.8	23.7	30.1	37	18.6	26.9	35.8	45.4	55.7	23.1	33.5	44.8	56.9	69.7
		0.60	0.60	10.8	16.4	22.3	28.7	35.6	16.8	25	33.9	43.5	53.7	20.8	31.1	42.5	54.5	67.2
	UDL	0.05	0.30	13.9	18.4	23.2	28.5	34.1	19.6	26.3	33.6	41.6	50	24.2	32.8	42.2	52.3	63.1
		0.05	0.40	13.8	17.4	22.1	27.2	32.8	18.4	25	32.1	39.8	48.1	22.7	31.1	40.2	50.1	60.6
		0.05	0.50	12.2	16.5	21.1	26.2	31.6	17.3	23.7	30.7	38.3	46.3	21.3	29.6	38.5	48.2	58.4
		0.05	0.60	11.4	15.6	20.2	25.1	30.4	16.2	22.5	29.3	36.7	44.6	19.9	28	36.7	46.2	56.3
		0.30	0.30	13.6	18	22.8	28	33.6	19.2	25.8	33	40.9	49.3	23.7	32.2	41.5	51.5	62.2
		0.40	0.40	12.4	16.8	21.4	26.4	31.9	17.6	24.1	31	38.7	46.8	21.7	30	38.9	48.6	59
		0.50	0.50	11.3	15.5	20	24.9	30.2	15.9	22.2	29	36.4	44.3	19.6	27.7	36.4	45.9	55.9
		0.60	0.60	10	14.2	18.6	23.4	28.6	14.2	20.4	27	34.3	42	17.4	25.3	33.9	43.1	52.9
	3PL	0.05	0.30	12.3	15.9	19.7	23.9	28.3	16.7	22.1	27.8	34.1	40.8	20.5	27.4	34.8	42.9	51.5
		0.05	0.40	11.4	14.9	18.7	22.7	27.1	15.5	20.7	26.3	32.5	39	19	25.7	33	40.8	49.3
		0.05	0.50	10.5	14	17.7	21.7	26	14.3	19.4	25	31	37.5	17.5	24.1	31.2	39	47.3
		0.05	0.60	9.69	13.1	16.8	20.7	25	13.1	18.2	23.7	29.7	36.1	16	22.6	29.7	37.3	45.5
		0.30	0.30	11.8	15.2	19	22.9	27.1	15.9	21.1	26.6	32.6	39	19.6	26.2	33.3	41	49.2
		0.40	0.40	10.5	13.8	17.4	21.2	25.2	14.1	19.1	24.4	30.1	36.2	17.3	23.7	30.5	37.8	45.6
		0.50	0.50	9.13	12.4	15.8	19.5	23.4	12.3	17.1	22.2	27.7	33.5	14.9	21.1	27.7	34.7	42.2
		0.60	0.60	7.73	10.9	14.3	17.8	21.6	10.3	15	20	25.3	30.9	12.5	18.5	24.9	31.7	39

Notes: M_{design} is the design sagging moment ; M_1 is the ratio of first support to span design moment; M_2 is the ratio of second support to span design moment; Rotations in mrads

Table 6-2: Composite connection rotation capacity requirement to reach $0.90M_p$ span moment (continued)

				Span to depth ratio = 15					Span to depth ratio = 20					Span to depth ratio = 25				
Steel grade	Load case	End moments		Maximum dead load stress, σ_{dl}					Maximum dead load stress, σ_{dl}					Maximum dead load stress, σ_{dl}				
		M_1	M_2	$0.0\sigma_y$	$0.25\sigma_y$	$0.5\sigma_y$	$0.75\sigma_y$	$1.0\sigma_y$	$0.0\sigma_y$	$0.25\sigma_y$	$0.5\sigma_y$	$0.75\sigma_y$	$1.0\sigma_y$	$0.0\sigma_y$	$0.25\sigma_y$	$0.5\sigma_y$	$0.75\sigma_y$	$1.0\sigma_y$
S355	2PL	0.05	0.30	13	18	23.4	29.6	36.2	19.3	27.5	36.5	46.2	57	26	37	49.2	62.7	77.4
		0.05	0.40	12	16.7	21.7	27.4	33.7	17.4	24.9	33.5	42.7	52.7	23.2	33.6	45.1	57.7	71.4
		0.05	0.50	11	15.5	20.3	25.7	31.6	15.8	22.8	30.9	39.7	49.3	20.8	30.6	41.6	53.6	66.6
		0.05	0.60	10.1	14.5	19.1	24.2	29.8	14.4	21.1	28.7	37.1	46.3	18.8	28.1	38.5	50.1	62.5
		0.30	0.30	13.6	19.9	26.4	33.1	41	22.5	31.3	42.3	54.2	66.9	30.7	43.1	58.2	74.4	91.5
		0.40	0.40	12.4	18.6	24.9	31.6	39.4	20.7	29.4	40.2	52	64.5	28.4	40.6	55.6	71.6	88.4
		0.50	0.50	11.1	17.2	23.5	30.1	37.8	18.9	27.5	38.2	49.8	62.2	26	38.1	52.9	68.7	85.4
		0.60	0.60	9.74	15.8	22.1	28.6	36.2	16.9	25.5	36.1	47.7	59.8	23.5	35.5	50.2	65.9	82.1
	UDL	0.05	0.30	13.6	18.8	24.2	30	36.3	20.2	28	36.7	46.2	56.4	26.6	37.2	49.1	62.2	76.1
		0.05	0.40	12.7	17.8	23.1	28.7	34.9	18.9	26.5	35	44.3	54.3	25	35.3	46.9	59.6	73.2
		0.05	0.50	11.9	16.9	22	27.6	33.6	17.7	25.1	33.5	42.6	52.3	23.4	33.6	44.9	57.4	70.6
		0.05	0.60	11.1	16	21	26.5	32.4	16.5	23.8	32	40.9	50.5	21.8	31.8	42.9	55.1	68.1
		0.30	0.30	13.3	18.4	23.8	29.6	35.8	19.7	27.4	36.1	45.5	55.7	26	36.5	48.3	61.2	75
		0.40	0.40	12.2	17.1	22.3	27.9	33.9	18.1	25.5	33.9	43	52.8	23.8	34	45.4	57.9	71.3
		0.50	0.50	10.9	15.8	20.8	26.3	32.2	16.3	23.5	31.7	40.6	50.1	21.5	31.4	42.6	54.7	67.7
		0.60	0.60	9.66	14.4	19.4	24.7	30.4	14.4	21.6	29.6	38.2	47.4	19.1	28.8	39.7	51.5	63.9
	3PL	0.05	0.30	12.3	16.6	21.1	25.9	31	17.2	23.7	30.8	38.3	46.5	22.1	30.9	40.4	50.7	61.9
		0.05	0.40	11.3	15.6	20	24.7	29.6	15.8	22.2	29.1	36.5	44.5	20.4	29	38.3	48.4	59.3
		0.05	0.50	10.4	14.6	18.9	23.6	28.4	14.6	20.8	27.6	34.9	42.8	18.7	27.2	36.3	46.3	57.0
		0.05	0.60	9.55	13.7	18	22.5	27.3	13.3	19.5	26.3	33.5	41.2	17.2	25.5	34.6	44.4	55.0
		0.30	0.30	11.7	16	20.3	25	29.8	16.4	22.7	29.5	36.7	44.5	21	29.4	38.6	48.4	59.1
		0.40	0.40	10.4	14.5	18.7	23.1	27.8	14.4	20.5	27	34	41.4	18.5	26.6	35.3	44.8	54.9
		0.50	0.50	9	13	17	21.3	25.8	12.4	18.3	24.6	31.3	38.4	15.8	23.7	32.2	41.3	51.0
		0.60	0.60	7.54	11.4	15.4	19.6	23.8	10.3	16.1	22.2	28.7	35.4	13.1	20.8	29	37.7	46.8

Notes: M_{design} is the design sagging moment ; M_1 is the ratio of first support to span design moment; M_2 is the ratio of second support to span design moment; Rotations in mrads

Table 6-3: Composite connection rotation capacity requirement to reach $0.95M_p$ span moment

				Span to depth ratio = 15					Span to depth ratio = 20					Span to depth ratio = 25				
Steel grade	Load case	End moments		Maximum dead load stress, σ_{dl}					Maximum dead load stress, σ_{dl}					Maximum dead load stress, σ_{dl}				
		M_1	M_2	$0.0\sigma_y$	$0.25\sigma_y$	$0.5\sigma_y$	$0.75\sigma_y$	$1.0\sigma_y$	$0.0\sigma_y$	$0.25\sigma_y$	$0.5\sigma_y$	$0.75\sigma_y$	$1.0\sigma_y$	$0.0\sigma_y$	$0.25\sigma_y$	$0.5\sigma_y$	$0.75\sigma_y$	$1.0\sigma_y$
S275	2PL	0.05	0.30	16.8	22.5	28.7	35.8	43.1	25.2	34.1	43.6	53.6	64.3	31.2	42.3	54.1	66.5	79.6
		0.05	0.40	15	20.3	26.1	32.6	39.4	22.4	30.6	39.5	48.8	58.9	27.6	38	49.1	60.8	73.2
		0.05	0.50	13.6	18.4	23.9	30.1	36.5	20	27.7	36.1	44.9	54.4	24.6	34.5	45	56	67.9
		0.05	0.60	12.4	16.9	22	28	34.1	18	25.3	33.3	41.7	50.8	22.1	31.4	41.5	52.1	63.4
		0.30	0.30	21.7	28.6	36.1	45.5	54.4	32.8	44.1	55.6	67.4	80.1	39.7	53.2	67	81.2	96.2
		0.40	0.40	20.5	27.3	34.7	43.9	52.7	31	42.2	53.6	65.2	77.7	37.5	50.8	64.4	78.4	93.2
		0.50	0.50	19.1	25.9	33.2	42.4	51.1	29.2	40.2	51.5	63	75.5	35.1	48.3	61.8	75.7	90.3
		0.60	0.60	17.7	24.5	31.8	40.9	49.6	27.2	38.2	49.5	60.9	73.3	32.7	45.8	59.2	73	87.6
	UDL	0.05	0.30	17.5	22.8	28.7	35.5	42.4	25.5	34	43	52.4	62.6	31.3	41.9	53	64.8	77.2
		0.05	0.40	16.5	21.7	27.4	34.1	40.8	24.1	32.4	41.2	50.4	60.2	29.6	39.9	50.7	62.2	74.3
		0.05	0.50	15.6	20.8	26.3	32.9	39.4	22.9	31	39.6	48.6	58.2	28	38.1	48.7	59.9	71.7
		0.05	0.60	14.7	19.7	25.2	31.6	38	21.5	29.5	37.9	46.7	56.2	26.3	36.2	46.6	57.6	69.2
		0.30	0.30	17.1	22.4	28.2	35	41.8	25	33.4	42.3	51.7	61.7	30.7	41.1	52.2	63.8	76.1
		0.40	0.40	15.8	21	26.6	33.2	39.7	23.2	31.3	39.9	49	58.7	28.4	38.5	49.2	60.4	72.4
		0.50	0.50	14.5	19.5	25	31.4	37.8	21.3	29.2	37.6	46.4	55.8	26	35.8	46.3	57.2	68.8
		0.60	0.60	13.1	18	23.4	29.6	35.9	19.3	27.1	35.3	43.8	53.1	23.5	33.2	43.3	54	65.3
	3PL	0.05	0.30	14.1	18.3	22.9	28	33.3	19.9	26.4	33.3	40.7	48.7	24.5	32.7	41.5	50.9	60.9
		0.05	0.40	13.2	17.3	21.7	26.7	31.9	18.5	24.9	31.7	38.9	46.7	22.8	30.8	39.4	48.6	58.4
		0.05	0.50	12.2	16.3	20.7	25.6	30.7	17.3	23.5	30.2	37.3	45	21.2	29.1	37.6	46.6	56.2
		0.05	0.60	11.4	15.4	19.7	24.6	29.6	16.1	22.3	28.9	35.9	43.5	19.7	27.5	35.9	44.8	54.3
		0.30	0.30	13.4	17.5	21.8	26.6	31.7	18.8	25	31.6	38.6	46.2	23.1	31	39.4	48.2	57.8
		0.40	0.40	12	15.9	20	24.6	29.4	16.8	22.7	29	35.7	42.9	20.6	28.1	36.1	44.5	53.6
		0.50	0.50	10.5	14.3	18.3	22.7	27.3	14.7	20.4	26.4	32.8	39.7	17.9	25.1	32.8	41	49.7
		0.60	0.60	8.99	12.6	16.5	20.8	25.2	12.5	18	23.9	30.1	36.8	15.2	22.2	29.7	37.5	45.9

Notes: M_{design} is the design sagging moment ; M_1 is the ratio of first support to span design moment; M_2 is the ratio of second support to span design moment; Rotations in mrads

Table 6-3: Composite connection rotation capacity requirement to reach $0.95M_p$ span moment (continued)

Steel grade	Load case	End moments		Span to depth ratio = 15 Maximum dead load stress, σ_{dl}					Span to depth ratio = 20 Maximum dead load stress, σ_{dl}					Span to depth ratio = 25 Maximum dead load stress, σ_{dl}				
		M_1	M_2	$0.0\sigma_y$	$0.25\sigma_y$	$0.5\sigma_y$	$0.75\sigma_y$	$1.0\sigma_y$	$0.0\sigma_y$	$0.25\sigma_y$	$0.5\sigma_y$	$0.75\sigma_y$	$1.0\sigma_y$	$0.0\sigma_y$	$0.25\sigma_y$	$0.5\sigma_y$	$0.75\sigma_y$	$1.0\sigma_y$
S355	2PL	0.05	0.30	15.6	21.5	28.1	35.2	43.2	25.7	35.6	46.2	59.1	72.2	35	49.2	64.7	81	98.7
		0.05	0.40	14.1	19.4	25.7	32.5	39.9	22.8	32.1	42	53.8	66	31.1	44.2	58.5	73.7	90.2
		0.05	0.50	12.8	17.8	23.7	30.2	37.2	20.4	29.1	38.6	49.6	61	27.8	40.1	53.5	67.8	83.4
		0.05	0.60	11.7	16.5	22.1	28.1	35	18.3	26.6	35.7	46.2	57	24.9	36.7	49.4	63	77.8
		0.30	0.30	18.8	24.7	33.5	42.2	52.5	33.3	46.5	59.8	76.3	92.3	46.5	64.9	84.1	104	124
		0.40	0.40	17.5	23.3	31.9	40.6	50.7	31.4	44.5	57.6	73.9	89.7	44	62.2	81.2	100	121
		0.50	0.50	16.1	21.8	30.4	38.9	49	29.4	42.3	55.3	71.5	87.1	41.4	59.5	78.2	97.2	118
		0.60	0.60	14.6	20.3	28.9	37.3	47.2	27.3	40.2	53.1	69.1	84.4	38.7	56.7	75.3	94	114
	UDL	0.05	0.30	16.3	21.8	28.4	35.3	43	26	35.8	46.2	58.5	70.9	35.2	49	63.8	79.3	96
		0.05	0.40	15.3	20.7	27.1	33.8	41.4	24.6	34.1	44.2	56.2	68.3	33.3	46.7	61.1	76.2	92.5
		0.05	0.50	14.4	19.7	25.9	32.6	40	23.2	32.6	42.6	54.2	66.2	31.5	44.7	58.8	73.6	89.5
		0.05	0.60	13.5	18.7	24.8	31.3	38.5	21.8	31	40.7	52.2	63.8	29.6	42.5	56.4	70.8	86.4
		0.30	0.30	16	21.4	27.9	34.7	42.4	25.5	35.2	45.5	57.6	70	34.5	48.2	62.8	78.2	94.7
		0.40	0.40	14.6	20	26.2	32.9	40.3	23.5	32.9	42.9	54.7	66.6	31.9	45.2	59.3	74.2	90.2
		0.50	0.50	13.3	18.5	24.6	31	38.3	21.5	30.7	40.3	51.8	63.4	29.3	42.1	55.9	70.3	85.9
		0.60	0.60	11.9	17	23	29.3	36.2	19.4	28.4	37.8	48.9	60	26.5	39.1	52.5	66.4	81.3
	3PL	0.05	0.30	13.7	18.4	23.6	29.1	35.1	20.4	28	36.1	45.4	55.1	26.9	37.4	48.8	61	74.2
		0.05	0.40	12.7	17.3	22.4	27.7	33.6	19	26.4	34.3	43.4	52.9	25	35.3	46.5	58.4	71.3
		0.05	0.50	11.7	16.3	21.2	26.5	32.3	17.6	24.9	32.7	41.7	51	23.2	33.4	44.4	56.1	68.8
		0.05	0.60	10.8	15.3	20.2	25.4	31.1	16.3	23.5	31.3	40.1	49.3	21.6	31.6	42.5	54	66.5
		0.30	0.30	13.1	17.6	22.6	27.8	33.6	19.3	26.6	34.3	43.2	52.4	25.3	35.4	46.2	57.8	70.3
		0.40	0.40	11.6	16	20.8	25.8	31.2	17.1	24.1	31.5	39.9	48.7	22.4	32.1	42.4	53.5	65.4
		0.50	0.50	10.1	14.3	18.9	23.8	29	14.8	21.6	28.8	36.8	45.2	19.4	28.7	38.7	49.3	60.6
		0.60	0.60	8.5	12.7	17.1	21.8	26.8	12.5	19.1	26	33.8	41.6	16.4	25.4	35	45	55.6

Notes: M_{design} is the design sagging moment ; M_1 is the ratio of first support to span design moment; M_2 is the ratio of second support to span design moment; Rotations in mrads

Table 6-4: Percentage increase of $\theta_{required}$ of unpropped compared with propped construction for different dead load stress [L/D= 15 to 20, $M_{support}/M_{span}$ varies between 0.3 to 0.6]

Steel Grade	Loading	$\sigma_{d.l.} = 0.25\,\sigma_y$		$\sigma_{d.l.} = 0.50\,\sigma_y$		$\sigma_{d.l.} = 0.75\,\sigma_y$		$\sigma_{d.l.} = \sigma_y$	
		Internal Beam	External beam	Internal Beam	External beam	Internal Beam	External beam	Internal Beam	External beam
S275	$0.85M_p$	39-46%	31-35%	80-100%	64-73%	124-155%	101-118%	170-217%	143-167%
	$0.90M_p$	40-46%	34-38%	83-93%	73-81%	129-145%	117-120%	178-201%	164-180%
	$0.95M_p$	35-39%	35-38%	72-81%	74-79%	114-125%	117-122%	156-173%	162-168%
S355	$0.85M_p$	44-58%	39-45%	93-120%	79-92%	152-185%	121-144%	215-259%	168-202%
	$0.90M_p$	44-53%	41-44%	99-108%	83-94%	156-165%	132-149%	215-232%	185-208%
	$0.95M_p$	35-46%	39-43%	86-96%	84-89%	138-149%	133-140%	200-205%	188-195%

Table 6-5: Relative proportions of elastic and plastic rotations – tests by Culver [1961]

Test	Loads	δ_{el}	θ_{el}	θ_{pl}	θ_{pl}^*	$\theta_{el}/\theta_{pl}^*$
B1-T1	2PL	8.42	0.0084	0.0323	0.0120	0.70
B2-T1	2PL	8.42	0.0084	0.0296	0.0106	0.76
B3-T1	2PL	8.42	0.0084	0.0300	0.0108	0.76

Table 6-6: Limiting design values for the maximum stress prior to hardening of the slab concrete (σ_{dl})

Steel grade	Beam location	Span to depth ratio = 15			Span to depth ratio = 20			Span to depth ratio = 25		
		2PL	UDL	3PL	2PL	UDL	3PL	2PL	UDL	3PL
S355	Internal	$\sigma_{dl} \le 0.89\sigma_y$	$\sigma_{dl} = 1.0\sigma_y$	$\sigma_{dl} = 1.0\sigma_y$	$\sigma_{dl} \le 0.44\sigma_y$	$\sigma_{dl} \le 0.53\sigma_y$	$\sigma_{dl} \le 0.73\sigma_y$	$\sigma_{dl} \le 0.21\sigma_y$	$\sigma_{dl} \le 0.29\sigma_y$	$\sigma_{dl} \le 0.44\sigma_y$
	External	$\sigma_{dl} = 1.0\sigma_y$	$\sigma_{dl} = 1.0\sigma_y$	$\sigma_{dl} = 1.0\sigma_y$	$\sigma_{dl} \le 0.54\sigma_y$	$\sigma_{dl} \le 0.51\sigma_y$	$\sigma_{dl} \le 0.67\sigma_y$	$\sigma_{dl} \le 0.30\sigma_y$	$\sigma_{dl} \le 0.26\sigma_y$	$\sigma_{dl} \le 0.39\sigma_y$
S275	Internal	$\sigma_{dl} \le 0.68\sigma_y$	$\sigma_{dl} \le 0.80\sigma_y$	$\sigma_{dl} = 1.0\sigma_y$	$\sigma_{dl} \le 0.31\sigma_y$	$\sigma_{dl} \le 0.40\sigma_y$	$\sigma_{dl} \le 0.58\sigma_y$	$\sigma_{dl} \le 0.13\sigma_y$	$\sigma_{dl} \le 0.18\sigma_y$	$\sigma_{dl} \le 0.31\sigma_y$
	External	$\sigma_{dl} \le 0.81\sigma_y$	$\sigma_{dl} \le 0.78\sigma_y$	$\sigma_{dl} = 1.0\sigma_y$	$\sigma_{dl} \le 0.42\sigma_y$	$\sigma_{dl} \le 0.38\sigma_y$	$\sigma_{dl} \le 0.53\sigma_y$	$\sigma_{dl} \le 0.21\sigma_y$	$\sigma_{dl} \le 0.16\sigma_y$	$\sigma_{dl} \le 0.28\sigma_y$

Note: Values assume support to span moment ration (M_{sup}/M_{span}) ≥ 0.3 and the maximum design sagging moment is $0.85M_p$

Chapter 7 - Assessment of the effect of strain hardening on the flexural strength of steel beams

---

Papers published based on this chapter:

1. Byfield, M. P., M. Dhanalakshmi, (2002). Analysis of strain hardening in steel beams using mill tests, *International conferences on advances in steel structures*, Hong Kong, 139-146.

2. Byfield, M. P., Davies, J. M. and M. Dhanalakshmi. (2004). "Calculation of the strain hardening behaviour of steel structures based on mill tests", Journal of Constructional Steel Research, Vol. 61, 133-150.

7.1 Introduction

The early research into plastic design theory by Baker (1963) demonstrated that the plastic moment capacity (M_p), determined as the product of the yield stress and the plastic section modulus, leads to a marginal underestimation of the strength because it ignores the effect of strain hardening, see Figure 7-1a.

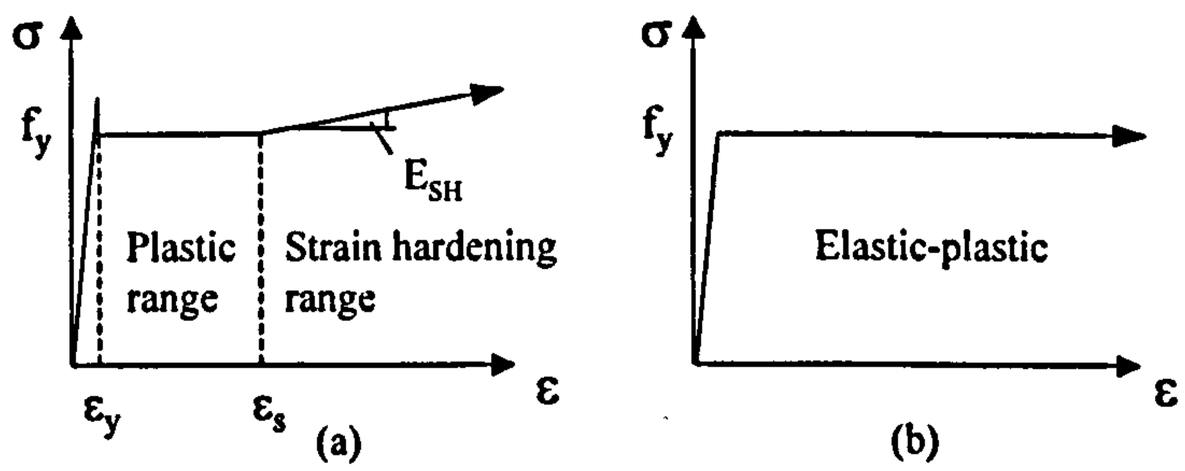

Figure 7-1. Stress-strain curves for mild steel; (a) actual (b)simplified for design

This conservatism was found to be useful, because it was shown to off-set the reduction in the collapse load of rigid-jointed sway frames due to the changes in geometry caused by deflexions, also known as second-order effects or frame instability, that occurs during the successive formation of plastic hinges. Calculations based on the elastic-plastic stress-strain relationship in Figure 7-1b were justified because the conservatism due to the neglect of strain hardening was found to be approximately balanced by the reduction in load capacity due to second order effects. However, relatively recent research by Davies (1990) has shown that portal frames are much more sensitive to second order effects than was previously known. Therefore, it is necessary to characterise the strain-hardened performance of modern structural steels in ordered to establish the safety of modern portal framed buildings.

The recent experimental testing of 12 hot rolled sections by Byfield and Nethercot (1998), showed that M_p underestimated flexural strength by an average of 18%. The tests were carried out in uniform bending on beams that were fully restrained against lateral movement. Tensile testing of the sections showed that the steel demonstrated no significant zone of plasticity, with strain hardening beginning shortly after initial yielding. A further 20 sections were tested with lateral restraints positioned such that the non-dimensional slenderness ($\bar{\lambda}_{LT}$) was set to just less than 0.4, corresponding to the limit of applicability of the M_p resistance function in accordance with Eurocode 3: Part 1.1. Despite the wide spacing of the lateral restraints the observed bending strengths exceeded M_p by an average of 14%. Thus, the M_p formula was shown to significantly underestimate strength.

The calculations of M_p used for establishing the accuracy of the design formula were based on measured geometric and material properties based on mill tests. Mill tests define a yield stress corresponding to a 0.5% proof strain. They do not therefore refer to either the upper or lower yield point. Mill tests are carried out at a relatively high rate of strain beyond 1% strain, although all strain rates conform to the limits defined in EN10025 (CEN, 1990). Mill tests were used because they represent the industry standard measure of yield stress. A full account of the differences between mill and conventional coupon tests is given in Kemp *et al* (2002).

The tests upon which Byfield and Nethercot's (1998) findings are based were carried out on relatively light-weight sections (203x102x23UB and 152x152x30UC). It is not clear whether the results are transferable to the heavier sections more common in commercial rigidly jointed frames. Scale effects are particularly important since the conservatism observed in the calculation of M_p may have been due to unrepresentative or unusual material properties of the small sample of sections tested. Moreover, the yield stress of hot rolled steel is well known to be affected by material thickness. Thus, a method by which strain hardened flexural strength can be quantified directly from mill tests is required in order to extend the scope of the research.

The conservatism in the M_p formula is compounded by the results of mill tests of steel often revealing significantly higher strengths than the nominal yield stress assumed during design. A survey based on over 7000 material and geometric properties of structural steels, Byfield and Nethercot (1997), showed that the average tensile strength of steel (using mill tests) was some 16% higher than the nominal yield stress, where the flange thickness was greater than 10mm. In sections with a flange thickness of less than 10mm, average mill stress exceeded the nominal yield stress by 37%. The survey also showed that the geometric properties of rolled steel sections are close to the nominal values and have little impact on strength.

The above discussion is concerned with increases in the value of M_p in uniform bending. Another even more favourable manifestation of strain hardening occurs when a plastic hinge forms at a location where there is a significant bending moment gradient (e.g. below a point load, at the eaves of a portal frame or where a beam frames into a column). Here, the shape of the moment gradient constrains the spread of plasticity and, as the plastic hinge rotates, the strain hardening associated with the increasing strain causes a more marked increase in the bending moment at the hinge position.

Davies (1966) showed that the increased moment due to strain hardening, δM, associated with a plastic hinge rotation θ_p is given to a good approximation by:

$$\delta M = \frac{EI}{kh}\theta_p \qquad (1)$$

where E = elastic modulus of the steel;

I = second moment of area of the steel member

h = a parameter termed the "equivalent cantilever" which depends on the shape of the bending moment diagram in the vicinity of the plastic hinge (Figure 7-2)

k = a dimensionless strain hardening parameter which is a property of the steel

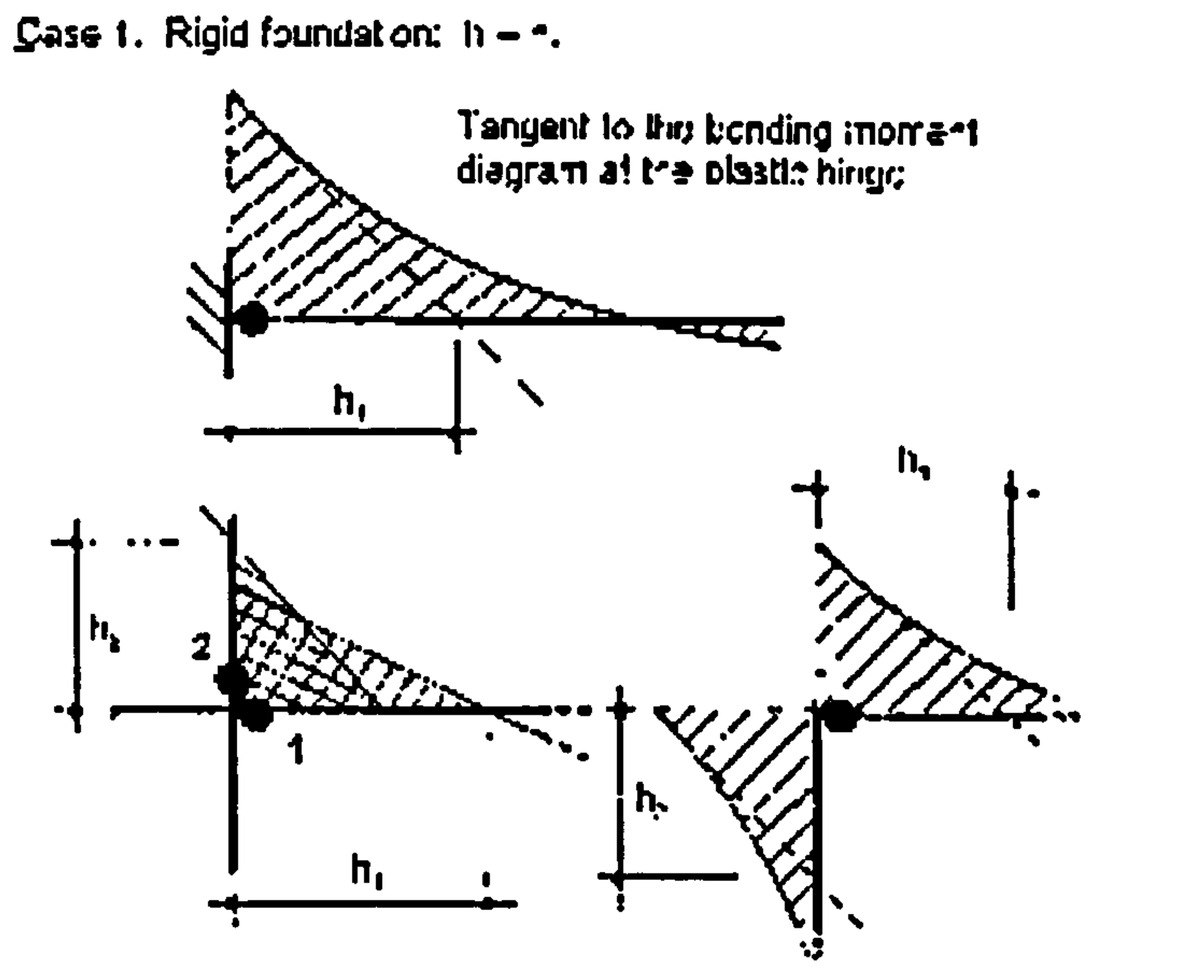

Figure 7-2. "Equivalent cantilever" h as a function of the shape of the bending moment diagram

Equation (1) arises from a proposal made originally by Horne (1960). Horne suggested that when the strain at the "strain centre" of a section reached the value ε_s (see Figure 1) at the onset of strain hardening, the cross-section would lock, thus forcing the plastic zone to spread outwards away from the section of maximum bending moment. The strain centre was located at a distance r_s from the neutral axis of the section where:

$$r_s = \frac{I}{S} \tag{2}$$

and S is the plastic modulus of the section. In this original proposal, the dimensionless quantity 'k' was the ratio of ε_s to the strain at yield.

The above concept offers a simple and convenient treatment of strain hardening for the purposes of structural analysis, Davies (2002). It was investigated in some detail in the 1960's (Horne and Medland (1966), Davies (1966) and (1966a)) and it was found that it was adequate for practical design provided that 'k' was determined by bending tests on simply supported beams subject to a single point load, rather than from the stress-strain curve as originally proposed.

The above formulation is particularly suitable for inclusion in computer programs for the second-order elastic-plastic analysis of plane frames based on the displacement method. There is, therefore, considerable interest in confirming its validity for current steel qualities and section shapes and, in particular, determining an appropriate value (or values) for 'k'.

This chapter provides an up to date assessment of the strain hardening factor that may be incorporated into computer programs for second-order elastic-plastic analysis. A survey of tensile tests (mill tests) is presented which shows that the strain hardening behaviour is independent of material thickness and steel grade. This allows a generalisation of the stress-strain relationship for hot rolled steel to be defined and thus the characteristic stress-strain relationship is define..

The modelling technique which is presented in Chapter 4 allows the non-linear moment-deformation behaviour of beams to be accurately predicted using the mill test data. A parametric study has been carried out using the modelling technique based on the defined characteristic stress-strain data. The study covers different cross sections (203x102x23 UB, 533x210x82UB), span to depth ratio (L/D=10 to 60) and loading conditions (UDL,

2PL and 1PL). The moment-rotation results obtained from the parametric study are used to estimate values of the strain hardening factor to be used during elastic-plastic design.

7.2 Survey of mill tests

A total of 50 mill tests taken from hot rolled I and H sections, with varying flange thickness and steel grade (S275 and S355) are presented, see Table 7-1.

Table 7-1. Results from the survey of mill tests

Steel grade	Sample size	Mean flange thickness (mm)	Mean 0.5RT (N/mm^2)	E_{SH} (N/mm^2)
S275	10	10.4	326	2502
S275	8	20.0	302	2435
S275	7	34.9	293	2554
S355	8	11.1	399	2963
S355	9	20.0	395	2235
S355	8	37.8	374	2527

The tests were carried out at the Corus (British Steel) Lackenby Mill, locating at Redcar in the UK. The Lackenby mill is a modern beam mill and the steel sampled was produced using the continuous casting process. Table 7-1 lists average values for yield stress, where the yield stress corresponds to the stress at 0.5% total strain (0.5RT). The tests were in accordance with the Specification EN10025 (CEN, 1990), which specifies that test coupons must be cut from the flanges, in contrast with US practice, in which coupons are typically sampled from web material.

The stress strain curves from the 50 mill tests surveyed for steel grade S275 and S355 are shown in Figure 7-3 and Figure 7-4 respectively. The tests demonstrate that all the samples exhibit approximately the same rate of strain hardening beyond strains of 1 to 1.5%.

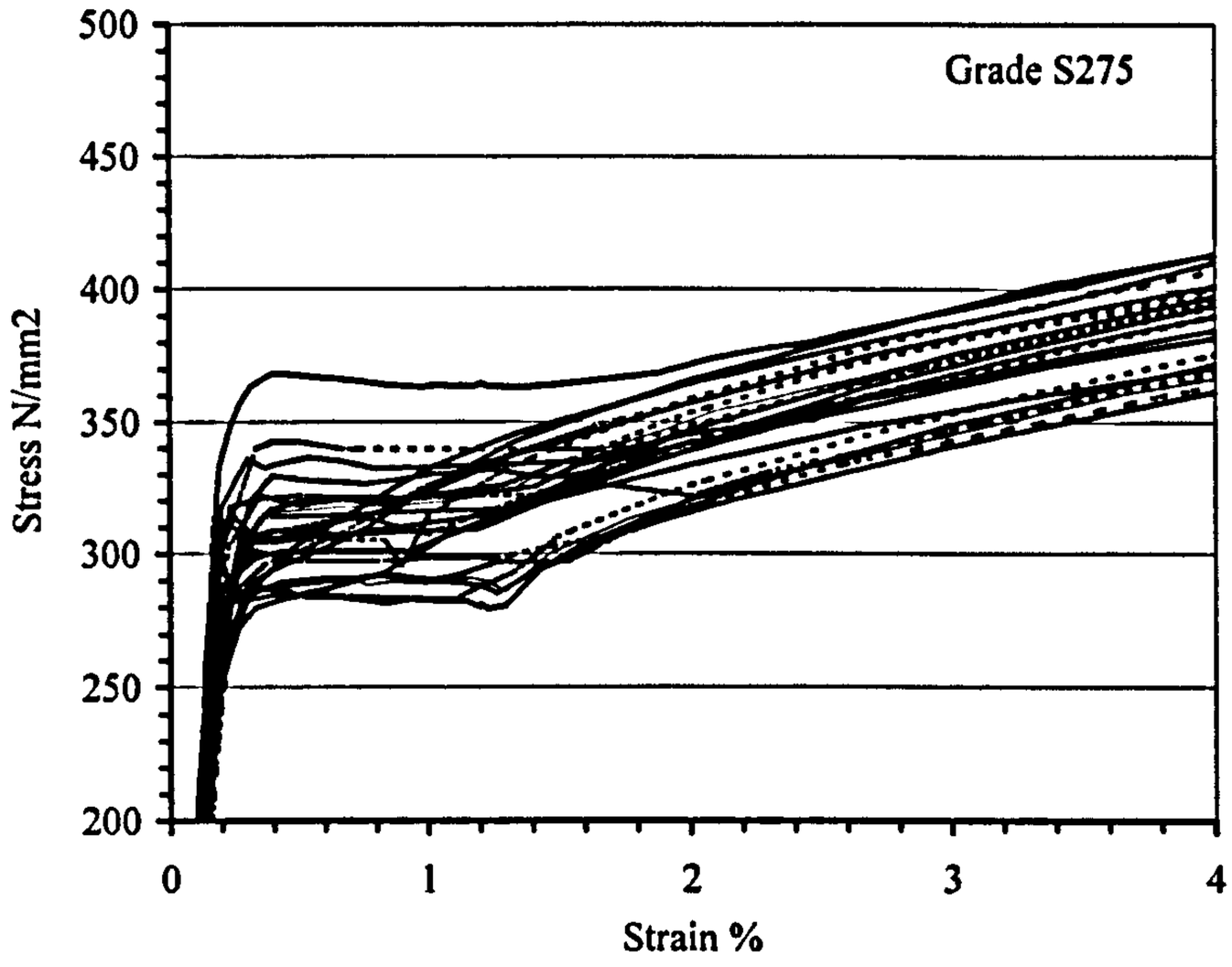

Figure 7-3. Combined results from 50 mill tests for S275 grade steel

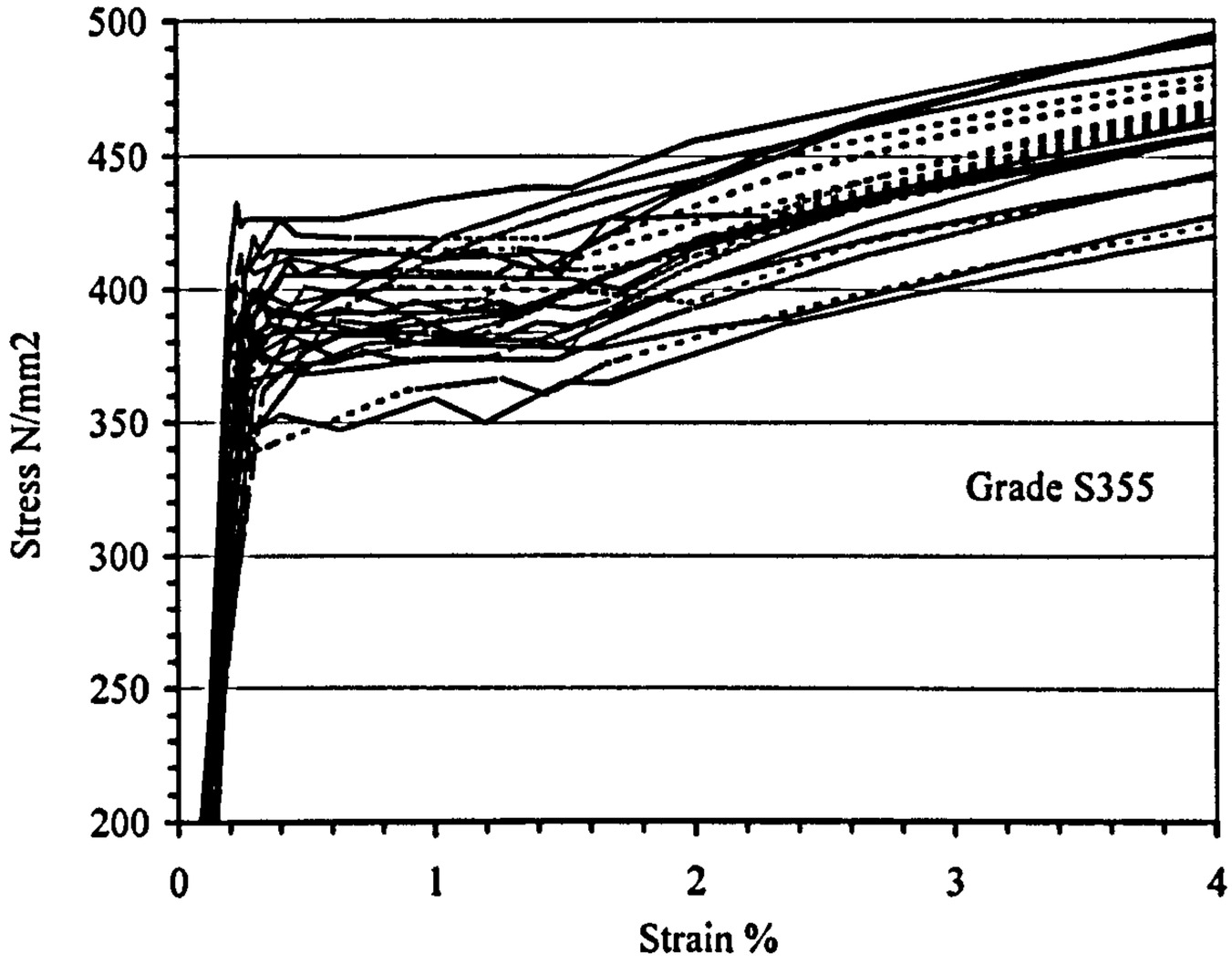

Figure 7-4. Combined results from 50 mill tests for S355 steel

Table 7-2 lists the average strain hardening modulus E_{SH} derived from the tests, where E_{SH} is defined as the slope taken between 1.5% and 4% strain. Inspection of Table 7-2 shows that the rate of strain hardening is independent of material thickness. In addition,

the rate of strain hardening seems to differ little between the S275 and S355 steel grades. This is encouraging because it suggests that the practical treatment of the influence of strain hardening (e.g. '*k*' in equation (1)) may be harmonised over the current range of section shapes and steel grades. A clear link between the yield point and material thickness is also demonstrated, although this effect is already well documented by Byfield and Nethercot (1997), amongst others.

Table 7-2. Comparison of strain hardening properties

Reference	E_{SH}	ε_{sh}
Horne (1981)	$\cong 0.05E$ (10000 N/mm^2)	6-10 ε_y
Lay and Smith (1965)	2550N/mm^2	$11\varepsilon_y$
Byfield and Dhanalakshmi	2700N/mm^2	$6\varepsilon_y$

The mean values of stress strain curves, together with the 95% upper and lower confidence limits are shown in Figure 7-5 (based on the data presented in Figure 7-3 and Figure 7-4). It is generally accepted that nominal values of yield stress are characteristic values, i.e. they correspond to the lower 95% confidence limit. This assumption is confirmed from Figure 7-5, with the characteristic stress at 0.5% strain corresponding to the nominal values of 275N/mm^2 and 355N/mm^2. Based on these characteristic stress-strain responses, the value for strain hardening modulus, E_{SH}, was found to be 2700N/mm^2. Furthermore, strain hardening was found to commence at a strain equal to 6 times the yield strain, i.e., $\varepsilon_s = 6\varepsilon_y$, see Figure 7-1a. These values have been compared with those found by other researchers in Table 7-2. Good agreement is found with Lay and Smith's findings, although significantly less strain hardening was observed than predicted by Horne.

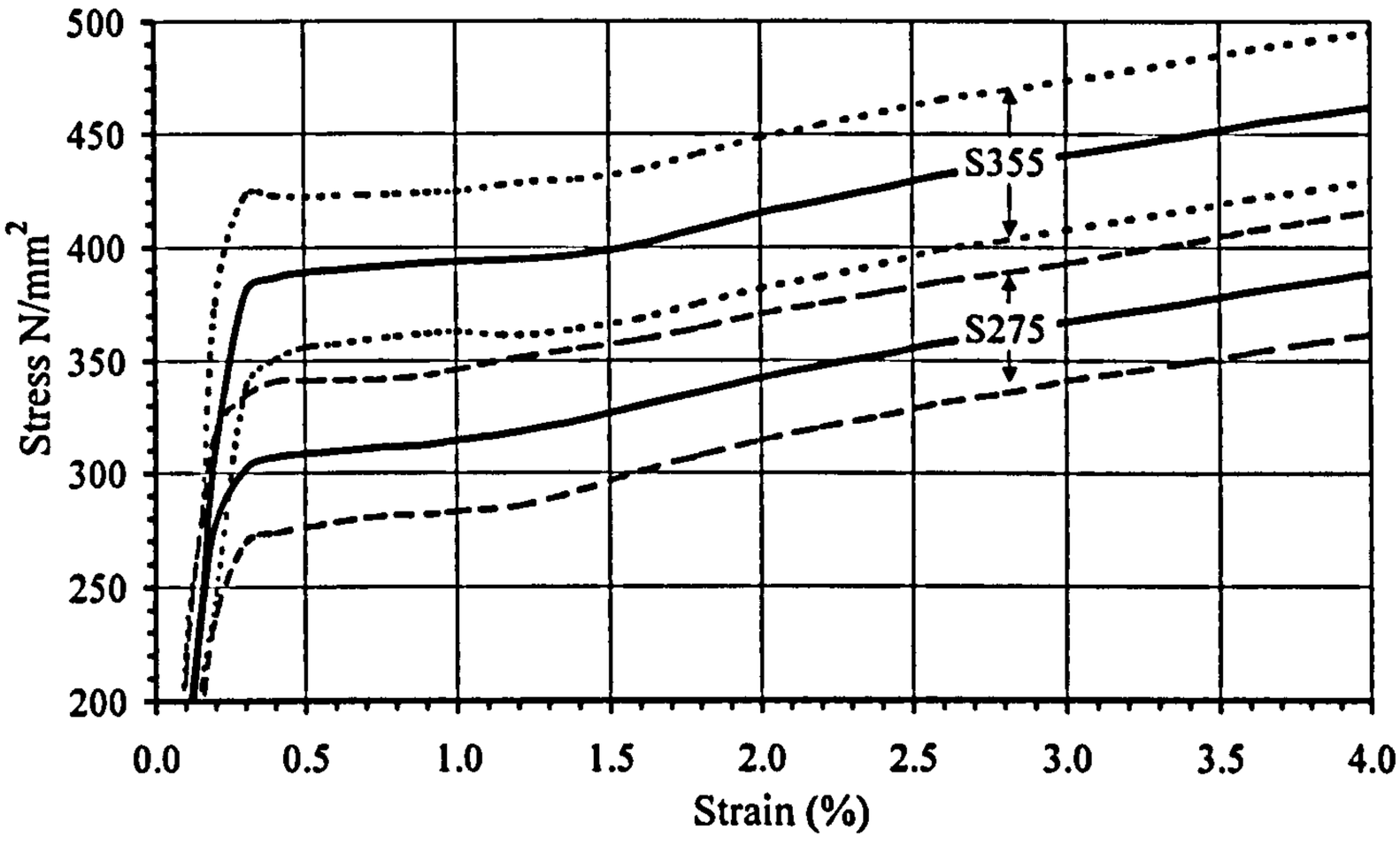

Figure 7-5. Stress-strain curves – mean (solid lines), upper and lower 95% confidence limits

7.3 Modelling of moment deformation using mill tests

In order to evaluate the significance of strain hardening in the light of the available test data, there are three generic cases to consider, as shown in Figure 7-6. For each of the three cases, the line diagram is shown above the corresponding bending moment diagram. Figure 7-6(a) shows the case that has been frequently tested although it hardly ever occurs in practice. It is characterised by a long region of uniform bending moment so that, when full plasticity occurs, it extends over the full distance between the loads. This evidently reduces the influence of strain hardening on bending strength. Figure 7-6(b) shows a plastic hinge occurring below a distributed load. Here, although the bending moment diagram is non-uniform at the plastic hinge position, it has zero slope and is only changing slowly. Although the scope for spread of plasticity is not unlimited, it is considerable so that the increase in M_p due to strain hardening is likely to be similar to case (a). Figure 7-6(c) shows a plastic hinge occurring below a significant point load. Here the spread of plasticity is limited by the shape of the bending moment diagram, which leads to quite different considerations. The numerical model described in Chapter 4 can deal with each of these situations.

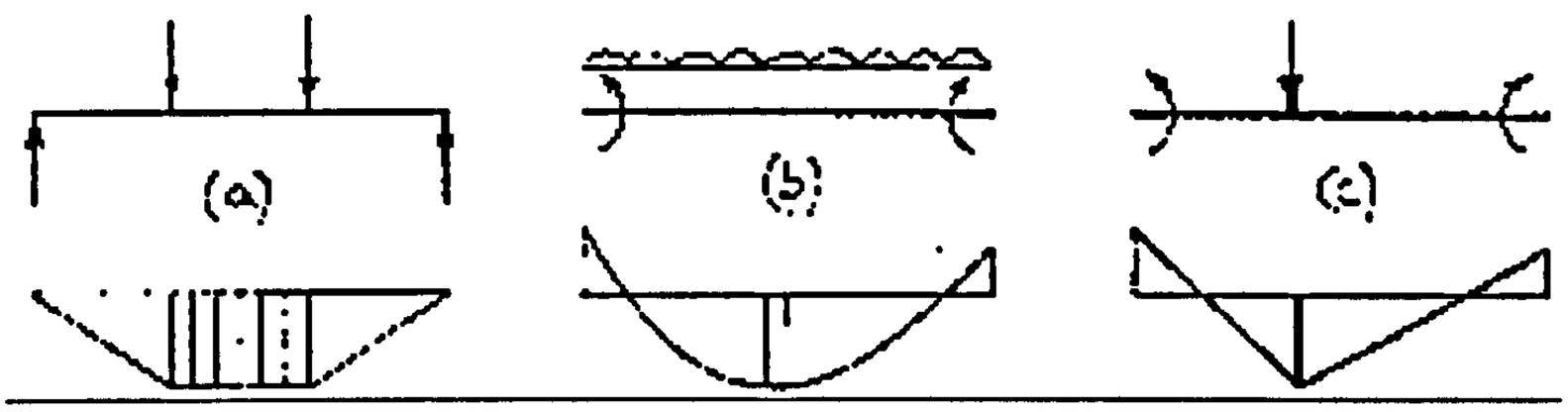

Figure 7-6. Generic cases of strain hardening in plastic hinges

Equation (1) only applies to the situation shown in Figure 7-6(c). For the cases shown in Figure 7-6(a) and (b), the "equivalent cantilever" $h = \infty$ (tangent to the bending moment at the plastic hinge is asymptotic), so that there is no increase in bending moment with plastic hinge rotation. This chapter shows that there may, however, be an increase in the moment of resistance M_p due to strain hardening.

7.4 Comparison between predicted and experimental moment vs. end rotation (M-θ) responses

Figure 7-7 and Figure 7-8 show the experimental M-θ response to 4-point loading based on the average results from 6 identical bending tests for each of two sections (203x102x23UB and 152x152x30UC) reported by Byfield and Nethercot (1998) respectively.

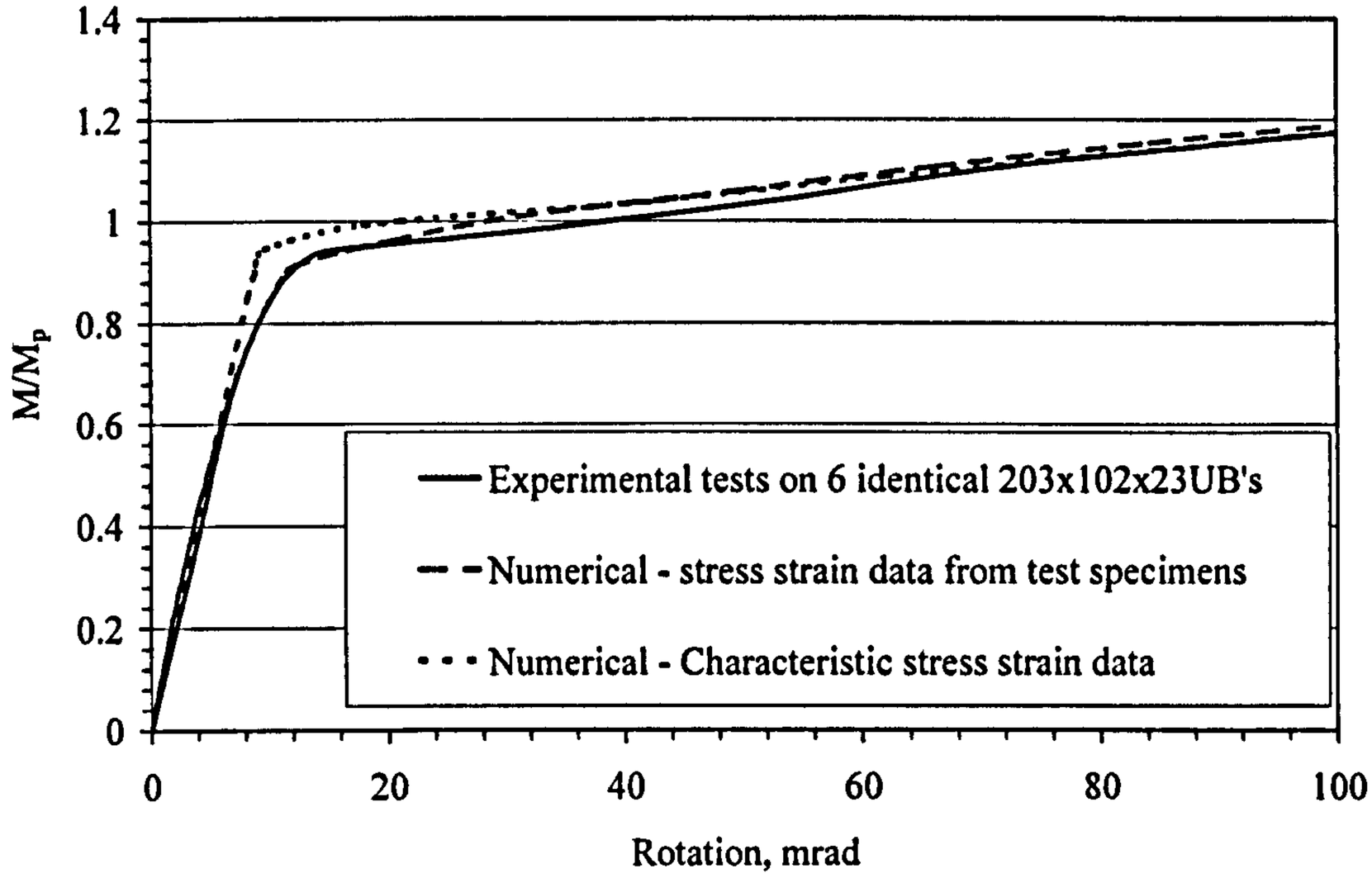

Figure 7-7. Comparison between experimental and predicted M-θ for Nottingham test beam section 203x102x23UB

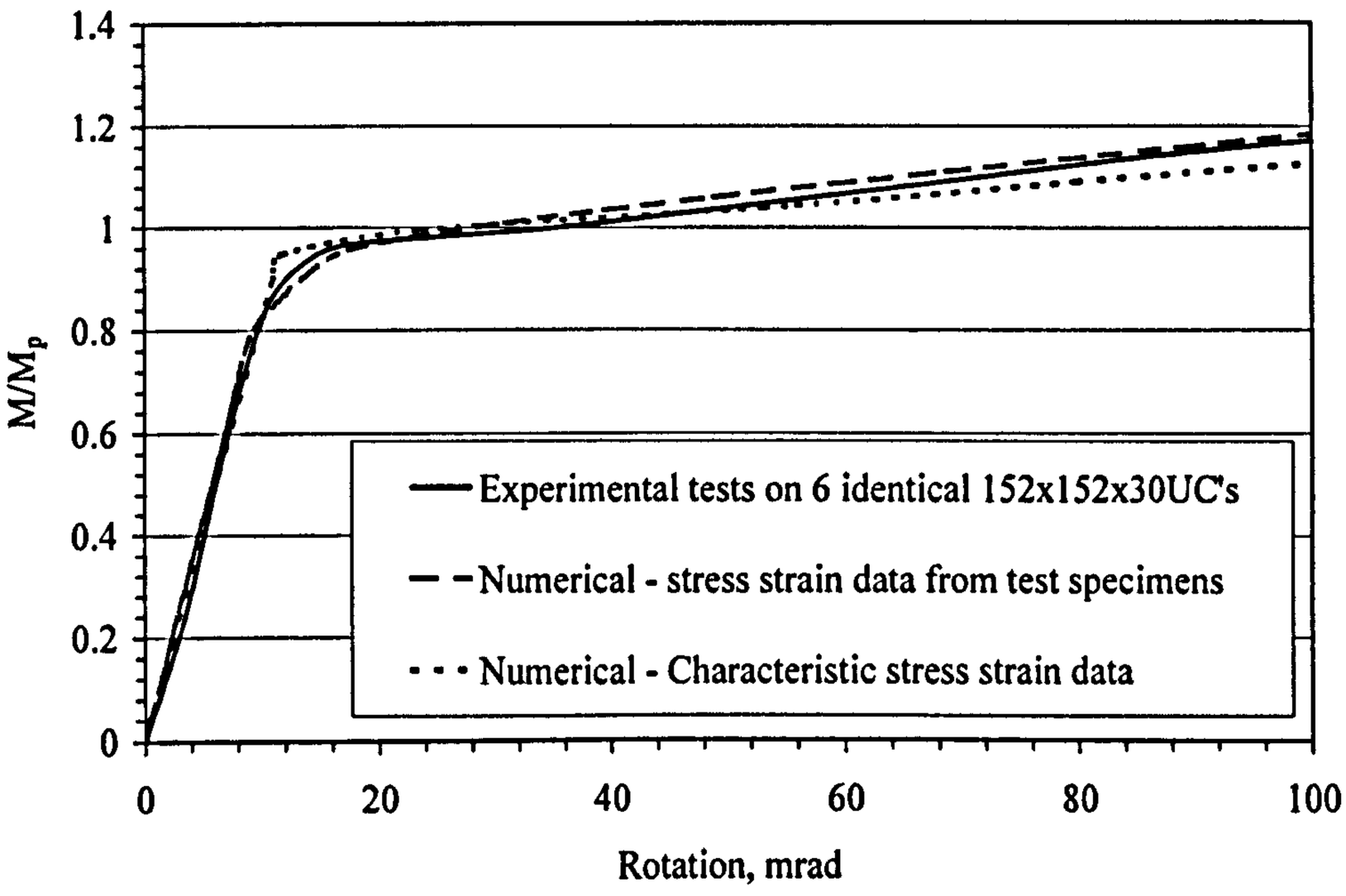

Figure 7-8. Comparison between experimental and predicted M-θ for Nottingham test beam section 152x152x30UC

These figures also show two theoretical M-θ responses calculated using the numerical method described in Chapter 4. The first was calculated using the average of the mill test stress-strain curves taken from the 6 test specimens (2 tests per specimen) for each sections. This method reduced statistical variations and therefore allows the method to fully demonstrate the degree of accuracy with which it is able to predict strength vs. ductility. The model can clearly be seen to achieve a good degree of conformity with experimental behaviour.

Figure 7-7 and Figure 7-8 also show the predicted M-θ relationship based on the characteristic stress strain relationship shown in Figure 7-5 for S275 steel. Again, good conformity between experimental and theoretical behaviour is demonstrated. The divergence between experimental and theoretical behaviour below 1 degree of end-rotation is due to the characteristic value of elastic modulus being significantly below 205,000N/mm^2. Mill tests are a poor method of measuring elastic modulus; they have therefore produced a poor prediction of M-θ within the elastic range.

7.5 Parametric study

A parametric study was carried out based on 203x102x23UB (light section) and 533x210x82UB (heavy section) with the L/D varying from 10 to 60 in order to assess the influence of the span. Uniformly distributed (UDL), single (1PL) and two points loading (2PL) have been considered, i.e. the three generic cases shown in Figure 7-6. A total of 36 cases have been studied in a combination of steel grade, span to depth ratio and loading type, giving the results presented in Table 7-3 and Table 7-4 for each of the sections considered. The analysis was carried out using the characteristic stress strain relationship established as part of this study, i.e. E_{SH} = 2700N/mm^2 and $\varepsilon_{sh} = 6\varepsilon_y$. The various parameters are described in detail below.

7.5.1 Section size

Comparison of Table 7-3 and Table 7-4 shows the difference in required rotation to achieve design sagging moment of 1.0Mp, 1.1Mp, 1.15Mp for the two sections

considered in the study is negligible. Figure 7-9 shows the predicted M-θ responses of the two sections considered for L/D ratio of 10 and for all the load cases considered. This analysis of the predicted M-θ responses for sections of different weight but identical span to depth ratio (L/D) showed that section size did not significantly affect strain hardening.

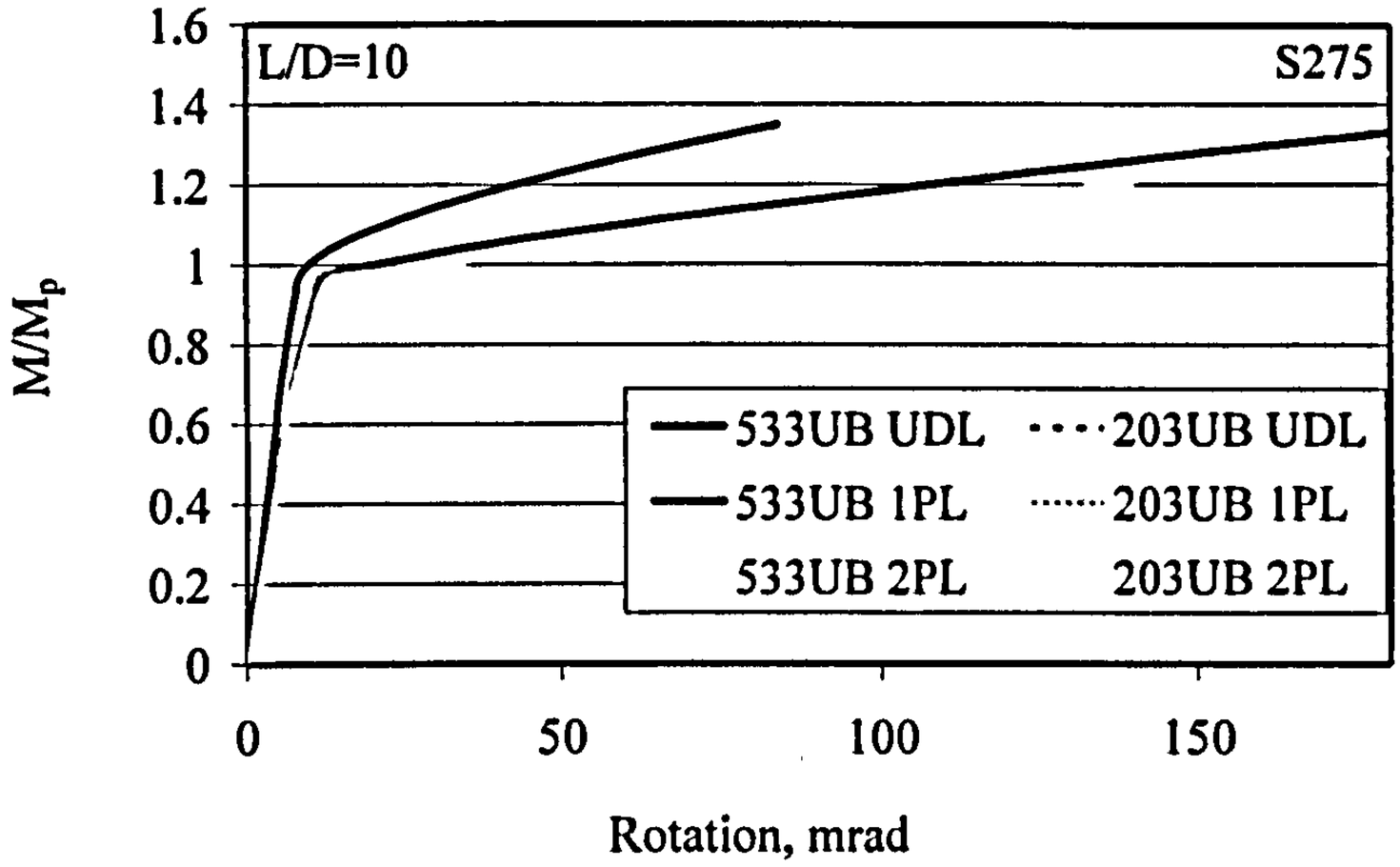

Figure 7-9. Effect of section size on strain hardening

7.5.2 Steel grade

As would be expected, higher grade steel was found to require greater end rotation than low grade steel in order to strain-harden, see Table 7-3 and Table 7-4. S355 steel required 20% greater end rotation to develop $1.0M_p$ if subjected to a single point load, 25% greater if subjected to a UDL and 56% greater rotation if subjected to 2-point loads. These increases vary slightly depending on the L/D ratio considered, but the exact figures can be determined from the data presented in Table 7-3 and Table 7-4. The loading type did not significantly effect the rotation required to achieve either 1.1 or $1.15M_p$. In both cases approximately 28% extra end rotation was required for S355, in comparison with S275 steel.

7.5.3 Loading type

The curvature distributions developed by a S275, 203x102x23UB, resisting loads from zero up to $1.15M_p$ are shown in Figure 7-10.

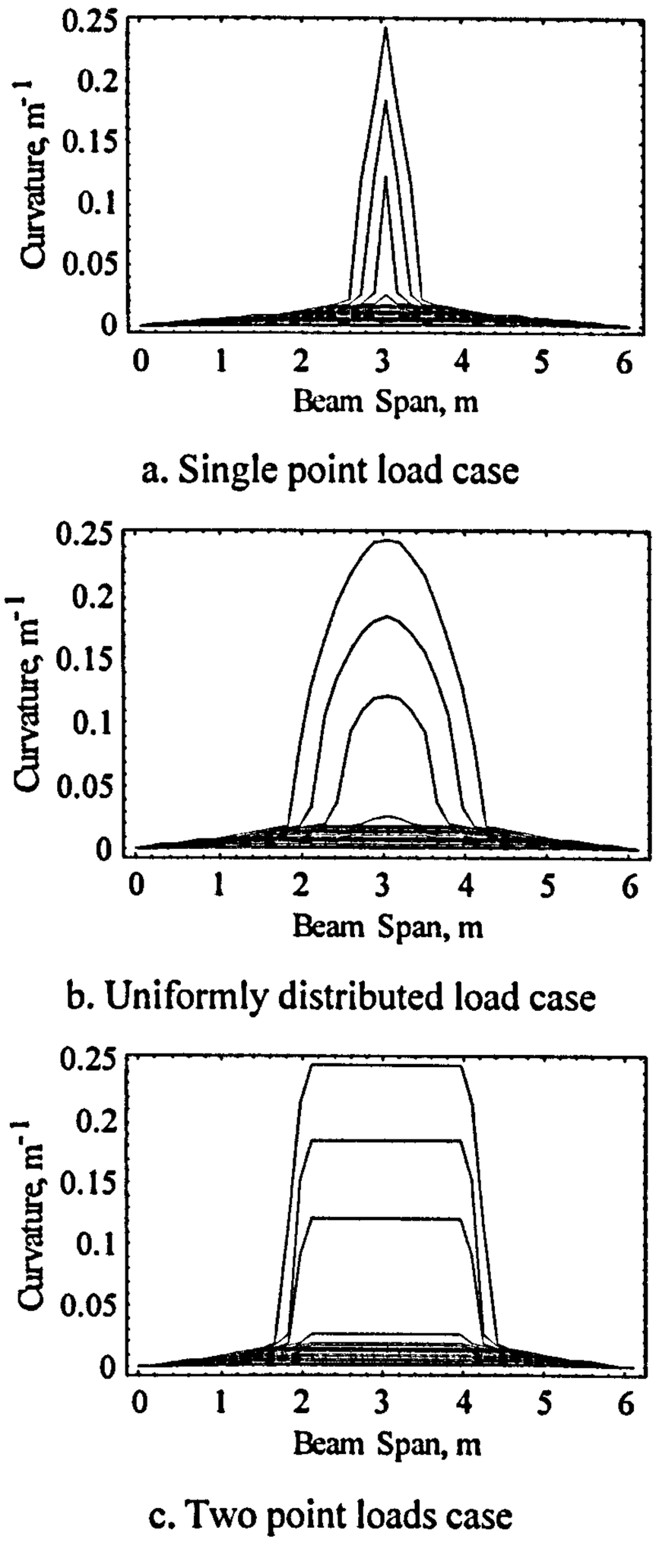

a. Single point load case

b. Uniformly distributed load case

c. Two point loads case

Figure 7-10. Curvature distribution along the span of the 203x102x23UB beam

The extended zone of plasticity visible in these figures help to explain why, as predicted earlier, the rotation requirement of beams resisting 2PL's (at third span points) is

substantially greater than for beams loaded by either UDL's or single point loads. Figure 7-10c shows that for the 2PL case, the plastic moment region extends over the mid one-third length of the span. Therefore the integral of curvature between the support and the point of maximum deflection (i.e. the end rotation) is substantially greater than for the 1PL case or the UDL case, Figure 7-10a & b respectively. Inspection of Table 7-3 and Table 7-4 reveals that for S275 grade steel, the percentage increase in end rotation is of the order of 200% to 280% from 1PL to 2PL, whereas for the UDL this increase is between 30% to 50%. For steel grade S355, the percentage increase is between 250% to 290% from 1PL to 2PL, whereas for the UDL this increase is 30% to 80%.

7.5.4 Span to Depth ratio (L/D)

The *L/D* ratio has been found to critically influence the capacity for strain hardening, as is shown in Figure 7-11 and Figure 7-12, in which predictions were based on all the three load cases considered. This comparison of normalised M-θ for different *L/D* ratios shows that higher ratio beams require substantially greater end rotation in order to generate M_p. The rotation requirements to achieve moments of 1.0, 1.1 and 1.15M_p are listed in Table 7-3 and Table 7-4 for different load cases and steel grades for both sections considered. These data demonstrate that the rotation requirement increases linearly with *L/D* ratio, regardless of load case and steel grade.

The bending tests carried out by Byfield and Nethercot (1998) were on a simply supported beam with a *L/D* ratio of 10. Figure 7-11 and Figure 7-12 explain why these tests demonstrated such a pronounced capacity for strain hardening. If the same sections had been tested with a span to depth ratio of 60, then 175mrad of end rotation would have been required to develop 1.0M_p.

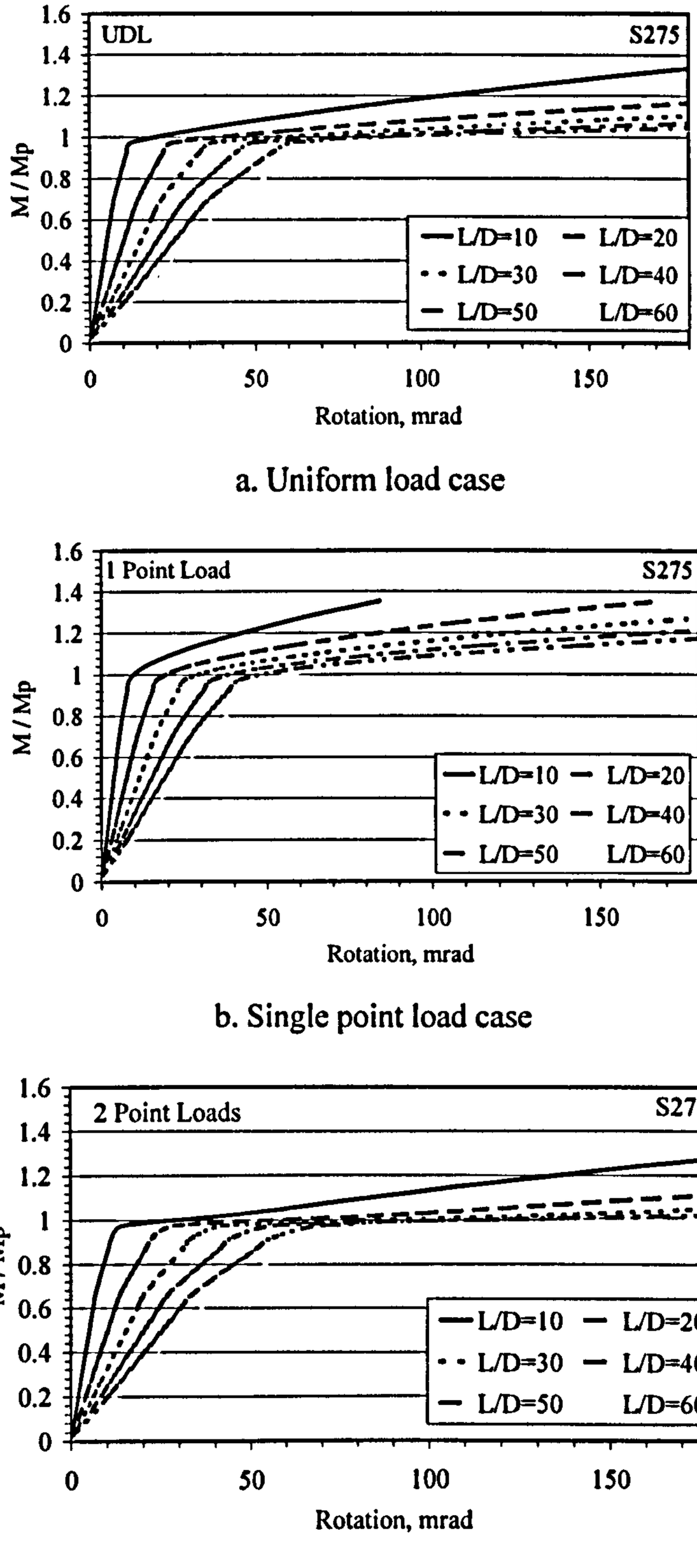

a. Uniform load case

b. Single point load case

c. Two points load case

Figure 7-11. Normalised M-θ curves for different L/D ratios – S275 grade

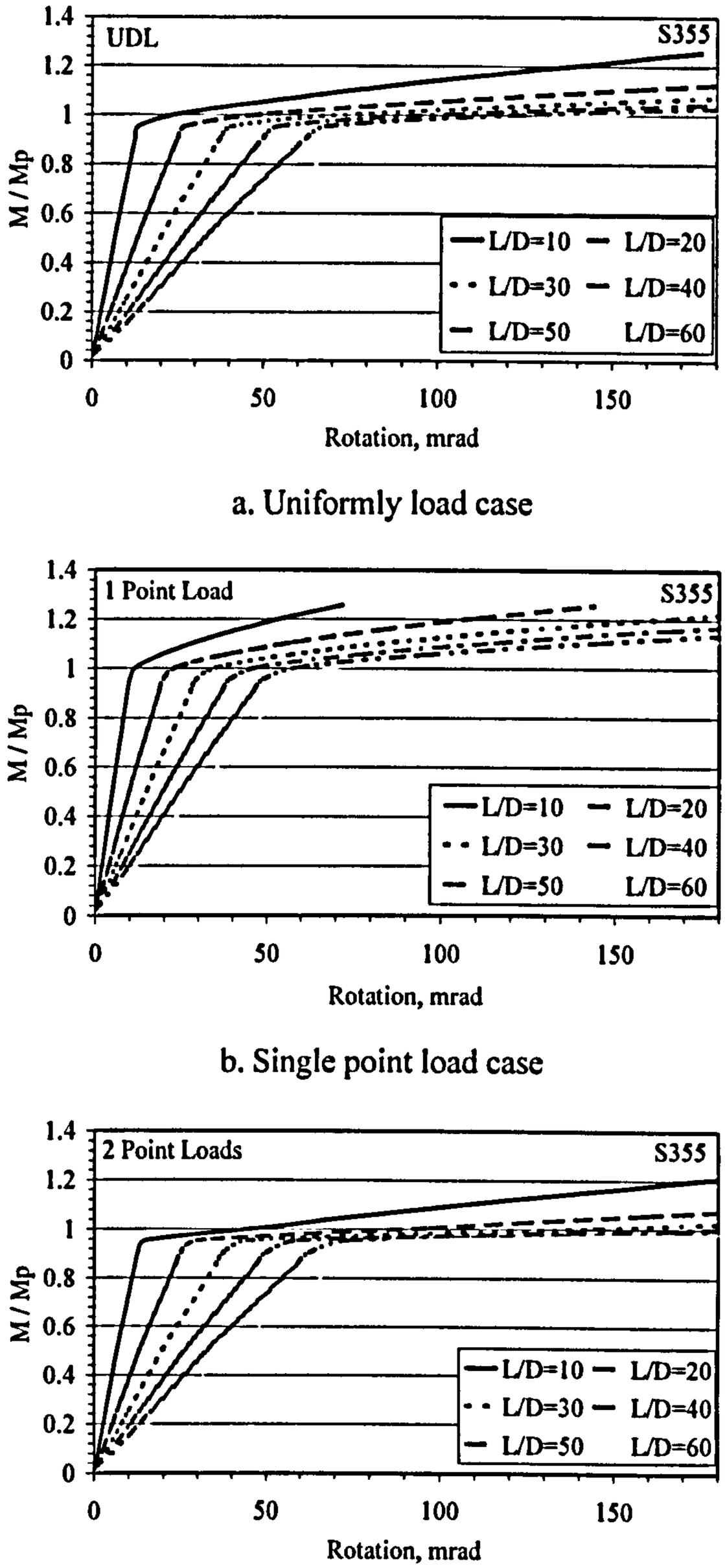

a. Uniformly load case

b. Single point load case

c. Two points load case

Figure 7-12. Normalised M-θ curves for different L/D ratios – S355 grade

7.5.4 Strain hardening factor ['*k*' value for computer analysis]

A particularly important outcome of this research is the information that it gives regarding appropriate values for the strain hardening constant '*k*' in equation (1).

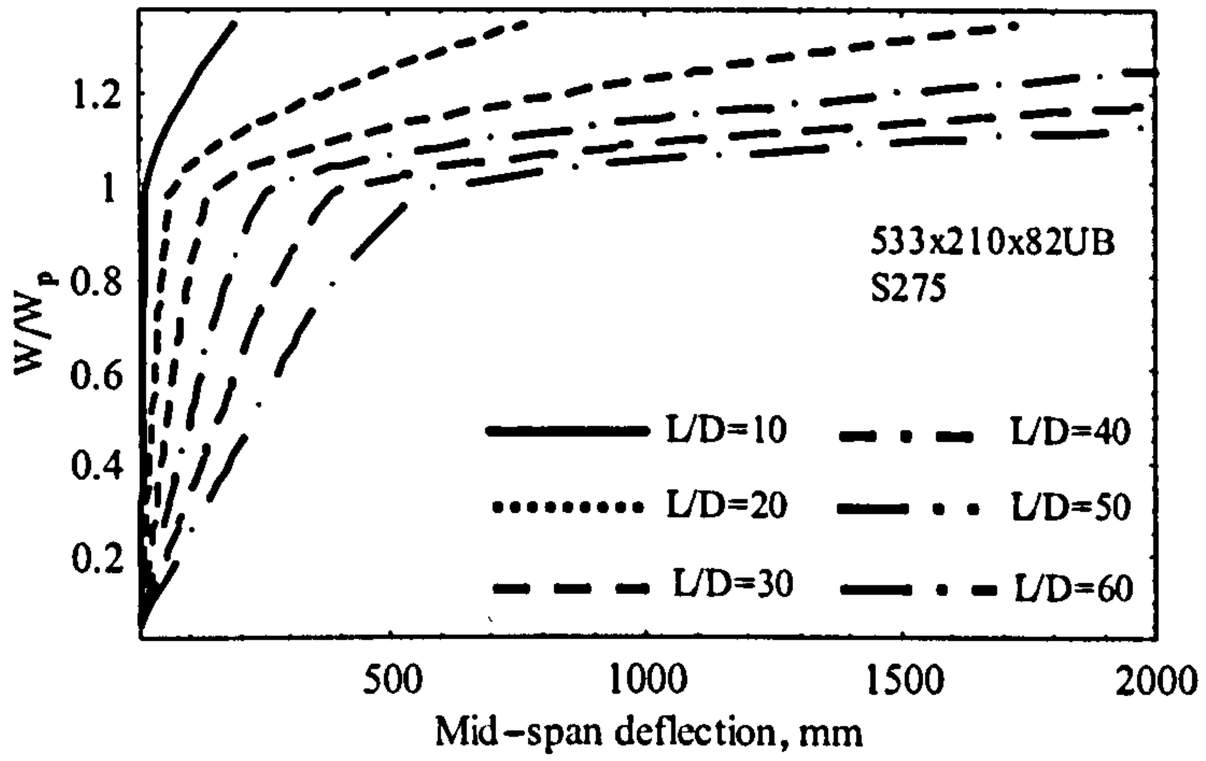

Single point load case

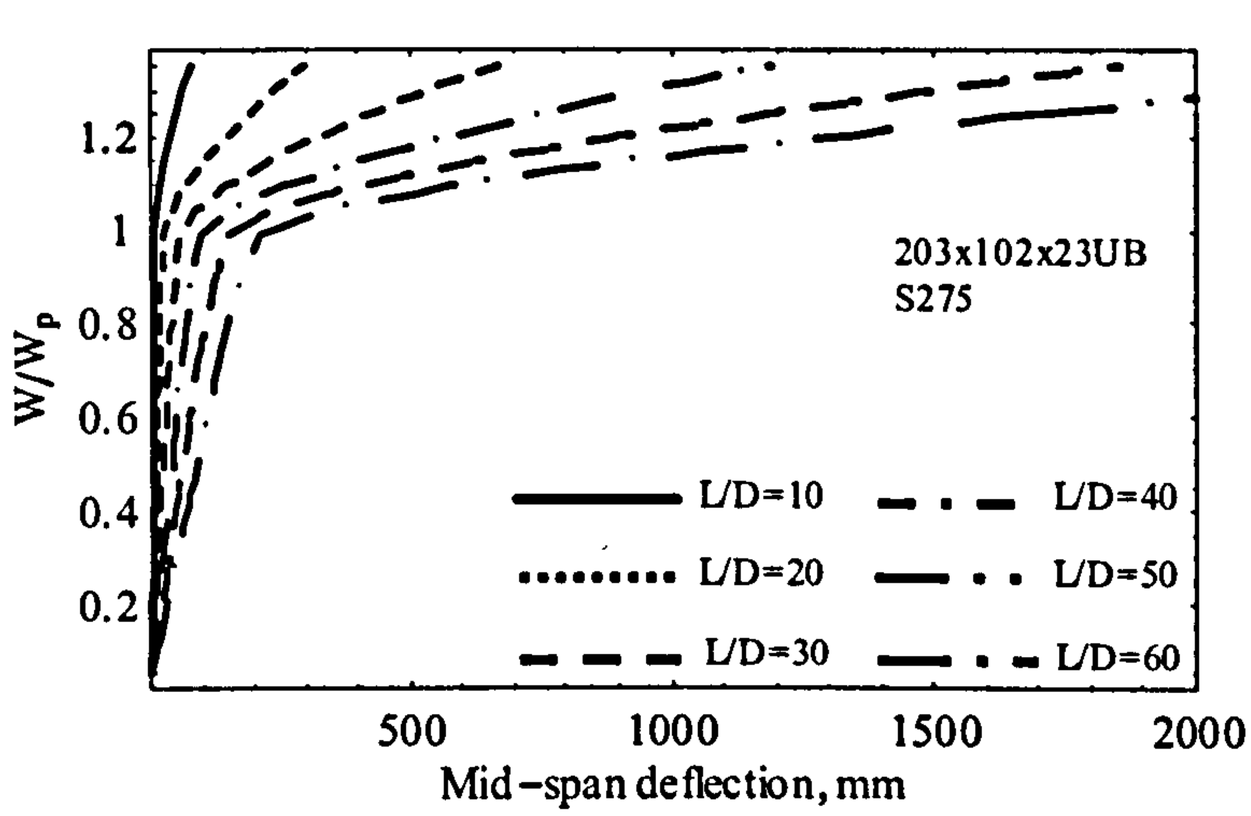

Single point load case

Figure 7-13. Normalised W-Δ curve for different L/D ratios – S275 grade

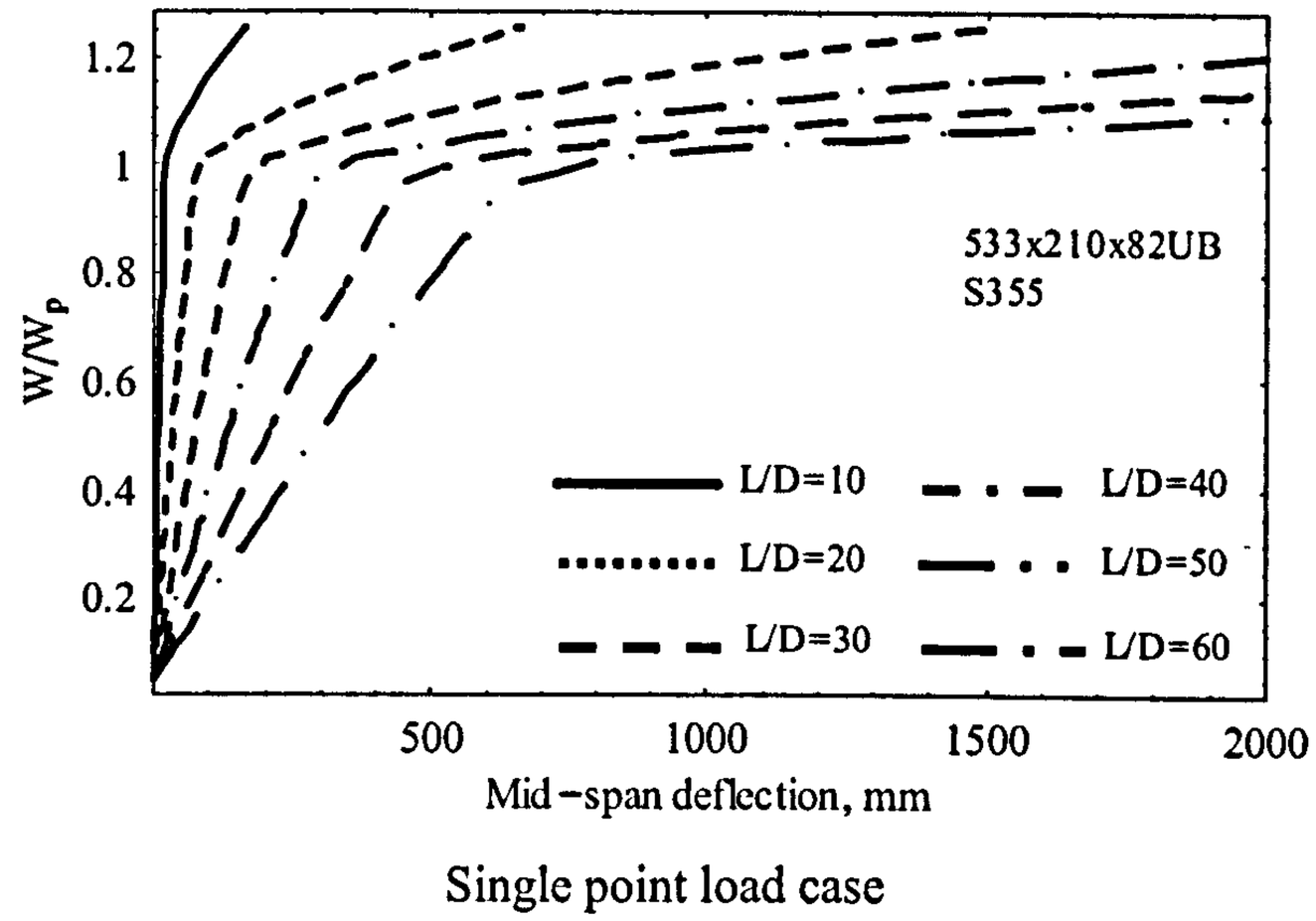

Single point load case

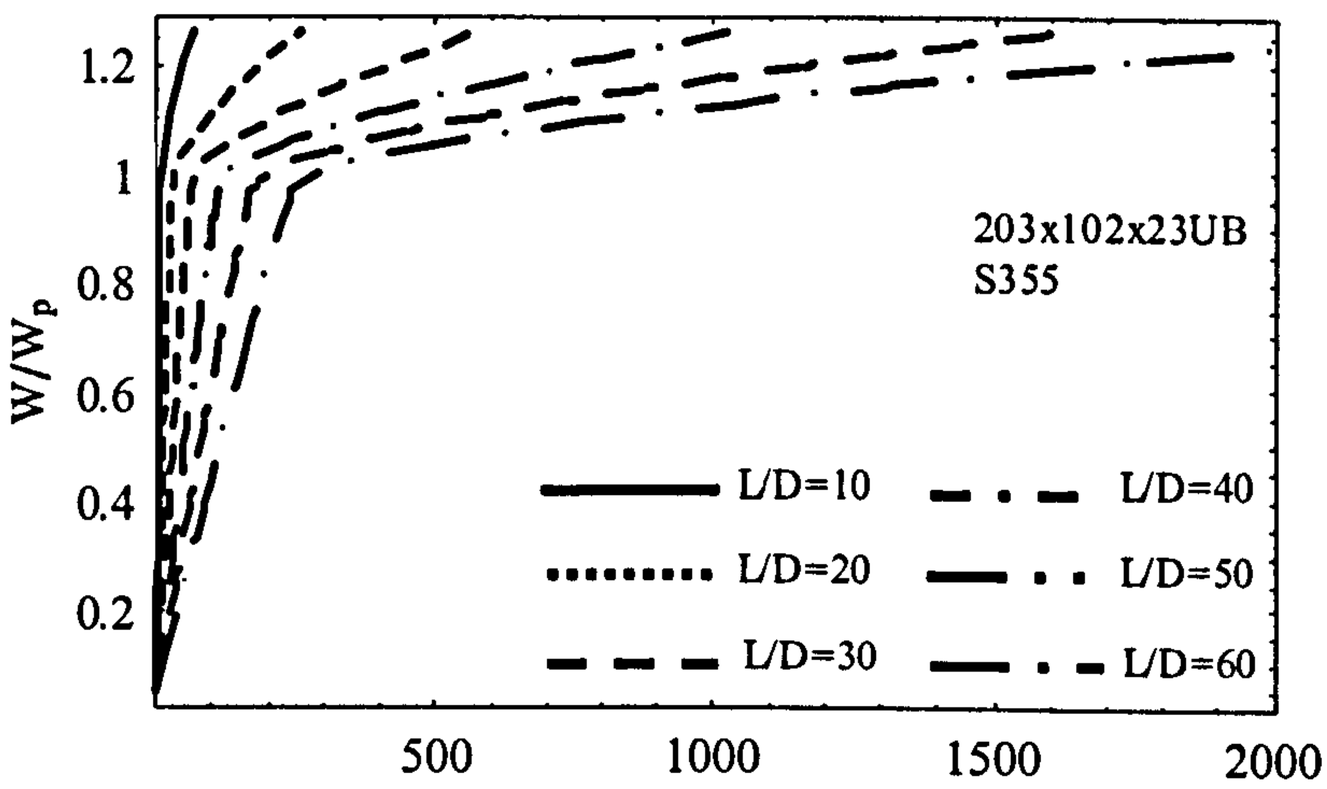

Single point load case

Figure 7-14. Normalised W-Δ curve for different L/D ratios – S355 grade

'*k*' value from the load-deflection curve (W-Δ curve)

The '*k*' value can be found from the slopes of the strain hardening parts of the load-deflection [Horne and Chin] for the single point load case. Figure 7-13 and Figure 7-14 show the normalised load vs. central deflection of the cases considered for the single point

load case. Figure 7-15 shows a beam in three-point bending with the associated bi-linear load deflection behaviour. In the elastic range the slope of the elastic part of the curve,

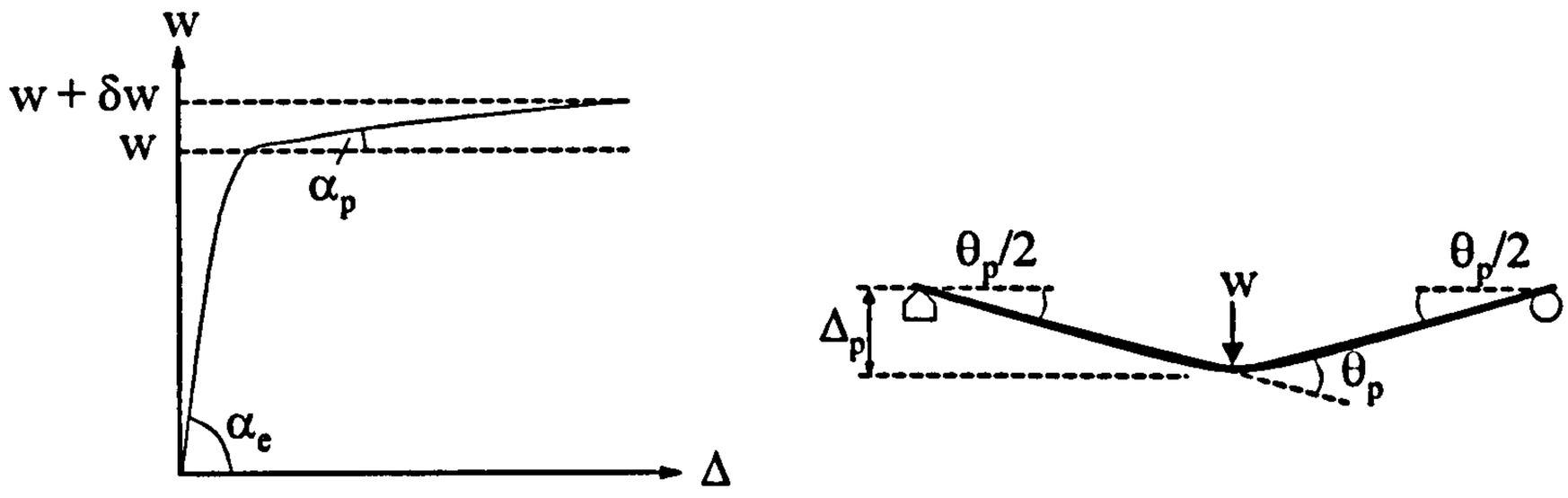

(a) (b)

Figure 7-15. Derivation of k-factor from load deflection curve

$$\alpha_e = \frac{w}{\Delta_e} \tag{3}$$

but

$$\Delta_e = \frac{wL^3}{48EI} \tag{4}$$

$$\therefore \alpha = \frac{48EI}{L^3} \tag{5}$$

Note that the notation is described in Figure 7-15. In the plastic range:

$$\delta m = \frac{\delta wL}{4} \tag{6}$$

$$\text{plastic deflection, } \Delta_p = \frac{\theta_p}{2}.\frac{L}{2} \tag{7}$$

$$\alpha_p = \frac{\delta w}{\Delta_p} = \frac{4\delta m}{L} \cdot \frac{4}{\theta_p L} = \frac{16\delta m}{L^2 \theta_p} \tag{8}$$

$$\therefore \delta m = \frac{\alpha_p L^2}{16} \theta_p \tag{9}$$

but "h" = l in equation (1)

$$\therefore \frac{\delta m}{\theta_p} = \frac{\alpha_p L^2}{16} = \frac{EI}{kh} = \frac{L^3 \alpha}{48} \cdot \frac{1}{kL} \tag{10}$$

$$\int_A \sigma_z dA = 0 \tag{11}$$

$$\therefore k = \frac{\alpha_e}{3\alpha_p} \tag{12}$$

i.e. 'k' can be determined directly from the relative slopes of the elastic and plastic regions of the load deflection curves.

Table 7-5 presents the strain hardening factor ('k') determined from the load-deflection values based on equations 3 to 12 for the cases considered. The plastic part of the curve is not generally precisely linear and it is considered to be sufficient to take a linear approximation to the initial part of the curve which intersects the elastic line at W = W_p. This procedure gives rise to the values of 'k' 8.84 for S275 and 9.1 for S355 steel, irrespective of span to depth ratio.

'k' value from the moment-rotation curve (M-θ curve)

Alternatively, k can be determined from the graphs of moment vs. end rotation, see Figure 7-16 with notation. In the elastic range:

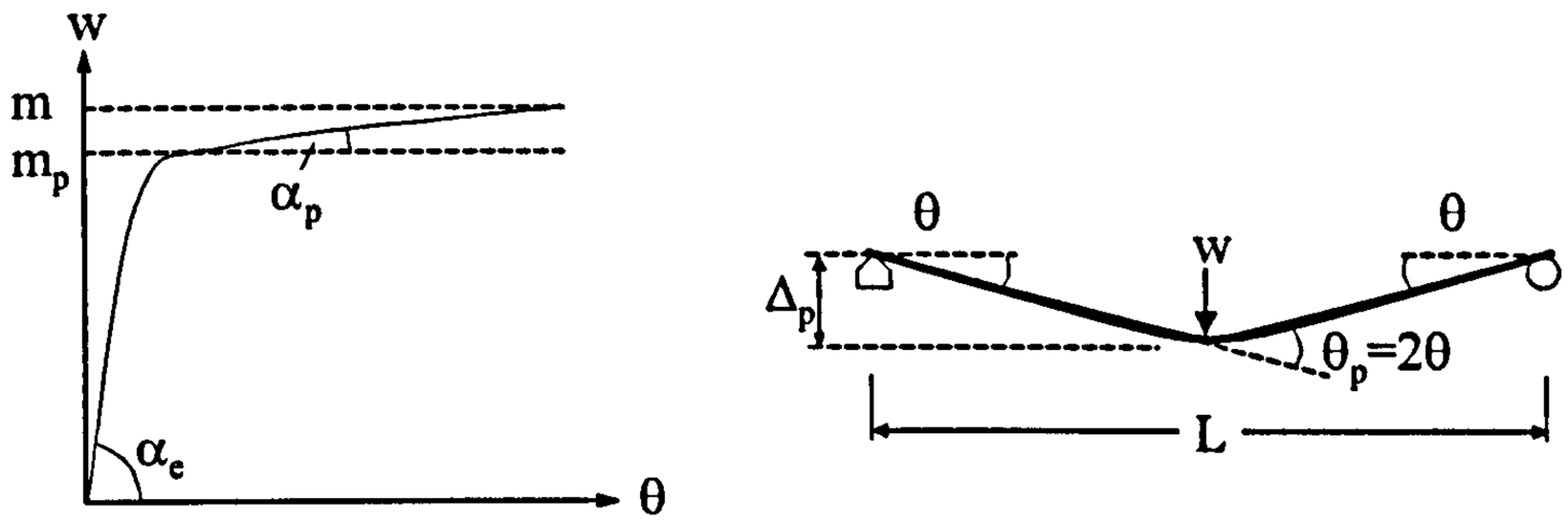

(a) (b)

Figure 7-16. Derivation of k-factor from moment-end rotation curve

$$\alpha_e = \frac{m}{\theta} \tag{13}$$

and

$$\theta_e = \frac{wL^2}{16EI} = \frac{mL}{4EI} \tag{14}$$

$$\therefore \alpha_e = \frac{m}{\theta} = \frac{4EI}{L} \tag{15}$$

In the plastic range:

$$\alpha_p = \frac{\delta m}{\theta} = \frac{2\delta m}{\theta_p} \tag{16}$$

$$\therefore \delta m = \frac{\alpha_p}{2}\theta_p \tag{17}$$

From equation (1)

$$\delta m = \frac{EI}{kL}\theta_p \tag{18}$$

$$\therefore \frac{EI}{kh} = \frac{\alpha_p}{2} \tag{19}$$

i.e.

$$\frac{1}{k} \cdot \frac{\alpha_e}{4} = \frac{\alpha_p}{2} \tag{20}$$

$$\therefore k = \frac{\alpha_e}{2\alpha_p} \tag{21}$$

Therefore, by using equation (1) with a little elementary structural mechanics, it has been shown that, $k = \alpha_e/(3\alpha_p)$ for a load-deflection curve or $k = \alpha_e/(2\alpha_p)$ for a M-θ curve (as in this paper), where α_e is the slope of the elastic part of the curve and α_p is the slope of the plastic part of the curve.

Table 7-6 presents the strain hardening factor ('k') determined from the moment-rotation values based on equations 13 to 21 for the cases considered. The plastic part of the curve is not generally precisely linear and it is considered to be sufficient to take a linear approximation to the initial part of the curve which intersects the elastic line at $M = M_p$. This procedure gives rise to the values of 'k' 10.3 for S275 and 10.2 for S355 steel, irrespective of span to depth ratio. These values are slightly higher than the 'k' values calculated from the W-Δ values as presented in Table 7-5. Given that increased strain hardening lowers the k value, a slightly conservative $k = 10$ seems to be a value that is adequate and safe for practical usage.

7.6 Conclusions

A survey of mill tests has shown that the onset of strain hardening and the strain hardening modulus are independent of section size and steel grade. This offers the opportunity to harmonise the treatment of strain hardening. Moreover, for the S275 and S355 grade steels, the onset of strain hardening has been found to occur at a strain of

approximately 6 times the yield strain, and the strain hardening modulus has been found to consistently approximate to 2700N/mm^2.

The accuracy of the numerical model presented in Chapter 4 has been established by comparing the predicted moment vs. end rotation behaviour of restrained steel beams with the behaviour observed through 12 identical bending tests. The results demonstrate that the numerical model, based on mill test data, provides accurate predictions of actual response to load. Using the model and the characteristic stress-strain properties of the steel derived from the survey of mill test data, a parametric study has been carried out in order to assess the influence that span to depth ratio (L/D), loading set up, steel grade and section size have on strain hardening.

Results show that, in regions of approximately uniform bending moment (e.g. below distributed loads), the ability to strain-harden is closely related to the *L/D* ratio. Low *L/D* ratio beams can be expected to significantly exceed their plastic moment capacities. In contrast, beams with high L/D ratios will require of the order of 10 degrees of end rotation in order to develop their plastic moment capacity alone. Such beams therefore, cannot be relied upon to generate enhanced strengths due to strain hardening, unless considerable end rotation can be accommodated before failure via either the local or lateral torsional buckling type mechanisms.

In regions where there is a significant moment gradient at a plastic hinge position, a simple equation is available which relates the increase in bending moment to the plastic hinge rotation. It has been shown that this equation can be used with confidence with modern steels and section sizes and an appropriate value of the strain hardening parameter is proposed. This formulation is particularly suitable for inclusion in computer programs for the elastic-plastic-stability analysis of plane steel frames where strain hardening can be advantageously used to offset the deleterious effects of frame instability.

Table 7-3. Required rotation to achieve 1.0Mp, 1.1Mp and 1.15Mp for 203x102x23UB

		L/D = 10			L/D = 20			L/D = 30			L/D = 40			L/D = 50			L/D = 60		
Grade	Load	1PL	UDL	2PL	1PL	UDL	2PL	1PL	UDL	2PL	1PL	UDL	2PL	1PL	UDL	2PL	1PL	UDL	2PL
S275	1.0Mp	9.6	18.8	28.3	19	37.5	56.5	28.6	56.5	84.6	38.2	75.4	112.9	47.8	94.1	141.2	57.4	113.1	169.5
S275	1.1Mp	21.6	58.3	82.9	43.3	116.6	165.6	65.1	175.1	248.7	86.7	233.4	331.4	108.4	291.6	414.5	130	349.9	497.2
S275	1.15Mp	30.9	81.3	108.4	61.8	162.5	216.6	92.7	243.8	325	123.7	325.2	433.4	154.5	406.3	541.6	185.5	487.6	650
S355	1.0Mp	11.3	23.6	44	22.9	47.1	88	34.2	70.7	131.8	45.7	94.4	175.8	57.1	118	219.7	68.6	141.5	263.7
S355	1.1Mp	27.4	74.7	106.6	54.8	149.4	213.3	82.2	224.1	319.9	109.8	298.8	426.6	137.2	373.3	533.2	164.6	448	639.8
S355	1.15Mp	39.4	104.4	139.5	78.7	208.7	278.9	118.2	313.1	418.5	157.6	417.5	558	196.9	521.9	697.4	236.3	626.2	836.9

Table 7-4. Required rotation to achieve 1.0Mp, 1.1Mp and 1.15Mp for 533x210x82UB

		L/D = 10			L/D = 20			L/D = 30			L/D = 40			L/D = 50			L/D = 60		
Grade	Load	1PL	UDL	2PL	1PL	UDL	2PL	1PL	UDL	2PL	1PL	UDL	2PL	1PL	UDL	2PL	1PL	UDL	2PL
S275	1.0Mp	9.9	25.5	30.6	19.7	40.0	61.3	29.6	60.0	91.9	39.5	80.0	122.5	49.4	100.0	153.2	59.2	120.0	183.8
S275	1.1Mp	22.1	59.3	84.0	44.3	118.6	168.1	66.4	177.9	252.1	88.5	237.1	336.2	110.7	296.4	420.2	132.8	355.7	504.3
S275	1.15Mp	31.5	82.5	109.8	63.0	165.0	219.7	94.5	247.5	329.5	125.9	330.1	439.4	157.4	412.6	549.2	188.9	495.1	659.1
S355	1.0Mp	11.9	24.3	44.9	23.7	48.7	89.7	35.6	73.0	134.6	47.4	97.3	179.5	59.3	121.7	224.4	71.1	146.0	269.2
S355	1.1Mp	28.1	76.0	108.2	56.2	152.0	216.4	84.3	228.0	324.5	112.4	304.0	432.7	140.5	380.1	540.9	168.6	456.1	649.1
S355	1.15Mp	40.2	106.1	141.5	80.4	212.1	283.0	120.6	318.2	424.5	160.8	424.2	566.0	201.0	530.3	707.5	241.2	636.3	849.0

Table 7-5. Calculation of strain hardening factor using W-Δ curves

	p_y	L/D	D	L	I	S	α_e	W_p	Δ_e	Δ_p @ 1.1W_p	α_p	κ	θ_p @ 1.15W_p	α_p	κ
Section size	N/mm^2		mm	mm	mm^4	mm^3	N/mm	Nmm	rad	Rad	N/mm		rad	N/mm	
203x102x23UB	275	10	203	2032	20641828	229577	24209	124279	5.133638	16.9322	1053	7.66	25.5456	913	8.84
	275	20	203	4064	20641828	229577	3026	62139	20.534551	67.7289	132	7.66	102.1820	114	8.84
	275	30	203	6096	20641828	229577	897	41426	46.202739	152.3900	39	7.66	229.9100	34	8.84
	275	40	203	8128	20641828	229577	378	31070	82.138202	270.9160	16	7.66	408.7290	14	8.84
	275	50	203	10160	20641828	229577	194	24856	128.340941	423.3060	8	7.66	638.6390	7	8.84
	275	60	203	12192	20641828	229577	112	20713	184.810955	609.5600	5	7.66	919.6410	4	8 84
	355	10	203	2032	20641828	229577	24209	160433	6.627059	22.1663	1032	7.82	33.4850	896	9.01
	355	20	203	4064	20641828	229577	3026	80216	26.508238	88.6654	129	7.82	133.9400	112	9.01
	355	30	203	6096	20641828	229577	897	53478	59.643535	199.4970	38	7.82	301.3650	33	9.01
	355	40	203	8128	20641828	229577	378	40108	106.032952	354.6610	16	7.82	535.7610	14	9.01
	355	50	203	10160	20641828	229577	194	32087	165.676487	554.1590	8	7.82	837.1260	7	9.01
	355	60	203	12192	20641828	229577	112	26739	238.574142	797.9880	5	7.82	1205.4600	4	9.01
533x210x82UB	275	10	528	5283	466867600	2024267	31156	421483	13.527975	45.0851	1336	7.78	67.7449	1166	8.91
	275	20	528	10566	466867600	2024267	3895	210741	54.111901	180.3410	167	7.78	270.9800	146	8.91
	275	30	528	15849	466867600	2024267	1154	140494	121.751777	405.7660	49	7.78	609.7040	43	8.91
	275	40	528	21132	466867600	2024267	487	105371	216.447603	721.3620	21	7.78	1083.9200	18	8.91
	275	50	528	26415	466867600	2024267	249	84297	338.199380	1127.1300	11	7.78	1693.6200	9	8.91
	275	60	528	31698	466867600	2024267	144	70247	487.007108	1623.0600	6	7.78	2438.8200	5	8.91
	355	10	528	5283	466867600	2024267	31156	544096	17.463386	59.1663	1305	7.96	88.9229	1142	9.09
	355	20	528	10566	466867600	2024267	3895	272048	69.853545	236.6650	163	7.96	355.6920	143	9.09
	355	30	528	15849	466867600	2024267	1154	181365	157.170476	532.4960	48	7.96	800.3060	42	9.09
	355	40	528	21132	466867600	2024267	487	136024	279.414179	946.6600	20	7.96	1422.7700	18	9.09
	355	50	528	26415	466867600	2024267	249	108819	436.584655	1479.1600	10	7.96	2223.0700	9	9.09
	355	60	528	31698	466867600	2024267	144	90683	628.681903	2129.9900	6	7.96	3201.2200	5	9.09

where $\alpha_e = 48\ EI/L^3$; $W_p = 4p_y\ S/L$; $\Delta_e = W_p\ L^3/\ 48EI$;Δ_p from Figure 7-13 and Figure 7-14; $\alpha_p = 0.1\ W_p/\ (\Delta_p - \Delta_e)$;$\kappa = \alpha_e/3\alpha_p$

Table 7-6. Calculation of strain hardening factor using M-θ curves

	p_y	L/D	D	L	I	S	α_e	M_p	θ_e	θ_p @ 1.1M_p	α_p	κ	θ_p @ 1.15M_p	α_p	κ
Section size	N/mm^2		mm	mm	mm^4	mm^3	N/mm	Nmm	rad	Rad	N/mm		rad	N/mm	
203x102x23UB	275	10	203	2032	20641828	229577	8329871632	63133675	0.007579	0.0216	450285486	9.28	0.0309	406077277	10.26
	275	20	203	4064	20641828	229577	4164935816	63133675	0.015158	0.0433	224342708	9.28	0.0618	203038638	10.26
	275	30	203	6096	20641828	229577	2776623877	63133675	0.022738	0.0651	149032226	9.28	0.0927	135359092	10.26
	275	40	203	8128	20641828	229577	2082467908	63133675	0.030317	0.0867	111972410	9.28	0.1237	101410607	10.26
	275	50	203	10160	20641828	229577	1665974326	63133675	0.037896	0.1084	89546164	9.28	0.1545	81215455	10.26
	275	60	203	12192	20641828	229577	1388311939	63133675	0.045475	0.1300	74692431	9.28	0.1855	67631212	10.26
	355	10	203	2032	20641828	229577	8329871632	81499835	0.009784	0.0274	462647826	9.00	0.0394	412783415	10.08
	355	20	203	4064	20641828	229577	4164935816	81499835	0.019568	0.0548	231323913	9.00	0.0787	206740744	10.08
	355	30	203	6096	20641828	229577	2776623877	81499835	0.029352	0.0822	154215942	9.00	0.1182	137594472	10.08
	355	40	203	8128	20641828	229577	2082467908	81499835	0.039136	0.1098	115334598	9.00	0.1576	103195854	10.08
	355	50	203	10160	20641828	229577	1665974326	81499835	0.048920	0.1372	92319937	9.00	0.1969	82612472	10.08
	355	60	203	12192	20641828	229577	1388311939	81499835	0.058704	0.1646	76962341	9.00	0.2363	68835974	10.08
533x210x82UB	275	10	528	5283	466867600	2024267	72464779922	556673337	0.00768	0.0221	3852826299	9.40	0.0315	3508200635	10.33
	275	20	528	10566	466867600	2024267	36232389961	556673337	0.01536	0.0443	1926401514	9.40	0.0630	1754100317	10.33
	275	30	528	15849	466867600	2024267	24154926641	556673337	0.02305	0.0664	1284270262	9.40	0.0945	1169400212	10.33
	275	40	528	21132	466867600	2024267	18116194981	556673337	0.03073	0.0885	963203666	9.40	0.1259	877050159	10.33
	275	50	528	26415	466867600	2024267	14492955984	556673337	0.03841	0.1107	770561537	9.40	0.1574	701640127	10.33
	275	60	528	31698	466867600	2024267	12077463320	556673337	0.04609	0.1328	642008524	9.40	0.1889	584698677	10.33
	355	10	528	5283	466867600	2024267	72464779922	718614671	0.00992	0.0281	3952414928	9.17	0.0402	3560430490	10.18
	355	20	528	10566	466867600	2024267	36232389961	718614671	0.01983	0.0562	1976207464	9.17	0 0804	1780210113	10.18
	355	30	528	15849	466867600	2024267	24154926641	718614671	0.02975	0.0843	1317471643	9.17	0.1206	1186807883	10.18
	355	40	528	21132	466867600	2024267	18116194981	718614671	0.03967	0.1124	988103732	9.17	0.1608	890105057	10.18
	355	50	528	26415	466867600	2024267	14492955984	718614671	0.04958	0.1405	790484503	9.17	0.2010	712086098	10.18
	355	60	528	31698	466867600	2024267	12077463320	718614671	0.05950	0.1686	658736875	9.17	0.2412	593406222	10.18

where $\alpha_e = 4EI/L$; $M_p = p_y S$; $\theta_e = M_p L / 4EI$; θ_p from Table 7-3 and Table 7-4; $\alpha_p = 0.1 M_p / (\theta_p - \theta_e)$; $\kappa = \alpha_e / 2\alpha_p$

Chapter 8 – Conclusions

8.1 Conclusions

During propped construction the steel-concrete composite action resists dead as well as imposed loads. Conversely, the steel section alone resists the floor self-weight in unpropped beams. Relatively few studies have been carried out to assess the rotation requirements for unpropped semi-continuous composite beams. This research overcame the difficulties involved modelling the composite and non-composite stages by using a numerical integration technique developed using the basic principles of structural mechanics. The method incorporates the fully non-linear material properties and requires very little assumption. The technique was initially validated using the experimental results from plain steel beam bending tests. The subsequent comparison between the model predictions and the results from the large-scale frame test reported, showed that the method is capable of predicting non-elastic load vs. end rotation behaviour to within a high degree of accuracy. Thus the model can be used with confidence in order to predict the connection rotation requirements for a wider range of loading configurations than is practically possible from experimental testing alone.

The rotation capacity required from the composite connections is a function of the method of construction, span to depth ratio, location within the building frame, ratio between the support (connection) moment capacity and the span (beam) moment capacity, loading type, steel grade and the percentage of the beam strength utilised during design. The current industry standard design guidance (designed primarily for propped constructions) recommends limits on some of these parameters in order to ensure that the required rotation does not exceed the available rotation. The primary restriction is that the maximum design sagging moment in the beam must be restricted to $0.85M_p$ and the ratio between the support and span design moments must not be less than 0.3. Furthermore, for beams subject to UDL's, multiple-point loads or single central-point loads, a span

to depth ratio should not exceed 25. For beams subject to two-point loads, a span to depth ratio of less than or equal to 20 should be observed. Since the standard connections are capable of achieving at least 30% of the beam moment capacity, it is possible to exploit the advantages of composite connections with beams propped during construction.

In unpropped construction the top half of the steel section is subjected to compression stresses which are in effect locked in during whilst supporting the dead weight from the steelwork, together with the weight from the wet concrete slab. Subsequent loads are resisted by the combined steel-concrete composite action. However, in order to achieve the ultimate limit state flexural moment the beam must undergo substantial additional curvature. This is necessary in order to convert these locked in compressive stresses into tensile stresses at or near to the yield stress. This additional curvature requirement leads to a substantial increase in end rotation, as the rotation is the integral of curvature. This increase is considerably because the strains in the bottom flange are non-elastic. They therefore produce a disproportionately large amount of curvature. Thus, the rotation requirement for unpropped beams is governed to a large extent by the ratio between the maximum dead load stress in the beam and the yield stress (σ_{dl}/σ_y).

Whilst the rotation requirement increases for unpropped beams, this is to some extent off-set by an increase in the available rotation capacity of the connections. This is because the connection reinforcing bars remain unstrained when resisting the dead weight of the slab. However, this additional rotation capacity has been shown to be only 10% to 15% greater for unpropped beams, in comparison with their propped counterparts. The available rotation capacity of a given connection is mainly governed by the ductility of the reinforcement. Approximately one third of the ductility requirement is due to the elastic strain, with the remaining two thirds due to plastic strain. Approximately 40% of elastic strain is due to the dead load. Hence the contribution of 10% to 15% of total strain due to dead load is the gain in the available rotation capacity in the case of unpropped construction.. This

marginal increase provides an available rotation capacity of 32mrad for connections to S355 beams, and 25mrad for S275 beams. Although the available rotation capacity of a given connection is primarily governed by the ductility of the reinforcement, the contribution from slip of shear connectors and compressive strain in the lower flange and web are also significant. Deformation of reinforcement and slip of shear connectors are not affected by the steel grade. However the compressive strain in the lower flange or beam is dependent on the steel grade and it is higher for S355 beams and hence the increase in the available rotation capacity for S355 grade sections. These values assume that connections are detailed in accordance with industry standard specifications, as described in the "green-book".

Comparing the rotation capacity available from the connections with the rotation requirement predicted using the numerical model, a parametric study was carried out to assess the applicability of composite connections with the unpropped mode of construction. In this study, the effects of all the parameters listed previously were assessed.

Due to the increased strains, the rotation requirement was found to be 10 to 20% higher for S355, than for S275 beams, irrespective of the mid-span design moment. Typically, the rotation requirement ($\theta_{required}$) increases by 25% as the ratio between the support moment and span moment decreases from 0.6 to 0.3 irrespective of the steel grade, span to depth (L/D) ratio, end conditions, sagging design moment and degree of propping. When the design sagging moment reduces from 0.95 to $0.85M_p$, the percentage reduction in $\theta_{required}$ is typically higher for internal beams than for external beams. When the design sagging moment reduces from 0.95 to $0.85M_p$ the percentage reduction in $\theta_{required}$ is typically lower as the dead load stress to yield stress ratio increases. Typically, $\theta_{required}$ increases by 10 to 90% as the L/D ratio increases from 15 to 25, depending on the design sagging moment and the steel grade. On average, $\theta_{required}$ is 20-60% higher for the 2-point loads case than for the 3-point loads case. In the case of 2-point loading, the plastic moment region extends over the mid one-third length of

the span and therefore the integral of curvature between the support and the point of maximum deflection is substantially greater than for the 3-point load case. Internal beams subjected to a UDL required slightly more end rotation than equivalent beams subjected to 3 point loads. This is as expected given that the zone of plasticity is extended for the UDL case. The rotation requirement of internal beams subjected to 2-point loads is substantially greater than that for external beams. This is because the lack of symmetry at external locations results in a sloping bending moment diagram and a resulting reduction in the zone of plasticity in the beam. Externally located beams subjected to UDL's required more end rotation than equivalent beams subjected to 2-point loads. This is due to the effect of non-symmetrical distribution of curvature on the loading type. The effect of lack of symmetry is more pronounced in the case of 2-point loading than in the UDL loading.

The ratio between the maximum bending stress (during this non composite stage) and the yield stress (σ_{dl}/σ_y) was found to be the critical factor effecting the rotation required from the connections. For every 0.25 increment in σ_{dl}/σ_y, $\theta_{required}$ increased by an average of 50%. This was irrespective of steel grades and beam location.

The investigation clearly showed that, generally, composite connections cannot be used with unpropped semi-continuous composite frame construction. If composite connections are used with unpropped construction, then the bending stress in the steel section due to the factored construction stage loads must be restricted to below 50% of the yield stress. This restriction becomes mandatory because the initial stress on the steel section due to absence of props significantly amplifies the final rotation required to achieve the design moment in the beam. As stated previously, this increase in rotation requirement is only partially offset by a moderate increase in available rotation capacity. Therefore, it has been concluded that limits must be imposed on the construction stage bending stress in order to limit the rotation requirement. In S355 beams where the span to depth ratio is less than or equal to 15 and subjected to two point loading, $\sigma_{dl} \leq 0.89\sigma_y$. If less than or

equal to 20, then the σ_{dl} limit falls to $0.44\sigma_y$. If less than or equal to 25, then the σ_{dl} limit falls to $0.21\sigma_y$. These limits can be relaxed for many configurations. For example the limits are less restrictive for beams supported by nominally pinned connections at one end due to the sloping bending moment diagram. Lower limits are also placed on beams subjected to 3 point loads or uniformly distributed loads. This is due to the more localised nature of the zone of plasticity. When beams are made from S275 steel the stress limits are more onerous. The rotation requirements are less onerous for S275 grade steel due to the lower elastic strains, the increase in available rotation capacity for S275 steel is lower in proportion to the increase in rotation requirement.

A full range of limiting σ_{dl}/σ_y ratios for different span to depth ratios, steel grades and loading types have been presented in this thesis for design purposes. Before relying on the ductility of standard composite connections when used in unpropped construction, designers should pay careful attention to the values given and ensure that the factored dead load stresses fall within the implied limits. An increase in steel beam size, or strength, may be necessary.

The test reported provides important information on the strength and ductility of composite connections when used with unpropped beams. The standard composite connections used at the interior column were shown to comfortably achieve their design moment capacity, although the limit on post construction ductility was shown to be 23mrads. The failure of the connection reinforcing bars initiated the decline in strength and this sudden failure of the rebars highlights the ductility problems associated with composite connections.

The experiment provided an opportunity to investigate the behaviour of a modified form of composite connection detail for use at perimeter columns (single-sided composite connections) with improved rebar anchorage. The investigation showed this perimeter composite connection to be capable of achieving close to an equivalent design moment as internal connections. Importantly, the cranks in the reinforcement provided additional ductility to the

connection, at the expense of absolute flexural strength. For this reason the connection failed to reach the design moment within an acceptable degree of rotation. Importantly, the top rows of bolts were shown to have failed at all of the composite connections, which again raise questions concerning the ductility of this form of connection detail.

The nominally pinned connection was shown to possess a considerable moment capacity, formed by a couple between the bolts and the bottom flange of the beam after only relatively low beam end rotations. This couple imposed considerable strain on the bolt/end plate assembly, which could have led to a sudden connection failure since the connection was designed to resist only shear loading. Since the allowed gap between bottom beam flange and column flange is approximately 10mm in the standard pin connection detail, the prying action becomes unavoidable. Thus, the ductility of this standard form of connection was shown to be lacking in the ultimate limit state condition.

The analysis clearly shows that the flexural strength of the test beam substantially exceeds the nominal beam strength. This was due to conservative design assumptions regarding material and geometric properties. The test was terminated due to concern regarding the rupturing of connection bolts. However at this stage the beam had achieved a large mid-span deflection of 300mm. It is possible that strain hardening would have provided further increases in flexural strength if the test had been continued, because the sagging moment region of the beam was showing no signs of buckling. However, further loading may have let to a connection fracture.

In the process of the development of the semi-continuous composite beam model an opportunity was taken to investigate the effects of strain hardening in plain steel beams. This is of interest because the elasto-plastic method of design used for portal frame structures incorporates an allowance for strain hardening, in order to partially off-set destabilising second-order effects from frame deflections. In recent years there has been a need to re-evaluate the strain-hardening effect, given

changes to the processes in steel production since the strain hardening factor was last calibrated in the 1960's. Moreover, there is now an increasing awareness of the destabilising effects of deflections on the load capacity of very slender modern sway frames.

Towards this purpose a survey of mill tests was carried out. It was found that the onset of strain hardening occurs at a strain of approximately 6 times the yield strain, and that the strain hardening modulus is approximately 2700 N/mm^2 for the S275 as well as S355 grades. A parametric study was then carried out using the numerical model for steel beams, based on the characteristic stress-strain curve from mill tests. The study assessed the influence that span to depth ratio (L/D), loading type, steel grade and section size have on the capacity for strain hardening. In regions of approximately uniform bending moment, the ability to strain-harden is closely related to the *L/D* ratio. Low L/D ratio beams subjected to uniformly distributed loads demonstrate a significant reserve of strength due to strain hardening. Conversely, high L/D ratio beams subjected to uniformly distributed loads require very high end rotations in order to achieve their flexural strength. Such sections cannot therefore be relied upon to develop enhanced capacity due to strain hardening. Section size was not found to effect strain hardening behaviour. However, S355 grade steel was found to require 28% greater end rotation than S275 grade steel in order to strain-harden. Two-point loading requires 280% higher end rotation than single point loading and 80% more than uniformly distributed loading. In the case of 2-point loading, the plastic moment region extends over the mid one-third length of the span and therefore the integral of curvature between the support and the point of maximum deflection is substantially greater than for the 3-point load case and UDL point load case. The strain hardening factor was calculated from the elastic and plastic slopes of the moment-rotation graphs produced by the numerical model. Results from an extensive parametric study have been assessed and a practical value for the strain hardening factor has been calibrated at 10, irrespective of the steel grade. This factor can be incorporated into the elastic-plastic design software used commercially for portal frame design.

8.2 Proposed future work

Associated areas of research where the work described in this thesis may be extended include the following:

(a) This research focus mainly the ultimate limit state requirements of the composite connections under unpropped construction. Clearly research is needed to meet the serviceability requirements of the composite connections under unpropped construction.

(b) It is clearly understood from this research there is a lack ductility in the standard connections proposed by the 'SCI Green book' due to the low percentage of reinforcement. A research could be carried out to improve the ductility by increasing the percentage of reinforcement. It appears that safe designs will require limits to be set on this parameter.

(c) This research shows the standard composite connection (flush end plate) detail used in the test achieved higher strength than the theoretical strength. This implies that connections such as angle cleat, partial depth end plate, fin plate connections which will have eventually less strength but more ductility can be used as standard composite connections. A research is needed to include these connections to be composite connections of more ductility in future composite connections design guide.

(d) Ignoring strain-hardening effect and over strength steel effect in calculating the flexural strength of the composite beam underestimates the true strength of the composite beams. The robustness of frames depends on the harmonious interaction between the weak beam members and strong connections. Underestimating the true flexural beam strength could result in the transfer of weak point of the frames from the beams to the connections and endanger the frame robustness. Hence the estimation of true strength of

composite beam is necessary. Research could be carried out to quantify the upper-bound strength of composite beams.

(e) It is understood that strain hardening will not have much effect when the desirable design sagging moment is only $0.85M_p$. However, for research purposes it is useful to establish this fact and also to quantify the required rotation for design sagging moments greater than $0.85M_p$. Again, this can be done through the numerical model developed as it is a generic model that can be used for both strain-hardening and non strain-hardening stress-strain relationships.

(f) The standard nominally pin connection detail in current design guides would benefit from improved ductility in order to avoid the prying action as observed in this study.

(g) All the standard connection details assume that the primary beam is connected to the major axis of the column. A study can be made for unpropped construction to investigate whether or not the connection to the minor axis of the column has a positive or negative effect on the strength and ductility of internal and external composite connections.

References

1 Ahmed, B. and Nethercot, D. A. (1995). "Numerical modelling of composite flush end-plate connections". Journal of Singapore Structural Steel Society, 6:1, 87-102.

2 Ahmed, B. and Nethercot, D. A. (1997). "Prediction of Initial Stiffness and Available Rotation Capacity of Major Axis Composite Flush Endplate Connections", Journal of Constructional Steel Research, Vol. 41, 31-60.

3 Ammerman, D. and Leon, R. T. (1987). "Behaviour of semi-rigid composite connections". AISC engineering journal, Second quarter, June.

4 Anderson, D, Aribert, J. M, Bode, H, and Kronenburger, H, J. (2000). "Design Rotation Capacity of Composite Joints", The Structural Engineer, Vol. 78, no. 6.

5 Anderson, D. and Johnson, R. P. (1992). A review of Eurocode 4: Part 1 for buildings, Department of engineering, University of Warwick, Research report CE3.

6 Anderson, D., and Najafi, A. A. (1994). "Performance of composite connections: major axis end plate joints", Journal of Constructional Steel Research, Volume 31, Issue 1, 31-57.

7 Anderson, D. and Najafi, A. A. (1997). Ductile steel-concrete composite joints. *Composite construction - Conventional and Innovative*, Innsbruck, Conference Report.

8 Aribert, J. M., Lachal, A., Muzeau, J.P., and Racher, P. (1994). Recent tests on steel and composite connections in France, *COST-C1 Proceedings second state-of-the-art workshop*, Brussels, European commission, 61-75.

9 Armer, G. S. T. and Moore, D. B. "Full scale testing on composite multi-storey structures". The structural engineer, 72(2).

10 Baker J. F. (1963). *Plastic Design in Steel to BS 968*. Publication No. 21, British Constructional Steelwork Association, London.

11 Baker, J. F. (1956) *The steel skeleton. Volume II: Plastic behaviour and design.* Cambridge University Press.

12 Barnard, P. R. (1970). Innovations in Composite Floor Systems. *Canadian Structural Engineering Conference Proceedings*, Canadian Steel Industries Construction Council, 13.

13 BCSA and SCI. (1991). *Joints in simple construction, Vol. 1: design methods.* The Steel Construction Institute, Publication No. 205.

14 BCSA and SCI. (1995). *Joints in steel construction – moment connections.* The Steel Construction Institute, Publication No. 207.

15 BCSA and SCI (1998). *Joints in steel construction – composite connections.* The Steel Construction Institute. Publication No. 213.

16 Bode, H., Ramm, W., Elz, S., and Kronenberger, H.-J. (1996). Composite connections: Experimental results, Semi-rigid structural connection, *IABSE colloquium*, Istanbul, 31-41.

17 Bose, B. and Hughes, A. F. (1995). Verifying the performance of standard ductile connections for semi-continuous frames, *Proceedings of the Institution of Civil Engineers, Structures and Buildings*, November.

18 Brett, P. R., Nethercot, D.A. & Owens, G. W. (1987). "Continuous construction in steel for roofs and composite floors", The Structural Engineer, Vol. 65A, no. 10, 355-63.

19 Brozzetti J. (1992). *Design of connections in the Eureka Cimsteel project, Connections in steel structures II: behaviour, strength and design*, R. Bjorhovde, A. Colson, G. Haaijer and J. W. B. Stark (eds), AISC, Chicago, 254-262.

20 Brugger, R. (1993). Zur Schubtragfahigkeit von Verbundknoten. PhD Thesis, University of Innsbruck, Austria.

21 BSI. (1990). *BS EN10002-1.*

22 BSI (1990). *BS 5950: Structural use of steelwork in building, part 1:1990: Code of practice for design in simple and continuous construction: hot rolled sections.*

23 BSI (1997). *BS 8110: Structural use of concrete, part 1:1997: Code of practice for design and construction.*

24 BSI. (1984). *BS 5400: Steel, concrete and composite bridges.*

25 BSI. (1988). BS 4449: *Specification for carbon steel bars for the reinforcement of concrete.*

26 BSI. (1990). *BS 5950: Structural use of steelwork in building, part 1*: Code of practice for design in simple and continuous construction: hot rolled sections.

27 BSI. (1990). *BS 5950: Part 3.1, Code of practice for design of simple and continuous composite beams*, London.

28 Byfield, M. P. and Dhanalakshmi, M. (2002). Analysis of strain hardening in steel beams using mill tests. *International conference on advances in Steel Structures (ICASS 02)*, Hong Kong, 139-146.

29 Byfield, M. P., Dhanalakshmi, M. and Goyder, H. G. D. (2004). "Modelling of un-propped semi-continuous composite beams". Journal of Constructional steel research, Volume 60, 1353-1367.

30 Byfield, M. P. and Nethercot, D. A. (1997). "Material and geometric properties of structural steel for use in design". The Structural Engineer, Vol. 75, no. 21, 363-373.

31 Byfield, M. P. and Nethercot, D. A. (1998). An analysis of the true bending strength of steel beams. Structures and Buildings. *Proceeding of the. Institution of Civil Engineers,* 128, 188-197.

32 Caughey, R A and Basil Scott, W. A Practical Method for the Design of I-Beams Haunched in Concrete.

33 CEN (1990). "EN10025: Hot rolled products for non-alloy structural steels", European Committee for Standardisation, Brussels.

34 Chapman, J. C. and Balakrishnan, S. (1964). "Experimental tests on composite beams". The Structural Engineer, 42(11), 369-383.

35 Climenhaga, J. J., and Johnson, R. P. (1972). "Local buckling in continuous composite beams". The Structural Engineer, Vol. 50, London, September, 367 – 374.

36 COST C1. (1997). European Co-operation in the field of scientific & technical research: *Semi-rigid behaviour of civil engineering structural connections*, Composite steel-concrete joints in braced frames for buildings. Editor Anderson, D., Luxembourg, European Commission.

37 Couchman, G. H. (1995). Design of continuous composite beams allowing for rotation capacity. Thesis No. 1308, Ecole Polytechnique Federale, Lausanne.

38 Couchman, G. H. (1997). Design of semi-continuous braced frames, Steel Construction Institute, Ascot, Publication No. 183.

39 Couchman, G. H., and Way, A. (2000). Ductility requirements for composite connections, Draft paper, The Steel Construction Institute.

40 Culver, C. G. and Coston, R. (1961). "Tests of composite beams with stud shear connectors". Journal of the Structural Division of the ASCE, 87(ST1), 1-17.

41 Davidson, J. B. (1987). Strength of beam-columns in flexibly connected steel frames, PhD Thesis, Department of civil and structural engineering, University of Sheffield.

42 Davidson, J., Lam, D. and Nethercot, D. (1990). "Semi-rigid action of composite joints", The Structural Engineer, Vol. 68, no. 24.

43 Davies J. M. (1966). "Frame instability and strain hardening in plastic theory". ASCE, Journal of Structural Engineering Division. ST3, June, 1-15.

44 Davies J. M. (1966a) Discussion of Horne and Medland, *Proceeding of the. Institution of Civil Engineers*, December, 684-686.

45 Davies J. M. (1990). "In plane stability in portal frames". The Structural Engineer, Vol. 68, No. 8, April, 141-147.

46 Davies J. M. (2002). "Second-order elastic-plastic analysis of plane frames". Journal of Construction Steel Research, 58, 1315-1330.

47 Davison, J. B., Kirby, P.A., and Nethercot, D.A. (1987). Rotational stiffness characteristics of steel beam-to-column connections. Journal of Constructional Steel Research, Vol. 8, 17-54.

48 Dhanalakshmi, M., Byfield, M. P. and Couchman, G. H. (2002). Composite connections at perimeter locations in unpropped composite floors, *International Conference on Advances in Steel Structures (ICASS 02)*, Hongkong, 261-268.

49 Driscoll, G. C. (1957). Rotation capacity of a continuous beam, Fritz engineering laboratory report, No. 268.2, Lehigh University.

50 ENV 1992-1-1. Eurocode 2: Design of concrete structures: Part1.1 General rules and rules for buildings, CEN, Brussels.

51 ENV 1993-1-1. (1998). Eurocode 3: Design of steel structures: Part1.1 General rules and rules for buildings/A2, CEN, Brussels.

52 ENV 1994-1-1. (1992). Eurocode 4, Design of composite steel and concrete structures: Part 1-1: General rules and rules for buildings, European committee for standardisation, Brussels, CEN.

53 European Convention for Constructional Steelwork: ECCS - Technical Committee 11-Composite Structures. (1999). Design of composite joints for buildings, No 109.

54 Ewing, J. A. (1899). *The strength of materials*, Cambridge.

55 Gibbons, C. (1990). The strength of biaxially loaded beam-columns in flexibly connected steel frames, PhD Thesis, Department of civil and structural engineering, University of Sheffield.

56 Gibbons, C. (1992). Partial strength moment resisting connections in composite frames. The Steel Construction Institute, Report RT-257.

57 Griffs, L. G. (1992) *Composite Frame Construction*, Ch. 4. 5, Constructional Steel Design – An International Guide, Ed by Dowling *et al*, 523-553.

58 Hope-Gill, M. C. (1979). "Redistribution in composite beams". The Structural Engineer, Vol. 57B, No. 1, London, March, 7-10.

59 Hope-Gill, M. C., and Johnson, R. P. (1976). Tests on three three–span continuous composite beams. *Proceedings of the Institution of Civil Engineers Part 2*, Vol. 61, London, 367 - 381.

60 Horne M. R and Medland I C. (1966) The collapse loads of steel frameworks, *Proceeding of the. Institution of Civil Engineers*, Vol. 33, March.

61 Horne M. R. (1960) Instability and the plastic theory of structures, *Transport Engineering Institute of Canada*, Vol. 4, No. 2.

62 Horne M. R. (1981). *Plastic design of low-rise frames*. Granada Publishing Ltd, UK.

63 Horne, M. R. and Chin, M. W., Plastic design of portal frames in steel to BS968, Report, BCSA.

64 Huber, G. and Tschemmernegg, F. (1998). Modelling of beam-to-column joints, Journal of constructional steel research, Vol. 45, No. 2, 199-216.

65 Johnson, R. P and Hope-Gill, M. (1972). Semi-Rigid Joints in Composite Frames, *Preliminary Report of the Ninth Congress of the International Association for Bridge and Structural Engineering*, Amsterdam, May, 133-144.

66 Johnson, R. P. and Chen, S. (1991). Local buckling and moment redistribution in Class 2 composite beams. *Structural Engineering International 4*, IABSE, Zurich, 27-34.

67 Johnson, R. P. and Fan, C. K. R. (1988). Strength of continuous composite beams designed to Eurocode 4. *IABSE Periodical 2*, Zurich, 33-44.

68 Johnson, R. P. and Law, C. L. C. (1981). Semi-rigid Joints for Composite Frames, *Proceedings of International Conference on Joints in Structural Steelwork*, ed. J. H. Howlett, Pentech Press, London, 3.3 – 3.19.

69 Johnson, R. P., and Hope-Gill, M. C. (1976). Applicability of simple plastic theory to continuous composite beams. *Proceedings of the Institution of Civil Engineers*, Vol. 61, London, March, 127-143.

70 Johnson, R. P., Moment redistribution in fixed ended beam, Computer program, Sydney University, Australia.

71 Kemp, A. R. (1987). Quantifying ductility in continuous composite beams, *Proceedings of the engineering foundation conference on composite construction*, Henniker, New Hampshire.

72 Kemp, A. R. (1988). Simplified modelling of material non-linearity in structural frames, Technical paper, Die Siviele Ingenieur in Suid-Afrika, September.

73 Kemp, A. R. (1990). Quantifying limit-states of rotation capacity in flexural members. *Proceedings of the Institution of Civil Engineers-Part 2*, September, London, Vol. 89, 387 – 406.

74 Kemp, A. R. and Dekker, N. W. (1991). "Available rotation capacity in steel and composite beams". The Structural Engineer, Vol. 69, no. 5, pp. 88 – 97.

75 Kemp, A. R., Nethercot, D. A. (2001). Required and available rotations in continuous composite beams with semi-rigid connections. Journal Of Constructional Steel Research, Vol. 57, Issue 4, 375-400.

76 Kubo, M. and Galambos, T. V. (1988). "Plastic collapse load of continuous composite plate girders". Engineering Journal, AISC, Vol. 25, no. 4, Chicago, pp. 517 – 529.

77 Latham, M. (1994). Constructing The Team, Final Report of the Government / Industry Review of Procurement and Contractual Arrangements in The UK Construction Industry HMSO, London.

78 Lawson, M and Wickens, P. (1992). *Composite beams*. In steel designers manual, 5th edition, Editors: G. W. Owens & P. R. Knowles, Blackwell Scientific Publications, Oxford, 592-619

79 Lawson, R. M., and Gibbons, C. (1995). Moment connections in composite construction: Interim guidance for end-plate connections, Technical report, SCI publication 143.

80 Leon, R. T. (1987). "Semi-rigid composite steel frames", AIC Engineering Journal, Fourth quarter.

81 Leon, R. T. (1987). *Behaviour of semi-rigid composite frame, composite steel structures: advance, design and construction*, edited by R. Narayanan, Elsevier applied science, London.

82 Li, T. Q. (1994). The analysis and ductility requirements of semi-rigid composite frames. PhD Thesis, Department of Civil Engineering, University of Nottingham.

83 Li, T. Q., Choo, B. S., and Nethercot, D. A. (1995). "Determination of rotation capacity requirements for steel and composite beams". Journal of Constructional Steel Research, Vol. 32, 303-332.

84 Li, T. Q., Nethercot, D. A. & Lawson, R. M. (2000). "Required rotation of composite connections". Journal of Constructional steel research, Vol. 56, 151-173.

85 Li, T. Q., Nethercot, D. A., and B. S. Choo. (1996). "Behaviour of Flush End-plate Composite Connections with Unbalanced Moment and Variable Shear/Moment Ratios--I. Experimental Behaviour", Journal of Constructional Steel Research, Volume 38, Issue 2, June, 125-164.

86 Li, T. Q., Nethercot, D. A., and B. S. Choo. (1996). "Behaviour of Flush End-plate Composite Connections with Unbalanced Moment and Variable Shear/Moment Ratios--II. Prediction of Moment Capacity", Journal of Constructional Steel Research, Volume 38, Issue 2, June, 165-198.

87 Li, T. Q., Nethercot, D. A., and Lawson, R. M. (2000). "Required rotation of composite connections". Journal of Constructional Steel Research, Vol. 56, Issue 2, 151-173.

88 Li, T. Q., Ahmed, B. and Lawson, R.M. (1996). Required rotation composite connections, The Steel Construction Institute, Ascot.

89 Li, T. Q., Choo, B. S. and Nethercot, D.A. (1993). Moment-curvature relations for steel and composite beams. Journal of the Singapore Structural Steel Society, 4(1), 35-51.

90 Lloyd, R. M. and Wright, H. D. (1992). "Insitu testing of a composite floor system", The structural engineer, Vol. 70, No. 12.

91 Moore, D. B. (1999). Ductility requirements for composite connections, Interim report No. 2, DETR Environment Transport Regions.

92 Moore, D. B and Couchman, G. H. (1998). "The development of a design guide for standardised composite connections", Journal of constructional steel research, Vol. 46, Nos. 1-3, 235.

93 Najafi, A. A. (1992). End plate connections and their influence on steel and composite structures, PhD Thesis, University of Warwick.

94 Najafi, A. A. and Anderson, D. (1997). Ductile steel-concrete composite joints, *Composite construction-Conventional and innovative*, Innsbruck, Report, IABSE, 427-432.

95 Narayanan, R. (1988). *Steel-Concrete Composite Structures-Stability and Strength.* Elsevier Applied Science, London.

96 Nethercot, D.A. (1995). "Semi-rigid joint action and the design of non-sway composite frames", Engineering structures, Vol. 17, No. 8, 554-567.

97 Nethercot D. A. (1989). *Frame analysis and the link between connection behaviour and frame performance: Frame and slab structure – Chapter 3*, edited by Armer, G. S. T., and Moore, D. B., Butterworths.

98 Nethercot, D. A., Li, T. Q. Choo, B. S. (1995). "Required rotations and moment redistribution for composite frames and continuous beams". Journal of Constructional Steel Research, Vol. 35, 121-163.

99 Oehlers, D. J. and Bradford, M. A. (1995). *Composite steel and concrete structural members*, Chapter 5, Elsevier Applied Science, 119.

100 Owens, G. W and C. B. Echeta. (1981). A Semi-Rigid Design Method for Composite Frames, *Proceedings of International Conference on Joints in Structural Steelwork*, Pentech Press, London, 320-338.

101 Packer, J. A. and Morris, L. J. (1977). "Limit state design method for the tension region of bolted beam-column connections", Structural Engineer, Vol. 55, no. 10, 446-458.

102 Ren, P and Crisinel, M. (1995). Prediction Method for Moment-Rotation Behaviour of Composite Beam to Steel Column Connection.

103 SCI (1992). *Partial strength moment resisting connections in composite frames*, Report RT-257, April, Revision 0.

104 SCI (1993). Design of composite connections – interim guidance for end-plate type connections. Report No. SCI-RT-330, July, Revision 1.

105 SCI. (1992). Partial strength moment resisting connections in composite frames. Document no. SCI-RT-275, Revision 0, April.

106 SCI. (1993). SCI-P-055: Design of composite slabs and beams with steel decking. The Steel Construction Institute.

107 Slutter, R. G. and Driscoll, C. G. (1965). "Flexural strength of steel-composite beams". Journal of the structural division of the ASCE, 91(ST2) , 71-99.

108 Stelmack, T. W., Marley, M. J. and Gerstle, K. H. (1986). "Analysis and tests of flexibly connected steel frames". Journal of structural engineering, ASCE, No.7, Vol. 112.

109 Tschemmernegg, F., Huber and Pavlov, G. (1995). Tension Region in the Panel Zone of a Composite Joint. Paper T4, *COST-C1/ECCS TC11 Drafting Group for Composite Connections*, University of Innsbruck, Austria.

110 Tschemmernegg, F., Huber, G. and Rubin, D. (1997). Composite joints for semi-continuous framing, Technical paper T14, Institute for Steel and Timber Construction, University of Innsbruck, October.

111 Weeks, G. (1969). Laboratory testing of large structures, I.A.T.R.L.M.S., Methodology and testing structures no. 3–Tests of full-scale structures, International colloquium, Rilem, Bucharest.

112 Wright, H. D., Evans, H. R. and Harding, P. W. (1987). "The Use of Profiled Steel Sheeting in Floor Construction", Journal of Constructional Steel Research, Vol. 7, 279-295

113 Xiao Y. (1994). Behaviour of Composite Connections in Steel and Concrete, PhD Thesis, University of Nottingham.

114 Xiao Y., D. A. Nethercot, and B. S. Choo. (1992). Moment Resistance of Composite Connections in Steel and Concrete, *Proceedings of the first world conference on constructional steel design*, Mexico, November.

115 Xiao, R. (1994). Behaviour of composite connections in steel and concrete, PhD Thesis, Department of civil engineering, University of Nottingham.

116 Xiao, Y, Choo, B. S., and Nethercot, D. A. (1994). Design of semi-rigid composite beam-column connections. *Building the future: Innovation in Design, Materials and Construction*, London, First Edition, 391 – 406.

117 Young, W. C. (1989). *Roark's formulas for stress and strain*. 6th Edition, McGraw Hill.

118 Zandonini, R. (1989). *Semi-Rigid Composite Joints, Structural Connections-Stability and Strength, Chapter 3*, edited by R. Narayanan, Elsevier Applied Science, 63-120.

Appendix A: Calculation of moment capacity of the test beam

A.1. Design flexural strength of the test beam

Composite test beam: 533 UB + 130 slab + 60 decking

$f_{cu} = 30\ N/mm^2$

North beam:

Effective width, $B_e = 0.7$ span/4 = 0.7 11400/4 = 1995 mm

Compressive resistance of concrete flange,

$R_c = 0.45\ B_e (D_s - D_p) = 0.45 \times 1995 \times (130-60) \times 30 \times 10^{-3} = 1885.3\ kN$

Tensile resistance of steel beam, $R_s = A_s p_y = 104 \times 10^2 \times 275 \times 10^{-3} = 2860\ kN$

$R_s > R_c$

Moment capacity of the beam,

$$M_{pc} = R_s \frac{D}{2} + R_c \left(\frac{D_s + D_p}{2} \right) - \frac{(R_s - R_c)^2}{R_f} \frac{T}{4}$$

$$M_{pc} = 2860 \frac{528.3}{2} + 1885.3 \left(\frac{130+60}{2} \right) - \frac{(2860-1885.3)^2}{13.2 x 208.8} \frac{13.2}{4} = 933\ \text{kN.m}$$

South beam:

Effective width, $B_e = 0.8$ span/4 = 0.8 11400/4 = 2280 mm

Compressive resistance of concrete flange,

$R_c = 0.45 B_e (D_s - D_p) = 0.45 \times 2280 \times (130-60) \times 30 \times 10^{-3} = 2154.6\ kN$

Tensile resistance of steel beam, $R_s = A_s p_y = 104 \times 10^2 \times 275 \times 10^{-3} = 2860\ kN$

$R_s > R_c$

Moment capacity of the beam,

$$M_{pc} = R_s \frac{D}{2} + R_c \left(\frac{D_s + D_p}{2} \right) - \frac{(R_s - R_c)^2}{R_f} \frac{T}{4}$$

$$M_{pc} = 2860 \frac{528.3}{2} + 2154.6 \left(\frac{130+60}{2} \right) - \frac{(2860-2154.6)^2}{13.2 x 208.8} \frac{13.2}{4} = 960\ \text{kN.m}$$

A.2. Flexural strength of the test beam based on measured material and geometric properties

Composite test beam: 533UB + 140 slab + 60 decking

$f_{cu} = 42$ N/mm^2

Stress values are taken from the experimental stress-strain curve as shown in Figure 3-11.

Slab effective width, $B_e = 3000$ mm

Compressive resistance of concrete flange,

$R_c = 0.45\ B_e (D_s - D_p) = 0.45 \times 3000 \times (140-60) \times 42 \times 10^{-3} = 4536\ kN$

Tensile resistance of steel beam,

$R_s = A_s p_y = 2 \times 13.2 \times 208.8 \times 298 \times 10^{-3} + 9.6 \times (528.3-2 \times 13.2) \times 330 \times 10^{-3} = 3233\ kN$

Therefore, neutral axis in slab. NA 57mm below top of slab, i.e. ,

$R_c = 0.45 \times 3000 \times 57 \times 42 \times 10^{-3} = 3232$ kN

Taking moments about centre of slab, M_{pc} =

+298 x 208.8 x 13.2 x (-13.2/2+528.3+140-57/2)

+330 x 9.6 x (528.3-2 x 13.2) x (528.3/2+140-57/2)

+298 x 208.8 x 13.2 x (140-57/2+13.2/2)

M_{pc} =520 + 597.3 + 97 = 1214 kN.m

A.3. Flexural strength of the test beam based on measured geometric properties and strain hardening in the flange and the web (Assume 3% strain in the Bottom flange and the web)

Composite test beam: 533UB + 140 slab + 60 decking

$f_{cu} = 42$ N/mm^2

Stress values are taken from the experimental stress-strain curve as shown in Figure 3-11.

Compressive resistance of concrete flange, $R_c = 0.45\ B_e\ (D_s - D_p)$

$= 0.45 \times 3000 \times (140-60) \times 42 \times 10^{-3} = 4536\ kN$

Tensile resistance of steel beam, $R_s = A_s\ p_y$

$= 13.2 \times 208.8 \times 360 \times 10^{-3} + 9.6 \times (528.3 - 2 \times 13.2) \times 380 \times 10^{-3} + 13.2 \times 208.8 \times 298 \times 10^{-3}$

$= 2756.16 \times 360 \times 10^{-3} + 4818.24 \times 380 \times 10^{-3} + 2756.16 \times 298 \times 10^{-3}$

$= 992.2176 + 1830.9312 + 821.336$

$= 3645\ kN$

Therefore, neutral axis in slab. NA 64.3mm below top of slab, i.e. ,

$R_c = 0.45 \times 3000 \times 64.3 \times 42 \times 10^{-3} = 3646$ kN

Taking moments about centre of slab, M_{pc} =

+360 x 208.8 x 13.2 x (-13.2/2+528.3+140-64.3/2)

+380 x 9.6 x(528.3-2x13.2)x(528.3/2+140-64.3/2)

+298 x 208.8 x 13.2 x (140-64.3/2+13.2/2)

M_{pc} =625 + 681 + 94 = 1400 kN.m

Appendix B – Numerical modelling of semi-continuous composite beam

MOMENT CURVATURE MODULES

MATERIAL NON-LINEARITY

```
stressSteelData[Ystress_, EMod_, Esh_, shno_] :=
  Module[{Ystrain, Shstrain, Maxstrain, strain1, strain2, strain3, Stressvalues1, Stressvalues2, Stressvalues3,
    Steelstressstrain, Webstressstrain},

   Ystrain = Ystress 100 / EMod;
   Shstrain = shno * Ystrain;
   Maxstrain = 10.;

   strain1 = Ystrain / 300;
   strain2 = (Shstrain - (Ystrain + strain1)) / 20;
   strain3 = (Maxstrain - (Shstrain + strain2)) / 30;

   Stressvalues1 = Table[{x, EMod * x/100}, {x, 0, Ystrain, strain1}];
   Stressvalues2 = Table[{x, Ystress}, {x, Ystrain + strain1, Shstrain, strain2}];
   Stressvalues3 = Table[{x, Ystress + (Esh * (x - Shstrain)/100)}, {x, Shstrain + strain2, Maxstrain, strain3}];

   Steelstressstrain = Union[Stressvalues1, Stressvalues2, Stressvalues3];
   Webstressstrain = Union[Stressvalues1, Stressvalues2, Stressvalues3];

   {Steelstressstrain, Webstressstrain}
  ];

stressstrainconcreteData[fcu_, γ_] := Module[{α, x0, y0, x1, y1, Stressvalues4, Stressvalues5, Concretestressstrain},
   α = 5.5 1000 Sqrt[fcu/γ];
   x0 = 0.0;
   y0 = 0.0;
   x1 = 2.4/10000 Sqrt[fcu/γ];
   y1 = 0.67 fcu/γ;
   Stressvalues4 = Table[{100 x, α/(2 (x0 - x1)) (x - x0)^2 + (x - x0)}, {x, x0, x1, (x1 - x0)/50}];
   Stressvalues5 = Table[{100 x, α/(2 (x0 - x1)) (x1 - x0)^2 + (x1 - x0)}, {x, x1, 0.1, (0.1 - x1)/50}];
   Concretestressstrain = Union[Stressvalues4, Stressvalues5];

   {Concretestressstrain}
];
```

```
stressstrainrebarData[YstressR_, EModR_] :=
  Module[{Ystrain, Maxstrain, strain1, strain2, Stressvalues1, Stressvalues2, Steelstressstrain, Webstressstrain},

   Ystrain = 100 YstressR / (1.05 EModR);
   Maxstrain = 15.;

   strain1 = Ystrain/300;
   strain2 = (Maxstrain - (Ystrain + strain1))/20;

   Stressvalues1 = Table[{x, EModR* x/100}, {x, 0, Ystrain - strain1, strain1}];
   Stressvalues2 = Table[{x, EModR* Ystrain/100}, {x, Ystrain + strain1, Maxstrain, strain2}];

   Rebarstressstrain = Union[Stressvalues1, Stressvalues2];

   {Rebarstressstrain}
  ];
```

INTERPOLATION

```
stresssteelInt[Ystress_, EMod_, Esh_, shno_] :=
  Module[{Steelstressstrain, Webstressstrain, steelintstr, websteelintstr},
   {Steelstressstrain, Webstressstrain} = stresssteelData[Ystress, EMod, Esh, shno];
   steelintstr = Interpolation[Steelstressstrain, InterpolationOrder → 1];
   websteelintstr = Interpolation[Webstressstrain, InterpolationOrder → 1];
   {steelintstr, websteelintstr}
  ];

stressstrainconcreteInt[fcu_, γ_] := Module[{Concretestressstrain, concreteintstr},
   {Concretestressstrain} = stressstrainconcreteData[fcu, γ];
   concreteintstr = Interpolation[Concretestressstrain, InterpolationOrder → 1];
   {concreteintstr}
  ];

stressstrainrebarInt[YstressR_, EModR_] := Module[{Rebarstressstrain, rebarintstr},
   {Rebarstressstrain} = stressstrainrebarData[YstressR, EModR];
   rebarintstr = Interpolation[Rebarstressstrain, InterpolationOrder → 1];
   {rebarintstr}
  ];
```

STEEL STRESS FUNCTION

```
stresssteel[Ystress_, EMod_, Esh_, shno_] := Module[{steelintstr, websteelintstr, σs, ϵ, σsweb},
    {steelintstr, websteelintstr} = stresssteelInt[Ystress, EMod, Esh, shno];
    σs[ϵ_/; ϵ ≥ 0] := steelintstr[ϵ];
    σs[ϵ_/; ϵ < 0] := -steelintstr[-ϵ];
    σsweb[ϵ_/; ϵ ≥ 0] := websteelintstr[ϵ];
    σsweb[ϵ_/; ϵ < 0] := -websteelintstr[-ϵ];
    {σs, σsweb}
  ];
```

CONCRETE STRESS FUNCTION

```
stressstrainconcrete[fcu_, γ_] := Module[{concreteintstr, ϵ, σc},
    {concreteintstr} = stressstrainconcreteInt[fcu, γ];
    σc[ϵ_/; ϵ ≥ 0] := 0;
    σc[ϵ_/; ϵ < 0] := -concreteintstr[-ϵ];
    {σc}
  ];
```

REBAR STRESS FUNCTION

```
stressstrainrebar[YstressR_, EModR_] := Module[{rebarintstr, ϵ, σr},
    {rebarintstr} = stressstrainrebarInt[YstressR, EModR];
    σr[ϵ_/; ϵ ≥ 0] := rebarintstr[ϵ];
    σr[ϵ_/; ϵ < 0] := -rebarintstr[-ϵ];
    {σr}
  ];
```

MATERIAL NON-LINEARITY PLOTS

```
stressPlot[Ystress_, EMod_, Esh_, shno_, fcu_, γ_, YstressR_, EModR_] := Module[
  {Steelstressstrain, Webstressstrain, Concretestressstrain, Rebarstressstrain, steelintstr, websteelintstr,
    concreteintstr, rebarintstr, σs, σsweb, σc, σr, plotσs, plotσsweb, plotσc, plotσr, x},

  {Steelstressstrain, Webstressstrain} = stresssteelData[Ystress, EMod, Esh, shno];
  {Concretestressstrain} = stressstrainconcreteData[fcu, γ];
  {Rebarstressstrain} = stressstrainrebarData[YstressR, EModR];

  {steelintstr, websteelintstr} = stresssteelInt[Ystress, EMod, Esh, shno];
  {concreteintstr} = stressstrainconcreteInt[fcu, γ];
  {rebarintstr} = stressstrainrebarInt[YstressR, EModR];

  {σs, σsweb} = stresssteel[Ystress, EMod, Esh, shno];
  {σc} = stressstrainconcrete[fcu, γ];
  {σr} = stressstrainrebar[YstressR, EModR];
```

```
ListPlot[Steelstressstrain, PlotJoined → False, FrameLabel → {"Strain, %", "Stress, N mm^-2"}];
Plot[steelintstr[x], {x, 0, 5}, Axes → False, FrameLabel → {"Strain, %", "Stress, Nmm^-2"}];
plotσs = Plot[σs[x], {x, -10, 10}, FrameLabel → {"Strain, %", "Stress, Nmm^-2"}];

ListPlot[Webstressstrain, PlotJoined → False, FrameLabel → {"Strain, %", "Stress, N mm^-2"}];
Plot[websteelintstr[x], {x, 0, 10}, Axes → False, FrameLabel → {"Strain, %", "Stress, Nmm^-2"}];
plotσsweb = Plot[σsweb[x], {x, -10, 10}, FrameLabel → {"Strain, %", "Stress, Nmm^-2"}];

ListPlot[Concretestressstrain, PlotJoined → False, FrameLabel → {"Strain, %", "Stress, N mm^-2"}];
Plot[concreteintstr[x], {x, 0, 0.35}, Axes → False, FrameLabel → {"Strain, %", "Stress, Nmm^-2"}];
Plot[σc[x], {x, -10, 10}, Axes → False, FrameLabel → {"Strain, %", "Stress, Nmm^-2"}];

ListPlot[Rebarstressstrain, PlotJoined → False, FrameLabel → {"Strain, %", "Stress, N mm^-2"}];
Plot[rebarintstr[x], {x, 0, 15}, Axes → False, FrameLabel → {"Strain, %", "Stress, Nmm^-2"}];
plotσr = Plot[σr[x], {x, -15, 15}, FrameLabel → {"Strain, %", "Stress, Nmm^-2"}];
];
```

GEOMETRIC NON-LINEARITY

STEEL GEOMETRY

```
Steelgeometry := Module[{b1, b2, t1, t2, tw, d, swidth, y},
  b1 = 177.9;
  b2 = 177.9;
  t1 = 12.8;
  t2 = 12.8;
  tw = 7.9;
  d = 406.4;
  swidth[y_/; d/2 - t1 ≤ y] := b1;
  swidth[y_/; d/2 + t2 ≤ y ≤ d/2 - t1] := tw;
  swidth[y_/; y ≤ -d/2 + t2] := b2;
  {b1, b2, t1, t2, tw, d, swidth}
 ];
```

CONCRETE GEOMETRY

```
Concretegeometry[L_] := Module[{ds, dp, dc, beff, cwidth},
  ds = 120;
  dp = 50;
  dc = ds - dp;
  beff = L/4;

  cwidth[y_/; y ≤ dp] := beff/2;
  cwidth[y_/; y > dp] := beff;

  {ds, dp, dc, beff, cwidth}
];
```

REBAR GEOMETRY

```
Rebargeometry := Module[{dr, radius, dlimit, rebarwidth},

    dr = 80;
    radius = 8;
    dlimit = dr + radius;
    rebarwidth[y_/; y < (dr - radius)] := 0;
    rebarwidth[y_/; (dr - radius) ≤ y ≤ (dr + radius)] := 4 2 √(radius^2 - (dr - y)^2) ;

    {dr, radius, dlimit, rebarwidth}
];
```

GEOMETRY ELASTIC STRAIN & STRESS

```
geoelasticprop[Ystress_, EMod_, Esh_, shno_] := Module[{YM, ϵy, ρy, σs, MI},

    {σs, σsweb} = stressssteel[Ystress, EMod, Esh, shno];
    {b1, b2, t1, t2, tw, d, swidth} = Steelgeometry;

    YM = EMod;
    MI = b1 d^3 / 12  (b1  tw) (d - t1 - t2)^3 / 12 ;
    ϵy = Ystress 100 / YM ;
    ρy = σs[ϵy];
    {YM, ϵy, ρy, MI}
];
```

GEOMETRIC PROPERTY

```
geometryprop[L_, Ystress_, EMod_, Esh_, shno_, fcu_, γ_] :=
  Module[{b1, b2, t1, t2, tw, d, ds, dc, beff, YM, ρy, EM, A, Rs, Rc, Rf, Rw, Mpc, ElasticMoment},
   {σs, σsweb} = stressssteel[Ystress, EMod, Esh, shno];
   {b1, b2, t1, t2, tw, d, swidth} = Steelgeometry;
   {ds, dp, dc, beff, cwidth} = Concretegeometry[L];
   {YM, ϵy, ρy, MI} = geoelasticprop[Ystress, EMod, Esh, shno];
   EM = MI 2 / d;
   A = b1 t1 + b2 t2 + (d - t1 - t2) tw;
   Rs = ρy A;
   Rf = ρy b1 t1;
   Rw = ρy (d - t1 - t2) tw;
   Rc = 0.67 fcu dc beff / γ;
   If[Rc > Rs, Mpc = Rs (d/2 + ds - Rs/Rc (dc/2)) / 10^6, Mpc = (Rs d/2 + Rc ((ds + dp)/2) - (Rs - Rc)^2 / Rf t1/4) / 10^6];
   ElasticMoment = ρy EM / 10^6;
   Mpc
  ];
```

STEEL AND CONCRETE - TOTAL DEPTH

```
SteelConcretegeometry[L_] := Module[{d, DD, ds},
   {b1, b2, t1, t2, tw, d, swidth} = Steelgeometry;
   {ds, dp, dc, beff, cwidth} = Concretegeometry[L];
   DD = d + ds;
   DD
  ];
```

GEOMETRIC NON-LINEARITY PLOTS

```
geometryPlot[L_] := Module[{d, ds, beff, dlimit, swidth, cwidth, rebarwidth, cg1, cg2, cg3, y},
   {b1, b2, t1, t2, tw, d, swidth} = Steelgeometry;
   {ds, dp, dc, beff, cwidth} = Concretegeometry[L];
   {dr, radius, dlimit, rebarwidth} = Rebargeometry;
   cg1 = Plot[swidth[y], {y, -d/2, d/2}, FrameLabel → {"Section Depth, mm", "Width, mm"}];
   cg2 = Plot[cwidth[y], {y, 0, ds}, PlotRange → {{0, ds}, {0, beff}}, FrameLabel → {"Section Depth, mm", "Width, mm"}];
   cg3 = Plot[rebarwidth[y], {y, 0, dlimit}, PlotRange → All, FrameLabel → {"Section Depth, mm", "Width, mm"}];
  ];
```

Strain,Stress,Force, Nacom and Natot Equations

$$M\phi\epsilon[L\_, Ystress\_, EMod\_, Esh\_, shno\_, upperwidth\_, upperdepth\_, upperstress\_] := Module[$$

{t1, t2, d, swidth, ϵtot, ϵecon, ϵecom, y, nacom, Fs, Fc, stresstot, Nacom, Natot, σs, σsweb},

{σs, σsweb} = stressSteel[Ystress, EMod, Esh, shno];

{b1, b2, t1, t2, tw, d, swidth} = Steelgeometry;

$$\epsilon tot[\epsilon ecom\_, \epsilon econ\_, nacom\_][y\_ /; y < 0] := \frac{\left(\frac{d}{2} \quad y\right)}{\frac{d}{2}} \; econ + \frac{y + nacom}{d + nacom} \; ecom;$$

$$tot[\; ecom\_, \; econ\_, nacom\_][y\_ /; y \geq 0] := \frac{y + nacom}{d + nacom} \; ecom;$$

$$stresstot[\; ecom\_, \; econ\_, nacom\_][y\_ /; \; d \leq y \leq \; d + t2] := \sigma s\left[\frac{\left(\frac{d}{2} + y\right)}{\frac{d}{2}} \; econ + \frac{y + nacom}{d + nacom} \; ecom\right];$$

$$stresstot[\; ecom\_, \; econ\_, nacom\_][y\_ /; \; d + t2 \leq y \leq \; t1] := \sigma sweb\left[\frac{\left(\frac{d}{2} + y\right)}{\frac{d}{2}} \; econ + \frac{y + nacom}{d + nacom} \; ecom\right];$$

$$stresstot[\; ecom\_, \; econ\_, nacom\_][y\_ /; \; t1 \leq y \leq 0] := \sigma s\left[\frac{\left(\frac{d}{2} + y\right)}{\frac{d}{2}} \; econ + \frac{y + nacom}{d + nacom} \; ecom\right];$$

$$stresstot[\; ecom\_, \; econ\_, nacom\_][y\_ /; y \geq 0] := upperstress\left[\frac{y + nacom}{d + nacom} \; ecom\right];$$

Fs[ecom_, econ_, nacom_] :=

$$NIntegrate\left[\; 1/10\text{^}3 \, \sigma s\left[\frac{\left(\frac{d}{2} + y\right)}{\frac{d}{2}} \; econ + \frac{y + nacom}{d + nacom} \; ecom\right] swidth\left[y + \frac{d}{2}\right], \{y, \; d, \; d + t2\},\right.$$

$$\left. MinRecursion \to 4, MaxRecursion \to 10, AccuracyGoal \to 3, WorkingPrecision \to 24\right] +$$

$$NIntegrate\left[\; 1/10\text{^}3 \, \sigma sweb\left[\frac{\left(\frac{d}{2} + y\right)}{\frac{d}{2}} \; econ + \frac{y + nacom}{d + nacom} \; ecom\right] swidth\left[y + \frac{d}{2}\right], \{y, \; d + t2, \; t1\},\right.$$

$$\left. MinRecursion \to 4, MaxRecursion \to 10, AccuracyGoal \to 3, WorkingPrecision \to 24\right] +$$

$$NIntegrate\left[\; 1/10\text{^}3 \, \sigma s\left[\frac{\left(\frac{d}{2} + y\right)}{\frac{d}{2}} \; econ + \frac{y + nacom}{d + nacom} \; ecom\right] swidth\left[y + \frac{d}{2}\right], \{y, \; t1, \; 0\},\right.$$

$$\left. MinRecursion \to 4, MaxRecursion \to 10, AccuracyGoal \to 3, WorkingPrecision \to 24\right];$$

$$Fc[\; ecom\_, \; econ\_, nacom\_] := NIntegrate\left[\; 1/10\text{^}3 \; upperstress\left[\frac{y + nacom}{d + nacom} \; ecom\right] upperwidth[y],\right.$$

$$\left. \{y, 0, upperdepth\}, MinRecursion \to 4, MaxRecursion \to 10, AccuracyGoal \to 3, WorkingPrecision \to 24\right];$$

Nacom[ecom_, econ_] :=

FindRoot[Fs[ecom, econ, na] + Fc[ecom, econ, na] == 0, {na, -(d - upperdepth)/2, upperdepth},

MaxIterations → 30][[1, 2]];

$$Natot[\epsilon ecom\_, \epsilon econ\_, nacom\_] := nacom \,/; \frac{nacom}{d + nacom} \; \epsilon ecom > \epsilon econ;$$

$$Natot[\epsilon ecom\_, \epsilon econ\_, nacom\_] := \frac{\epsilon econ + \epsilon ecom \, \frac{nacom}{nacom + d}}{\epsilon econ \, \frac{2}{d} \quad \frac{ecom}{nacom + d}} \; /; \frac{nacom}{d + nacom} \; ecom \leq \; econ;$$

{ tot, stresstot, Fs, Fc, Nacom, Natot}

];

Strain,Stress,Force, Nacom and Natot Plots - For sagging section

```
MϕϵConcretePlot[L_, Ystress_, EMod_, Esh_, shno_, fcu_, γ_, want2check_, want2plotTot_, want2plotNatot_,
  want2plotNacom_] :=
 Module[
  {cwidth, ds, σc},
  {σc} = stressstrainconcrete[fcu, γ];
  {ds, dp, dc, beff, cwidth} = Concretegeometry[L];
  MϕϵPlot[L, Ystress, EMod, Esh, shno, cwidth, ds, σc, want2check, want2plotTot, want2plotNatot, want2plotNacom];
 ];
```

Strain,Stress,Force, Nacom and Natot Plots - For hogging section

```
MϕϵRebarPlot[L_, Ystress_, EMod_, Esh_, shno_, YstressR_, EModR_, want2check_, want2plotTot_,
  want2plotNatot_, want2plotNacom_] :=
 Module[
  {rebarwidth, dlimit, σr},
  {σr} = stressstrainrebar[YstressR, EModR];
  {dr, radius, dlimit, rebarwidth} = Rebargeometry;
  MϕϵPlot[L, Ystress, EMod, Esh, shno, rebarwidth, dlimit, σr, want2check, want2plotTot, want2plotNatot,
   want2plotNacom];
 ];
```

M-ϕ-ϵ Equations

```
Moment[Nacom_, Natot_, {d_, t1_, t2_, upperdepth_}, swidth_, upperwidth_, {σs_, σsweb_, upperstress_}][
  ϵecom_, ϵecon_] :=
 Module[{na, nacom, natot},
  nacom = Nacom[ϵecom, ϵecon];
  natot = Natot[ϵecom, ϵecon, Nacom[ϵecom, ϵecon]];
  {ϵecom, ϵecon, nacom, natot, (ϵecom + ϵecon - (-(d/2))/(d/2) econ - nacom/(d + nacom) ecom)} / 100 1/d,
  -{NIntegrate[ 1/10^6 σs[(-(d/2 + y))/(d/2) econ + (-y + nacom)/(d + nacom) ecom] (y - natot) swidth[y + d/2],
    {y, -d, -d + t2}, MinRecursion → 4, MaxRecursion → 10, AccuracyGoal → 3, WorkingPrecision → 24] +
   NIntegrate[ 1/10^6 σsweb[(-(d/2 + y))/(d/2) econ + (-y + nacom)/(d + nacom) ecom] (y - natot) swidth[y + d/2],
    {y, -d + t2, -t1}, MinRecursion → 4, MaxRecursion → 10, AccuracyGoal → 3, WorkingPrecision → 24] +
   NIntegrate[ 1/10^6 σs[(-(d/2 + y))/(d/2) econ + (-y + nacom)/(d + nacom) ecom] (y - natot) swidth[y + d/2],
    {y, -t1, 0}, MinRecursion → 4, MaxRecursion → 10, AccuracyGoal → 3, WorkingPrecision → 24] +
   NIntegrate[ 1/10^6 upperstress[(-y + nacom)/(d + nacom) ecom] (y - natot) upperwidth[y], {y, 0, upperdepth},
    MinRecursion → 4, MaxRecursion → 10, AccuracyGoal → 3, WorkingPrecision → 24]}
 ];
```

```
MomentData[L_, Ystress_, EMod_, Esh_, shno_, upperwidth_, upperdepth_, upperstress_, want2loaddata_,
    want2savedata_, filename_] :=
  Module[
   {σs, σsweb, b1, b2, t1, t2, tw, d, swidth, YM, ϵy, ρy, MI, DD, ϵtot, stresstot, Fs, Fc, Nacom, Natot,
     myfile, const, const1, const2, nbcon, nbcom, data},
   {σs, σsweb} = stresssteel[Ystress, EMod, Esh, shno];
   {b1, b2, t1, t2, tw, d, swidth} = Steelgeometry;
   {YM, ϵy, ρy, MI} = geoelasticprop[Ystress, EMod, Esh, shno];
   DD = SteelConcretegeometry[L];
   {ϵtot, stresstot, Fs, Fc, Nacom, Natot} = Mϕϵ[L, Ystress, EMod, Esh, shno, upperwidth, upperdepth, upperstress];
   myfile = StringJoin[filename, ToString[L/DD], "_", ToString[Ystress], "_", ToString[EMod], "_", ToString[Esh],
     "_", ToString[shno], "_", "data.mx"];
   maxstr = 10;
   nbcon = 11;
   nbcom = 40;
   If[want2loaddata == 1, If[First[Dimensions[FileNames[myfile]]] == 1, data = Get[myfile],
     data = Table[Moment[Nacom, Natot, {d, t1, t2, upperdepth}, swidth, upperwidth, {σs, σsweb, upperstress}][
         ϵccom, ϵccon], {ϵccom, 0, maxstr - ϵy, (maxstr - ϵy)/nbcom}, {ϵccon, -ϵy, ϵy, (2 * ϵy)/nbcon}]],
    data = Table[Moment[Nacom, Natot, {d, t1, t2, upperdepth}, swidth, upperwidth, {σs, σsweb, upperstress}][
        ϵccom, ϵccon], {ϵccom, 0, maxstr - ϵy, (maxstr - ϵy)/nbcom}, {ϵccon, -ϵy, ϵy, (2 * ϵy)/nbcon}]];
   If[want2savedata == 1, Put[data, myfile]];
   data
  ];
```

SAGGING MOMENT DATA

```
MomentDataConcrete[L_, Ystress_, EMod_, Esh_, shno_, fcu_, γ_, want2loaddata_, want2savedata_, filename_] :=
  Module[
   {σc, ds, dp, dc, beff, cwidth},
   {σc} = stressstrainconcrete[fcu, γ];
   {ds, dp, dc, beff, cwidth} = Concretegeometry[L];
   MomentData[L, Ystress, EMod, Esh, shno, cwidth, ds, σc, want2loaddata, want2savedata, filename]
  ];
```

HOGGING MOMENT DATA

```
MomentDataRebar[L_, Ystress_, EMod_, Esh_, shno_, YstressR_, EModR_, want2loaddata_, want2savedata_, filename_] :=
  Module[
   {σr, dr, radius, dlimit, rebarwidth},
   {σr} = stressstrainrebar[YstressR, EModR];
   {dr, radius, dlimit, rebarwidth} = Rebargeometry;
   MomentData[L, Ystress, EMod, Esh, shno, rebarwidth, dlimit, σr, want2loaddata, want2savedata, filename]
  ];
```

3D M-ϕ-ϵ Interploation

M-ϕ-ϵ Interpolation Function

```
MPhiDLintPlot[intfunction_, econvalues_, amin_, amax_, mybound_, mybound2_] :=
  Module[{myplota, myplotb, myplotc},
   myplota = Plot3D[intfunction[x, y], {x, Min[econvalues], Max[econvalues]}, {y, amax - mybound, amax},
     Mesh → True, PlotPoints → {25, 10}, DisplayFunction → Identity];
   myplotc = Plot3D[intfunction[x, y], {x, Min[econvalues], Max[econvalues]},
     {y, amax - mybound2 - mybound, amax - mybound}, Mesh → True, PlotPoints → {25, 5},
     DisplayFunction → Identity];
   myplotb = Plot3D[intfunction[x, y], {x, Min[econvalues], Max[econvalues]}, {y, amin, amax - mybound2 - mybound},
     Mesh → True, PlotPoints → {25, 25}, DisplayFunction → Identity];
   Show[myplota, myplotb, myplotc, Epilog → {
     Text[StyleForm["Curvature , mm ⁻¹", FontSize → 13, FontFamily → "Times New Roman"], {-0.22, 0.45},
      {0, 0}, {-0.13, 1}],
     Text[StyleForm["D L S t r a i n , %", FontSize → 11, FontFamily → "Times New Roman"],
      {0.25, 0.05}, {0, 0}, {1, -0.4}],
     Text[StyleForm["M o m e n t , kN.m", FontSize → 11, FontFamily → "Times New Roman"],
      {0.95, 0.2}, {0, 0}, {1, 1.5}]},
    PlotRange → All, PlotRegion → {{0.15, 0.9}, {-0.6, 1.6}}, DisplayFunction → $DisplayFunction];
  ];
```

M-ϕ-ϵ 3-D Plot

```
MPhiDLmyphi[L_, want2plot_, filename_, mybound_, mybound2_] := Module[
  {data, SMomentCurvature, St, Mo, Cu, amin, amax, nb, moment, econvalues, aa, aaaa, endmincurv,
   endmaxcurv, newaaa, phia, phigrid, myphi},
  If[First[Dimensions[FileNames[filename]]] == 1, data = Get[filename]];
  SMomentCurvature = Table[{Flatten[data, 1][[i]][[2]], Flatten[data, 1][[i]][[6]], Flatten[data, 1][[i]][[5]]},
    {i, 1, Length[Flatten[data, 1]]}];
  St = Table[{Flatten[data, 1][[i]][[2]]}, {i, 1, Length[Flatten[data, 1]]}];
  Mo = Table[{Flatten[data, 1][[i]][[6]]}, {i, 1, Length[Flatten[data, 1]]}];
  Cu = Table[{Flatten[data, 1][[i]][[5]]}, {i, 1, Length[Flatten[data, 1]]}];
  amin = Min[Mo];
  amax = Max[Mo];
  nb = 500;
  moment = Table[x, {x, amin, amax, (amax - amin) / nb}];
  econvalues = Table[data[[1]][[i]][[2]], {i, 1, Length[data[[1]]]}];
  phigrid = {};
  For[i = 1, i ≤ Length[econvalues], i++,
   aa = Select[SMomentCurvature, #1[[1]] == econvalues[[i]] &];
   aaaa = Sort[Table[{aa[[i]][[2]], aa[[i]][[3]]}, {i, 1, Length[aa]}], #1[[1]] < #2[[1]] &];
   endmincurv = aaaa[[1]][[2]];
   endmaxcurv = aaaa[[Length[aaaa]]][[2]];
   newaaa = Union[{{amin, endmincurv}}, aaaa, {{amax, endmaxcurv}}];
   phia = Interpolation[newaaa, InterpolationOrder → 1];
   AppendTo[phigrid, Table[{econvalues[[i]], x, phia[x]}, {x, amin, amax, (amax - amin) / nb}]];
  ];
  myphi = Flatten[phigrid, 1];
  intfunction = Interpolation[myphi, InterpolationOrder → 1];
  If[want2plot == 1, MPhiDLintPlot[intfunction, econvalues, amin, amax, mybound, mybound2]];
  intfunction
 ];
```

PIN REGION

PIN M-ϕ Equations

```
PinM[{d_, t1_, t2_}, swidth_, {σs_, σsweb_}][see_] := Module[{y},
    NIntegrate[ 1/10^6 σs[2 y/d see] y swidth[y], {y, d/2, d/2  t2}, MinRecursion → 4, MaxRecursion → 10,
      AccuracyGoal → 3, WorkingPrecision → 24] +
    NIntegrate[ 1/10^6 σsweb[2 y/d see] y swidth[y], {y, d/2 + t2, d/2  t1}, MinRecursion → 4,
      MaxRecursion → 10, AccuracyGoal → 3, WorkingPrecision → 24] +
    NIntegrate[ 1/10^6 σs[2 y/d see] y swidth[y], {y, d/2  t1, d/2}, MinRecursion → 4, MaxRecursion → 10,
      AccuracyGoal → 3, WorkingPrecision → 24]
  ];
```

PIN M-ϕ Data Aquisition

```
PinMoment[Ystress_, EMod_, Esh_, shno_, want2loadPindata_, want2savePindata_, filename_] :=
  Module[
    {σs, σsweb, t1, t2, d, swidth, see, Pinmyfile, nbsee, Steelmomentdata},
    {σs, σsweb} = stressstee[Ystress, EMod, Esh, shno];
    {b1, b2, t1, t2, tw, d, swidth} = Steelgeometry;
    {YM, εy, ρy, MI} = geoelasticprop[Ystress, EMod, Esh, shno];
    Pinmyfile = StringJoin[filename, ToString[Ystress], "_", ToString[EMod], "_", ToString[Esh], "_",
      ToString[shno], "_", "Pindata.mx"];
    nbsee = 100.;
    If[want2loadPindata == 1,
      If[First[Dimensions[FileNames[Pinmyfile]]] == 1, Steelmomentdata = Get[Pinmyfile],
        Steelmomentdata = Table[{PinM[{d, t1, t2}, swidth, {σs, σsweb}][see], see/100 2/d},
          {see, -10.0, 10.0, (2 * 10.)/nbsee}];,
      Steelmomentdata = Table[{PinM[{d, t1, t2}, swidth, {σs, σsweb}][see], see/100 2/d},
          {see, -10.0, 10.0, (2 * 10.)/nbsee}];
    ];
    If[want2savePindata == 1, Put[Steelmomentdata, Pinmyfile]];
    Steelmomentdata
  ];
```

Pin 2D M-ϕ Interploation

```
MPhiPinintPlot[Steelintmom_, Steelmomentdata_] := Module[{myplotpin, x},
  myplotpin = Plot[Steelintmom[x], {x, Min[Steelmomentdata], Max[Steelmomentdata]}, PlotRange → All,
    Axes → True, AxesLabel → {"Moment, kN.m", "Curvature, mm^-1"}];]
```

MEMBER RESPONSE MODULES

Sagging 3D Moment-Curvature-DLstrain relationship

```
SagIntfunctions[L_, filedata_] := Module[
    {intphi},
    intphi = MPhiDLmyphi[L 1000, 0, filedata, 0, 0];
    intphi
  ];
```

Hogging 3D Moment-Curvature-DLstrain relationship

```
HogIntfunctions[L_, fileRebardata_] := Module[
    {Rebarintphi},
    Rebarintphi = MPhiDLmyphi[L 1000, 0, fileRebardata, 0, 0];
    Rebarintphi
  ];
```

Pin 2D Moment-Curvature relationship

```
PinIntfunctions[L_, fileSteelmoment_] := Module[
    {Steelintmom},
    Steelintmom = MPhiPinint[fileSteelmoment, 0];
    Steelintmom
  ];
```

Maximum Sagging Moment

```
MaximumSaMom[L_, filedata_] := Module[
    {data, SMomentCurvature, i, Mo, amax},
    If[First[Dimensions[FileNames[filedata]]] == 1, data = Get[filedata]];
    SMomentCurvature = Table[{Flatten[data, 1][[i]][[2]], Flatten[data, 1][[i]][[6]], Flatten[data, 1][[i]][[5]]},
      {i, 1, Length[Flatten[data, 1]]}];
    Mo = Table[{Flatten[data, 1][[i]][[6]]}, {i, 1, Length[Flatten[data, 1]]}];
    amax = Max[Mo];
    amax
  ];

maxmo[L_, Ystress_, EMod_, Esh_, shno_] := Module[
    {maxm, listm},
    maxm = geometryprop[L, Ystress, EMod, Esh, shno, 30, 1.5];
    listm = {0.85 maxm, 0.90 maxm, 0.95 maxm};
    {listm, maxm}
];
```

TWO POINT LOADS EQUATIONS - EXTERNAL and INTERNAL BEAMS

Dead Load Equation

```
Deadloadstrain[L_, con1M_, con2M_, Ystress_, EMod_, Esh_, shno_] := Module[
  {b1, b2, t1, t2, tw, d, swidth, YM, ϵy, ρy, MI, L1, L2, DLstrain, x, p1, p2, dld, load1},
  {b1, b2, t1, t2, tw, d, swidth} = Steelgeometry;
  {YM, ϵy, ρy, MI} = geoelasticprop[Ystress, EMod, Esh, shno];
  L1 = L/3;
  L2 = L/3;
  DLstrain[x_/; 0 ≤ x < L1, p1_, p2_] := 100/YM d 10^6/(2 MI) (((((p1 (L - L1) + p2 (L - L1 - L2))/L) x)
      - (((((p1 (L - L1)  p2 (L - L1 - L2))/L) L/2) - (p1 (L/2 - L1))) (con1M  ((con2M - con1M) x)/L));
  DLstrain[x_/; L1 ≤ x < L1  L2, p1_, p2_] :=
    100/YM d 10^6/(2 MI) (((((p1 (L - L1)  p2 (L - L1 - L2))/L) x) - (p1 (x - L1))
      - (((((p1 (L - L1)  p2 (L - L1 - L2))/L) L/2) - (p1 (L/2 - L1))) (con1M  ((con2M - con1M) x)/L));
  DLstrain[x_/; L1  L2 ≤ x ≤ L, p1_, p2_] :=
    100/YM d 10^6/(2 MI) (((((p1 (L - L1)  p2 (L - L1 - L2))/L) x) - (p1 (x - L1)) - (p2 (x - L1 - L2))
      - (((((p1 (L - L1)  p2 (L - L1 - L2))/L) L/2) - (p1 (L/2 - L1))) (con1M  ((con2M - con1M) x)/L));
  dld = FindRoot[DLstrain[L1, load1, load1] == ϵy, {load1, 1}][[1, 2]];
  {DLstrain, dld}
];
```

Whole moment Equation

```
Moment[L_, con1M_, con2M_, Ystress_, EMod_, Esh_, shno_, filedata_] := Module[
  {Mo, DLstrain, dld, L1, L2, Wholemoment, x, p1, p2, p4, p5, lld},
  Mo = MaximumSaMom[L, filedata];
  {DLstrain, dld} = Deadloadstrain[L, con1M, con2M, Ystress, EMod, Esh, shno];
  L1 = L/3;
  L2 = L/3;
  Wholemoment[x_/; 0 ≤ x < L1, p1_, p2_, p4_, p5_] :=
    (((p1 (L - L1) + p2 (L - L1 - L2))/L) x) + (((p4 (L - L1) + p5 (L - L1 - L2))/L) x) +
    - (con1M + ((con2M - con1M) x)/L)
    (((((p1 (L - L1) + p2 (L - L1 - L2))/L) L/2) - (p1 (L/2 - L1))) + (((((p4 (L - L1) + p5 (L - L1 - L2))/L) L/2) -
    (p4 (L/2 - L1)));
```

```
Wholemoment[x_/; L1 ≤ x < L1 + L2, p1_, p2_, p4_, p5_] :=
  (((p1 (L - L1) + p2 (L - L1 - L2))/L) x) (p1 (x  L1)) + (((p4 (L  L1) + p5 (L  L1  L2))/L) x)
  (p4 (x  L1)) + (con1M + ((con2M  con1M) x)/L)
   (((((p1 (L  L1) + p2 (L  L1  L2))/L) L/2) (p1 (L/2  L1)) + (((p4 (L  L1) + p5 (L  L1  L2))/L) L/2)
    (p4 (L/2  L1)));
Wholemoment[x_/; L1 + L2 ≤ x ≤ L, p1_, p2_, p4_, p5_] :=
  (((p1 (L  L1) + p2 (L  L1  L2))/L) x) (p1 (x  L1)) (p2 (x  L1  L2)) + (((p4 (L  L1) + p5 (L  L1  L2))/L) x)
  (p4 (x  L1)) (p5 (x  L1  L2)) +
   (con1M + ((con2M  con1M) x)/L)
   (((((p1 (L  L1) + p2 (L  L1  L2))/L) L/2) (p1 (L/2  L1)) + (((p4 (L  L1) + p5 (L  L1  L2))/L) L/2)
    (p4 (L/2  L1)));

 lkl = FindRoot[Wholemoment[L1, dkl, dkl, p4, p4] == Mo, {p4, 0}][[1, 2]];
 {Wholemoment, lkl}
 ];

MomentFull[L_, con1M_, con2M_, Ystress_, EMod_, Esh_, shno_] := Module[
  {Mo, DLstrain, dkl, L1, L2, Wholemoment, x, p1, p2, p4, p5, lkl},
  {DLstrain, dkl} = Deadloadstrain[L, con1M, con2M, Ystress, EMod, Esh, shno];
  Mo = maxmo[L 1000, Ystress, EMod, Esh, shno][[2]];
  L1 = L/3;
  L2 = L/3;
  Wholemoment[x_/; 0 ≤ x < L1, p1_, p2_, p4_, p5_] :=
   (((p1 (L - L1) + p2 (L - L1 - L2))/L) x) + (((p4 (L - L1) + p5 (L - L1 - L2))/L) x) +
   -(con1M + ((con2M - con1M) x)/L)
   (((((p1 (L - L1) + p2 (L - L1 - L2))/L) L/2) - (p1 (L/2 - L1)) + (((p4 (L - L1) + p5 (L - L1 - L2))/L) L/2) -
    (p4 (L/2 - L1)));
Wholemoment[x_/; L1 ≤ x < L1 + L2, p1_, p2_, p4_, p5_] :=
 (((p1 (L - L1) + p2 (L - L1 - L2))/L) x) - (p1 (x - L1)) + (((p4 (L - L1) + p5 (L - L1 - L2))/L) x) -
  (p4 (x - L1)) + -(con1M + ((con2M - con1M) x)/L)
   (((((p1 (L - L1) + p2 (L - L1 - L2))/L) L/2) - (p1 (L/2 - L1)) + (((p4 (L - L1) + p5 (L - L1 - L2))/L) L/2) -
    (p4 (L/2 - L1)));
Wholemoment[x_/; L1 + L2 ≤ x ≤ L, p1_, p2_, p4_, p5_] :=
 (((p1 (L - L1) + p2 (L - L1 - L2))/L) x) - (p1 (x - L1)) - (p2 (x - L1 - L2)) + (((p4 (L - L1) + p5 (L - L1 - L2))/L) x) -
  (p4 (x - L1)) - (p5 (x - L1 - L2)) +
  -(con1M + ((con2M - con1M) x)/L)
   (((((p1 (L - L1) + p2 (L - L1 - L2))/L) L/2) - (p1 (L/2 - L1)) + (((p4 (L - L1) + p5 (L - L1 - L2))/L) L/2) -
    (p4 (L/2 - L1)));

 lkl = FindRoot[Wholemoment[L1, dkl, dkl, p4, p4] == Mo, {p4, 0}][[1, 2]];
 {Wholemoment, lkl}
];
```

Curvature, Deflection and Slope Equation

```
CurvDeflSlope[select_, L_, filedata_, fileRebardata_, fileSteelmoment_, con1M_, con2M_, Ystress_, EMod_, Esh_, shno_] :=
 Module[
  {b1, b2, t1, t2, tw, d, swidth, YM, ϵy, ρy, MI, L1, L2, intphi, Rebarintphi, DLstrain, dld, Wholemoment,
   lld, α, β, zzz1, Steelintmom, sss1, mmm1, x, p1, p2, p4, p5, zzz2, zzz3, sss2, sss3, mmm2, mmm3,
   ILϕ, Deflection, Deflectionxx},
  {b1, b2, t1, t2, tw, d, swidth} = Steelgeometry;
  {YM, ϵy, ρy, MI} = geoelasticprop[Ystress, EMod, Esh, shno];
  intphi = SagIntfunctions[L, filedata];
  Rebarintphi = HogIntfunctions[L, fileRebardata];
  {DLstrain, dld} = Deadloadstrain[L, con1M, con2M, Ystress, EMod, Esh, shno];
  {Wholemoment, lld} = Moment[L, con1M, con2M, Ystress, EMod, Esh, shno, filedata];
  L1 = L/3;
  L2 = L/3;
  α = lld/lld;
  β = dld/dld;
  zzz1[sss1_/; sss1 ≥ 0, mmm1_/; mmm1 ≥ 0] := intphi[sss1, mmm1];
  zzz1[sss1_/; sss1 ≤ 0, mmm1_/; mmm1 ≥ 0] := intphi[sss1, mmm1];
  If[select == "pin-comp",
   Steelintmom = PinIntfunctions[L, fileSteelmoment];
   zzz1[sss1_/; sss1 ≤ 0, mmm1_/; mmm1 ≤ 0] := -Steelintmom[-mmm1];];
  If[select == "comp-comp",
   zzz1[sss1_/; sss1 ≤ 0, mmm1_/; mmm1 ≤ 0] := -Rebarintphi[sss1, -mmm1];];
  ILϕ[x_/; 0 ≤ x < L1, p1_, p2_, p4_, p5_] :=
   zzz1[
    100/YM d 10^6/(2 MI) (((((p1 (L-L1)+p2 (L-L1-L2))/L) x)+
      -(((((p1 (L-L1)+p2 (L-L1-L2))/L) L/2)-(p1 (L/2-L1)))) (con1M+((con2M-con1M) x)/L)),
    (((p1 (L-L1)+p2 (L-L1-L2))/L) x)+(((p4 (L-L1)+p5 (L-L1-L2))/L) x)+
     -(con1M+((con2M-con1M) x)/L)
      (((((p1 (L-L1)+p2 (L-L1-L2))/L) L/2)-(p1 (L/2-L1)))+(((p4 (L-L1)+p5 (L-L1-L2))/L) L/2)-
       (p4 (L/2-L1))))];
  zzz2[sss2_/; sss2 ≥ 0, mmm2_/; mmm2 ≥ 0] := intphi[sss2, mmm2];
  zzz2[sss2_/; sss2 ≤ 0, mmm2_/; mmm2 ≥ 0] := intphi[sss2, mmm2];
  zzz2[sss2_/; sss2 ≤ 0, mmm2_/; mmm2 ≤ 0] := -Rebarintphi[sss2, -mmm2];
  ILϕ[x_/; L1 ≤ x < L1+L2, p1_, p2_, p4_, p5_] :=
   zzz2[
    100/YM d 10^6/(2 MI) ((((p1 (L-L1)+p2 (L-L1-L2))/L) x)-(p1 (x-L1))+
      -(((((p1 (L-L1)+p2 (L-L1-L2))/L) L/2)-(p1 (L/2-L1)))) (con1M+((con2M-con1M) x)/L)),
    (((p1 (L-L1)+p2 (L-L1-L2))/L) x)-(p1 (x-L1))+(((p4 (L-L1)+p5 (L-L1-L2))/L) x)-
     (p4 (x-L1))+-(con1M+((con2M-con1M) x)/L)
      (((((p1 (L-L1)+p2 (L-L1-L2))/L) L/2)-(p1 (L/2-L1)))+(((p4 (L-L1)+p5 (L-L1-L2))/L) L/2)-
       (p4 (L/2-L1))))];
```

```
zzz3[sss3_/; sss3 ≥ 0, mmm3_/; mmm3 ≥ 0] := intphi[sss3, mmm3];
  zzz3[sss3_/; sss3 ≤ 0, mmm3_/; mmm3 ≥ 0] := intphi[sss3, mmm3];
  zzz3[sss3_/; sss3 ≤ 0, mmm3_/; mmm3 ≤ 0] := - Rebarintphi[sss3, - mmm3];
  ILϕ[x_/; L1 + L2 ≤ x ≤ L, p1_, p2_, p4_, p5_] :=
    zzz3[
     100/YM d 10^6/(2 MI) (((p1 (L - L1) + p2 (L - L1 - L2))/L) x) (p1 (x - L1)) (p2 (x - L1 - L2)) +
          (((p1 (L - L1) + p2 (L - L1 - L2))/L) L/2) (p1 (L/2 - L1))) (con1M + (con2M - con1M) x/L)).
     (((p1 (L - L1) + p2 (L - L1 - L2))/L) x) (p1 (x - L1)) (p2 (x - L1 - L2)) +
      (((p4 (L - L1) + p5 (L - L1 - L2))/L) x) (p4 (x - L1)) (p5 (x - L1 - L2)) +
       (con1M + (con2M - con1M) x/L)
          (((p1 (L - L1) + p2 (L - L1 - L2))/L) L/2) (p1 (L/2 - L1)) + (((p4 (L - L1) + p5 (L - L1 - L2))/L) L/2)
            (p4 (L/2 - L1)))];
  Deflection[p1_, p4_] :=
    Module[{y, sol}, sol = NDSolve[{y''[x] == 1000 ILϕ[x, p1, β p1, p4, α p4], y[0] == 0, y[L] == 0}, y,
        {x, 0, L}, MaxSteps → 10000];
      First[y /. sol]];
  Deflectionxx[p1_, p4_][x_] := Module[{y}, y = Deflection[p1, p4];
      y[x]];
  {α, β, ILϕ, Deflectionxx}
  ];
```

Moment, Curvature, Deflection and Slope Graphs - Table Equation

---

```
ResponseGraphTable[select_, L_, filedata_, fileRebardata_, fileSteelmoment_, con1M_, con2M_, Ystress_,
    EMod_, Esh_, shno_, ndld_, nlld_, nx_] :=
  Module[
   {x, p1, p4, α, β, dld, lld, i, j, k, DLstrain, Wholemoment, ILϕ, Deflectionxx, momtable1, momtable2,
     momtable3, curtable1, curtable2, curtable3, deftable1, deftable2, deftable3, slotable1, slotable2, slotable3},
   {DLstrain, dld} = Deadloadstrain[L, con1M, con2M, Ystress, EMod, Esh, shno];
   {Wholemoment, lld} = Moment[L, con1M, con2M, Ystress, EMod, Esh, shno, filedata];
   {α, β, ILϕ, Deflectionxx} = CurvDefISlope[select, L, filedata, fileRebardata, fileSteelmoment, con1M,
      con2M, Ystress, EMod, Esh, shno];
   momtable1 = Table[Wholemoment[x, p1, β p1, p4, α p4], {p1, 0, dld, dld/ndld}, {p4, 0, lld, lld/nlld}];
   momtable2 = Table[{x, Evaluate[momtable1]}, {x, 0, L, L/nx}];
   momtable3 = Table[{momtable2[[i, 1]], momtable2[[i, 2]][[j, k]]}, {j, 1, ndld + 1}, {k, 1, nlld + 1}, {i, 1, nx + 1}];
   curtable1 = Table[1000 ILϕ[x, p1, β p1, p4, α p4], {p1, 0, dld, dld/ndld}, {p4, 0, lld, lld/nlld}];
   curtable2 = Table[{x, Evaluate[curtable1]}, {x, 0, L, L/nx}];
   curtable3 = Table[{curtable2[[i, 1]], curtable2[[i, 2]][[j, k]]}, {j, 1, ndld + 1}, {k, 1, nlld + 1}, {i, 1, nx + 1}];
   deftable1 = Table[Deflectionxx[p1, p4][x], {p1, 0, dld, dld/ndld}, {p4, 0, lld, lld/nlld}];
   deftable2 = Table[{x, Evaluate[deftable1]}, {x, 0, L, L/nx}];
   deftable3 = Table[{deftable2[[i, 1]], deftable2[[i, 2]][[j, k]]}, {j, 1, ndld + 1}, {k, 1, nlld + 1}, {i, 1, nx + 1}];
   slotable1 = Table[Derivative[1][Deflectionxx[p1, p4]][y], {p1, 0, dld, dld/ndld}, {p4, 0, lld, lld/nlld}];
   slotable2 = Table[{y, Evaluate[slotable1]}, {y, 0, L, L/nx}];
   slotable3 = Table[{slotable2[[i, 1]], 1000 slotable2[[i, 2]][[j, k]]}, {j, 1, ndld + 1}, {k, 1, nlld + 1}, {i, 1, nx + 1}];
   {momtable3, curtable3, deftable3, slotable3}
  ];
```

Moment vs. Rotation Graphs - Table Equation

```
MomRotTable[select_, L_, filedata_, fileRebardata_, fileSteelmoment_, con1M_, con2M_, Ystress_, EMod_,
    Esh_, shno_, ndld_, nlld_, nx_] :=
  Module[
   {DLstrain, dld, Wholemoment, lld, α, β, ILϕ, Deflectionxx, momtable4, x, p1, p4, momtable5, momtable6,
     i, j, k, slotable4, y, slotable5, slotable6},
   {DLstrain, dld} = Deadloadstrain[L, con1M, con2M, Ystress, EMod, Esh, shno];
   {Wholemoment, lld} = Moment[L, con1M, con2M, Ystress, EMod, Esh, shno, filedata];
   {α, β, ILϕ, Deflectionxx} = CurvDeflSlope[select, L, filedata, fileRebardata, fileSteelmoment, con1M,
     con2M, Ystress, EMod, Esh, shno];
   momtable4 = Table[Wholemoment[x, p1, β p1, p4, α p4], {p1, 0, dld, dld/ndld}, {p4, 0, lld + dld - p1, (lld + dld - p1)/nlld}];
   momtable5 = Table[{x, Evaluate[momtable4]}, {x, 0, L, L/nx}];
   momtable6 = Table[{momtable5[[i, 1]], momtable5[[i, 2]][[j, k]]}, {j, 1, ndld + 1}, {k, 1, nlld + 1}, {i, 1, nx + 1}];
   slotable4 = Table[Derivative[1][Deflectionxx[p1, p4]][y], {p1, 0, dld, dld/ndld}, {p4, 0, lld + dld - p1, (lld + dld - p1)/nlld}];
   slotable5 = Table[{y, Evaluate[slotable4]}, {y, 0, L, L/nx}];
   slotable6 = Table[{slotable5[[i, 1]], 1000 slotable5[[i, 2]][[j, k]]}, {j, 1, ndld + 1}, {k, 1, nlld + 1}, {i, 1, nx + 1}];
   {momtable6, slotable6}
  ];
```

Moment vs. Rotation - Plots Equations - Compo Connection
End

```
MRradians[select_, t_, L_, filedata_, fileRebardata_, fileSteelmoment_, con1M_, con2M_, Ystress_, EMod_,
    Esh_, shno_, ndld_, nlld_, nx_] :=
  Module[
   {MRrad1, MRrad2, MRradC1, MRradC2, momtable6, slotable6},
   {momtable6, slotable6} = MomRotTable[select, L, filedata, fileRebardata, fileSteelmoment, con1M,
     con2M, Ystress, EMod, Esh, shno, ndld, nlld, nx];
   MRrad2 = Table[{slotable6[[t, i, nx + 1, 2]], Max[momtable6[[t, i]]]}, {i, 1, nlld + 1}];
   MRradC2 = Insert[MRrad2, {0, 0}, 1];
   MRrad1 = Table[{- slotable6[[t, i, 1, 2]], Max[momtable6[[t, i]]]}, {i, 1, nlld + 1}];
   MRradC1 = Insert[MRrad1, {0, 0}, 1];
   {MRradC1, MRradC2}
  ];
```

THREE POINT LOADS EQUATIONS - EXTERNAL and INTERNAL BEAMS

Dead Load Equation

```
DeadloadstrainPL[L_, con1M_, con2M_, Ystress_, EMod_, Esh_, shno_] :=
  Module[{b1, b2, t1, t2, tw, d, swidth, YM, ϵy, ρy, MI, L1, L2, L3, DLstrain, x, p1, p2, p3, dkl, load1},
   {b1, b2, t1, t2, tw, d, swidth} = Steelgeometry;
   {YM, ϵy, ρy, MI} = geoelasticprop[Ystress, EMod, Esh, shno];
   L1 = L/4;
   L2 = L/4;
   L3 = L/4;
   DLstrain[x_/; 0 ≤ x < L1, p1_, p2_, p3_] :=
    100/YM d 10^6/(2 MI) (((1/L (p1 (L - L1) + p2 (L - L1 - L2) + p3 (L - L1 - L2 - L3))) x) +
      -(((1/L (p1 (L - L1) + p2 (L - L1 - L2) + p3 (L - L1 - L2 - L3))) L/2) - (p1 (L/2 - L1)))
       (con1M + ((con2M - con1M) x)/L));
   DLstrain[x_/; L1 ≤ x < L1 + L2, p1_, p2_, p3_] :=
    100/YM d 10^6/(2 MI) (((1/L (p1 (L - L1) + p2 (L - L1 - L2) + p3 (L - L1 - L2 - L3))) x) - (p1 (x - L1)) +
      -(((1/L (p1 (L - L1) + p2 (L - L1 - L2) + p3 (L - L1 - L2 - L3))) L/2) - (p1 (L/2 - L1)))
       (con1M + ((con2M - con1M) x)/L));
   DLstrain[x_/; L1 + L2 ≤ x < L1 + L2 + L3, p1_, p2_, p3_] :=
    100/YM d 10^6/(2 MI) (((1/L (p1 (L - L1) + p2 (L - L1 - L2) + p3 (L - L1 - L2 - L3))) x) - (p1 (x - L1)) -
      (p2 (x - L1 - L2)) + -(((1/L (p1 (L - L1) + p2 (L - L1 - L2) + p3 (L - L1 - L2 - L3))) L/2) - (p1 (L/2 - L1)))
       (con1M + ((con2M - con1M) x)/L));
   DLstrain[x_/; L1 + L2 + L3 ≤ x ≤ L, p1_, p2_, p3_] :=
    100/YM d 10^6/(2 MI) (((1/L (p1 (L - L1) + p2 (L - L1 - L2) + p3 (L - L1 - L2 - L3))) x) - (p1 (x - L1)) -
      (p2 (x - L1 - L2)) - (p3 (x - L1 - L2 - L3)) +
      -(((1/L (p1 (L - L1) + p2 (L - L1 - L2) + p3 (L - L1 - L2 - L3))) L/2) - (p1 (L/2 - L1)))
       (con1M + ((con2M - con1M) x)/L));
   dkl = FindRoot[DLstrain[L1 + L2, load1, load1, load1] == ϵy, {load1, 1.}][[1, 2]];
   {DLstrain, dkl}
  ];
```

Whole moment Equation

```
MomentPL[L_, con1M_, con2M_, Ystress_, EMod_, Esh_, shno_, filedata_] :=
  Module[{Mo, DLstrain, dld, L1, L2, L3, Wholemoment, x, p1, p2, p3, p4, p5, p6, lld},
   Mo = MaximumSaMom[L, filedata];
   {DLstrain, dld} = DeadloadstrainPL[L, con1M, con2M, Ystress, EMod, Esh, shno];
   L1 = L/4;
   L2 = L/4;
   L3 = L/4;
   Wholemoment[x_ /; 0 ≤ x < L1, p1_, p2_, p3_, p4_, p5_, p6_] :=
    (((1/L) (p1 (L - L1) + p2 (L - L1 - L2) + p3 (L - L1 - L2 - L3))) x) +
    (((1/L) (p4 (L - L1) + p5 (L - L1 - L2) + p6 (L - L1 - L2 - L3))) x) +
    -(con1M + ((con2M - con1M) x)/L)
     ((((1/L) (p1 (L - L1) + p2 (L - L1 - L2) + p3 (L - L1 - L2 - L3))) L/2) - (p1 (L/2 - L1)) +
      (((1/L) (p4 (L - L1) + p5 (L - L1 - L2) + p6 (L - L1 - L2 - L3))) L/2) - (p4 (L/2 - L1)));
  Wholemoment[x_ /; L1 ≤ x < L1 + L2, p1_, p2_, p3_, p4_, p5_, p6_] :=
   (((1/L) (p1 (L - L1) + p2 (L - L1 - L2) + p3 (L - L1 - L2 - L3))) x) - (p1 (x - L1)) +
   (((1/L) (p4 (L - L1) + p5 (L - L1 - L2) + p6 (L - L1 - L2 - L3))) x) - (p4 (x - L1)) +
   -(con1M + ((con2M - con1M) x)/L)
    ((((1/L) (p1 (L - L1) + p2 (L - L1 - L2) + p3 (L - L1 - L2 - L3))) L/2) - (p1 (L/2 - L1)) +
     (((1/L) (p4 (L - L1) + p5 (L - L1 - L2) + p6 (L - L1 - L2 - L3))) L/2) - (p4 (L/2 - L1)));
  Wholemoment[x_ /; L1 + L2 ≤ x < L1 + L2 + L3, p1_, p2_, p3_, p4_, p5_, p6_] :=
   (((1/L) (p1 (L - L1) + p2 (L - L1 - L2) + p3 (L - L1 - L2 - L3))) x) - (p1 (x - L1)) - (p2 (x - L1 - L2)) +
   (((1/L) (p4 (L - L1) + p5 (L - L1 - L2) + p6 (L - L1 - L2 - L3))) x) - (p4 (x - L1)) - (p5 (x - L1 - L2)) +
   -(con1M + ((con2M - con1M) x)/L)
    ((((1/L) (p1 (L - L1) + p2 (L - L1 - L2) + p3 (L - L1 - L2 - L3))) L/2) - (p1 (L/2 - L1)) +
     (((1/L) (p4 (L - L1) + p5 (L - L1 - L2) + p6 (L - L1 - L2 - L3))) L/2) - (p4 (L/2 - L1)));
  Wholemoment[x_ /; L1 + L2 + L3 ≤ x ≤ L, p1_, p2_, p3_, p4_, p5_, p6_] :=
   (((1/L) (p1 (L - L1) + p2 (L - L1 - L2) + p3 (L - L1 - L2 - L3))) x) - (p1 (x - L1)) - (p2 (x - L1 - L2)) -
   (p3 (x - L1 - L2 - L3)) + (((1/L) (p4 (L - L1) + p5 (L - L1 - L2) + p6 (L - L1 - L2 - L3))) x) -
   (p4 (x - L1)) - (p5 (x - L1 - L2)) - (p6 (x - L1 - L2 - L3)) +
   -(con1M + ((con2M - con1M) x)/L)
    ((((1/L) (p1 (L - L1) + p2 (L - L1 - L2) + p3 (L - L1 - L2 - L3))) L/2) - (p1 (L/2 - L1)) +
     (((1/L) (p4 (L - L1) + p5 (L - L1 - L2) + p6 (L - L1 - L2 - L3))) L/2) - (p4 (L/2 - L1)));
  lld = FindRoot[Wholemoment[L1 + L2, dld, dld, dld, p4, p4, p4] == Mo, {p4, 0}][[1, 2]];
  {Wholemoment, lld}
];
```

Curvature, Deflection and Slope Equation

```
CurvDeflSlopePL[select_, L_, filedata_, fileRebardata_, fileSteelmoment_, con1M_, con2M_, Ystress_, EMod_,
  Esh_, shno_] :=
 Module[{b1, b2, t1, t2, tw, d, swidth, YM, ϵy, ρy, MI, L1, L2, intphi, Rebarintphi, DLstrain, dld, Wholemoment,
   lld, α, β, zzz1, Steelintmom, sss1, mmm1, x, p1, p2, p3, p4, p5, p6, zzz2, zzz3, zzz4, sss2, sss3,
   sss4, mmm2, mmm3, mmm4, ILϕ, Deflection, Deflectionxx},
  {b1, b2, t1, t2, tw, d, swidth} = Steelgeometry;
  {YM, ϵy, ρy, MI} = geoelasticprop[Ystress, EMod, Esh, shno];
  intphi = SagIntfunctions[L, filedata];
  Rebarintphi = HogIntfunctions[L, fileRebardata];
  {DLstrain, dld} = DeadloadstrainPL[L, con1M, con2M, Ystress, EMod, Esh, shno];
  {Wholemoment, lld} = MomentPL[L, con1M, con2M, Ystress, EMod, Esh, shno, filedata];
  L1 = L/4;
  L2 = L/4;
  L3 = L/4;
  α = lld/lld;
  β = dld/dld;
  zzz1[sss1_/; sss1 ≥ 0, mmm1_/; mmm1 ≥ 0] := intphi[sss1, mmm1];
  zzz1[sss1_/; sss1 ≤ 0, mmm1_/; mmm1 ≥ 0] := intphi[sss1, mmm1];
  If[select == "pin-comp",
   Steelintmom = PinIntfunctions[L, fileSteelmoment];
   zzz1[sss1_/; sss1 ≤ 0, mmm1_/; mmm1 ≤ 0] := -Steelintmom[-mmm1];];
  If[select == "comp-comp",
   zzz1[sss1_/; sss1 ≤ 0, mmm1_/; mmm1 ≤ 0] := -Rebarintphi[sss1, -mmm1];];
  ILϕ[x_/; 0 ≤ x < L1, p1_, p2_, p3_, p4_, p5_, p6_] :=
   zzz1[
    100/YM d 10^6/(2 MI) (((1/L (p1 (L - L1) + p2 (L - L1 - L2) + p3 (L - L1 - L2 - L3))) x) +
       -(((1/L (p1 (L - L1) + p2 (L - L1 - L2) + p3 (L - L1 - L2 - L3))) L/2) - (p1 (L/2 - L1))))
        (con1M + (con2M - con1M) x/L)),
    ((1/L (p1 (L - L1) + p2 (L - L1 - L2) + p3 (L - L1 - L2 - L3))) x) +
     ((1/L (p4 (L - L1) + p5 (L - L1 - L2) + p6 (L - L1 - L2 - L3))) x) +
     -(con1M + (con2M - con1M) x/L)
      (((1/L (p1 (L - L1) + p2 (L - L1 - L2) + p3 (L - L1 - L2 - L3))) L/2) - (p1 (L/2 - L1)) +
       ((1/L (p4 (L - L1) + p5 (L - L1 - L2) + p6 (L - L1 - L2 - L3))) L/2) - (p4 (L/2 - L1))))];
```

```
zzzz2[sss2_/; sss2 ≥ 0, mmm2_/; mmm2 ≥ 0] := intphi[sss2, mmm2];
zzzz2[sss2_/; sss2 ≤ 0, mmm2_/; mmm2 ≥ 0] := intphi[sss2, mmm2];
zzzz2[sss2_/; sss2 ≤ 0, mmm2_/; mmm2 ≤ 0] := - Rebarintphi[sss2, - mmm2];
ILϕ[x_/; L1 ≤ x < L1 + L2, p1_, p2_, p3_, p4_, p5_, p6_] :=
  zzzz2[
   100/YM d 10^6/(2 MI) (((1/L (p1 (L - L1) + p2 (L - L1 - L2) + p3 (L - L1 - L2 - L3))) x) - (p1 (x - L1)) +
     -(((1/L (p1 (L - L1) + p2 (L - L1 - L2) + p3 (L - L1 - L2 - L3))) L/2) - (p1 (L/2 - L1)))
      (con1M + (con2M - con1M) x/L)),
    ((1/L (p1 (L - L1) + p2 (L - L1 - L2) + p3 (L - L1 - L2 - L3))) x) - (p1 (x - L1)) +
     ((1/L (p4 (L - L1) + p5 (L - L1 - L2) + p6 (L - L1 - L2 - L3))) x) - (p4 (x - L1)) +
     -(con1M + (con2M - con1M) x/L)
      (((1/L (p1 (L - L1) + p2 (L - L1 - L2) + p3 (L - L1 - L2 - L3))) L/2) - (p1 (L/2 - L1)) +
       ((1/L (p4 (L - L1) + p5 (L - L1 - L2) + p6 (L - L1 - L2 - L3))) L/2) - (p4 (L/2 - L1)))];
zzzz3[sss3_/; sss3 ≥ 0, mmm3_/; mmm3 ≥ 0] := intphi[sss3, mmm3];
zzzz3[sss3_/; sss3 ≤ 0, mmm3_/; mmm3 ≥ 0] := intphi[sss3, mmm3];
zzzz3[sss3_/; sss3 ≤ 0, mmm3_/; mmm3 ≤ 0] := - Rebarintphi[sss3, - mmm3];
ILϕ[x_/; L1 + L2 ≤ x < L1 + L2 + L3, p1_, p2_, p3_, p4_, p5_, p6_] :=
  zzzz3[
   100/YM d 10^6/(2 MI) (((1/L (p1 (L - L1) + p2 (L - L1 - L2) + p3 (L - L1 - L2 - L3))) x) - (p1 (x - L1)) -
     (p2 (x - L1 - L2)) + -(((1/L (p1 (L - L1) + p2 (L - L1 - L2) + p3 (L - L1 - L2 - L3))) L/2) - (p1 (L/2 - L1)))
      (con1M + (con2M - con1M) x/L)),
    ((1/L (p1 (L - L1) + p2 (L - L1 - L2) + p3 (L - L1 - L2 - L3))) x) - (p1 (x - L1)) - (p2 (x - L1 - L2)) +
     ((1/L (p4 (L - L1) + p5 (L - L1 - L2) + p6 (L - L1 - L2 - L3))) x) - (p4 (x - L1)) - (p5 (x - L1 - L2)) +
     -(con1M + (con2M - con1M) x/L)
      (((1/L (p1 (L - L1) + p2 (L - L1 - L2) + p3 (L - L1 - L2 - L3))) L/2) - (p1 (L/2 - L1)) +
       ((1/L (p4 (L - L1) + p5 (L - L1 - L2) + p6 (L - L1 - L2 - L3))) L/2) - (p4 (L/2 - L1)))];
```

```
zzzz4[sss4_/; sss4 ≥ 0, mmm4_/; mmm4 ≥ 0] := intphi[sss4, mmm4];
  zzzz4[sss4_/; sss4 ≤ 0, mmm4_/; mmm4 ≥ 0] := intphi[sss4, mmm4];
  zzzz4[sss4_/; sss4 ≤ 0, mmm4_/; mmm4 ≤ 0] := - Rebarintphi[sss4, - mmm4];
  IIL𝜙[x_/; L1 + L2 + L3 ≤ x ≤ L, p1_, p2_, p3_, p4_, p5_, p6_] :=
    zzzz4[
      100/YM d10^6/(2 MI) ((((1/L (p1 (L - L1) + p2 (L - L1 - L2) + p3 (L - L1 - L2 - L3))) x) - (p1 (x - L1)) -
          (p2 (x - L1 - L2)) - (p3 (x - L1 - L2 - L3)) +
          -((((1/L (p1 (L - L1) + p2 (L - L1 - L2) + p3 (L - L1 - L2 - L3))) L/2) - (p1 (L/2 - L1))))
           (con1M + (con2M - con1M) x/L)),
      (((1/L (p1 (L - L1) + p2 (L - L1 - L2) + p3 (L - L1 - L2 - L3))) x) - (p1 (x - L1)) - (p2 (x - L1 - L2)) -
       (p3 (x - L1 - L2 - L3)) + (((1/L (p4 (L - L1) + p5 (L - L1 - L2) + p6 (L - L1 - L2 - L3))) x) -
       (p4 (x - L1)) - (p5 (x - L1 - L2)) - (p6 (x - L1 - L2 - L3)) +
       -(con1M + (con2M - con1M) x/L)
        ((((1/L (p1 (L - L1) + p2 (L - L1 - L2) + p3 (L - L1 - L2 - L3))) L/2) - (p1 (L/2 - L1)) +
          ((1/L (p4 (L - L1) + p5 (L - L1 - L2) + p6 (L - L1 - L2 - L3))) L/2) - (p4 (L/2 - L1))))];
Deflection[p1_, p4_] :=
  Module[{y, sol}, sol = NDSolve[{y'[x] == 1000 IIL𝜙[x, p1, β p1, β p1, p4, α p4, α p4], y[0] == 0, y[L] == 0},
      y, {x, 0, L}, MaxSteps → 10000];
    First[y /. sol]];
Deflectionxx[p1_, p4_][x_] := Module[{y}, y = Deflection[p1, p4];
    y[x]];
{α, β, IIL𝜙, Deflectionxx}
];
```

Moment, Curvature, Deflection and Slope Graphs - Table Equation

---

```
ResponseGraphTablePL[select_, L_, filedata_, fileRebardata_, fileSteelmoment_, con1M_, con2M_, Ystress_,
  EMod_, Esh_, shno_, ndld_, nlld_, nx_] :=
 Module[{x, p1, p4, α, β, dld, lld, i, j, k, DLstrain, Wholemoment, IL𝜙, Deflectionxx, momtable1, momtable2,
   momtable3, curtable1, curtable2, curtable3, deftable1, deftable2, deftable3, slotable1, slotable2, slotable3},
  {DLstrain, dld} = DeadloadstrainPL[L, con1M, con2M, Ystress, EMod, Esh, shno];
  {Wholemoment, lld} = MomentPL[L, con1M, con2M, Ystress, EMod, Esh, shno, filedata];
  {α, β, IL𝜙, Deflectionxx} = CurvDeflSlopePL[select, L, filedata, fileRebardata, fileSteelmoment, con1M,
    con2M, Ystress, EMod, Esh, shno];
  momtable1 = Table[Wholemoment[x, p1, β p1, β p1, p4, α p4, α p4], {p1, 0, dld, dld/ndld}, {p4, 0, lld, lld/nlld}];
  momtable2 = Table[{x, Evaluate[momtable1]}, {x, 0, L, L/nx}];
  momtable3 = Table[{momtable2[[i, 1]], momtable2[[i, 2]][[j, k]]}, {j, 1, ndld + 1}, {k, 1, nlld + 1}, {i, 1, nx + 1}];
  curtable1 = Table[1000 IIL𝜙[x, p1, β p1, β p1, p4, α p4, α p4], {p1, 0, dld, dld/ndld}, {p4, 0, lld, lld/nlld}];
  curtable2 = Table[{x, Evaluate[curtable1]}, {x, 0, L, L/nx}];
  curtable3 = Table[{curtable2[[i, 1]], curtable2[[i, 2]][[j, k]]}, {j, 1, ndld + 1}, {k, 1, nlld + 1}, {i, 1, nx + 1}];
```

```
deftable1 = Table[Deflectionxx[p1, p4][x], {p1, 0, dld, dld/ndld}, {p4, 0, lld, lld/nlld}];
deftable2 = Table[{x, Evaluate[deftable1]}, {x, 0, L, L/nx}];
deftable3 = Table[{deftable2[[i, 1]], deftable2[[i, 2]][[j, k]]}, {j, 1, ndld + 1}, {k, 1, nlld + 1}, {i, 1, nx + 1}];
slotable1 = Table[Derivative[1][Deflectionxx[p1, p4]][y], {p1, 0, dld, dld/ndld}, {p4, 0, lld, lld/nlld}];
slotable2 = Table[{y, Evaluate[slotable1]}, {y, 0, L, L/nx}];
slotable3 = Table[{slotable2[[i, 1]], 1000 slotable2[[i, 2]][[j, k]]}, {j, 1, ndld + 1}, {k, 1, nlld + 1}, {i, 1, nx + 1}];
{momtable3, curtable3, deftable3, slotable3}
];
```

Moment vs. Rotation Graphs - Table Equation

```
MomRotTablePL[select_, L_, filedata_, fileRebardata_, fileSteelmoment_, con1M_, con2M_, Ystress_, EMod_,
  Esh_, shno_, ndld_, nlld_, nx_] :=
 Module[{DLstrain, dld, Wholemoment, lld, α, β, ILϕ, Deflectionxx, momtable4, x, p1, p4, momtable5,
   momtable6, i, j, k, slotable4, y, slotable5, slotable6},
  {DLstrain, dld} = DeadloadstrainPL[L, con1M, con2M, Ystress, EMod, Esh, shno];
  {Wholemoment, lld} = MomentPL[L, con1M, con2M, Ystress, EMod, Esh, shno, filedata];
  {α, β, ILϕ, Deflectionxx} = CurvDeflSlopePL[select, L, filedata, fileRebardata, fileSteelmoment, con1M,
    con2M, Ystress, EMod, Esh, shno];
  momtable4 = Table[Wholemoment[x, p1, β p1, β p1, p4, α p4, α p4], {p1, 0, dld, dld/ndld},
    {p4, 0, lld + dld - p1, (lld + dld - p1)/nlld}]; momtable5 = Table[{x, Evaluate[momtable4]}, {x, 0, L, L/nx}];
  momtable6 = Table[{momtable5[[i, 1]], momtable5[[i, 2]][[j, k]]}, {j, 1, ndld + 1}, {k, 1, nlld + 1}, {i, 1, nx + 1}];
  slotable4 = Table[Derivative[1][Deflectionxx[p1, p4]][y], {p1, 0, dld, dld/ndld}, {p4, 0, lld + dld - p1, (lld + dld - p1)/nlld}];
  slotable5 = Table[{y, Evaluate[slotable4]}, {y, 0, L, L/nx}];
  slotable6 = Table[{slotable5[[i, 1]], 1000 slotable5[[i, 2]][[j, k]]}, {j, 1, ndld + 1}, {k, 1, nlld + 1}, {i, 1, nx + 1}];
  {momtable6, slotable6}
 ];
```

Moment vs. Rotation - Plots Equations - Compo Connection end

```
MRradiansPL[select_, t_, L_, filedata_, fileRebardata_, fileSteelmoment_, con1M_, con2M_, Ystress_, EMod_,
  Esh_, shno_, ndld_, nlld_, nx_] := Module[{MRrad1, MRrad2, MRradC1, MRradC2, momtable6, slotable6},
  {momtable6, slotable6} = MomRotTablePL[select, L, filedata, fileRebardata, fileSteelmoment, con1M,
    con2M, Ystress, EMod, Esh, shno, ndld, nlld, nx];
  MRrad2 = Table[{slotable6[[t, i, nx + 1, 2]], Max[momtable6[[t, i]]]}, {i, 1, nlld + 1}];
  MRradC2 = Insert[MRrad2, {0, 0}, 1];
  MRrad1 = Table[{- slotable6[[t, i, 1, 2]], Max[momtable6[[t, i]]]}, {i, 1, nlld + 1}];
  MRradC1 = Insert[MRrad1, {0, 0}, 1];
  {MRradC1, MRradC2}
 ];
```

UDL EQUATIONS - EXTERNAL and INTERNAL BEAMS

Dead Load Equation

```
DeadloadstrainUDL[L_, con1M_, con2M_, Ystress_, EMod_, Esh_, shno_] := Module[
  {b1, b2, t1, t2, tw, d, swidth, YM, ϵy, ρy, MI, L1, DLstrain, DLstrainfind, x, p1, dld, load1},
  {b1, b2, t1, t2, tw, d, swidth} = Steelgeometry;
  {YM, ϵy, ρy, MI} = geoelasticprop[Ystress, EMod, Esh, shno];
  DLstrainfind[x_/; 0 ≤ x ≤ L, p1_] := 100/YM d 10^6/(2 MI) (((p1 L/2) x - p1 x x/2)
      -((p1 L L/8)(con1M (con2M - con1M) x/L)));
  L1 = FindMinimum[-DLstrainfind[x, 100.0], {x, {L/2, L/3}}][[2, 1, 2]];
  DLstrain[x_/; 0 ≤ x < L1, p1_] := 100/YM d 10^6/(2 MI) (((p1 L/2) x - p1 x x/2)
      -((p1 L L/8)(con1M (con2M - con1M) x/L)));
  DLstrain[x_/; L1 ≤ x ≤ L, p1_] := 100/YM d 10^6/(2 MI) (((p1 L/2) x - p1 x x/2)
      -((p1 L L/8)(con1M (con2M - con1M) x/L)));
  dld = FindRoot[DLstrain[L1, load1] == ϵy, {load1, 1}][[1, 2]];
  {DLstrain, dld, L1}
];
```

Whole moment Equation

```
MomentUDL[L_, con1M_, con2M_, Ystress_, EMod_, Esh_, shno_, filedata_] := Module[
  {Mo, DLstrain, dld, L1, Wholemoment, x, p1, p4, lld},
  Mo = MaximumSaMom[L, filedata];
  {DLstrain, dld, L1} = DeadloadstrainUDL[L, con1M, con2M, Ystress, EMod, Esh, shno];
  Wholemoment[x_/; 0 ≤ x < L1, p1_, p4_] :=
   (((p1 L/2) x - p1 x x/2) ((p4 L/2) x - p4 x x/2)) -(con1M (con2M - con1M) x/L)((p1 L L/8) (p4 L L/8));
  Wholemoment[x_/; L1 ≤ x ≤ L, p1_, p4_] :=
   (((p1 L/2) x - p1 x x/2) ((p4 L/2) x - p4 x x/2)) -(con1M (con2M - con1M) x/L)((p1 L L/8) (p4 L L/8));
  lld = FindRoot[Wholemoment[L1, dld, p4] == Mo, {p4, 0}][[1, 2]];
  {Wholemoment, lld}
];
```

Curvature, Deflection and Slope Equation

```
CurvDeflSlopeUDL[select_, L_, filedata_, fileRebardata_, fileSteelmoment_, con1M_, con2M_, Ystress_,
    EMod_, Esh_, shno_] :=
  Module[
   {b1, b2, t1, t2, tw, d, swidth, YM, ϵy, ρy, MI, L1, intphi, Rebarintphi, DLstrain, dld, Wholemoment, lld,
     α, β, zzz1, Steelintmom, sss1, mmm1, x, p1, p4, zzz2, sss2, mmm2, ILϕ, Deflection, Deflectionxx},
   {b1, b2, t1, t2, tw, d, swidth} = Steelgeometry;
   {YM, ϵy, ρy, MI} = geoelasticprop[Ystress, EMod, Esh, shno];
   intphi = SagIntfunctions[L, filedata];
   Rebarintphi = HogIntfunctions[L, fileRebardata];
   {DLstrain, dld, L1} = DeadloadstrainUDL[L, con1M, con2M, Ystress, EMod, Esh, shno];
   {Wholemoment, lld} = MomentUDL[L, con1M, con2M, Ystress, EMod, Esh, shno, filedata];
   α = lld / lld;
   β = dld / dld;
   zzz1[sss1_ /; sss1 ≥ 0, mmm1_ /; mmm1 ≥ 0] := intphi[sss1, mmm1];
   zzz1[sss1_ /; sss1 ≤ 0, mmm1_ /; mmm1 ≥ 0] := intphi[sss1, mmm1];
   If[select == "pin-comp",
    Steelintmom = PinIntfunctions[L, fileSteelmoment];
    zzz1[sss1_ /; sss1 ≤ 0, mmm1_ /; mmm1 ≤ 0] := - Steelintmom[- mmm1];];
   If[select == "comp-comp",
    zzz1[sss1_ /; sss1 ≤ 0, mmm1_ /; mmm1 ≤ 0] := - Rebarintphi[sss1, - mmm1];];

   ILϕ[x_ /; 0 ≤ x < L1, p1_, p4_] := zzz1[100/YM d 10^6/(2 MI) (((p1 L/2) x - p1 x x/2)
       - ((p1 L L/8)(con1M - (con2M - con1M) x/L))),
     (((p1 L/2) x - p1 x x/2) ((p4 L/2) x - p4 x x/2)) - (con1M - (con2M - con1M) x/L)((p1 L L/8) (p4 L L/8))];
   zzz2[sss2_ /; sss2 ≥ 0, mmm2_ /; mmm2 ≥ 0] := intphi[sss2, mmm2];
   zzz2[sss2_ /; sss2 ≤ 0, mmm2_ /; mmm2 ≥ 0] := intphi[sss2, mmm2];
   zzz2[sss2_ /; sss2 ≤ 0, mmm2_ /; mmm2 ≤ 0] := - Rebarintphi[sss2, - mmm2];
   ILϕ[x_ /; L1 ≤ x ≤ L, p1_, p4_] := zzz2[100/YM d 10^6/(2 MI) (((p1 L/2) x - p1 x x/2)
       - ((p1 L L/8)(con1M - (con2M - con1M) x/L))),
     (((p1 L/2) x - p1 x x/2) ((p4 L/2) x - p4 x x/2)) - (con1M - (con2M - con1M) x/L)((p1 L L/8) (p4 L L/8))];
   Deflection[p1_, p4_] :=
    Module[{y, sol}, sol = NDSolve[{y'[x] == 1000 ILϕ[x, p1, p4], y[0] == 0, y[L] == 0}, y, {x, 0, L}, MaxSteps → 10000];
     First[y /. sol]];
   Deflectionxx[p1_, p4_][x_] := Module[{y}, y = Deflection[p1, p4];
      y[x]];
   {α, β, ILϕ, Deflectionxx}
  ];
```

Moment, Curvature, Deflection and Slope Graphs - Table Equation

```
ResponseGraphTableUDL[select_, L_, filedata_, fileRebardata_, fileSteelmoment_, con1M_, con2M_, Ystress_,
    EMod_, Esh_, shno_, ndld_, nlld_, nx_] :=
  Module[
   {x, p1, p4, α, β, dld, lld, i, j, k, DLstrain, L1, Wholemoment, ILϕ, Deflectionxx, momtable1, momtable2,
     momtable3, curtable1, curtable2, curtable3, deftable1, deftable2, deftable3, slotable1, slotable2, slotable3},
   {DLstrain, dld, L1} = DeadloadstrainUDL[L, con1M, con2M, Ystress, EMod, Esh, shno];
   {Wholemoment, lld} = MomentUDL[L, con1M, con2M, Ystress, EMod, Esh, shno, filedata];
   {α, β, ILϕ, Deflectionxx} = CurvDeflSlopeUDL[select, L, filedata, fileRebardata, fileSteelmoment,
     con1M, con2M, Ystress, EMod, Esh, shno];
   momtable1 = Table[Wholemoment[x, p1, p4], {p1, 0, dld, dld/ndld}, {p4, 0, lld, lld/nlld}];
   momtable2 = Table[{x, Evaluate[momtable1]}, {x, 0, L, L/nx}];
   momtable3 = Table[{momtable2[[i, 1]], momtable2[[i, 2]][[j, k]]}, {j, 1, ndld + 1}, {k, 1, nlld + 1}, {i, 1, nx + 1}];
   curtable1 = Table[1000 ILϕ[x, p1, p4], {p1, 0, dld, dld/ndld}, {p4, 0, lld, lld/nlld}];
   curtable2 = Table[{x, Evaluate[curtable1]}, {x, 0, L, L/nx}];
   curtable3 = Table[{curtable2[[i, 1]], curtable2[[i, 2]][[j, k]]}, {j, 1, ndld + 1}, {k, 1, nlld + 1}, {i, 1, nx + 1}];
   deftable1 = Table[Deflectionxx[p1, p4][x], {p1, 0, dld, dld/ndld}, {p4, 0, lld, lld/nlld}];
   deftable2 = Table[{x, Evaluate[deftable1]}, {x, 0, L, L/nx}];
   deftable3 = Table[{deftable2[[i, 1]], deftable2[[i, 2]][[j, k]]}, {j, 1, ndld + 1}, {k, 1, nlld + 1}, {i, 1, nx + 1}];
   slotable1 = Table[Derivative[1][Deflectionxx[p1, p4]][y], {p1, 0, dld, dld/ndld}, {p4, 0, lld, lld/nlld}];
   slotable2 = Table[{y, Evaluate[slotable1]}, {y, 0, L, L/nx}];
   slotable3 = Table[{slotable2[[i, 1]], 1000 slotable2[[i, 2]][[j, k]]}, {j, 1, ndld + 1}, {k, 1, nlld + 1}, {i, 1, nx + 1}];
   {momtable3, curtable3, deftable3, slotable3}
  ];
```

Moment vs. Rotation Graphs - Table Equation

```
MomRotTableUDL[select_, L_, filedata_, fileRebardata_, fileSteelmoment_, con1M_, con2M_, Ystress_,
    EMod_, Esh_, shno_, ndld_, nlld_, nx_] :=
  Module[
   {DLstrain, dld, L1, Wholemoment, lld, α, β, ILϕ, Deflectionxx, momtable4, x, p1, p4, momtable5,
     momtable6, i, j, k, slotable4, y, slotable5, slotable6},
   {DLstrain, dld, L1} = DeadloadstrainUDL[L, con1M, con2M, Ystress, EMod, Esh, shno];
   {Wholemoment, lld} = MomentUDL[L, con1M, con2M, Ystress, EMod, Esh, shno, filedata];
   {α, β, ILϕ, Deflectionxx} = CurvDeflSlopeUDL[select, L, filedata, fileRebardata, fileSteelmoment,
     con1M, con2M, Ystress, EMod, Esh, shno];
   momtable4 = Table[Wholemoment[x, p1, p4], {p1, 0, dld, dld/ndld}, {p4, 0, lld + dld - p1, (lld + dld - p1)/nlld}];
   momtable5 = Table[{x, Evaluate[momtable4]}, {x, 0, L, L/nx}];
   momtable6 = Table[{momtable5[[i, 1]], momtable5[[i, 2]][[j, k]]}, {j, 1, ndld + 1}, {k, 1, nlld + 1}, {i, 1, nx + 1}];
   slotable4 = Table[Derivative[1][Deflectionxx[p1, p4]][y], {p1, 0, dld, dld/ndld}, {p4, 0, lld + dld - p1, (lld + dld - p1)/nlld}];
   slotable5 = Table[{y, Evaluate[slotable4]}, {y, 0, L, L/nx}];
   slotable6 = Table[{slotable5[[i, 1]], 1000 slotable5[[i, 2]][[j, k]]}, {j, 1, ndld + 1}, {k, 1, nlld + 1}, {i, 1, nx + 1}];
   {momtable6, slotable6}
  ];
```

```
MRradiansUDL[select_, t_, L_, filedata_, fileRebardata_, fileSteelmoment_, con1M_, con2M_, Ystress_,
    EMod_, Esh_, shno_, ndld_, nlld_, nx_] :=
  Module[
   {MRrad1, MRrad2, MRradC1, MRradC2, momtable6, slotable6},

   {momtable6, slotable6} = MomRotTableUDL[select, L, filedata, fileRebardata, fileSteelmoment, con1M,
      con2M, Ystress, EMod, Esh, shno, ndld, nlld, nx];

   MRrad2 = Table[{slotable6[[t, i, nx + 1, 2]], Max[momtable6[[t, i]]]}, {i, 1, nlld + 1}];
   MRradC2 = Insert[MRrad2, {0, 0}, 1];

   MRrad1 = Table[{- slotable6[[t, i, 1, 2]], Max[momtable6[[t, i]]]}, {i, 1, nlld + 1}];
   MRradC1 = Insert[MRrad1, {0, 0}, 1];

   {MRradC1, MRradC2}
  ];
```

Appendix C – Results from the parametric study of semi-continuous composite beam

C.1 EFFECT OF DEAD LOAD STRESS

C.1.1 External beam, L/D=15, 2PL

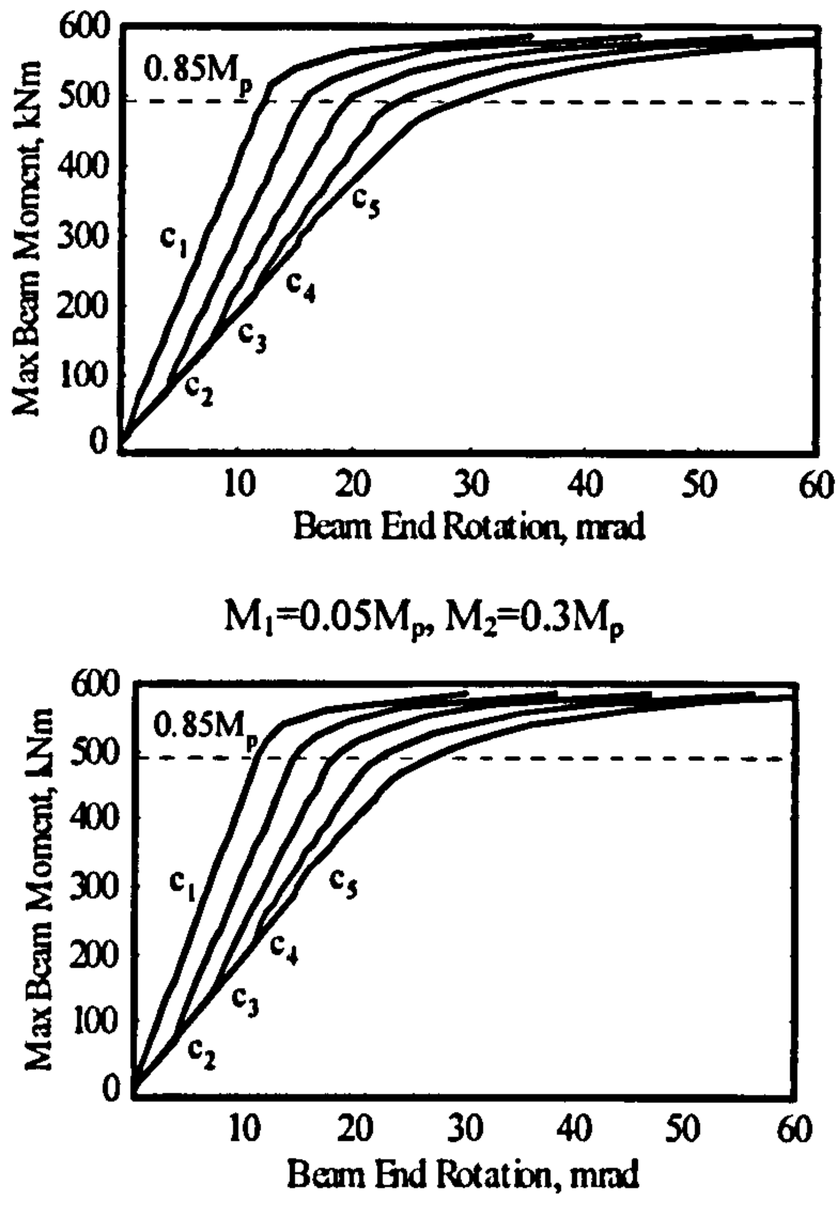

M_1=0.05M_p, M_2=0.3M_p

M_1=0.05M_p, M_2=0.4M_p

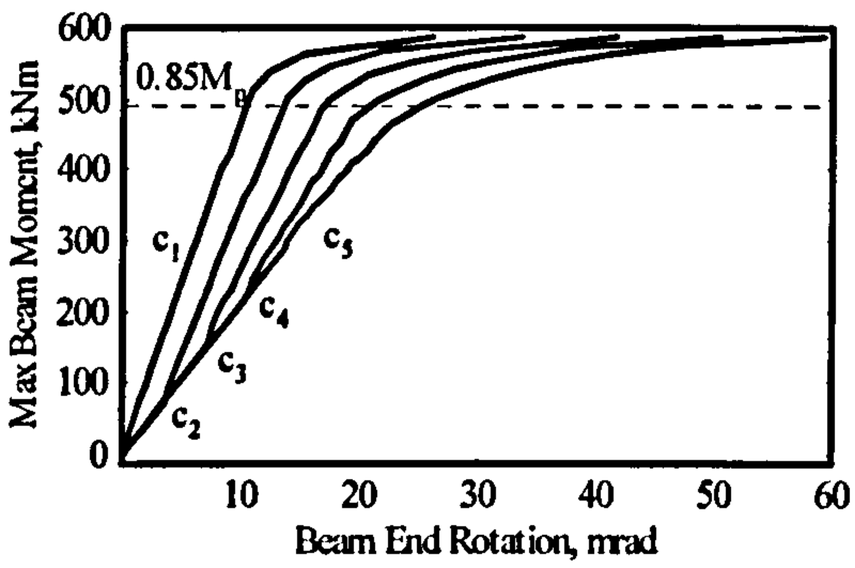

M_1=0.05M_p, M_2=0.5M_p

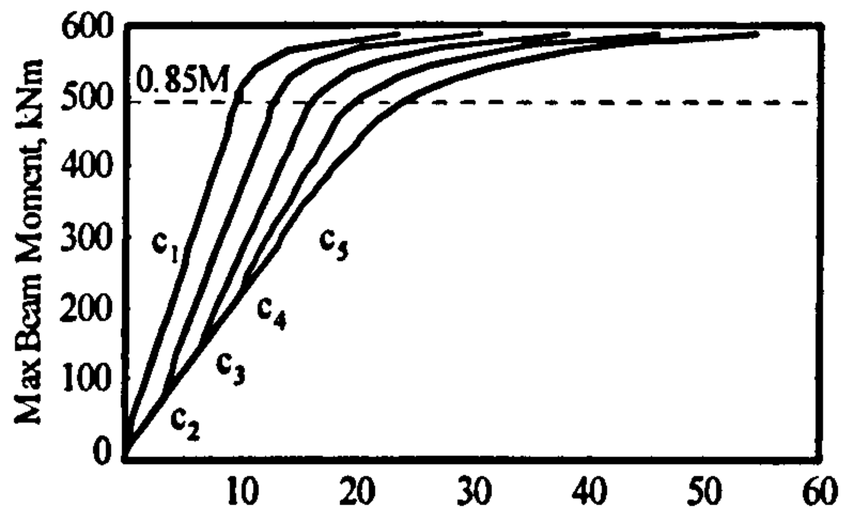

M_1=0.05M_p, M_2=0.6M_p

Grade S275

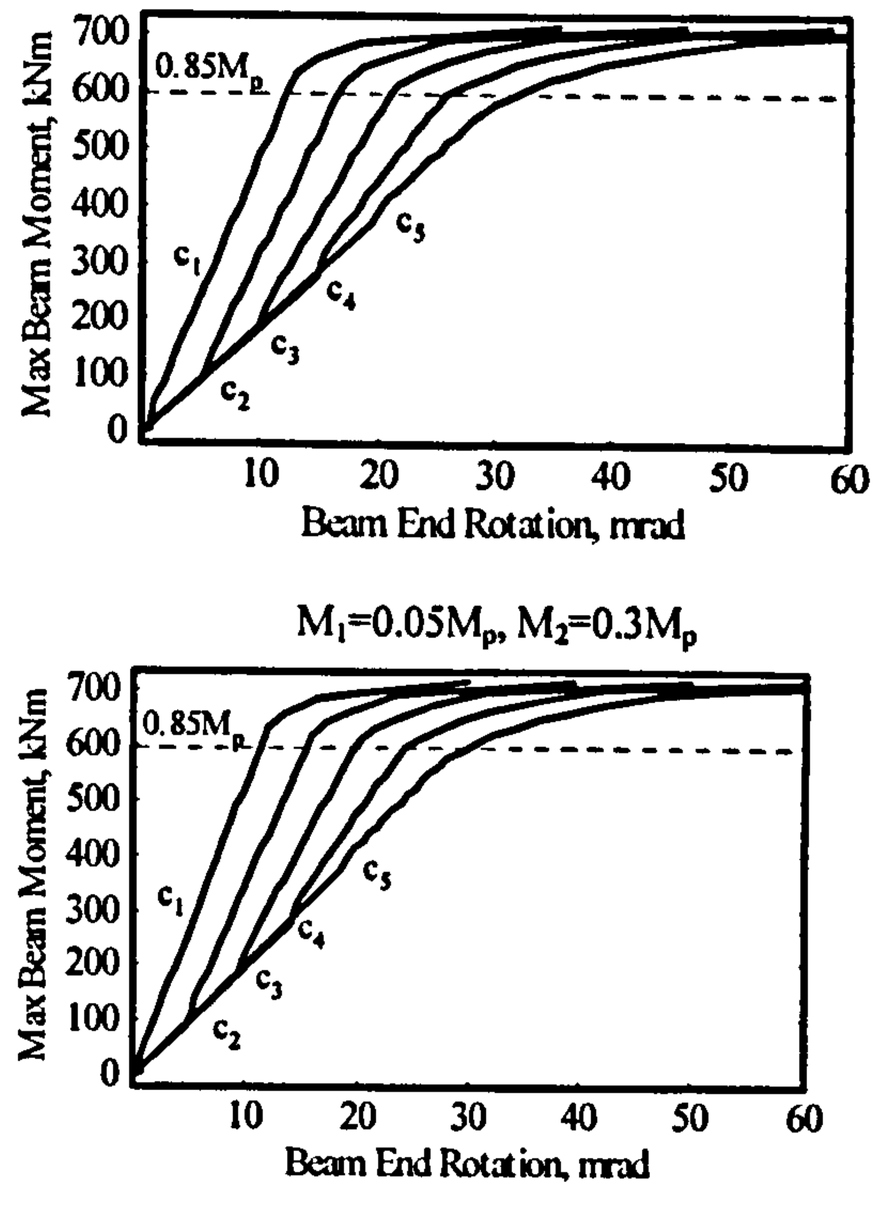

M_1=0.05M_p, M_2=0.3M_p

M_1=0.05M_p, M_2=0.4M_p

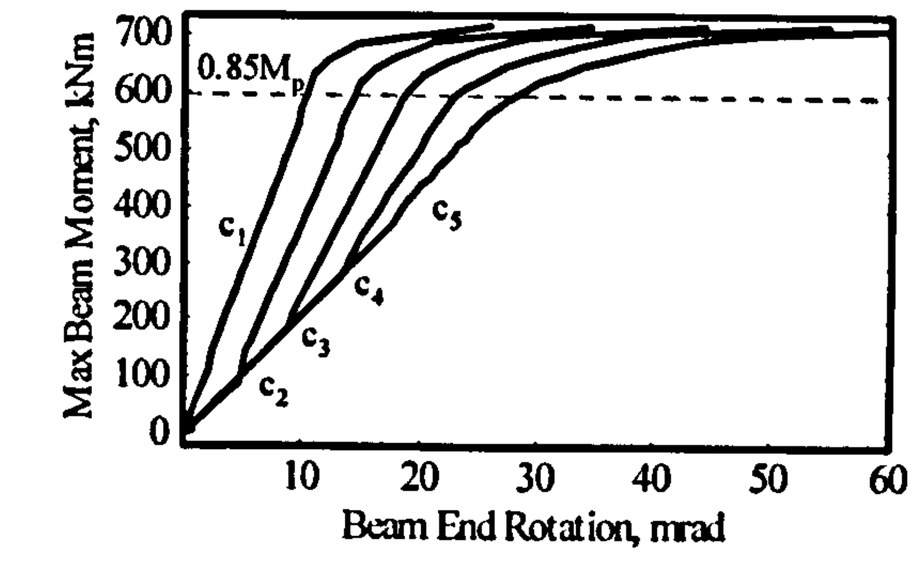

M_1=0.05M_p, M_2=0.5M_p

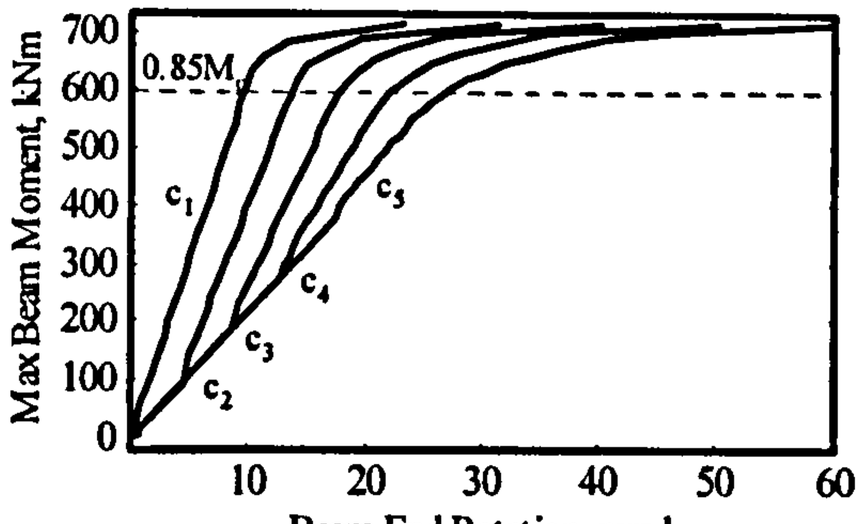

M_1=0.05M_p, M_2=0.6M_p

Grade S355

Figure C1-1. Moment vs. end rotation relationship for various maximum dead load stress levels (c_1:σ_{dl}=0; c_2:σ_{dl}=0.25σ_y; c_3:σ_{dl}=0.50σ_y; c_4:σ_{dl}=0.75σ_y; c_5:σ_{dl}=σ_y)

C.1.2 External beam, L/D=20, 2PL

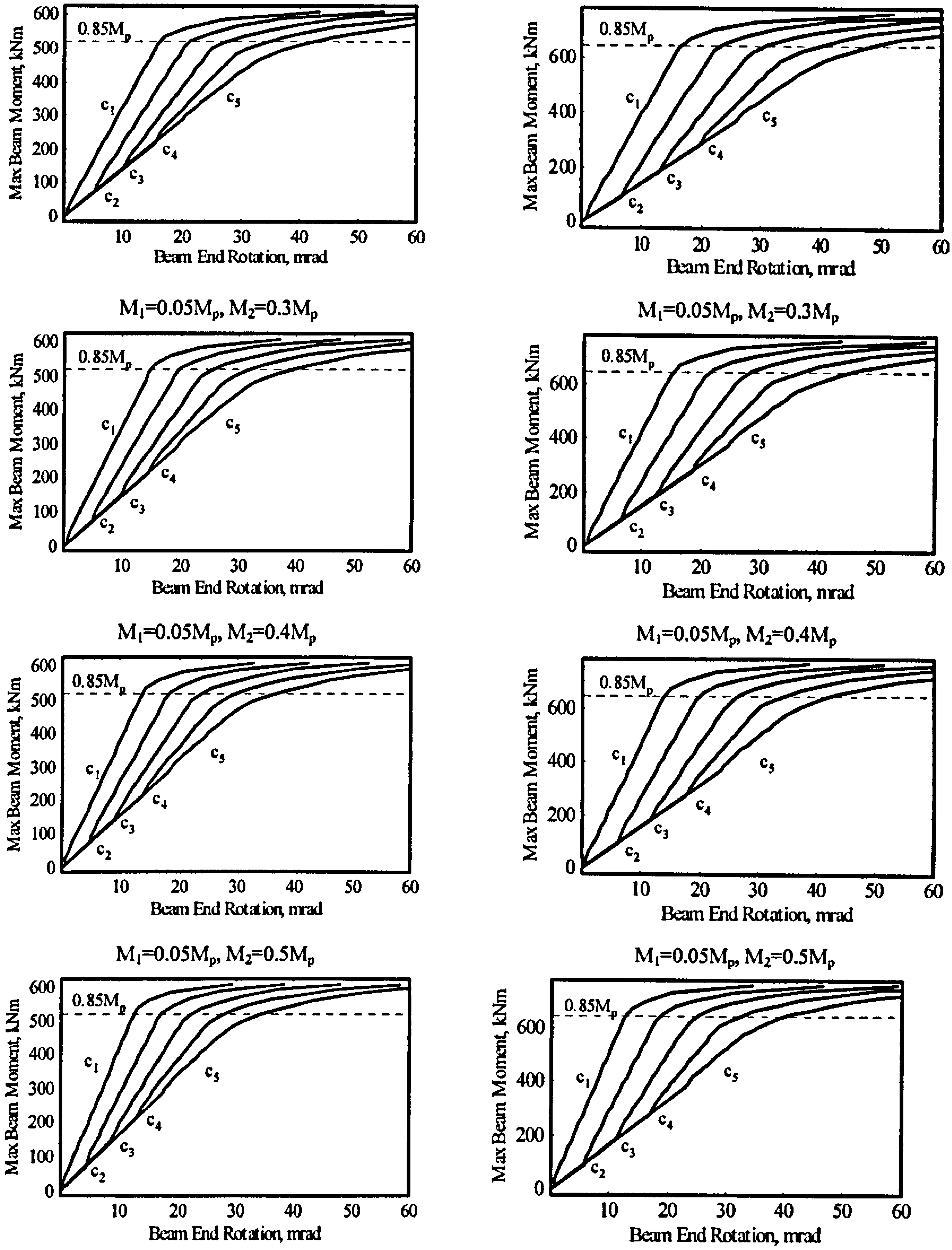

M_1=0.05M_p, M_2=0.3M_p | M_1=0.05M_p, M_2=0.3M_p

M_1=0.05M_p, M_2=0.4M_p | M_1=0.05M_p, M_2=0.4M_p

M_1=0.05M_p, M_2=0.5M_p | M_1=0.05M_p, M_2=0.5M_p

M_1=0.05M_p, M_2=0.6M_p | M_1=0.05M_p, M_2=0.6M_p

Grade S275 | Grade S355

Figure C1-2. Moment vs. end rotation relationship for various maximum dead load stress levels (c_1:σ_{dl}=0; c_2:σ_{dl}=0.25σ_y; c_3:σ_{dl}=0.50σ_y; c_4:σ_{dl}=0.75σ_y; c_5:σ_{dl}=σ_y)

C.1.3 External beam, L/D=25, 2PL

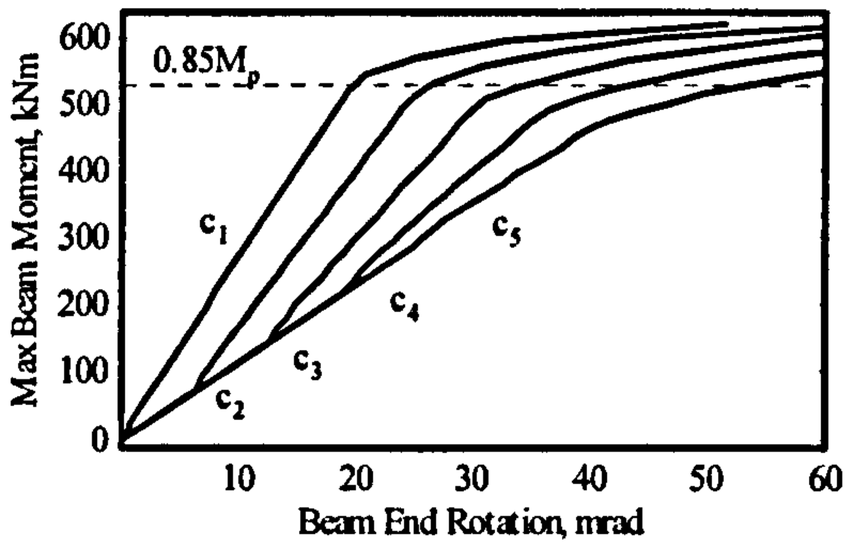

M_1=0.05M_p, M_2=0.3M_p

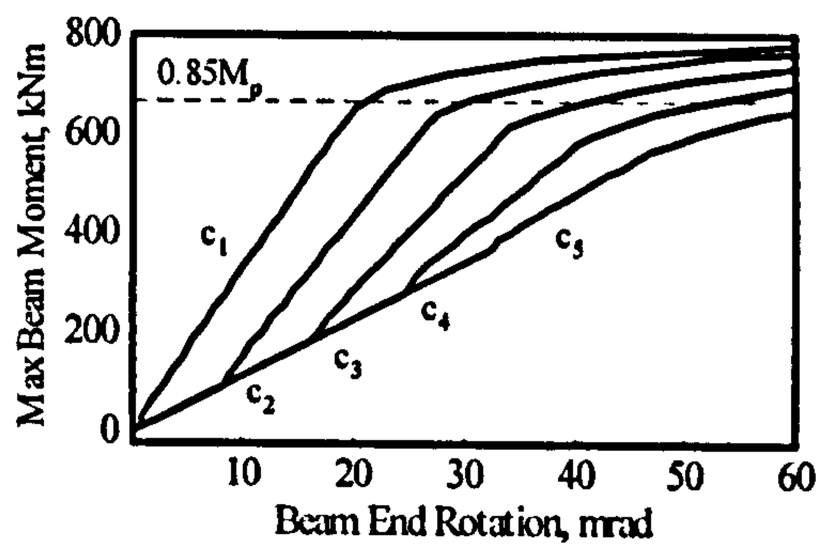

M_1=0.05M_p, M_2=0.3M_p

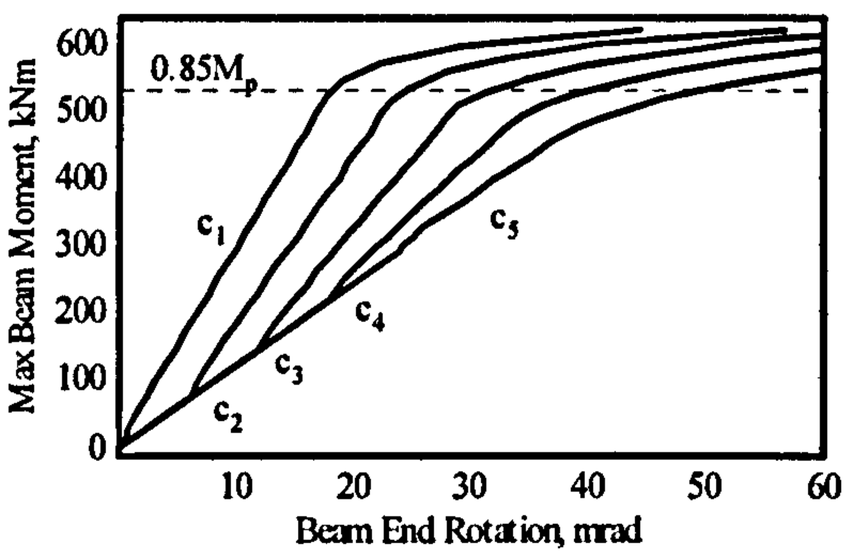

M_1=0.05M_p, M_2=0.4M_p

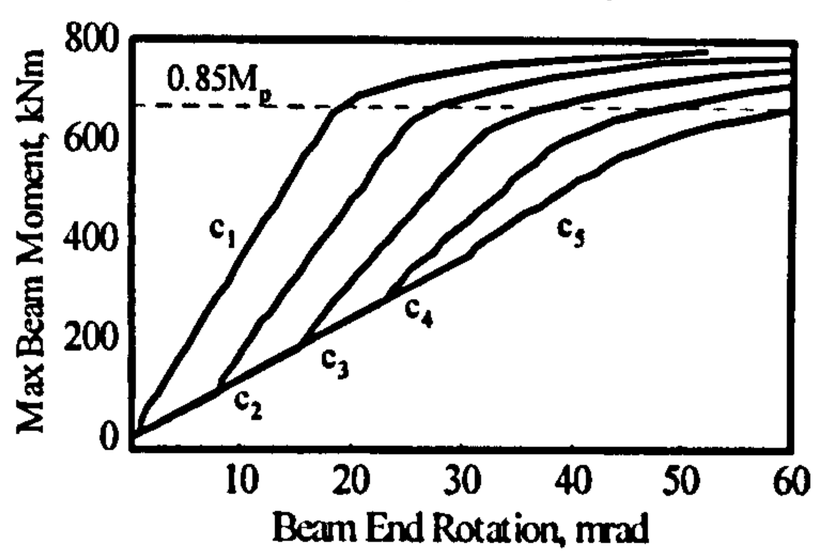

M_1=0.05M_p, M_2=0.4M_p

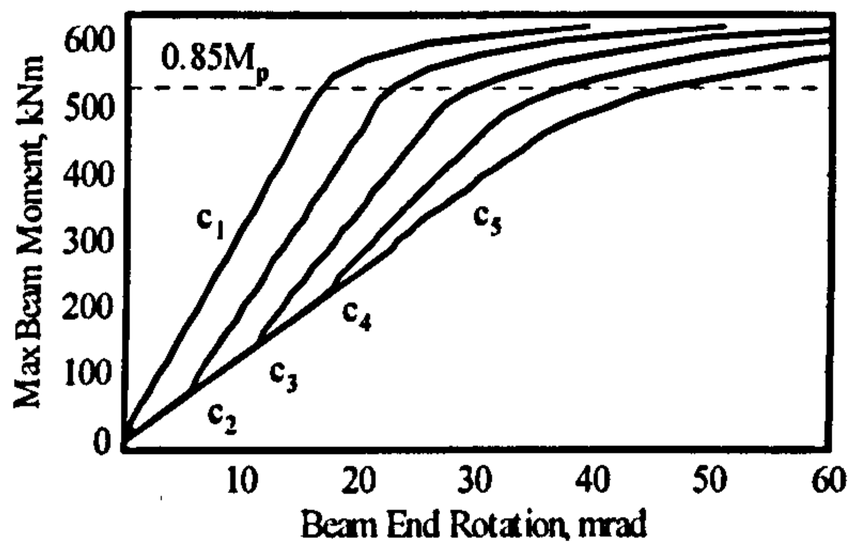

M_1=0.05M_p, M_2=0.4M_p

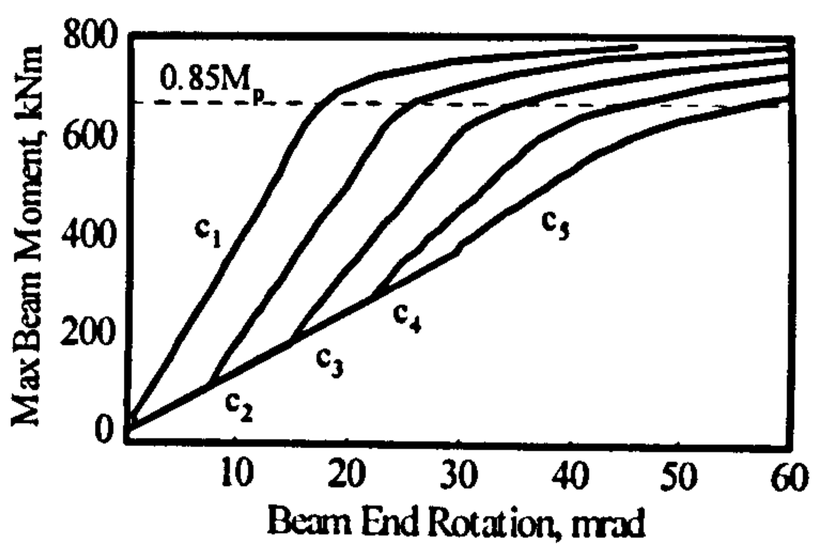

M_1=0.05M_p, M_2=0.5M_p

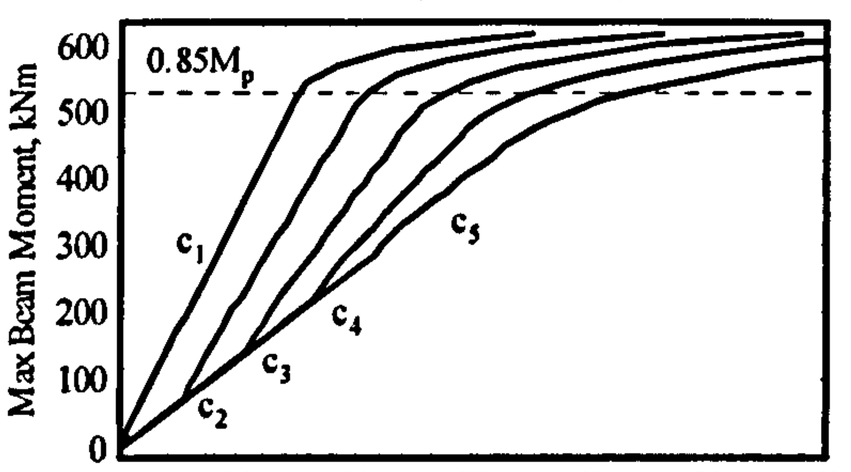

M_1=0.05M_p, M_2=0.5M_p

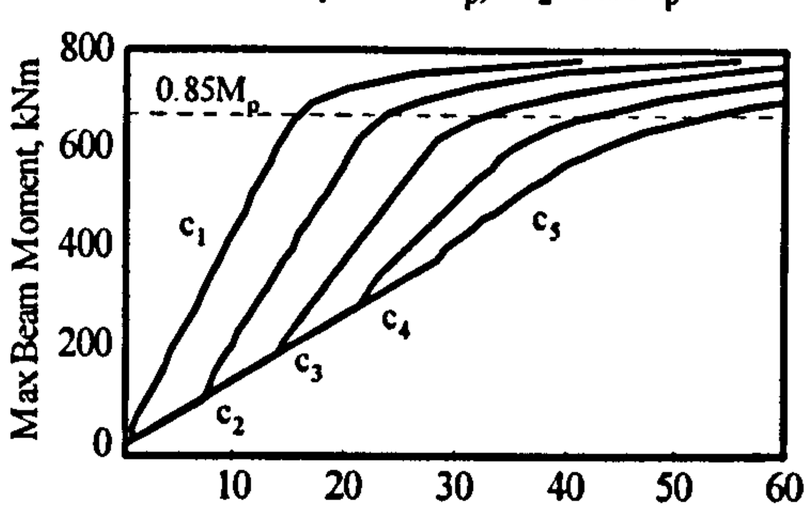

M_1=0.05M_p, M_2=0.6M_p

Grade S275

M_1=0.05M_p, M_2=0.6M_p

Grade S355

Figure C1-3. Moment vs. end rotation relationship for various maximum dead load stress levels (c_1:σ_{dl}=0; c_2:σ_{dl}=0.25σ_y; c_3:σ_{dl}=0.50σ_y; c_4:σ_{dl}=0.75σ_y; c_5:σ_{dl}=σ_y)

C.1.4 Internal beam, L/D=15, 2PL

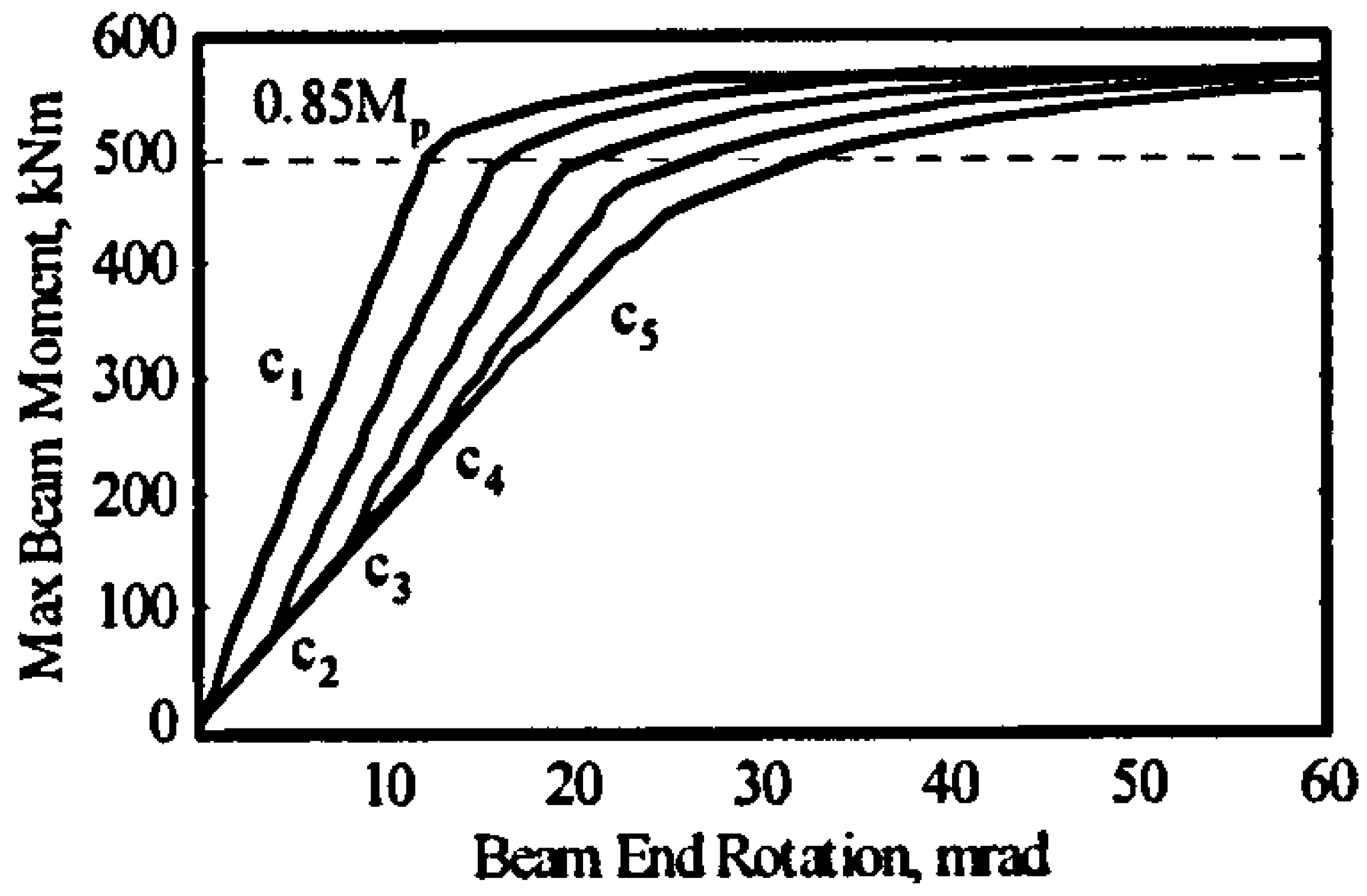

$M_1=0.3M_p$, $M_2=0.3M_p$

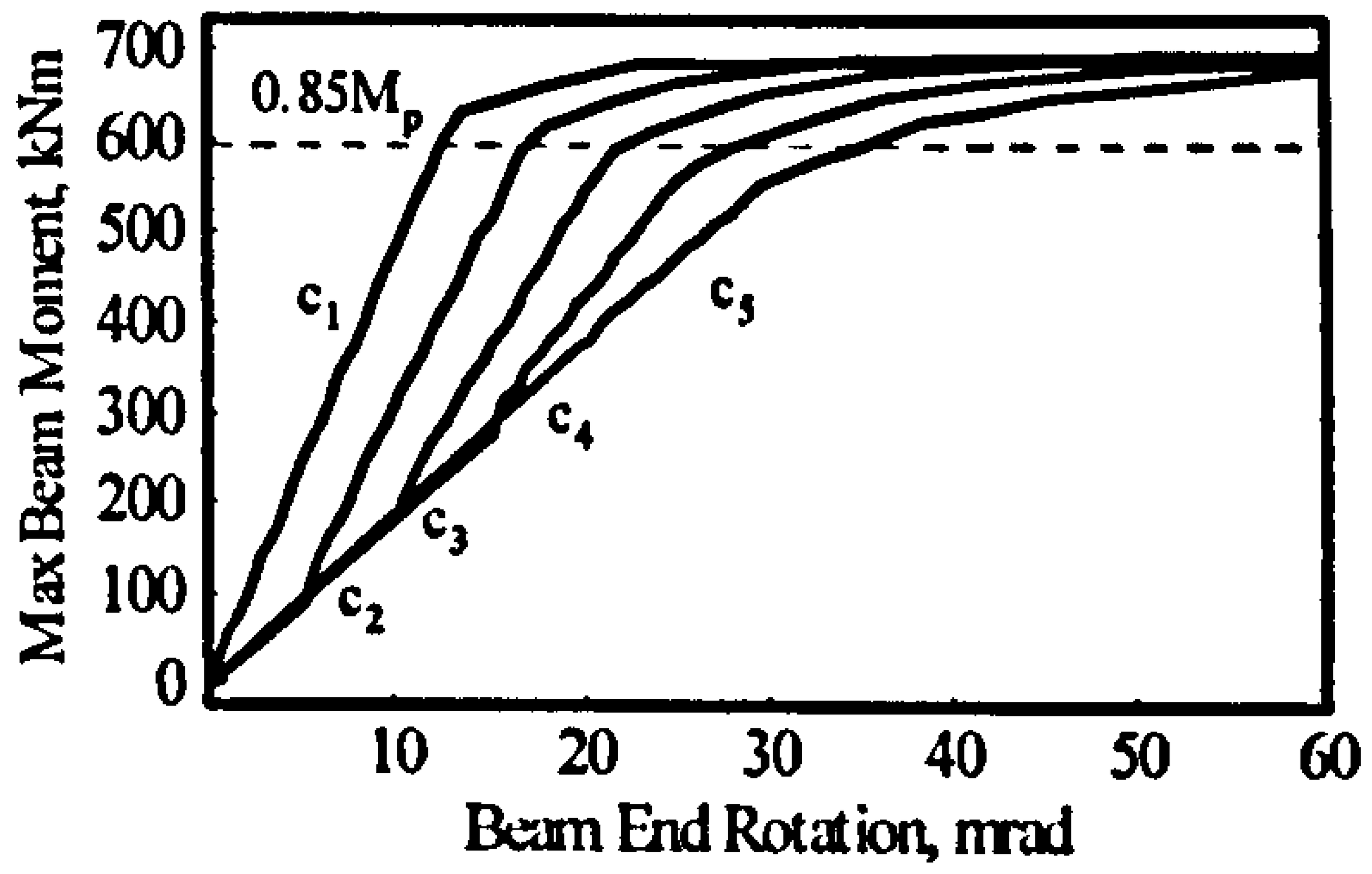

$M_1=0.3M_p$, $M_2=0.3M_p$

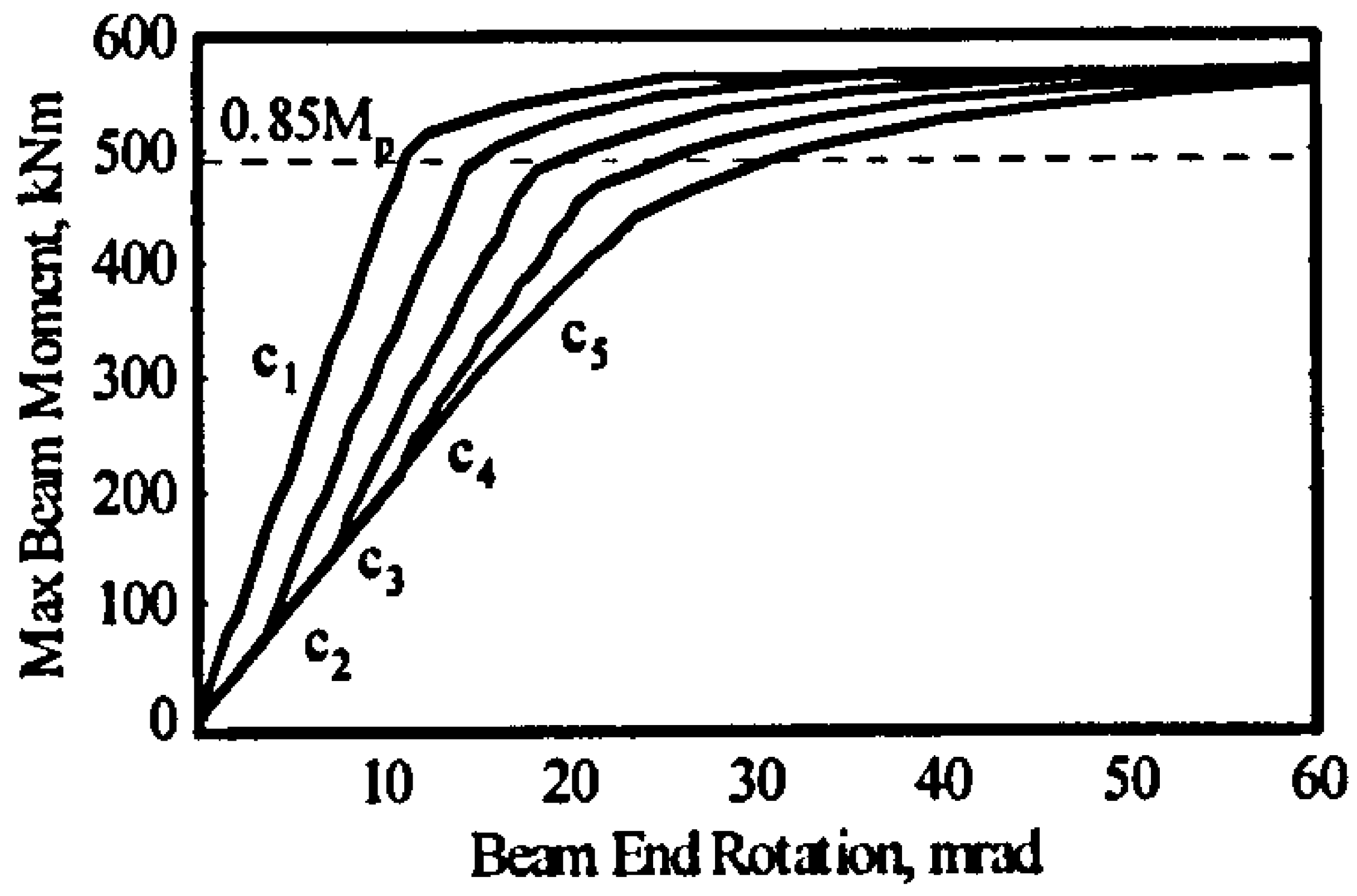

$M_1=0.4M_p$, $M_2=0.4M_p$

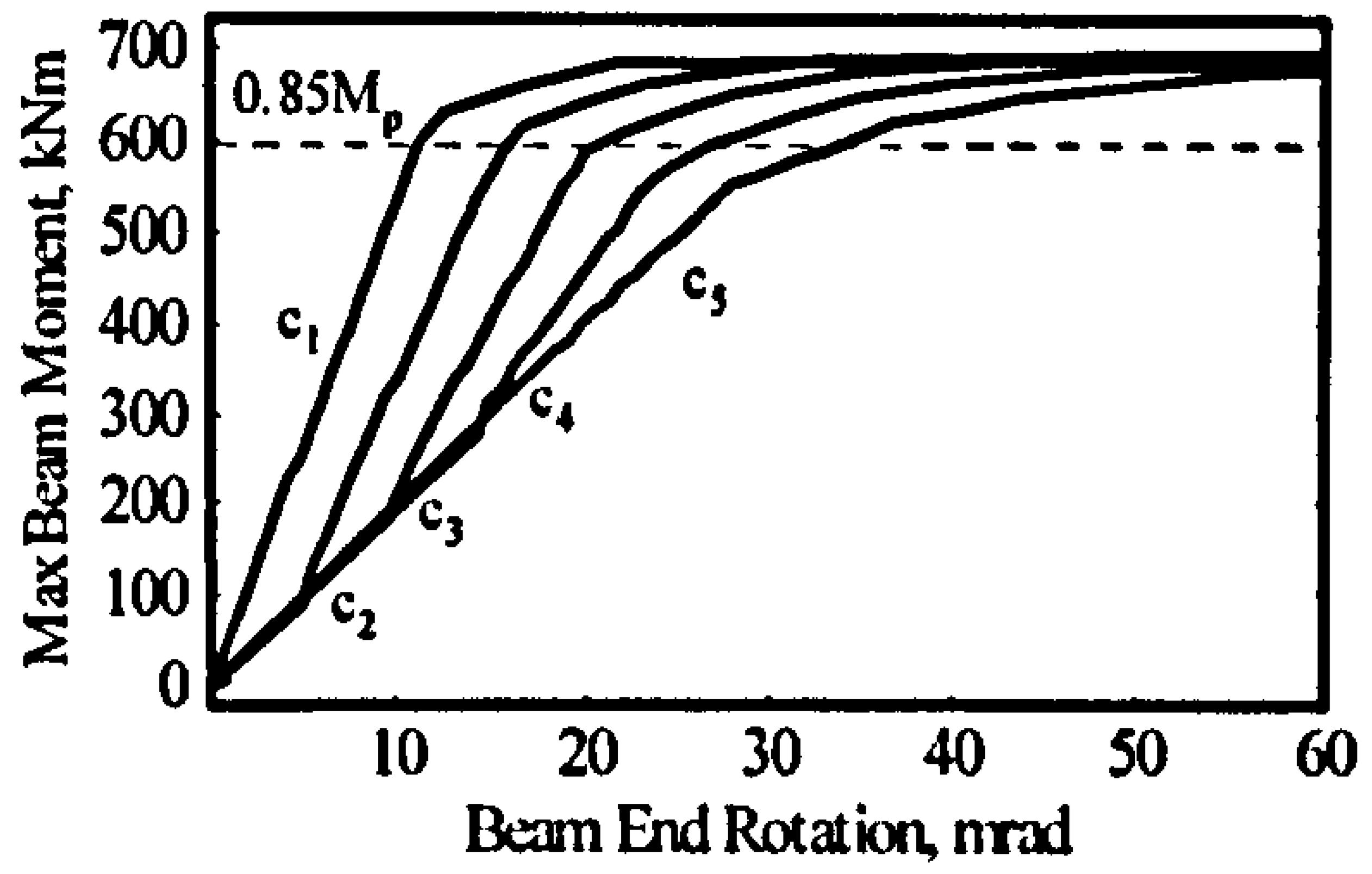

$M_1=0.4M_p$, $M_2=0.4M_p$

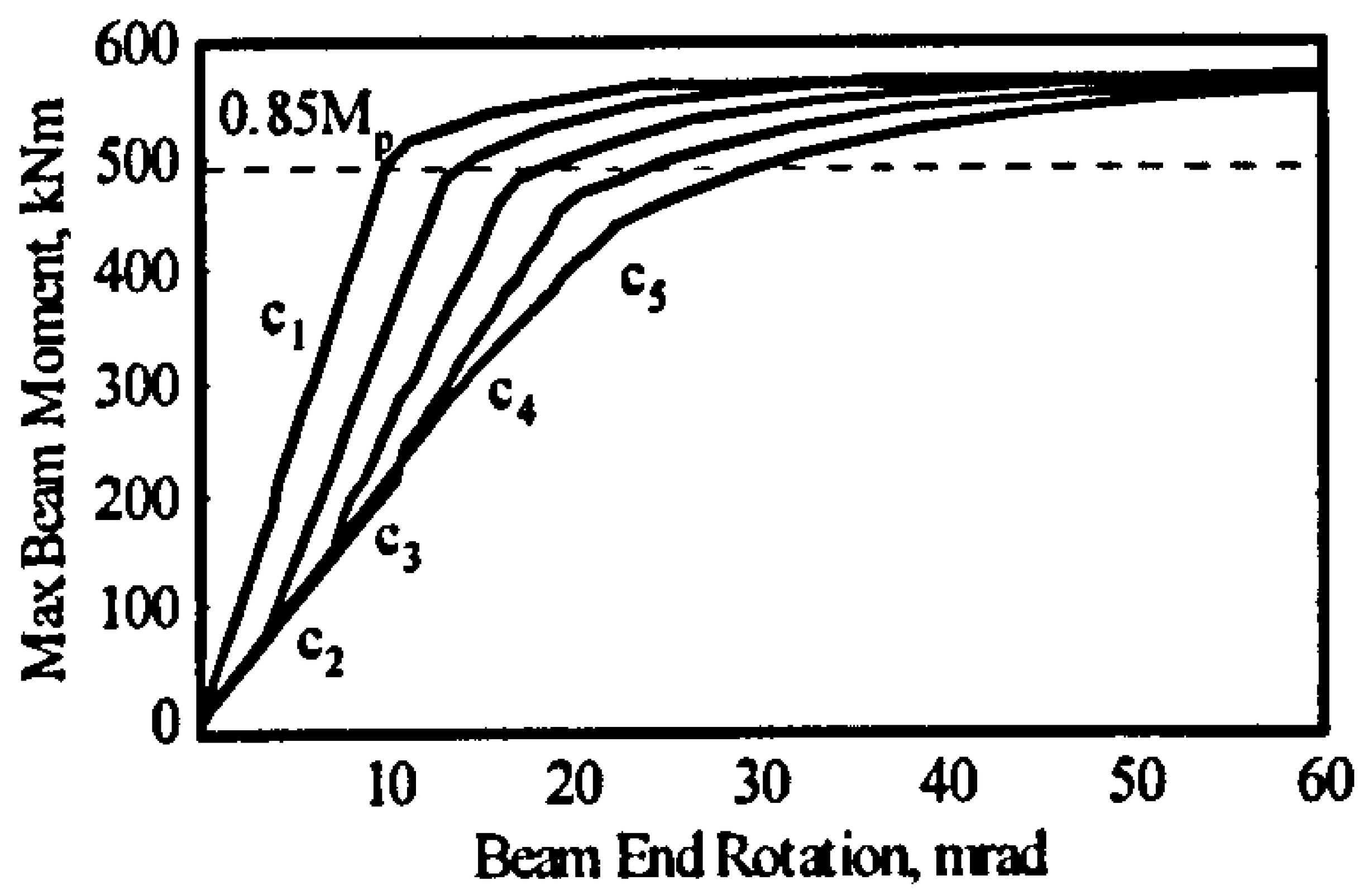

$M_1=0.5M_p$, $M_2=0.5M_p$

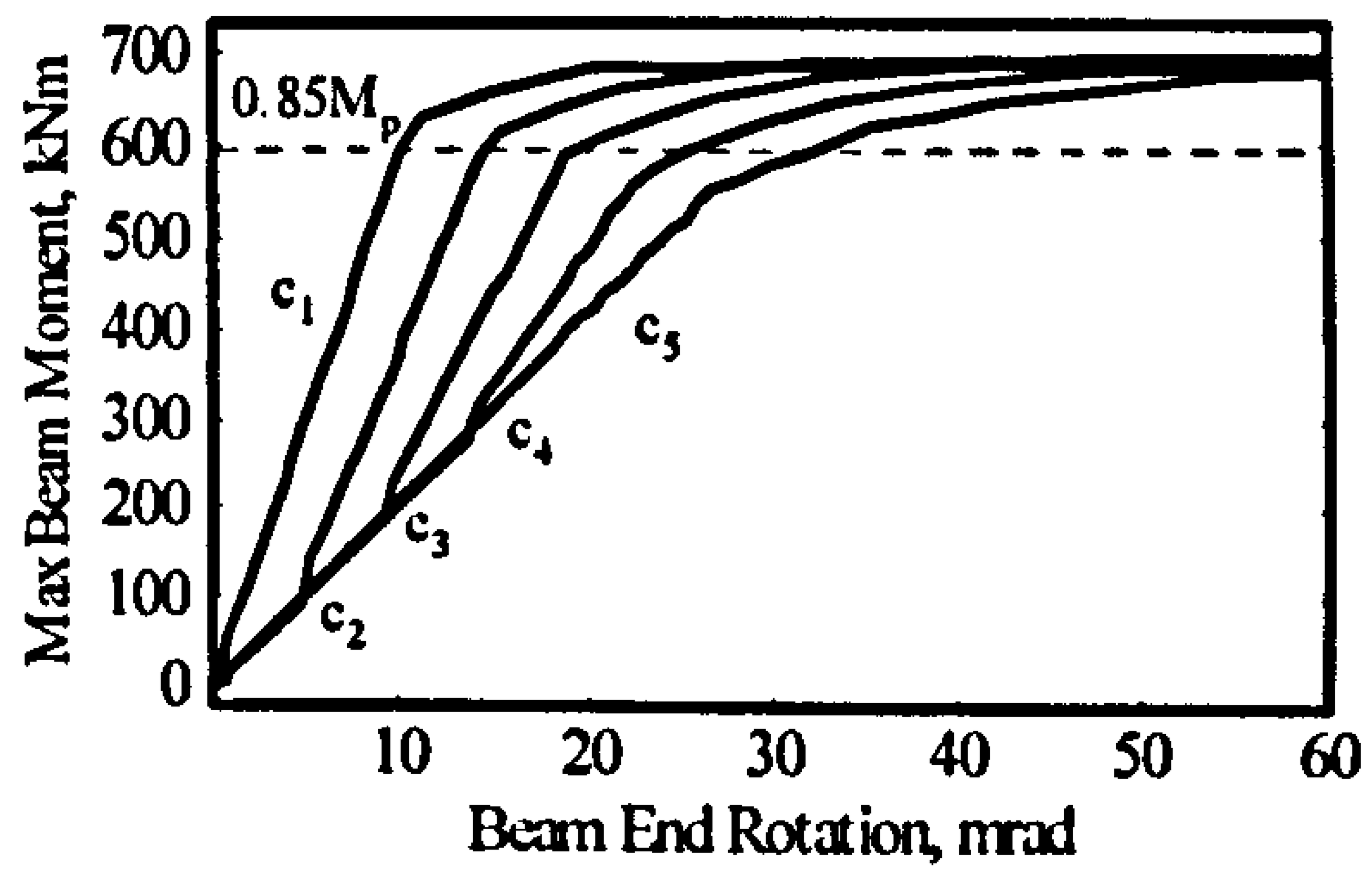

$M_1=0.5M_p$, $M_2=0.5M_p$

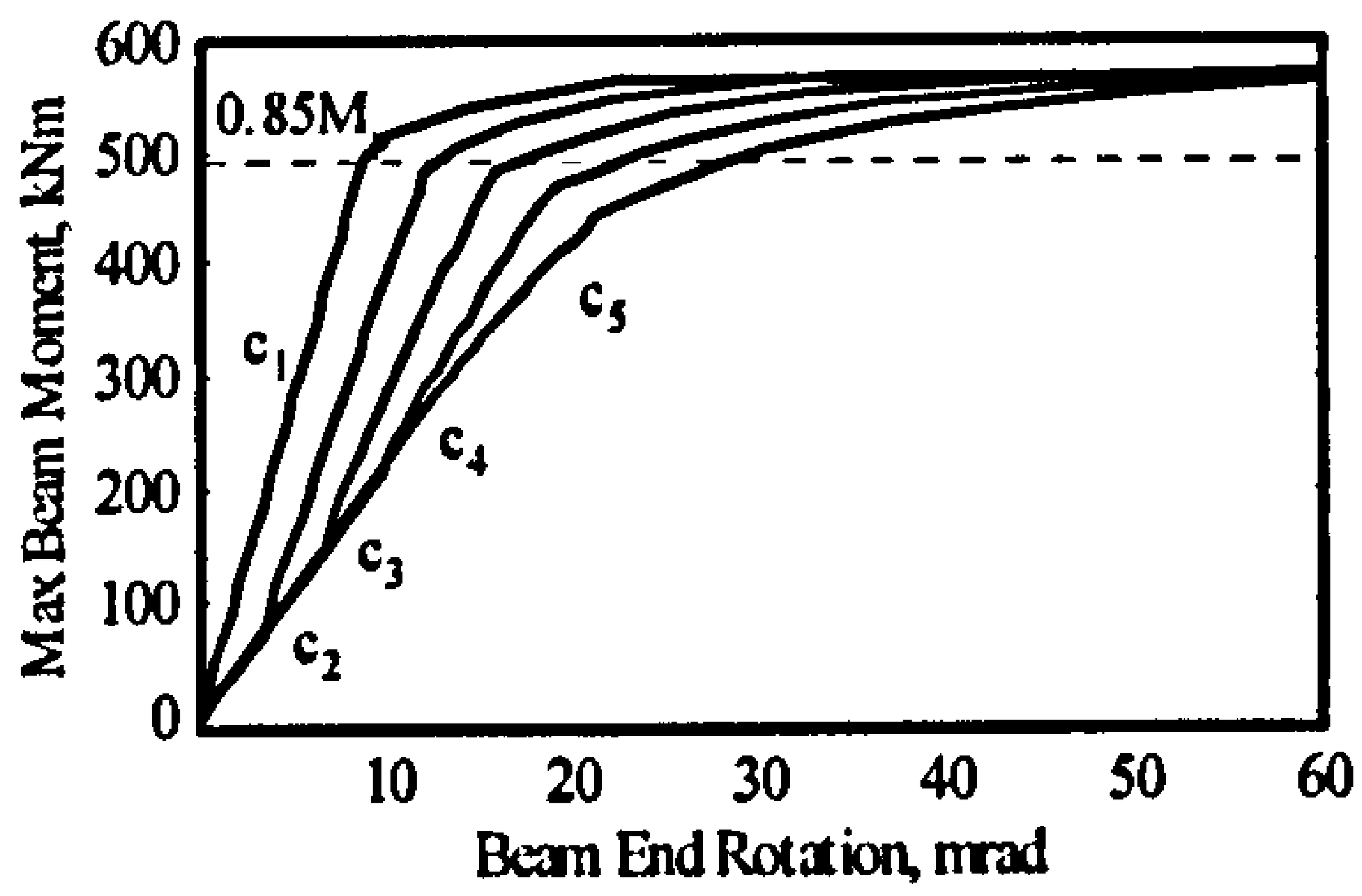

$M_1=0.6M_p$, $M_2=0.6M_p$

Grade S275

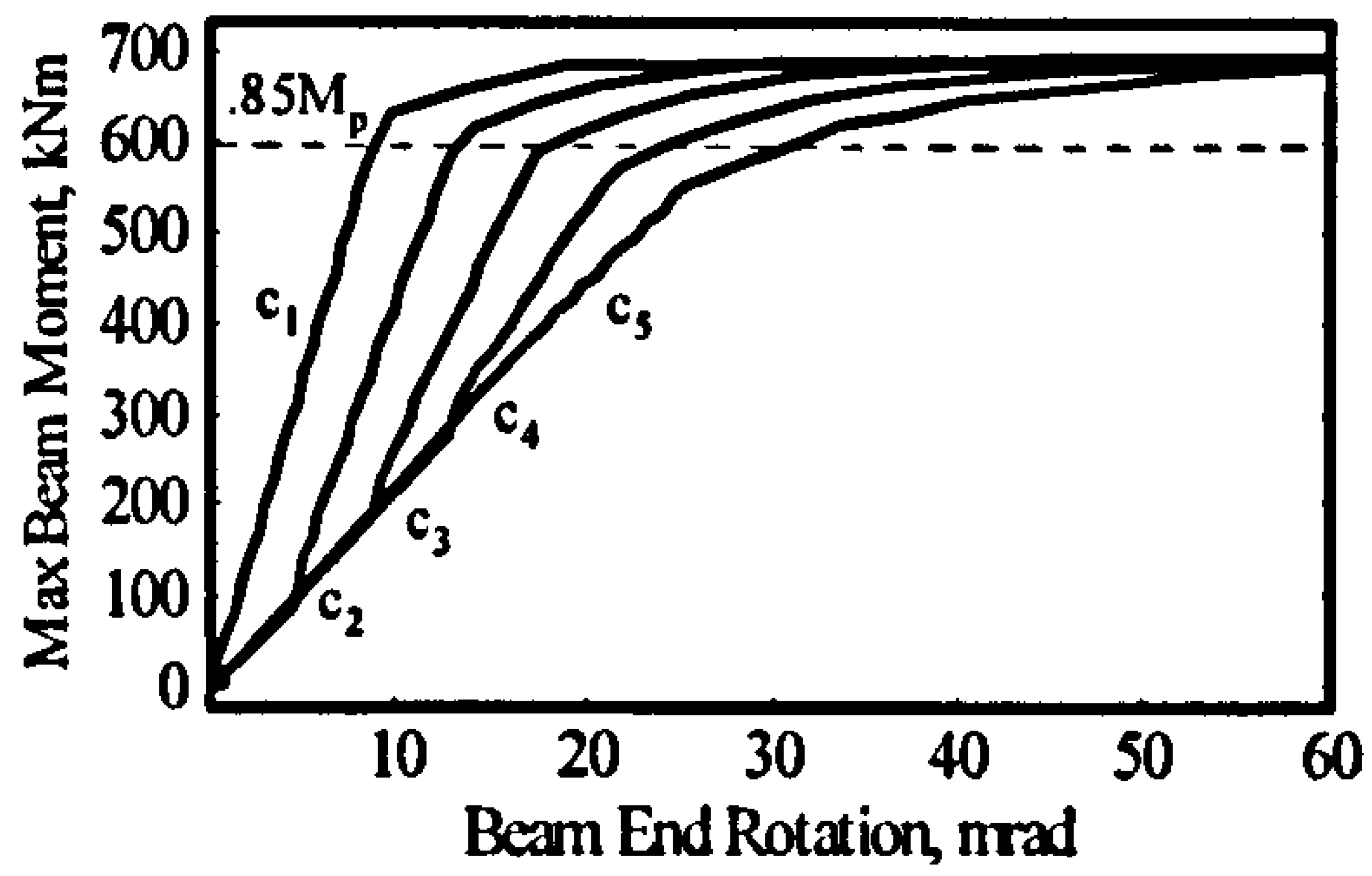

$M_1=0.6M_p$, $M_2=0.6M_p$

Grade S355

Figure C1-4. Moment vs. end rotation relationship for various maximum dead load stress levels (c_1: $\sigma_{dl}=0$; c_2: $\sigma_{dl}=0.25\sigma_y$; c_3: $\sigma_{dl}=0.50\sigma_y$; c_4: $\sigma_{dl}=0.75\sigma_y$; c_5: $\sigma_{dl}=\sigma_y$)

C.1.5 Internal beam, L/D=20, 2PL

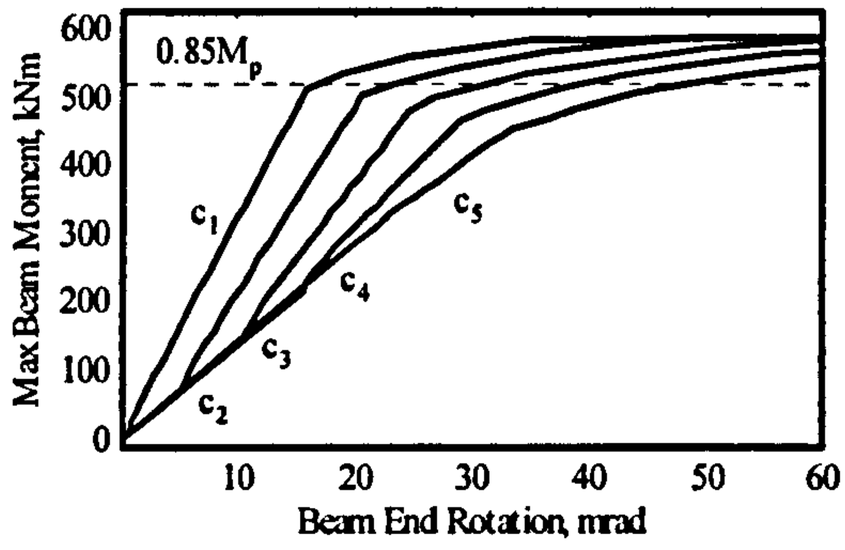

$M_1=0.3M_p$, $M_2=0.3M_p$

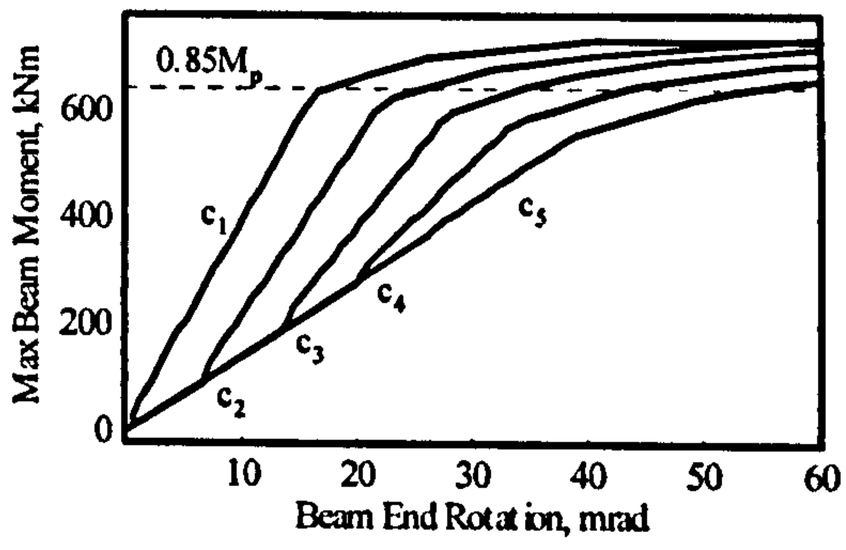

$M_1=0.3M_p$, $M_2=0.3M_p$

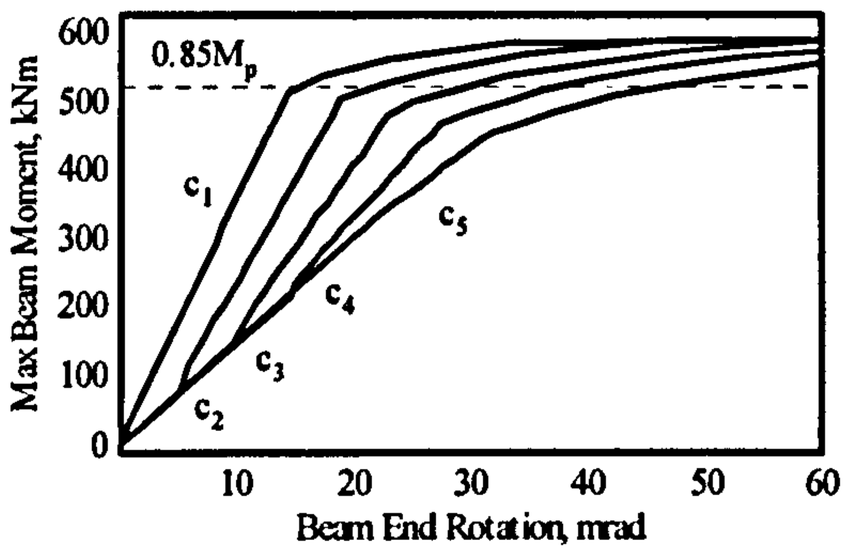

$M_1=0.4M_p$, $M_2=0.4M_p$

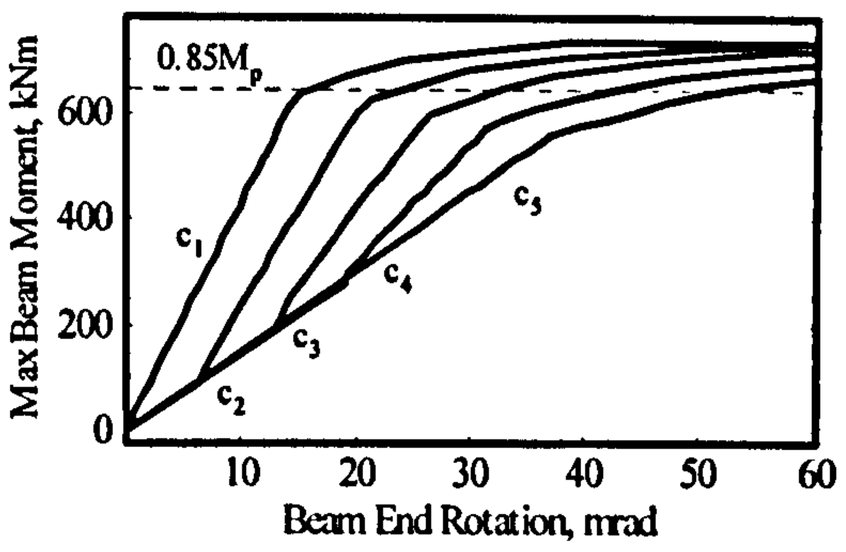

$M_1=0.4M_p$, $M_2=0.4M_p$

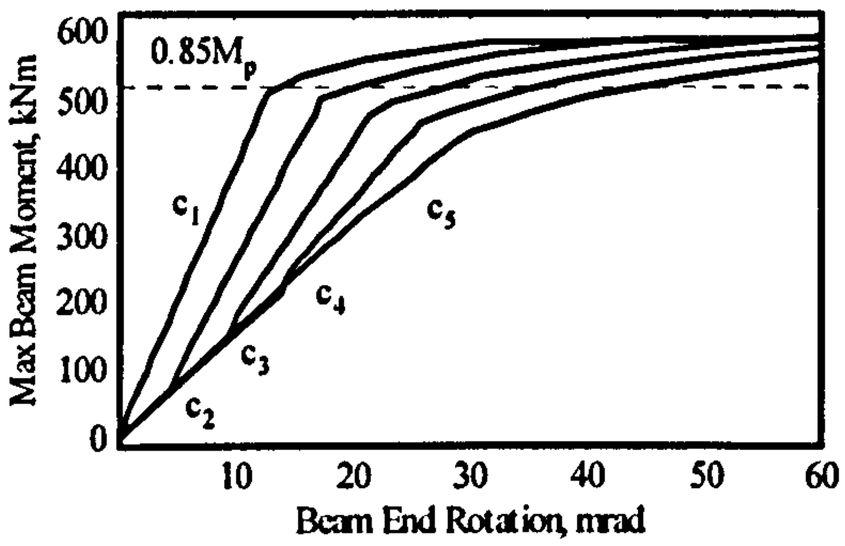

$M_1=0.4M_p$, $M_2=0.4M_p$

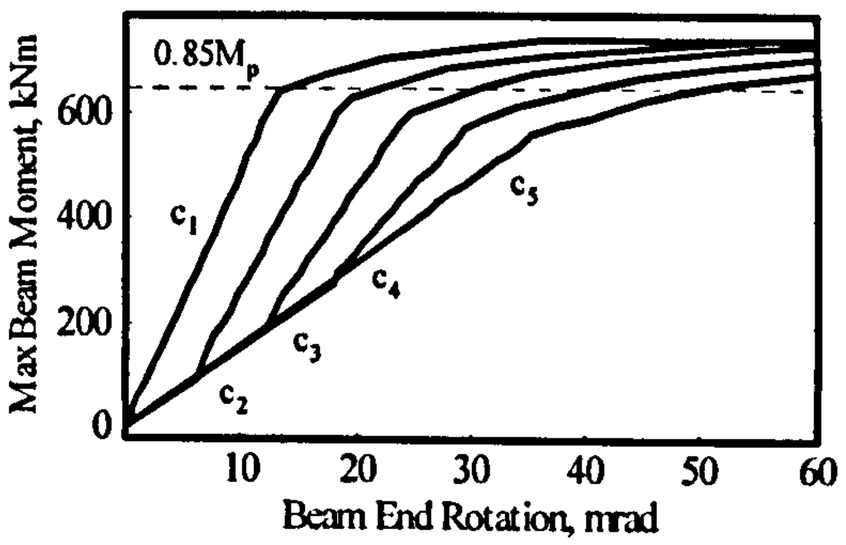

$M_1=0.5M_p$, $M_2=0.5M_p$

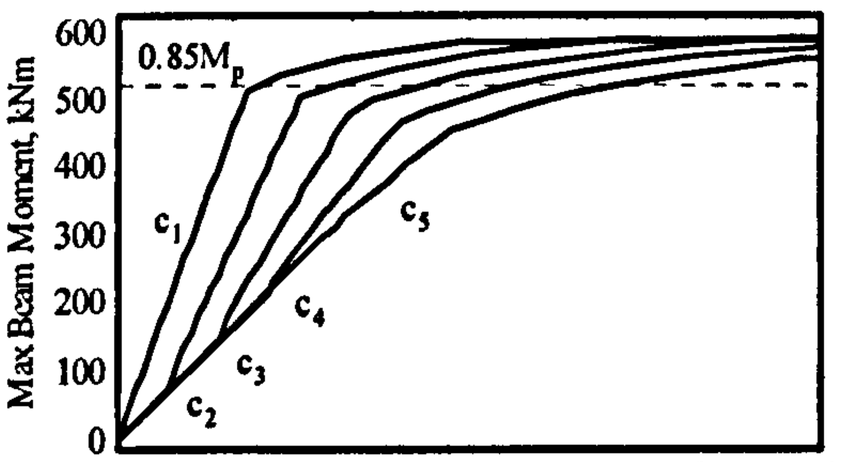

$M_1=0.5M_p$, $M_2=0.5M_p$

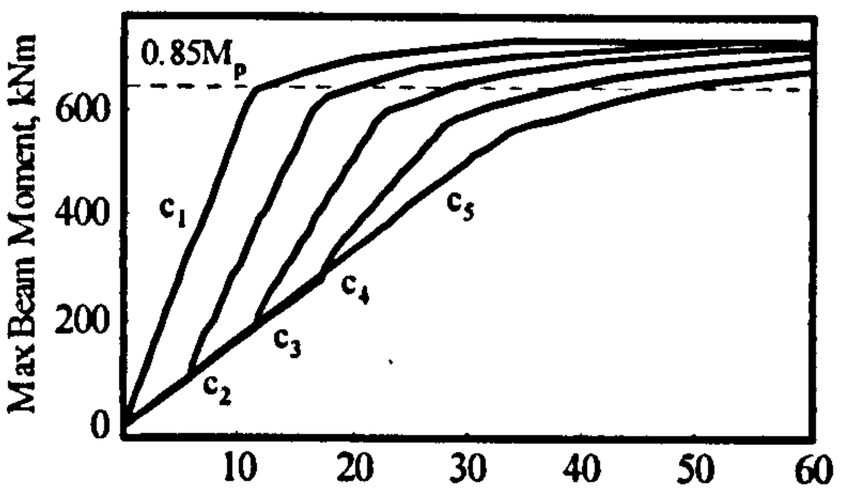

$M_1=0.6M_p$, $M_2=0.6M_p$

Grade S275

$M_1=0.6M_p$, $M_2=0.6M_p$

Grade S355

Figure C1-5. Moment vs. end rotation relationship for various maximum dead load stress levels (c_1:σ_{dl}=0; c_2:σ_{dl}=0.25σ_y; c_3:σ_{dl}=0.50σ_y; c_4:σ_{dl}=0.75σ_y; c_5:σ_{dl}=σ_y)

C.1.6 Internal beam, L/D=25, 2PL

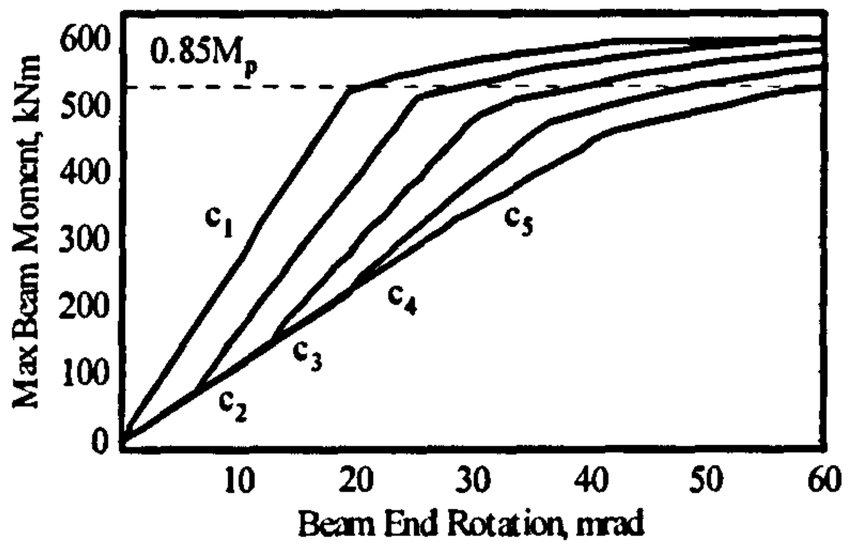

M_1=0.3M_p, M_2=0.3M_p

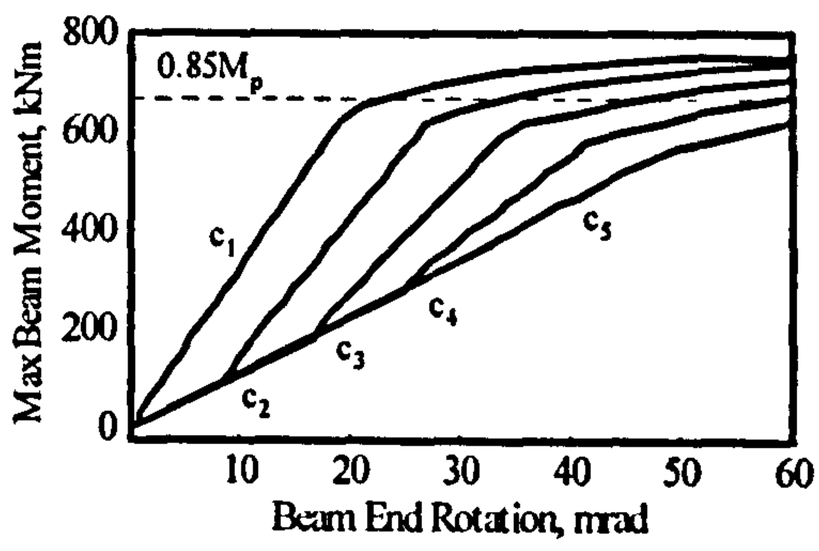

M_1=0.3M_p, M_2=0.3M_p

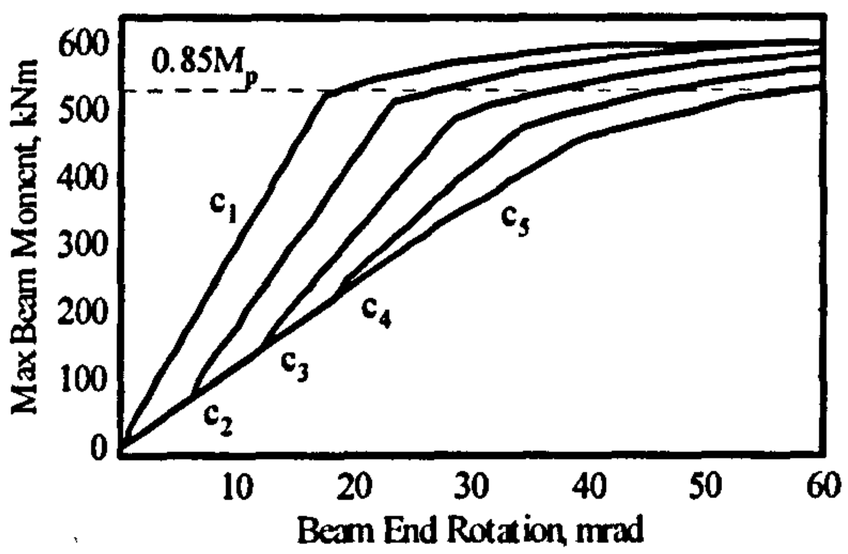

M_1=0.4M_p, M_2=0.4M_p

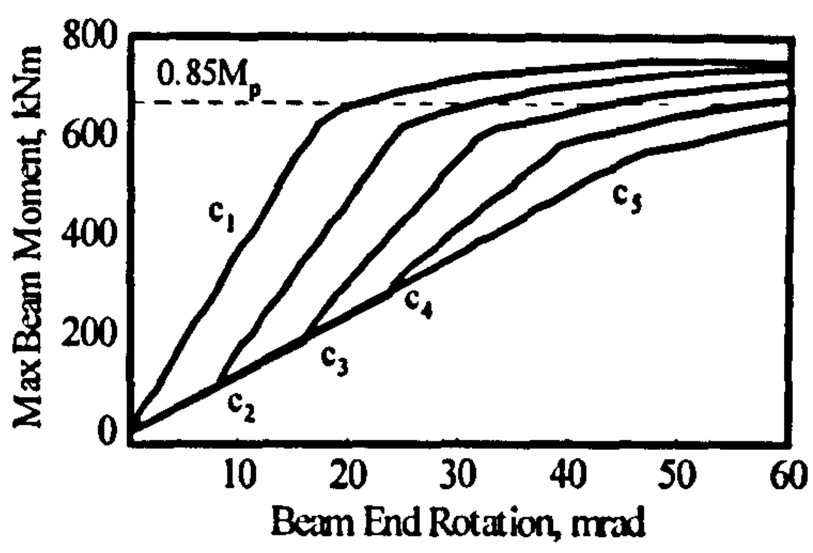

M_1=0.4M_p, M_2=0.4M_p

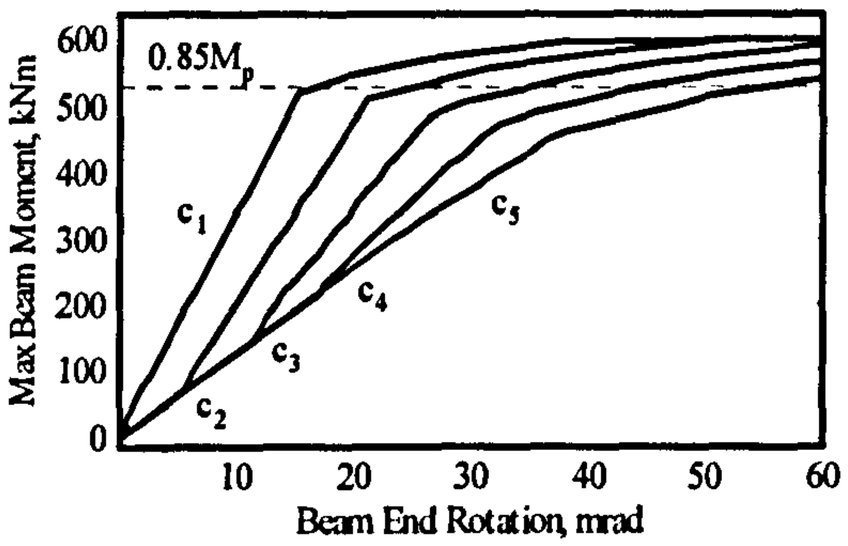

M_1=0.5M_p, M_2=0.5M_p

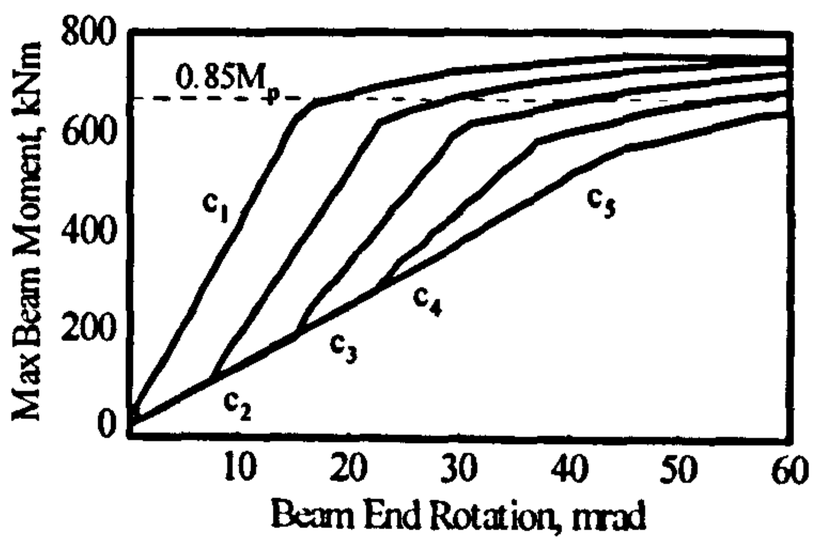

M_1=0.5M_p, M_2=0.5M_p

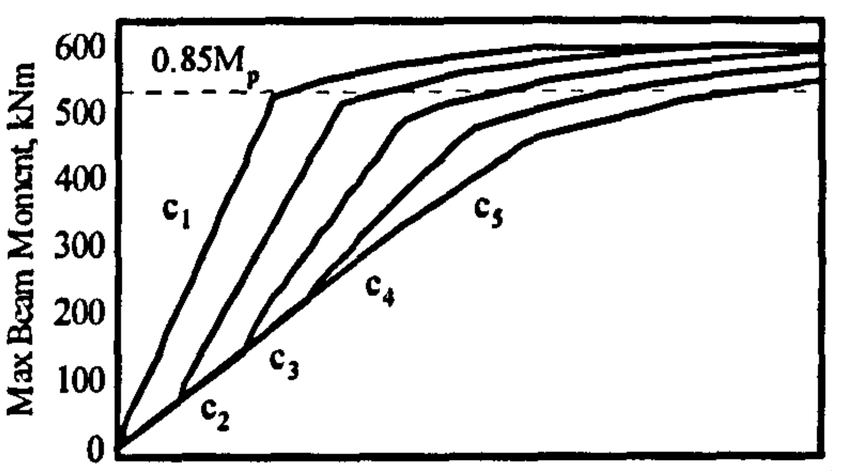

M_1=0.6M_p, M_2=0.6M_p

Grade S275

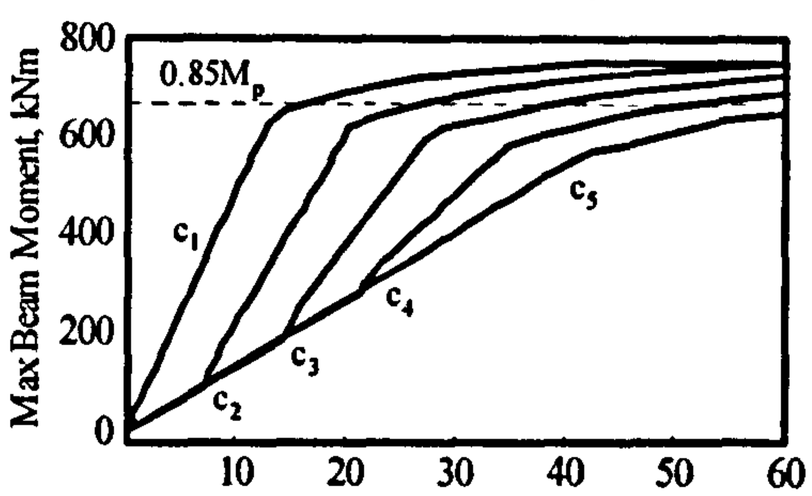

M_1=0.6M_p, M_2=0.6M_p

Grade S355

Figure C1-6. Moment vs. end rotation relationship for various maximum dead load stress levels (c_1:σ_{dl}=0; c_2:σ_{dl}=0.25σ_y; c_3:σ_{dl}=0.50σ_y; c_4:σ_{dl}=0.75σ_y; c_5:σ_{dl}=σ_y)

C.1.7 External beam, L/D=15, 3PL

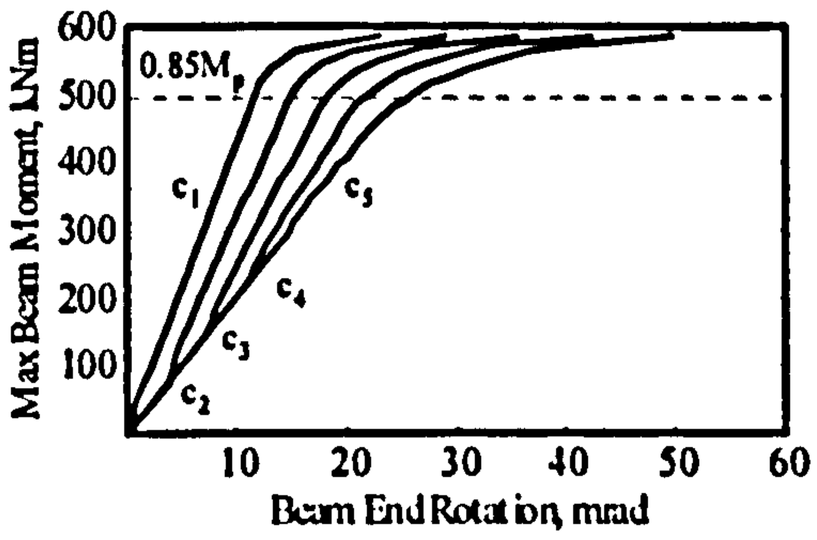

M_1=0.05M_p, M_2=0.3M_p

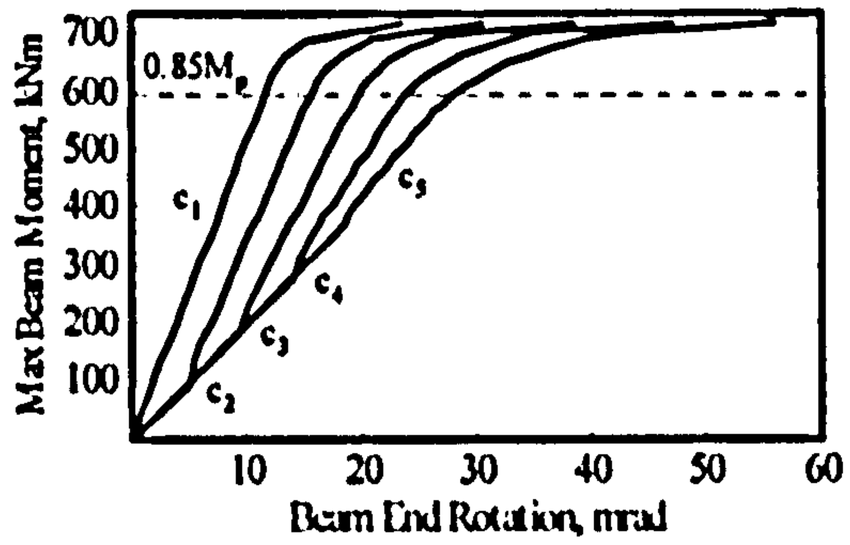

M_1=0.05M_p, M_2=0.3M_p

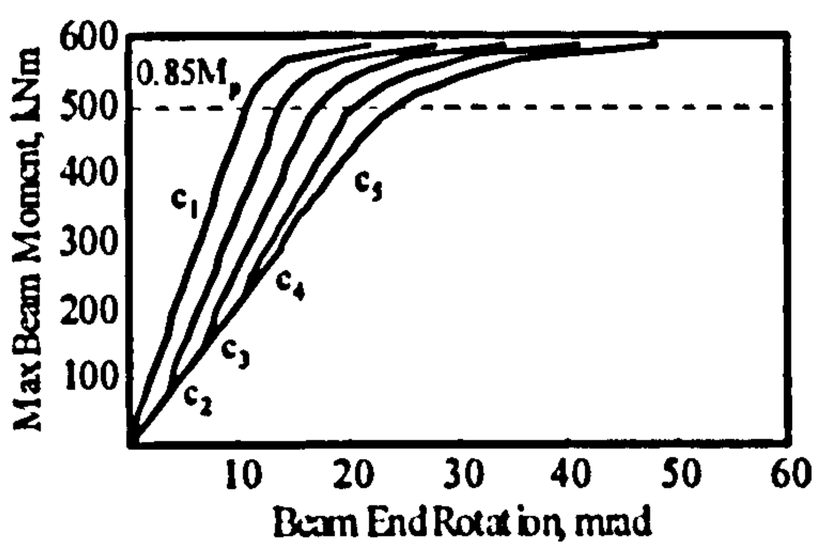

M_1=0.05M_p, M_2=0.4M_p

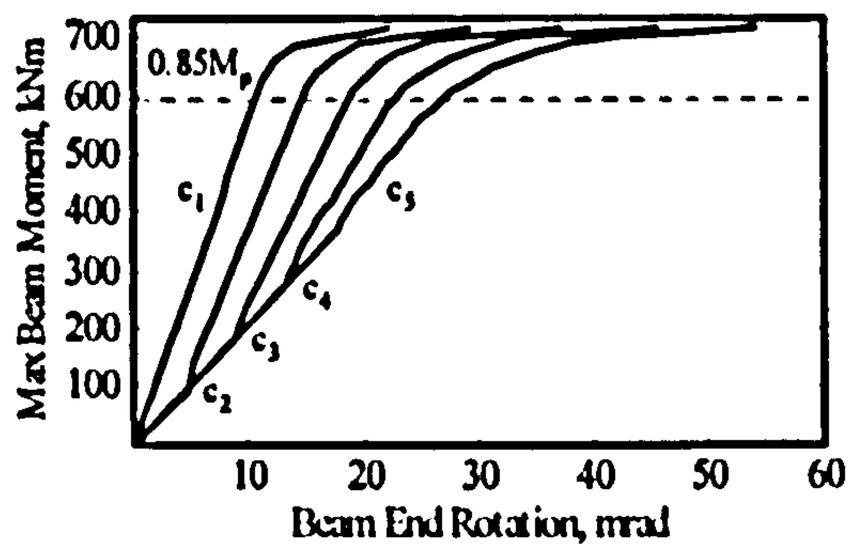

M_1=0.05M_p, M_2=0.4M_p

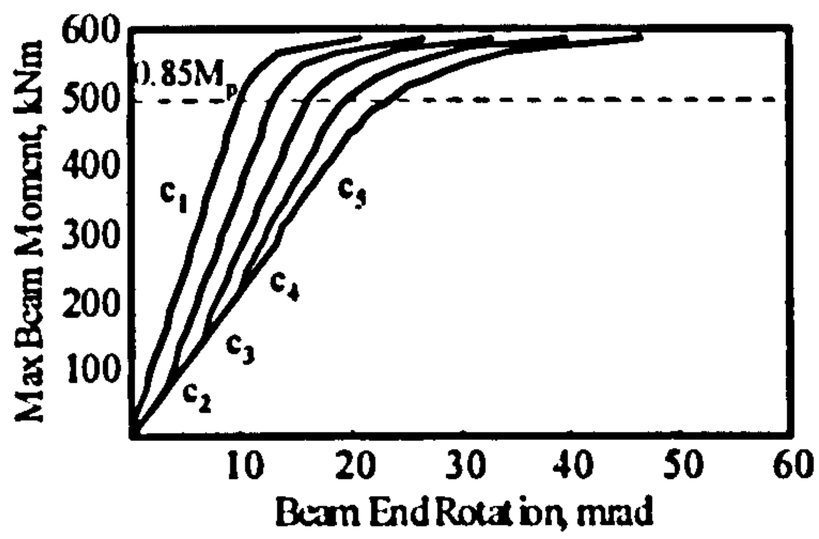

M_1=0.05M_p, M_2=0.4M_p

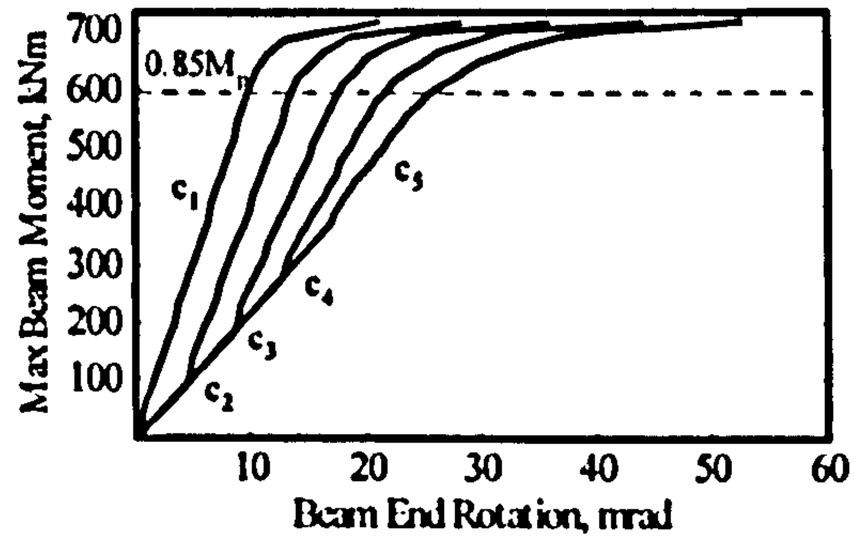

M_1=0.05M_p, M_2=0.5M_p

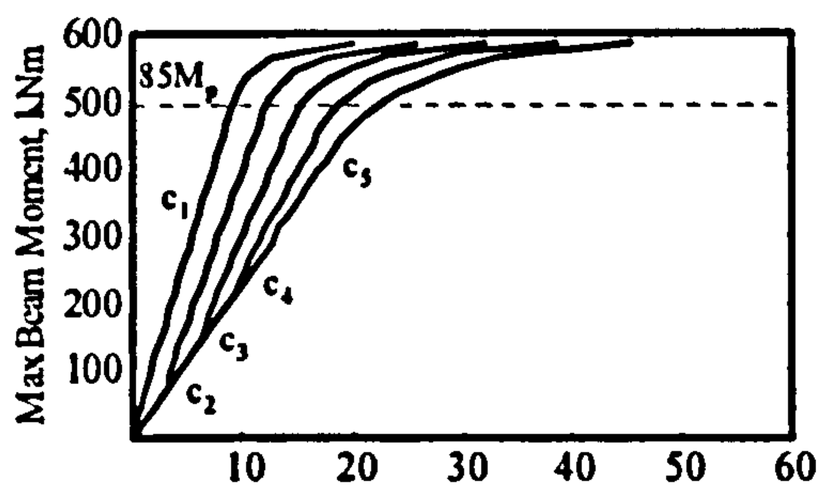

M_1=0.05M_p, M_2=0.5M_p

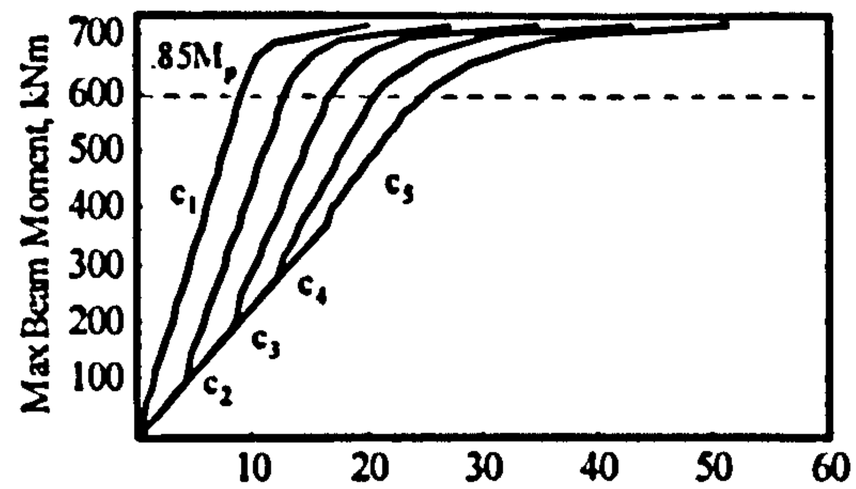

M_1=0.05M_p, M_2=0.6M_p

Grade S275

M_1=0.05M_p, M_2=0.6M_p

Grade S355

Figure C1-7. Moment vs. end rotation relationship for various maximum dead load stress levels (c_1:σ_{dl}=0; c_2:σ_{dl}=0.25σ_y; c_3:σ_{dl}=0.50σ_y; c_4:σ_{dl}=0.75σ_y; c_5:σ_{dl}=σ_y)

C.1.8 External beam, L/D=20, 3PL

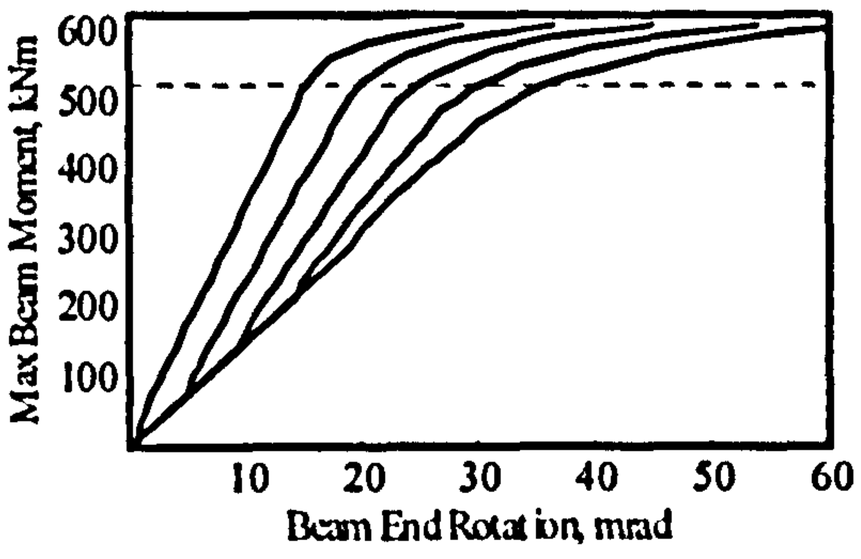

M_1=0.05M_p, M_2=0.3M_p

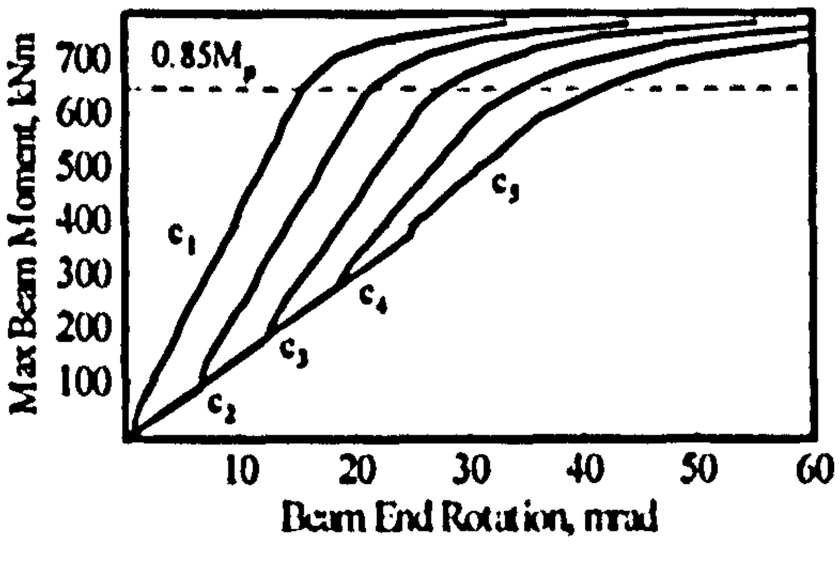

M_1=0.05M_p, M_2=0.3M_p

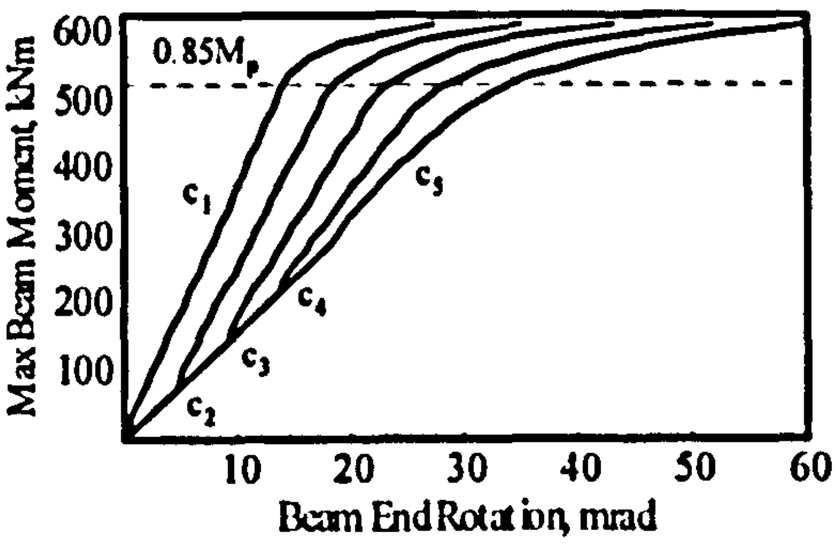

M_1=0.05M_p, M_2=0.4M_p

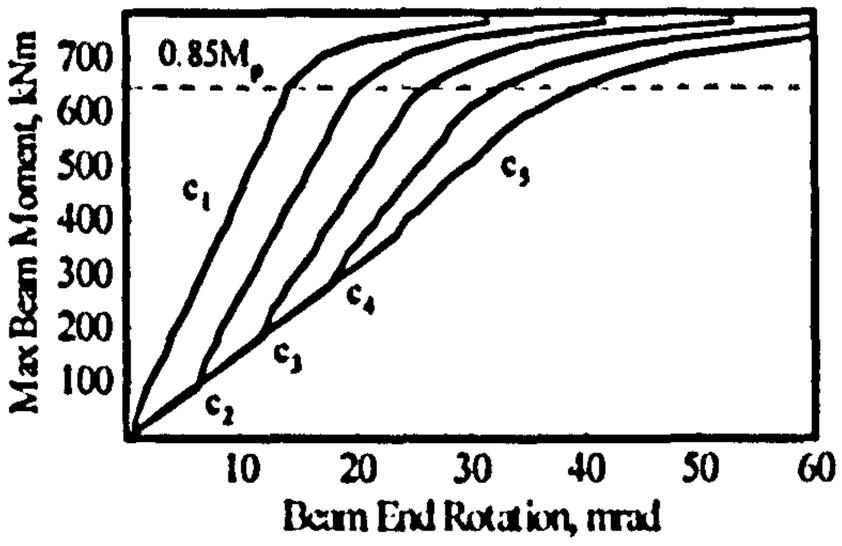

M_1=0.05M_p, M_2=0.4M_p

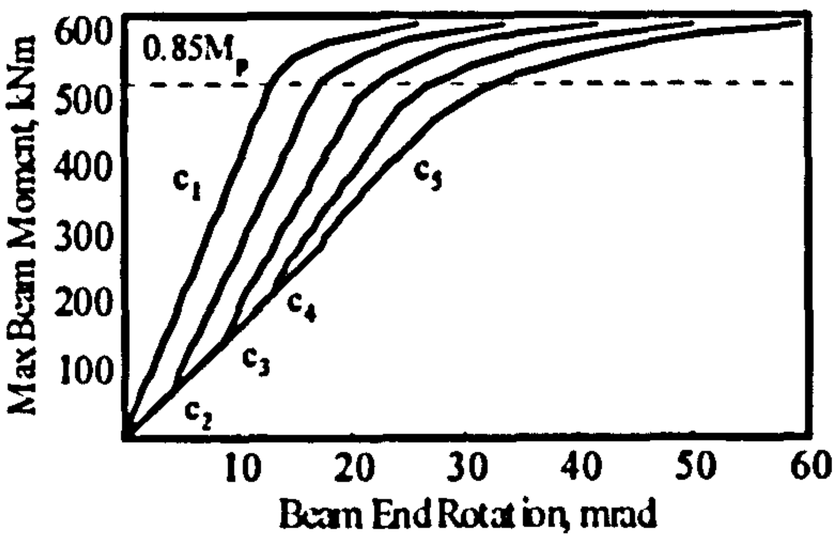

M_1=0.05M_p, M_2=0.5M_p

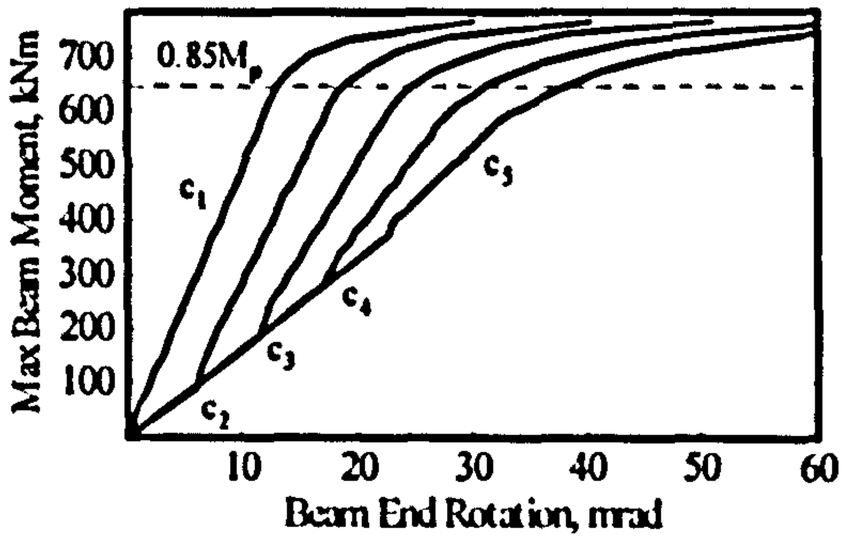

M_1=0.05M_p, M_2=0.5M_p

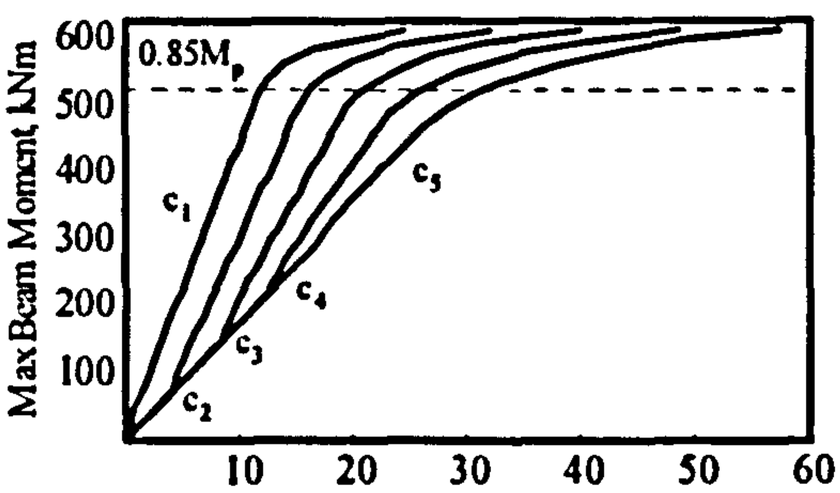

M_1=0.05M_p, M_2=0.6M_p

Grade S275

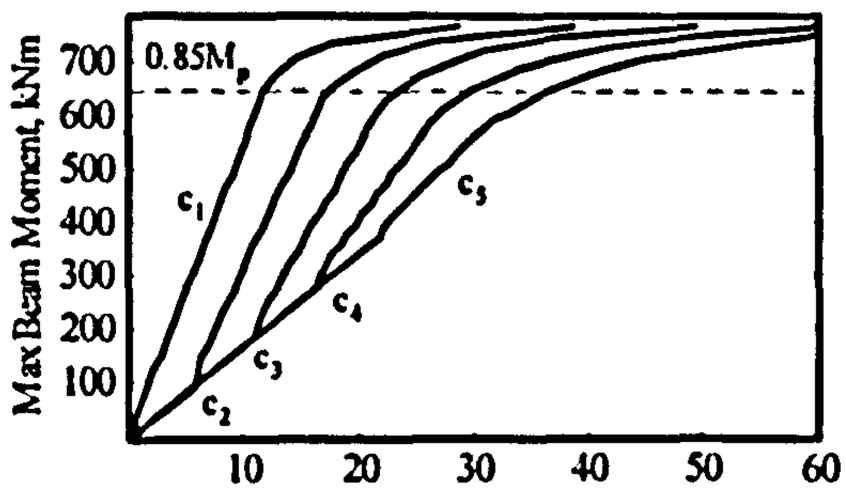

M_1=0.05M_p, M_2=0.6M_p

Grade S355

Figure C1-8. Moment vs. end rotation relationship for various maximum dead load stress levels (c_1:σ_{dl}=0; c_2:σ_{dl}=0.25σ_y; c_3:σ_{dl}=0.50σ_y; c_4:σ_{dl}=0.75σ_y; c_5:σ_{dl}=σ_y)

C.1.9 External beam, L/D=25, 3PL

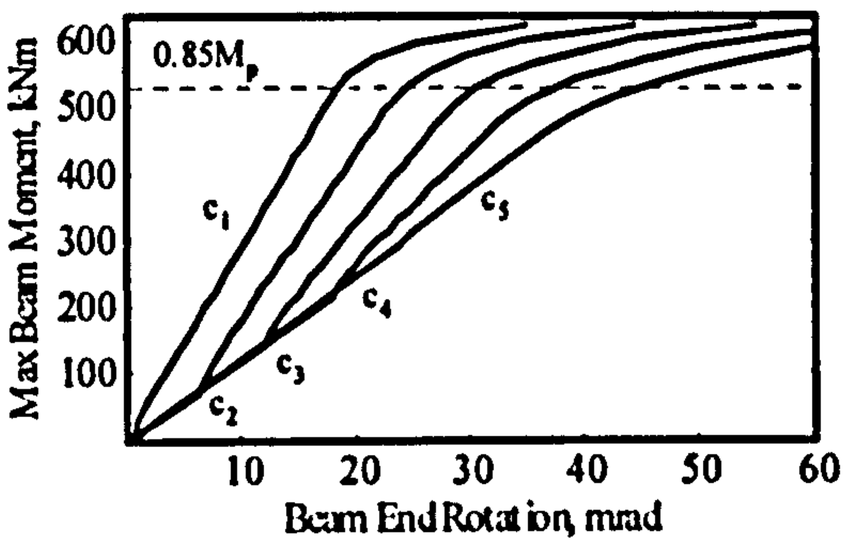

M_1=0.05M_p, M_2=0.3M_p

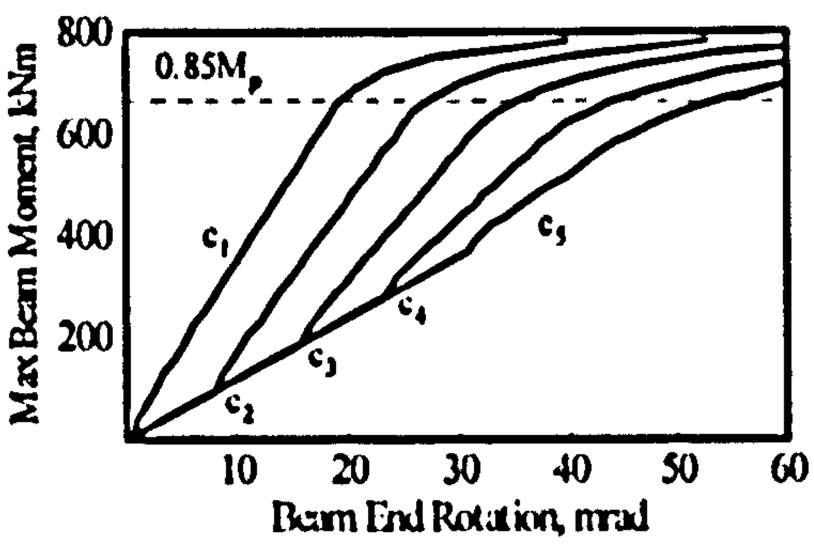

M_1=0.05M_p, M_2=0.3M_p

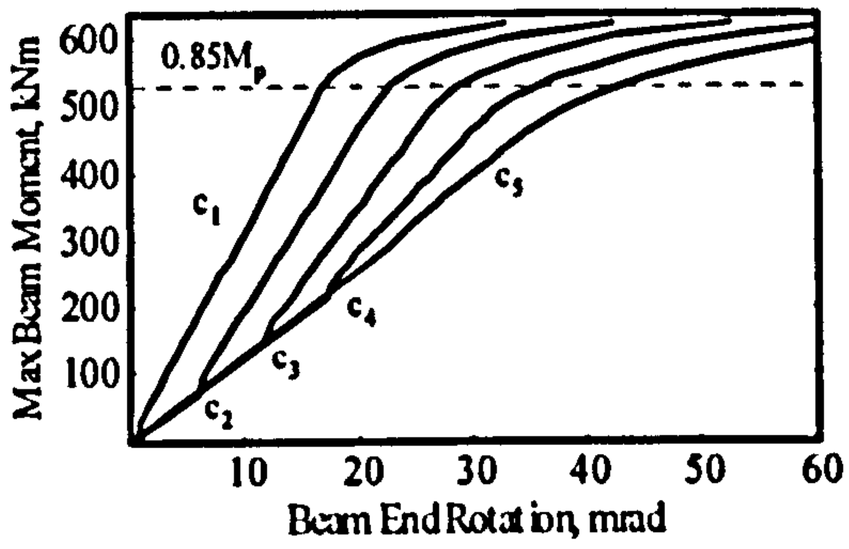

M_1=0.05M_p, M_2=0.4M_p

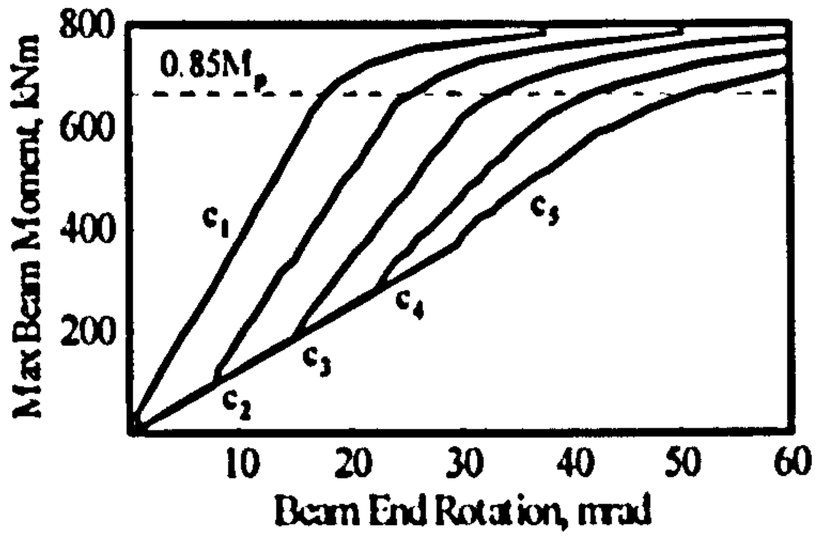

M_1=0.05M_p, M_2=0.4M_p

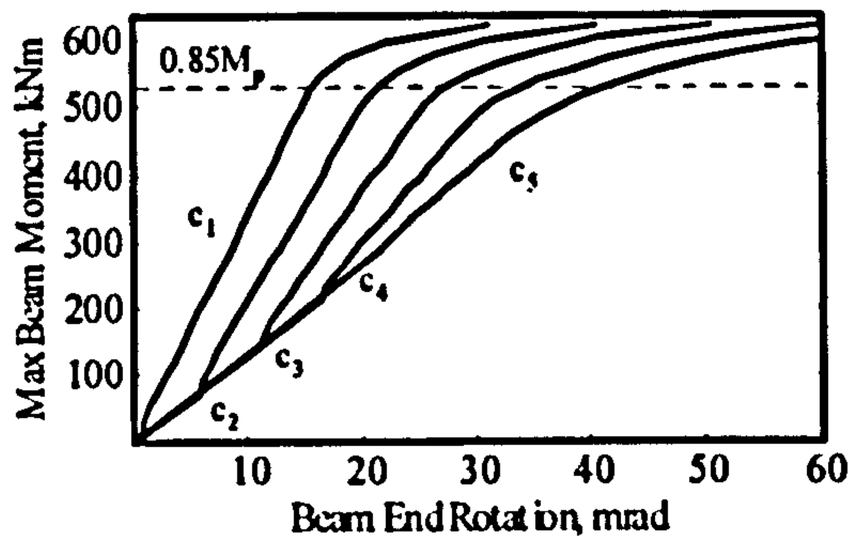

M_1=0.05M_p, M_2=0.4M_p

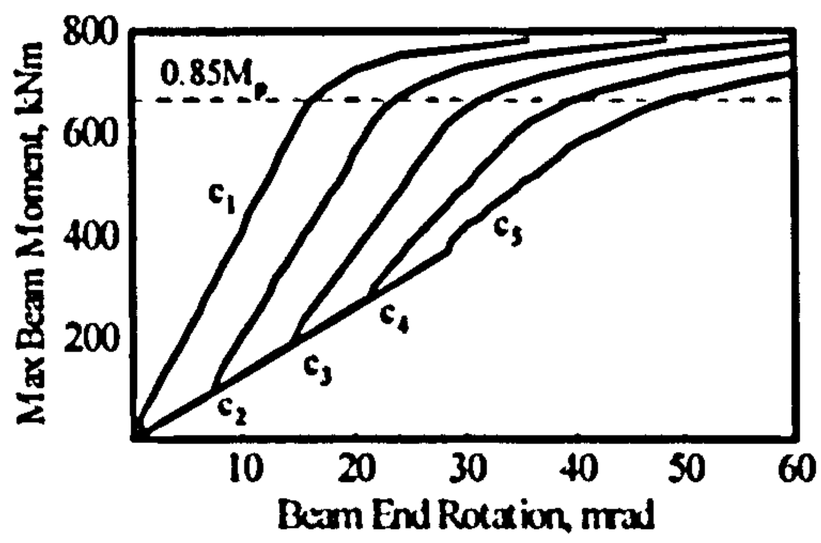

M_1=0.05M_p, M_2=0.5M_p

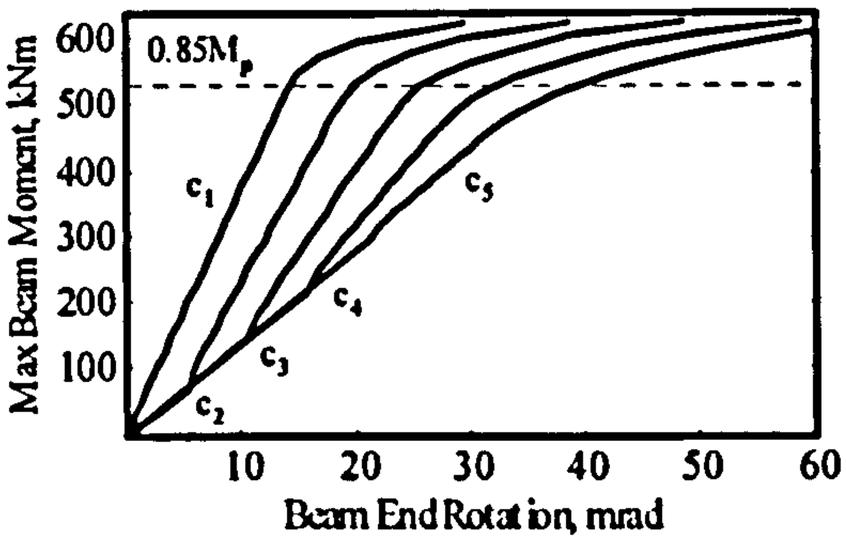

M_1=0.05M_p, M_2=0.5M_p

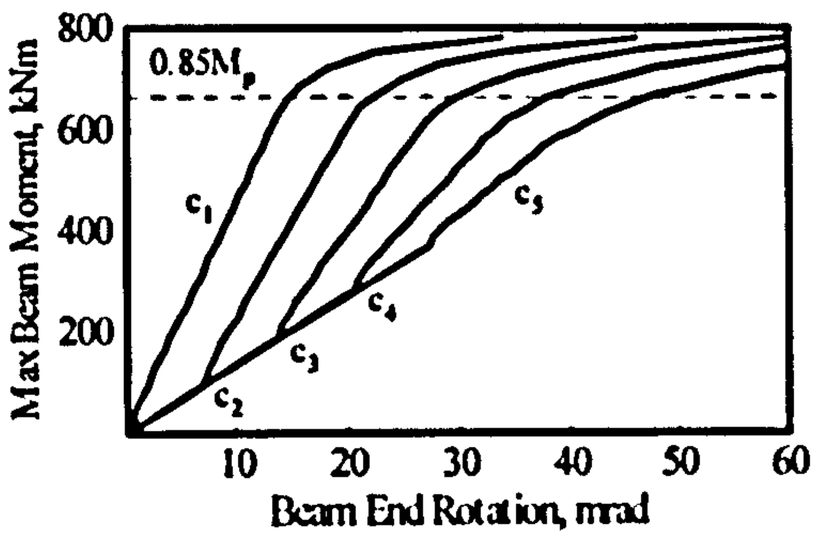

M_1=0.05M_p, M_2=0.6M_p

Grade S275

M_1=0.05M_p, M_2=0.6M_p

Grade S355

Figure C1-9. Moment vs. end rotation relationship for various maximum dead load stress levels (c_1: σ_{dl}=0; c_2: σ_{dl}=0.25σ_y; c_3: σ_{dl}=0.50σ_y; c_4: σ_{dl}=0.75σ_y; c_5: σ_{dl}=σ_y)

C.1.10 Internal beam, L/D=15, 3PL

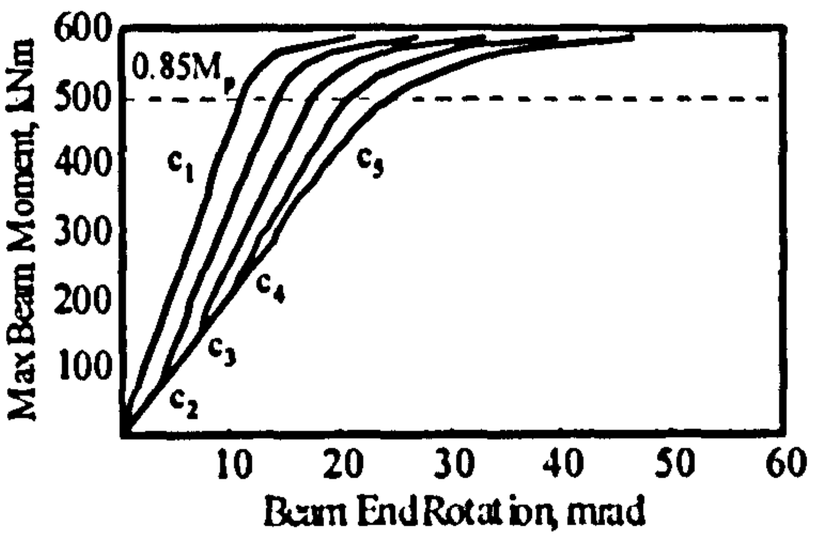

M_1=0.3M_p, M_2=0.3M_p

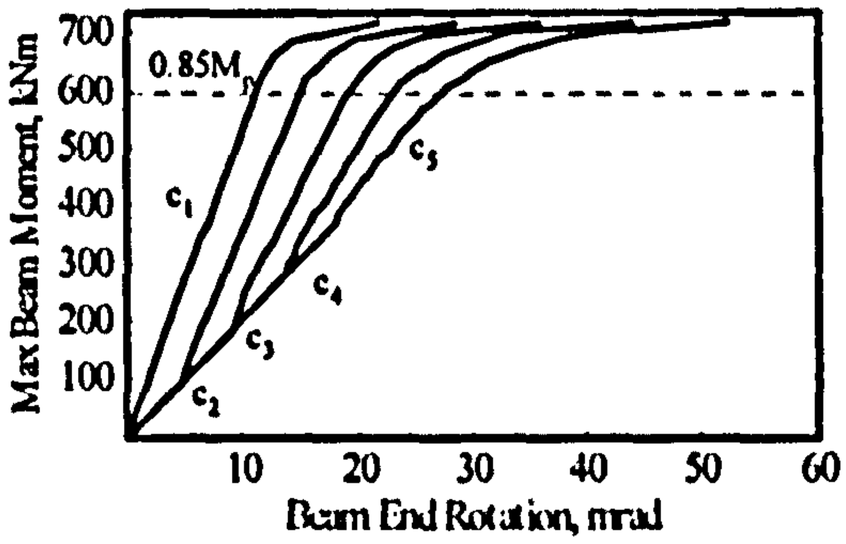

M_1=0.3M_p, M_2=0.3M_p

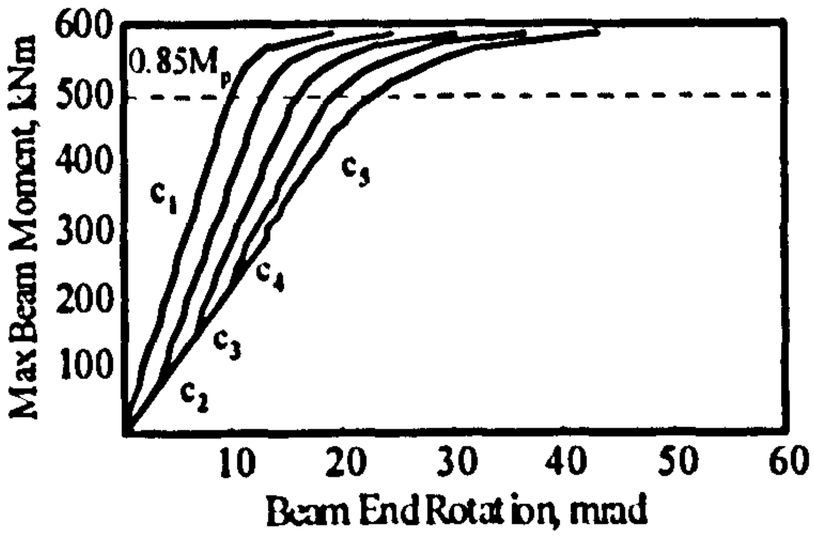

M_1=0.4M_p, M_2=0.4M_p

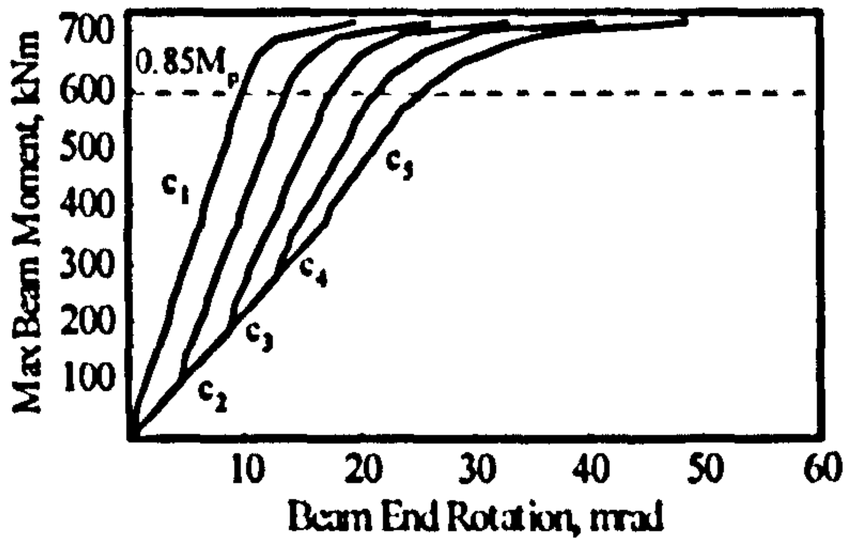

M_1=0.4M_p, M_2=0.4M_p

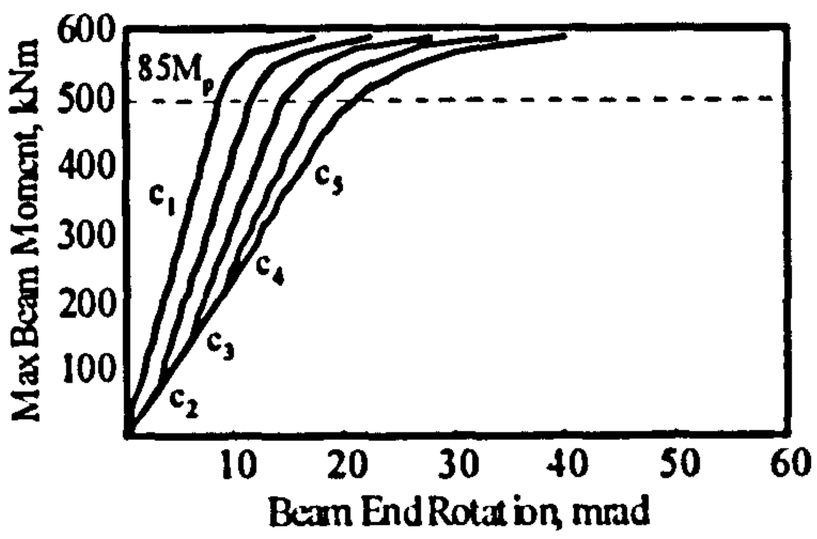

M_1=0.4M_p, M_2=0.4M_p

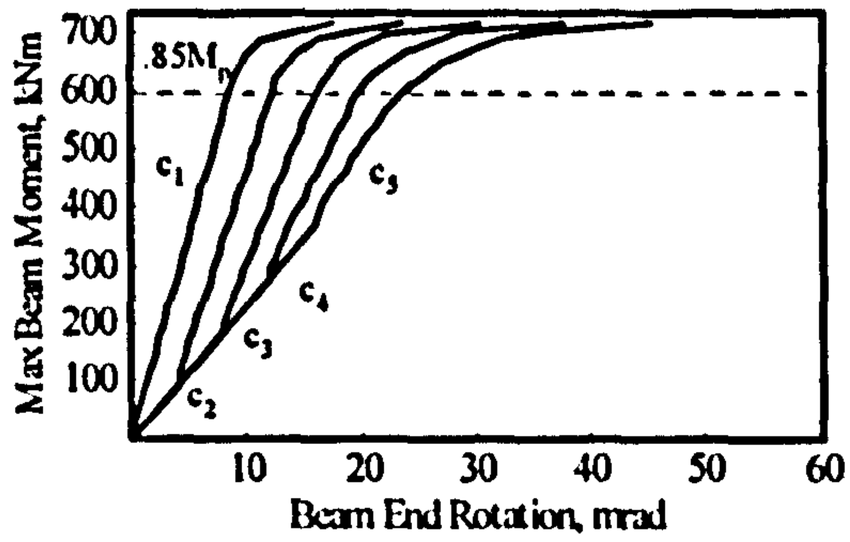

M_1=0.5M_p, M_2=0.5M_p

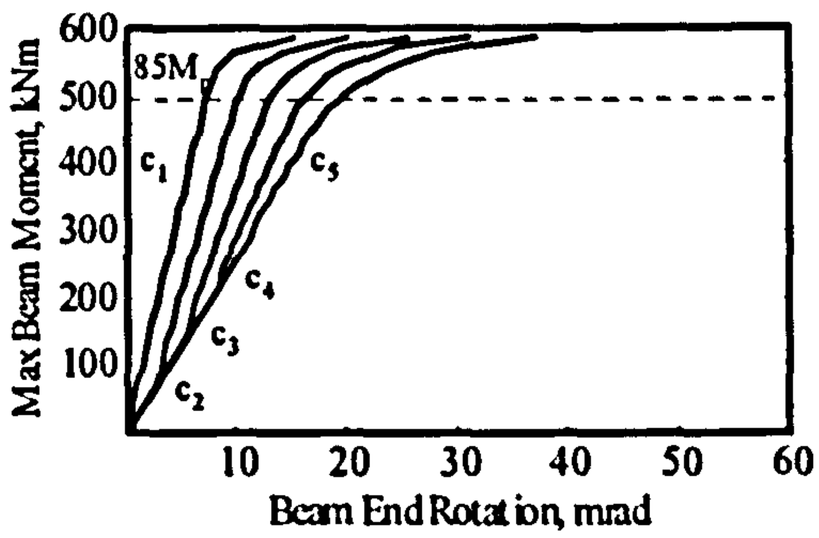

M_1=0.5M_p, M_2=0.5M_p

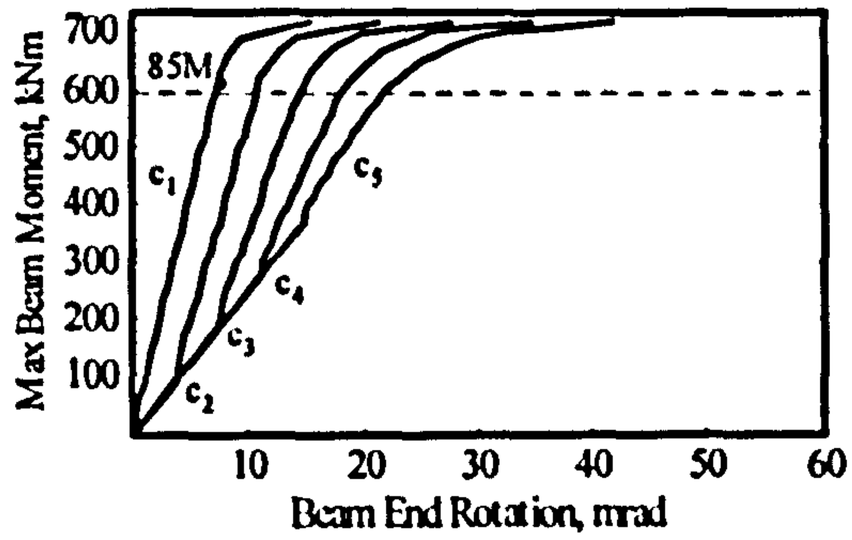

M_1=0.6M_p, M_2=0.6M_p

Grade S275

M_1=0.6M_p, M_2=0.6M_p

Grade S355

Figure C1-10. Moment vs. end rotation relationship for various maximum dead load stress levels (c_1: σ_{dl}=0; c_2: σ_{dl}=0.25σ_y; c_3: σ_{dl}=0.50σ_y; c_4: σ_{dl}=0.75σ_y; c_5: σ_{dl}=σ_y)

C.1.11 Internal beam, L/D=20, 3PL

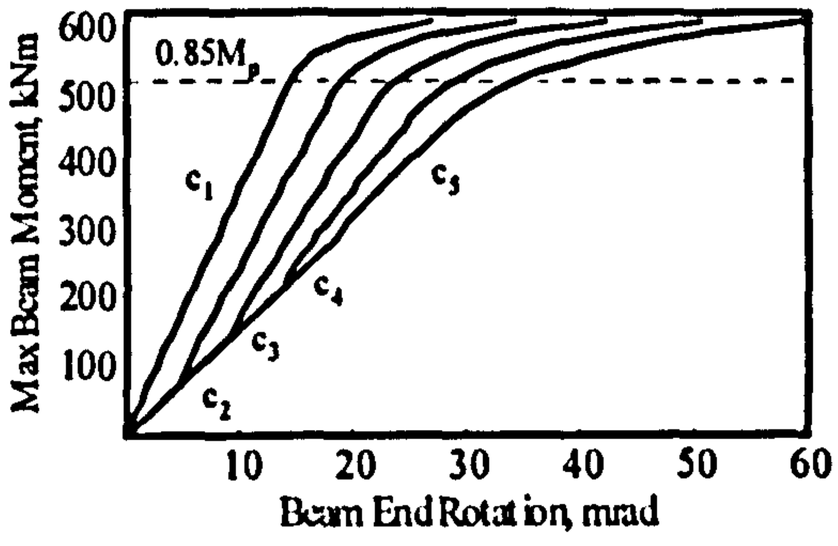

M_1=0.3M_p, M_2=0.3M_p

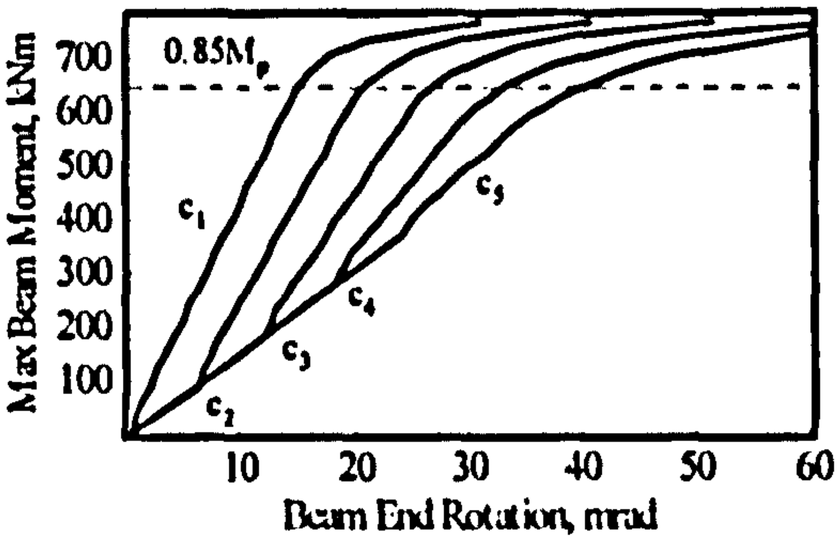

M_1=0.3M_p, M_2=0.3M_p

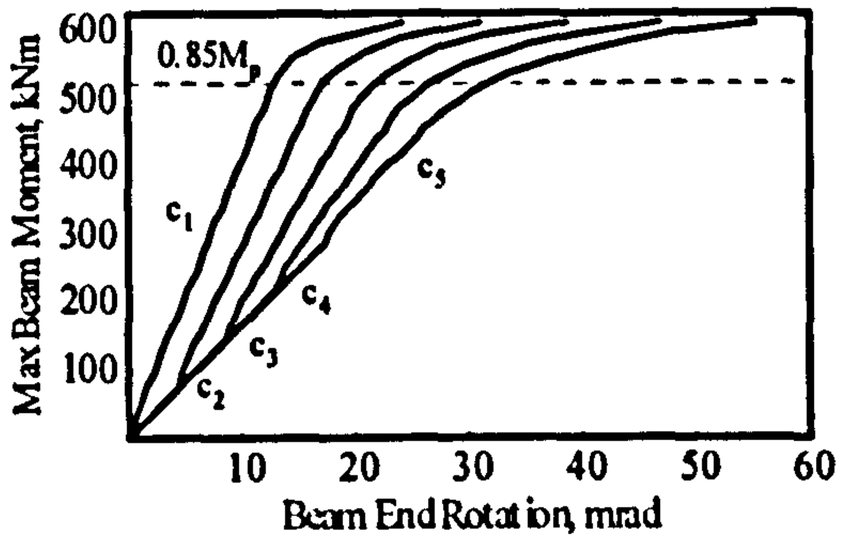

M_1=0.4M_p, M_2=0.4M_p

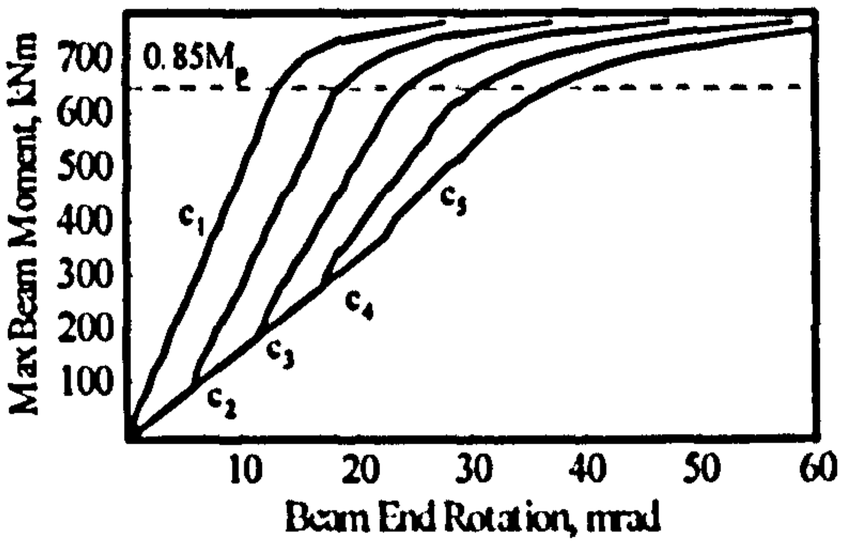

M_1=0.4M_p, M_2=0.4M_p

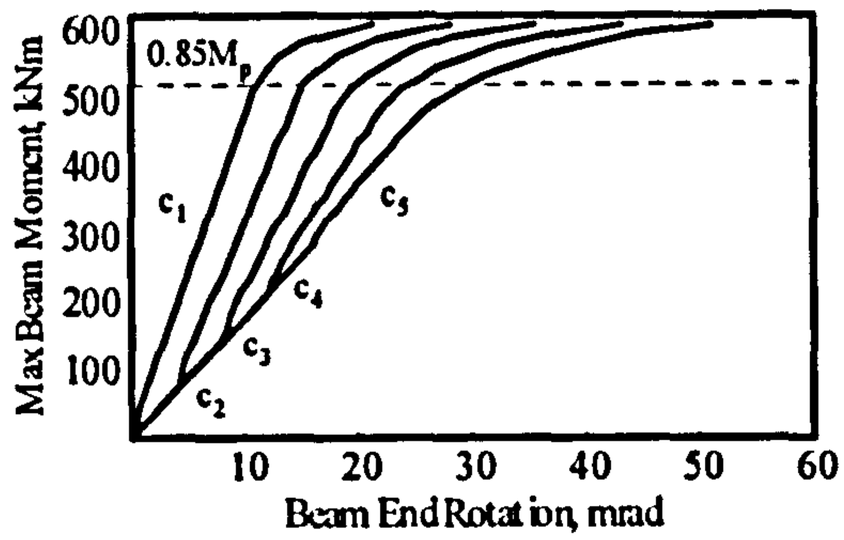

M_1=0.5M_p, M_2=0.5M_p

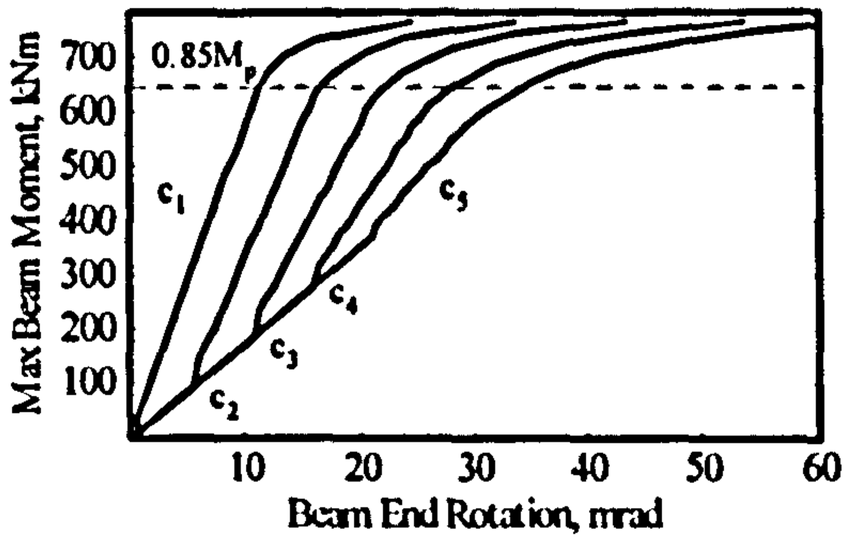

M_1=0.5M_p, M_2=0.5M_p

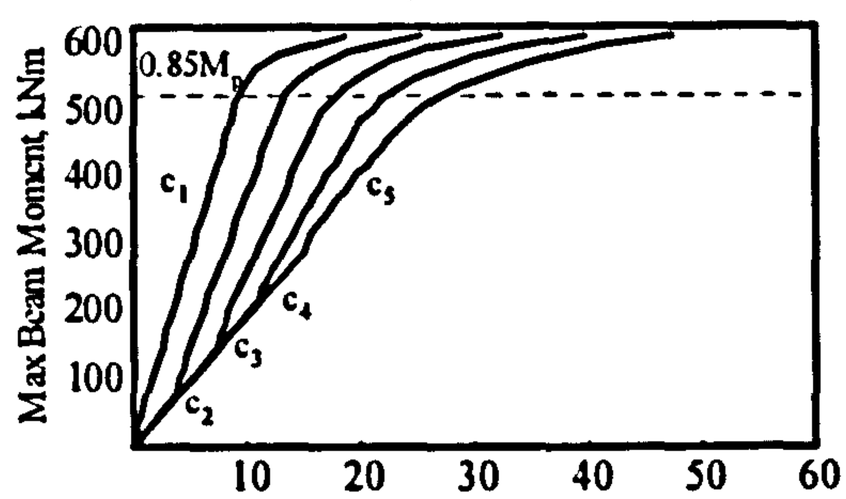

M_1=0.6M_p, M_2=0.6M_p

Grade S275

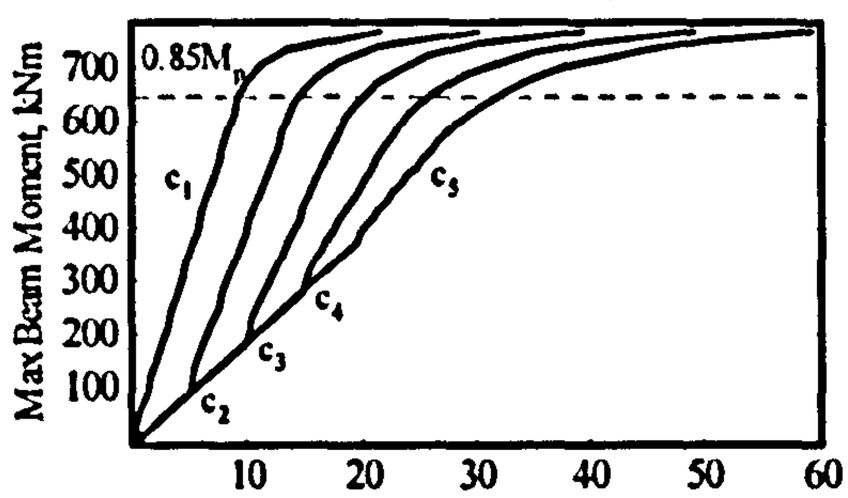

M_1=0.6M_p, M_2=0.6M_p

Grade S355

Figure C1-11. Moment vs. end rotation relationship for various maximum dead load stress levels (c_1:σ_{dl}=0; c_2:σ_{dl}=0.25σ_y; c_3:σ_{dl}=0.50σ_y; c_4:σ_{dl}=0.75σ_y; c_5:σ_{dl}=σ_y)

C.1.12 Internal beam, L/D=25, 3PL

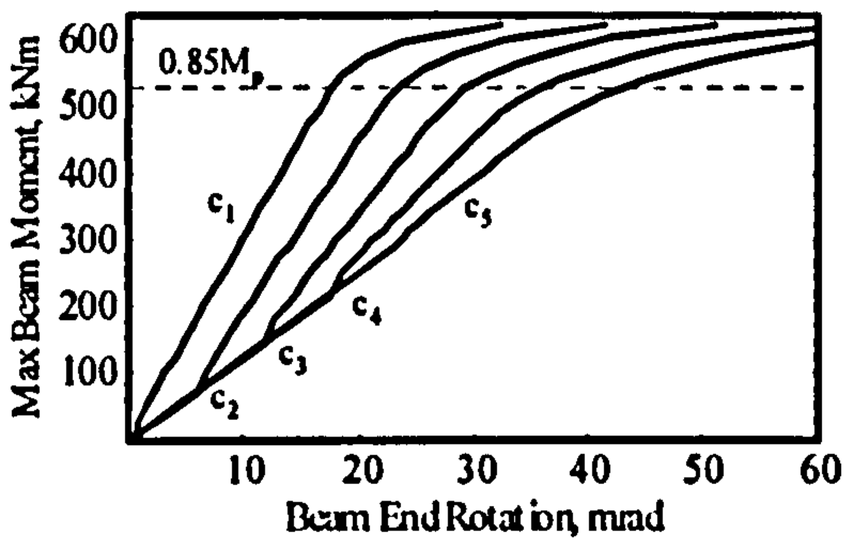

M_1=0.3M_p, M_2=0.3M_p

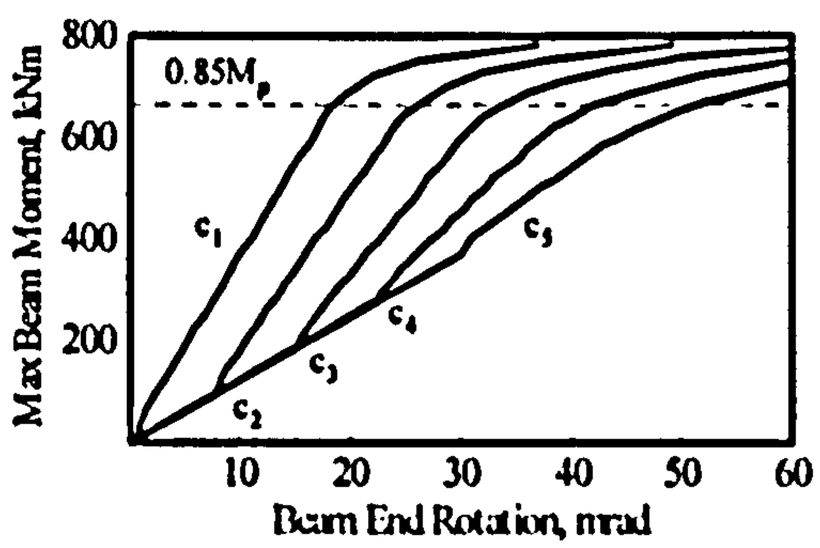

M_1=0.3M_p, M_2=0.3M_p

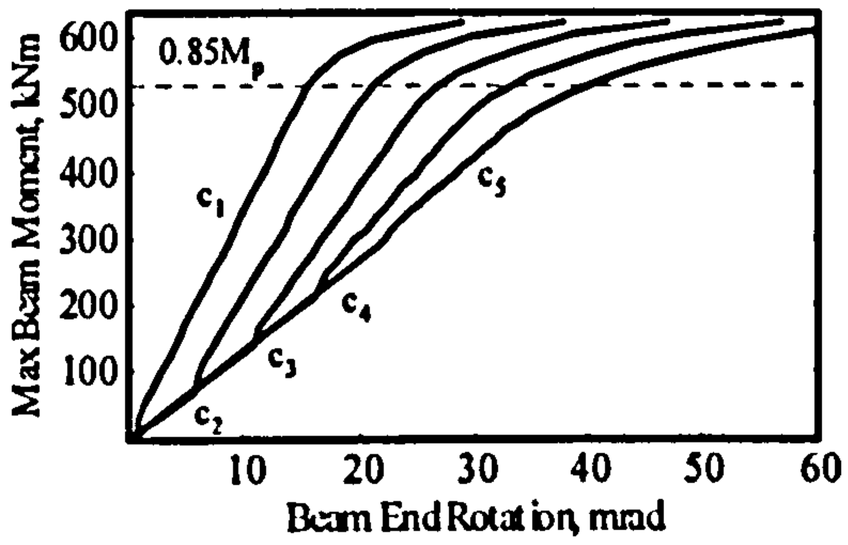

M_1=0.4M_p, M_2=0.4M_p

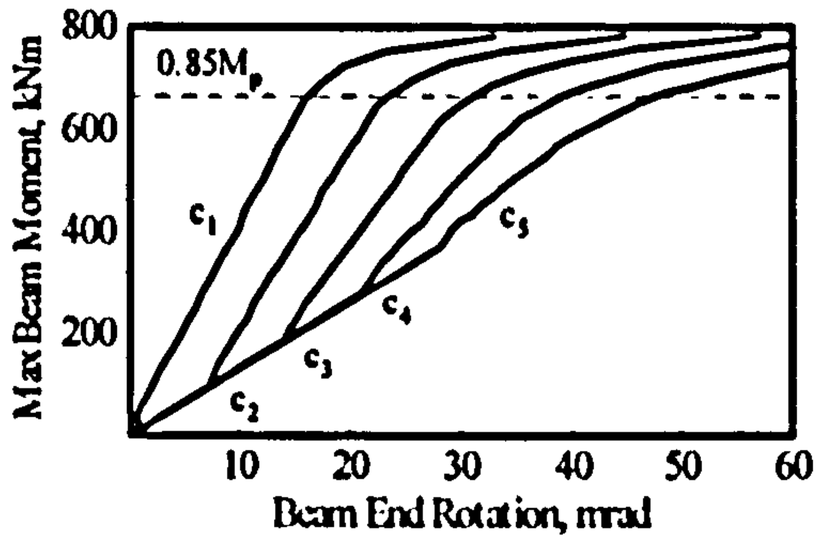

M_1=0.4M_p, M_2=0.4M_p

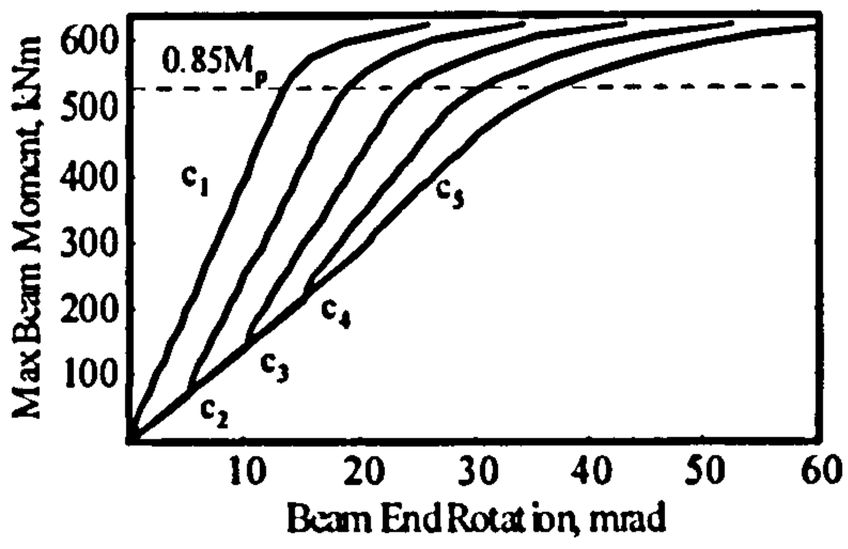

M_1=0.5M_p, M_2=0.5M_p

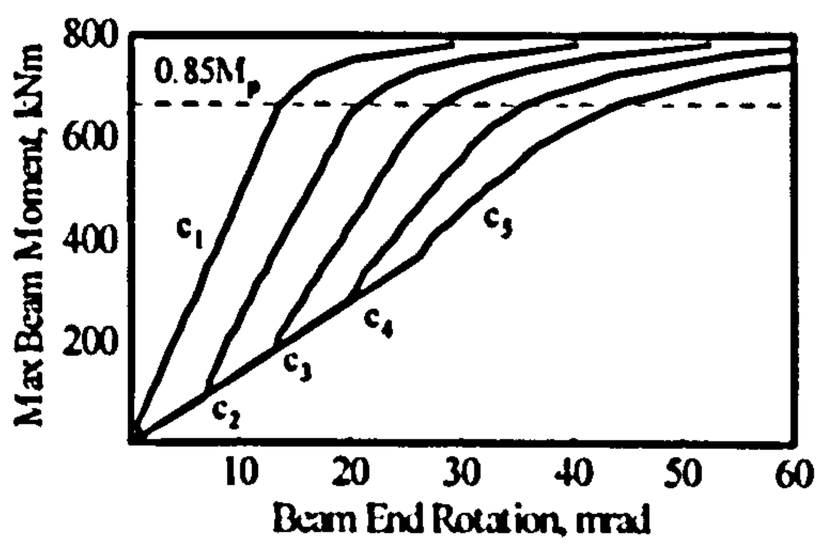

M_1=0.5M_p, M_2=0.5M_p

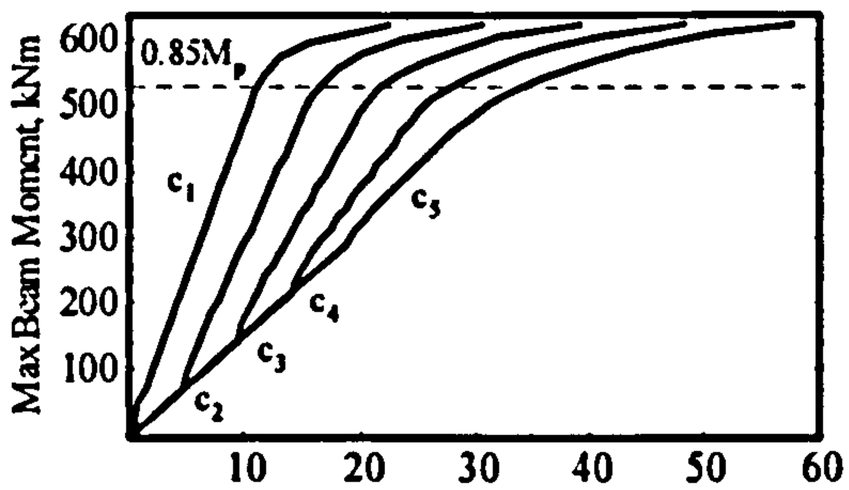

M_1=0.6M_p, M_2=0.6M_p

Grade S275

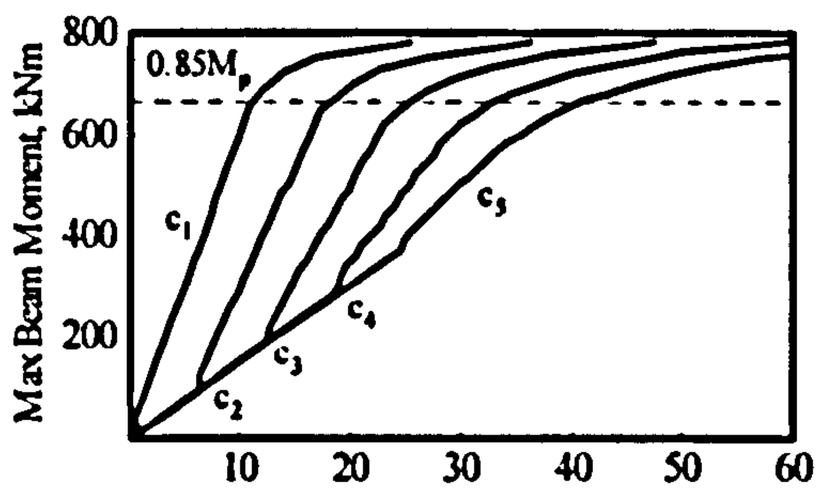

M_1=0.6M_p, M_2=0.6M_p

Grade S355

Figure C1-12. Moment vs. end rotation relationship for various maximum dead load stress levels (c_1:σ_{dl}=0; c_2:σ_{dl}=0.25σ_y; c_3:σ_{dl}=0.50σ_y; c_4:σ_{dl}=0.75σ_y; c_5:σ_{dl}=σ_y)

C.1.13 External beam, L/D=15, UDL

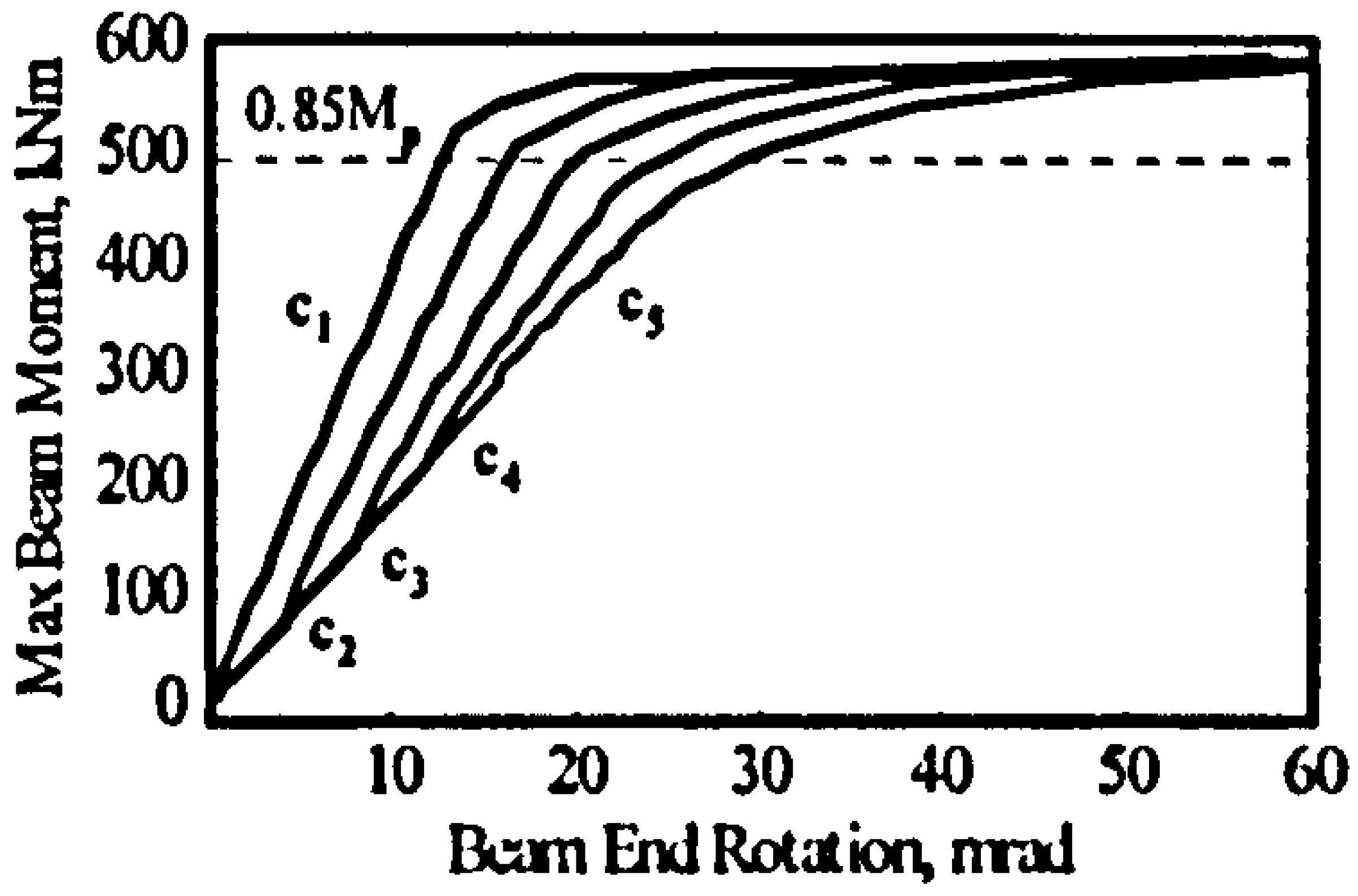

M_1=0.05M_p, M_2=0.3M_p

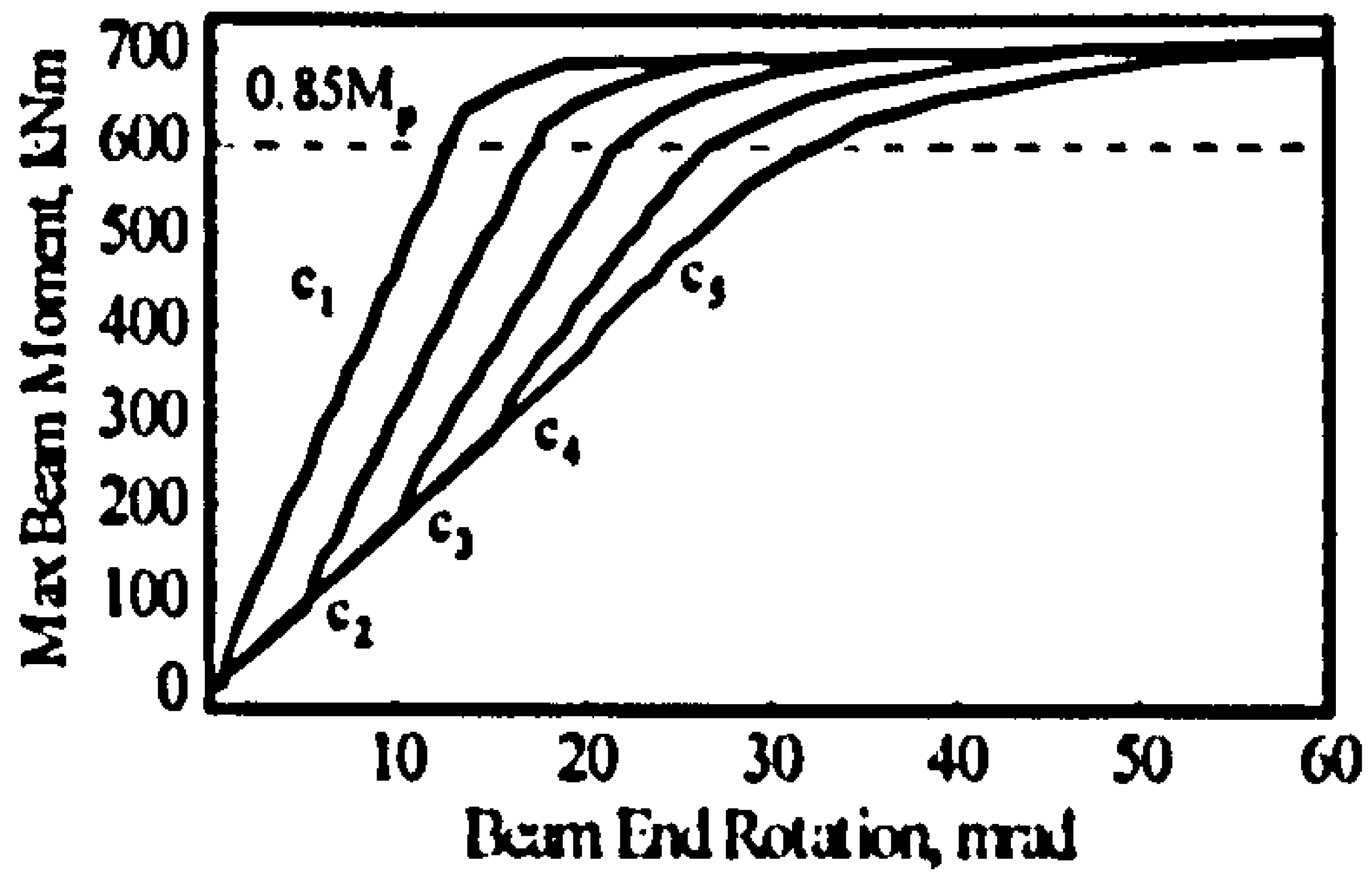

M_1=0.05M_p, M_2=0.3M_p

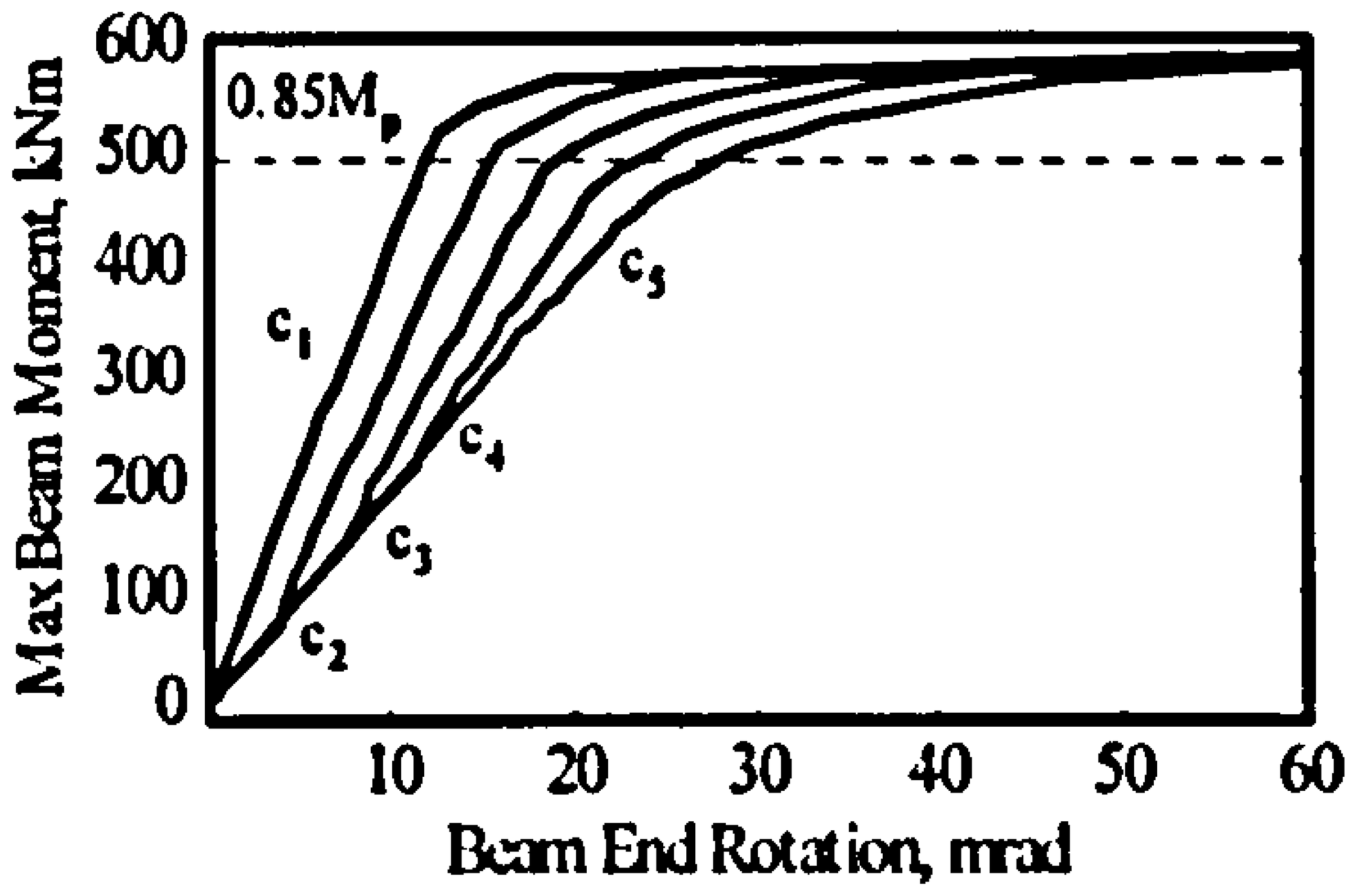

M_1=0.05M_p, M_2=0.4M_p

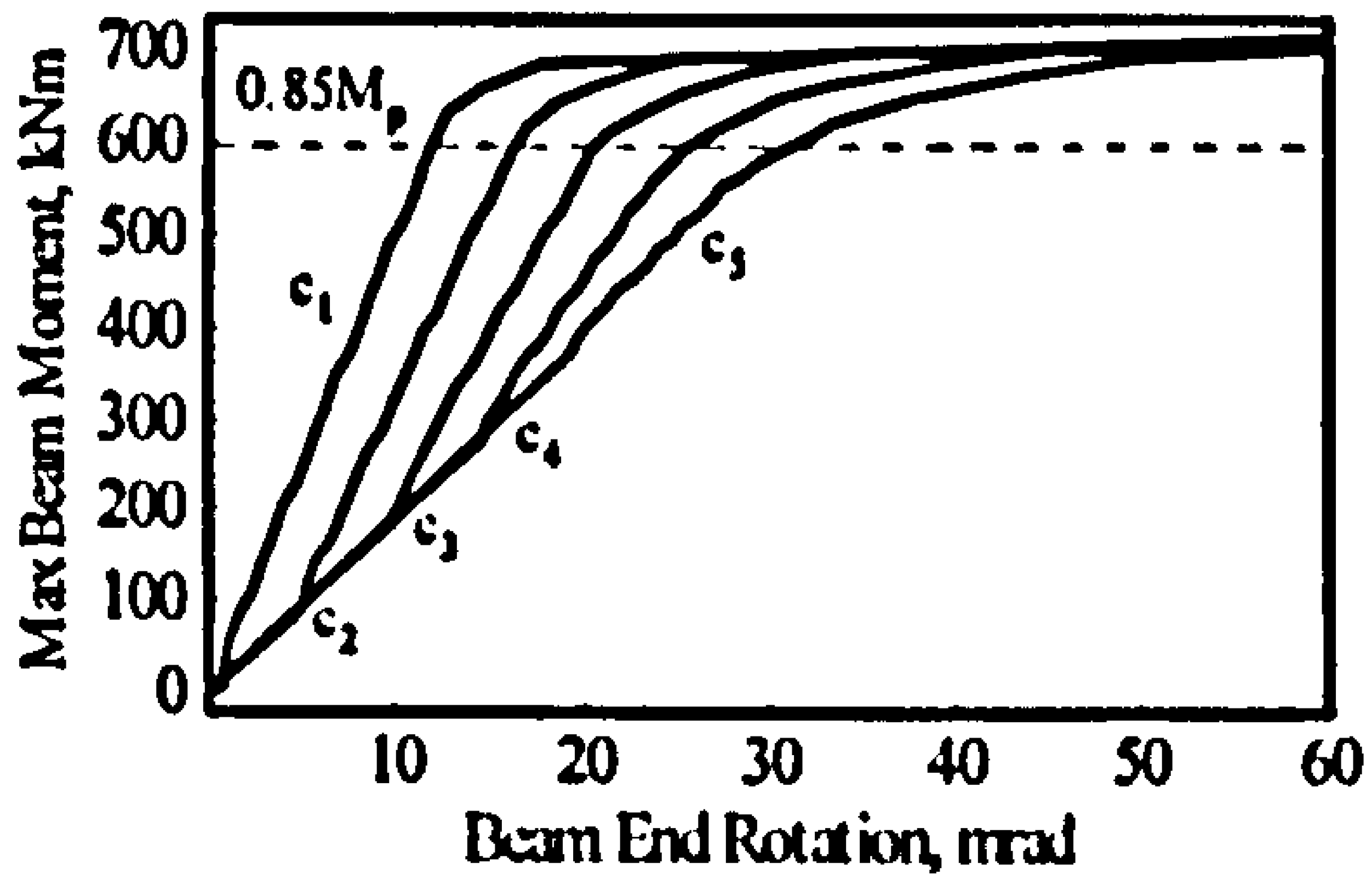

M_1=0.05M_p, M_2=0.4M_p

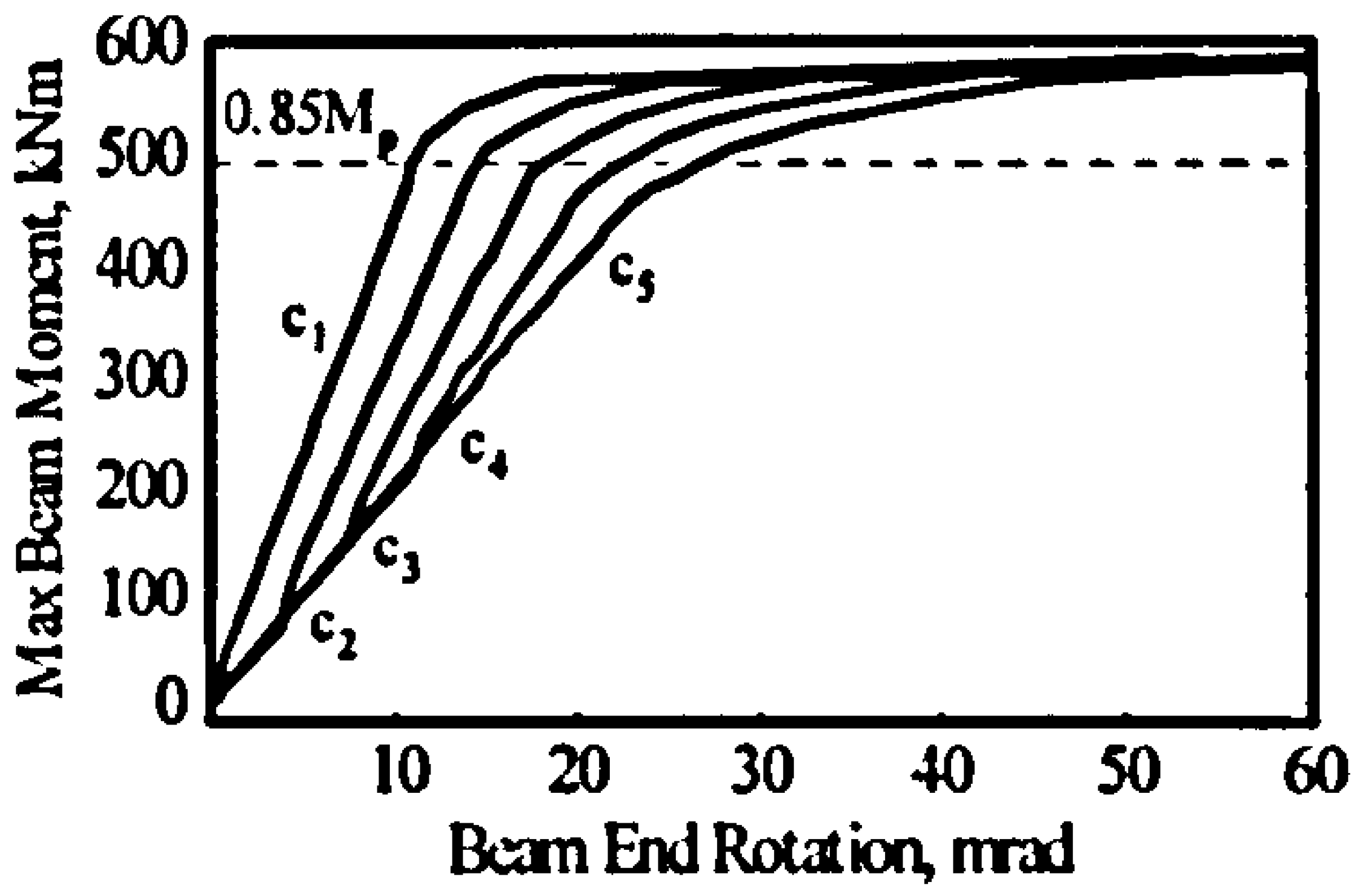

M_1=0.05M_p, M_2=0.5M_p

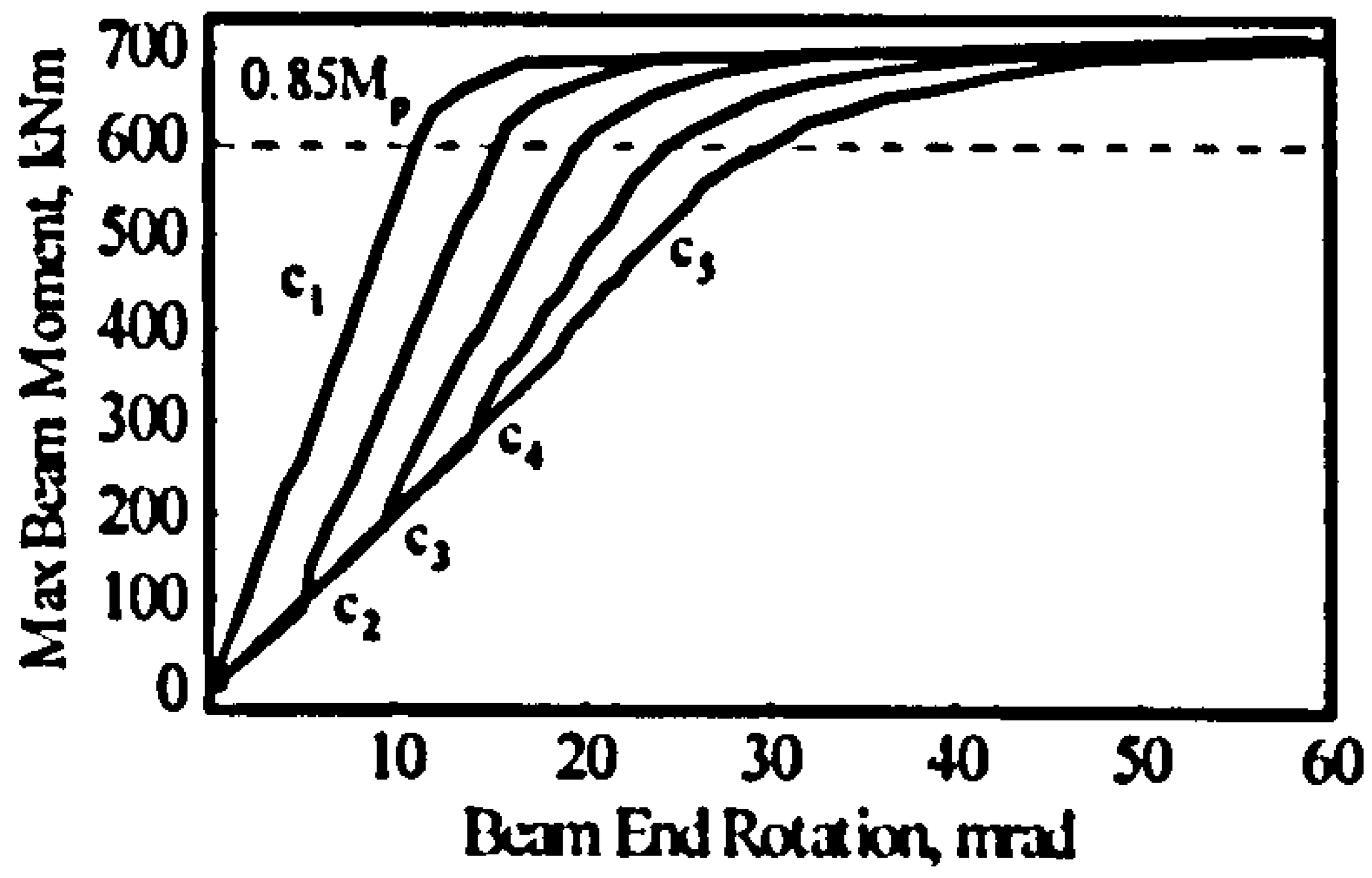

M_1=0.05M_p, M_2=0.5M_p

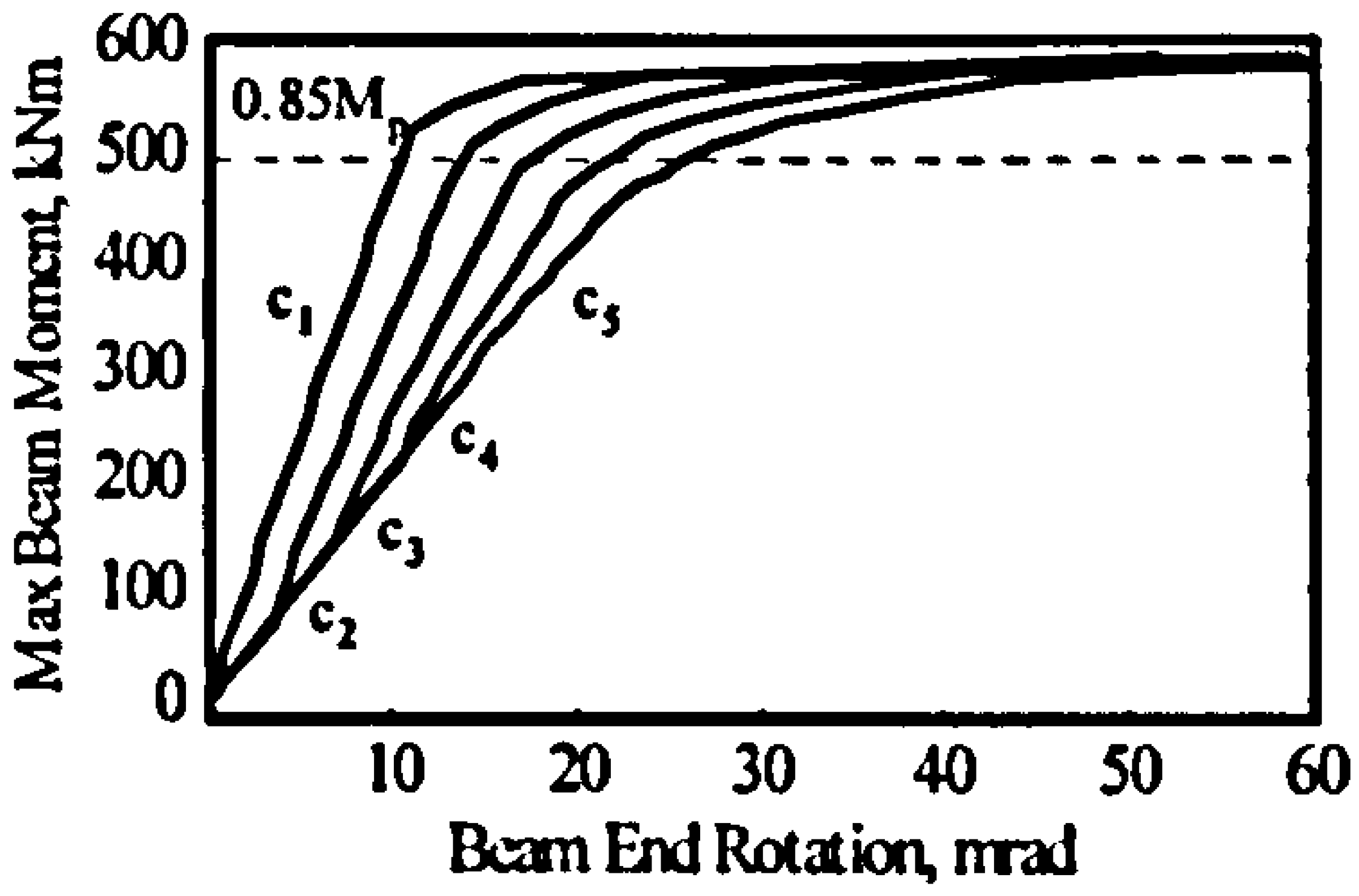

M_1=0.05M_p, M_2=0.6M_p

Grade S275

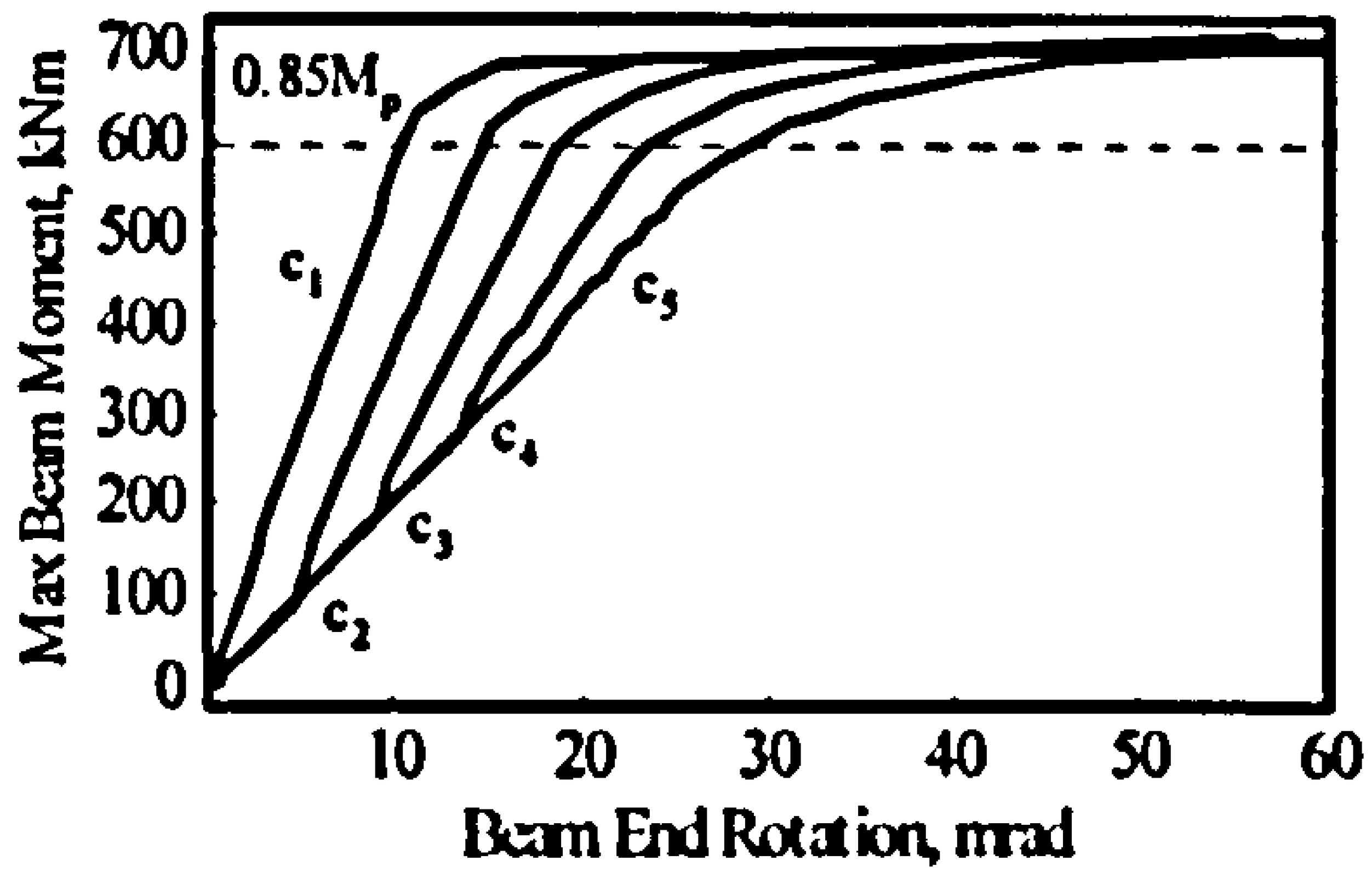

M_1=0.05M_p, M_2=0.6M_p

Grade S355

Figure C1-13. Moment vs. end rotation relationship for various maximum dead load stress levels (c_1:σ_{dl}=0; c_2:σ_{dl}=0.25σ_y; c_3:σ_{dl}=0.50σ_y; c_4:σ_{dl}=0.75σ_y; c_5:σ_{dl}=σ_y)

C.1.14 External beam, L/D=20, UDL

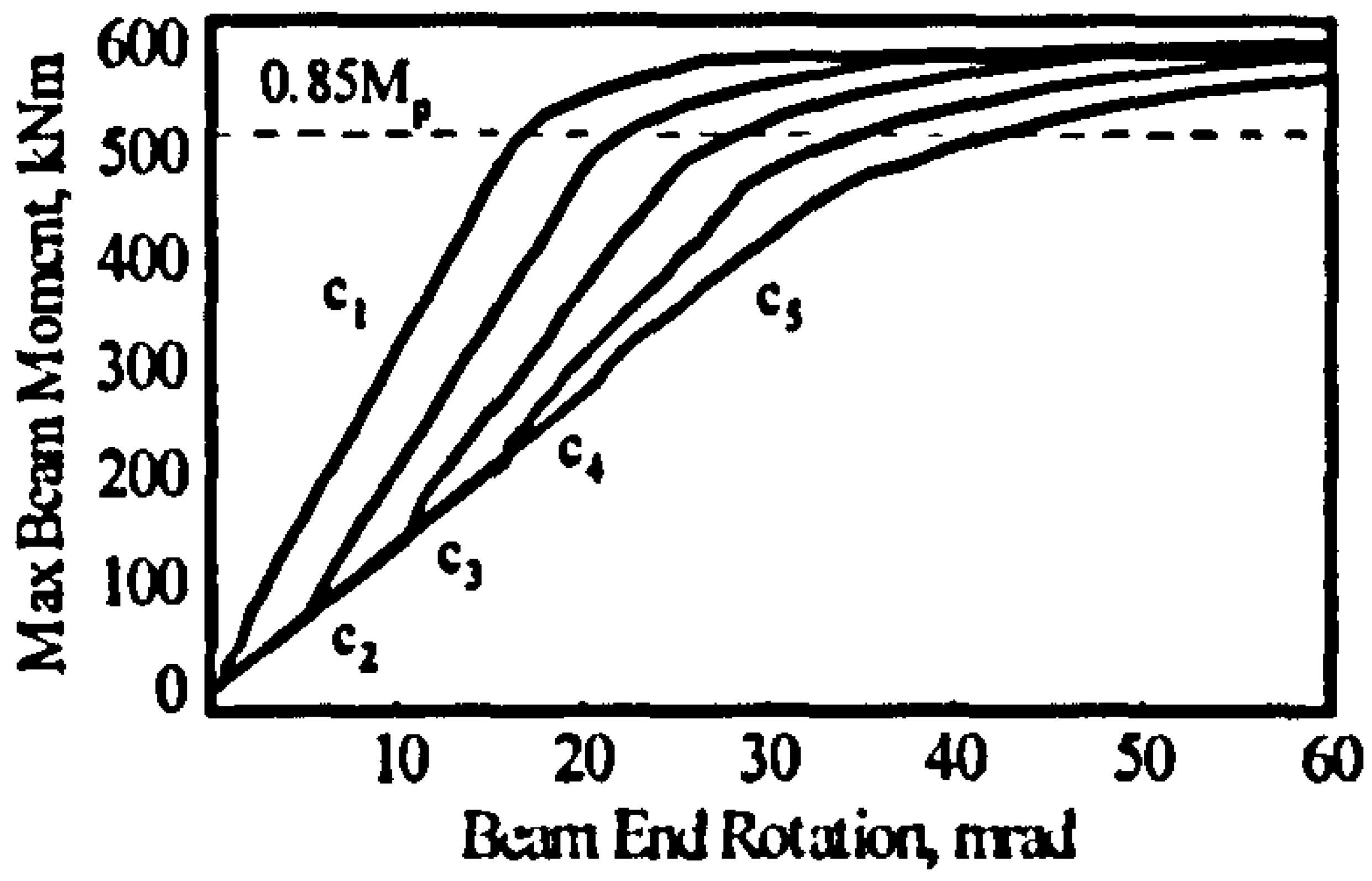

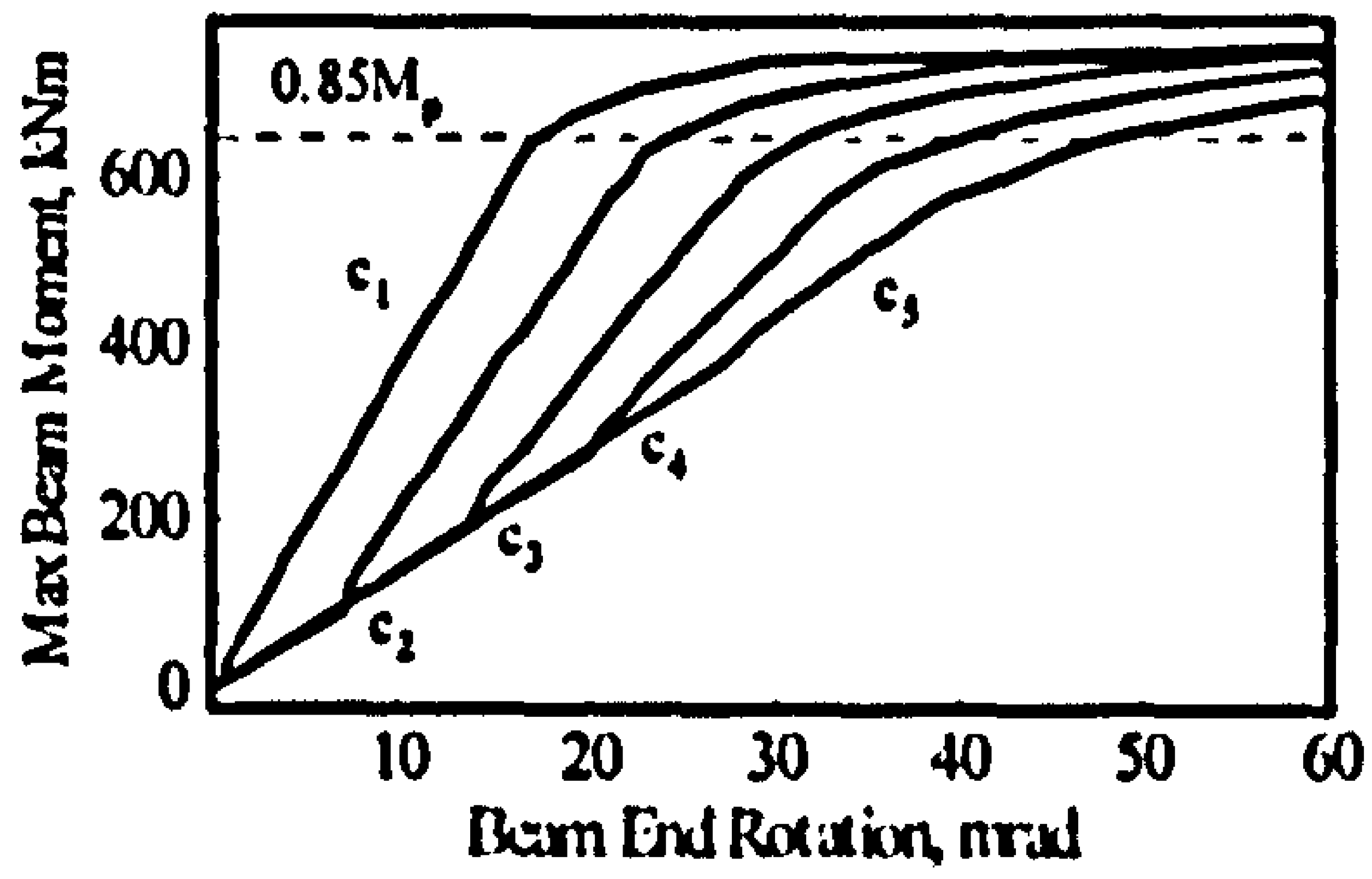

M_1=0.05M_p, M_2=0.3M_p

M_1=0.05M_p, M_2=0.3M_p

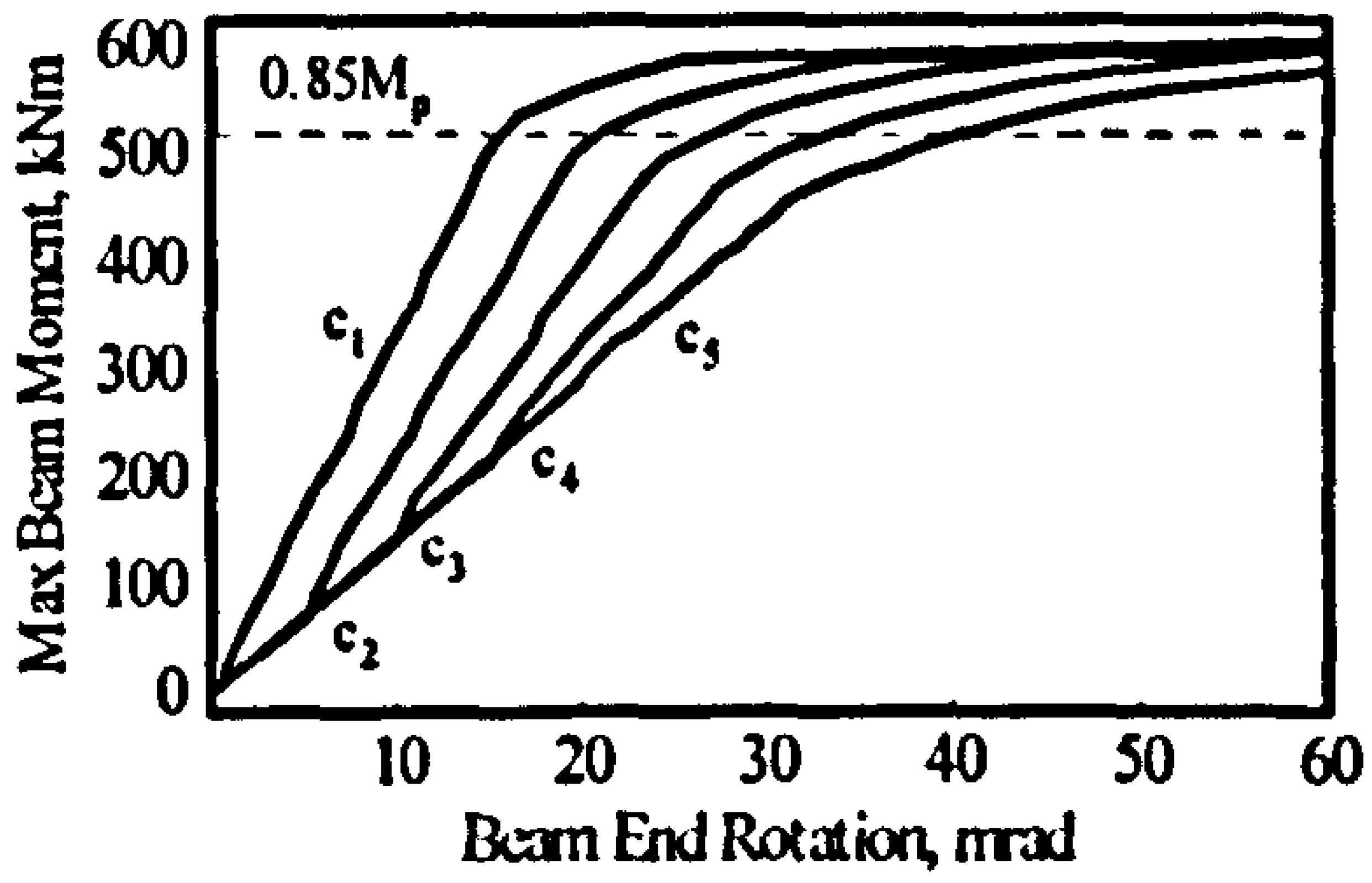

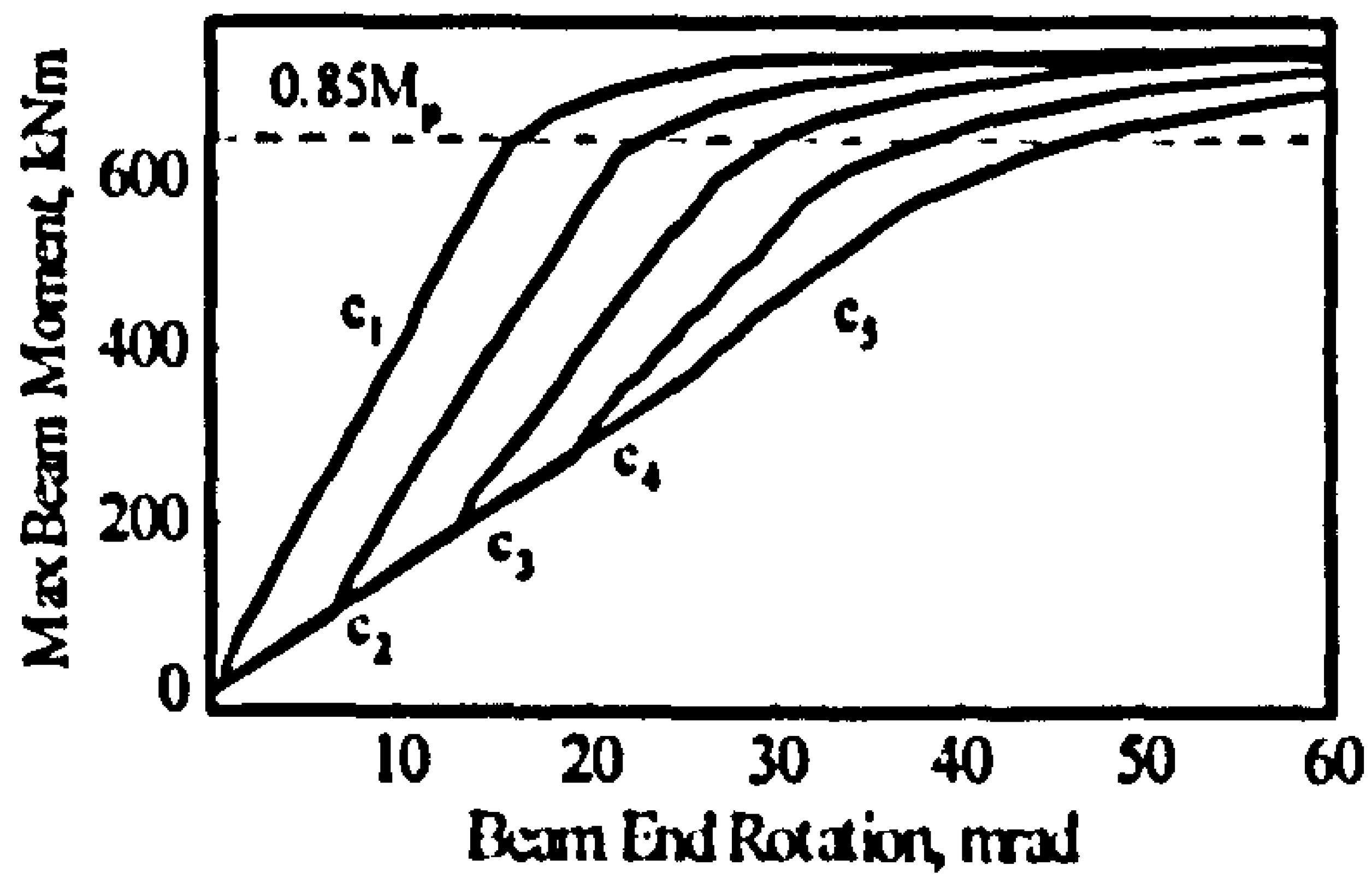

M_1=0.05M_p, M_2=0.4M_p

M_1=0.05M_p, M_2=0.4M_p

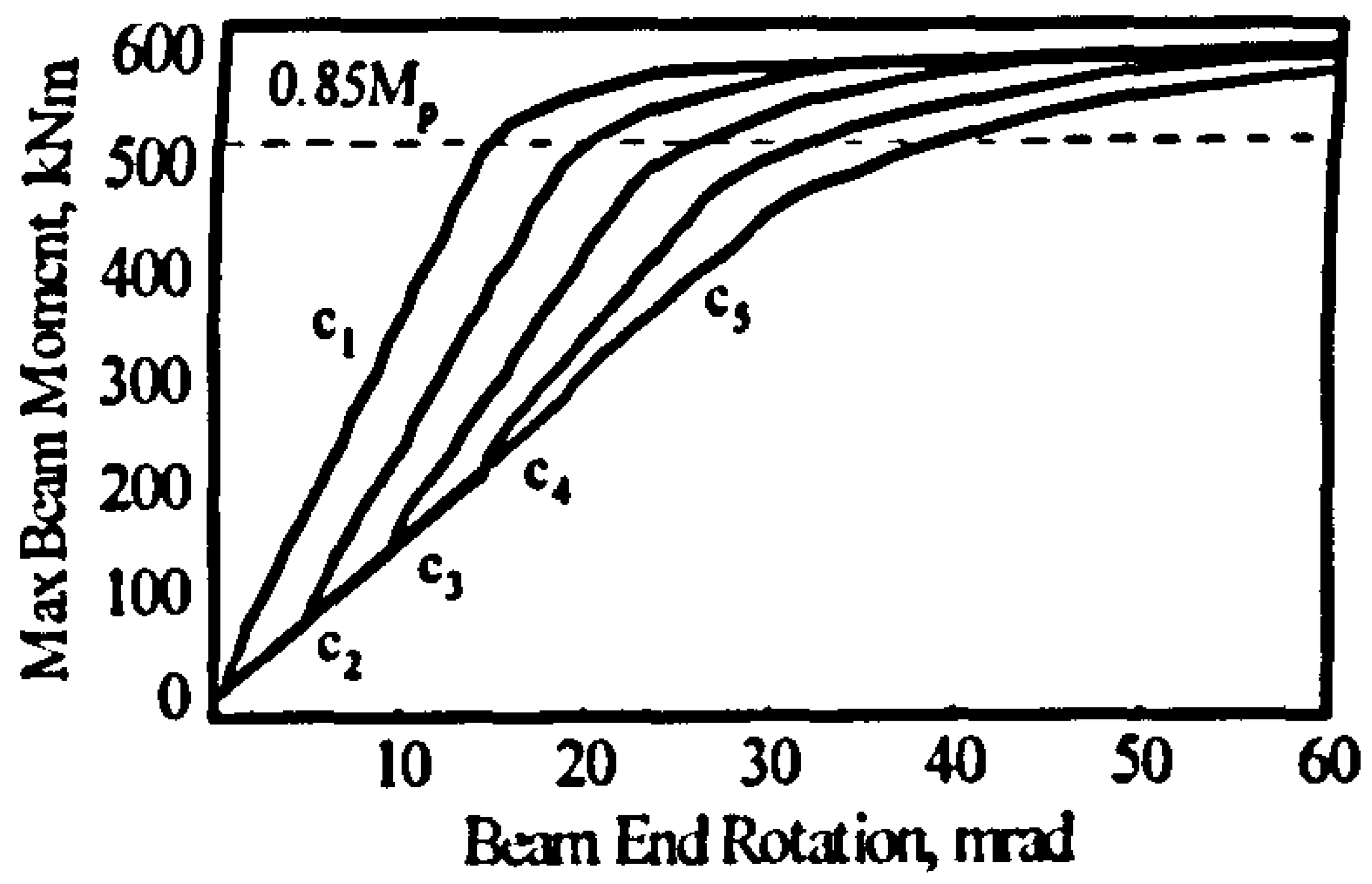

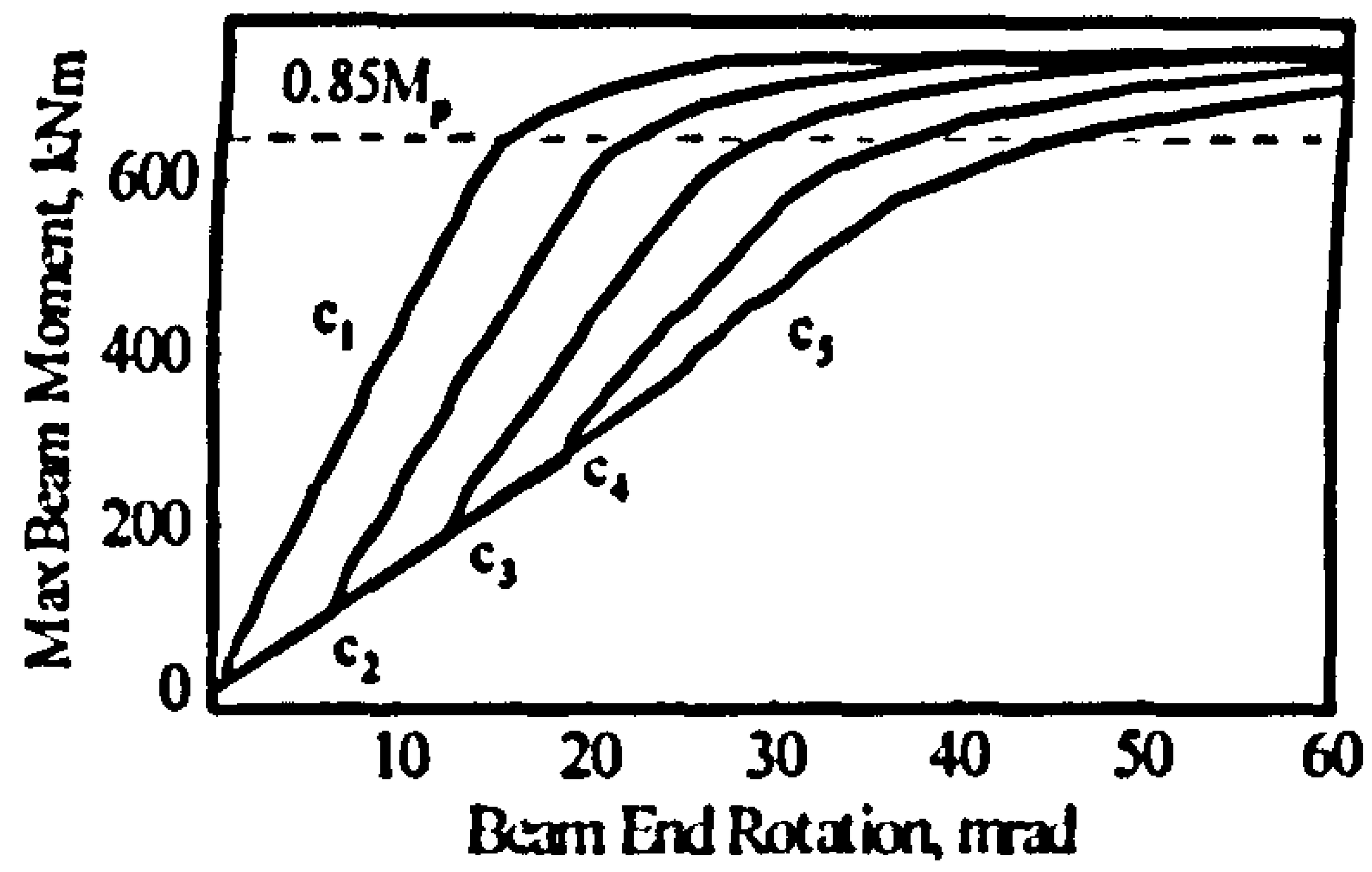

M_1=0.05M_p, M_2=0.5M_p

M_1=0.05M_p, M_2=0.5M_p

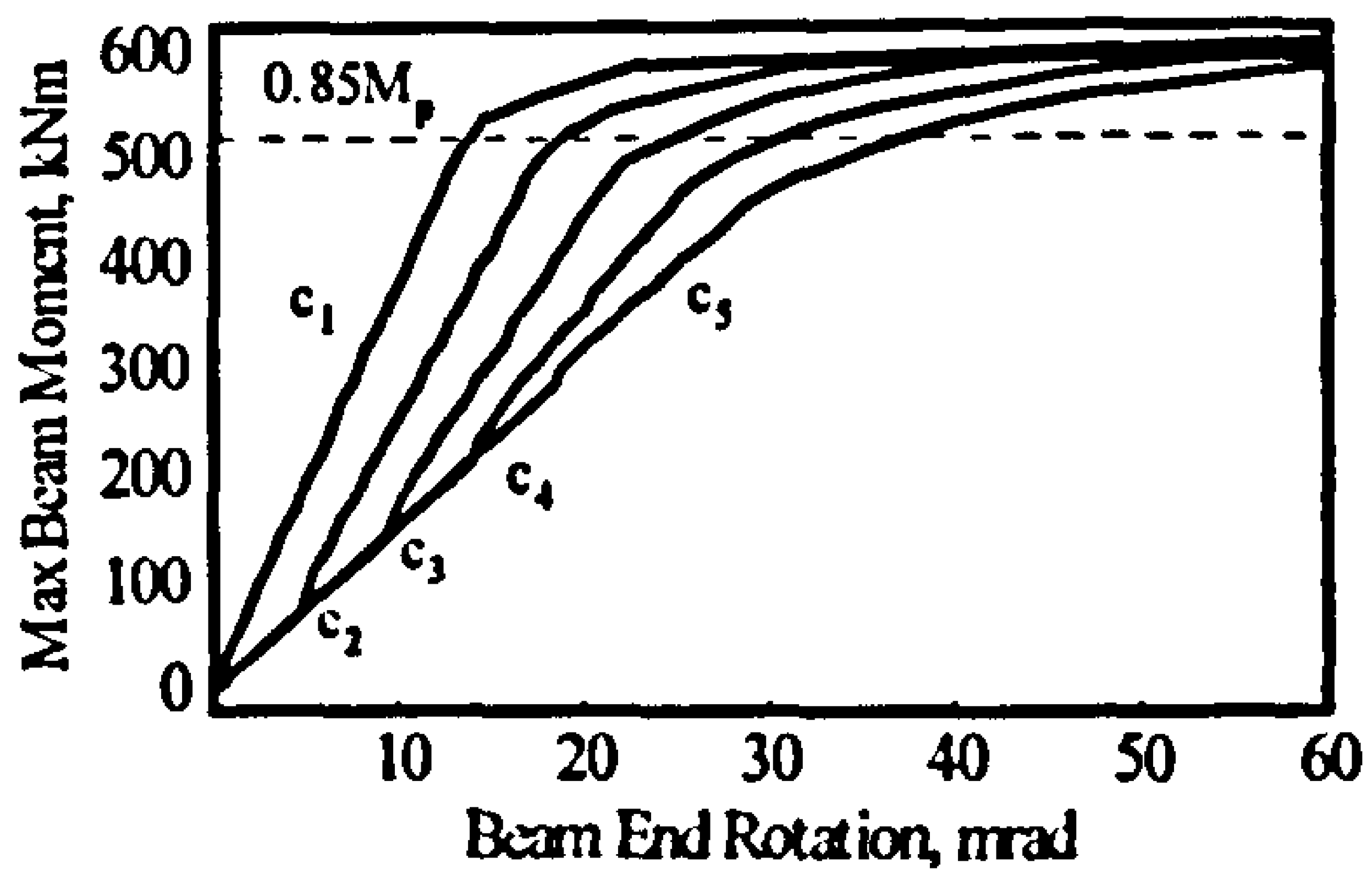

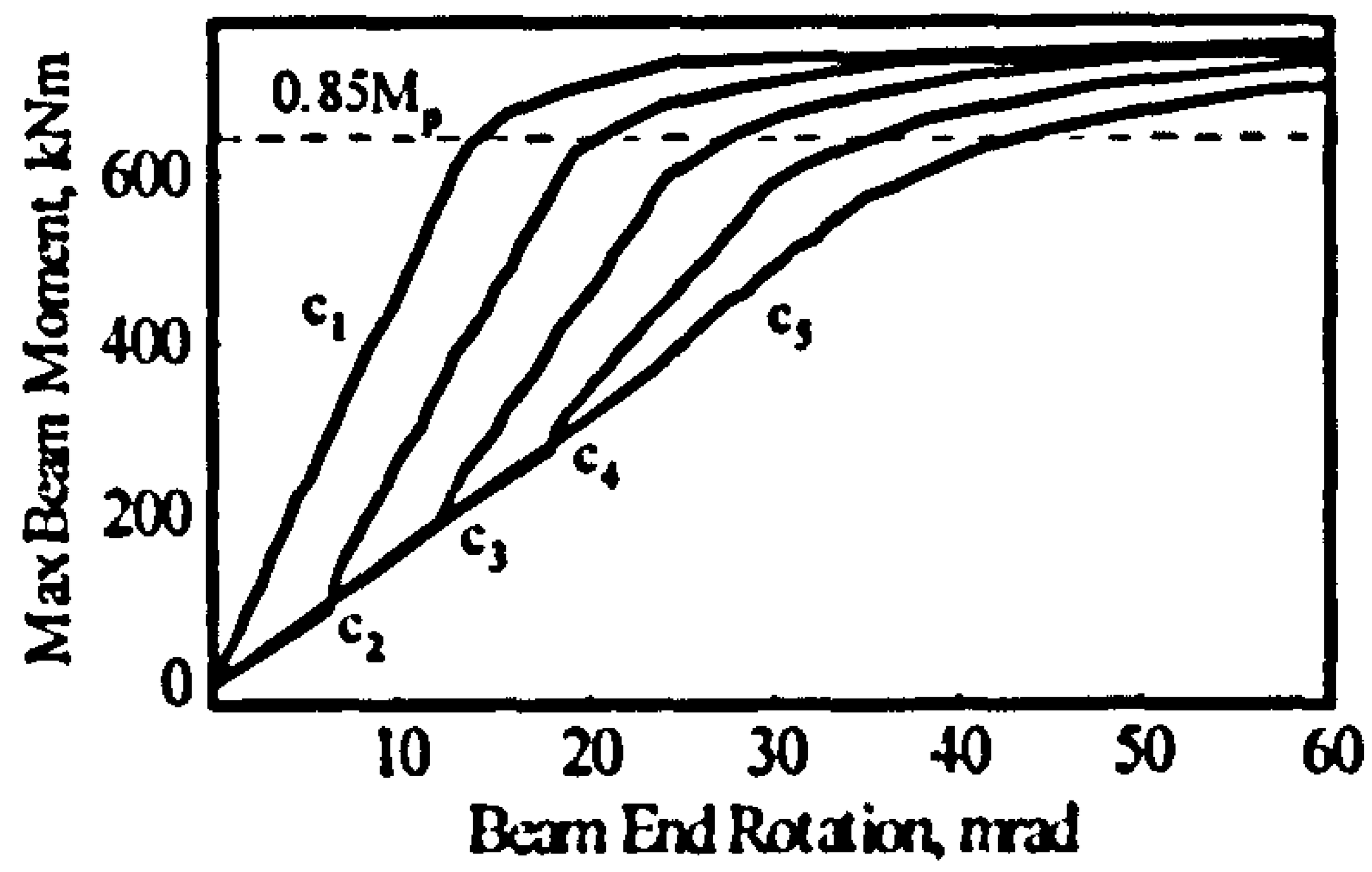

M_1=0.05M_p, M_2=0.6M_p

Grade S275

M_1=0.05M_p, M_2=0.6M_p

Grade S355

Figure C1-14. Moment vs. end rotation relationship for various maximum dead load stress levels (c_1:σ_{dl}=0; c_2:σ_{dl}=0.25σ_y; c_3:σ_{dl}=0.50σ_y; c_4:σ_{dl}=0.75σ_y; c_5:σ_{dl}=σ_y)

C.1.15 External beam, L/D=25, UDL

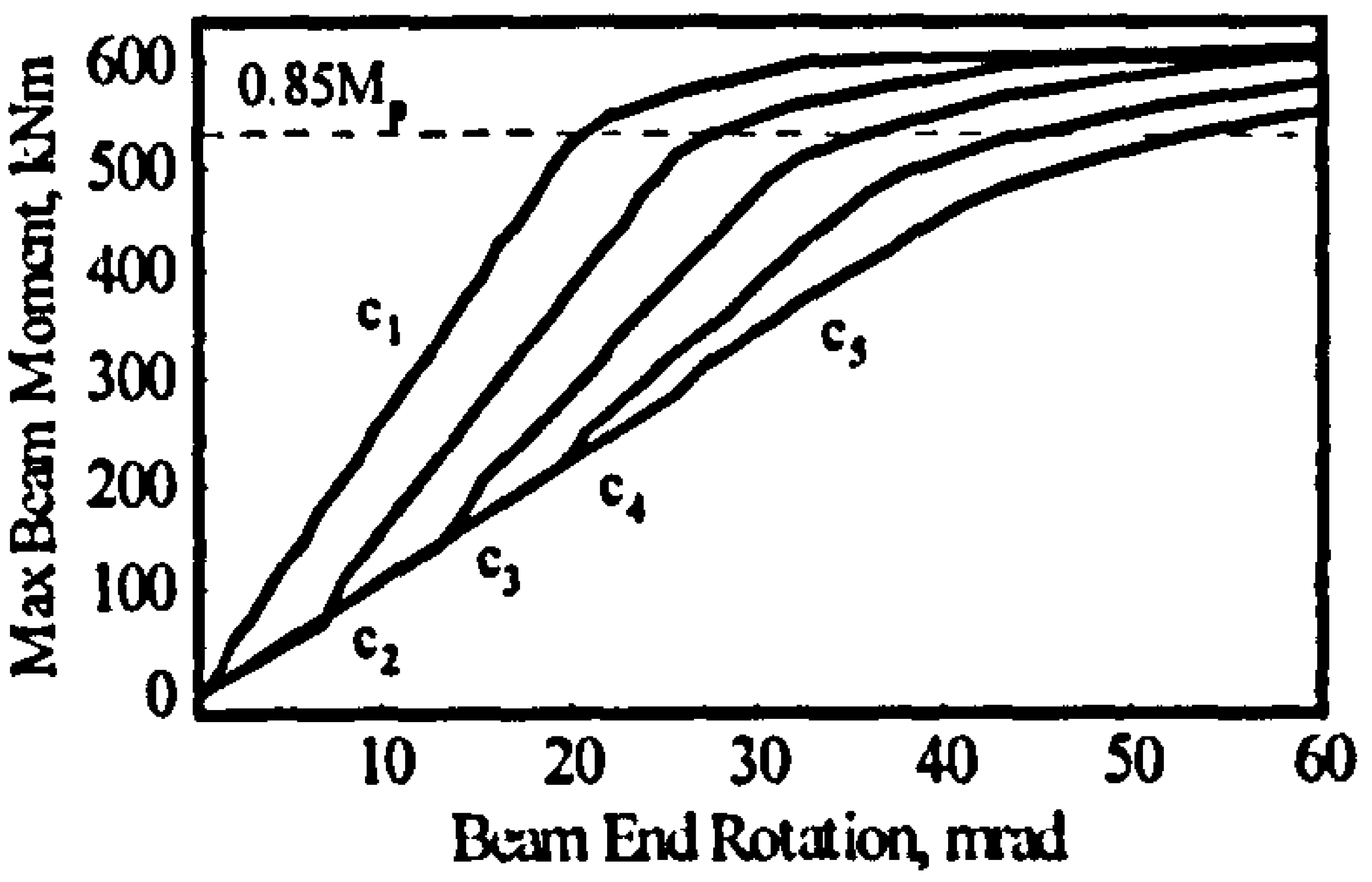

M_1=0.05M_p, M_2=0.3M_p

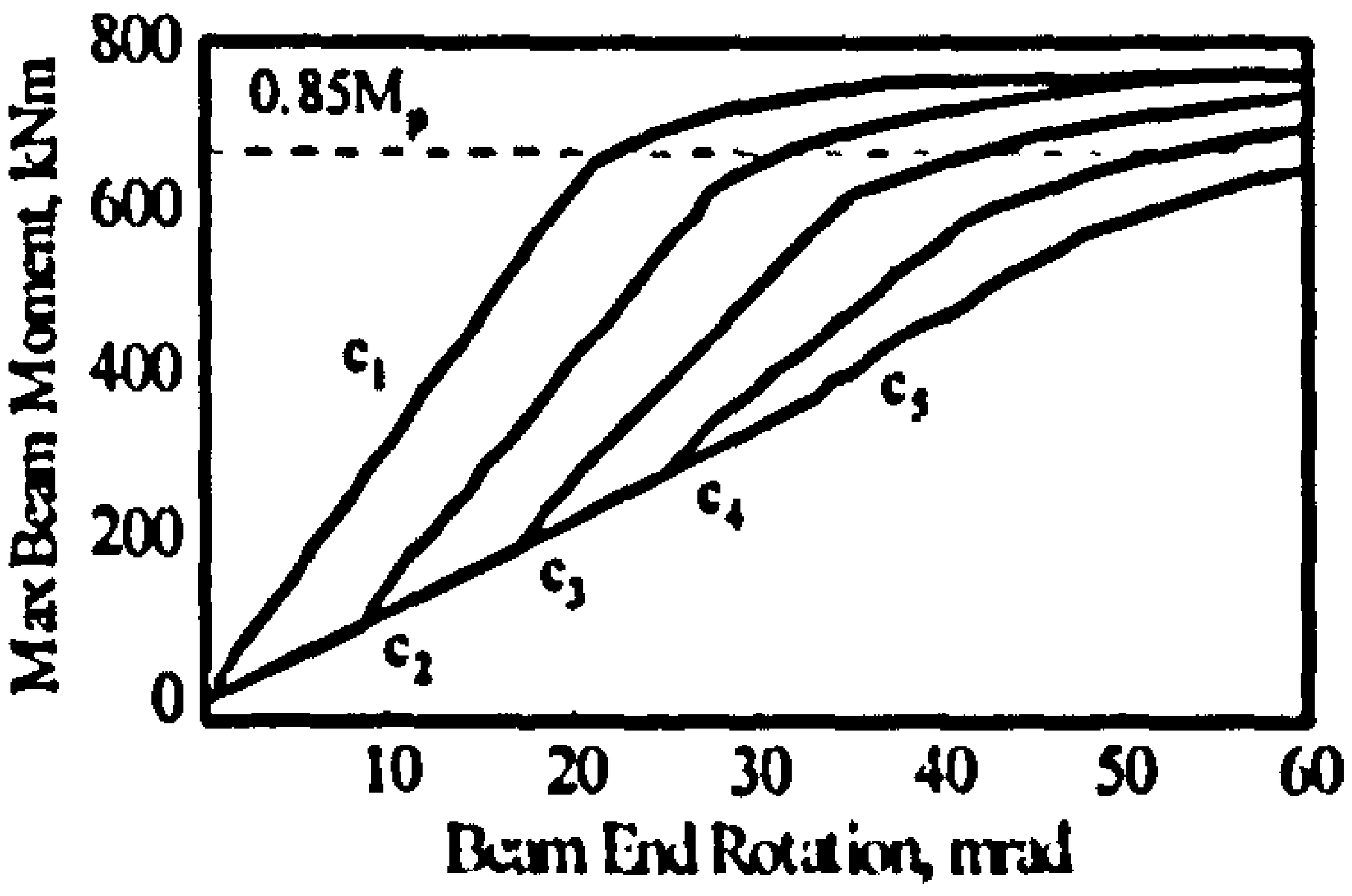

M_1=0.05M_p, M_2=0.3M_p

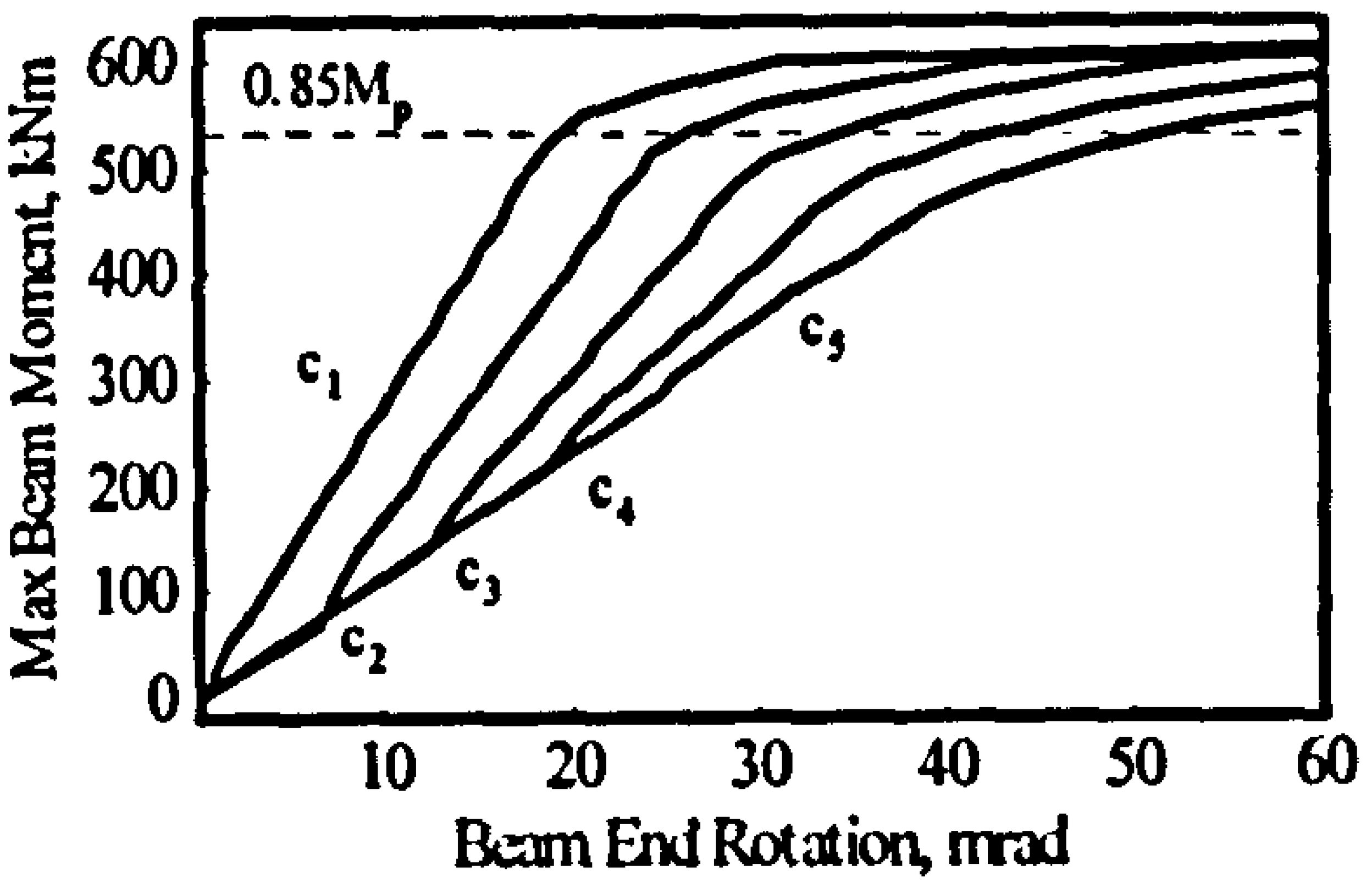

M_1=0.05M_p, M_2=0.4M_p

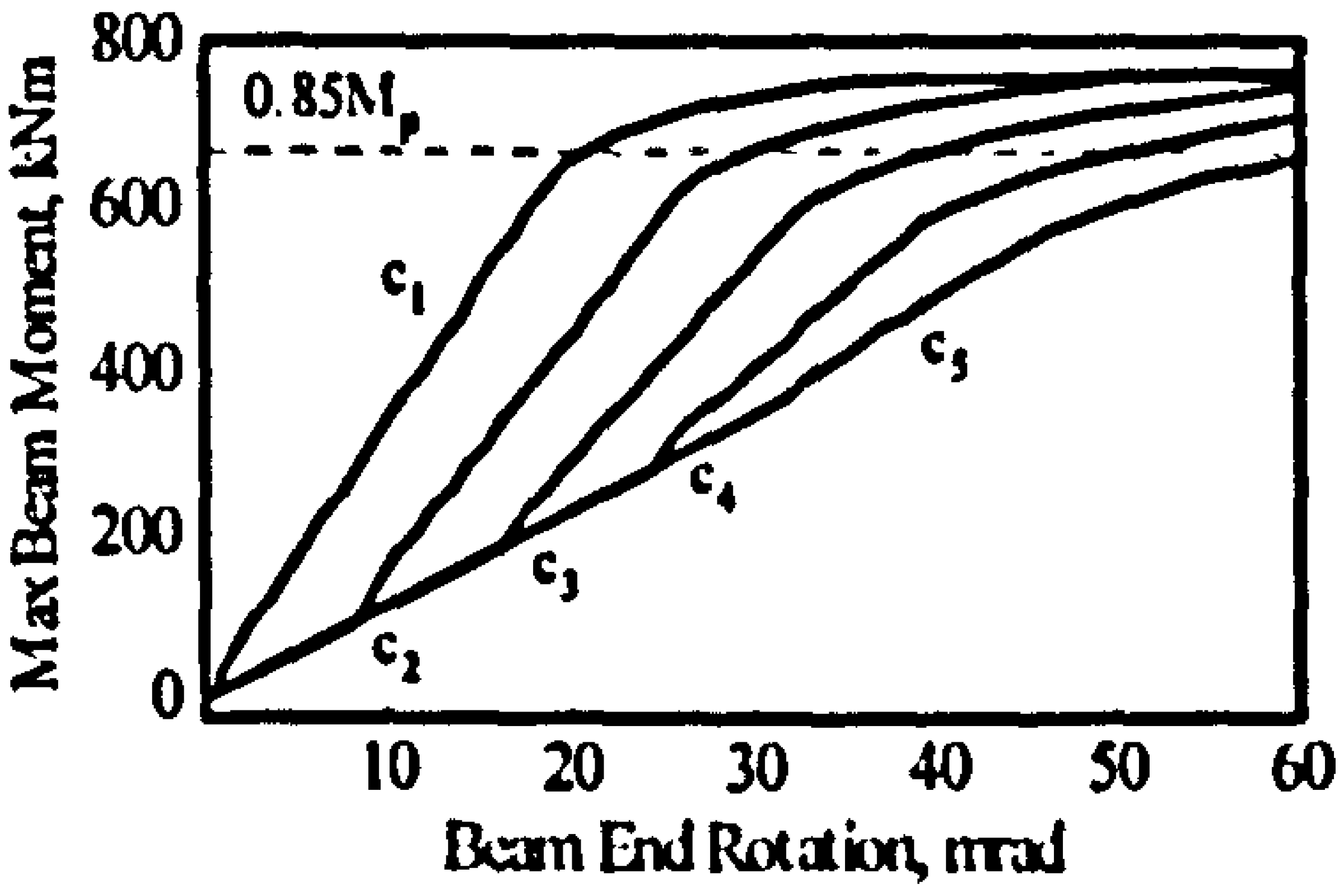

M_1=0.05M_p, M_2=0.4M_p

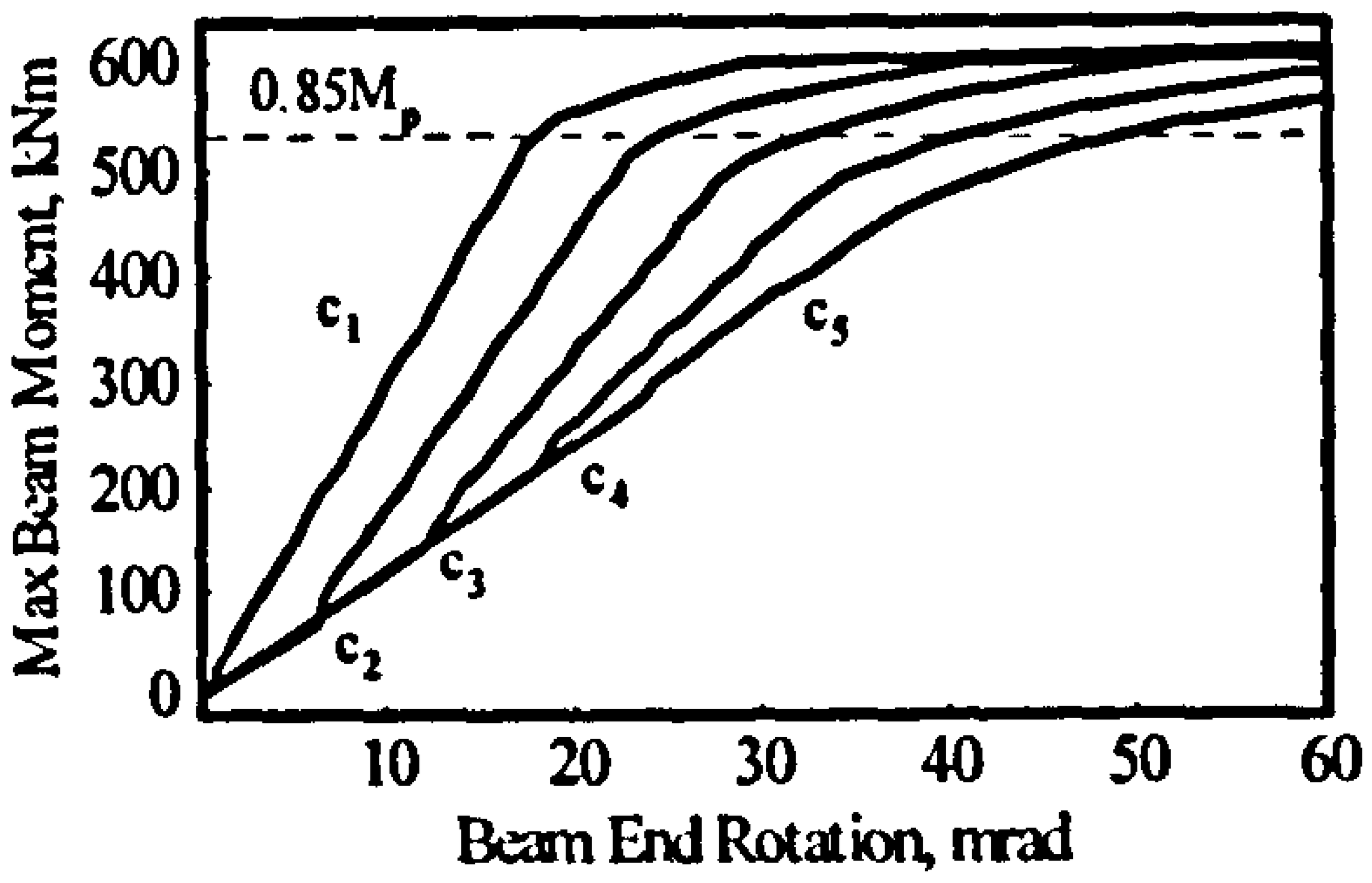

M_1=0.05M_p, M_2=0.5M_p

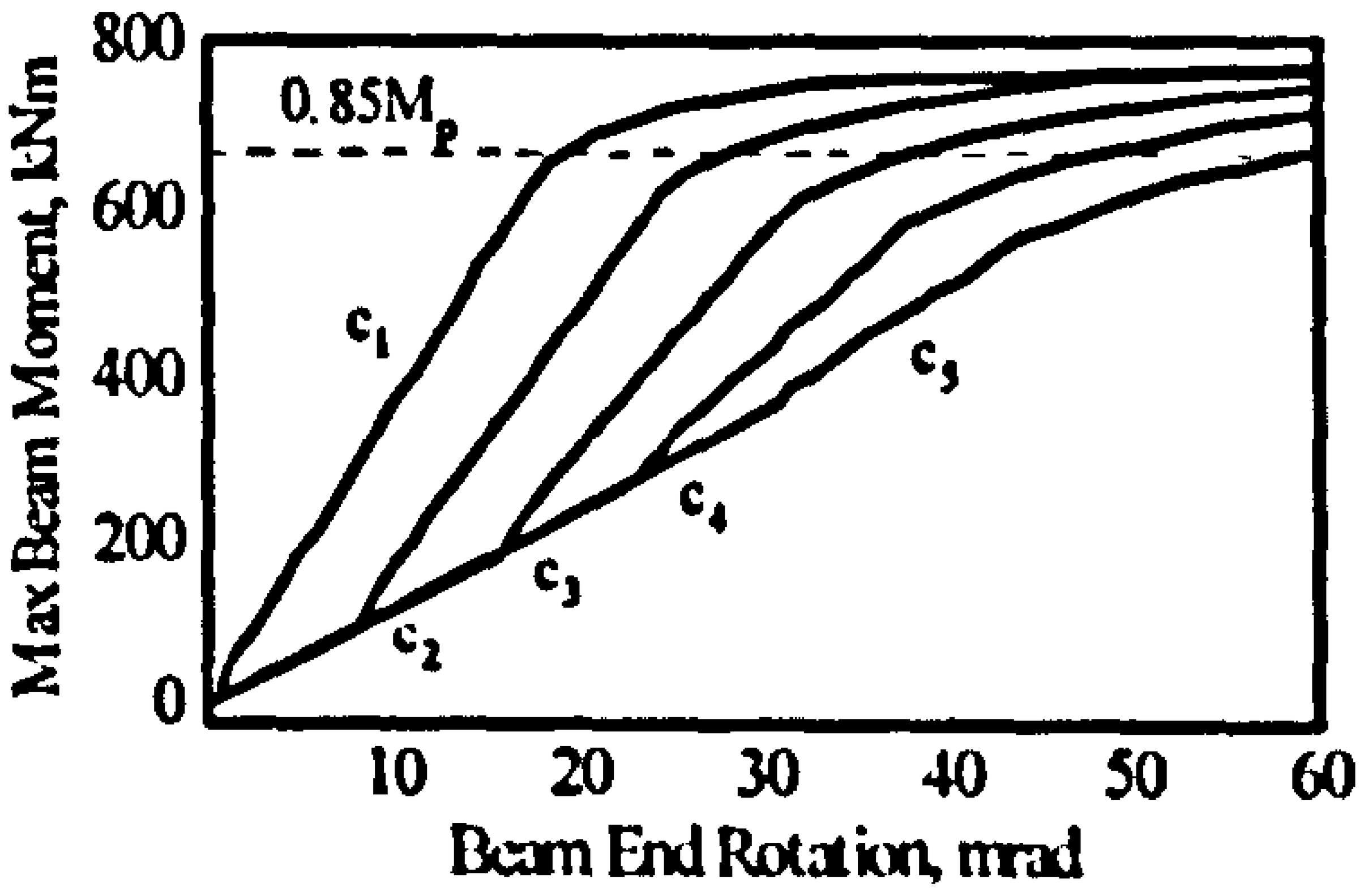

M_1=0.05M_p, M_2=0.5M_p

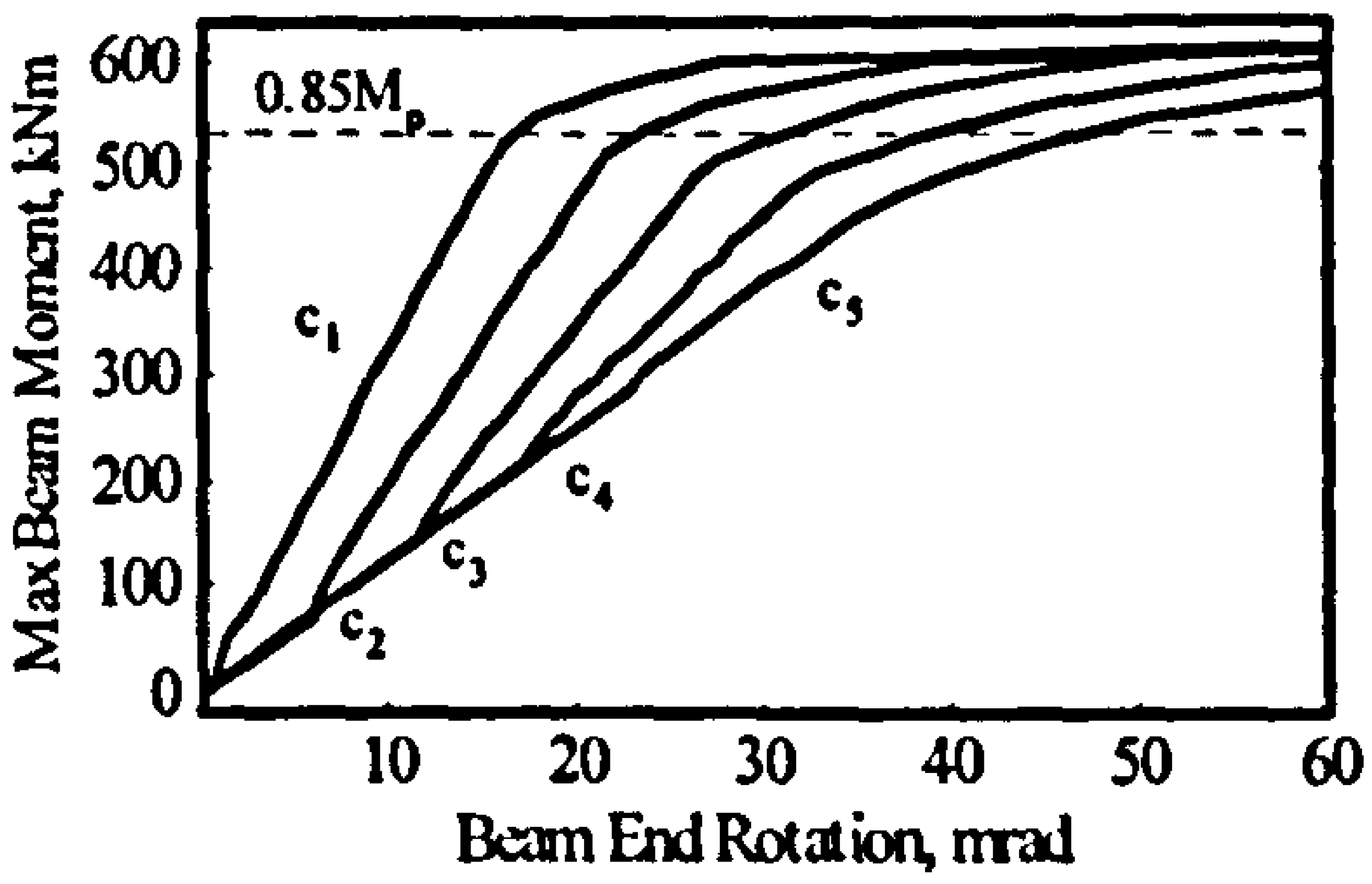

M_1=0.05M_p, M_2=0.6M_p

Grade S275

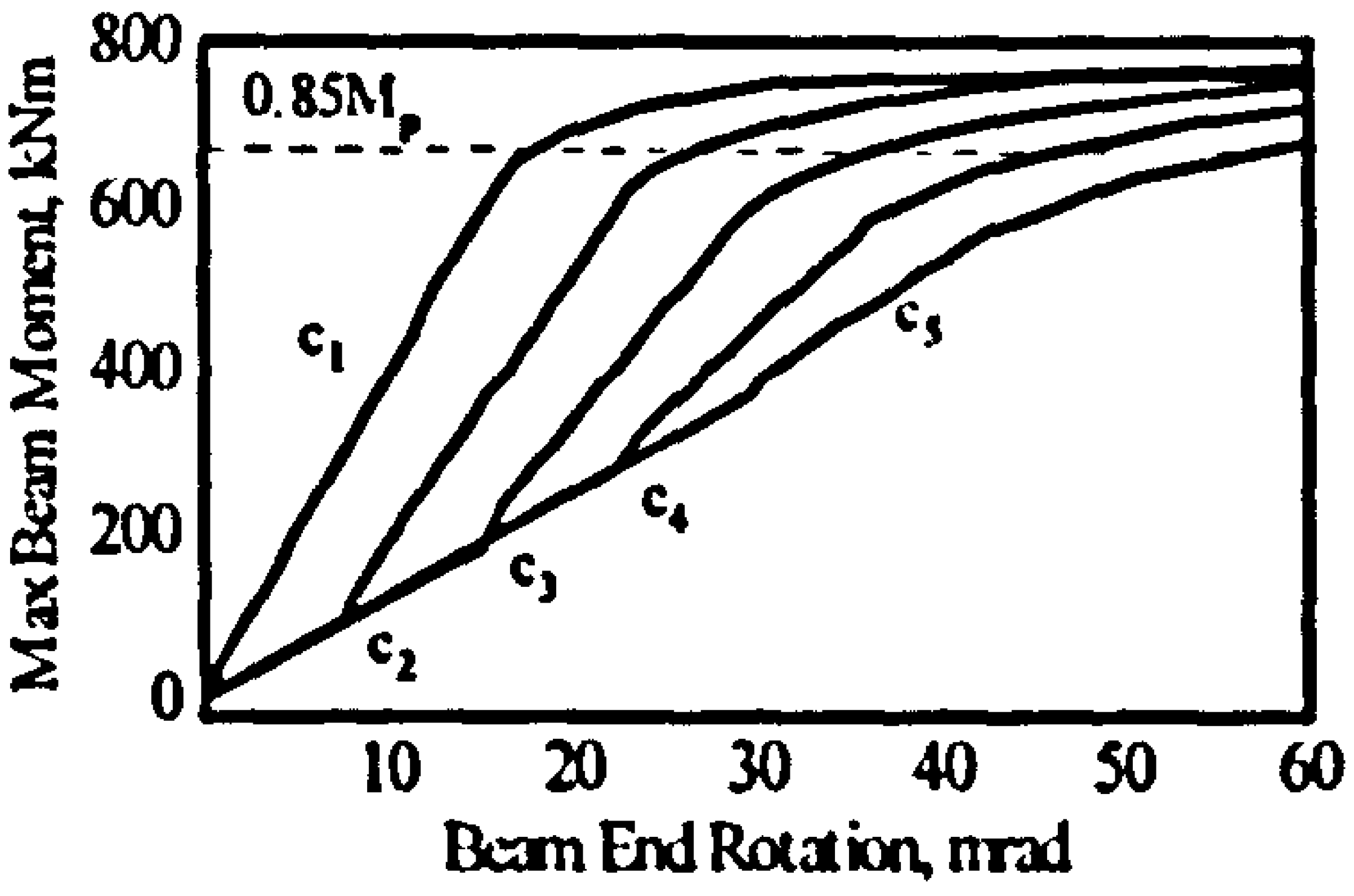

M_1=0.05M_p, M_2=0.6M_p

Grade S355

Figure C1-15. Moment vs. end rotation relationship for various maximum dead load stress levels (c_1:σ_{dl}=0; c_2:σ_{dl}=0.25σ_y; c_3:σ_{dl}=0.50σ_y; c_4:σ_{dl}=0.75σ_y; c_5:σ_{dl}=σ_y)

C.1.16 Internal beam, L/D=15, UDL

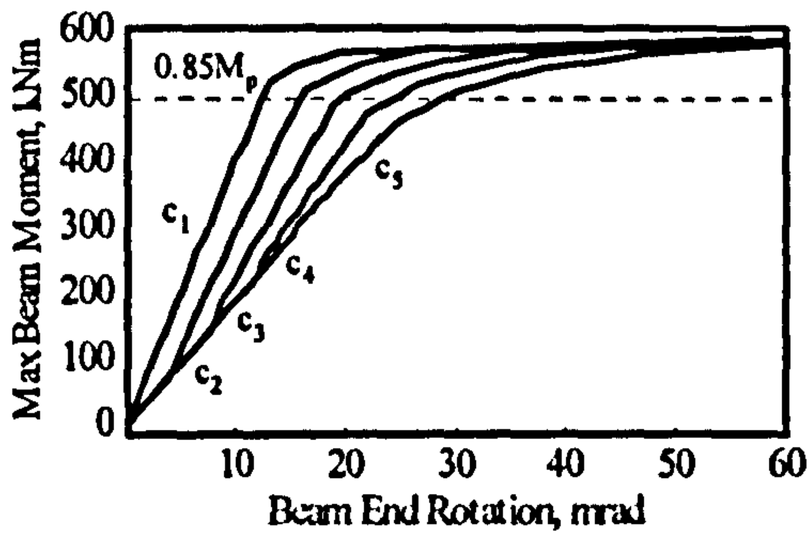

M_1=0.3M_p, M_2=0.3M_p

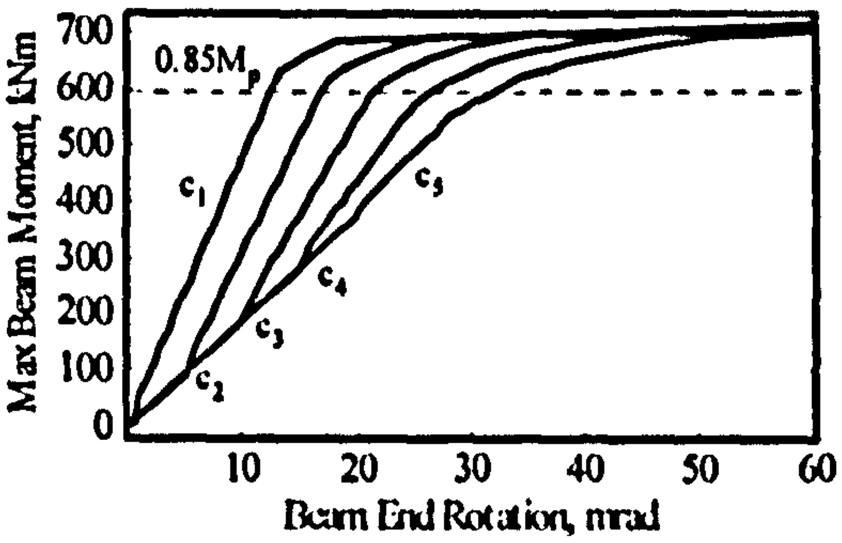

M_1=0.3M_p, M_2=0.3M_p

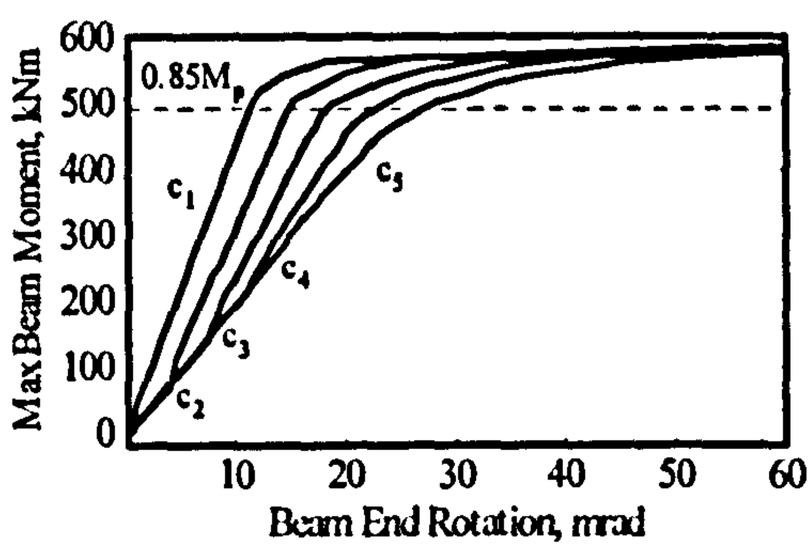

M_1=0.4M_p, M_2=0.4M_p

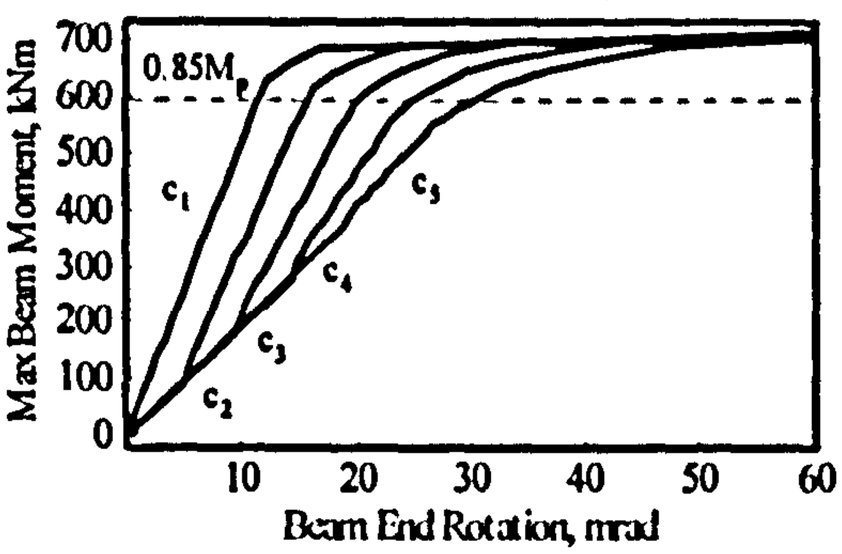

M_1=0.4M_p, M_2=0.4M_p

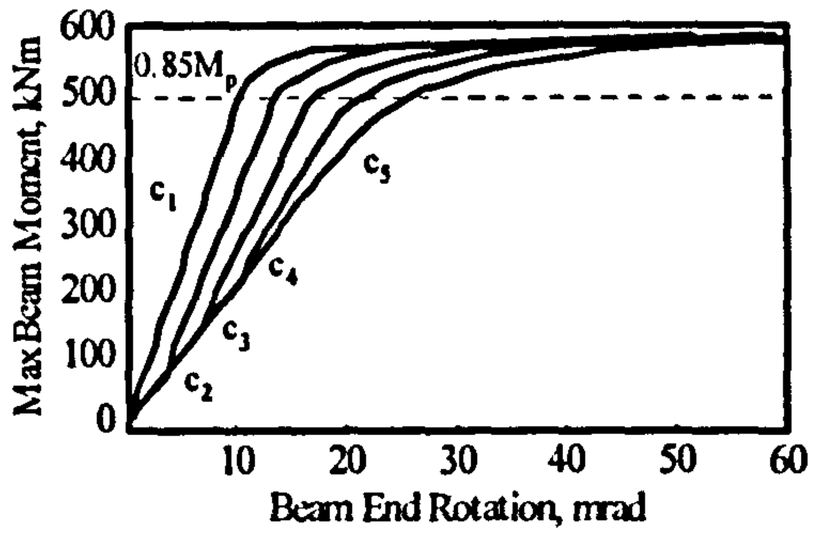

M_1=0.5M_p, M_2=0.5M_p

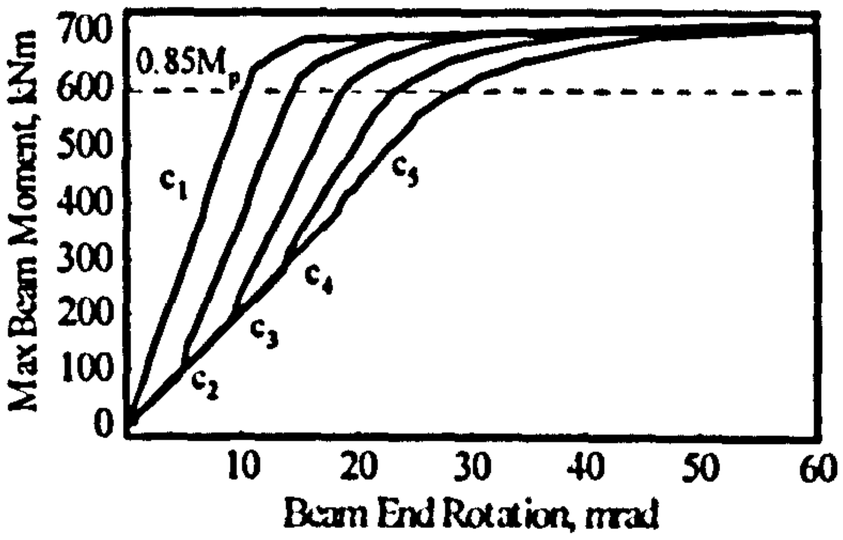

M_1=0.5M_p, M_2=0.5M_p

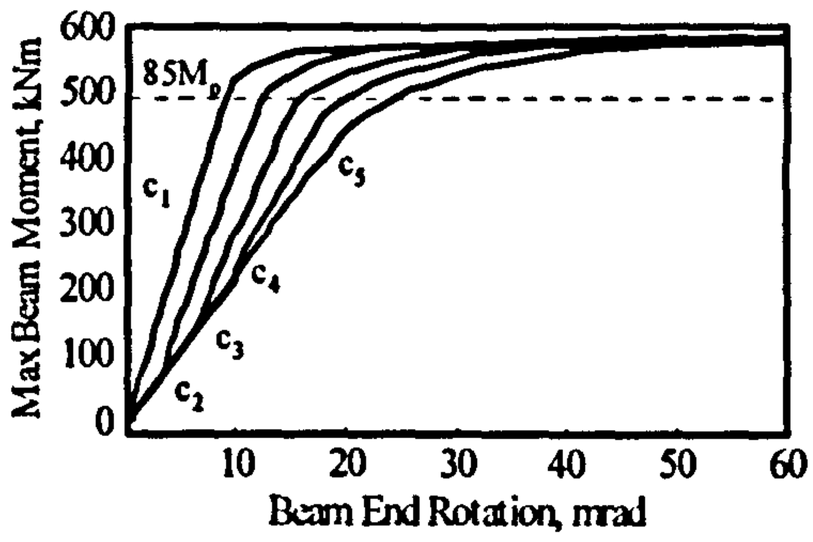

M_1=0.6M_p, M_2=0.6M_p

Grade S275

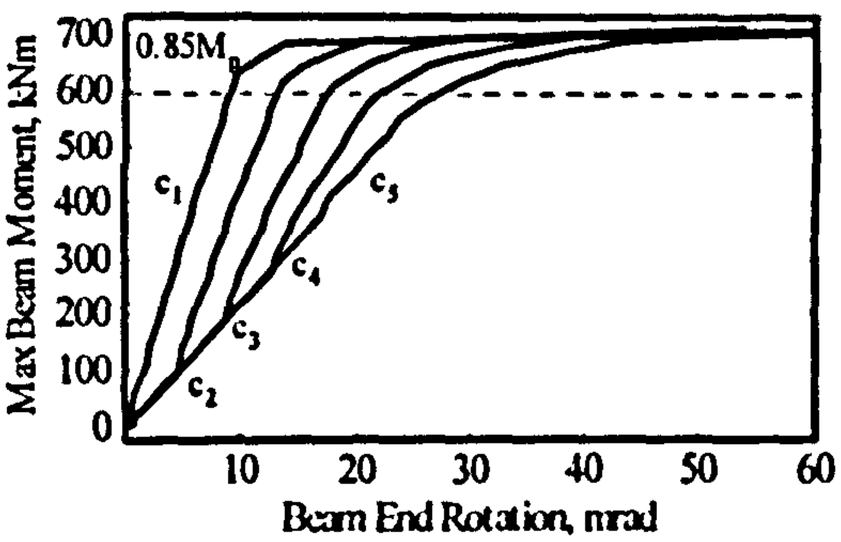

M_1=0.6M_p, M_2=0.6M_p

Grade S355

Figure C1-16. Moment vs. end rotation relationship for various maximum dead load stress levels (c_1: σ_{dl}=0; c_2: σ_{dl}=0.25σ_y; c_3: σ_{dl}=0.50σ_y; c_4: σ_{dl}=0.75σ_y; c_5: σ_{dl}=σ_y)

C.1.17 Internal beam, L/D=20, UDL

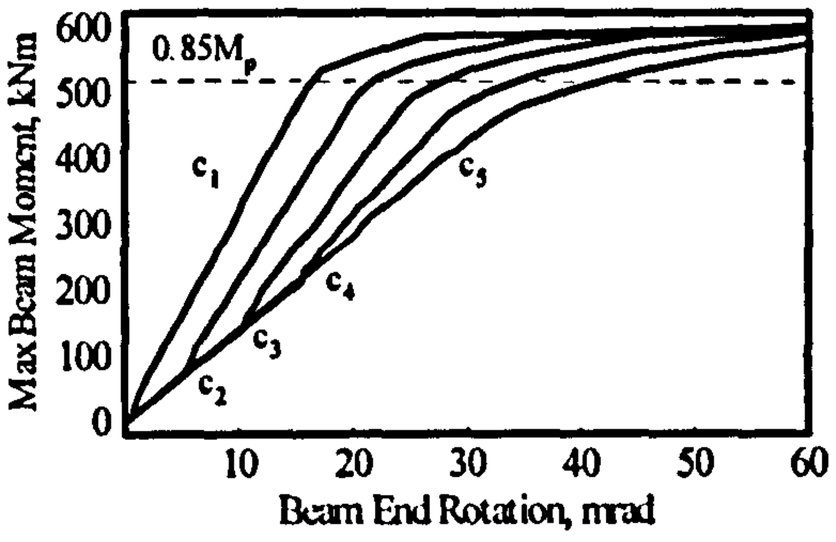

M_1=0.3M_p, M_2=0.3M_p

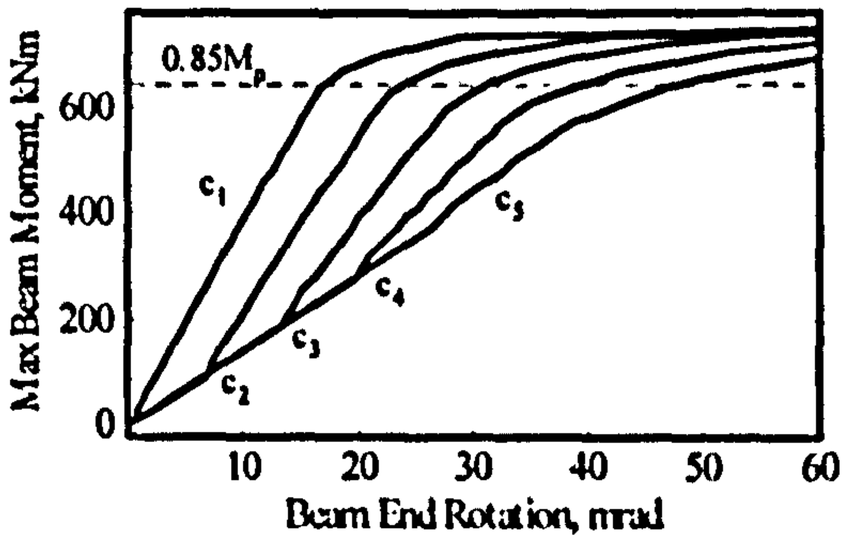

M_1=0.3M_p, M_2=0.3M_p

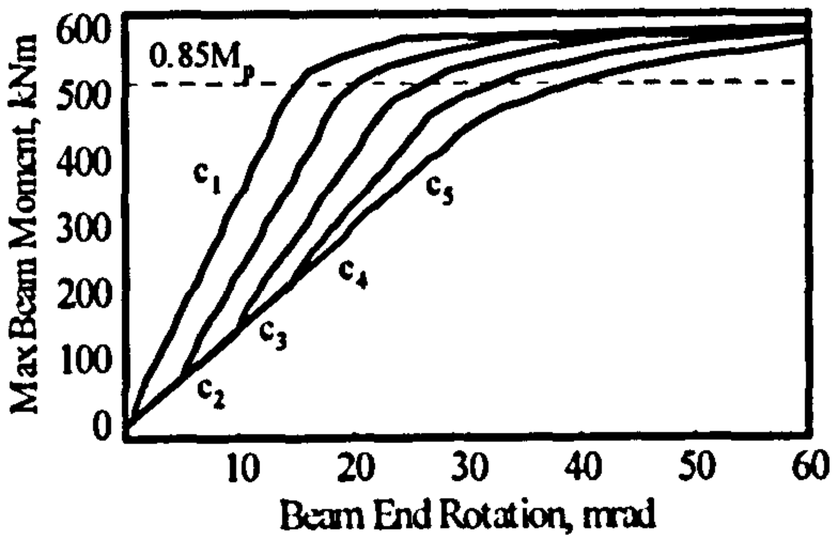

M_1=0.4M_p, M_2=0.4M_p

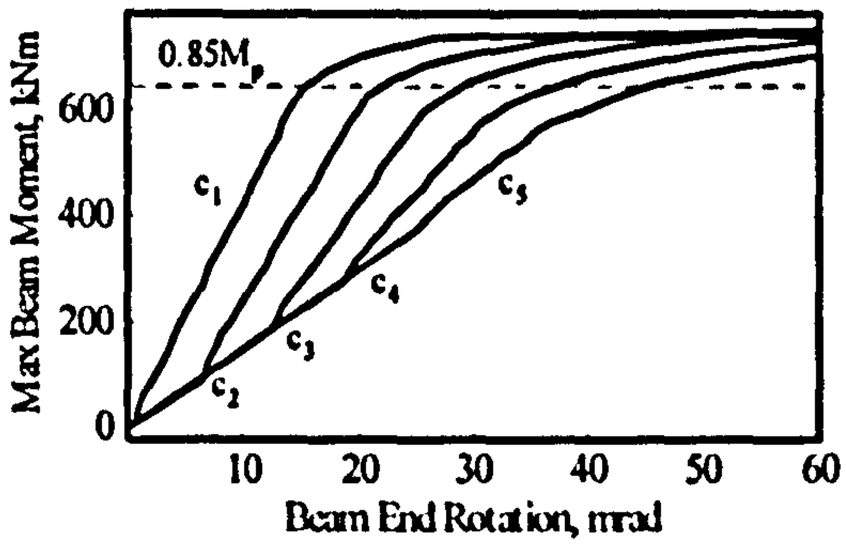

M_1=0.4M_p, M_2=0.4M_p

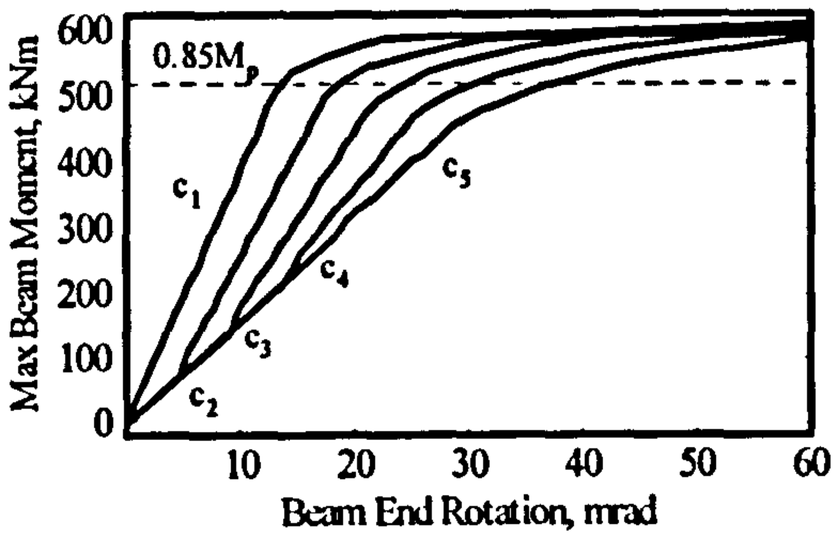

M_1=0.5M_p, M_2=0.5M_p

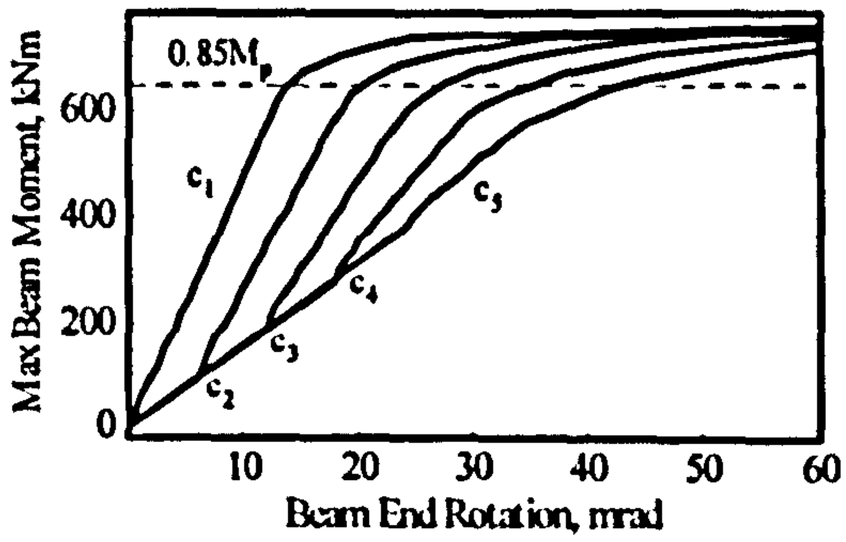

M_1=0.5M_p, M_2=0.5M_p

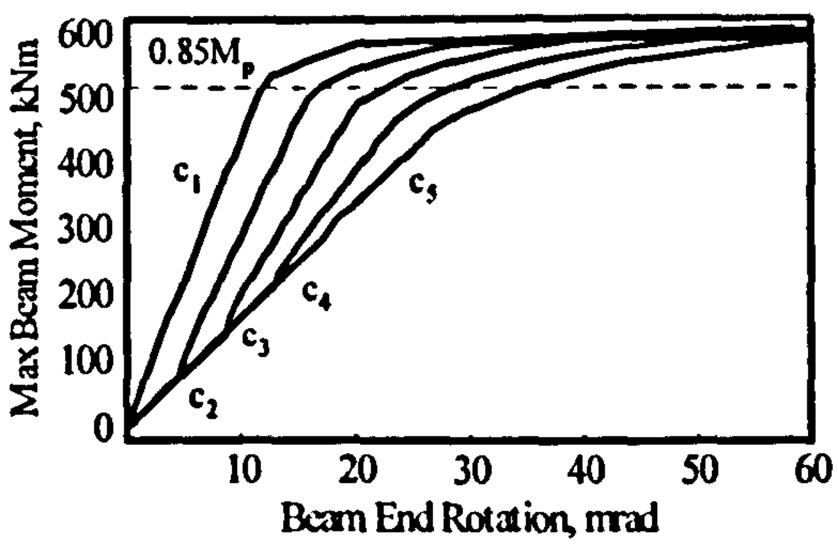

M_1=0.6M_p, M_2=0.6M_p

Grade S275

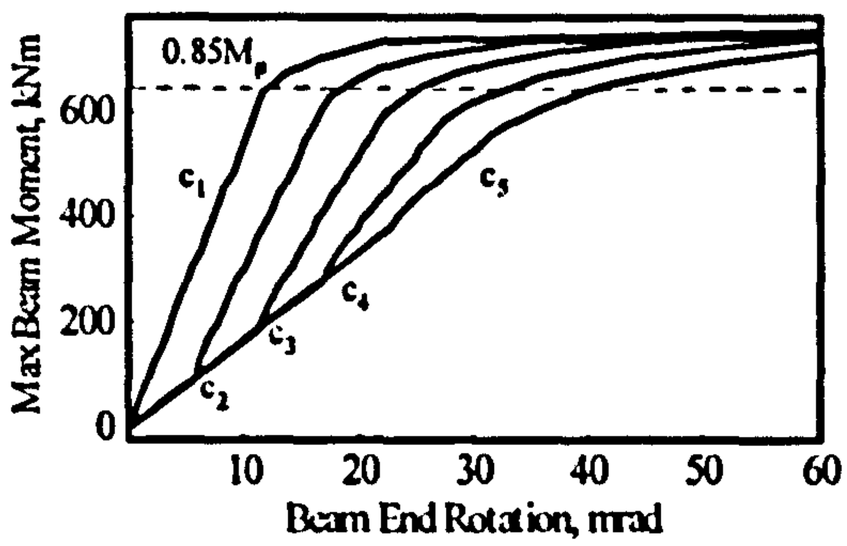

M_1=0.6M_p, M_2=0.6M_p

Grade S355

Figure C1-17. Moment vs. end rotation relationship for various maximum dead load stress levels (c_1:σ_{dl}=0; c_2:σ_{dl}=0.25σ_y; c_3:σ_{dl}=0.50σ_y; c_4:σ_{dl}=0.75σ_y; c_5:σ_{dl}=σ_y)

C.1.18 Internal beam, L/D=25, UDL

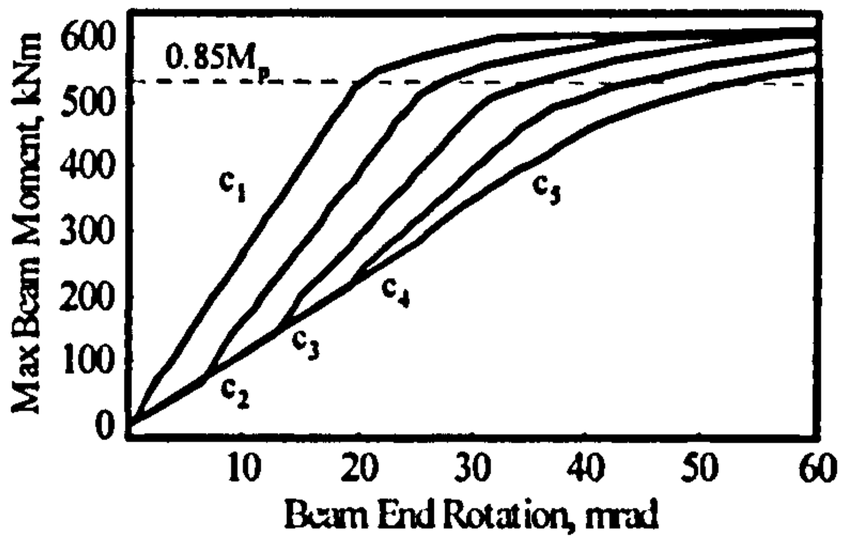

M_1=0.3M_p, M_2=0.3M_p

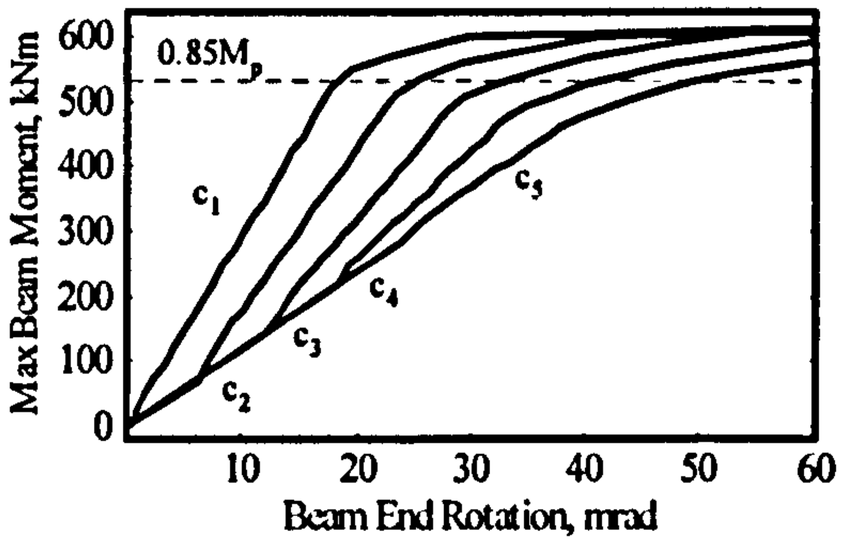

M_1=0.4M_p, M_2=0.4M_p

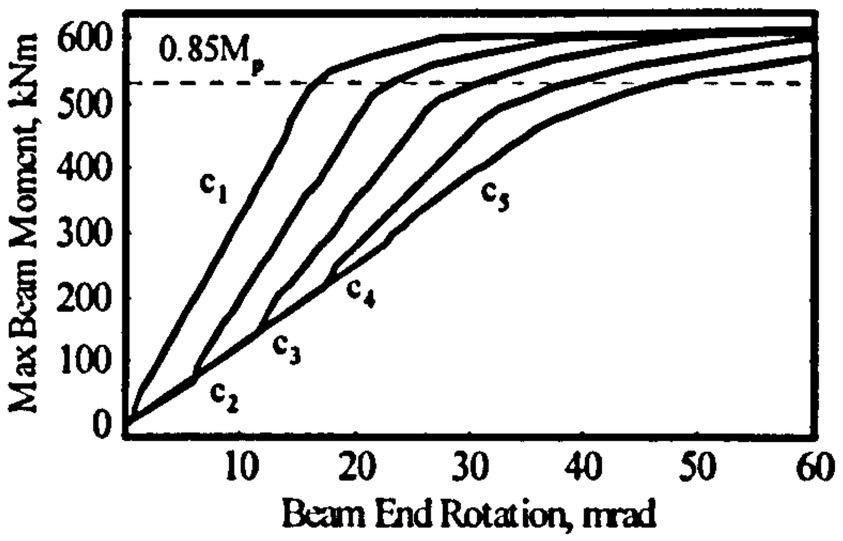

M_1=0.5M_p, M_2=0.5M_p

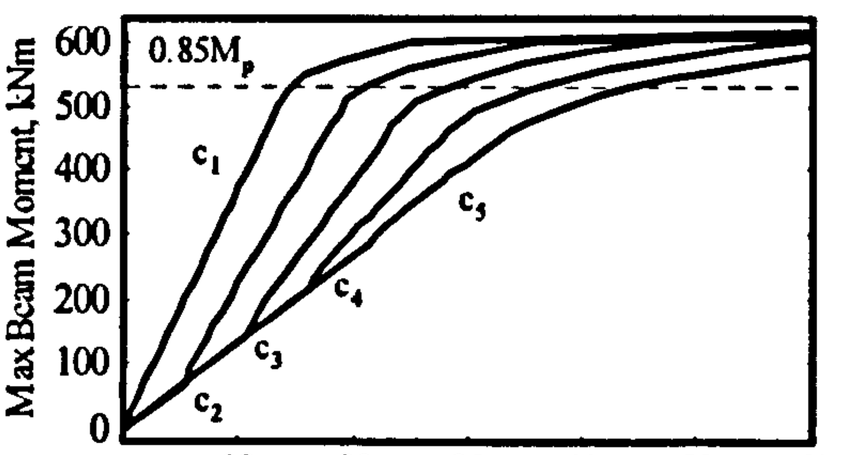

M_1=0.6M_p, M_2=0.6M_p

Grade S275

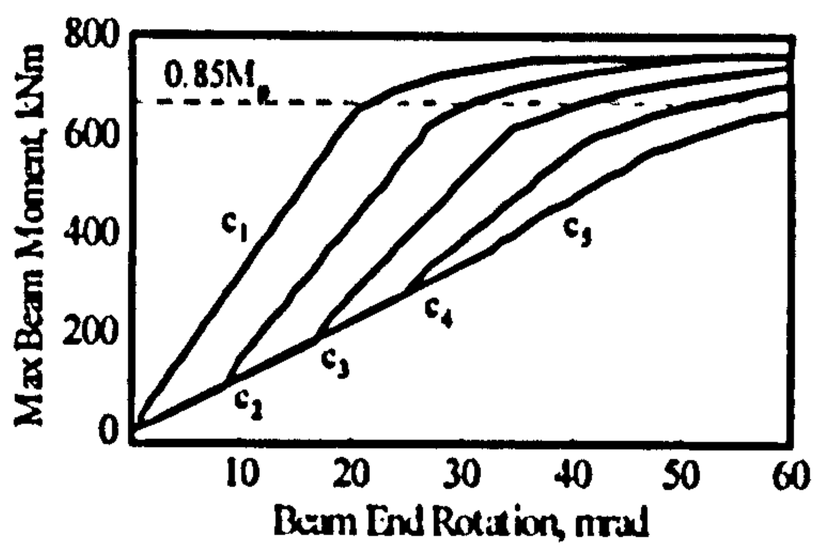

M_1=0.3M_p, M_2=0.3M_p

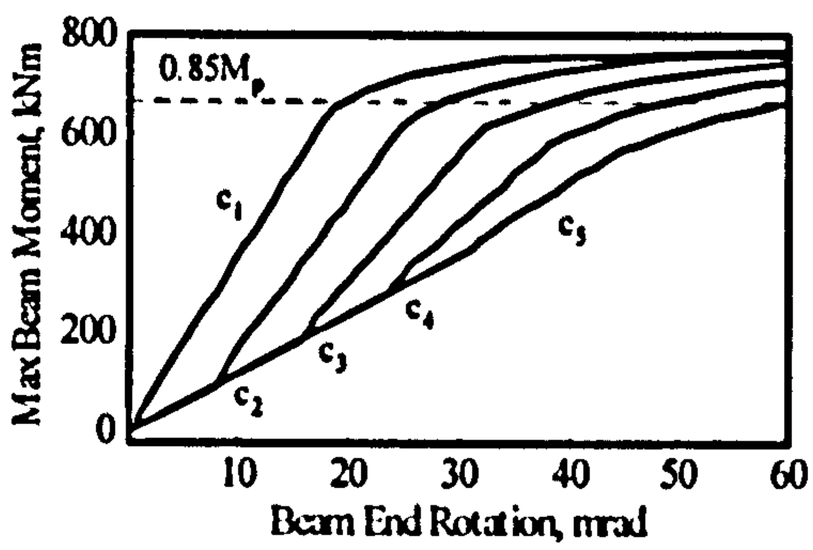

M_1=0.4M_p, M_2=0.4M_p

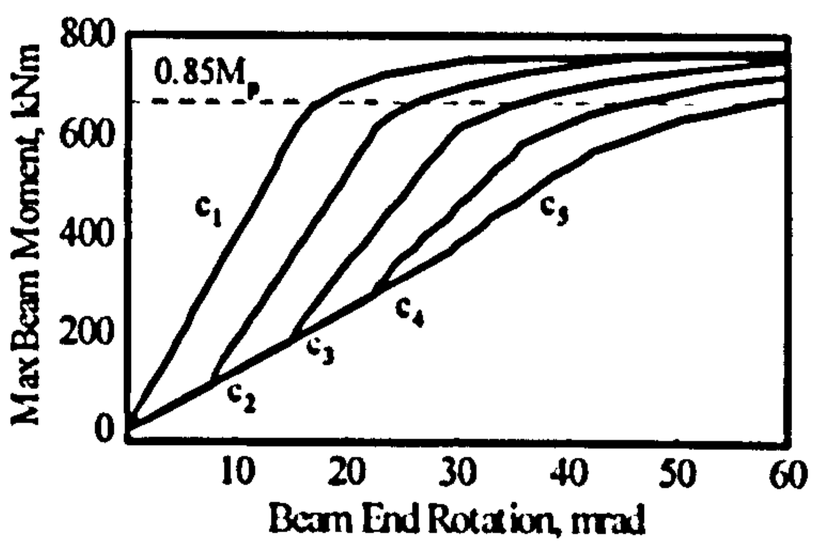

M_1=0.5M_p, M_2=0.5M_p

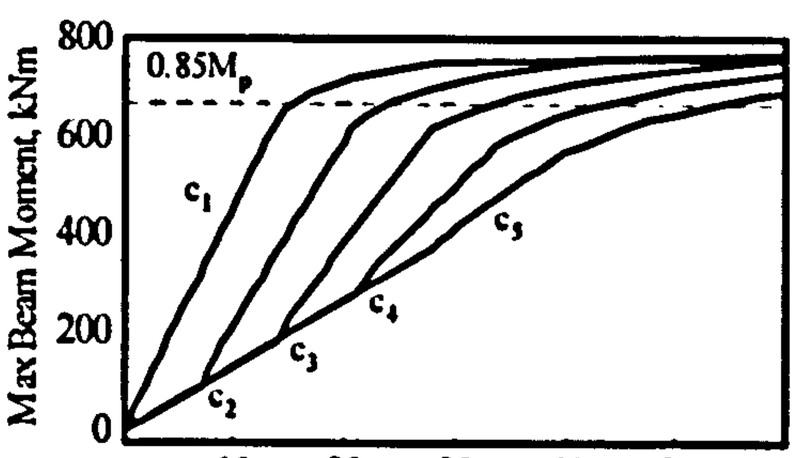

M_1=0.6M_p, M_2=0.6M_p

Grade S355

Figure C1-18. Moment vs. end rotation relationship for various maximum dead load stress levels (c_1:σ_{dl}=0; c_2:σ_{dl}=0.25σ_y; c_3:σ_{dl}=0.50σ_y; c_4:σ_{dl}=0.75σ_y; c_5:σ_{dl}=σ_y)

C.2 REQUIRED ROTATION

C.2.1 External beam, S275:

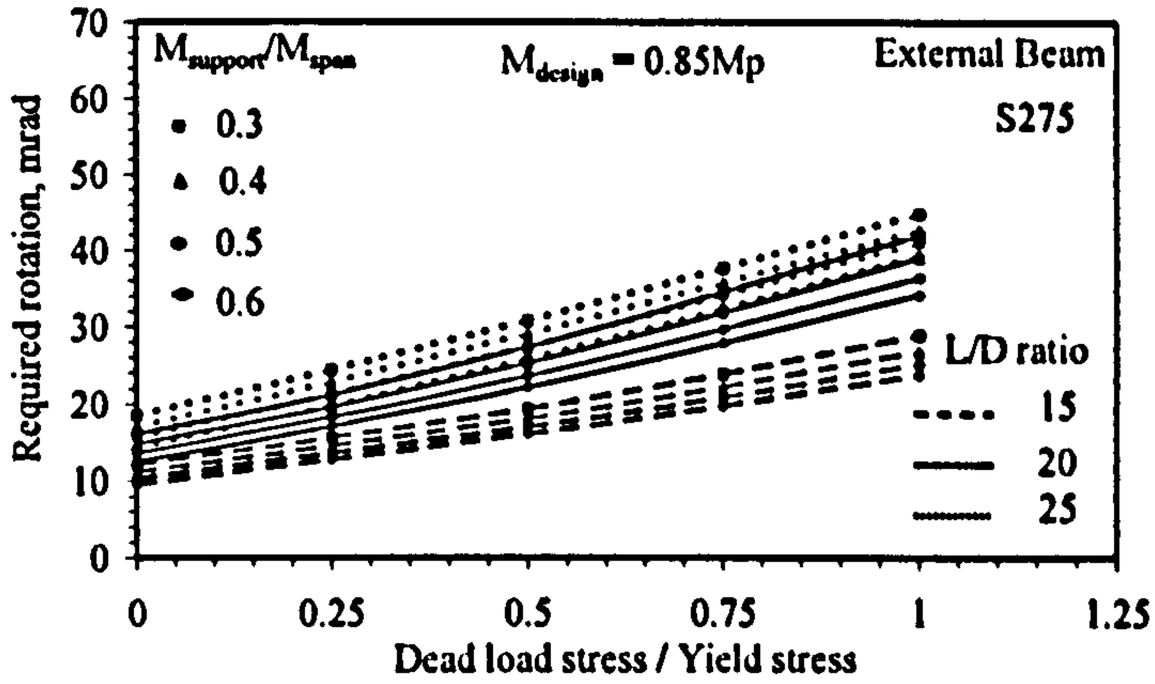

Figure C2-1. Required rotations to achieve 0.85 M_p – S275, External beam

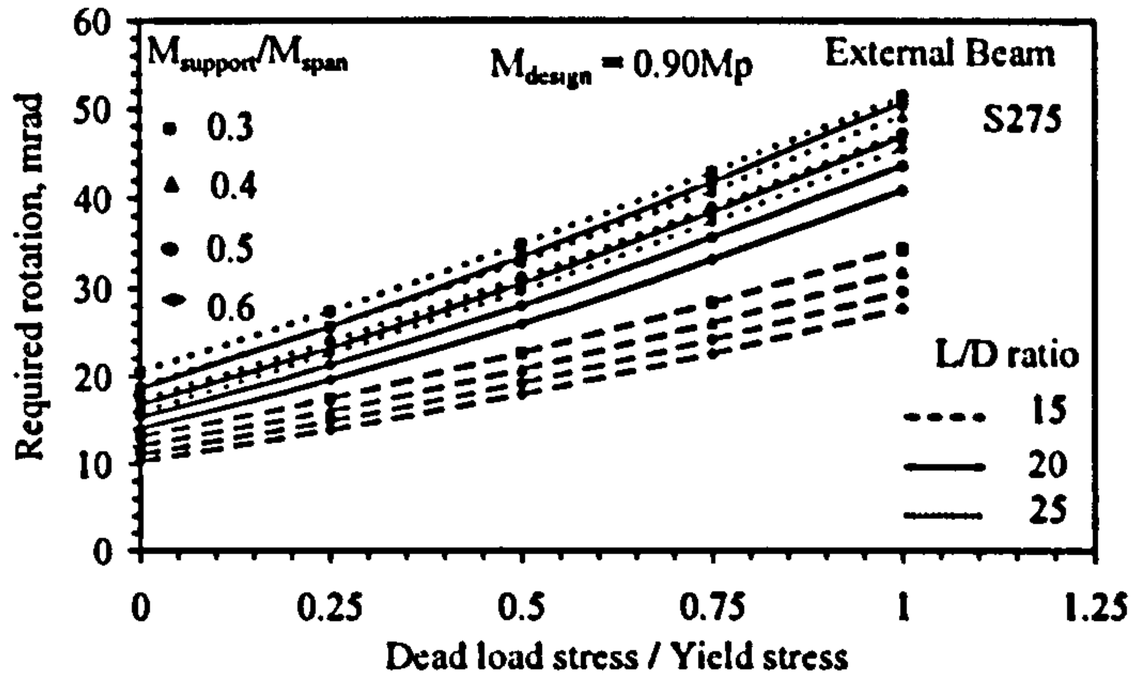

Figure C2-2. Required rotations to achieve 0.90 M_p – S275, External beam

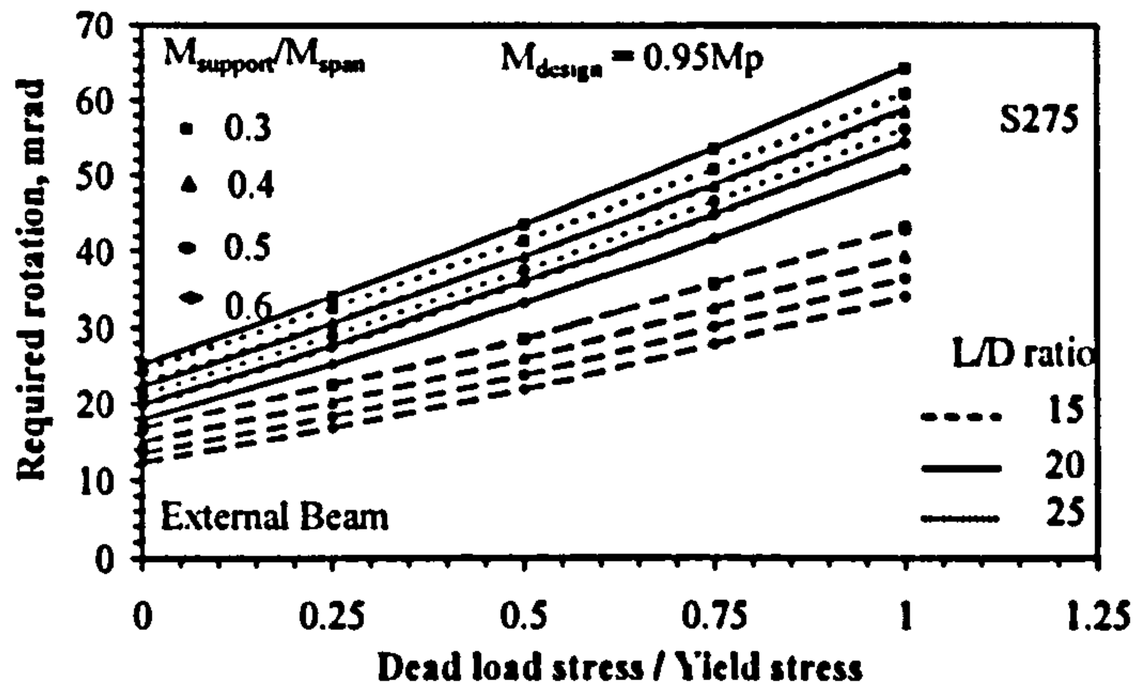

Figure C2-3. Required rotations to achieve 0.95 M_p – S275, External beam

C.2.2 External beam, S355

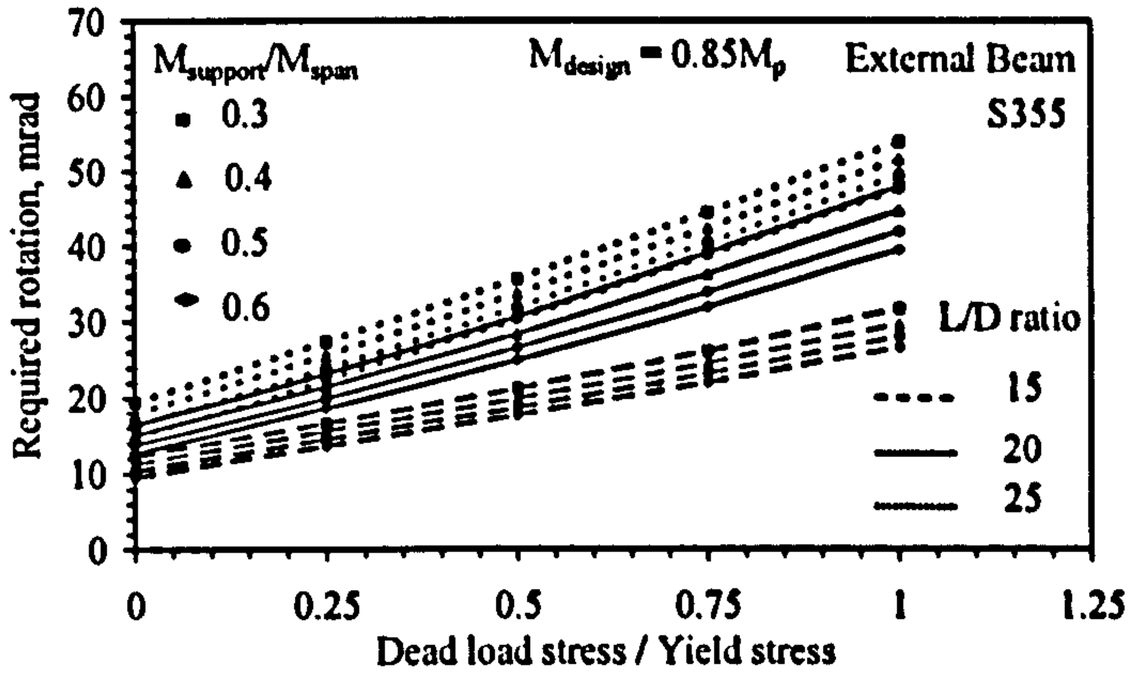

Figure C2-4. Required rotations to achieve 0.85 M_p – S355, External beam

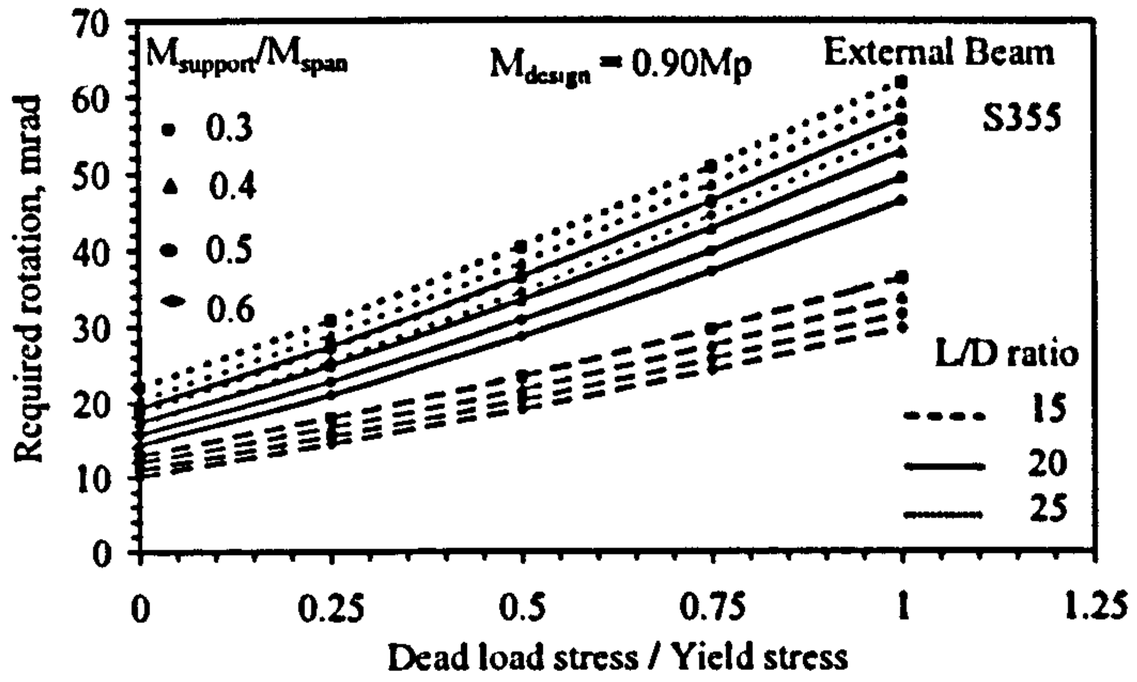

Figure C2-5. Required rotations to achieve 0.90 M_p – S355, External beam

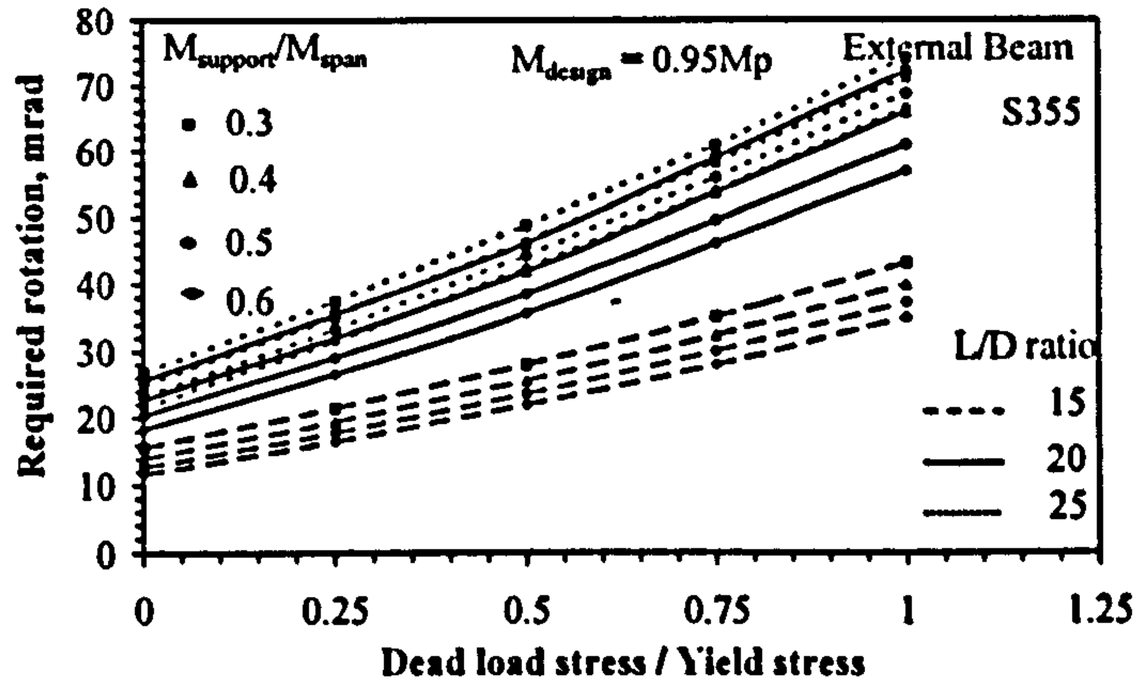

Figure C2-6. Required rotations to achieve 0.95 M_p – S355, External beam

C.2.3 Internal beam, S275:

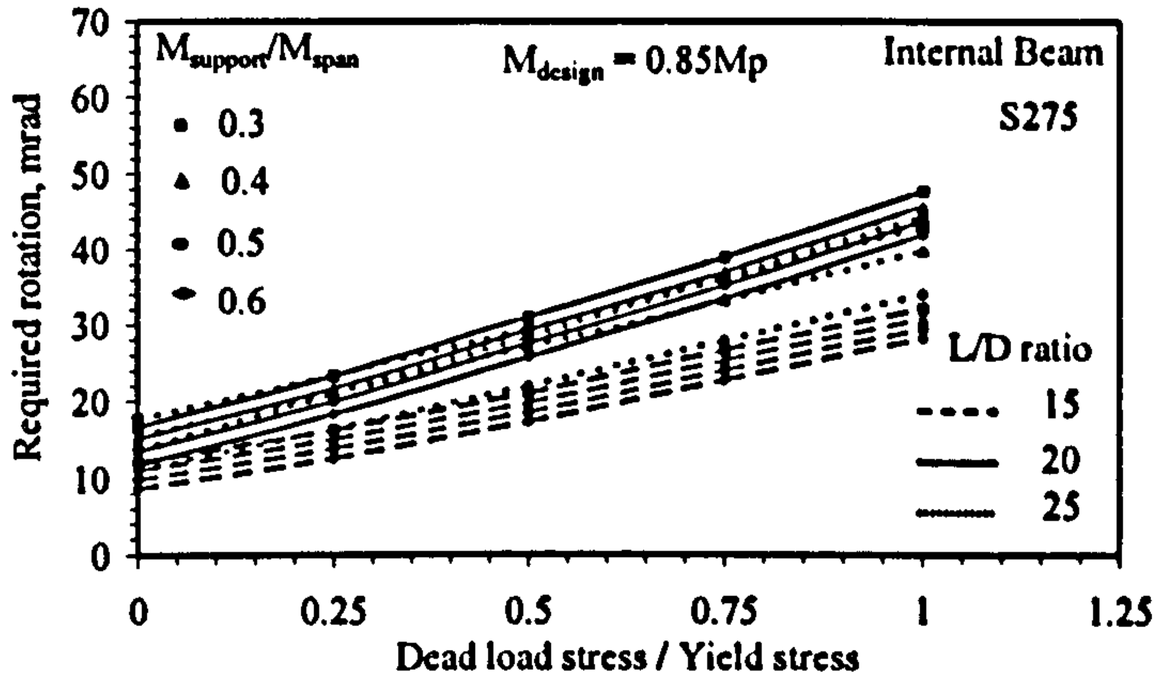

Figure C2-7. Required rotations to achieve 0.85 M_p – S275, Internal beam

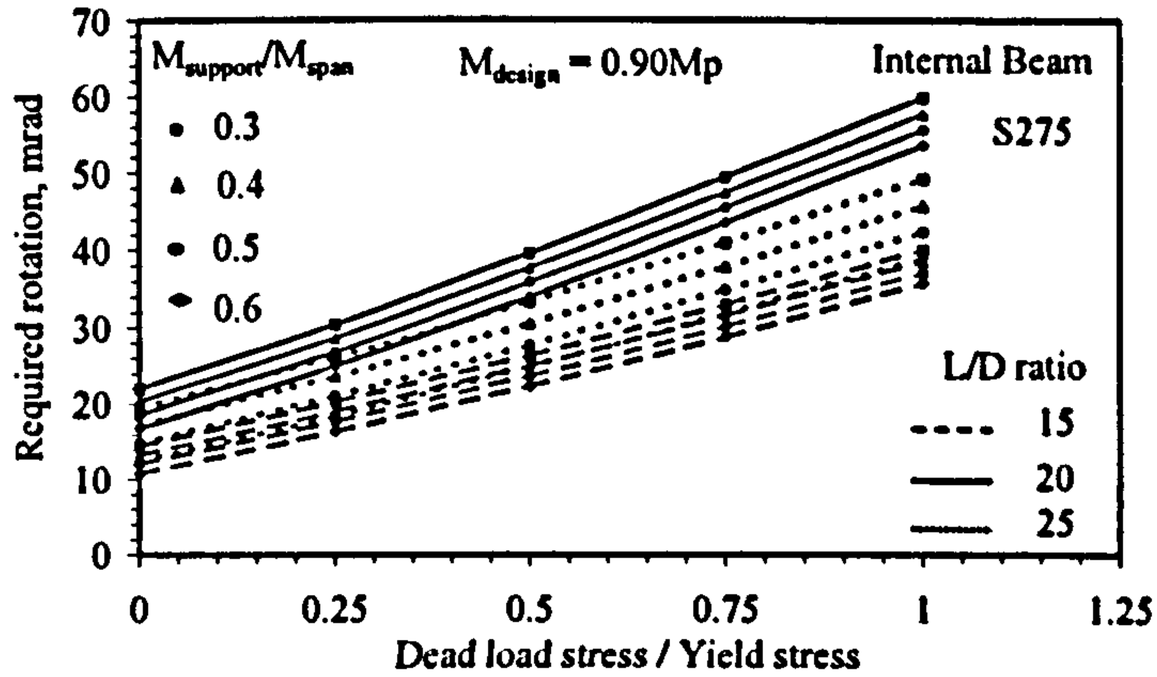

Figure C2-8. Required rotations to achieve 0.90 M_p – S275, Internal beam

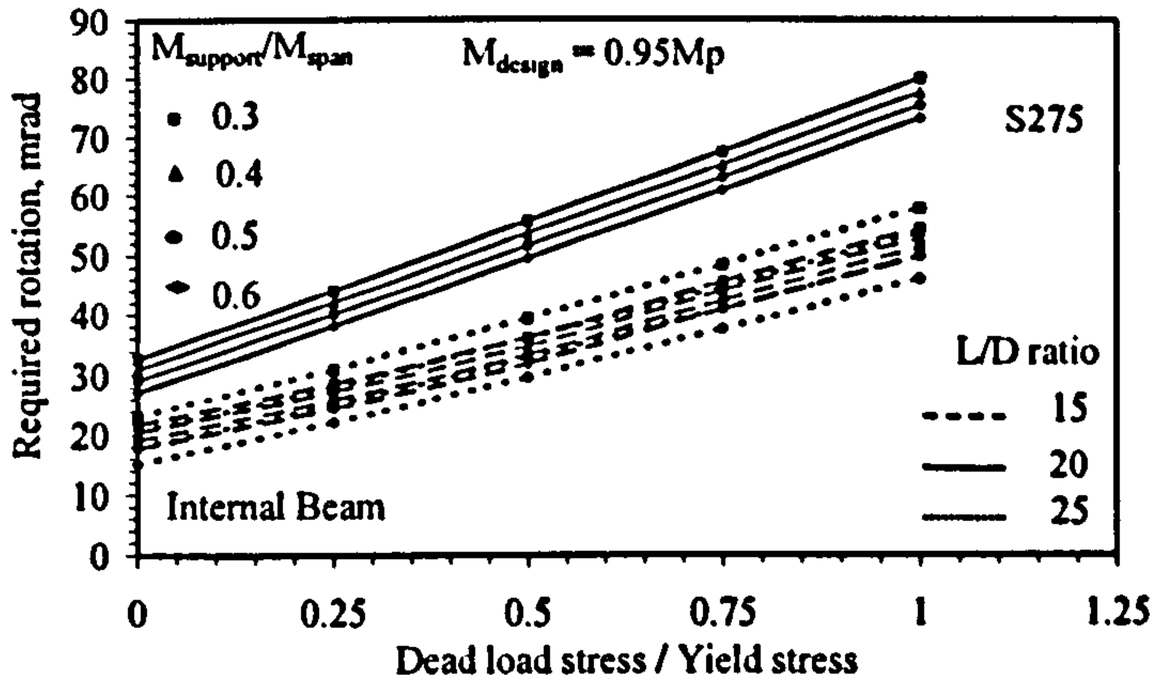

Figure C2-9. Required rotations to achieve 0.95 M_p – S275, Internal beam

C.2.4 Internal beam, S355:

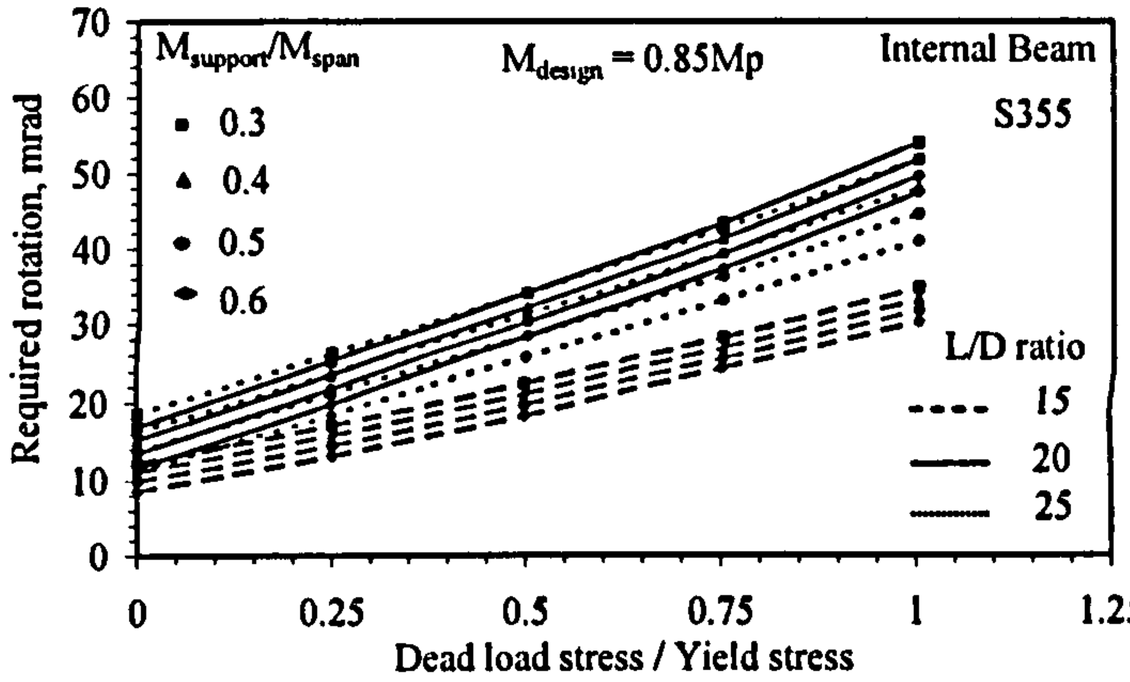

Figure C2-10. Required rotations to achieve 0.85 M_p – S355, Internal beam

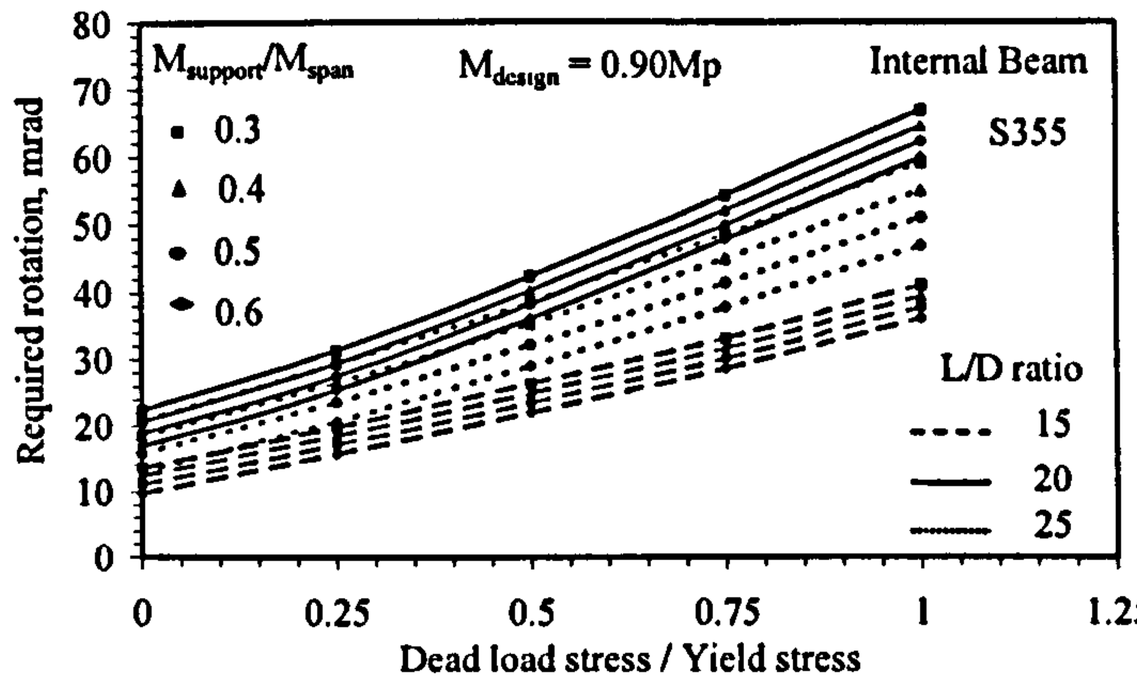

Figure C2-11. Required rotations to achieve 0.90 M_p – S355, Internal beam

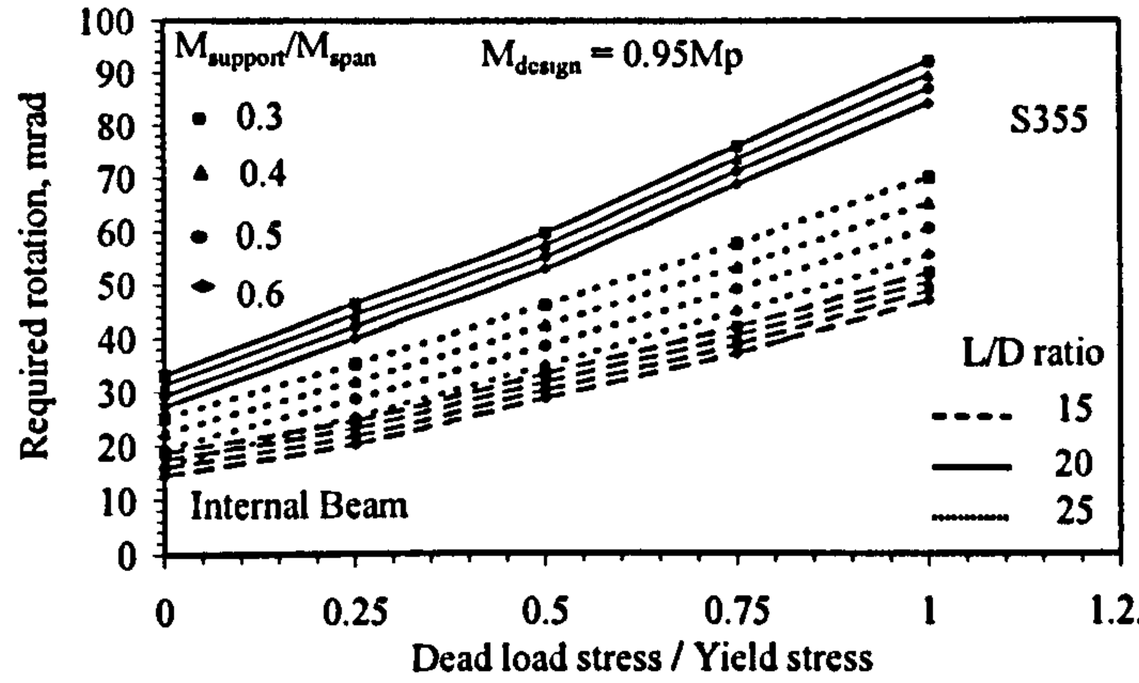

Figure C2-12. Required rotations to achieve 0.95 M_p – S355, Internal beam

C.3 EFFECT OF STEEL GRADE

C.3.1 External beam

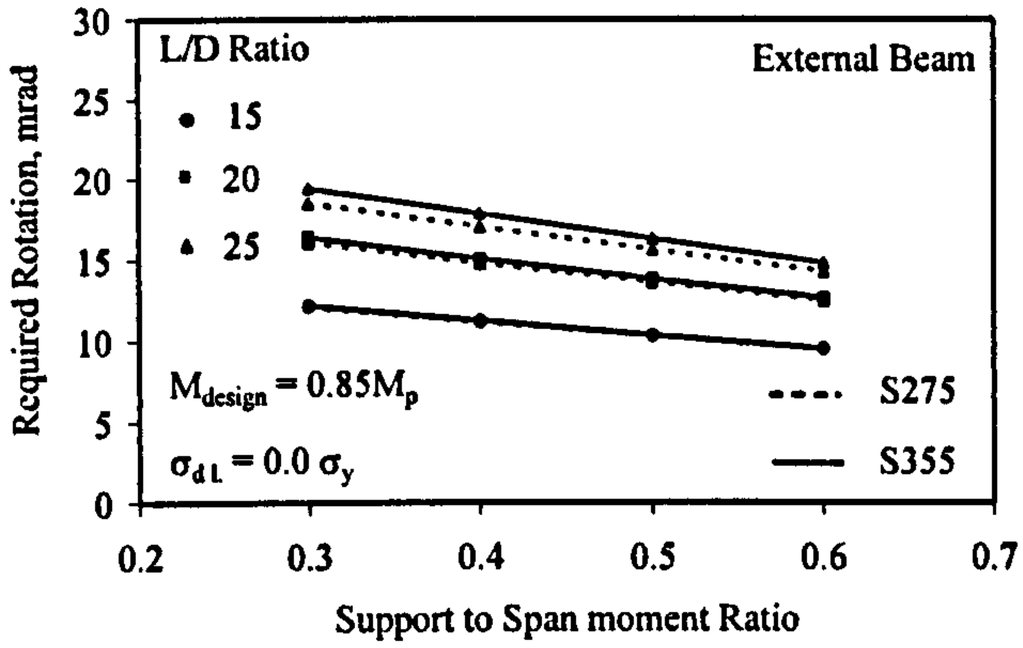

Figure C3-1. Effect of Steel grade on the required rotation at $\sigma_{dl} = 0.0\ \sigma_y$

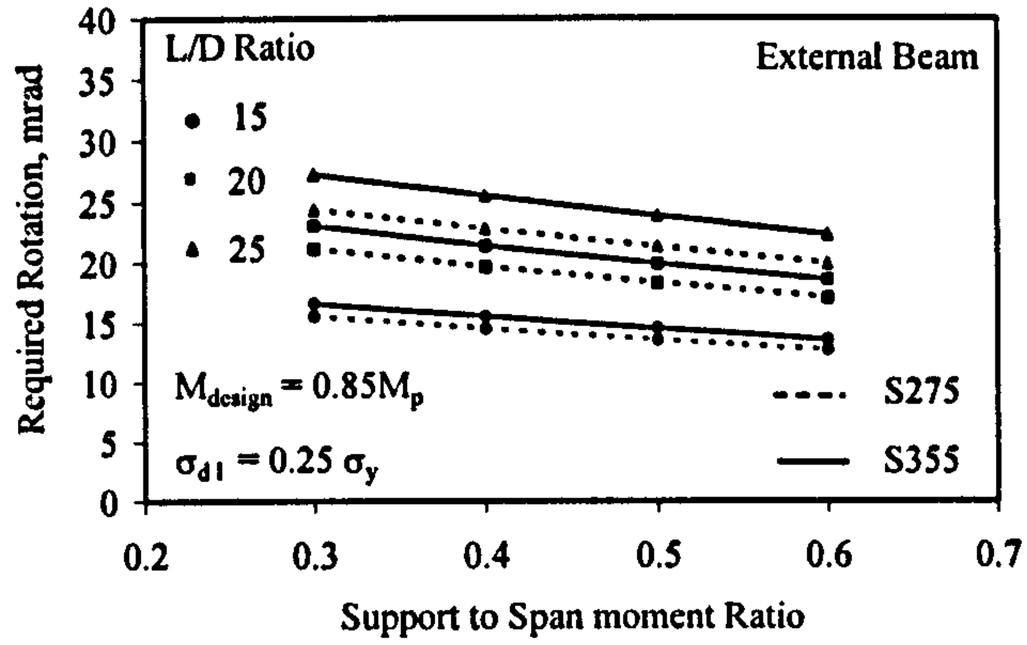

Figure C3-2. Effect of Steel grade on the required rotation at $\sigma_{dl} = 0.25\ \sigma_y$

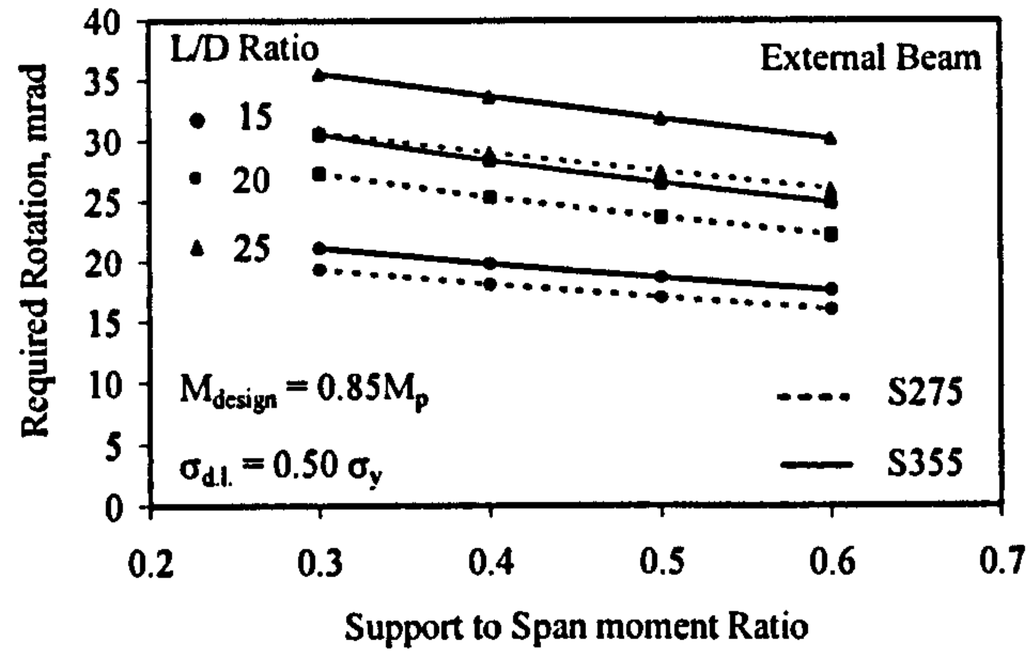

Figure C3-3. Effect of Steel grade on the required rotation at $\sigma_{dl} = 0.50\ \sigma_y$

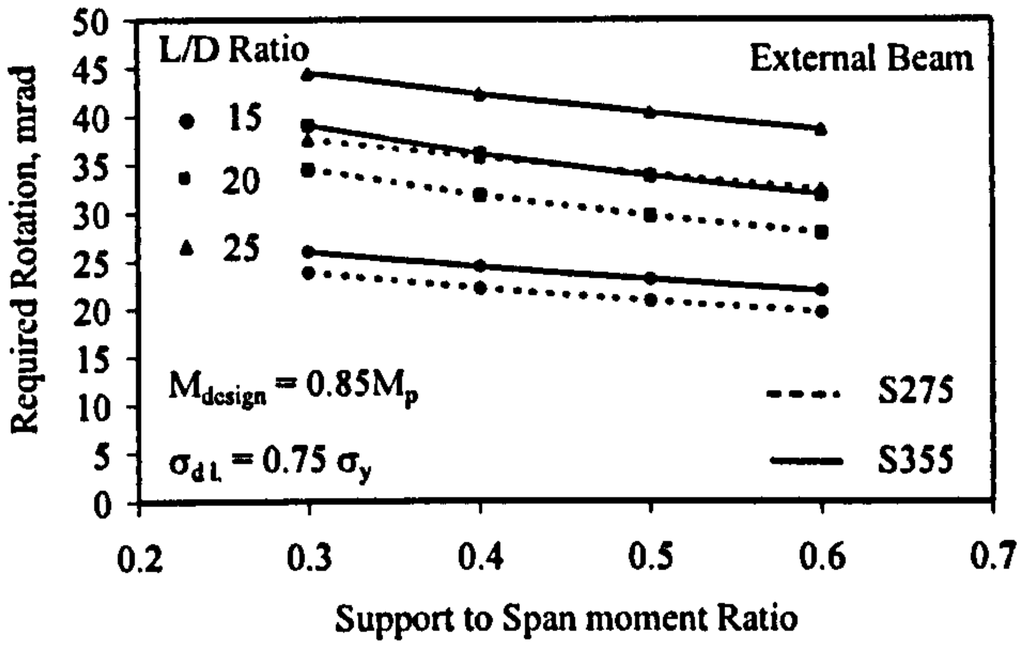

Figure C3-4. Effect of Steel grade on the required rotation at $\sigma_{dl} = 0.75\ \sigma_y$

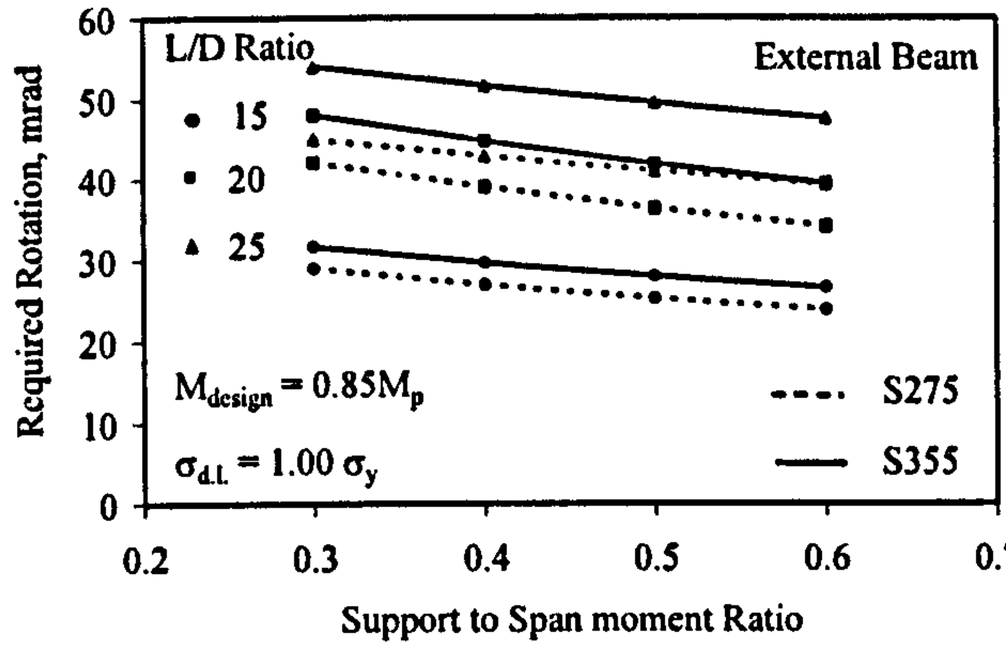

Figure C3-5. Effect of Steel grade on the required rotation at $\sigma_{dl} = 1.0\ \sigma_y$

C.3.2 Internal beam

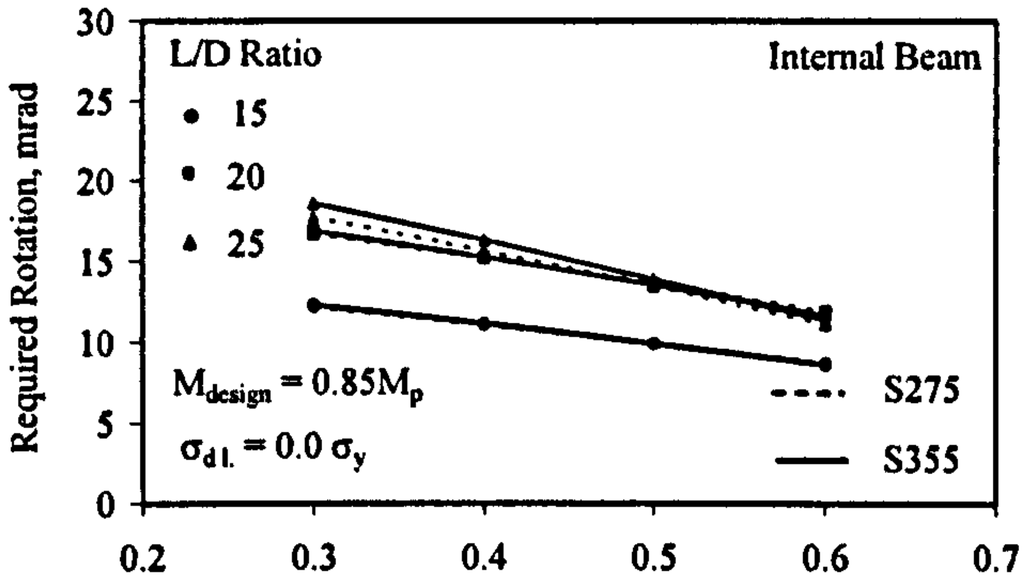

Figure C3-6. Effect of Steel grade on the required rotation at $\sigma_{dl} = 0.0\ \sigma_y$

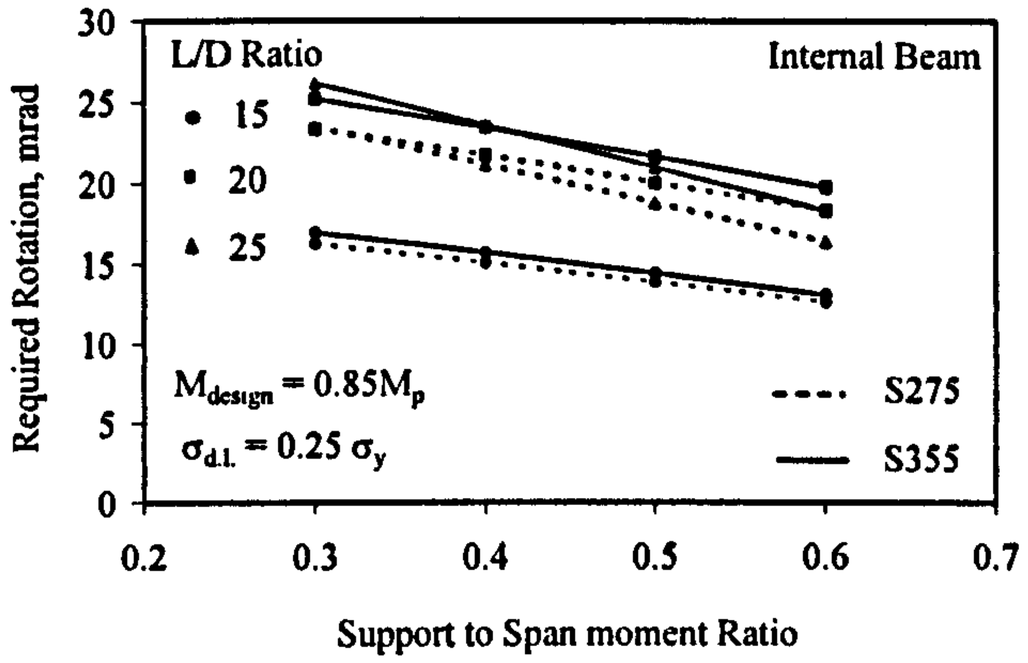

Figure C3-7. Effect of Steel grade on the required rotation at $\sigma_{dl} = 0.25\ \sigma_y$

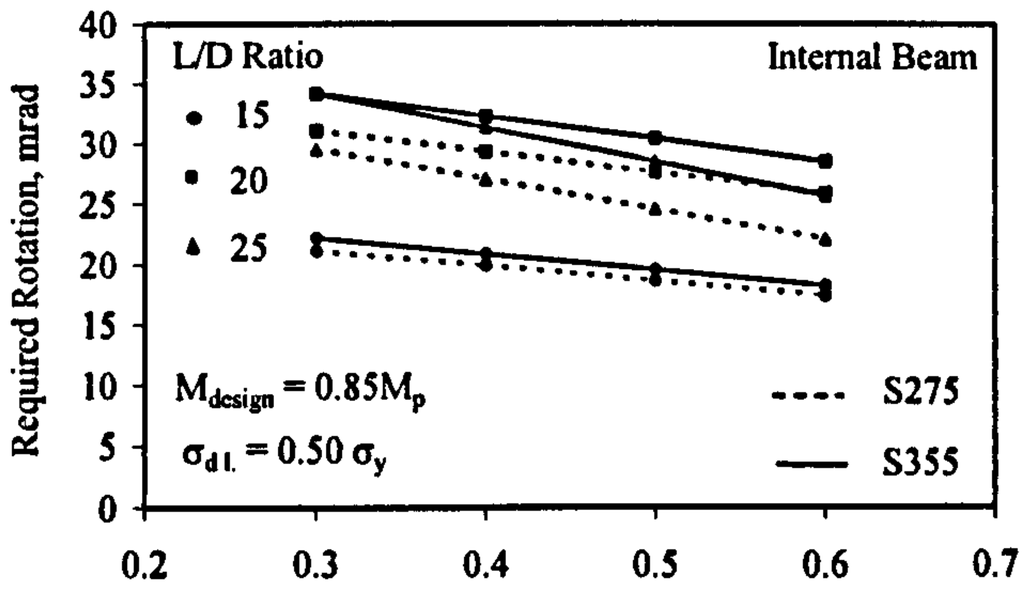

Figure C3-8. Effect of Steel grade on the required rotation at $\sigma_{dl} = 0.50\ \sigma_y$

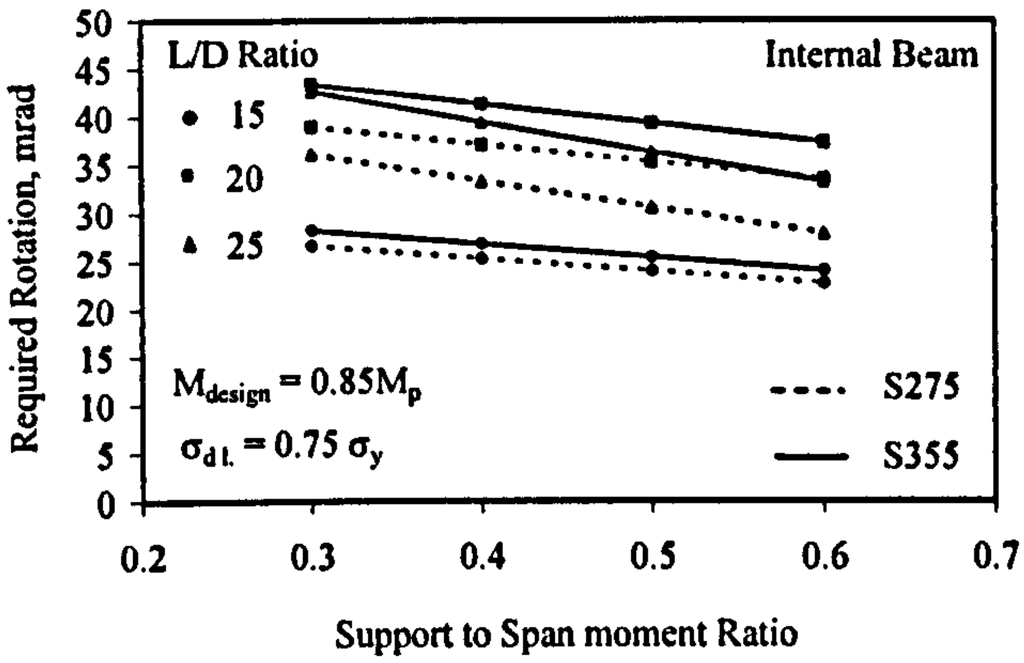

Figure C3-9. Effect of Steel grade on the required rotation at $\sigma_{dl} = 0.75\ \sigma_y$

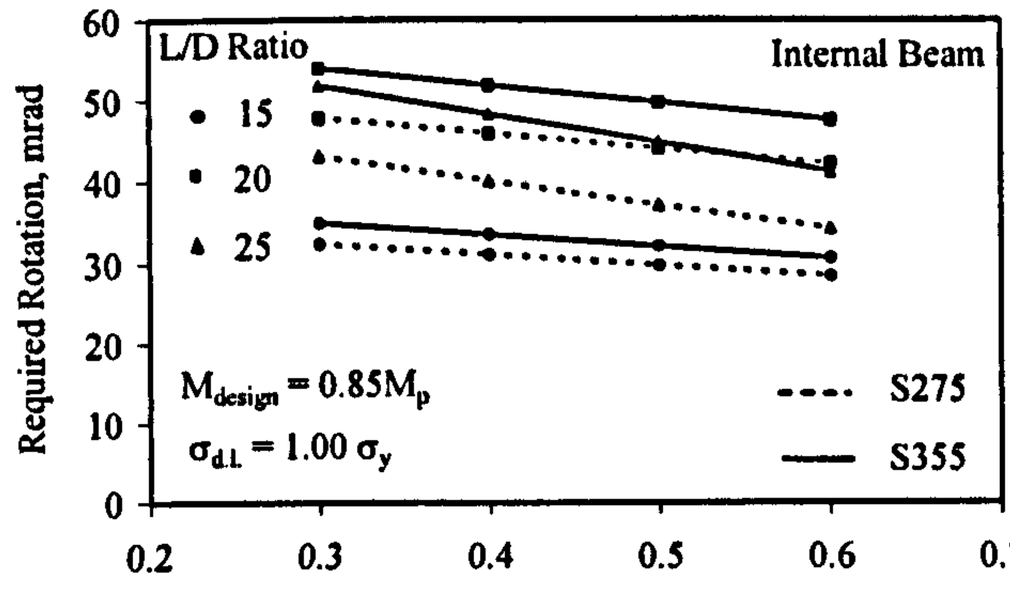

Figure C3-10. Effect of Steel grade on the required rotation at $\sigma_{dl} = 1.0\ \sigma_y$

C.4 EFFECT OF DESIGN MOMENT

C.4.1 Grade S275

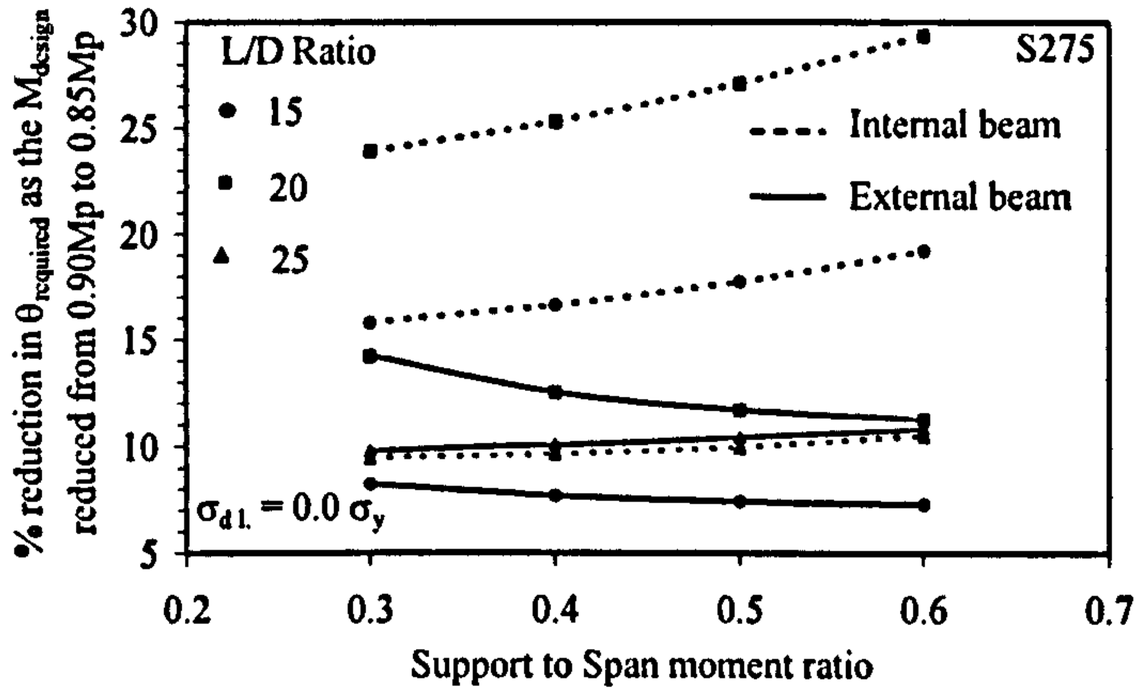

Figure C4-1. Percentage reduction in required rotation as the design moment reduced from 0.90 M_p to 0.85 M_p for unpropped form of construction: $\sigma_{dl} = 0.0\sigma_y$

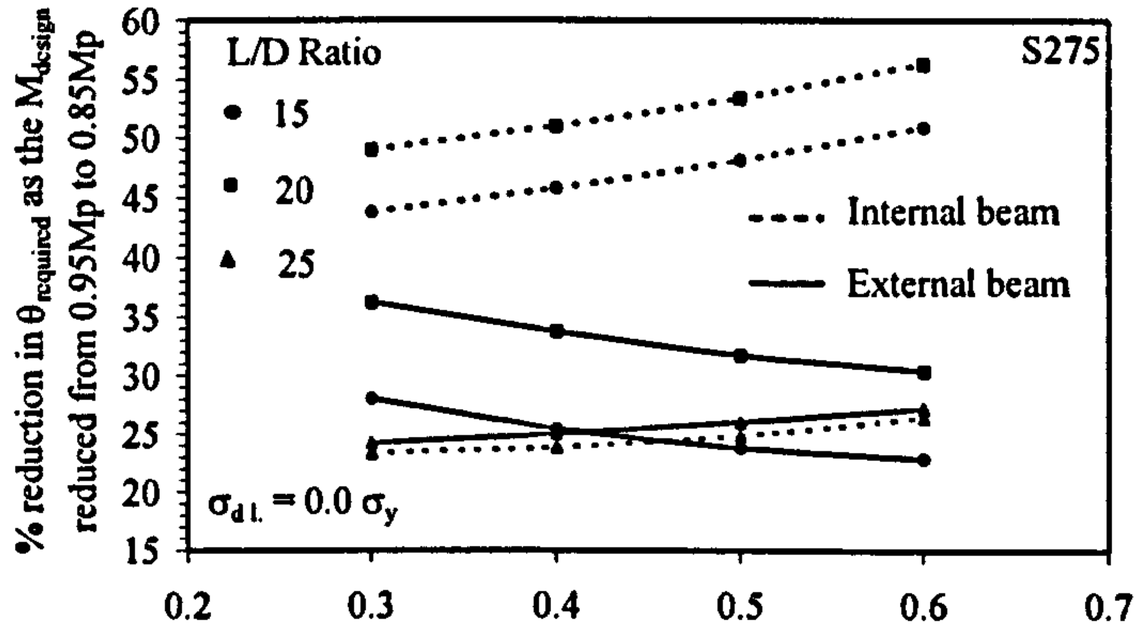

Figure C4-2. Percentage reduction in required rotation as the design moment reduced from 0.95 M_p to 0.85 M_p for unpropped form of construction: $\sigma_{dl} = 0.0\sigma_y$

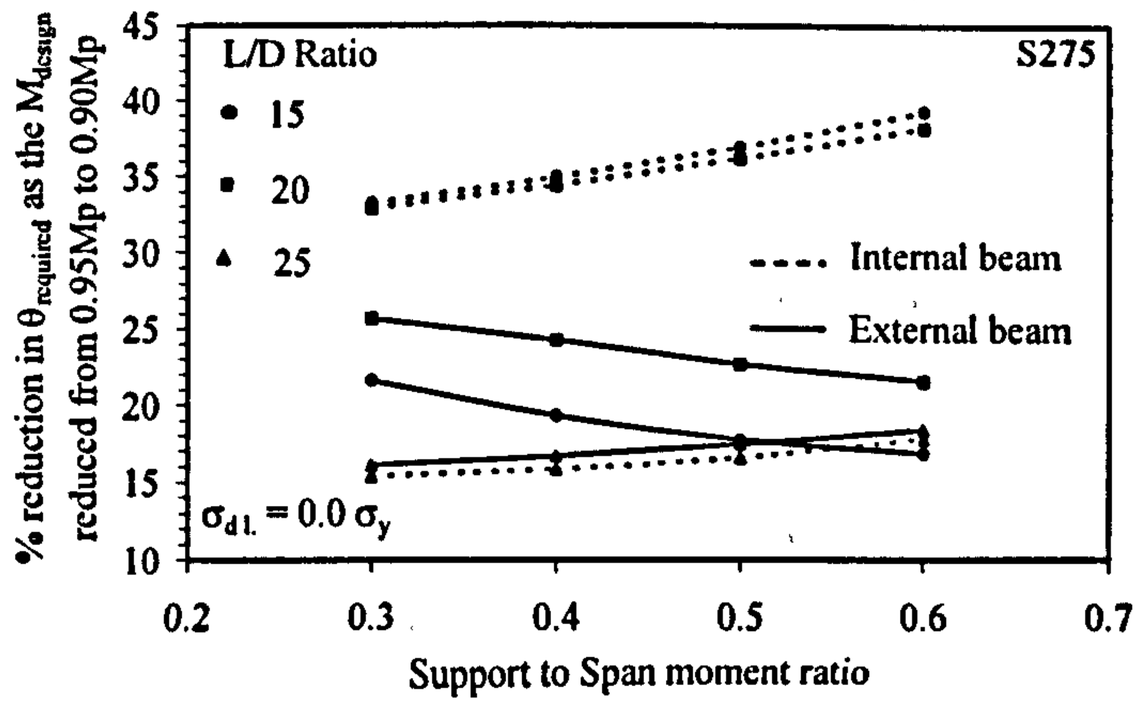

Figure C4-3. Percentage reduction in required rotation as the design moment reduced from 0.95 M_p to 0.90 M_p for unpropped form of construction: $\sigma_{dl} = 0.0\sigma_y$

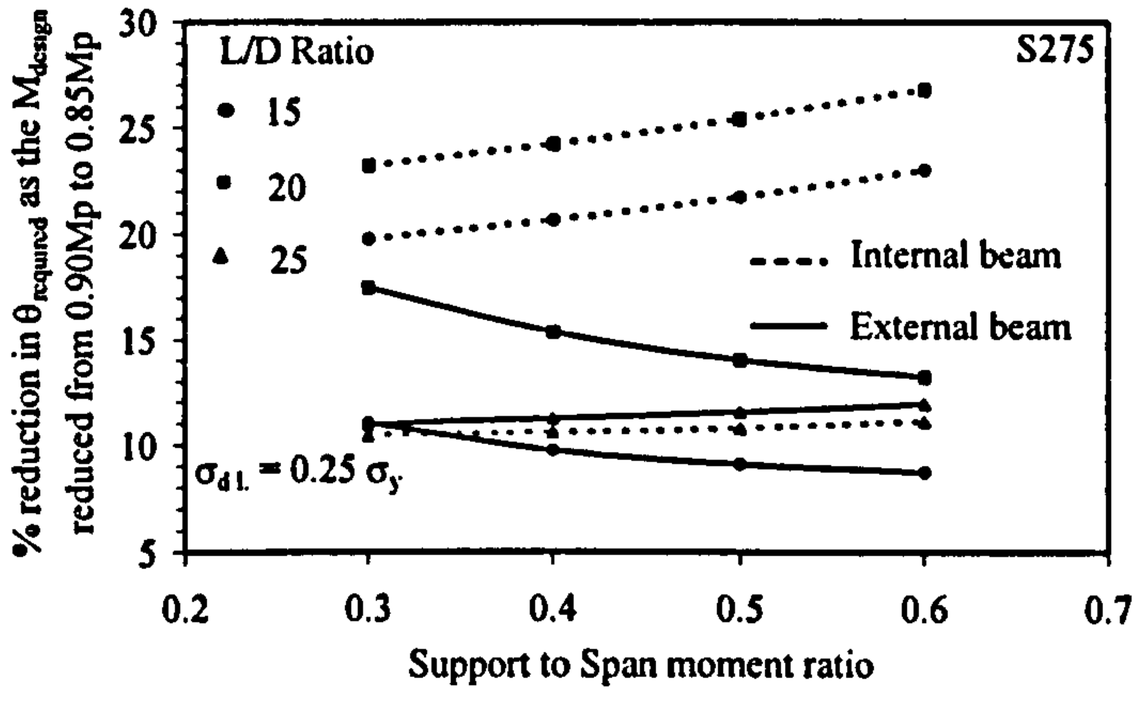

Figure C4-4. Percentage reduction in required rotation as the design moment reduced from 0.90 M_p to 0.85 M_p for unpropped form of construction: $\sigma_{dl} = 0.25\sigma_y$

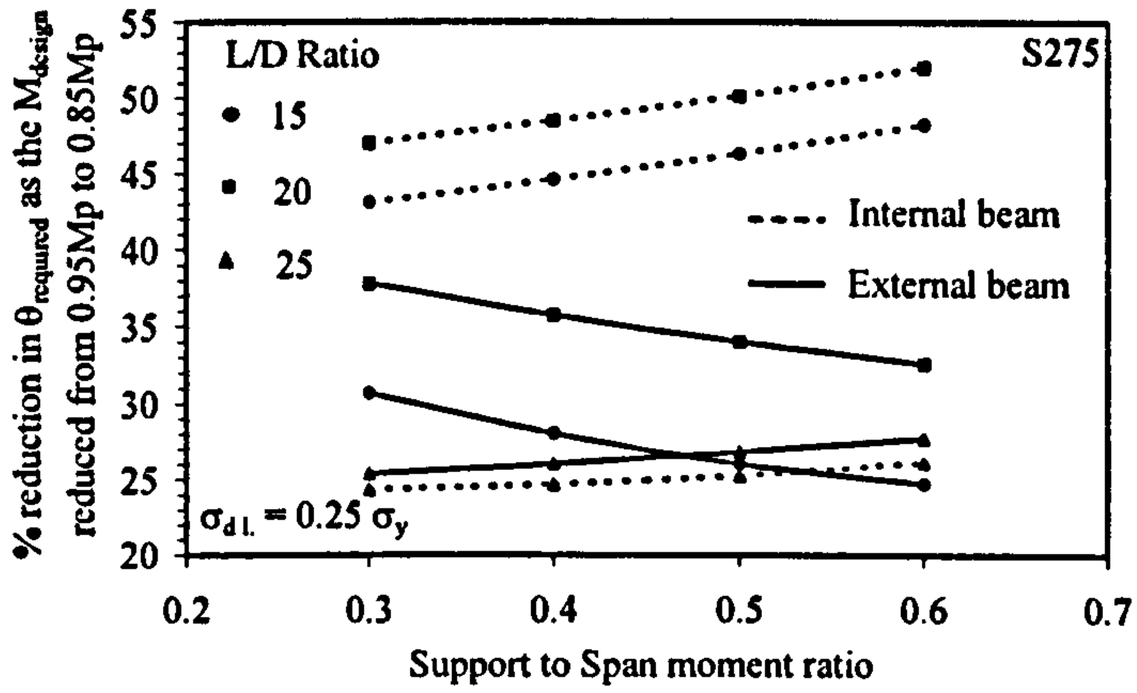

Figure C4-5. Percentage reduction in required rotation as the design moment reduced from 0.95 M_p to 0.85 M_p for unpropped form of construction: $\sigma_{dl} = 0.25\sigma_y$

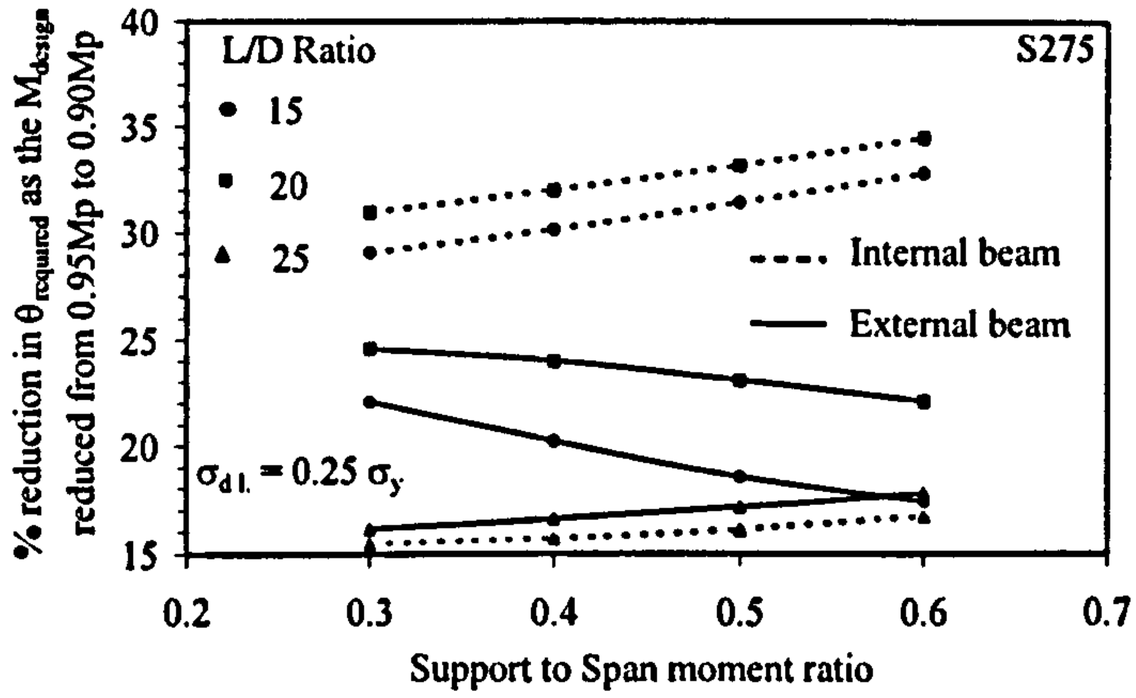

Figure C4-6. Percentage reduction in required rotation as the design moment reduced from 0.95 M_p to 0.90 M_p for unpropped form of construction: $\sigma_{dl} = 0.25\sigma_y$

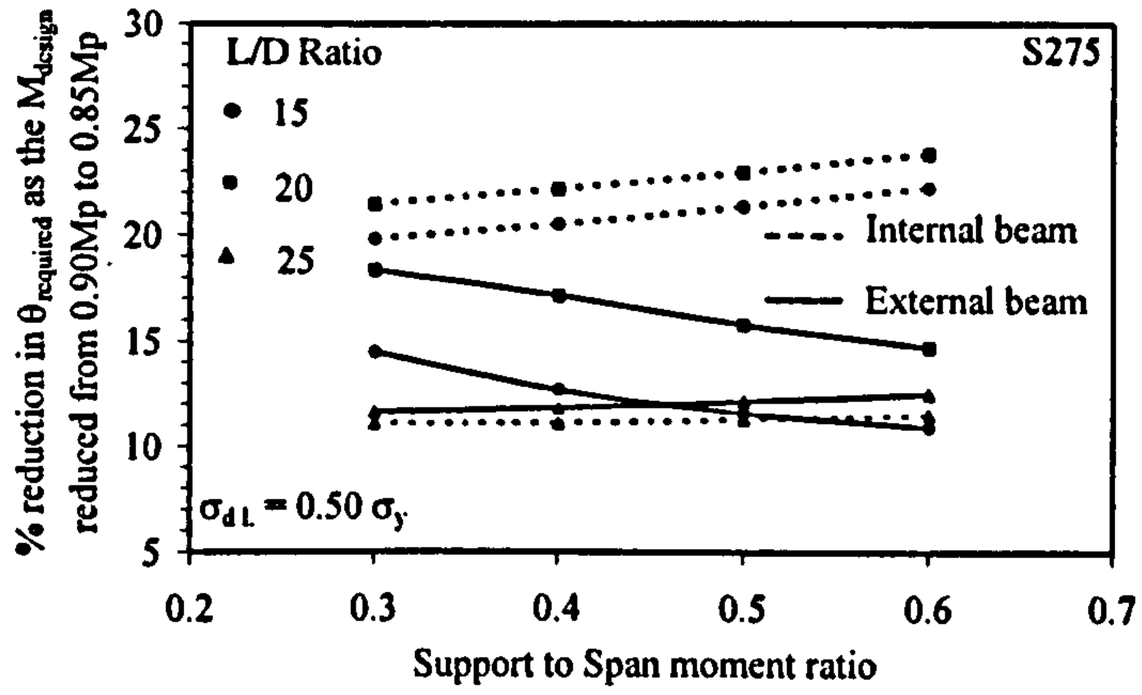

Figure C4-7. Percentage reduction in required rotation as the design moment reduced from 0.90 M_p to 0.85 M_p for unpropped form of construction: $\sigma_{dl} = 0.50\sigma_y$

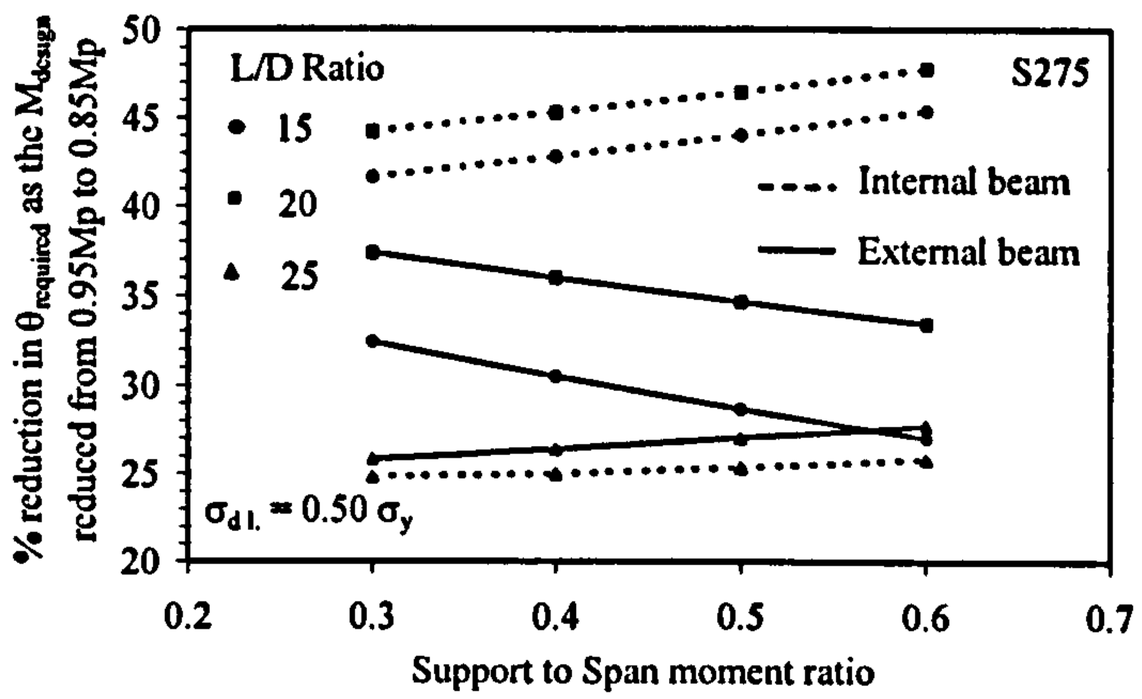

Figure C4-8. Percentage reduction in required rotation as the design moment reduced from 0.95 M_p to 0.85 M_p for unpropped form of construction: $\sigma_{dl} = 0.50\sigma_y$

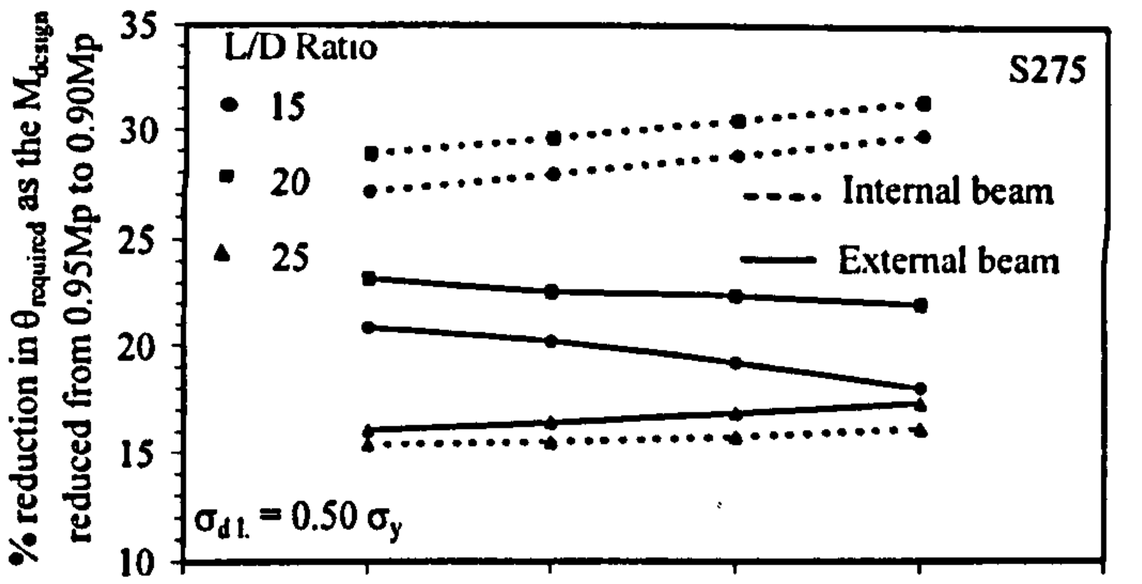

Figure C4-9. Percentage reduction in required rotation as the design moment reduced from 0.95 M_p to 0.90 M_p for unpropped form of construction: $\sigma_{dl} = 0.50\sigma_y$

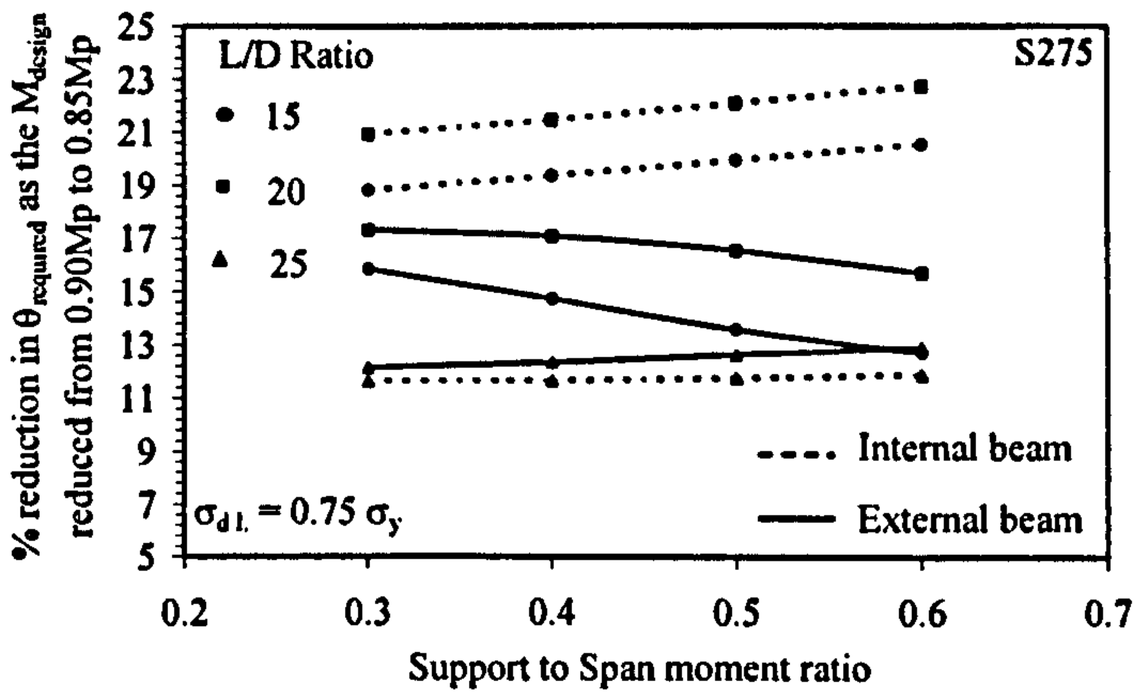

Figure C4-10. Percentage reduction in required rotation as the design moment reduced from 0.90 M_p to 0.85 M_p for unpropped form of construction: $\sigma_{dl} = 0.75\sigma_y$

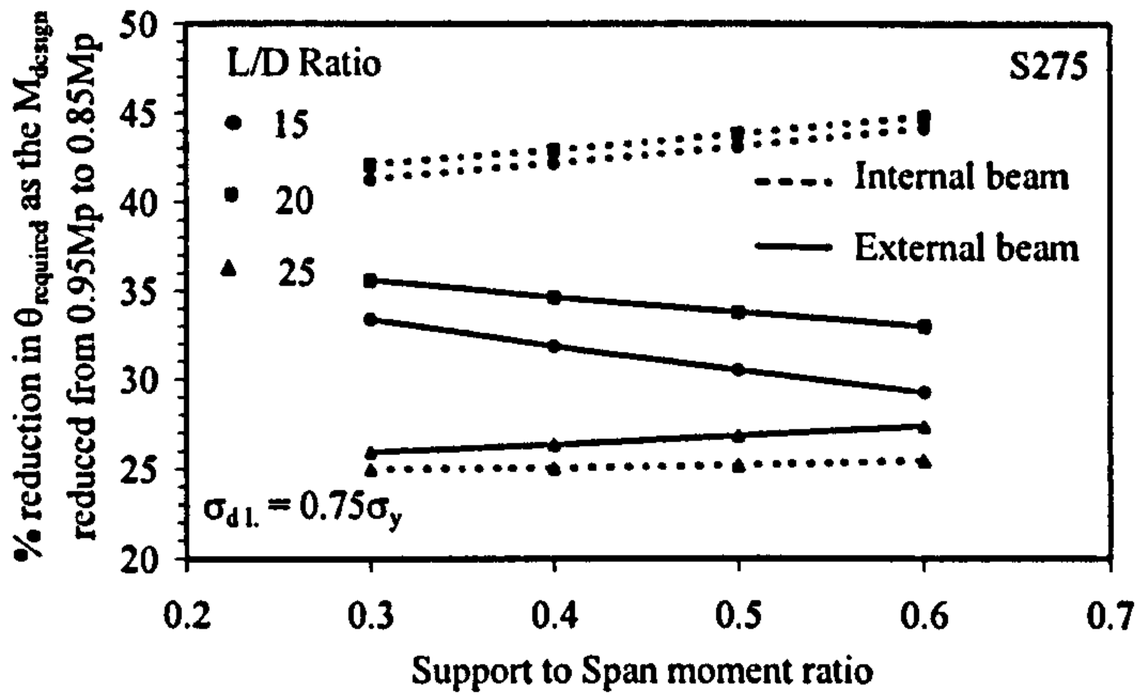

Figure C4-11. Percentage reduction in required rotation as the design moment reduced from 0.95 M_p to 0.85 M_p for unpropped form of construction: $\sigma_{dl} = 0.75\sigma_y$

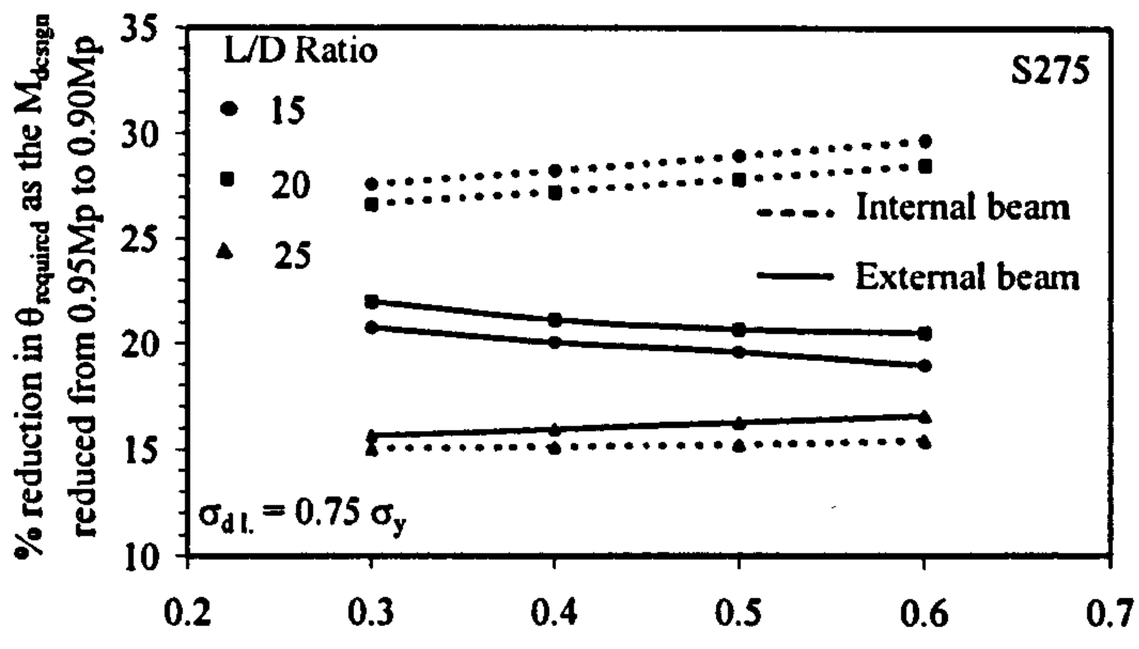

Figure C4-12. Percentage reduction in required rotation as the design moment reduced from 0.95 M_p to 0.90 M_p for unpropped form of construction: $\sigma_{dl} = 0.75\sigma_y$

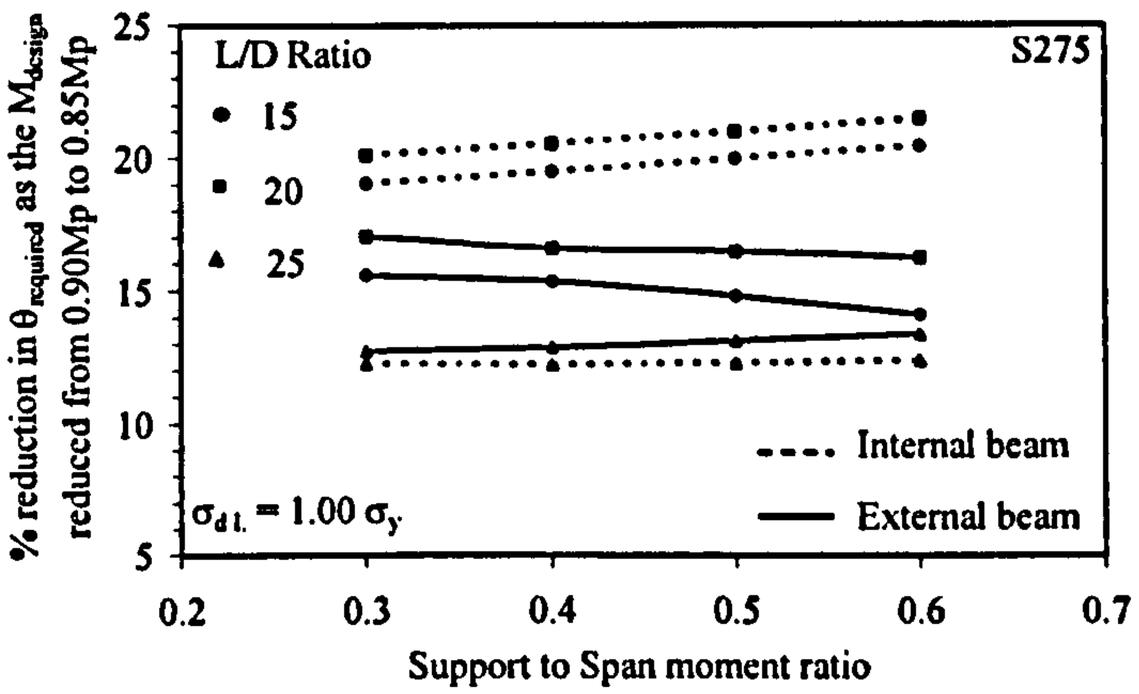

Figure C4-13. Percentage reduction in required rotation as the design moment reduced from 0.90 M_p to 0.85 M_p for unpropped form of construction: $\sigma_{dl} = 1.00\sigma_y$

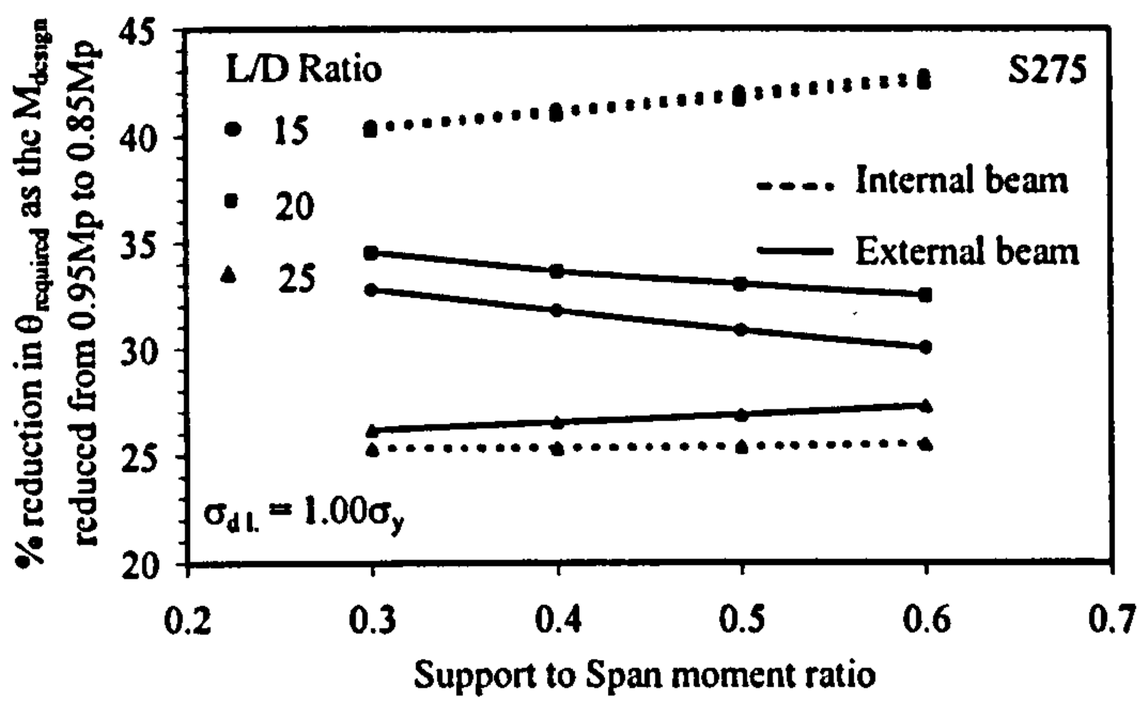

Figure C4-14. Percentage reduction in required rotation as the design moment reduced from 0.95 M_p to 0.85 M_p for unpropped form of construction: $\sigma_{dl} = 1.00\sigma_y$

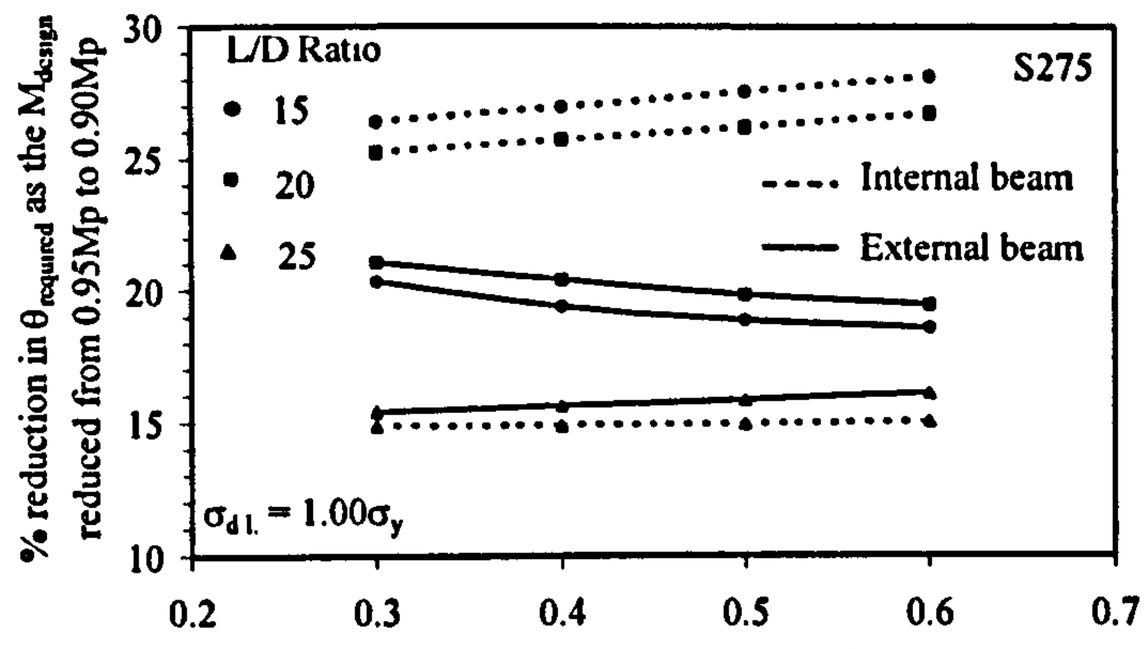

Figure C4-15. Percentage reduction in required rotation as the design moment reduced from 0.95 M_p to 0.90 M_p for unpropped form of construction: $\sigma_{dl} = 1.00\sigma_y$

C.4.2 Grade S355

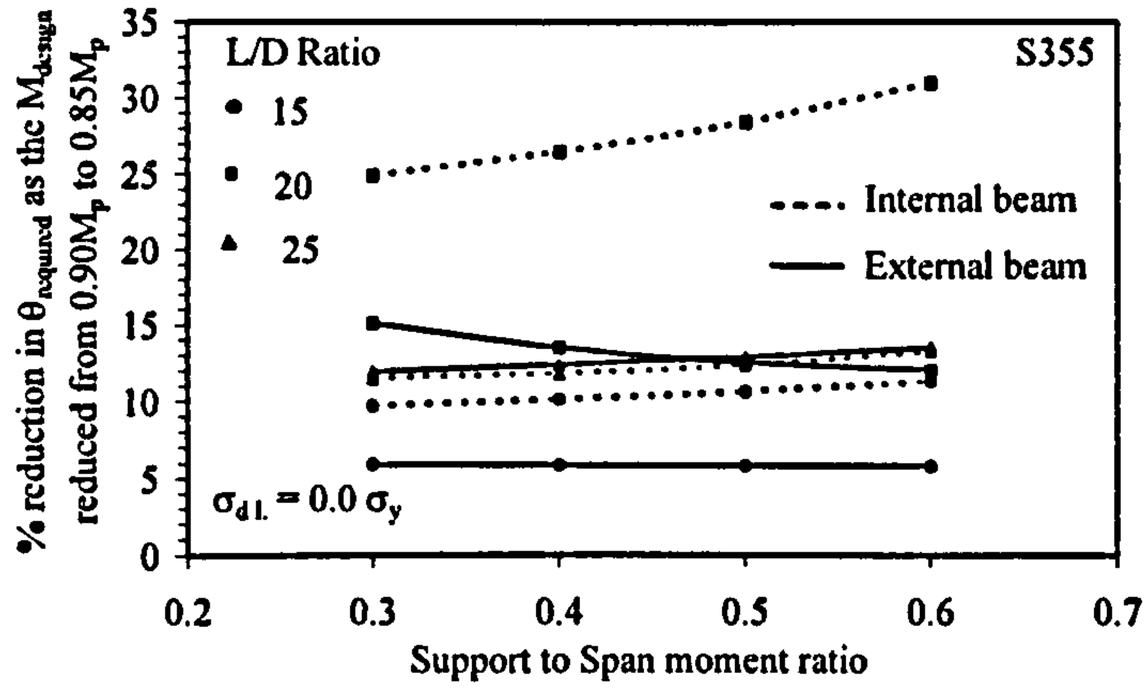

Figure C4-16. Percentage reduction in required rotation as the design moment reduced from 0.90 M_p to 0.85 M_p for unpropped form of construction: $\sigma_{dl} = 0.0\sigma_y$

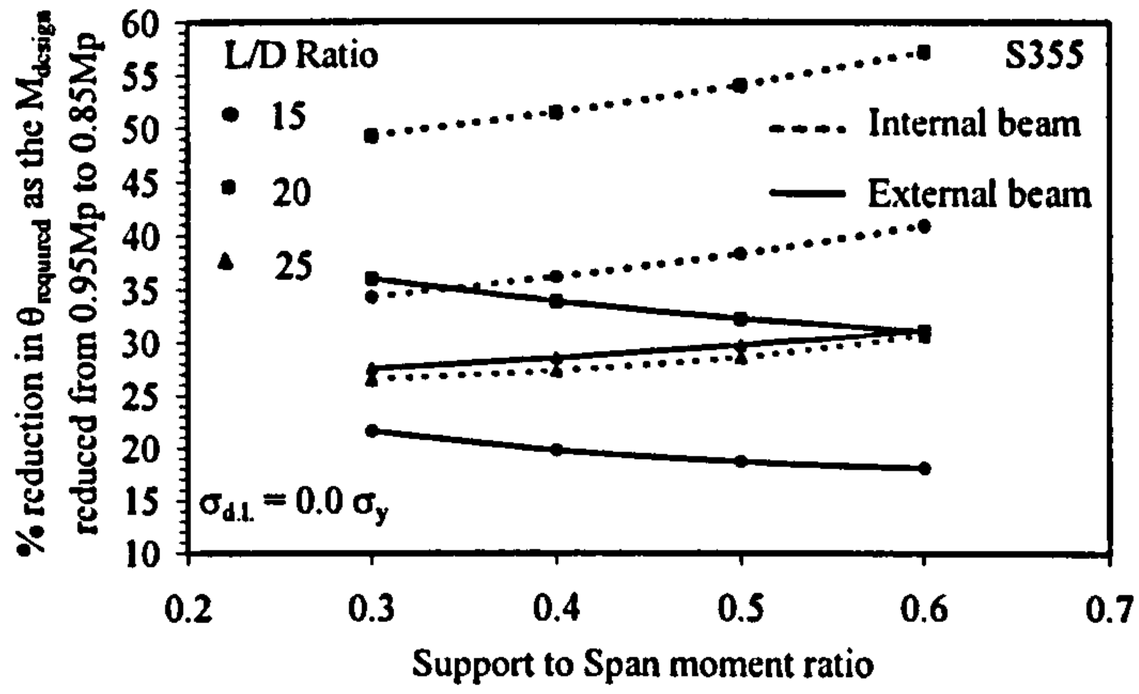

Figure C4-17. Percentage reduction in required rotation as the design moment reduced from 0.95 M_p to 0.85 M_p for unpropped form of construction: $\sigma_{dl} = 0.0\sigma_y$

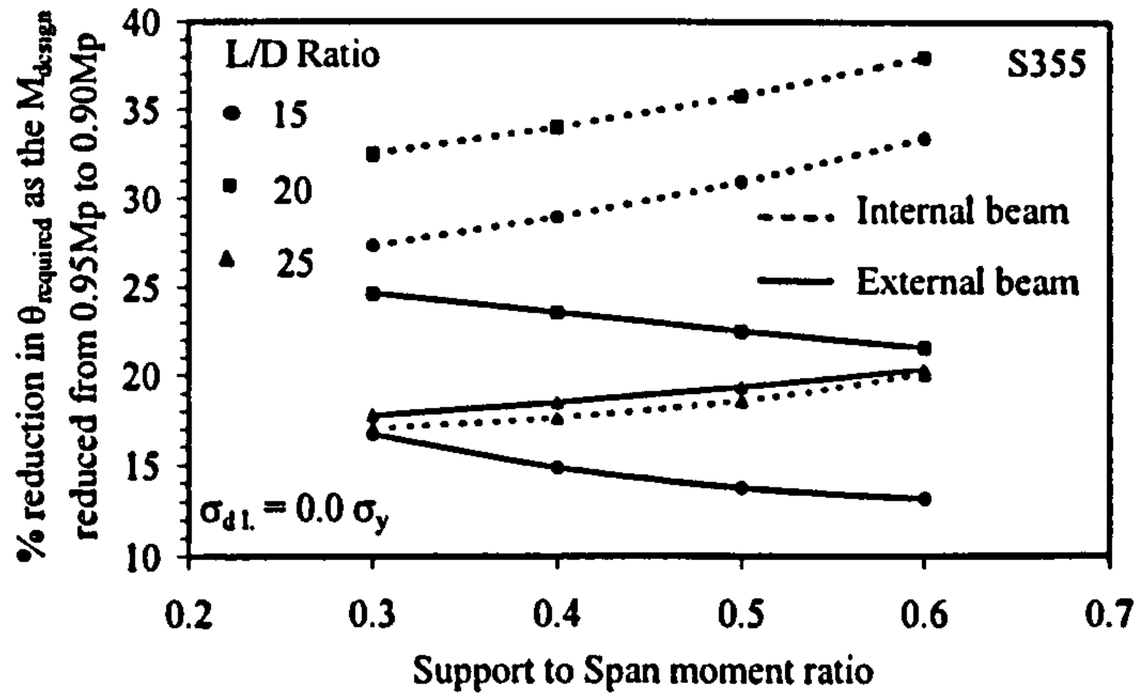

Figure C4-18. Percentage reduction in required rotation as the design moment reduced from 0.95 M_p to 0.90 M_p for unpropped form of construction: $\sigma_{dl} = 0.0\sigma_y$

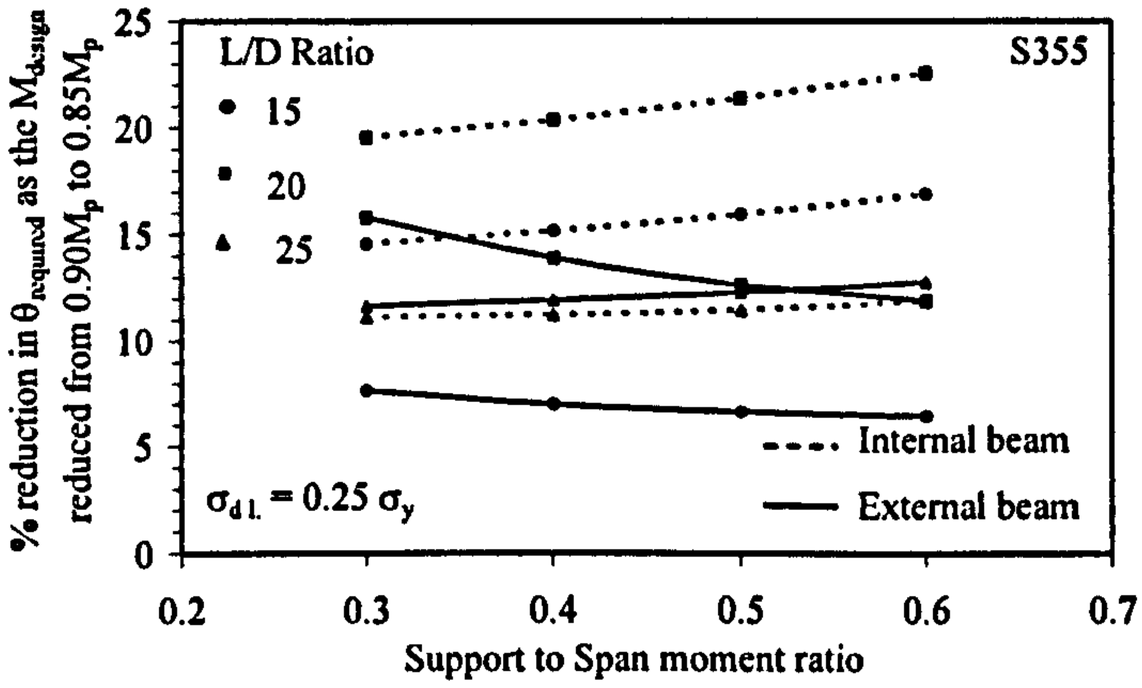

Figure C4-19. Percentage reduction in required rotation as the design moment reduced from 0.90 M_p to 0.85 M_p for unpropped form of construction: $\sigma_{dl} = 0.25\sigma_y$

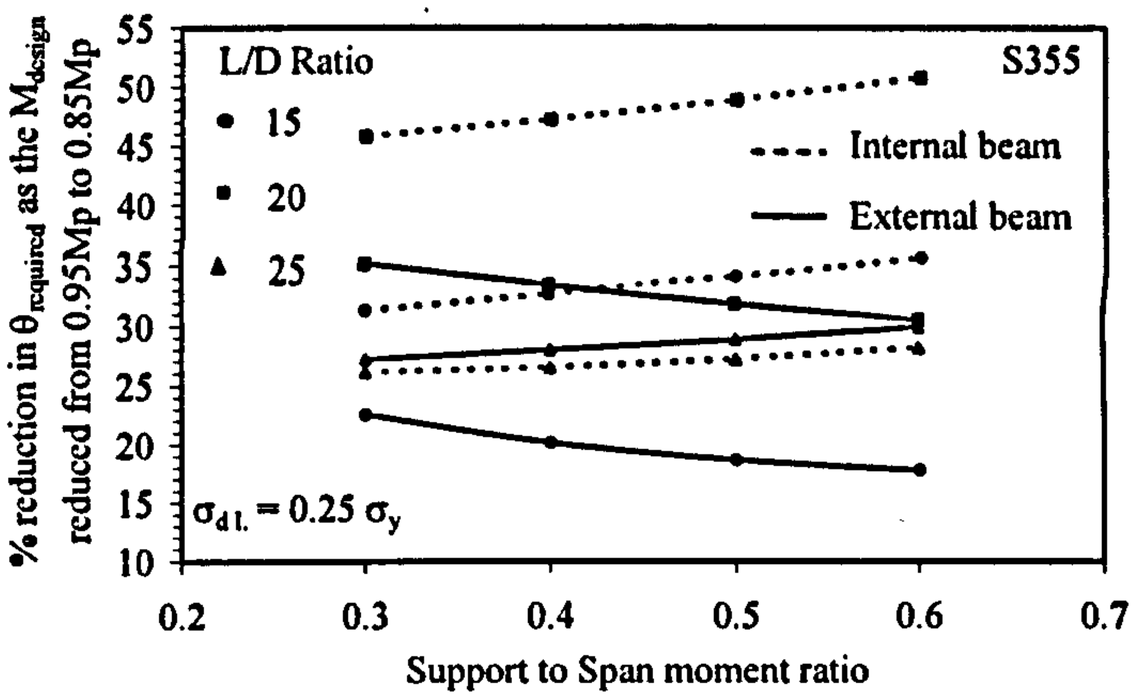

Figure C4-20. Percentage reduction in required rotation as the design moment reduced from 0.95 M_p to 0.85 M_p for unpropped form of construction: $\sigma_{dl} = 0.25\sigma_y$

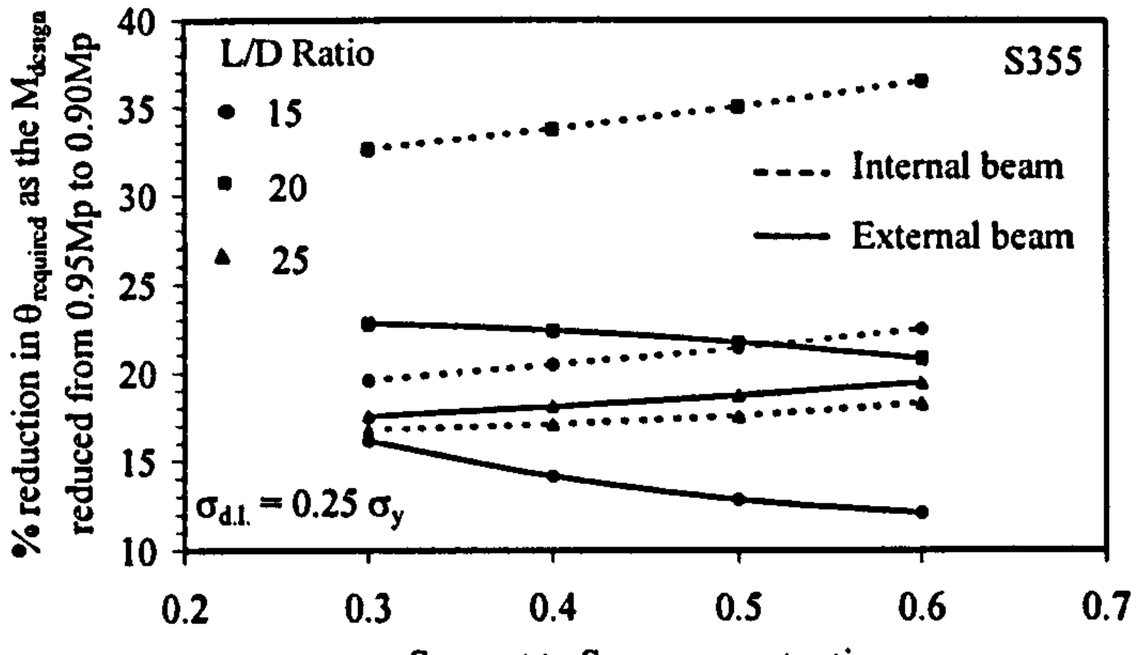

Figure C4-21. Percentage reduction in required rotation as the design moment reduced from 0.95 M_p to 0.90 M_p for unpropped form of construction: $\sigma_{dl} = 0.25\sigma_y$

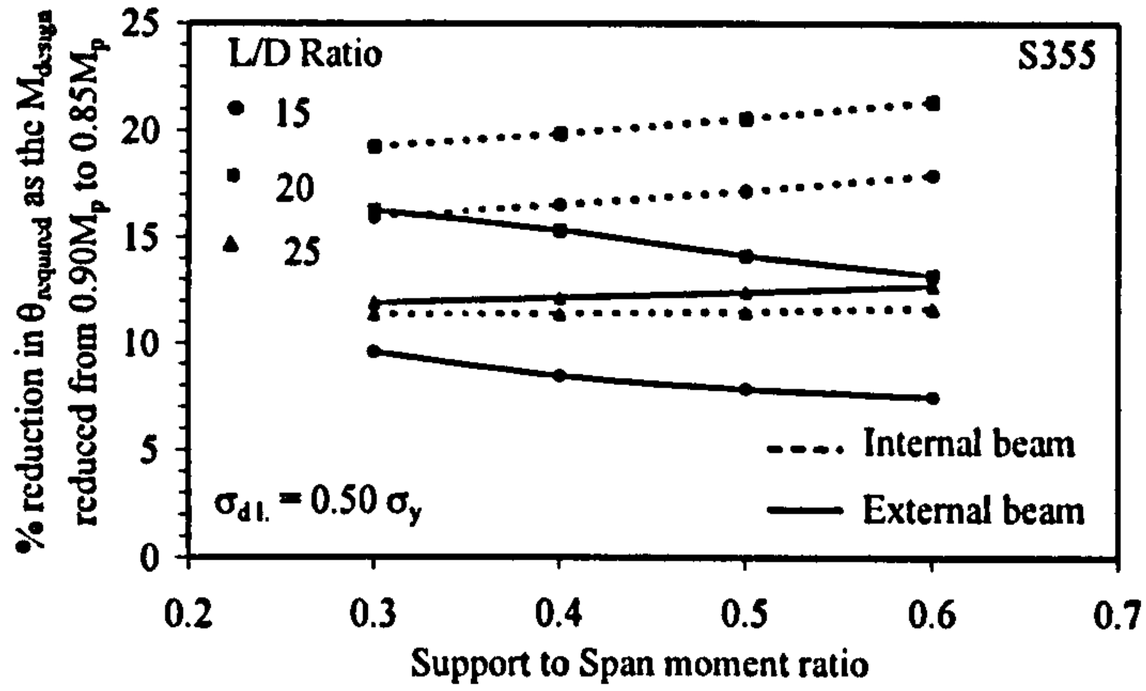

Figure C4-22. Percentage reduction in required rotation as the design moment reduced from 0.90 M_p to 0.85 M_p for unpropped form of construction: $\sigma_{dl} = 0.50\sigma_y$

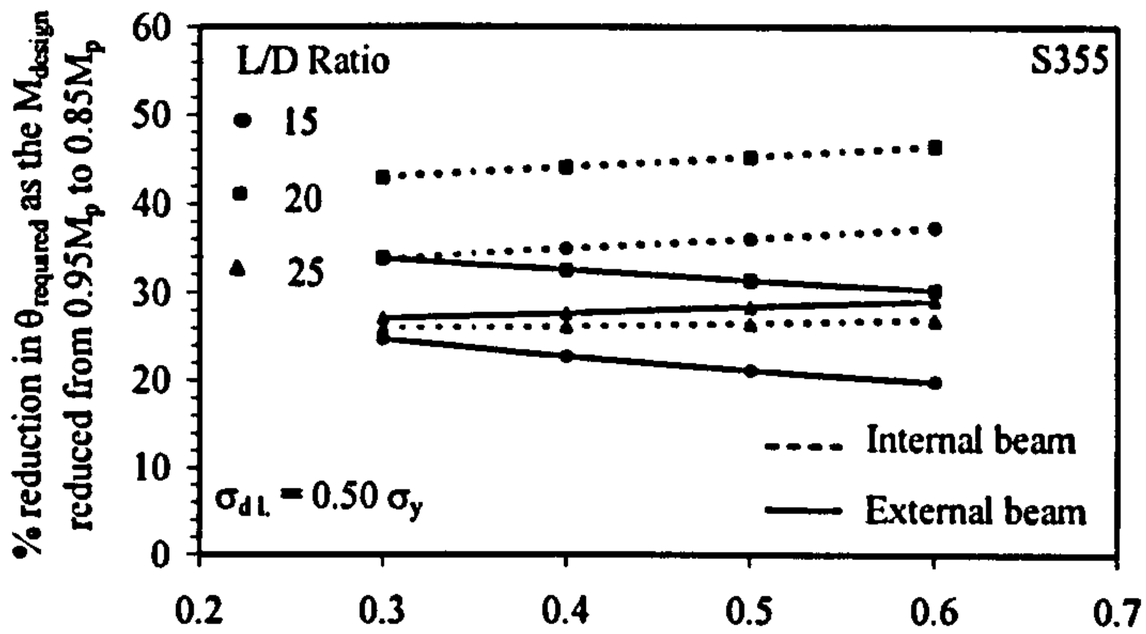

Figure C4-23. Percentage reduction in required rotation as the design moment reduced from 0.95 M_p to 0.85 M_p for unpropped form of construction: $\sigma_{dl} = 0.50\sigma_y$

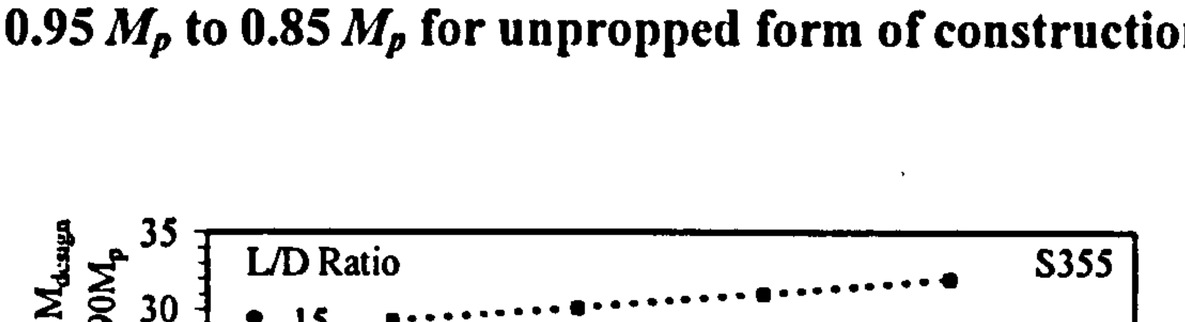

Figure C4-24. Percentage reduction in required rotation as the design moment reduced from 0.95 M_p to 0.90 M_p for unpropped form of construction: $\sigma_{dl} = 0.50\sigma_y$

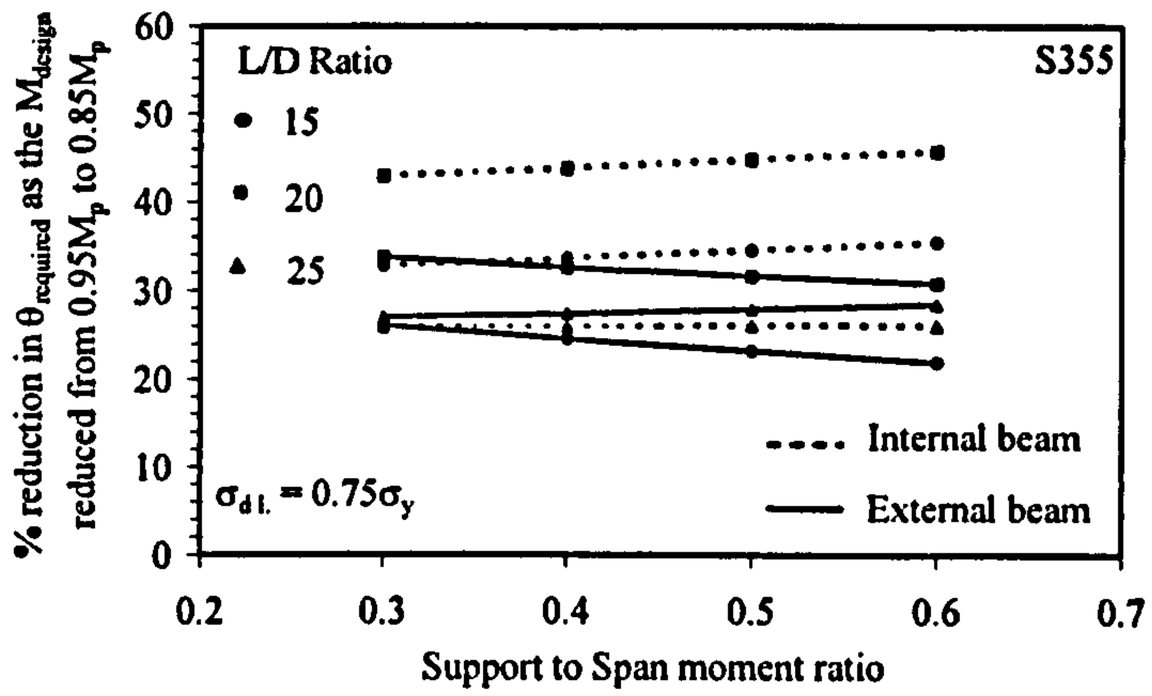

Figure C4-25. Percentage reduction in required rotation as the design moment reduced from 0.90 M_p to 0.85 M_p for unpropped form of construction: $\sigma_{dl} = 0.75\sigma_y$

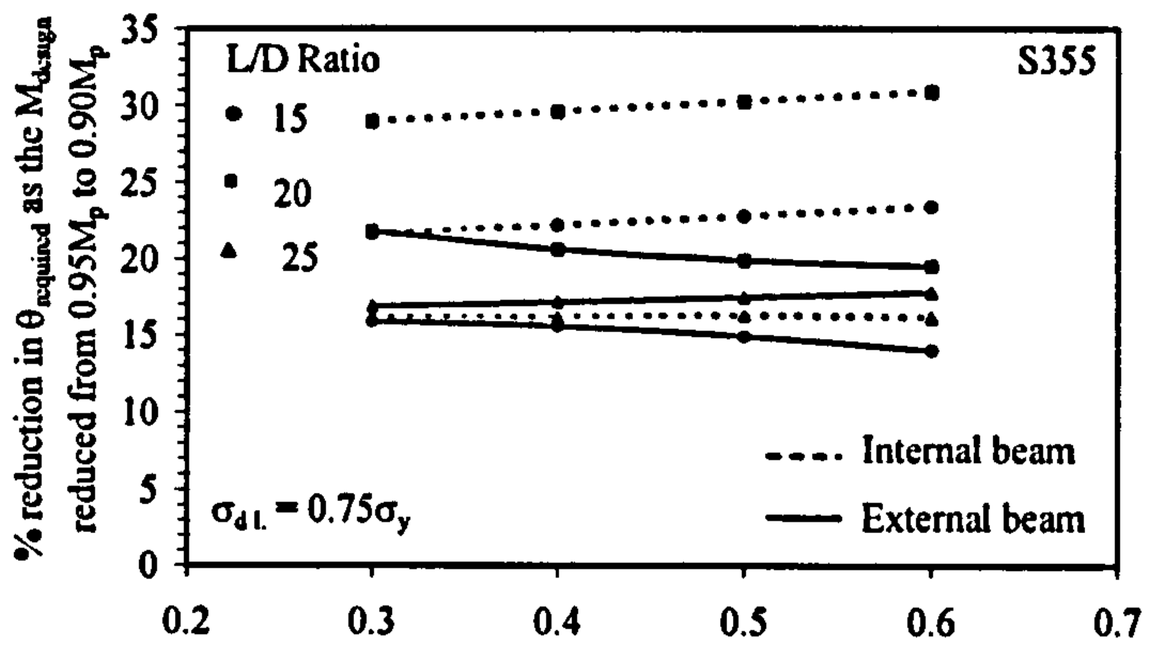

Figure C4-26. Percentage reduction in required rotation as the design moment reduced from 0.95 M_p to 0.85 M_p for unpropped form of construction: $\sigma_{dl} = 0.75\sigma_y$

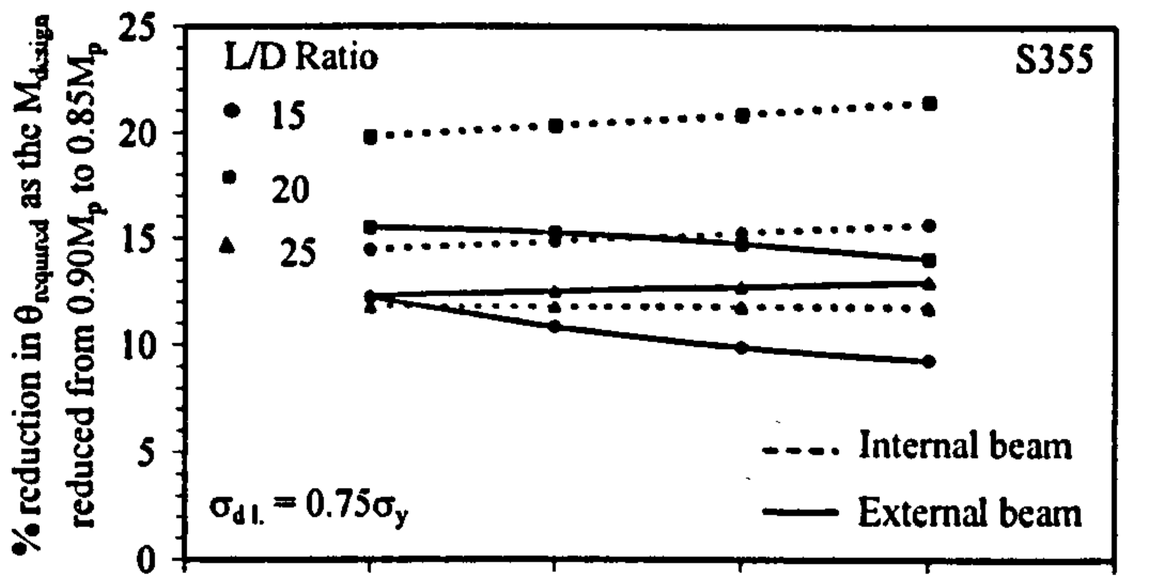

Figure C4-27. Percentage reduction in required rotation as the design moment reduced from 0.95 M_p to 0.90 M_p for unpropped form of construction: $\sigma_{dl} = 0.75\sigma_y$

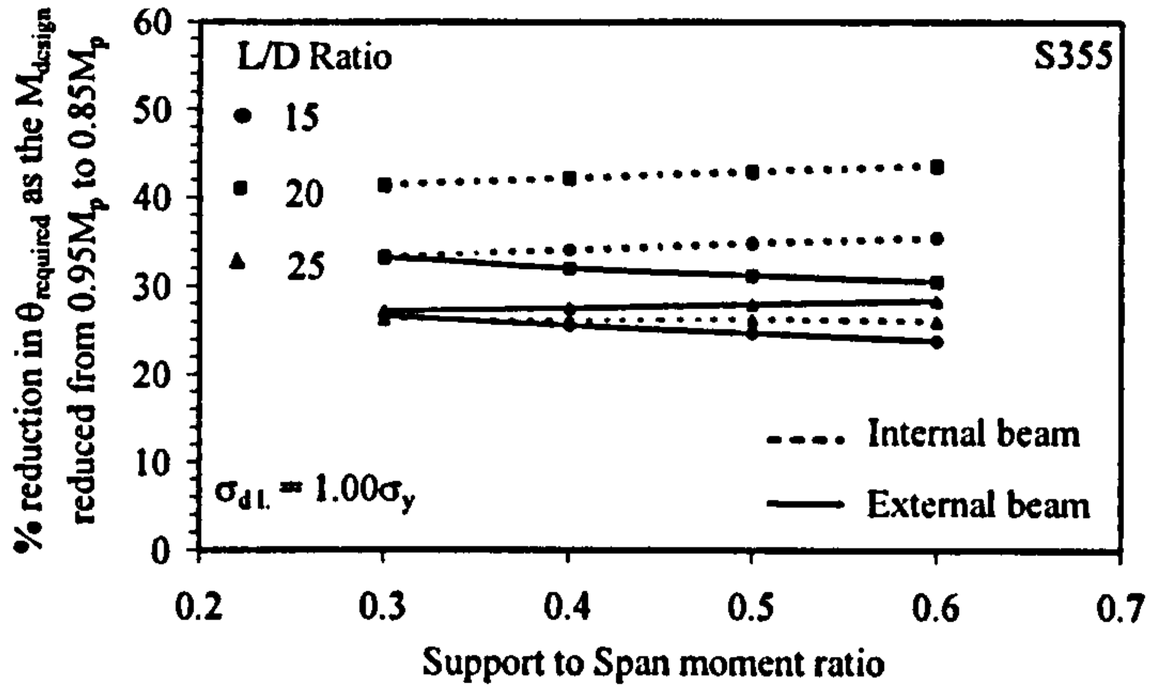

Figure C4-28. Percentage reduction in required rotation as the design moment reduced from 0.90 M_p to 0.85 M_p for unpropped form of construction: $\sigma_{dl} = 1.00\sigma_y$

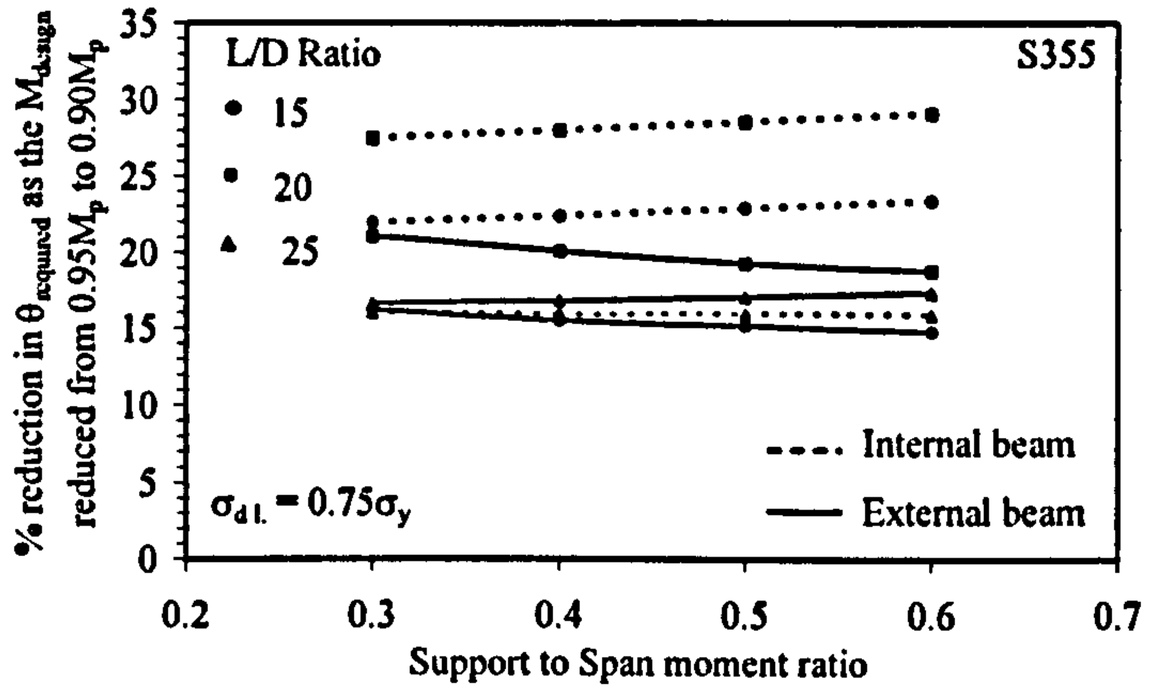

Figure C4-29. Percentage reduction in required rotation as the design moment reduced from 0.95 M_p to 0.85 M_p for unpropped form of construction: $\sigma_{dl} = 1.00\sigma_y$

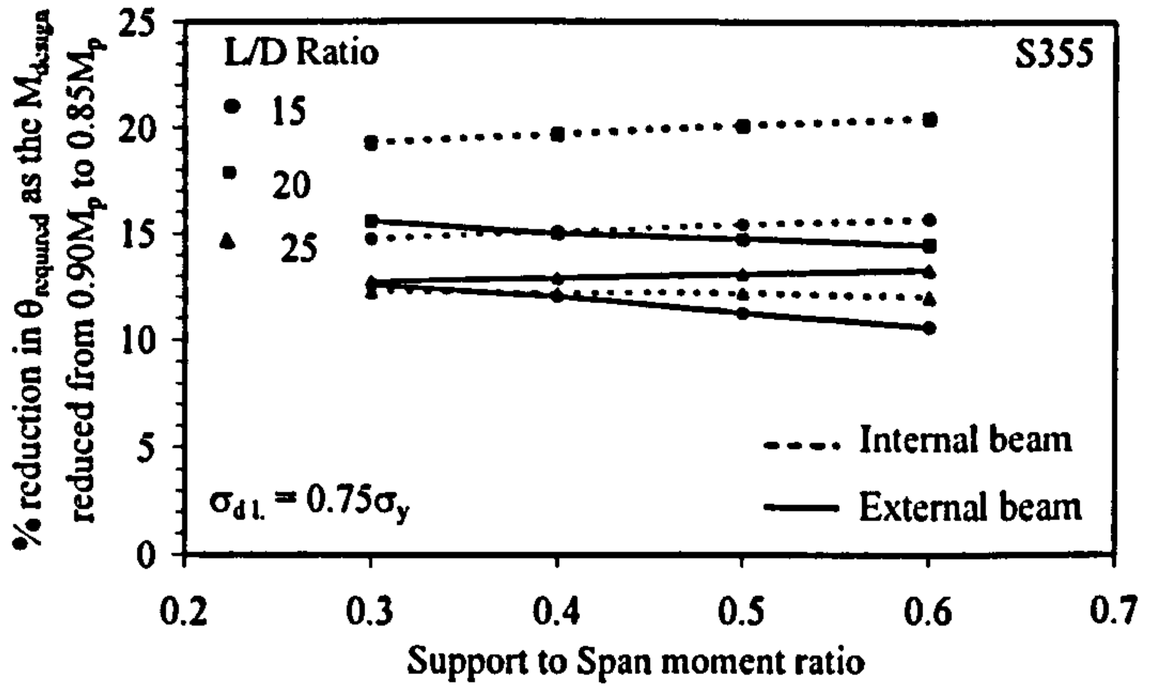

Figure C4-30. Percentage reduction in required rotation as the design moment reduced from 0.95 M_p to 0.90 M_p for unpropped form of construction: $\sigma_{dl} = 1.00\sigma_y$

Appendix D:

Worked example of unpropped semi-continuous composite beam

D1: Basic design data

Scheme	: Semi-continuous composite beam
Construction type	: Unpropped
Location within the frame	: Internal
Composite beam span	= 10m
Loaded width	= 3m

D.2 Composite beam geometry

457 x 152 x 60UB, Class 1 section, S275

Steel beam depth, D =454.6mm

Slab depth, D_s = 120mm

Profile depth, D_p = 60mm

Assume full shear connection

D.3 Construction stage loading

Dead load	= 3 kN/m^2
Imposed load	= 0.5 kN/m^2
ULS design load	= 1.4 x 3.0 + 1.6 x 0.5 = 5 kN/m^2
Design moment	= 10^2 x 3 x 5 / 8 = 188 kN.m

D.4 Composite stage loading

Dead load	= 3 kN/m^2
Imposed load and partitions	= 6 kN/m^2
ULS design load	= 1.4 x 3.0 + 1.6 x 6 = 13.8 kN/m^2
Design moment	= 10^2 x 3 x 13.8 / 8 = 518 kN.m

D.5 Steel beam properties

Area of the steel beam section, A = 7620 mm^2

Second moment of area of the steel section, I = 25500 x 10^4 mm^4

Elastic section modulus of the steel section, $Z = 1.1 \times 10^6\ mm^3$

Plastic moment capacity of steel beam = $1.2 \times 275 \times 1.1 \times 10^6 = 364$ kN.m

D.6 Composite beam properties

Effective width = 10000/4 = 2500mm

modular ratio, $\alpha_e = 15$

Second moment of area of an uncracked section,

$$I_c = I_x + \frac{B_e (D_s - D_p)^3}{12\alpha_e} + \frac{A B_e (D_s - D_p)(D + D_s + D_p)^2}{4\{A\alpha_e + B_e (D_s - D_p)\}}$$

$$I_c = 25500x10^4 + \frac{2500(120-60)^3}{12x15} + \frac{7620x2500(120-60)(454.6+120+60)^2}{4\{7620x15+2500(120-60)\}} = 69340x10^4\ mm^4$$

Neutral axis position, $y_e = \frac{A\alpha_e (D + 2D_s) + B_e (D_s - D_p)^2}{2\{A\alpha_e + B_e (D_s - D_p)\}}$

$$y_e = \frac{7620x15(454.6+2x120)+2500(120-60)^2}{2\{7620x15+2500(120-60)\}} = 167mm$$ (From the top of the slab)

Elastic section modulus for the concrete flange,

$$Z_c = \frac{I_c \alpha_e}{y_e} = \frac{69340x10^4 x15}{167} = 62281x10^3\ mm^3$$

Elastic section modulus of the steel member,

$$Z_s = \frac{I_c}{(D + D_s - y_e)} = \frac{69340x10^4}{(454.6+120-167)} = 1701x10^3\ mm^3$$

Plastic moment capacity of composite beam = 621 kN.m (Ref: SCI, Green book)

Design moment capacity of composite beam = 0.85Mp = 0.85 x 621 = 528 kN.m

D.7 Construction stage design

D.7.1 ULS design for semi-continuous steel beam

A moment connection having strength equal to approximately 30% of the beam moment capacity will be used at each end of the span, therefore the maximum applied sagging moment is taken as 77% of the free moment.

[Note: If the moment connection strength equal to approximately 60% of the beam moment capacity is used at each end of the span, then the maximum applied sagging moment will be taken as 63% of the free moment.]

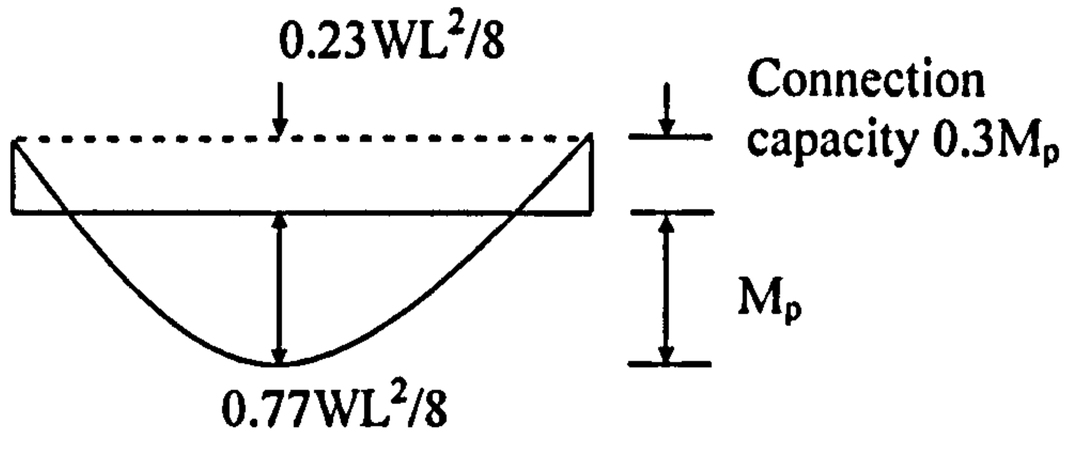

Free moment due to construction stage loading = 10^2 x 3 x 5 / 8 = 188 kN.m

Applied sagging moment, $M_{applied}$ = 0.77 x 188 = 145 kN.m < 364 kN.m Pass

D.7.2 Moment connection design

From SCI guide P-183, provide moment connection comprising 2 rows of M20 8.8 bolts with 200x12mm thick S275 flush end plate. This arrangement gives connection moment capacity of 122kN.m.

Minimum connection moment = 0.3Mp = 109 kN.m < Connection capacity

Maximum connection moment = 0.6Mp = 218 kN.m > Connection capacity Pass

D.7.3 SLS design for semi-continuous steel beam

a. Deflection check

Ref: BS 5950 Part 3: Section 2.4.2

Deflection under dead load for unpropped construction:

Serviceability dead load = 1.0 x 3 = 3 kN/m^2

Dead load deflection, $\delta_{dead} = \beta\, wL^4 / 384\, EI$

For an internal beam, with connections having a strength less than 0.45Mp, β=3.5

Dead load deflection, δ_{dead} = 3.5 (3 x 3) 10000^4 / (384 x 205000 x 2.51 x 10^8)

= 16mm < 25mm in the non-composite stage to limit ponding of the concrete <u>Pass</u>

<u>b. Bending stress check</u>

Max. stress in steel section due to factored construction stage loading, (dead load stress)

= $M_{applied}$ /z = 145 x 10^6 / 1.1 x 10^6 = 132 N/mm^2

Dead load stress / Yield stress = 132 / 275 = 0.48 N/mm^2

[Note: For connection moment equal to 0.6M_p, Dead load stress / Yield stress = 118 / 275 = 0.39 N/mm^2]

<u>c. Vibration response</u>

Dead load deflection assuming simple supports = 5 wL^4 / 384 EI = 23mm

Natural frequency of the beam = 18 / $(23)^{1/2}$ = 3.8. This exceeds the lower limit of 3Hz, so a check of beam response to dynamic loading is not required. <u>Pass</u>

D.8 Composite stage design

D.8.1 ULS design for semi-continuous composite beam

A composite connection having a strength equal to approximately 30% of the beam moment capacity will be used at each end of the span, design sagging moment of the composite beam is taken as $0.85M_p$, therefore the maximum applied sagging moment is taken as 87% of the free moment.

[Note: If a composite connection having a strength equal to approximately 60% of the beam moment capacity is used at each end of the span and the design sagging moment of the composite beam is taken as $0.85M_p$ then the maximum applied sagging moment will be taken as 67% of the free moment.]

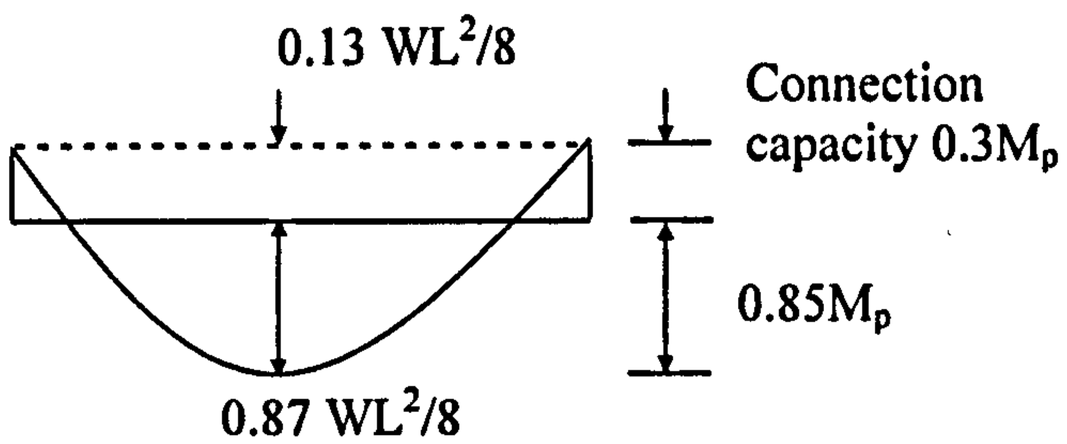

Free moment due to composite stage loading= 10^2 x 3 x 13.8 / 8 = 518 kN.m

Applied sagging moment = 0.87 x 518 = 451 kN.m < 528 kN.m Pass

D.8.2 composite connection design

From SCI guide 213/98, provide composite connection comprising 4 nos. ϕ16 rebars and 2 rows of M20 8.8 bolts with 200x12mm thick S275 flush end plate. This arrangement gives composite connection moment capacity of 303 kN.m.

Minimum connection moment = 0.3Mp = 186 kN.m < Connection capacity

Maximum connection moment = 0.6Mp = 373 kN.m > Connection capacity Pass

D.8.3 SLS design for semi-continuous composite beam

a. Deflection check

Ref: BS 5950 Part 3: Section 2.4.2

Deflection under unfactored imposed load:

Serviceability imposed load = 1.0 x 6 = 6 kN/m^2

Imposed load deflection, $\delta_{imposed} = \beta\, wL^4 / 384\, EI_c$

For an internal beam, with connections having a strength less than 0.45Mp, β=3.5

Imposed load deflection, $\delta_{imposed}$ $= 3.5\ (6 \times 3)\ 10000^4 / (384 \times 205000 \times 69340 \times 10^4)$

$= 12mm < Span/360$

<u>b. Bending stress check</u>

Bending moment due to unfactored dead load = $3 \times 3 \times 10^2/8 = 113 kN.m$

Bending moment due to unfactored impose load = $6 \times 3 \times 10^2/8 = 225 kN.m$

Max. stress in steel due to unfactored dead load = $\frac{113 \times 10^6}{1.1 \times 10^6} = 103\, N/mm^2$

Max. stress in steel due to unfactored impose load = $\frac{225 \times 10^6}{1.7 \times 10^6} = 132\, N/mm^2$

Combined stress = $103+132 = 235\ N/mm^2 < 275\ N/mm^2$

Max. stress in concrete = $\frac{225 \times 10^6}{62.281 \times 10^6} = 3.6\, N/mm^2 < 0.45 f_{cu}$

<u>c. Vibration response</u>

Dead load deflection assuming simple supports = $5\ wL^4 / 384\ EI$

Dead load deflection, δ_{dead} $= 5\ (3 \times 3)\ 10000^4 / (384 \times 205000 \times 69340 \times 10^4) = 8mm$

Natural frequency of the beam = $18 / (8)^{1/2} = 6.2$ Hz

This exceeds the lower limit of 4Hz, so a check of composite beam response to dynamic loading is not required.

LIST OF PUBLICATIONS

1. Byfield, M. P., M. Dhanalakshmi, Couchman, G. H. and Goyder, H. G. D. (2005) Limitations in the use of composite connections with unpropped construction, *Eurosteel 2005 conference*.
2. Byfield, M. P., M. Dhanalakshmi and Couchman. G. H. (2004). "Assessment of the use of composite connections with unpropped composite beams", Journal of Constructional Steel Research, Volume 60, 1369-1386.
3. Byfield, M. P., Dhanalakshmi, M. and Goyder, H. G. D. (2004). "Modelling of un-propped semi-continuous composite beams". Journal of Constructional steel research, Volume 60, 1353-1367.
4. Byfield, M. P., Davies, J. M. and M. Dhanalakshmi. (2004). "Calculation of the strain hardening behaviour of steel structures based on mill tests", Journal of Constructional Steel Research, Vol. 61, 133-150.
5. Dhanalakshmi, M., Byfield, M. P. and Couchman, G. H. (2002). Composite connections at perimeter locations in unpropped composite floors, *International Conference on Advances in Steel Structures (ICASS 02)*, Hong Kong, 261-268.
6. Byfield, M. P., M. Dhanalakshmi, (2002). Analysis of strain hardening in steel beams using mill tests, *International conferences on advances in steel structures*, Hong Kong, 139-146.
7. Dhanalakshmi, M. and Byfield, M.P. (2002) *Strength and Ductility of Composite connections*, The Structural Engineer, Volume 80, Number 20